Advances in INSECT PHYSIOLOGY

INSECT MECHANICS AND CONTROL

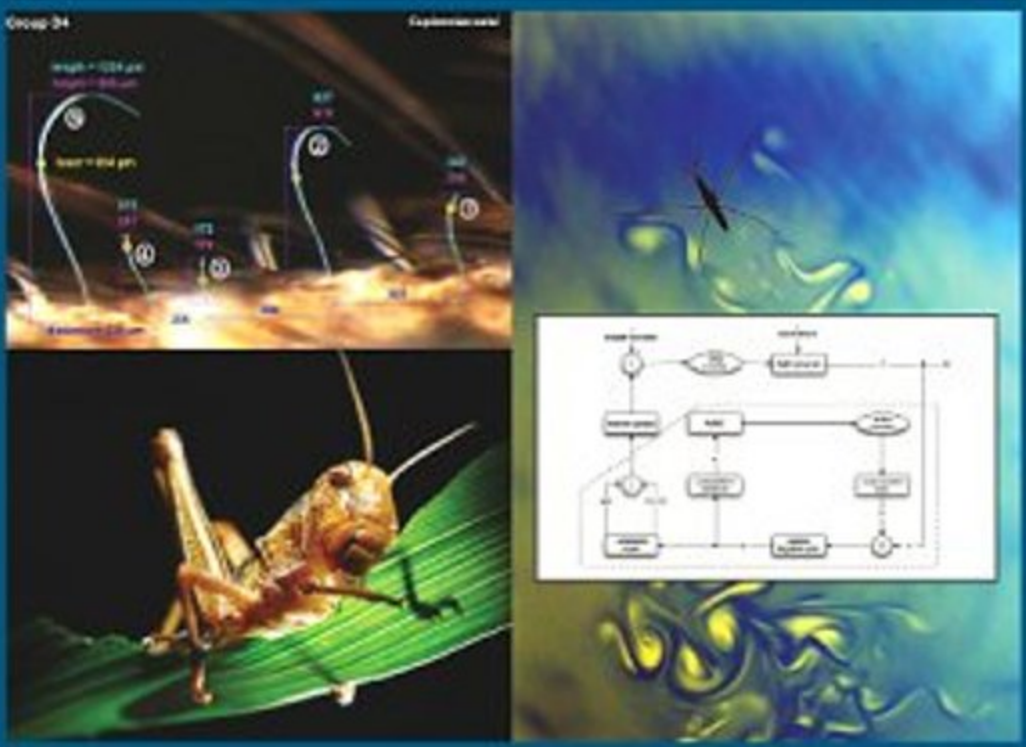

Volume 34

Edited by JÉRÔME CASAS
and STEPHEN J. SIMPSON

Series Editor STEPHEN J. SIMPSON

AP

Contributors

F.G. Barth
Department of Neurobiology and Cognition Research, Life Sciences, University of Vienna, Wien, Austria

A. Büschges
Department of Animal Physiology, Zoological Institute, University of Cologne, D-50923 Cologne, Germany

J.W.M. Bush
Department of Mathematics, MIT, Cambridge, MA 02139, USA

J. Casas
Institut de Recherche en Biologie de l'Insecte, CNRS and Université de Tours, Tours, France

F.J. Clissold
Behaviour, Physiology and Ecology Research Group, School of Biological Sciences, The University of Sydney, Australia

S.N. Gorb
Evolutionary Biomaterials Group, Department of Thin Films and Biosystems, Max Planck Institute for Metals Research, D-70569 Stuttgart, Germany

M. Gruhn
Department of Animal Physiology, Zoological Institute, University of Cologne, D-50923 Cologne, Germany

D.L. Hu
The Courant Institute of Mathematical Sciences, NYU, New York, NY, USA

J.A.C. Humphrey
Department of Mechanical and Aerospace Engineering, Department of Biology, University of Virginia, Charlottesville, VA 22904-4746, USA

H.G. Krapp
Department of Bioengineering, Imperial College London, South Kensington Campus, London, SW7 2AZ, UK

M. Prakash
Center for Bits and Atoms, MIT, Cambridge, MA, USA

S.J. Simpson
School of Biological Sciences, The University of Sydney, Sydney, Australia

G.K. Taylor
Department of Zoology, University of Oxford, Tinbergen Building, South Parks Road, Oxford, OX1 3PS, UK

Introduction

This special thematic volume of *Advances in Insect Physiology* is the first book ever published with a focus on insect mechanics and control. Reasons for such a late interest in an otherwise important field are numerous and include the traditional disregard of physics by biologists, as Steve Vogel regrets in his book '*Comparative Biomechanic*s'. An impediment to many biologists is a fear of equations and a limited understanding of the latest technological tools available within the large domains of biological physics, nanobiotechnology and chemical biology. Although many of the present generation of biologists are superbly well equipped in the techniques of genomics and molecular biology, the more instrumental sciences have tended to pass us by. An exception is insect flight, an area which has seen a major upsurge of interest recently among biologists, spurred on by the involvement and interest of physicists and engineers. The publication of the second edition of the long since out of press book by Akira Azuma '*The Biomechanics of Flying and Swimming*' by the *American Institute of Aeronautics and Astronautics* is a telling example of the growing interest among physical scientists in biology. Our hope in drawing together the authors for the present volume was that we might provide an accessible synthesis of a series of topics in insect mechanics and control – topics, which although dealt with in isolation, have never been brought together in one place.

Although the topics covered are original and at the fore front of the interface between organismal biology, physics, engineering and applied mathematics, the spirit with which the selected chapters have been conceived remains true to the *Advances in Insect Physiology* series: deep insights gained by specialist researchers, presented in detailed, scholarly monograph form. At a time in which major review journals ask authors to reduce the number of references in their 'reviews' to a bare minimum, sometimes with a bias for the latest ones, the *Advances in Insect Physiology* series represents one of the last venues to present a comprehensive and well-rounded story supported by ample equations and graphs. We strongly believe that only a serious wrestling with any subject matter sheds sufficient light to spark analogies and generalities. This is the reason why the *Advances in Insect Physiology* series was the most appropriate venue to convey the message of the book.

The average insect weighs only a few milligrams, yet they are capable of extraordinary feats of behavioural control, belying the traditional view of them as simple, hard-wired automata. Indeed, the combination of small size and behavioural sophistication is probably the key to the success of the insects. But being tiny poses physical challenges, and the physical world in which these creatures live is unlike ours. For example, getting wet poses life-threatening risks, yet moving upside down on the ceiling is a trivial task. If we are to understand the behavioural ecology of insects, we must be able to make sense of the physical worlds in which they live. But there are challenges to seeking a physical understanding of insects. First, even among the insects there is a huge range of sizes, from minute fairy flies with wings spans of 0.5 mm to beetles and moths weighing tens of grams. A flying thrips has little in common with a hovering hawkmoth, and a scientist interested in these tiny creatures might be well served by looking at the hydrodynamics of swimming copepods. Second, insects typically occupy an awkward region in physical parameter space, in which one despairs of searching for some terms to drop in equations: the values are not extremely small, yet neither are they extremely large! As an example, let us think of a wolf spider pursuing its cricket prey among the forest litter and let us assume that one is interested in the kind of flow the spider is producing ahead of it; a valuable source of information which is used by the escaping cricket. The Reynolds Number of the spider will be somewhere between 10 and 100, leaving any analytical approximation of the Navier–Stokes equation looking somewhat suspicious. One is then tempted to resort to numerical solution of the full equation.

This is where high-tech comes into play. Nowadays, one can numerically solve increasingly complex phenomena on a desktop computer, which is a boon for biological problems that are difficult to cast into neat analytical equations. But progress in understanding is secured only once the output is backed by hard facts. Luckily, the following chapters are replete with technology which enables us to measure and visualize the results. Examples are laser-based Particle Image Velocity (PIV), Atomic Force Microscopy (AFM) and high-speed cameras of many kinds, including the latest combinations for 3D vision. These new tools, hardly available a decade ago, enable us to look at last at processes occurring at the very same size scale at which the animal is experiencing a force or making its behavioural decisions. Interestingly, these new technical tools offer to reinvigorate a field which was until recently considered as *passé*: functional morphology. This discipline had to some degree stagnated and, wrongly, become seen as less relevant than modern molecular approaches. Quantifying complex phenotypes and describing how they relate to, and are regulated by, the interaction between genes and the physical and biological environments during development is of paramount importance in a post-genomic world.

The association between insects and high-tech is, however, a two-way relationship. Bionics and biomimetics initiatives are increasingly supported by public, industrial and private agencies worldwide, in the accelerating quest for energy-sparse locomotion, smart materials and solutions to complex decision and control problems. Insect mechanics and control has a huge potential to offer in this respect, from Micro-Electronical-Mechanical Systems (MEMS) design, to flapping flight Micro Air Vehicles (MAV) and robotics. The millions of insects on earth are millions of solutions to specific problems: an endless source of inspiration.

This book shows very clearly that the mechanics of sensors, locomotory appendages and mouth parts, no matters how well understood in terms of physical quantities, cannot be fully understood without being integrated into their neural control systems. We are, however, still very far from understanding the distributed processing of information gathering by thousands of sensors of different kinds, let alone the operation of the central neural control networks. Much progress has been made by neurobiologists, both conceptually and in terms of the fine detail of sensors and circuits, but there is a long way to go. Further away yet, at the far horizon, is the merging of insect mechanics with other fields, for example life history theory or insect chemoecology. For example, the processes occurring in the physico-chemical boundary layers during antennal olfaction have hardly attracted attention, despite their obvious importance.

We hope that this book sparks interest in the field of insect mechanics and control, both among biologists and physical scientists. We thank the dozens of referees for their precious help, some of whom worked on large manuscripts under strong time pressure. We are extremely grateful to Pedro Telleria Teixeira and Pat Gonzalez for their tremendous efforts in helping with the formatting and style checking of submitted manuscripts. Finally, we must thank the authors for doing such a wonderful job. The work of J. Casas on insect mechanics is supported by the two bionics EU-grants CICADA (IST-2001-34718) and CILIA (IST-016039), while Steve Simpson edited this volume with an ARC Federation Fellow at the University of Sydney.

Jérôme Casas
Stephen J. Simpson

Medium Flow-Sensing Hairs: Biomechanics and Models

Joseph A.C. Humphrey[a] and Friedrich G. Barth[b]

[a]*Department of Mechanical and Aerospace Engineering, Department of Biology, University of Virginia, Charlottesville, VA, USA*

[b]*Department of Neurobiology and Cognition Research, Life Sciences, University of Vienna, Wien, Austria*

1 Introduction: medium flow-sensing hairs in the animal kingdom 2
1.1 Functional morphology 4
1.2 Hair arrays 11
2 Hair motion physical–mathematical models 15
2.1 Single hairs: physically exact and approximate model approaches 16
2.2 Hair suspension: torsional restoring constant S and damping constant R 28
2.3 Model validation: comparison between measurements and calculations 31
2.4 Hair arrays: the question of viscosity-mediated coupling 36
3 Parameter effects 40
3.1 Medium contributions to hair inertia and damping and to flow-induced forces 40
3.2 Dependence of hair motion on the geometry and physical properties of the hair, and on medium dynamics and physical properties 43
4 Discussion 51
4.1 Sensitivity and selectivity 51
4.2 Sensory ecology 54
4.3 Evolution through selective pressures on different parameters 61
5 Bio-inspired artificial motion sensors 63
5.1 Motivation and applications 63
5.2 Enabling materials and fabrication technologies 64
5.3 Some practical considerations 68
Notation (dimensions in SI units) 69
Acknowledgements 72
References 73
Appendix A Determination of the frequency corresponding to the maximum slope of the maximum angular velocity of an oscillating hair 77
Appendix B Filiform hair response to a transient pulsating boundary layer flow 78

ADVANCES IN INSECT PHYSIOLOGY VOL. 34
ISBN 978-0-12-373714-4
DOI: 10.1016/S0065-2806(07)34001-0

Abstract

Arthropods use fluid medium motion-sensing filiform hairs on their exoskeleton to detect aerodynamic or hydrodynamic stimuli in their surroundings that affect their behaviour. The hairs, often of different lengths and organized in groups or arrays, respond to particular fluid motion amplitudes and frequencies produced by prey, predators, or conspecifics, even in the presence of background noise peculiar to the environment. While long known to biologists and experimentally investigated by them, it is only relatively recently that comprehensive physical–mathematical models have emerged offering an alternative methodology for investigating the biomechanics of filiform hair motion. These models have been developed and applied to quantitatively predict the performance characteristics of filiform hairs in air and water as a function of the relevant parameters that affect their physical behaviour. They even allow the exploration of possible biological evolutionary paths for filiform hair changes resulting from physical selection pressures. In this chapter we review the state of knowledge of filiform hair biomechanics and discuss two physical–mathematical models to predict hair dynamical behaviour. One modelling approach is analytically exact, serving for quantitative purposes, while the other, derived from it, is approximate, serving for qualitative guidance concerning the parameter dependencies of hair motion. Using these models we look in turn at the influence of these parameters and the fluid media physical properties on hair motion, including the possibility of medium-facilitated viscous coupling between hairs. The models point to areas where data is currently lacking and future research could be focused. In addition, new results are presented pertaining to transient flows. We qualitatively explore the possibility of an overlapping water–air niches adaptation potential that may explain how, over many generations, the filiform hairs of an arthropod living in water could have evolved to function in air. Because flow-sensing hairs have served to inspire corresponding artificial medium motion microsensors, we discuss recent advances in this area. Significant challenges remain to be overcome, especially with respect to the materials and fabrication techniques used. In spite of the impressive technological advances made, nature still remains unrivalled.

1 Introduction: medium flow-sensing hairs in the animal kingdom

Life is immersed in fluids which are hardly ever motionless. Thus, living organisms are exposed to the flow of water and to the movement of air almost permanently. There are abiotic and biotic sources of medium flow, including the situation when an organism actively moves relative to the

fluid surrounding it. In many animals behaviour such as predation and escape are guided by medium flow. Therefore, it is not surprising that the sensory reception of medium flow is a capacity found in almost all animal groups and that it is highly developed in a number of them.

In fact, the reception of hydrodynamic stimuli informing an organism about its aquatic environment is known to occur in protozoans, coelenterates, flatworms, annelids, molluscs, crustaceans, echinoderms, chaetognaths, urochordates, cephalochordates, fishes, amphibians, and mammals (Budelmann, 1989; Bleckmann, 1994). Likewise, the reception of air movement by terrestrial animals is widespread among the arthropods such as the pseudoscorpions, scorpions, mites, spiders (Reißland and Görner, 1985), and insects, in particular the orthopterans.

Despite their widespread occurrence and different evolutionary origin, medium flow receptors share one conspicuous property: they all represent hair-like structures with the hair shaft forming a lever flexibly suspended in the skin or exoskeleton. In all cases the hair shaft responds to the viscous forces exerted by the medium flow and is more or less easily deflected by these forces. One or several sensory neurons at the hair base pick up the mechanical stimulus passed on to them by the movement of the inner end of the hair shaft.

Although sharing overall similarity, the medium flow sensors of different animal groups are likely not to be homologous in most cases. Instead, they represent a perfect example of convergent evolution, having responded to the same physical selection pressures relevant for a medium flow sensor. This also applies for different groups within the arthropods. Thus the filiform hair sensilla of insects like cockroaches, crickets, or locusts on the one hand, and the trichobothria of spiders and scorpions on the other, differ with regard to location on the body, number of sensory cells, and the way their dendritic ends are attached to the hair shaft. Even the homology of the trichobothria between spiders and scorpions is doubtful (Reißland and Görner, 1985).

Our review will concentrate on the terrestrial environment, that is, on the reception of air flow. It will mainly draw from research conducted with spiders and crickets and concentrate on biomechanical rather than neurobiological and behavioural aspects. It should be stressed at the outset, however, that the theoretical treatment which follows is applicable to both air and water treated as incompressible fluid media (motions induced by sound propagation playing no role), and indeed predicts a number of differences related to the differences in the physical properties of the two media (Devarakonda *et al.*, 1996; Humphrey *et al.*, 2001, 2003; Barth, 2004). Among the most relevant such differences are the following for hairs immersed in oscillating flows: (i) hair substrate boundary layer thickness: $\delta_{\text{water}} \approx 0.22 \times \delta_{\text{air}}$; (ii) force per unit hair length: $F_{\text{water}} \approx 43 \times F_{\text{air}}$; (iii) total moment of inertia per unit hair length: $I_{\text{t(water)}} \gg I_{\text{t(air)}}$.

The relevance for the functional morphology of a hair-like flow sensor is discussed later.

1.1 FUNCTIONAL MORPHOLOGY

1.1.1 *Absolute sensitivity*

One of the incentives to study the morphology of arthropod flow sensors is the remarkable sensitivity of some of them. In crickets and spiders the work needed to drive their flow-sensing hairs through one movement cycle at threshold deflection is between 2.5×10^{-20} J and 1.5×10^{-19} J (Thurm, 1982a,b; Humphrey *et al.*, 2003). According to Shimozawa *et al.* (2003), the cricket cercal filiform hairs at threshold work near the thermal noise of Brownian motion with signal enhancement by stochastic resonance. The given sensitivity values correspond to a fraction of the energy contained in a single quantum of green light allowing these arthropod flow sensors to operate at the limit of what is physically possible. In their frequency range of operation, their sensitivity is by no means inferior to that of our own most sensitive receptor cells in the eye and ear (Gitter and Klinke, 1989). Obviously, the hair–air interaction is highly perfected in arthropod air flow sensors.

Because the energy thresholds of arthropod flow sensors are close to $k_B T$ (k_B, Boltzmann constant, T absolute temperature; 4.1×10^{-21} J at 300 K), the sensors will be exposed to thermal noise when working at threshold. Direct evidence for this conjecture comes from experiments demonstrating the fluctuations of the timing of sensory cell action potentials in response to near-threshold sinusoidal stimulation (Shimozawa *et al.*, 2003). Thus the receptor cells are subject to an internal noise similar in magnitude to that of the response at threshold. Interestingly, the super-imposition of minute external noise elicits action potentials of the sensory cell when stimulated by a very weak sub-threshold stimulus. Such an enhancement of signal detection by the addition of noise is known as stochastic resonance (Douglass *et al.*, 1993).

In the case of cricket flow sensors the cell-intrinsic thermal noise is used by the sensory cells for stochastic sampling and signal detection (Shimozawa *et al.*, 2003). Stochastic resonance has also been demonstrated at the level of first-order interneurons in the terminal abdominal ganglion of a cricket (Levin and Miller, 1996). Signal encoding could be considerably improved through the addition of external noise in the stimulus regime close to threshold.

1.1.2 *Torsional restoring constant S and damping constant R*

Viewed in detail, the Bauplan of arthropod mechanically sensitive hair sensilla is a source of considerable variation. Figure 1, which is based on

spider hair sensilla, shows in a simplified way the commonalities and differences between a flow-sensing hair and a tactile hair (Barth, 2004).

Note that the torsional restoring constant S, which works to drive the deflected hair back to its resting position and thus counteracts deflection, is smaller by as much as three-to-four orders of magnitude in flow-sensing trichobothria ($S \sim 10^{-12}\,\mathrm{Nm\,rad^{-1}}$) than in tactile hair sensilla (Barth and Dechant, 2003). A related specialization of the flow sensor is that it does not bend when being deflected by the torque due to the viscous forces exerted by the medium flow along its shaft. In contrast, the tactile hair is usually stimulated from above and is bent substantially while being deflected (Dechant *et al.*, 2001). As a consequence, in the case of the air flow sensor the moment of inertia of the hair shaft is a critical parameter when considering its deflection by the viscous forces exerted by the air flow around it, whereas in the case of the tactile hair the Young's modulus, E, of the hair material and its distribution (J, second moment of area) along the length of the hair shaft are of crucial importance.

Like S, the damping constant R of a mechanically sensitive hair sensillum is a property inherent to the complex structure that supports the hair at its base. Also like S, the damping constant R counteracts hair deflection. Unlike S, however, R is more difficult to measure and experimental values are uncommon. In Section 2.2, two recently proposed methods for simultaneously determining S and R are presented. These approaches yield values of $R \sim 10^{-15}\,\mathrm{N\,m\,s\,rad^{-1}}$ for the trichobothria of *Cupiennius salei* (see, also, Humphrey *et al.*, 2001).

1.1.3 *Lever system*

As will be shown in Sections 2 and 3, the physics of the air–hair interaction is the initial step in a complex series of events transforming the input from the environment into the mechanical stimulus which finally elicits a nervous signal at the sensory cell membrane. Notwithstanding these complexities, the hair shaft forms a simple lever with its long arm exposed to the medium flow and its short arm coupled to the sensory cells. According to microscopic measurements in live slice preparations of the flow sensors of a spider (*C. salei*), a scorpion (*Euscorpius italicus*), a cricket (*Acheta domesticus*), and a cockroach (*Periplaneta americana*), the location of the axis of rotation is such that the length relation between the outer and the inner lever arm is large in all cases, reaching ratios of more than 1000:1. This is in good agreement with fine structural data (Christian, 1971, 1972; Gnatzy and Tautz, 1980; Anton, 1991; for review see Barth, 2002b). It implies that the displacement of the hair tip is scaled down considerably while the force at the same time is scaled up by the same factor and reminds of the

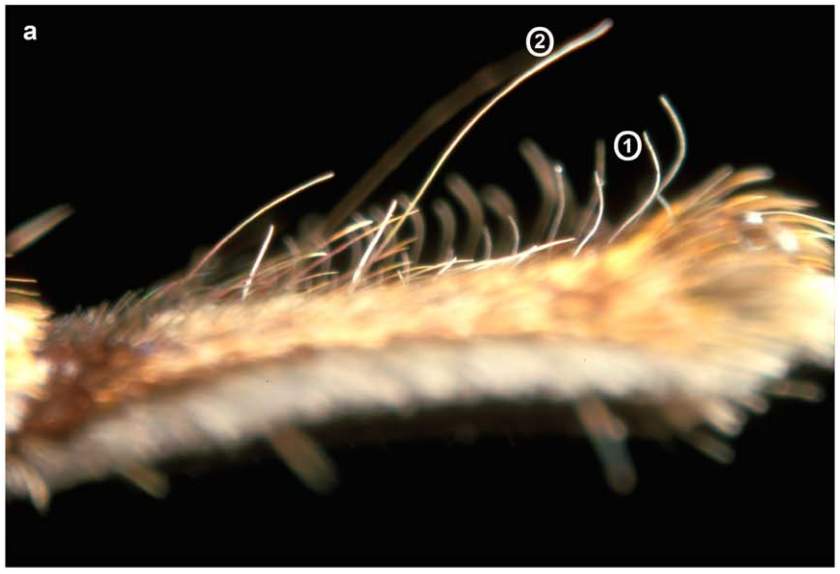
a
②
①

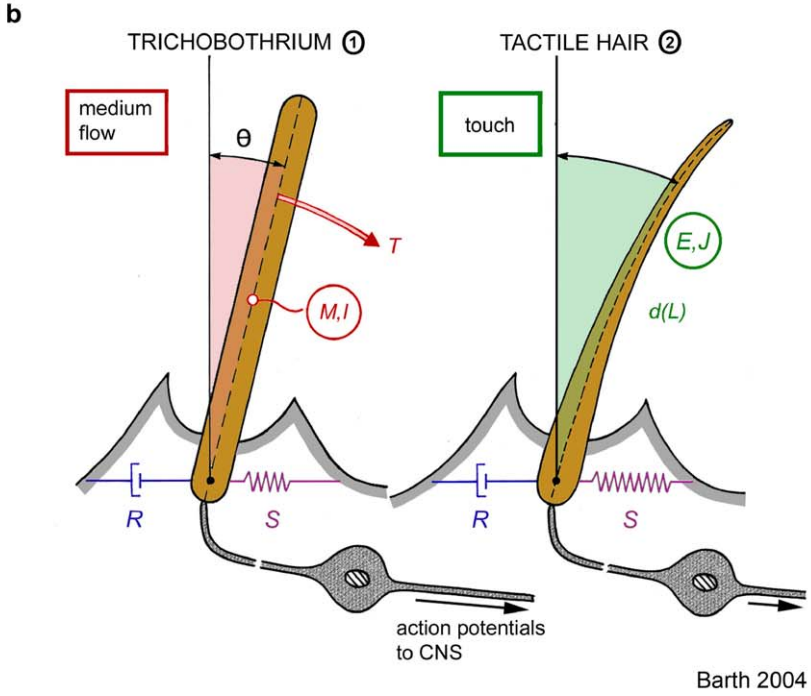
b
TRICHOBOTHRIUM ①
TACTILE HAIR ②
medium flow
θ
T
M,I
touch
E,J
d(L)
R
S
R
S
action potentials to CNS
Barth 2004

mechanical properties of the mammalian middle ear (22:1); however, the effect is much larger in the flow sensors.

From these data and the direct microscopic observation of slice preparations (Görner, 1965) the deflection of the hair shaft at the sensory cell membrane proper, that is the effective mechanical input transduced to a receptor potential, can be derived. Taking a displacement of the outer hair shaft of 1°, the inner end of the short lever arm moves by 30 nm in the case of the cercal hairs of the cricket *Gryllus bimaculatus* (Gnatzy and Tautz, 1980), and by about 7 nm in the case of the trichobothria of the spider *C. salei*. Taking a threshold displacement of 0.1° or even 0.01° (lowest value found) for spider trichobothria (Barth and Höller, 1999) the displacement close to the dendrite eliciting an impulse response reduces to 0.07 nm.

1.1.4 *Surface and mass*

In some air flow sensors like the trichobothria of *C. salei* the surface of the hair shaft is conspicuously feathery with 4–14 minute branches for each 10 μm hair length (Fig. 2). This is found in other spiders as well but by no means in all of them, the orb weaver *Nephila clavipes* being one of the exceptions with a more or less smooth surface (Barth, 2002b). These numerous structures (or branches) increase the drag force acting on the sensillum and thus its sensitivity. This is because the air flow around the trichobothrium is dominated by viscous forces at Reynolds numbers less than 1, typical of filiform hairs, and because the branches significantly increase the surface area available for the action of viscous drag. The proximity of the branches works to arrest the motion of air between them, effectively increasing the characteristic diameter of the hair upon which the viscous drag per unit length is based (Schlichting, 1979).

Along with this goes an optimization of the hair as a lightweight structure since, whereas the drag forces are determined by the outer contour of the hair, the 'inertial' diameter of the hair is much smaller. This saves building material without significantly changing the mechanical frequency response of the hair (Fletcher, 1978; Barth *et al.*, 1993).

FIG. 1 (a) The last segment (tarsus) of the walking leg of a spider (*C. salei*) with trichobothria (1) and tactile hairs (2) on its dorsal side. (b) Whereas the Bauplan is basically the same for the two hair sensilla, only a few differences turn them into an air flow sensor (trichobothrium) or a tactile hair, respectively, as is explained in the text. *Note: T*, torque induced by the air flow and deflecting the hair shaft; *M*, mass of the hair shaft; *I*, inertia due to *M*; *R*, damping constant; *S*, torsional restoring constant, like *R* resisting hair deflection; *E*, Young's modulus; *J*, second moment of area; *d*(*L*) diameter of hair shaft as a function of hair length. (From Barth, 2004; Current Opinion in Neurobiology 14: 415–422; with kind permission of Elsevier.) (see color plate section at the end of this book).

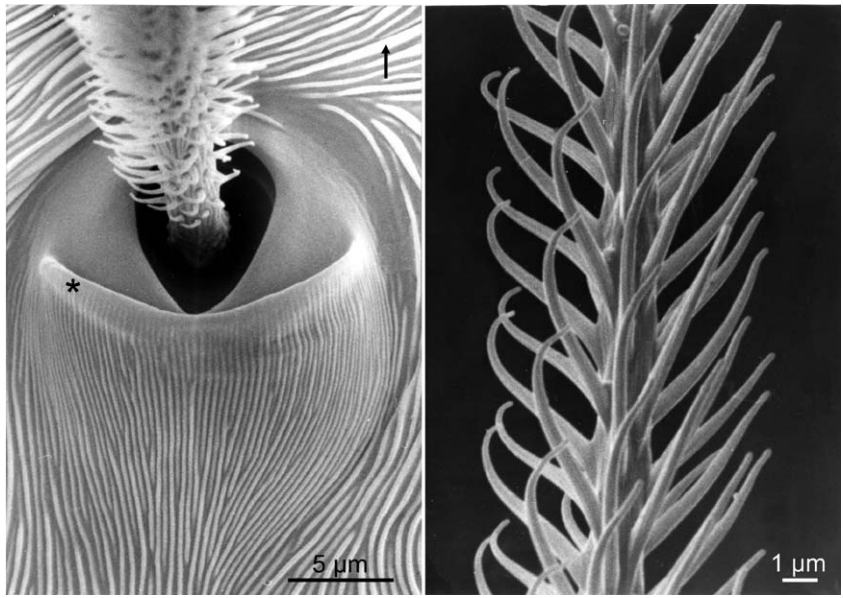

FIG. 2 Fine structure of cuticular cup surrounding the base of the hair shaft of a spider (*C. salei*) trichobothrium (left) and branches of the hair shaft (right) increasing the area available for the action of viscous drag.

1.1.5 *Coupling of dendrite(s)*

The coupling of the dendrite(s) to the inner end of the hair shaft differs substantially in different animal groups. Since this review concentrates on arthropod air flow reception, two examples of such differences are given here for insects and spiders, again arguing against a homology of the two cases. Figure 3 compares the fine structure of a cricket cercus filiform hair with that of a spider trichobothrium. In the case of the cricket the inner end of the hair shaft presses against the single dendrite of the only sensory cell innervating this sensillum by way of a small cuticular protrusion. This protrusion moves against the dendritic sheath when the hair shaft is deflected in the direction leading to depolarization. However, the spider trichobothrium is supplied by four dendrites belonging to four sensory cells. The dendrites terminate in a cuticular helmet-like structure. According to an old hypothesis supported by microscopic observations of live sensilla and electrophysiological experiments (Görner, 1965), the dendrites are stimulated by being slightly stretched (or compressed) when the lower rim of the helmet moves towards them as a result of hair shaft displacement. Depending on the direction of hair deflection different dendrites or sets of dendrites are stimulated. This implies that in spider

trichobothria different directions of hair deflection are represented by different sensory cells (Görner, 1965). Accordingly, in spider trichobothria (Reißland and Görner, 1978; Barth *et al.*, 1993) the mechanical directionality of hair shaft angular displacement is usually weak as compared to cricket (Landolfa and Jacobs, 1995) and cockroach filiform hairs (Nicklaus, 1965).

1.1.6 *Hair length and boundary layer thickness*

A conspicuous feature of terrestrial arthropod air flow-sensing hairs is the similarity of their lengths, which consistently vary within a narrow range roughly between 100 µm and 2000 µm, extreme lengths being those found in the bird spider *Sericopelma* (2500 µm) (Den Otter, 1974) and *G. bimaculatus* with 3000 µm (Gnatzy and Schmidt, 1971). Indeed, varying hair length within this range is the most effective way to modify the mechanical frequency response of a hair (Humphrey *et al.*, 2003). The reason for this is not just because of changes in hair mass and suspension elasticity as a function of hair length, but because of a match of hair length with the boundary layer thicknesses occurring at the frequencies contained in the biologically relevant air flows (Barth *et al.*, 1993; Steinmann *et al.*, 2006). Boundary layer thickness limits the hair mechanical response to low frequencies. Since the boundary layer thickness of an oscillating flow decreases with increasing frequency ($\delta \propto f^{-1/2}$), and since hair resonance frequency increases with decreasing hair length, we find that the frequency response of a hair correlates best with the frequency of an oscillating flow having a boundary layer thickness that scales with hair length. Above the leg of the spider *C. salei*, the boundary layer thickness varies between about 2600 and 600 µm within a frequency range of about 10–960 Hz. At low frequencies, short hairs increasingly remain in a zone of reduced flow velocities. We conclude that the lengths of the hair-like flow sensors found in terrestrial arthropods reflect this relationship. It should be noted that the optimal hair length at the resonance frequency is not larger than the boundary layer thickness. Simply increasing hair length into the free field flow to increase sensitivity would not work because in oscillating air flows the same air velocity amplitude at a larger distance from the hair suspension would then lead to increasingly smaller angular displacements of the hair.

As already shown by Görner and Andrews (1969), for spider trichobothria the angular displacement amplitude increases with hair length. However, as shown later, the displacement amplitude does not depend on hair length alone. Instead of just the angular displacement of the hair one can also employ the ratio of the maximum hair tip displacement at the hair's resonance frequency to the maximum air particle displacement (oscillating flow) as a measure of mechanical hair

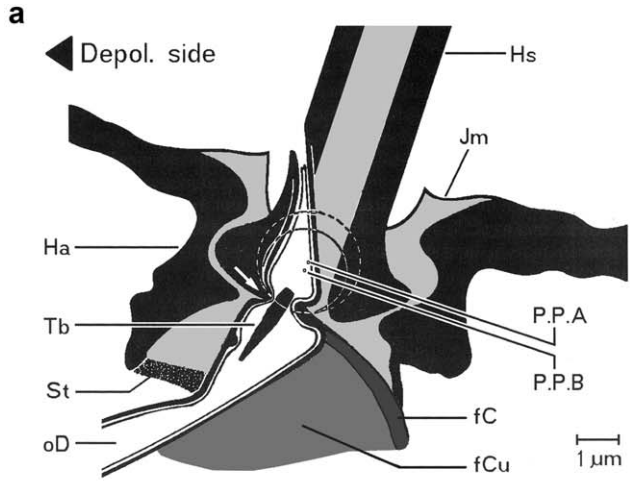

Gnatzy and Tautz 1980

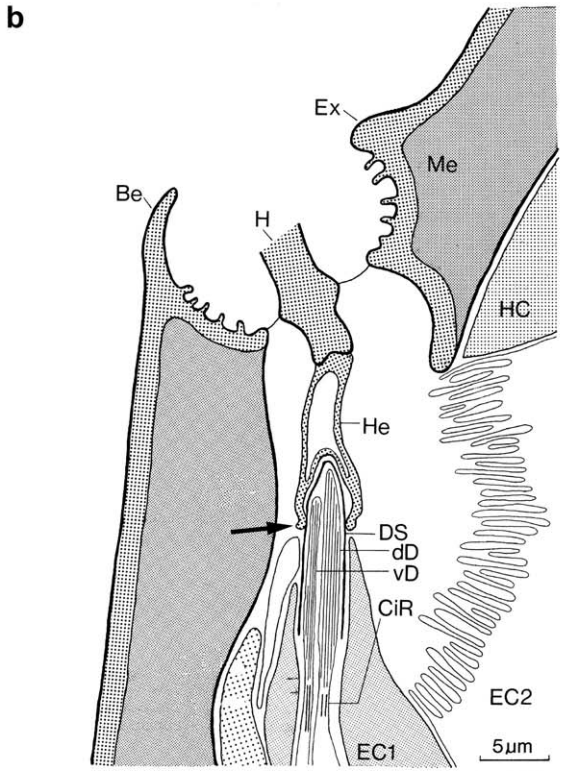

Anton 1991

sensitivity. In 78% of the 85 trichobothria studied in *C. salei* (Barth *et al.*, 1993) we found this ratio to be less than one. The upper frequency limit of such air flow sensors, however, is mainly determined by the mass of the hair through its moment of inertia. Humphrey *et al.* (2001) show that the resonance frequency of a hair of length L is $\omega_{\mathrm{res}(\theta)} \propto I_{\mathrm{t}}^{-1/2}$, where $I_{\mathrm{t}} \propto L^3$ is the total moment of inertia of the hair. It follows that $\omega_{\mathrm{res}(\theta)} \propto L^{-3/2}$ and, therefore, $\omega_{\mathrm{res}(\theta)}$ decreases with increasing L.

The mathematical models presented in this chapter permit predictions regarding the geometry and mechanical properties of flow sensors in water. Both the smaller boundary layer thicknesses (by 0.22) and the increased drag (by 43) in water as compared to air allow for even shorter hairs than those in air, with the same mechanical sensitivity (Devarakonda *et al.*, 1996; Humphrey *et al.*, 2001; Barth, 2004). In addition, the cumulative effects of viscosity are of much greater importance in water than in air. As a consequence, as opposed to hair length, hair diameter and mass hardly have any effect in water and the value of the damping constant R is less influential on frequency tuning. Morphologically and mechanically identical hairs are tuned to much lower frequencies in water than in air (Devarakonda *et al.*, 1996; Barth, 2002a,b).

1.2 HAIR ARRAYS

In most cases arthropod air flow sensors do not occur singly but in groups, forming characteristic patterns that are used as taxonomic characters and which, in some animal groups such as scorpions and pseudoscorpions, are very important clues for classification (Vachon, 1973; Mahnert, 1976; Reißland and Görner, 1985). Figure 4 presents three examples of arthropod air flow sensor arrangements.

FIG. 3 Stimulus transformation in hair-like arthropod medium flow sensors. (a) Cricket (*G. bimaculatus*) cercal filiform hair, modified from Gnatzy and Tautz (1980); the hair forms a lever with a long outer and a very short inner hair shaft and the axis of rotation between P.P.A and P.P.B. When the outer hair shaft is deflected in the direction of depolarization of the sensory cell (Depol. side), the dendritic end (oD) of the sensory cell is deformed as indicated by the white arrow. *Note:* Tb, tubular body within dendritic end; Jm, joint membrane of hair shaft (Hs) suspension; fC, fibrous cap; fCu, fibrous cushion presumably serving as an abutment when the hair is stimulated by deflection; St, cuticular connection. (b) Structure of basal part of spider (*C. salei*) trichobothrium (from Barth, 2002b after Anton, 1991). Cut base of the hair shaft (H) within cuticular cup (Be) and suspended by joint membrane; He, helmet-like structure into the inner end of which reach the dendritic endings of several (3–4) sensory cells. When the outer hair shaft is deflected, the rim of the inner end of the helmet presses against one or two of the dendrites eliciting a nervous response. CiR, ciliary region; DS, dendrite sheath; dD, vD, dorsal and ventral dendrite; EC1,2, sheath cells; Ex, exocuticle; HC, hypodermal cell; Me, mesocuticle. With kind permission of Springer Science and Business Media.

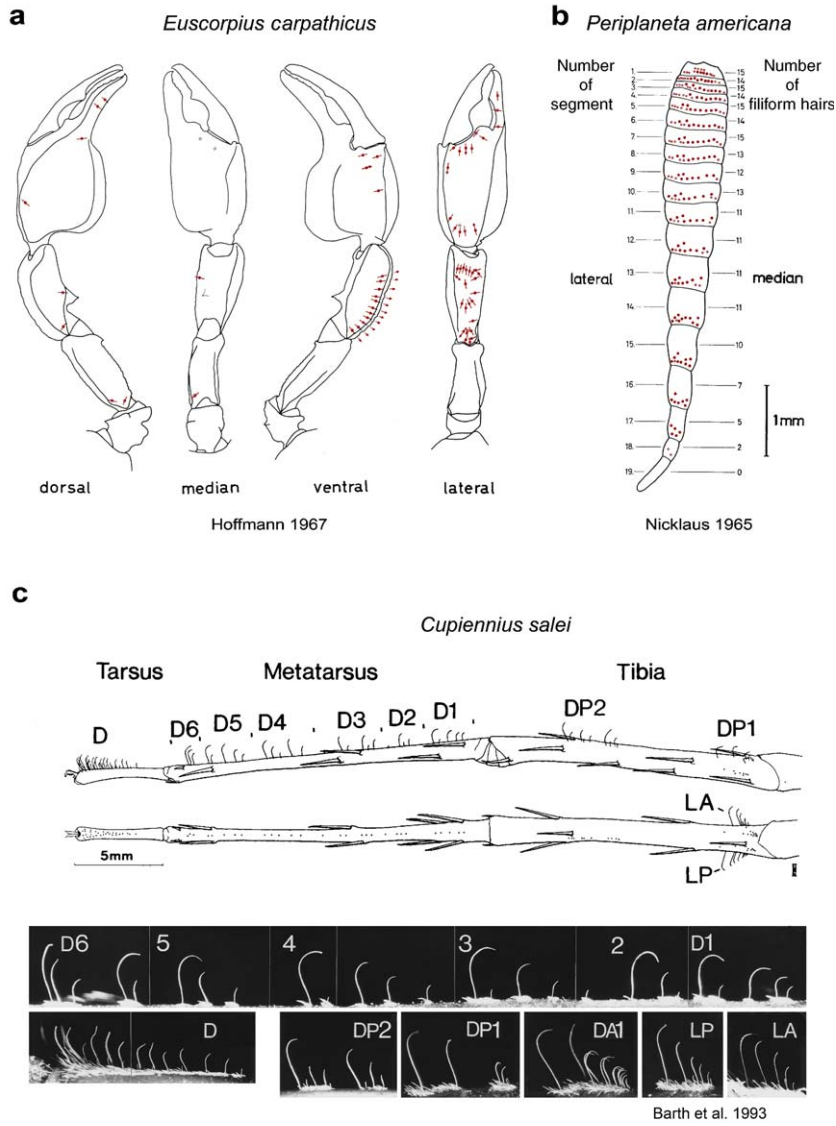

FIG. 4 Examples showing the arrangement of arrays of arthropod medium flow sensors on the pedipalp of a scorpion (a), on the cercus of a cockroach (b), and on the walking leg of a wandering spider (c). Arrows in (a) indicate the plane in which hairs are most easily deflected. The spider leg is shown from the side and from above, and the various groups of trichobothria denoted on the drawing are also seen on the photographs below. (a) Modified from Hoffmann (1967); (b) from Nicklaus (1965); (c) from Barth *et al.* (1993). (a) and (b): with kind permission of Springer Science and Business Media; (c) from Phil. Trans. R. Soc. BA and Proc. R. Soc. A, with kind permission of the Royal Society.

Among the major questions to be asked are (i) What can an array of air flow sensors do more and/or better than a single sensor? (ii) How do individual hairs in a formation potentially interact with each other due to fluid mechanical reasons? (iii) What are the particular functional advantages of having particular arrangements of sensors at particular locations of the exoskeleton?

Only rudimentary answers can be given at present, as much has still to be learned. This is because, so far, most attention has been given to understanding individual sensors and, as a consequence, there is a dearth of studies on air flow sensor ensembles and their significance.

(i) When the sensor hairs show obvious length gradation in a group such as those typical of spiders like *C. salei* (see Figs. 4c and 5), the group will cover a larger frequency range with high sensitivity as compared to a single hair. This was demonstrated experimentally by analysing the mechanical frequency responses of up to five neighbouring hairs (Barth *et al.*, 1993). Theoretically, the responses of differently tuned hairs in a group could be used for a spectral analysis of the flow stimulus (Fig. 5). According to Shimozawa *et al.* (2003), the torsional resistance within the hair base changes with hair length in cricket filiform hairs, matching the frictional resistance at air–hair contact and thereby maximizing energy transmission and thus sensitivity.

Directional fractionation of a stimulus is another possibility in cases where the individual hairs of a group differ in their mechanical directional sensitivity (Dechant *et al.*, 2006). This does not seem to be pronounced in the trichobothria of spiders (Barth *et al.*, 1993), but is certainly relevant for those of scorpions (Fig. 4; Hoffmann, 1967), and in the case of the cercal filiform hairs of cockroaches (Nicklaus, 1965) and crickets (Landolfa and Jacobs, 1995; Magal *et al.*, 2006).

(ii) Air flow sensors often form groups with relatively small spacings of tens to hundreds of micrometers between them. In a recent study, for the first time the possibility of viscous-mediated coupling between neighbouring hairs in an array was studied both experimentally and theoretically (Bathellier *et al.*, 2005). The question was whether a hair affects the flow field around it in a way that in turn changes the dynamics of neighbouring hairs. The main results for the case examined (trichobothria of the spider *C. salei*) are the following: (a) In the biologically relevant frequency range of 30–300 Hz viscous coupling between pairs of hairs is at most very small. (b) According to theory (consistent with Humphrey *et al.*, 1993), the relatively large spacing between the hairs (20–50 hair diameters) and the tuning to the above-mentioned frequencies explain the practical absence of coupling. (c) Larger hairs do not sense the perturbation of the flow by smaller hairs because their dynamics is mainly determined by the upper part of the hair shafts which are removed from the perturbation.

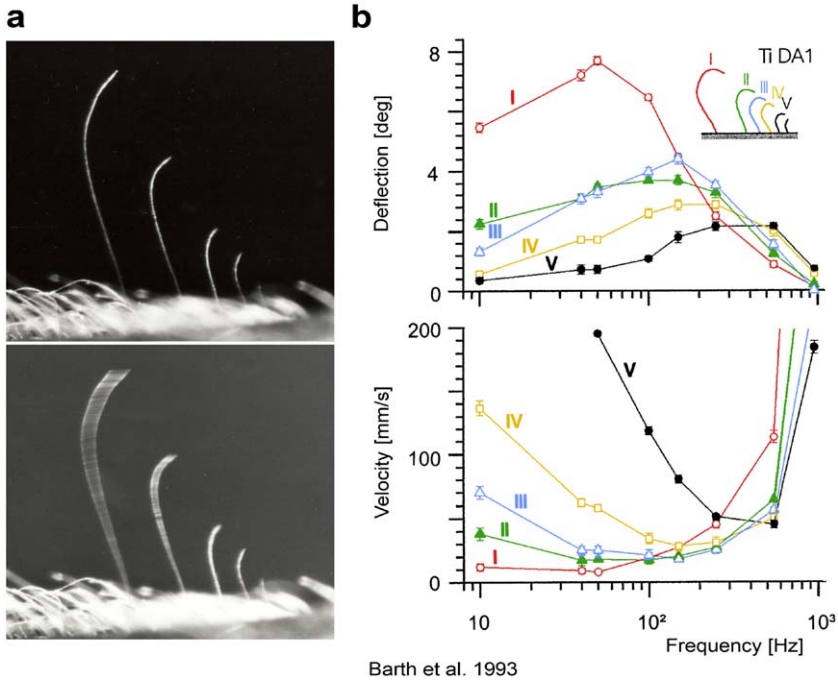

FIG. 5 Groups of spider trichobothria (*C. salei*) showing differences in hair length and mechanical properties. Whereas the longest hair measures 1150 μm, the shortest one is only 400 μm long. (a) Group of trichobothria on the walking leg tibia exposed to a flow field oscillating at 50 Hz. Clearly, hair deflection is correlated with hair length. (b) Group of trichobothria on the tibia; above: deflection of different hairs in flow fields oscillating at different frequencies but with a constant particle velocity amplitude of 50 mm s^{-1}; below: the particle velocity amplitude of air flow oscillating at different frequencies necessary to deflect the hair by 2.5°. Note differences in the mechanical frequency tuning of the hairs differing in length. (From Barth *et al.*, 1993; Phil. Trans. R. Soc. BA and Proc. R. Soc. A, with kind permission of the Royal Society.) (see color plate section at the end of this book).

(d) The typical arrangement of the trichobothria in *Cupiennius* reduces or eliminates interactions.

The results for the case of *Cupiennius* highlight important parameters to be considered but should not generate premature generalizations. In scorpions, most of the trichobothria groups we have observed show large spacing and no relevant interaction is expected (Fig. 4). The situation is similar for the filiform hairs of caterpillars (Markl and Tautz, 1975), but is expected to differ for the cricket and cockroach cercus (Magal *et al.*, 2006; Dangles *et al.*, 2007). Cummins *et al.* (2007) calculate significant viscous coupling among the more closely spaced hairs on the cricket cercus.

(iii) Like the first two questions above, the third needs much more attention than hitherto received and only a few generalizations seem

justified. The most striking of these may be the fact that in spiders the trichobothria form a widely spread out system, with up to about 100 flow sensors on every leg providing the animal with an all-around view regarding flows approaching from any horizontal and dorsal direction (Barth *et al.*, 1993; Brittinger, 1998). The large area covered by the trichobothria of spiders is reminiscent of other sensory systems for which spatial resolution of the stimulus is crucial: the fish lateral line system, the electroreceptors of weakly electric fish, the touch receptors in the human skin, to name just a few. There are good reasons to assume that the same applies to the spider case. *C. salei* is a hunting spider that uses its air flow sensors (in addition to substrate vibration sensors) to detect prey, even flying prey which it catches with a well-oriented jump (Brittinger, 1998; Barth, 2002b), a behaviour obviously demanding in regard to the detection, recognition, and localization of the stimulus source. In contrast, the air flow sensors of caterpillars are warning devices detecting the air flow generated by a flying predator approaching (wasp or parasitic fly). Depending on stimulus strength the caterpillars freeze or make winding movements until they fall from their plant and can no longer be detected by the predator. These sensors are just threshold detectors responding in a narrow frequency range only, corresponding to the frequencies contained in the predator signal (Tautz and Markl, 1978). Interestingly, in crickets and cockroaches with their flow sensors clustered on the cerci the mediation of a quick escape reaction is also the relevant behavioural context. In both these cases, however, the response is oriented (Camhi, 1984; Landolfa and Jacobs, 1995; Gnatzy, 1996; Paydar *et al.*, 1999).

2 Hair motion physical–mathematical models

In this section we present the theoretical foundations of a physical–mathematical model admitting closed-form analytical solutions for the angular displacement, velocity, and acceleration of filiform hairs due to the torques imposed by sinusoidally oscillating fluid media. The model applies to hairs in air or water and, despite certain approximations, is capable of generating accurate quantitative results. It is referred to as the 'Physically Exact Model' (PEM). We then derive a 'Physically Approximate Model' (PAM) version of the exact model from which qualitative information is more easily obtained. Three procedures for determining the torsional restoring constant S (N m rad^{-1}) and the damping constant R (N m s rad^{-1}) of filiform hairs, by combining experiments with calculations, are then explained. This is followed by a section on validation where selected experimental results are compared with corresponding PEM and PAM calculations. Hair arrays are discussed last within the context of the

PEM approach, focusing on conditions for which the motions of neighbouring hairs may be coupled through viscous fluid forces.

The theoretical material presented in this section draws mainly from the studies of Barth *et al.* (1993), Barth and Höller (1999), Devarakonda *et al.* (1996), Humphrey *et al.* (1993, 2001, 2003), Bathellier *et al.* (2005), and the text by Barth (2002b), all of which contain numerous references to the seminal work of many other authors, in particular T. Shimozawa and his collaborators. Except where otherwise noted, all quantities are expressed in SI units. A list of symbols and their SI units is provided in the Notation.

2.1 SINGLE HAIRS: PHYSICALLY EXACT AND APPROXIMATE MODEL APPROACHES

All physical–mathematical models represent a compromise between accurate physical representation and ease of formulation and calculation. The PEM presented here also requires some level of approximation in order to render fluid-driven hair motion calculable with reasonable resources and in a reasonable amount of time. Current computers, grid generation techniques, and numerical calculation methodologies make it possible to solve the coupled hair–fluid motion problem with considerable physical rigour. However, for this it is necessary to integrate at least two of the three components of the Navier–Stokes vector momentum conservation equation describing the motion of the fluid as a function of space and time while simultaneously solving the motion of the hair described as a forced, damped, harmonic oscillator. Even assuming incompressible, constant property, low Reynolds number fluid flow as is typical of the filiform hairs considered here (allowing non-linear inertial contributions to the balance of momentum to be neglected) and one-way coupling through viscous fluid forces (in which fluid motion affects hair motion but not the other way around) complexities relating to hair geometry (such as size, shape, surface morphology, and hair-to-hair spacing) render the single hair problem computationally demanding and the hair array problem formidable. This is largely because considerable spatial grid refinement is needed around each hair to accurately capture the velocity and pressure distributions of the fluid moving past it, from which to determine the drag force and torque acting on it. Therefore, in our two modelling approaches a number of approximations simplify calculation while retaining the essential physics of the problem, aiming for quantitative and qualitative accuracy in the PEM and PAM approaches, respectively. In contrast, for either model, the accuracy of numerical calculation is not an issue of concern.

As in our earlier work, the analyses presented in this section assume that the medium flow field driving hair motion oscillates periodically about a zero mean value of velocity, meaning that the fluid experiences zero net translation past the hair. Such a condition differs from the natural one wherein, generally, the medium oscillations generated by the walking or

flying motions of an insect and of interest to a spider, for example, are part of an unsteady continuous background flow due to the insect itself (Barth *et al.*, 1995; Barth and Höller, 1999; Klopsch *et al.*, 2007) and, possibly, the local atmospheric conditions (Barth, 2002b; see Section 4.2.2). Notwithstanding, the assumption is valid and convenient since: (i) The unsteady flow to which a filiform hair is naturally exposed can be decomposed into a mean, steady velocity component upon which the unsteady velocity component is superimposed. The steady component deflects the hair from its original angular orientation with respect to the exoskeletal surface to a new orientation around which the unsteady component causes it to oscillate. Thus, relative to the new orientation it is only the unsteady component of motion that matters. (ii) It is possible to set up an experiment using two loudspeakers in push–pull mode to generate an oscillating air flow field with zero mean velocity in which the amplitude and frequency of the oscillations are precisely controlled. Such a flow field allows a detailed investigation of the geometrical and dynamical factors affecting the response and performance characteristics of flow-sensing filiform hairs (Barth *et al.*, 1993). In combination with the kind of analysis presented here, such experimental data have been used to derive values for the torsional restoring constant, S, and the damping constant, R, of *C. salei* trichobothria (Barth *et al.*, 1993; Barth, 2002b; Humphrey *et al.*, 1993) and for the cercal hairs of the cricket *G. bimaculatus* (Shimozawa *et al.*, 1998). With S and R known, flow-driven hair motions resulting from the prescription of velocity fields corresponding to natural conditions can be calculated. An example of this, relating to the role of transient phenomena on hair motion sensing, is presented in Section 4.2.2.

2.1.1 *Physically exact model*

Medium flow-sensing filiform hairs have variable diameter along their length (Barth *et al.* 1993; Kumagai *et al.*, 1998; Humphrey *et al.*, 2001; Dangles *et al.*, 2007). In the case of the spider *Cupiennius* many trichobothria are also curved along the distal third of their length, approximately, and possess densely packed short branches along the entire hair length (Barth *et al.*, 1993; Barth, 2002b). With reference to Fig. 6, we approximate any such hair as a straight solid cylinder of effective diameter d and length L, and density ρ_h. The hair is attached to the exoskeletal surface in a way that allows it to oscillate about a pivot point near its base. In its resting position the hair is assumed to be oriented normal to the surface. The hair is surrounded by a fluid medium (air or water) of density ρ and dynamic viscosity μ (kinematic viscosity $\nu \equiv \mu/\rho$). The fluid medium is assumed to oscillate sinusoidally, in a direction parallel to the surface and normal to the hair, at frequency ω ($\equiv 2\pi f$) radians per second and with an approaching velocity V_f at location y along the hair shaft with respect to

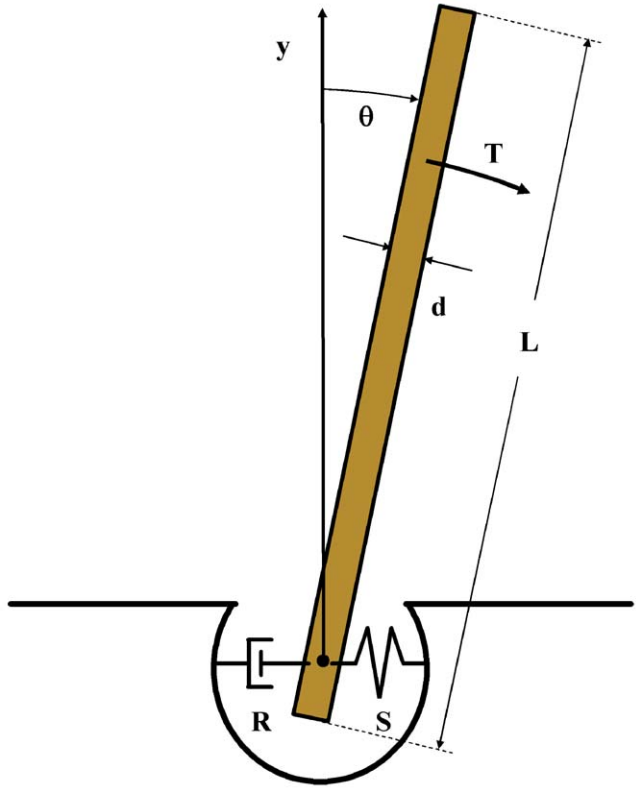

FIG. 6 Geometrical model of a flow-sensing filiform hair approximated as a cylinder of effective length L and diameter d with $L/d \gg 1$. At rest, the hair shaft is assumed to be aligned normal to the cuticle surface. The torque T (N m) created by fluid motion normal to the hair shaft is resisted by a restoring torque related to the hair torsional restoring constant S (N m rad^{-1}) and a damping torque related to the hair damping constant R (N m s rad^{-1}). At any instant in time, the sum of these torques (see Eq. 1) imparts an angular acceleration to the hair resulting in an angular displacement θ around a pivot point near its base. For $\theta \leq 10^{\circ}$ it follows that $\cos\theta > 0.98$ and the coordinate y normal to the cuticle essentially coincides with the hair shaft.

the pivot point at $y=0$ on the surface. At the same y location, the velocity of the cylindrically shaped hair is $V_c = y\dot{\theta}$, where $\dot{\theta}$ is the hair angular velocity, so that the relative velocity of the approaching fluid at location y is $V_r = V_f - V_c$. At any instant, the relative fluid motion induces a total torque T that acts on the hair. This is resisted by a restoring torque that is proportional to the hair angular displacement, θ , and by a damping torque due to the mechanical friction at the attachment point that is proportional to the hair angular velocity, $\dot{\theta}$. For these conditions, the

conservation of angular momentum for the hair about its pivot point is (Humphrey *et al.*, 1993)

$$I\ddot{\theta} = T - R\dot{\theta} - S\theta. \tag{1}$$

In Eq. (1) (and the equations below) superscript dots denote time derivatives, I is the moment of inertia of the hair with respect to the pivot point, and S and R are the hair torsional restoring constant and damping constant, respectively. The moment of inertia of the hair is determined from geometry and is given by

$$I = \frac{\pi\rho_{\mathrm{h}}d^2}{48}\left(4L^3 + \frac{3}{4}d^2L\right). \tag{2}$$

In contrast, because R and S are mechanical properties inherent to the hair, determined by the attachment structure and its material properties, they must be evaluated experimentally.

In principle, Eq. (1) provides a physically exact description of hair motion. In practice, the exactness and utility of its solution depend on the specification of T which is given by the expression

$$T = \int_0^L Fy \, \mathrm{d}y. \tag{3}$$

In Eq. (3), F is the force per unit length acting normal to the hair at location y along its length due to the relative motion of the fluid around it. As mentioned earlier, F could be determined from a rigorous numerical solution of the Navier–Stokes equation in component form subject to appropriate boundary conditions. However, the grid refinement required to resolve pressure and velocity gradients from which to determine F accurately as a function of time, and the need to simultaneously track the hair and redefine its position as it is displaced as a function of time, are so computationally intense as to render this approach impracticable. In an alternative, approximate method, F could be evaluated from theoretical or empirical drag relations obtained for steady flows around cylinders, the implied assumption being that fluid and hair velocities adjust instantaneously to changes in their values. We use this method in Section 4.2.2 to explore filiform hair motions under the action of transient flows more likely to arise in the natural environment. Yet a third and highly accurate approach is based on the theoretical analysis performed by Stokes (1851), described next.

In his classical paper, Stokes (1851) determined the functional form of the force exerted on a pendulum oscillating with small angular displacement amplitude in a quiescent, incompressible, constant property fluid. To facilitate his analysis, Stokes (1851) made the following approximations without significantly degrading physical accuracy: (i) the pendulum is approximated as a cylinder with length to diameter ratio $L/d \gg 1$; (ii) the

small displacement amplitude of the cylinder allows an analysis based on the assumption that it oscillates translationally in a direction normal to its longitudinal axis; (iii) the oscillation amplitude and frequency of the cylinder are such that the dimensionless parameter

$$s = \left(\frac{d}{4}\right)\left(\frac{2\pi f}{\nu}\right)^{1/2} \ll 1. \tag{4}$$

The condition expressed in Eq. (4) dictates that the characteristic Reynolds number of the cylinder, defined as $Re \equiv |V_r|(d/2)/\nu$, where $|V_r|$ is the absolute relative velocity of the approaching fluid with respect to the cylinder (a quantity that is essentially constant along the length of the cylinder because of the small amplitude constraint), should also be $Re \ll 1$. To see this, we note that Stokes (1851) analysed the motion of a cylinder oscillating in a quiescent fluid, so that $|V_r| = |V_c|$, and that the small amplitude constraint implies displacements of the cylinder that scale with its diameter, d. Since a typical displacement takes place in a half-period, $T_p/2$, a characteristic relative velocity is $|V_r| = |V_c| = d/(T_p/2) = 2df$. Substituting this result into the definition of Re gives $Re = d^2 f/\nu$, which is equal to s^2 within a constant of order one. Thus the condition that $s \ll 1$ implies that $Re \ll 1$ also, and both conditions are readily satisfied for the ranges of V_r, d, f, and ν of interest to this work.

For the above conditions, Stokes (1851) shows that the force F in Eq. (3) is composed of three terms, two associated with the fluid viscosity and one with the fluid density. Thus

$$F = F(\mu, V_r) + F(\mu, \dot{V}_r) + F(\rho, \dot{V}_r) \tag{5}$$

where

$$F(\mu, V_r) = 4\pi\mu G V_r \tag{6a}$$

$$F(\mu, \dot{V}_r) = -\frac{\pi\mu G \dot{V}_r}{2gf} \tag{6b}$$

$$F(\rho, \dot{V}_r) = \pi\rho(d/2)^2 \dot{V}_r. \tag{6c}$$

In these expressions the quantity G is given by

$$G = -\frac{g}{(g^2 + \pi^2/16)} \tag{7}$$

where

$$g = 0.577 + \ln(s) \tag{8}$$

with s given by Eq. (4).

The hair is itself an inverted cylindrically shaped pendulum oriented in its resting position normal to the exoskeletal surface. We restrict attention to angular displacements of 10° or less, corresponding to the bulk of our

previous experimental work. This requirement is imposed by the small oscillation amplitude constraint underpinning Stokes' theory. Since $\cos 10^\circ = 0.985$, for angles 10° or less the medium, which oscillates parallel to the exoskeletal surface, flows past the hair in a direction that is essentially normal to its shaft. In fact, much smaller angular displacements suffice to stimulate the sensory cells of a filiform hair. Kumagai *et al.* (1998) find 0.002–0.01° for the cercal hairs of *G. bimaculatus*; Barth and Höller (1999) report 0.01–0.1° for the trichobothria of *C. salei*; Wiese (1976) measures about 0.02° for the mechanoreceptors on the telson of the crayfish *Procambarus clarkii*. The hairs of interest here have $L/d \gg 1$, and the smallness of both d and V_r guarantee that the condition $Re \ll 1$ is met everywhere along their length. Therefore, for these conditions it is possible to apply Stokes' (1851) theory along the length of the hair.

Substitution of Eqs. (6) into Eq. (3) via Eq. (5), and of Eqs. (2) and (3) into Eq. (1), and rearranging the result with the help of $V_r = V_f - V_c$ to separate the terms involving hair motion from those involving fluid motion, yields

$$\begin{aligned}(I + I_\rho + I_\mu)\ddot{\theta} + (R + R_\mu)\dot{\theta} + S\theta \\ = 4\pi\mu G \int_0^L V_f y \, dy + \left(\frac{\pi\rho d^2}{4} - \frac{\pi^2 \mu G}{g\omega}\right) \int_0^L \dot{V}_f y \, dy.\end{aligned} \tag{9}$$

In Eq. (9) the quantities I_ρ, I_μ, and R_μ denote fluid medium contributions to the moment of inertia and the damping constant of the hair associated with the fluid medium density and viscosity. They are defined as

$$I_\rho = \frac{\pi\rho d^2 L^3}{12} \tag{10}$$

$$I_\mu = -\frac{\pi^2 \mu G L^3}{3g\omega} \tag{11}$$

$$R_\mu = \frac{4}{3}\pi\mu G L^3 \tag{12}$$

with G given by Eq. (7) and g by Eq. (8).

Typical values for I, I_ρ, I_μ, S, R, and R_μ are provided in Table 3, and for I_μ and R_μ as a function of frequency in Fig. 7, for the MeD1 hairs of *C. salei* (Barth *et al.*, 1993) and nominal hairs in water. The values of I_ρ, I_μ, and R_μ are determined from the expressions above using the medium physical properties given in Table 2. The values of S and R for MeD1 hairs (see Fig. 4c) are determined from the correlations given in Table 1, while the constant values used for nominal hairs in water are derived from arguments presented in Section 2.2. These results show that (i) $I_\rho \ll I \cong I_\mu$ for hairs

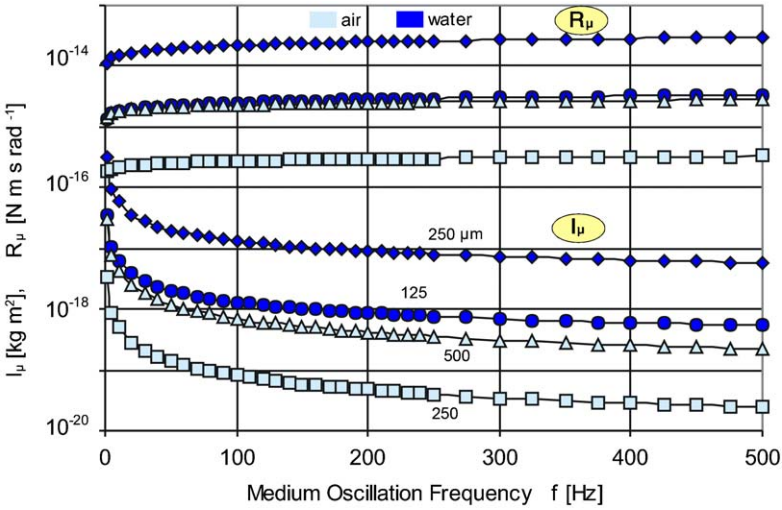

FIG. 7 Calculated values of viscous inertia, I_μ, and viscous damping, R_μ, for *C. salei* MeD1 spider filiform hairs in air and nominal filiform hairs in water as a function of medium oscillation frequency, f. Hair lengths are given in micrometers: circles (125 μm); diamonds (250 μm); squares (250 μm); triangles (500 μm).

TABLE 1 Density and experimental correlations for d, R, and S for spider *C. salei* MeD1 and TiDA1 hairs and cricket *G. bimaculatus* cercal hairs used in the calculations (Humphrey *et al.*, 2003)

	C. salei L (m)		*G. bimaculatus* L (m)
Physical property	MeD1 hairs	TiDA1 hairs	Cercal hairs
Density ρ_h (kg m^{-3})	1100	1100	1100
Diameter d (m)	$6.343 \times 10^{-5}\ L^{0.3063}$		$5.487 \times 10^{-4}\ L^{0.670}$
Damping constant R (N m s rad^{-1})	$2.031 \times 10^{-9}\ L^{1.909}$	$7.895 \times 10^{-9}\ L^{2.109}$	$5.880 \times 10^{-6}\ L^{2.770}$
Torsional restoring constant S (N m rad^{-1})	$1.272 \times 10^{-5}\ L^{2.030}$	$1.068 \times 10^{-9}\ L^{0.631}$	$1.944 \times 10^{-6}\ L^{1.670}$

Note: The cricket hair entry for R in this table was the value used in Humphrey *et al.* (2003) even though it was incorrectly printed on page 137 of that reference.

in air and $I_\mu \gg I \cong I_\rho$ for hairs in water; (ii) $R \cong R_\mu$ for both hairs in air and water; (iii) because of the L^3 dependence, long hairs have much larger values of I_μ and R_μ than short hairs; (iv) I_μ varies with frequency over a much larger range (10–200 Hz) than R_μ.

Together with a pair of initial boundary conditions, Eq. (9) can be solved numerically. Humphrey *et al.* (1993) have done so using a fourth-order Runge–Kutta method with an adaptive stepsize algorithm especially suited

for this class of initial value problem. Aside from its accuracy, the numerical solution approach allows the specification of fairly arbitrary distributions for the oscillating fluid velocity, V_f, in Eq. (9) as a function of location y along the hair shaft. This is the only way to solve Eq. (9) if, for example, V_f is specified from velocity measurements obtained in the natural environment.[1] However, for an accurate numerical solution it would be necessary to provide experimental values of V_f as a function of time and location along the hair shaft with such refinement as to make this approach impracticable. This is why much attention has been paid in earlier studies (Humphrey *et al.*, 1993; Devarakonda *et al.*, 1996; Shimozawa *et al.*, 1998; Steinmann *et al.*, 2006) to providing analytical functions for V_f that are biologically meaningful yet readily encoded for numerical calculation. Analytical expressions for the oscillating flow of a fluid parallel to and perpendicular to a cylindrical surface, such as a spider leg or a cricket cercus, have been used in Humphrey *et al.* (1993) and Steinmann *et al.* (2006). Even then, however, the numerical solution approach does not readily provide results of a general nature by means of which to explain the multiple parameter dependencies of the performance characteristics of flow-sensing filiform hairs (Humphrey *et al.*, 2001).

Fortunately, Eq. (9) admits an exact analytical solution for a class of oscillating fluid medium velocity distributions of considerable biological significance and of practical value for determining the torsional restoring constant S and the damping constant R. The substrate supporting the hair is, for example, either a leg in the case of a spider, or a cercus in the case of a cricket or cockroach, or a flagellum in the case of a crayfish. We assume the substrate is cylindrically shaped and of diameter D, with a length to diameter ratio much larger than one. Call δ the thickness of the boundary layer formed around the substrate as a consequence of the oscillating flow. Provided $\delta/(D/2) \ll 1$, the effects of substrate surface curvature on the flow are small and Stokes' (1851) solution for the velocity distribution of a fluid oscillating over a flat surface can be applied.[2] Since $\delta \propto (\nu/\omega)^{1/2}$ for a fluid oscillating over a flat surface (Panton, 1996), the condition translates into $((\nu/\omega)^{1/2})/(D/2) \ll 1$ or, equivalently, $fD^2/\nu \gg 2/\pi$.

[1]Note, however, that the natural environment flow field along the hair shaft must still conform to the assumptions and constraints underpinning Stokes' (1851) theory. For any flow field departing from Stokes' analysis, it is necessary to revert back to the numerical solution of Eq. (1) with all the attendant difficulties associated with evaluating the torque T acting on the hair shaft.

[2]This is strictly true for a fluid oscillating in a direction parallel to the longitudinal axis of a cylinder and approximately so for a fluid oscillating in a direction perpendicular to it. See Humphrey *et al.* (1993) for an in-depth discussion concerning this point and Steinmann *et al.* (2006) for velocity measurements of flows oscillating parallel and perpendicular to a cylinder.

In practice, for a cylindrical substrate of diameter $D = 2\,\text{mm}$, the condition is satisfied in air for $f > 25\,\text{Hz}$ and in water for $f > 2\,\text{Hz}$.

The velocity distribution for a fluid oscillating over a flat surface is (Panton, 1996)

$$V_\text{f} = U_\text{o}(-\cos(\omega t) + \cos(\omega t - \beta y)\text{e}^{-\beta y}) \tag{13}$$

where t is time, y an arbitrary location above the surface along a normal to it, $\omega(\equiv 2\pi f)$ the angular frequency, U_o the far-field amplitude of velocity corresponding to a very large value of y, and $\beta(\equiv(\omega/2\nu)^{1/2})$ the inverse of a characteristic viscous diffusion length scale related to the boundary layer thickness, δ, according to

$$\delta = 4.5/\beta. \tag{14}$$

With V_f given by Eq. (13), it is possible to solve Eq. (9) analytically. The methodology is provided in Appendix 1 of Humphrey *et al.* (1993) and the final steady periodic[3] solution for the hair angular displacement is

$$\theta = C_1\cos(\omega t) + C_2\sin(\omega t). \tag{15}$$

In Eq. (15)

$$C_1 = \frac{P(S - I_\text{t}\omega^2) - Q\omega R_\text{t}}{(S - I_\text{t}\omega^2)^2 + (\omega R_\text{t})^2} \tag{16a}$$

and

$$C_2 = \frac{P\omega R_\text{t} + Q(S - I_\text{t}\omega^2)}{(S - I_\text{t}\omega^2)^2 + (\omega R_\text{t})^2} \tag{16b}$$

[3]The general solution of Eq. (9) consists of two additive parts (Kreyszig, 1988): a solution of the homogeneous form of the equation, which corresponds to the transient solution; and a particular solution, which corresponds to the steady periodic solution. Because $R_\text{t}^2 < 4I_\text{t}S$ for the cricket and spider hairs examined in this chapter, we know that the system described by Eq. (9) is underdamped. In addition, the transient solution can be shown to be proportional to $\text{e}^{-t/\tau}$, where $\tau = 2I_\text{t}/R_\text{t}$. Using the values in Table 3 for MeD1 *Cupiennius* hairs, it can be shown that τ ranges from about $6 \times 10^{-4}\,\text{s}$ for a hair 250 μm long to about $2.5 \times 10^{-3}\,\text{s}$ for one that is 1000 μm long. It follows that the transient contribution to the general solution persists less than about 0.0025 s for a hair 250 μm long and less than about 0.01 s for one that is 1000 μm long. Thus, because of the short duration of the transient, even for long hairs, we are concerned here only with the steady periodic solution of Eq. (9).

with

$$I_t = I + I_\rho + I_\mu \tag{17}$$

$$R_t = R + R_\mu \tag{18}$$

$$P = A2\pi\mu G U_o L^2 + B\left(\frac{\pi\rho d^2 \omega U_o L^2}{8} - \frac{\pi^2 \mu G U_o L^2}{2g}\right) \tag{19a}$$

$$Q = B2\pi\mu G U_o L^2 + A\left(\frac{\pi^2 \mu G U_o L^2}{2g} - \frac{\pi\rho d^2 \omega U_o L^2}{8}\right) \tag{19b}$$

$$A = e^{-\beta L}[-(1/\beta L)\cos(-\beta L) - (1/\beta L + 1/(\beta L)^2)\sin(-\beta L)] - 1 \tag{20a}$$

$$B = e^{-\beta L}[(1/\beta L)\sin(-\beta L) - (1/\beta L + 1/(\beta L)^2)\cos(-\beta L)] + 1/(\beta L)^2. \tag{20b}$$

To within the approximations made, Eq. (15) and its first and second time derivatives provide a physically exact basis for calculating the time variation of angular displacement, velocity, and acceleration of flow-sensing hairs in oscillating air or water media. Further analysis (Humphrey *et al.*, 2001) yields expressions for the maximum angular displacement, maximum velocity, and maximum acceleration as a function of the flow oscillation frequency. The results are

$$\theta_{max}(\omega) = \left(\frac{P^2 + Q^2}{(S - I_t\omega^2)^2 + R_t^2\omega^2}\right)^{1/2} \tag{21a}$$

$$\dot{\theta}_{max}(\omega) = \omega\left(\frac{P^2 + Q^2}{(S - I_t\omega^2)^2 + R_t^2\omega^2}\right)^{1/2} \tag{21b}$$

$$\ddot{\theta}_{max}(\omega) = \omega^2\left(\frac{P^2 + Q^2}{(S - I_t\omega^2)^2 + R_t^2\omega^2}\right)^{1/2}. \tag{21c}$$

2.1.2 *Physically approximate model*

The quantities P, Q, I_t, and R_t in Eqs. (21) all depend non-linearly on ω. However, numerical evaluations for conditions typical of filiform hairs

oscillating in air and water reveal that they all tend towards constant asymptotic values for large frequencies ($f > 50\,\text{Hz}$), the asymptotic limit favouring hairs in air with $L \geq 500\,\mu\text{m}$ and in water with $L \geq 125\,\mu\text{m}$. The PAM assumes that these terms are constant for purposes of deriving approximate analytical expressions for the hair maximum angular displacement at resonance frequency, θ_{res}, the maximum angular velocity at resonance frequency,$\dot{\theta}_{\text{res}}$, and the corresponding resonance frequencies, $\omega_{\text{res}(\theta)}$ and $\omega_{\text{res}(\dot{\theta})}$, respectively.[4] The results are (Humphrey *et al.*, 2001)

$$\theta_{\text{res}} = \frac{2I_{\text{t}}}{R_{\text{t}}}\left(\frac{P^2+Q^2}{4I_{\text{t}}S - R_{\text{t}}^2}\right)^{1/2} \tag{22a}$$

$$\dot{\theta}_{\text{res}} = \frac{1}{R_{\text{t}}}\left(P^2+Q^2\right)^{1/2} \tag{22b}$$

$$\omega_{\text{res}(\theta)} = \left(\frac{S}{I_{\text{t}}} - \frac{R_{\text{t}}^2}{2I_{\text{t}}^2}\right)^{1/2} \tag{23a}$$

$$\omega_{\text{res}(\dot{\theta})} = \left(\frac{S}{I_{\text{t}}}\right)^{1/2}. \tag{23b}$$

The only physically acceptable solutions for Eqs. (22a, 22b) and (23a, 23b) correspond to conditions for which the quantities under the 1/2 exponents are positive. The most restrictive constraint is imposed by Eq. (23a) which requires $2I_{\text{t}}S - R_{\text{t}}^2 > 0$. As a consequence, there may be physical conditions for which this constraint is not observed and for which accurate values of θ_{res}, $\dot{\theta}_{\text{res}}$, $\omega_{\text{res}(\theta)}$, and $\omega_{\text{res}(\dot{\theta})}$ must be obtained from the PEM or the numerical solution of Eq. (9).

Using the information provided in Tables 1–3 it is possible to establish the practical implication of the constraint $2I_tS - R_t^2 > 0$ for the MeD1 hairs of *C. salei* (Barth *et al.*, 1993) and nominal hairs in water. The result is that for a hair of length L in air or water there is a maximum frequency above which the constraint is not observed (Fig. 8). Even though

[4]Strictly, the 'resonance frequency' of a mechanical system forced to oscillate sinusoidally corresponds to its 'natural frequency', ω_{o}, the frequency of the system's undamped motion. As the forcing frequency ω approaches ω_{o}, the amplitude of the undamped system's motion tends to infinity. In the presence of damping, as is the case for oscillating filiform hairs, the amplitude of the system's motion will be finite but may have a maximum depending on the forcing frequency, ω, and the damping constant. This is referred to as 'practical resonance' (Kreyszig, 1988) but, for simplicity, in this chapter, we use the words 'resonance frequency' noting that the terminology 'best frequency' is also used extensively in the biological literature.

TABLE 2 Medium physical properties (evaluated at 27 °C) used in the calculations

Physical Property	Air	Water
Density ρ ($\mathrm{kg\,m^{-3}}$)	1.1614	995.6
Dynamic viscosity μ ($\mathrm{kg\,m^{-1}\,s^{-1}}$)	1.85×10^{-5}	8.00×10^{-4}
Kinematic viscosity v ($\mathrm{m^2\,s^{-1}}$)	1.59×10^{-5}	8.04×10^{-7}

TABLE 3 Typical values of the parameters used in (or derived from) PEM calculations for MeD1 *C. salei* hairs in air and nominal hairs in water

Parameter	MeD1 Spider Hairs in Air			Nominal Hairs in Water		
L (m)	1.00×10^{-3}	5.00×10^{-4}	2.50×10^{-4}	2.50×10^{-4}	1.25×10^{-4}	6.25×10^{-5}
d (m)	7.65×10^{-6}	6.18×10^{-6}	5.00×10^{-6}	1.00×10^{-5}	7.50×10^{-6}	5.00×10^{-6}
I ($\mathrm{kg\,m^2}$)	1.68×10^{-17}	1.38×10^{-18}	1.13×10^{-19}	4.50×10^{-19}	3.17×10^{-20}	1.76×10^{-21}
I_ρ ($\mathrm{kg\,m^2}$)	1.78×10^{-20}	1.45×10^{-21}	1.19×10^{-22}	4.07×10^{-19}	2.86×10^{-20}	1.59×10^{-21}
I_μ ($\mathrm{kg\,m^2}$) (100 Hz)	6.28×10^{-18}	7.08×10^{-19}	8.02×10^{-20}	1.32×10^{-17}	1.31×10^{-18}	1.23×10^{-19}
R ($\mathrm{N\,m\,s\,rad^{-1}}$)	3.81×10^{-15}	1.01×10^{-15}	2.70×10^{-16}	1.00×10^{-15}	1.00×10^{-15}	1.00×10^{-15}
R_μ ($\mathrm{N\,m\,s\,rad^{-1}}$) (100 Hz)	1.93×10^{-14}	2.30×10^{-15}	2.74×10^{-16}	2.20×10^{-14}	2.49×10^{-15}	2.73×10^{-16}
S ($\mathrm{N\,m\,rad^{-1}}$)	1.03×10^{-11}	2.53×10^{-12}	6.20×10^{-13}	1.00×10^{-12}	1.00×10^{-12}	1.00×10^{-12}

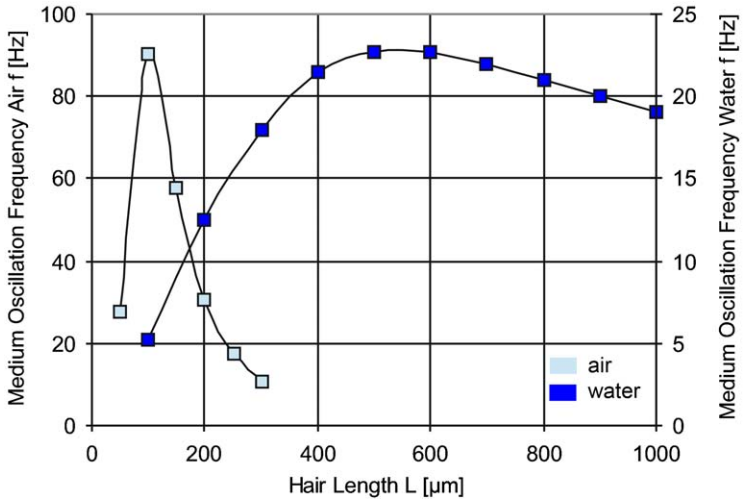

FIG. 8 Approximate values of the maximum medium oscillation frequency, f, for which the constraint $2I_tS - R_t^2 > 0$ is observed and the PAM applies, plotted as a function of filiform hair length, L: (a) *C. salei* MeD1 trichobothria in air (left ordinate); (b) nominal hairs in water (right ordinate).

approximate, this result indicates that the PAM is limited in its range of application. Notwithstanding, in the range where it applies and even beyond, the PAM yields relations that provide fundamental insight and useful qualitative guidance of a general nature concerning the parameter

TABLE 4 Approximate parameter functional dependencies for hair maximum angular displacement at resonance frequency, θ_{res}, and maximum angular velocity at resonance frequency, $\dot{\theta}_{\mathrm{res}}$, and of their associated resonance frequencies $\omega_{\mathrm{res}(\theta)}$ and $\omega_{\mathrm{res}(\dot{\theta})}$

	Hairs in Air	Hairs in Water
θ_{res}	$\dfrac{\rho_{\mathrm{h}}^{1/2} d L^{7/2} \mu U_{\mathrm{o}}}{S^{1/2}(R+\mu L^3)}\left(1+\dfrac{\mu L^{3/2}}{\rho_{\mathrm{h}}^{1/2} d S^{1/2}}\right)$	$\dfrac{\mu L^2 U_{\mathrm{o}}}{S}$
$\dot{\theta}_{\mathrm{res}}$	$\dfrac{\mu L^2 U_{\mathrm{o}}}{(R+\mu L^3)}$	$\dfrac{\mu L^2 U_{\mathrm{o}}}{(R+\mu L^3)}$
$\omega_{\mathrm{res}(\theta)}$	$\dfrac{S^{1/2}}{\rho_{\mathrm{h}}^{1/2} d L^{3/2}}$	$\dfrac{\mu L^3 S}{(R+\mu L^3)^2}$
$\omega_{\mathrm{res}(\dot{\theta})}$	$\dfrac{S^{1/2}}{\rho_{\mathrm{h}}^{1/2} d\, L^{3/2}}$	$\dfrac{S}{\mu L^3}$

Note: Coefficients of order one affecting the tabulated relations are omitted for clarity.

dependencies of hair motion. To obtain these relations we follow, and improve upon, the analysis outlined in Humphrey *et al.* (2001).

Earlier in this section we found that $I_\rho \ll I \cong I_\mu$ in air, and $I_\mu \gg I \cong I_\rho$ in water. This simplifies the specification of I_{t} in Eqs. (22a, b and 23a, b) and allows these equations to be written in a way amenable to series expansions of certain terms. Aided by their numerical evaluation it is possible to identify the dominant terms to within constants of order one. This order of magnitude analysis yields the relations given in Table 4. The relations for $\omega_{\mathrm{res}(\dot{\theta})}$ in air and water, and for $\omega_{\mathrm{res}(\theta)}$ in air, agree exactly with those in Table 1 of Humphrey *et al.* (2001). The remaining relations, while in qualitative agreement with their corresponding relations in Table 1 of Humphrey *et al.* (2001), represent more compact descriptions of the major parameter functional dependencies.[5]

2.2 HAIR SUSPENSION: TORSIONAL RESTORING CONSTANT *S* AND DAMPING CONSTANT *R*

The calculation of hair motion by any of the three procedures outlined earlier (numerical, physically exact, physically approximate) requires the

[5]The most notable difference between the relations in Table 4 of this work and Table 1 of Humphrey *et al.* (2001) is the complete absence of the fluid medium density, ρ, in Table 4. The present analysis recognizes that $\rho_{\mathrm{h}}/\rho \gg 1$ in air, so that only the dependence on ρ_{h} is retained in three of the relations for hairs in air. Similarly, because $\rho_{\mathrm{h}}/\rho \cong 1$ in water, neither of the two densities appears in the relations for hairs in water. A consequence of this, following from dimensional considerations, is that the values of the exponents of the various quantities in the relations can also differ between the two studies.

specification of the torsional restoring constant, S (N m rad^{-1}), and of the damping constant, R (N m s rad^{-1}). For hairs in air it is possible to determine S directly from static force measurements (Shimozawa and Kanou, 1984b). In contrast, direct measurements of R do not exist. However, by combining experimental measurements with numerical calculations based on the use of Eq. (9) it is possible to derive values for both R and S (Barth *et al.*, 1993; Humphrey *et al.*, 1993; Shimozawa *et al.*, 1998). For hairs in water we know of no S or R data for flow-sensing hairs and we use instead the procedure outlined in Humphrey *et al.* (2001) to specify approximate values.

There are at least two ways to combine measurements and calculations of hair mobility to derive S and R data. The first requires measurements of the phase difference between hair displacement and medium velocity, $\Delta\Phi$, as a function of medium oscillation frequency, ω. The quantities $\Delta\Phi$, S, and R are analytically related by an expression of the form

$$-\Delta\Phi = \tan^{-1}\left[f(S, R, I, I_\mu, I_\rho, R_\mu, g, \omega)\right] \tag{24}$$

where f is a simple algebraic function (Humphrey *et al.*, 1993). Substitution of a pair of ($\Delta\Phi$, ω) values into Eq. (24) yields two equations with two unknowns, S and R, since for a hair of known geometrical characteristics oscillating in air, the other parameters in the relation are known. In an extension of this approach, Shimozawa *et al.* (1998) have derived analytical expressions, valid for any instant in time in a sinusoidal oscillation cycle, for the hair angular displacement, velocity, and acceleration in terms of the experimentally known maximum angular displacement and phase shift, $\Delta\Phi$. These three quantities and the torque T are then calculated numerically at four instants in time in a cycle for different experimental frequencies ω. The results are substituted into Eq. (1) which yields four equations for three unknowns, I, S, and R for each value of ω. While only two of the four equations for each value of ω are independent, in combination with a least squares error analysis the total set of equations obtained is solved for I, S, and R.

A number of uncertainties affect the phase difference approach for determining S and R (Humphrey *et al.*, 1993). Of these, the most serious are uncertainties in (i) the substrate shape and dimensions; (ii) the assumed time-dependent velocity profile driving hair motion, which depends on the flow–substrate relative orientation; and (iii) the measurement of the phase shift $\Delta\Phi$. The last of these, in particular, represents a challenge. This is because, following the procedure of Humphrey *et al.* (1993), for example, in order to obtain S and R to within $\pm 10\%$, $\Delta\Phi$ must be known to within $\pm 5\%$. For cricket filiform hairs in an air flow oscillating at 176 Hz this translates into a maximum uncertainty of $\pm 3^\circ$ corresponding to a maximum uncertainty in time of $\pm 5 \times 10^{-5}$ s, approximately. As a

consequence we have proposed a considerably simpler procedure for determining S and R (Barth *et al.*, 1993). For a hair of known d and L this consists in searching for the pair of (S, R) values that will best match an experimentally measured $\theta_{max} = f(\omega)$ profile to calculations of θ_{max} obtained by solving Eq. (9) numerically or using the analytical result given by Eq. (21a). Although we have determined optimal (S, R) pairs for filiform hairs using this procedure by trial and error, it can be made more effective in combination with a least squares error minimization approach.

Table 1 summarizes correlations obtained for S and R as a function of hair length L for the cercal hairs of the cricket *G. bimaculatus* using the phase difference approach (Shimozawa *et al.*, 1998), and for the MeD1 and TiDA1 trichobothria of the spider *C. salei* using the alternative procedure proposed by Barth *et al.* (1993) (Humphrey *et al.*, 2001, 2003). Also tabulated are the allometric relations giving the average diameter $d = d(L)$ for these hairs. Figure 9 shows plots of the $S = S(L)$ and $R = R(L)$ correlations. For hair lengths $L \leq 700\,\mu m$, the S values of the cricket cercal hairs fall between the larger (TiDA1) and smaller (MeD1) values of the spider hairs. In contrast, for all hair lengths the R values of the cricket cercal hairs are larger than those of the TiDA1 and MeD1 hairs which, for any hair length, differ little between themselves.

In contrast to filiform hairs in air, we know of no data for S and R for flow-sensing hairs in water. It appears, however, that for comparable mechanical sensitivities, hydrodynamic mechanoreceptors can be much

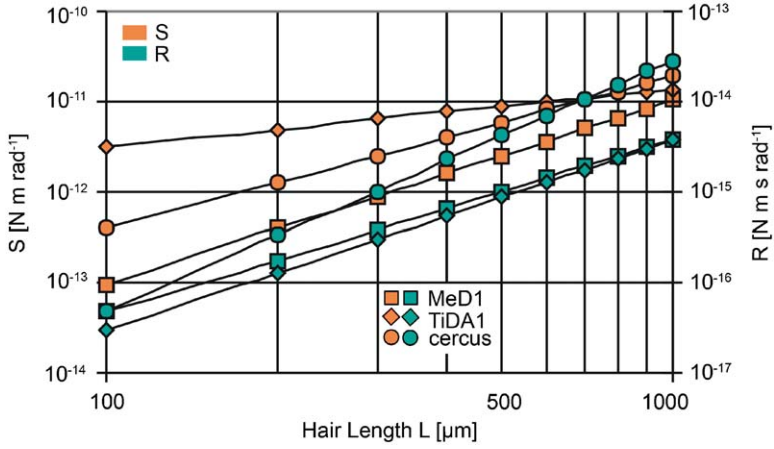

FIG. 9 Variation of the torsional restoring constant, S, and of the damping constant, R, with filiform hair length, L, from the correlations given in Table 1 for the MeD1 (squares) and TiDA1 (diamonds) hairs of the spider *C. salei*, and the cercal hairs (circles) of the cricket *G. bimaculatus*.

shorter than their aerodynamic counterparts (Barth *et al.*, 1993; Bleckmann, 1994; Devarakonda *et al.*, 1996) with resonance frequencies smaller than about 150 Hz as determined through the electrophysiologically measured cell response (Wiese, 1976). In the absence of experimental data, Humphrey *et al.* (2001) discuss a procedure for estimating S and R for hairs in water based on Eq. (23a). The equation is first rearranged to read $S = I_t\omega_{\mathrm{res}(\theta)}^2 + R_t^2/2I_t$ and values are fixed for the fluid medium and hair physical properties, hair length and diameter, and hair resonance frequency. Then, by varying R the equation yields values of S such that the (S, R) pairs obtained satisfy the values prescribed. When the calculation is done for *Cupiennius* MeD1 hairs of different length in air, the $S = S(R)$ curves obtained overlap markedly in the neighbourhood of $S = 4 \times 10^{-12}$ N m rad^{-1} and $R = 10^{-15}$ N m s rad^{-1}. This (S, R) pair falls well within the range determined from experiments using the methods described earlier. The expectation is that the same should be true for hairs in water which are found to overlap in the neighbourhood of $S = 2 \times 10^{-11}$ N m rad^{-1} and $R = 10^{-14}$ N m s rad^{-1}. However, there is an uncertainty affecting the $S = S(R)$ curves for hairs in water that does not affect the curves for hairs in air. For a hair in air we know from experiments the hair length, diameter, and resonance frequency to prescribe, but for a hair in water we can only make educated guesses of these quantities (Humphrey *et al.*, 2001). Notwithstanding, we conclude from the above results that the S and R values for hairs in water are somewhat larger than for hairs in air.

2.3 MODEL VALIDATION: COMPARISON BETWEEN MEASUREMENTS AND CALCULATIONS

In this chapter, the PEM is used to quantitatively evaluate the effects of various parameters (geometrical, dynamical, and relating to physical properties) on the mechanical response and performance characteristics of flow-sensing filiform hairs. Therefore, it is important to establish its predictive capabilities by reference to experimental results. In contrast, because of its qualitative nature, for the PAM it is important to verify that simplified relations obtained from it reproduce all major experimental trends.

Unless otherwise stated, all the calculations presented in this chapter are for the MeD1 and TiDA1 trichobothria on the metatarsus and tibia of the legs of the spider *C. salei*, the cercal hairs of the cricket *G. bimaculatus*, and what we refer to as 'nominal hairs' in water. Table 1 lists the correlations from which d, S, and R are obtained for spider and cricket hairs as a function of their length. Table 3, discussed below, gives values for d, L, S, and R used for the MeD1 hairs as well as the nominal hairs in water. For the physical properties of air and water used in the calculations see Table 2.

2.3.1 *Validation of the physically exact model*

The validation of the PEM is performed primarily by comparing measured and calculated values of hair maximum angular displacement, maximum angular displacement at resonance frequency, and the resonance frequency for spider trichobothria and cricket cercal hairs. As will be shown, agreement is good between the experimental and numerical results and we conclude that the PEM is capable of hair mobility calculations as accurate as the experimental measurements compared with.

Measured and calculated values of hair maximum angular displacement are compared in Fig. 10. The results are plotted as a function of medium frequency for an oscillating air flow with velocity amplitude $U_o = 50\,\mathrm{mm\,s^{-1}}$. The experimental and calculation conditions correspond to two of the MeD1 and one of the TiDA1 hairs of *C. salei* (Barth *et al.*, 1993). The calculations performed using the $S = S(L)$ and $R = R(L)$ correlations in Table 1 show good agreement with the measurements for the 1150 μm long TiDA1 hair and the 250 μm long MeD1 hair. However, the 750 μm long MeD1 hair calculations differ from their corresponding measurements by about 26% at the mechanical resonance frequency of

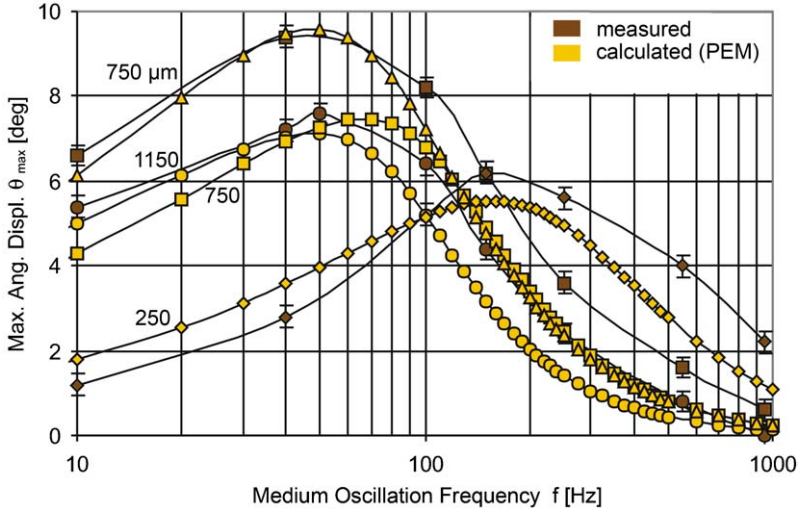

FIG. 10 Measured and calculated (PEM) values of *C. salei* MeD1 (squares and diamonds) and TiDA1 (circles) filiform hair maximum angular displacement, θ_{max}, plotted as a function of medium frequency, f, for an oscillating air flow with velocity amplitude $U_o = 50\,\mathrm{mm\,s^{-1}}$. Also shown is the calculated PEM result (triangle) for an MeD1 hair 750 μm long with S reduced by 30% from the Table 1 correlation value of 5.77×10^{-12} to $4.04 \times 10^{-12}\,\mathrm{N\,m\,rad^{-1}}$. Hair lengths are given in micrometers.

~ 55 Hz. Much better agreement is obtained for this hair if the value of S given by the correlation in Table 1 is decreased by 30%, from 5.77×10^{-12} N m rad^{-1} to 4.04×10^{-12} N m rad^{-1}. This finding points to three things: (i) the sensitivity of the calculations to the specification of S (and, to a less extent, of R); (ii) the experimental correlations for $S = S(L)$ (and $R = R(L)$) in Table 1 are subject to uncertainties difficult to quantify but which for S could be as large as $\pm 30\%$ for some hair lengths; (iii) the quantities S and R may be dependent on unknown viscoelastic properties inherent to the hair mechanical support. With respect to this last point, we note the following results from work in progress: (a) measurements of S for the trichobothria of *C. salei* obtained via surface force spectroscopy show a frequency dependence in the range 20–100 Hz (collaboration with V. Tsukruk, Georgia Institute of Technology); (b) atomic force microscope measurements of S for a beak-shaped putative mechanoreceptor on the flagellum of the crayfish *P. clarkii* reveal that it depends on the hair angular displacement (collaboration with E. Berger and D. Mellon, University of Virginia).

Measured and calculated values of MeD1 and TiDA1 hairs maximum angular displacement at resonance frequency, θ_{res}, and of the resonance frequency, $f_{\text{res}(\theta)}$, are respectively plotted as a function of hair length in Figs. 11 and 12. Again, the amplitude of velocity of the oscillating air flow

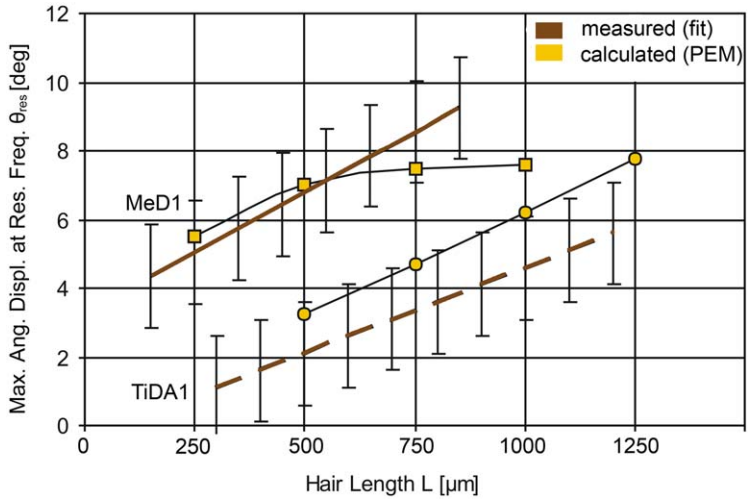

FIG. 11 Measured and calculated values of filiform hair maximum angular displacement at resonance frequency, θ_{res}, plotted as a function of hair length, L. Lines with uncertainty bars represent linear fits to the experimental data of Barth *et al.* (1993) for the MeD1 and TiDA1 hairs of the spider *C. salei*. Symbols correspond to PEM calculations of MeD1 (squares) and TiAD1 (circles) hairs. Both the measurements and calculations are for $U_o = 50$ mm s^{-1}.

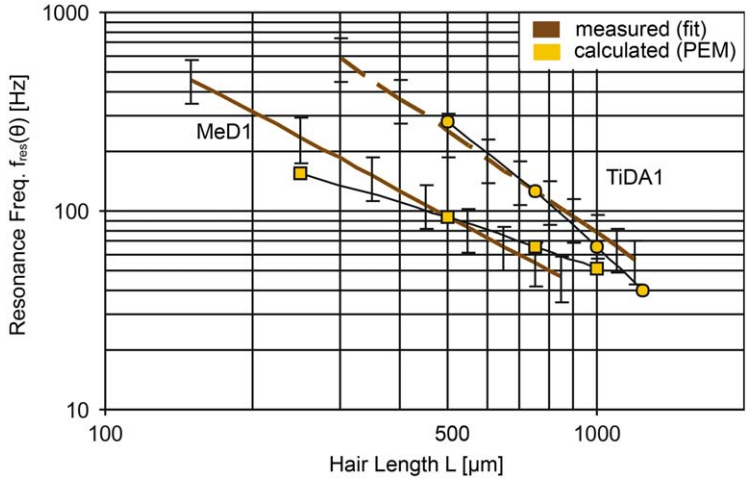

FIG. 12 Measured and calculated values of filiform hair resonance frequency, $f_{res(\theta)}$, plotted as a function of hair length, L. Lines with uncertainty bars represent fits to the experimental data of Barth *et al.* (1993) for the MeD1 and TiDA1 hairs of the spider *C. salei*. Symbols correspond to PEM calculations of MeD1 (squares) and TiDA1 (circles) hairs. Both the measurements and calculations are for $U_o = 50\,\text{mm}\,\text{s}^{-1}$, but note that $f_{res(\theta)}$ is independent of U_o.

is $U_o = 50\,\text{mm}\,\text{s}^{-1}$. Agreement is generally good between the measurements and calculations of both quantities, the calculations falling within or very close to the uncertainty bars of the measurements. The lower values of θ_{res} calculated for MeD1 hairs with $L > 750\,\mu\text{m}$ are, most likely, due to an uncertainty (or an unknown visco-elastic dependence) in the correlation for $S = S(L)$ in Table 1 for MeD1 hairs of this length (see previous paragraph). In similar comparisons between measurements and calculations for the cercal hair of a cricket in an oscillating air flow with $U_o = 1\,\text{mm}\,\text{s}^{-1}$ agreement is very good for θ_{res}, but for hairs with $L > 1000\,\mu\text{m}$ the calculated values of $f_{res(\theta)}$ are from 35% to 45% lower than measured (Figs. 13 and 14).

Given the number and nature of the approximations embedded in the PEM and the scatter in the experimental data, the degree of correspondence found between the above measurements and calculations is deemed to be good.

2.3.2 *Validation of the physically approximate model*

The validation of the PAM consists in showing that the relations in Table 4 correctly predict all major observed trends in hair mechanical behaviour as a function of the parameters upon which that behaviour depends. For hairs

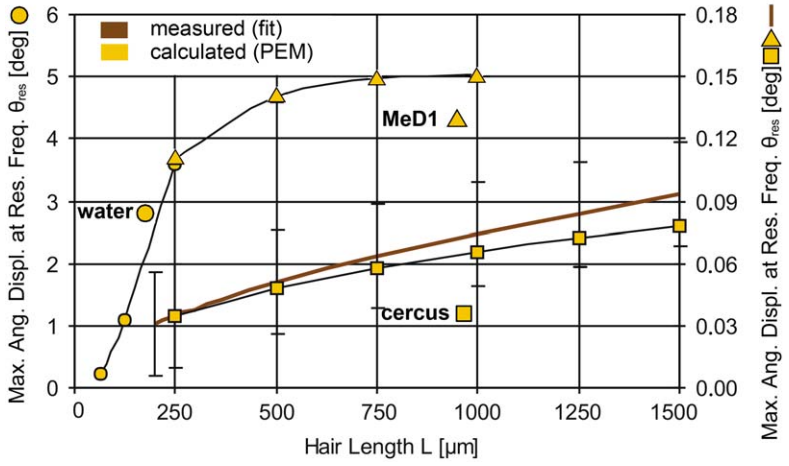

FIG. 13 Measured and calculated values of filiform hair maximum angular displacement at resonance frequency, θ_{res}, plotted as a function of hair length, L. Continuous line with uncertainty bars represents fit to the experimental data of Kumagai *et al.* (1998) for the cercal hairs of the cricket *G. bimaculatus* (right ordinate). Symbols correspond to PEM calculations of MeD1 spider hairs (triangles, right ordinate), cercal cricket hairs (squares, right ordinate), and nominal hairs in water (circles, left ordinate). Both the measurements and calculations are for $U_o = 1\,\mathrm{mm\,s^{-1}}$.

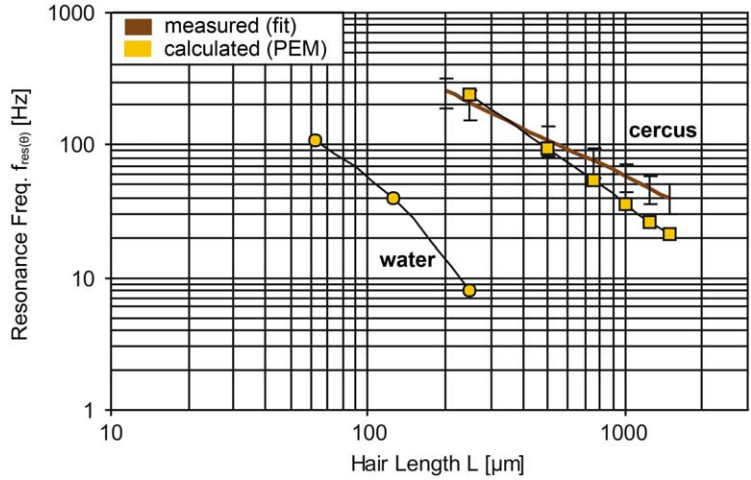

FIG. 14 Measured and calculated values of filiform hair resonance frequency, $f_{res(\theta)}$, plotted as a function of hair length, L. Continuous line with uncertainty bars represents fit to the experimental data of Kumagai *et al.* (1998) for the cercal hairs of the cricket *G. bimaculatus*. Symbols correspond to PEM calculations of cercal cricket hairs (squares) and nominal hairs in water (circles). Both the measurements and calculations are for $U_o = 1\,\mathrm{mm\,s^{-1}}$, but note that $f_{res(\theta)}$ is independent of U_o.

in air we refer to experimental data or to PEM calculations. For hairs in water we rely exclusively on comparisons with PEM calculations.

Hairs in air:

(i) The linear dependence of θ_{res} on U_o is in agreement with the observations of Shimozawa and Kanou (1984b), Barth *et al.* (1993), and Kumagai *et al.* (1998). The linear dependence of $\dot{\theta}_{res}$ on U_o is also displayed by corresponding PEM calculations.

(ii) The $L^{1/2}$ dependence of θ_{res} (given by the dominant term in the relation) is in agreement with the $L^{0.55}$ dependence observed by Kumagai *et al.* (1998). The L^{-1} dependence of $\dot{\theta}_{res}$ is also displayed by corresponding PEM calculations.

(iii) The $L^{-3/2}$ dependence of $\omega_{res(\theta)}$ agrees reasonably with the $L^{-0.92}$ dependence observed by Kumagai *et al.* (1998) and with the range of dependencies, $L^{-1.053}$ to $L^{-1.695}$, for different hair clusters observed by Barth *et al.* (1993).

(iv) While we are unaware of experimental data showing the functional dependencies of hair behaviour on ρ_h μ, d, S, and R, they arise as expected in all four of the relations in Table 4, and the trends given by these relations are also supported by corresponding PEM calculations.

Hairs in water:

All we can say is that the parameter functional dependencies also arise as expected in all four of the tabulated relations, and that the trends the relations yield are supported by PEM calculations.

2.4 HAIR ARRAYS: THE QUESTION OF VISCOSITY-MEDIATED COUPLING

In many arachnids and insects the filiform flow-sensing hairs form arrays and are near to neighbouring tactile or chemosensor hairs, or other hairs. As a consequence, the potential exists for viscosity-mediated coupling among hairs (Humphrey *et al.*, 1993). This problem has recently been investigated in some detail (Bathellier *et al.*, 2005; Cummins *et al.* 2007).

Scaling considerations suggest that viscous coupling between a pair of adjacent hairs with $L/d \gg 1$ should be negligible when $s/d \gg Re^{-1}$, where d is the hair diameter, s the spacing between the hairs, and Re the Reynolds number of the hair as defined in Section 2.1.1 (Humphrey *et al.*, 1993; Bathellier *et al.*, 2005). This criterion applies to a flow approaching normal to the plane containing the pair of hairs and is in agreement with correlations derived from the theoretical analysis of Cheer and Koehl (1987) for the flow normal to a pair of infinitely long cylinders in the range $10^{-5} \leq Re \leq 0.5$. The criterion suggests that viscosity-mediated coupling

should be negligible between pairs of hairs in an array for $s/d > 100$ in a flow with $Re > 0.01$ and for $s/d > 10$ in a flow with $Re > 0.1$.

In a combined experimental–theoretical investigation involving the trichobothria of *C. salei*, Bathellier *et al.* (2005) looked further into the matter of viscous coupling between pairs of hairs in in-line arrays, with the motion of the hairs taking place in the plane containing the array (that is, parallel to the leg supporting the hairs). In their experiments a coefficient characterizing the viscous coupling of a hair H1 of a pair of adjacent hairs (H1, H2) was defined by

$$\kappa_1 = \frac{\theta_{1(\mathrm{ref})} - \theta_1}{\theta_{1(\mathrm{ref})}} \tag{25}$$

where $\theta_{1(\mathrm{ref})}$ is a reference value equal to the maximum angular displacement of hair H1 in the absence of hair H2 that might affect it, and θ_1 ($\leq \theta_{1(\mathrm{ref})}$) is the maximum angular displacement of hair H1 in the presence of hair H2. In addition to a reference test measuring the flow-induced motion of hair H1 in the absence of hair H2, three tests were performed in which hair H1 was free to move while hair H2 was manipulated in two ways. In test one, both hairs H1 and H2 moved freely under the action of the oscillating flow. In test two, hair H2 was fixed in its equilibrium position while hair H1 moved freely under the action of the oscillating flow. In test three, hair H2 was mechanically driven at its base by a glass needle and hair H1 moved freely in response to any possible air motions induced by hair H2. These tests covered, approximately, a range of hair spacings $22.5 \leq s/d \leq 45$ in flow fields oscillating between 40 Hz and 150 Hz with a far-field velocity $U_o \leq 0.3\,\mathrm{m\,s^{-1}}$ for most of the experimental runs. For these conditions tests two and three revealed viscous coupling between hairs ($0.05 \leq \kappa_1 \leq 0.15$), whereas test one for a pair of freely moving hairs did not ($\kappa_1 \leq 0.05$).

Bathellier *et al.* (2005) also performed numerical calculations of viscous coupling between filiform hairs based on a theoretical analysis valid for the very low Reynolds number regimes characteristic of flow-driven oscillating hairs. They considered two identical TiDA1 hairs of length $L = 650\,\mu\mathrm{m}$ and diameter $d = 10\,\mu\mathrm{m}$, separated by a variable distance s/d immersed in an air flow oscillating uniformly at frequency f parallel to the common plane containing their axes. The near-field air velocity around the pair of hairs was analytically derived from Stokes' (1851) theory using linear superposition. This velocity distribution was then used to derive analytical expressions for the periodic drag forces and torques acting on each of the two hairs. Expressions for hair angular displacement were then obtained from the analytical solution of Eq. (1) from which, ultimately, values of the viscous coupling coefficient, κ_1, for hair H1 in the presence of hair H2 were calculated. The following ranges were explored in the

calculations: $5 \leq s/d \leq 55$ and $30 \leq f(\text{Hz}) \leq 200$ for flows with far-field amplitude of velocity $U_o = 0.3\,\text{m s}^{-1}$. Values of S and R for the hairs were set from correlations of the type shown in Table 1.

Values of κ_1 for hair H1 calculated for the three test cases were in good agreement with the experimental data and with the findings of Cheer and Koehl (1987). In addition, the theoretical results revealed four major findings (Fig. 15): (i) for all three of the test cases the viscous coupling coefficient κ_1 for hair H1 varies with frequency; (ii) likewise, for all three test cases κ_1 decreases quickly with increasing s/d (for $s/d > 50$ viscous coupling is essentially negligible); (iii) for fixed s/d and f, coupling is stronger when hair H2 is fixed or mechanically driven than when both hairs are free to move; (iv) when both hairs are free to move and the spacing between them is $s/d \cong 10$, the coupling coefficient for hair H1 is $\kappa_1 < 0.11$ at $f = 50$ Hz and $\kappa_1 < 0.03$ at $f = 200$ Hz. These findings apply to hairs of equal length. In the case of hairs of different length a large one affects a smaller one more strongly than the other way around.

Cummins *et al.* (2007) have developed a model that simulates the viscous coupling of arbitrarily positioned but closely spaced filiform hairs arranged in small groups as on the cricket cercus. The viscous coupling is estimated by means of a steady Stokes approximation to the Navier–Stokes

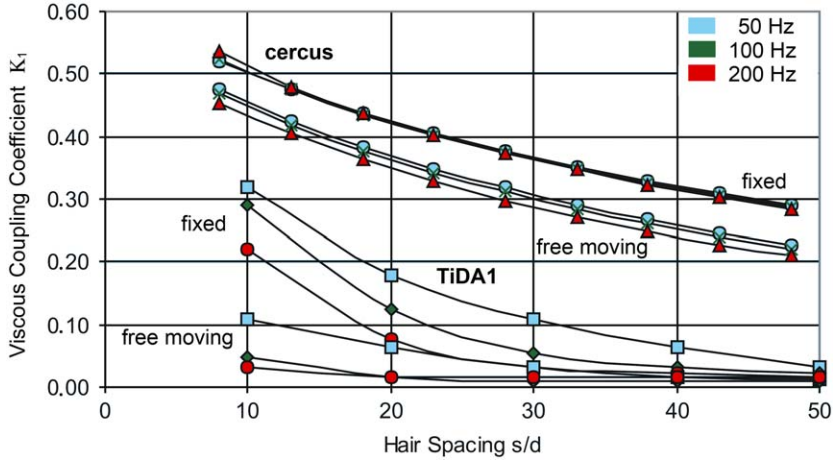

FIG. 15 Calculated variation of the viscous coupling coefficient, κ_1, for a free-moving hair in the presence of a second 'fixed' or 'free-moving' hair as a function of dimensionless hair spacing, s/d, at different flow oscillation frequencies (squares and circles, 50 Hz; diamonds and crosses, 100 Hz; circles and triangles, 200 Hz). The data for the cricket cercal hairs ($L = 200\,\mu\text{m}$, $d = 3\,\mu\text{m}$, $U_o = 0.05\,\text{m s}^{-1}$) were provided by B. Cummins for this chapter. The data for the TiDA1 hair of *Cupiennius* ($L = 650\,\mu\text{m}$, $d = 10\,\mu\text{m}$, $U_o = 0.3\,\text{m s}^{-1}$) are from Bathellier *et al.* (2005). Values for S and R in the calculations are specified from correlations of the type shown in Table 1.

equations valid for hair spacings $s/\ell_v \leq 1$, where $\ell_v (= 1/\beta \equiv (\omega/2\nu)^{-1/2})$, defined in Section 2.1.1, is a characteristic viscous diffusion length scale related to the boundary layer thickness, δ, of the flow oscillating about the cricket cercus. The approach is based on a special adaptation of the method of regularized Stokeslets (Cortez, 2001) that avoids singular velocity fields. Denote the maximum distance between any two points on a pair of adjacent filiform hairs by ℓ_M. For hairs with $\ell_M/\ell_v > 1$, unsteady effects may be significant and viscous coupling will likely be overestimated by the solution of the steady Stokes equations. Therefore, the model of Cummins *et al.* (2007) is most accurate in a low-to-moderate frequency regime for small groups of short, tightly packed filiform hairs, such as occur at the base of the cercus, where $s/d \sim 6$–8 for hairs of diameter $d \sim 5\,\mu m$. By discretizing the cercal system and applying the method of regularized Stokeslets the total velocity field about a group of hairs, which is the sum of the cercal boundary layer and the velocities due to viscous interactions among filiform hairs, is obtained.

Using this approach, Cummins *et al.* (2007) have calculated the motion of a free-moving cercal hair H1 with a neighbouring hair H2 adjacent to it that is fixed or also free to move. Both hairs have $L = 200\,\mu m$ and $d = 3\,\mu m$, approximately. The viscous coupling between the free-moving hair and its neighbour is quantified by κ_1 as defined by Eq. (25). Figure 15 shows κ_1 plotted as a function of the scaled distance s/d between the two hairs for air flow frequencies of 50, 100, and 200 Hz with oscillation amplitude of $U_o = 0.05\,m\,s^{-1}$. As in Bathellier *et al.* (2005), the results show that the motion of the free-moving reference hair is influenced more strongly by a fixed neighbouring hair than by one that is also free to move. This is intuitive since a fixed hair resists the air flow more than an oscillating hair. Relative to the calculated κ_1 results obtained by Bathellier *et al.* (2005), the data suggest that short cricket cercal hairs experience significantly larger viscous coupling than longer spider trichobothria. Partly contributing to this is the larger torsional restoring constant S of cricket cercal hairs (Fig. 9), which are less easily deflected by the medium flow (Fig. 13).

However, Cummins *et al.* (2007) have also applied their model to spider hairs of medium-to-long length that are more widely spaced, and still the values of κ_1 are larger than found by Bathellier *et al.* (2005) (data not shown). This could be due to the above-mentioned steady Stokes approximation. Thus, the viscous diffusion length scale, ℓ_v, has values 318, 225, and 159 μm at $f = 50$, 100, and 200 Hz, respectively. Since the largest distance between two points on two hairs is the diagonal connecting the tip of one hair with the base of the other hair, for $L = 200\,\mu m$ we find values of ℓ_M/ℓ_v equal to 0.67 (50 Hz), 0.95 (100 Hz), and 1.34 (200 Hz) for $s/d = 25$, and equal to 0.79 (50 Hz), 1.11 (100 Hz), and 1.57 (200 Hz) at $s/d = 50$. Therefore, the viscous coupling of a pair of cercal hairs 200 μm long is accurately captured at 50 Hz but may be overestimated at 200 Hz.

In contrast, for long cricket or spider hairs the steady Stokes approximation is likely to yield an overestimate except at low frequencies. Since the analytical model of Bathellier *et al.* (2005) works better than that of Cummins *et al.* (2007) for long hairs at high frequencies, it is not surprising that the latter exhibits contrary results. The two approaches represent complementary ways for exploring the different hair length and flow oscillation frequency regimes affecting filiform hair motion.

The main conclusion from the experiments and the theoretical analyses discussed earlier is that, for free-moving hairs in most trichobothria arrays, for which hair spacings fall in the range $20 \leq s/d \leq 50$, viscous coupling between pairs of neighbouring hairs is, at most, weak (see Figs. 6 and 7 and their discussion in Bathellier *et al.*, 2005). From the spider's point of view as a predator executing highly oriented movements there may be advantages to this because viscous coupling between or among hairs would degrade their independent performance. In contrast, from a cricket's point of view as a potential prey executing a comparatively simpler escape response there may be an advantage to viscous coupling among cercal hairs due to the larger number of simultaneously stimulated hairs alarming it (see also Dangles *et al.*, 2005, 2006a, and 2007; Magal *et al.*, 2006).

3 Parameter effects

In this section we first establish the relative importance of medium density and viscosity on the forces affecting hair motion for purely oscillatory flow. We then explore the effects of hair geometry and physical properties on the performance of a flow-sensing hair.

3.1 MEDIUM CONTRIBUTIONS TO HAIR INERTIA AND DAMPING AND TO FLOW-INDUCED FORCES

The angular displacement, velocity, and acceleration of a hair can be calculated using Eq. (1) or Eq. (9). Although Eq. (1) is more general, because Eq. (9) is based on Stokes' (1851) theory it has the advantage of grouping all the θ , $\dot{\theta}$, and $\ddot{\theta}$ dependent terms on the left-hand side and, as has been shown in Section 2.1.1, this allows the equation to be solved analytically for a biologically important class of fluid velocity distributions. Irrespective of whether Eq. (9) is solved analytically or numerically, we know from previous considerations that $I_\rho \ll I \cong I_\mu$ for hairs in air and $I_\mu \gg I \cong I_\rho$ for hairs in water, while $R \cong R_\mu$ for hairs both in air and in water. In addition, assuming a sinusoidal velocity for the oscillating fluid medium the three terms on the right-hand side of Eq. (9), per unit length of hair, are in the ratios

$$A : B : C = 4\pi\mu G : \pi\rho d^2\omega/4 : \pi^2\mu G/g. \tag{26}$$

For the range of flow oscillation frequencies, ω, of biological interest, $B \ll A \cong C$ for hairs in air and water. Thus, whether in air or in water, medium density plays little if any role in determining the motion characteristics of a hair. In contrast, medium viscosity works to dominate the moment of inertia for hairs in water and adds significantly to damping in both air and water.

A more rigorous way to establish the effects of medium density and viscosity on the motion characteristics of a hair is by examining the relative magnitudes of the three forces $F(\mu, V_r)$, $F(\mu, \dot{V}_r)$, and $F(\rho, \dot{V}_r)$ contributing to F in Eq. (5) which ultimately determines the torque T in Eq. (1). The quantity $F(\rho, \dot{V}_r)$ is the acceleration reaction due to the added mass of fluid surrounding the hair that must be accelerated with the hair. The quantities $F(\mu, V_r)$ and $F(\mu, \dot{V}_r)$ represent viscous drag forces associated with the relative velocity and acceleration, respectively. Estimates of the magnitudes of these three terms for a cylindrically shaped hair in translational oscillatory motion, obtained from Eqs. (6), are provided in Figs. 16 and 17 as a function of time and frequency, respectively. These results correspond to a nominal hair with $d = 10\,\mu m$ oscillating in a fluid with a relative fluid velocity given by $V_r = U_o \sin(2\pi ft)$. For the amplitude of the relative velocity we take $U_o \approx df$ from the PEM analysis in Section 2.1.1 which, for $d = 10\,\mu m$ and $f = 100\,Hz$, yields $U_o = 1\,mm\,s^{-1}$, a typical value in the frequency range of interest. The results in Fig. 16 are for a hair in air but the same findings and conclusions apply to a hair in water. They show that

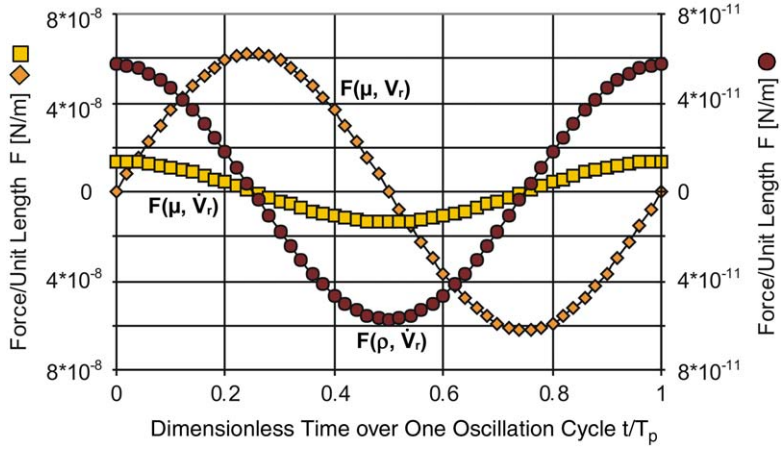

FIG. 16 Forces per unit length acting on a filiform hair plotted as a function of time for an oscillation cycle of period $T_p = 1/f = 1/100$ s. The hair is approximated as a cylinder of diameter $d = 10\,\mu m$ oscillating normal to its longitudinal axis in still air with a relative velocity given by $V_r = U_o \sin(2\pi ft)$, where $U_o = 1\,mm\,s^{-1}$. In the figure: $F(\mu, V_r)$(diamonds; left ordinate); $F(\mu, \dot{V}_r)$ (squares; left ordinate); $F(\rho, \dot{V}_r)$ (circles; right ordinate).

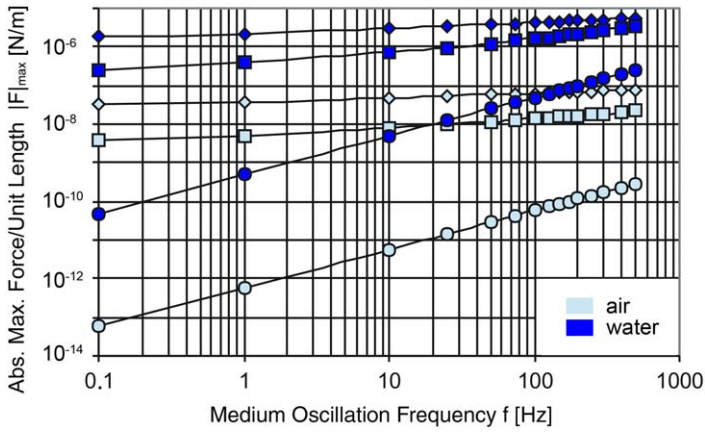

FIG. 17 Maximum absolute values (amplitudes) of the forces per unit length acting on a filiform hair plotted as a function of medium oscillation frequency. The hair is approximated as a cylinder of diameter $d = 10\,\mu\text{m}$ oscillating normal to its longitudinal axis in still air or water. The fluid relative velocity is given by $V_r = U_o \sin(2\pi f t)$, where $U_o = 1\,\text{mm}\,\text{s}^{-1}$. In the figure: $F(\mu, V_r)$ (diamonds), $F(\mu, \dot{V}_r)$ (squares), $F(\rho, \dot{V}_r)$ (circles).

(in terms of absolute values) over most of an oscillation cycle $|F(\mu, V_r)| > |F(\mu, \dot{V}_r)| \gg |F(\rho, \dot{V}_r)|$ and, as expected, that the velocity-dependent force is 90° out of phase with respect to the two acceleration-dependent forces. The plots in Fig. 17 show the maximum absolute values (amplitudes) of these forces over an oscillation cycle plotted as a function of frequency for a hair in air and a hair in water. Again, we find that $|F(\mu, V_r)| > |F(\mu, \dot{V}_r)| \gg |F(\rho, \dot{V}_r)|$ for both media in the frequency range $0.1 \leq f \leq 500\,\text{Hz}$. The ratio of the two viscosity-dependent forces, $\left|F|\mu, V_r|\right| / |F\mu, \dot{V}_r|$, ranges from 8.94 at 0.1 Hz to 3.52 at 500 Hz in air, and from 7.05 at 0.1 Hz to 1.63 at 500 Hz in water. In contrast, the ratio of the two acceleration-dependent forces, $\left|F|\mu, \dot{V}_r|\right| / F|\rho, \dot{V}_r|$, ranges from 6.37×10^4 at 0.1 Hz to 76.8 at 500 Hz in air, and from 5.14×10^3 at 0.1 Hz to 14.3 at 500 Hz in water. Clearly, for the ranges of the variables explored the acceleration reaction force $F(\rho, \dot{V}_r)$ is always quite small relative to the viscous forces $F(\mu, V_r)$ and $F(\mu, \dot{V}_r)$. The latter two, however, are comparable in magnitude at all frequencies in both air and water.

All these results are in agreement with those in Humphrey *et al.* (1993) and their later studies. Humphrey *et al.* (1993) defined a 'virtual mass' force given by $F_{VM} = F(\mu, \dot{V}_r) + F(\rho, \dot{V}_r)$, where the first term is associated with the diffusion of vorticity from the hair surface into the fluid medium and the second with the added mass of fluid surrounding the hair that must be accelerated with it. Humphrey *et al.* (1993) found that F_{VM} should not be neglected in calculating flow-induced oscillating hair motions because, even

though $F(\rho, \dot{V}_r)$ is negligibly small, $F(\mu, \dot{V}_r)$ is comparable to $F(\mu, V_r)$ and of obvious importance. As noted by Shimozawa *et al.* (1998), the F_{VM} notation is misleading since, strictly, $F(\mu, \dot{V}_r)$ does not contribute to the virtual mass of a hair. In spite of the use of this notation in Humphrey *et al.* (1993) and subsequent communications, the findings and conclusions of those studies are not altered. However, to avoid propagating further confusion in the literature we eschew the use of the F_{VM} notation in favour of that used in this chapter.

3.2 DEPENDENCE OF HAIR MOTION ON THE GEOMETRY AND PHYSICAL PROPERTIES OF THE HAIR, AND ON MEDIUM DYNAMICS AND PHYSICAL PROPERTIES

The motion of a filiform hair as a function of its geometry and physical properties, and as a function of its interactions with the fluid medium dynamics and its physical properties, can be investigated using the PEM or, for more arbitrary specifications of the fluid medium velocity that observe the conditions for which Stokes' (1851) theory applies, by solving Eq. (9) numerically. In this chapter, we pursue the first approach without incurring any fundamental limitations. However, before doing so the analytical results of the PAM, in particular the relations given in Table 4, are evaluated for qualitative guidance concerning the expected parameter dependencies of hair motion.

3.2.1 *Physically approximate model findings*

The relations in Table 4 show that

(a) For both air and water, the dynamic viscosity, μ, is the dominant physical medium property. Variations in μ will mainly be due to variations in temperature, with swings of $\pm 15\,^{\circ}C$ about an average of $27\,^{\circ}C$ causing changes in μ of about $\pm 4\%$ in air and $\pm 34\%$ in water. Because μ appears to the first power in all the relations for water, variations of it due to changes in temperature may significantly affect hair motion.

(b) Of the two geometrical dimensions, L appears in all relations for both air and water and has a much stronger effect on hair motion than d. The reason why d appears in the relations for air and not in those for water is because, as shown earlier, the moment of inertia of a hair, given by Eq. (2), plays a major role in determining hair motion in air but not in water.

(c) If the viscosity and hair length in air are such that $\mu L^{3/2}/\rho_h^{1/2} d S^{1/2} \gg 1$ and $\mu L^3/R \gg 1$, then the expression for θ_{res} in air simplifies to that given for water.

(d) For both air and water, the model predicts the experimentally observed increases of θ_{res} and $\dot{\theta}_{res}$ with increasing U_o.
(e) The torsional restoring constant S affects θ_{res}, $\omega_{res(\theta)}$ and $\omega_{res(\dot{\theta})}$ in both air and water. Increasing S decreases θ_{res} and increases $\omega_{res(\theta)}$ and $\omega_{res(\dot{\theta})}$.
(f) The damping constant R affects θ_{res} and $\dot{\theta}_{res}$ in air and $\dot{\theta}_{res}$ and $\omega_{res(\theta)}$ in water. Increasing R decreases all four of these quantities.
(g) $\omega_{res(\theta)}$ and $\omega_{res(\dot{\theta})}$ are of the same order of magnitude in air and the same is true for water if $\mu L^3/R \gg 1$.
(h) The relation for θ_{res} in air appears as the product of a dominant term times a second term of order unity and it follows that

$$\frac{(\theta_{res})_{wat}}{(\theta_{res})_{air}} \approx \frac{\left(\frac{\mu L^2 U_o}{S}\right)_{wat}}{\left(\frac{\rho_h^{1/2} d L^{7/2} \mu U_o}{S^{1/2}(R+\mu L^3)}\right)_{air}} = 29$$

for hairs of equal length $L = 250\,\mu m$ oscillating in air and water with the same amplitude of velocity U_o, using values of ρ_h, μ, d, R, and S given in Tables 1–3. For these conditions it also follows that

$$\frac{(\dot{\theta}_{res})_{wat}}{(\dot{\theta}_{res})_{air}} \approx \frac{\left(\frac{\mu L^2 U_o}{R+\mu L^3}\right)_{wat}}{\left(\frac{\mu L^2 U_o}{R+\mu L^3}\right)_{air}} = 1.8$$

and

$$\frac{\left(\omega_{res(\theta)}\right)_{wat}}{\left(\omega_{res(\theta)}\right)_{air}} \approx \frac{\left(\frac{\mu L^3 S}{\left(R+\mu L^3\right)^2}\right)_{wat}}{\left(\frac{S^{1/2}}{\rho_h^{1/2} d L^{3/2}}\right)_{air}} = 0.06.$$

Thus, in agreement with Devarakonda *et al.* (1996), for the same amplitude of velocity in the two oscillating media hairs in water experience significantly larger maximum angular displacements at higher maximum angular velocities than hairs of equal length in air. In addition, the maximum angular displacement resonance frequency of the hair in water is significantly smaller than that of the hair in air.[6]

[6]These results have been obtained assuming equal velocities in the two incompressible fluid media. If the incompressible flow condition is relaxed and fluid motion is caused, instead, by traveling sound waves, for equal sound intensities in the two media their amplitudes of velocity will be in the ratio $u_{air}/u_{water} = [(\rho c)_{water}/(\rho c)_{air}]^{1/2} \approx 60$, where ρ and c are the media density and speed of sound (Denny, 1993).

3.2.2 *Physically exact model findings*

All of the qualitative PAM model findings listed earlier are borne out by PEM model calculations. In addition, both the PAM and PEM findings of this work are in good agreement with many of the earlier results based on the numerical solution of Eq. (9) (Shimozawa and Kanou, 1984b; Barth *et al.*, 1993; Humphrey *et al.*, 1993; Devarakonda *et al.*, 1996; Kumagai *et al.*, 1998; Shimozawa *et al.*, 1998). The response and performance characteristics of filiform hairs as a function of the major parameters (d, L, S, R, ρ_h, ρ, μ, U_o, ω) that affect their motion have been extensively explored (Humphrey *et al.*, 1993; Devarakonda *et al.*, 1996). Here we remark on some additional quantitative results yielded by the PEM model. Except where otherwise noted, for hairs in air the allometric relations provided in Table 1 have been used throughout this chapter.

(a) PEM calculated values of maximum angular displacement (θ_{max}), velocity ($\dot{\theta}_{max}$), and acceleration ($\ddot{\theta}_{max}$) are plotted as a function of flow oscillation frequency in Fig. 18 for MeD1 *Cupiennius* filiform hairs in air and nominal hairs in water. The shapes of the profiles for θ_{max} in Fig. 18a are as expected (see also Fig. 10). They show how the resonance frequency of a hair, $f_{res(\theta)}(\equiv \omega_{res(\theta)}/2\pi)$, increases with decreasing hair length (see also Figs. 12 and 14) and how θ_{res} (the value of θ_{max} at $f=f_{res(\theta)}$) decreases with decreasing hair length (see also Figs. 11 and 13). These results were obtained setting $U_o = 10\,\text{mm}\,\text{s}^{-1}$ in both the air and water media and, as a consequence, the nominal hairs in water experience larger angular displacements than the hairs in air (see also Fig. 13 and refer to point 'h' in Section 3.2.1). It is also clear that for a given hair length, the value of $f_{res(\theta)}$ in water is smaller than in air (see Fig. 14).

(b) For hairs in air, plots of $\dot{\theta}_{max}$ (Fig. 18b) show that the maximum value of this quantity, $\dot{\theta}_{res}$, and its corresponding resonance frequency, $\omega_{res(\dot{\theta})}$, both increase with decreasing hair length. This is in agreement with the relations for $\dot{\theta}_{res}$ and $\omega_{res(\dot{\theta})}$ provided in Table 4. The corresponding plots of $\dot{\theta}_{max}$ for hairs in water show similar trends, except that instead of displaying maxima they tend to asymptotic limits in the parameter range explored (and such behaviour persists even if the values assumed for R and S are varied by $\pm 50\%$ for these hairs). Compared to the hairs in air the hairs in water experience larger angular velocities. Similarly, plots of $\ddot{\theta}_{max}$ (Fig. 18c) show that for $f > 100\,\text{Hz}$, approximately, this quantity also increases with decreasing hair length. However, for $f < 100\,\text{Hz}$ for hairs in air and $f < 50\,\text{Hz}$ for hairs in water the reverse is true (see Fig. 18d covering the frequency range

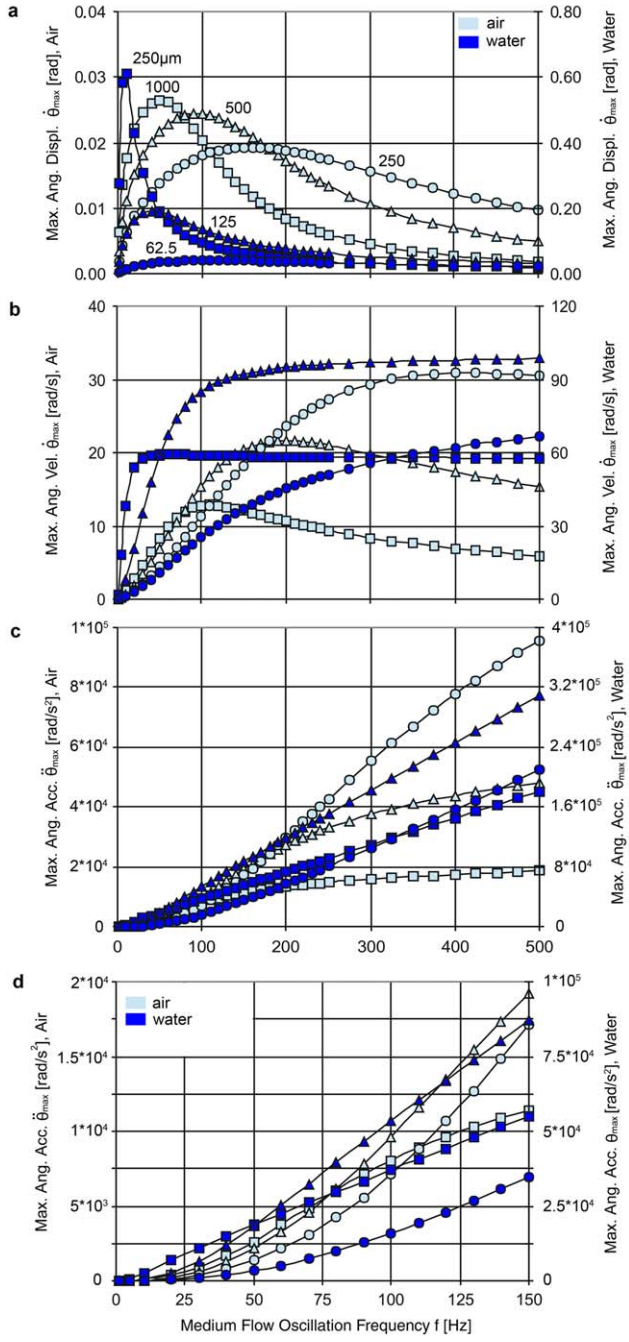
a
b
c
d
air
water
250μm
1000
500
250
125
62.5
Max. Ang. Displ. θ̇max [rad], Air
Max. Ang. Displ. θ̇max [rad], Water
Max. Ang. Vel. θ̇max [rad/s], Air
Max. Ang. Vel. θ̇max [rad/s], Water
Max. Ang. Acc. θ̈max [rad/s²], Air
Max. Ang. Acc. θ̈max [rad/s²], Water
Medium Flow Oscillation Frequency f [Hz]

$0 \leq f \leq 150$ Hz of Fig. 18c). In all cases, the hairs in water experience larger angular accelerations.

(c) Calculations of the dimensionless velocity of the tip of a hair, $V_{\text{hair}}/U_{\text{o}}$, and of the air medium velocity at the tip of the hair, $V_{\text{air}}/U_{\text{o}}$, are compared in Fig. 19 for an MeD1 trichobothrium 500 μm long. These results are characteristic of the dynamics at the tip of a hair. Notwithstanding, they serve to illustrate that, because of the complex coupling between hair motion and the y-dependent form of the oscillating medium flow velocity given by Eq. (13), there can be significant variations in the two velocities along the length of a hair which will alter its frequency response characteristics. Two cases are considered corresponding to air oscillation frequencies of 100 and 300 Hz, respectively, and in both cases the far-field amplitude of velocity is $10\,\text{mm}\,\text{s}^{-1}$. We denote by $V_{\text{r}}^{*} = (V_{\text{air}} - V_{\text{hair}})_{\text{air max}}/U_{\text{o}}$ the dimensionless relative air velocity at the tip of the hair, with V_{air} and V_{hair} both evaluated at the time corresponding to the maximum value of V_{air} in an oscillation cycle of period T_{p}. The dimensionless phase difference between $V_{\text{air}}/U_{\text{o}}$ and $V_{\text{hair}}/U_{\text{o}}$ is defined as $\phi = (t_{\text{air}}^{\text{max}} - t_{\text{hair}}^{\text{max}})/T_{\text{p}}$, where 'max' denotes the values of time corresponding to the maximum values of $V_{\text{air}}/U_{\text{o}}$ and $V_{\text{hair}}/U_{\text{o}}$ in an oscillation cycle. It is clear from the data in Fig. 19 that both V_{r}^{*} and ϕ depend on frequency. (Although not shown, similar time-dependent results have been obtained for nominal hairs in water.) From data like these it is possible to obtain plots of V_{r}^{*} and ϕ as a function of frequency for hairs of different length in air and water (Figs. 20 and 21). The hairs in air show a maximum in V_{r}^{*} at low frequency followed by a minimum at higher frequency. The locations of the maxima and minima depend on hair length, with the longest hair displaying the largest range of V_{r}^{*} and the shortest hair displaying the smallest. The hairs in water show similar variations in V_{r}^{*}, except that, in the parameter range explored, they do not display the minima observed for the hairs in air. The hairs in air have positive phase shift at low frequencies, but with increasing frequency the shift becomes negative for the hairs 1000 and 500 μm long. The hairs

FIG. 18 PEM calculated maximum values of *C. salei* MeD1 filiform hair angular displacement θ_{max} (a), angular velocity $\dot{\theta}_{\text{max}}$ (b), and angular acceleration $\ddot{\theta}_{\text{max}}$ (c, d) in air (left ordinate) and of a nominal hair in water (right ordinate) as a function of medium flow oscillation frequency with $U_{\text{o}} = 10\,\text{mm}\,\text{s}^{-1}$. Hair lengths are given in micrometers.

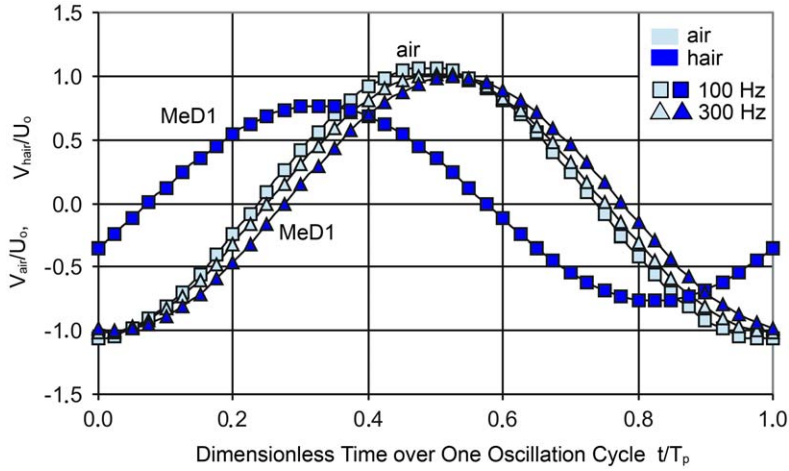

FIG. 19 PEM calculations of *C. salei* MeD1 filiform hair tip velocity, V_{hair}, and air velocity, V_{air}, at the hair tip plotted non-dimensionally as a function of time, t, over one cycle period, T_{p}, of a flow oscillating at 100 Hz (squares) and 300 Hz (triangles) with $U_{\text{o}} = 10\,\text{mm s}^{-1}$. Hair length is $L = 500\,\mu\text{m}$.

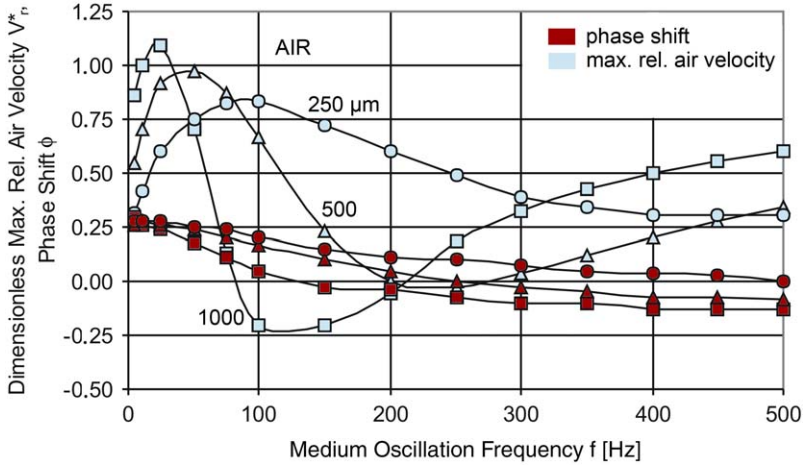

FIG. 20 PEM calculations of dimensionless maximum relative air velocity, V_{r}^{*}, and phase shift, ϕ, between air and filiform hair velocities as a function of medium oscillation frequency, f, for *C. salei* MeD1 hairs in air with $U_{\text{o}} = 10\,\text{mm s}^{-1}$. Hair lengths are given in micrometers (circles, 250 µm; triangles, 500 µm; squares, 1000 µm).

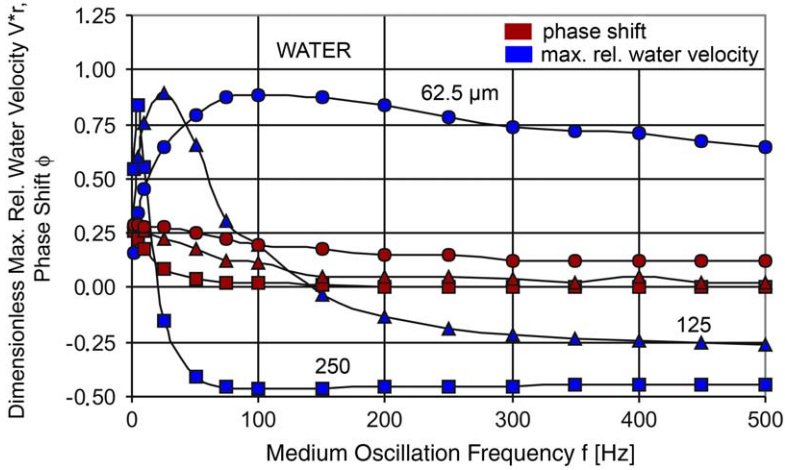

FIG. 21 PEM calculations of dimensionless maximum relative water velocity, V_r^*, and phase shift, ϕ, between water and filiform hair velocities as a function of medium oscillation frequency, f, for nominal hairs in water with $U_o = 10\,\text{mm}\,\text{s}^{-1}$. Hair lengths are given in micrometers (circles, 62.5 μm; triangles, 125 μm; squares, 250 μm).

in water have positive or zero phase shift for all frequencies in the range explored.

(d) A more realistic dimensionless parameter characterizing the mechanical sensitivity (or response) of a hair to the motion of an oscillating fluid medium is given by the rate of change of the hair tip maximum velocity with respect to the far-field amplitude of velocity, evaluated at the angular displacement resonance frequency; that is, $S^* \equiv \mathrm{d}(L\dot{\theta}_{\max})/\mathrm{d}U_o$ evaluated at $\omega_{\mathrm{res}(\theta)}$.[7] Using Eq. (21b) to evaluate $\mathrm{d}\dot{\theta}_{\max}/\mathrm{d}U_o$ it follows that

$$S^* = \left(\frac{\mathrm{d}\left(L\dot{\theta}_{\max}\right)}{\mathrm{d}U_o}\right)_{\omega_{\mathrm{res}(\theta)}} = L\left(\frac{\omega\theta_{\max}}{U_o}\right)_{\omega_{\mathrm{res}(\theta)}} = L\frac{\omega_{\mathrm{res}(\theta)}\theta_{\mathrm{res}}}{U_o}. \quad (27)$$

We are interested in the variation of S^* as a function of hair length non-dimensionalized by the boundary layer thickness δ as

[7]Note that this definition differs from that used in Humphrey *et al.* (2001, 2003) where the sensitivity parameter is defined as $S^* = \mathrm{d}(L\dot{\theta}_{\mathrm{res}})/\mathrm{d}U_o$. This quantity represents the rate of change of the hair tip maximum velocity with respect to the far-field amplitude of velocity evaluated at $\omega_{\mathrm{res}(\dot{\theta})}$, the angular velocity resonance frequency. The differences between the two definitions lead to differences in their plots.

defined by Eq. (14), also evaluated at $\omega_{\mathrm{res}(\theta)}$; that is

$$L^* = \left(\frac{L}{\delta}\right)_{\omega_{\mathrm{res}(\theta)}} = \frac{L}{6.34\left(\nu/\omega_{\mathrm{res}(\theta)}\right)^{1/2}}.$$

Figure 22 shows plots of S^* versus L^* obtained using the PEM to calculate θ_{res} and $\omega_{\mathrm{res}(\theta)}$, and using experimentally derived correlations for θ_{res} and $\omega_{\mathrm{res}(\theta)}$. The results show (i) good qualitative agreement between the experimentally derived and PEM calculations for MeD1 and cercus hairs, and similar trends between the two for TiDA1 hairs; (ii) because of the definitions of S^* and L^*, it is theoretically possible for two hairs to have the same value of L^* and different values of S^* (see the PEM calculated results for TiDA1 hairs at $L^* \approx 0.83$); (iii) all hairs have an $L^* < 1$, meaning that they are well immersed in the oscillating flow boundary layer (Barth *et al.*, 1993); (iv) the values of L^* are smaller for hairs in water than hairs in air; (v) the values of S^* are generally larger for hairs in air than hairs in water; (vi) the values of S^* are larger for spider hairs than cricket hairs. (Although not shown, plots of S^* versus L^* obtained using the PAM are in qualitative agreement with these results.) Note that because S^* is evaluated at the hair resonance frequency, it provides no indication concerning the frequency bandwidth a hair responds to.

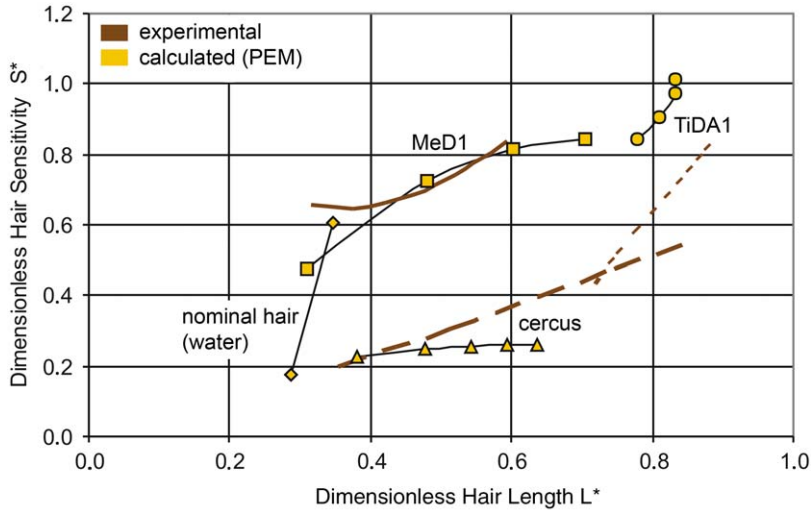

FIG. 22 Comparison between PEM calculated and experimentally derived values of filiform hair mechanical sensitivity (or response), S^*, plotted as a function of dimensionless hair length, L^*, for *C. salei* MeD1 and TiDA1 hairs, *G. bimaculatus* cercal hairs, and nominal hairs in water.

4 Discussion

In this section we focus primarily on the bearing of our model findings and related experimental observations in three important areas: (i) hair sensitivity and selectivity; (ii) motion sensing in air and water; (iii) the effects of selective pressures on the various parameters affecting hair motion.

4.1 SENSITIVITY AND SELECTIVITY

'Sensitivity' here refers to the change in the angular displacement, velocity, or acceleration of a flow-sensing hair relative to a change in any quantity of physical importance that affects its motion. Selectivity refers to the ability of a hair to preferentially react mechanically to a particular stimulus, usually by reference to its intensity, time course, and frequency content. Of course, the two are interconnected.

4.1.1 *Hair length, diameter, and surface area*

In contrast to hairs in air, for hairs in water their length, L, but not their diameter, d, appears in the relations given in Table 4. However, for hairs in air the two dimensions are known to be related by empirical allometric functions of the form $d = mL^n$ (Table 1; see also Shimozawa and Kanou, 1984a,b; Kumagai *et al.*, 1998; Humphrey *et al.*, 2003) and, in principle, this allows either d or L to be the sole characteristic dimension. From the form of the allometric relation it follows that the diameters and lengths of a long and short hair are related according to $d_L/d_S = (L_L/L_S)^n$. Therefore, doubling the length of a hair increases its diameter by a factor 2^n. The consequences to the surface areas and moments of inertia (see Eq. 2) of a pair of hairs are that $A_L/A_S = 2 \times 2^n$ and $I_L/I_S = 2^3 \times 2^{2n}$, where L and S refer to a long and short hair, respectively. The first term in these products denotes the contribution to the ratio due to the doubling of L, and the second is the contribution due to the associated 2^n increase in d. Thus, there is a significant effect on the moment of inertia of a hair in air due to increasing its length (2^3) and, by allometry, its diameter (2^{2n}).

What, however, is the potential significance of the area increase (2^n) due to d which ranges between 1.23 and 1.63, approximately? Does it significantly affect the drag experienced by a hair? The answer, surprisingly, is that it does not. To show this, consider the forces per unit length acting on a hair (Eqs. 6a–c). We have already shown that $F(\rho, \dot{V}_r)$ is negligible and that $F(\mu, V_r) > F(\mu, \dot{V}_r)$. For $F(\mu, V_r)$ and $F(\mu, \dot{V}_r)$, the dependence on d is embedded in their G and g terms as defined by Eqs. (7–8). For a pair of MeD1 hairs of length $L_L = 1000\,\mu m$ and $L_S = 500\,\mu m$ in a uniform flow oscillating at 100 Hz it can be shown

that

$$\frac{F(\mu, V_r)_L}{F(\mu, V_r)_S} = \frac{G_L}{G_S} = 1.05$$

and

$$\frac{F(\mu, \dot{V}_r)_L}{F(\mu, \dot{V}_r)_S} = \frac{G_L g_S}{G_S g_L} = 1.11.$$

This implies that increases in hair diameter (correlated with increases in hair length) do not significantly increase the forces acting on a hair. In contrast, because the integrals of these forces along the length of a hair are proportional to L^2 (Eq. 3), hair length emerges as the dominant geometrical dimension in determining the total torque acting on a hair in air. The conclusion is that, except for the moment of inertia of a hair in air, changes in hair diameter play a secondary role relative to changes in hair length in determining the performance characteristics of hair motion.[8] This analysis also illustrates how sensitivity and selectivity are intertwined since the length of a hair affects both.

4.1.2 *Torsional restoring constant S and damping constant R*

In Table 4, the torsional restoring constant, S, appears to the power 1/2 for hairs in air and to the power 1 for hairs in water. Thus, hairs in water are proportionally more sensitive to variations in the value of S than hairs in air. The damping constant R always appears in combination with the term $R_\mu \approx \mu L^3$. In general, $R \approx \mu L^3$ except for long hairs in air and water where $R \approx \mu L^3/10$ and short hairs in water where $R \approx 10 \times \mu L^3$, approximately (Table 3). However, as for L, once S and R are fixed they work (together with L and all the other parameters) to determine a hair's selectivity through the resulting resonance characteristics of the hair.

4.1.3 *Boundary layer thickness*

In Section 3.2.2, we defined a dimensionless parameter, $S^* = \mathrm{d}(L\dot{\theta}_{max})/\mathrm{d}U_o$, for characterizing the sensitivity of a hair to the motion of an oscillating fluid medium. Values for S^* plotted as a function of L^* (the hair length non-dimensionalized by the boundary layer thickness δ) with both S^* and L^* evaluated at the hair resonance frequency, are provided in Fig. 22.

[8] These considerations relate to the dependence of $F(\mu, V_r)$ and $F(\mu, \dot{V}_r)$ on changes in d due to changes in L. Clearly, changes in d independent of changes in L will affect these two forces directly, through the parameter s given by Eq. (4).

All hairs show values of $S^* \leq 1$ and $L^* < 1$, as expected from earlier considerations. Thus, all hairs are well immersed in their oscillating flow boundary layers with the values of L^* for hairs in water being significantly smaller than for hairs in air. In addition, for the parameter ranges explored, the data suggest that hairs in air are more sensitive than hairs in water, and that spider hairs are more sensitive than cricket hairs.

4.1.4 *Optimal hair sensitivity and selectivity occur at similar frequencies*

Returning to the issue of selectivity, Fig. 23 shows PEM calculated maximum angular displacements and velocities for a 500 μm long MeD1 *Cupiennius* hair plotted as a function of frequency for an air flow with far-field amplitude of velocity 2 mm s^{-1}. These are the conditions for which Barth and Höller (1999) obtained measurements of the action potentials per unit time fired by trichobothria sensory cells and their results are included in the figure. It is remarkable that the value of frequency corresponding to the maximum in the action potentials curve coincides closely with both the calculated hair resonance frequency, $f_{\mathrm{res}(\theta)}$, and the value of frequency that maximizes the slope of the maximum angular

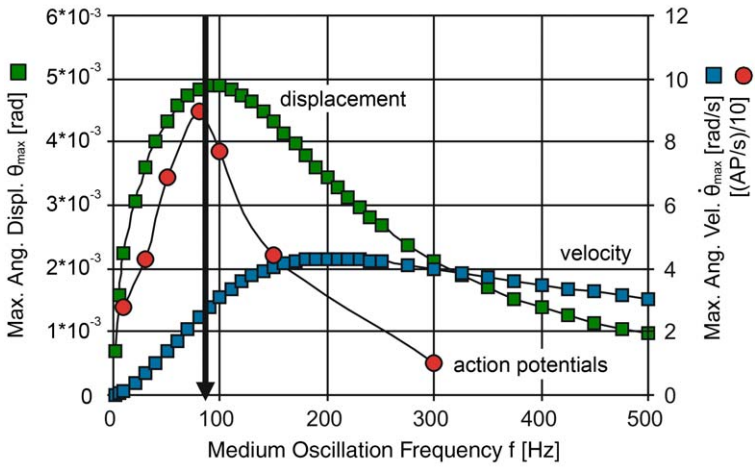

FIG. 23 PEM calculated maximum angular displacement, $\theta_{\max}$ and angular velocity, $\dot{\theta}_{\max}$, and measured action potential frequency, AP/s, for a 500 μm long MeD1 *C. salei* filiform hair (trichobothrium) plotted as a function of frequency, f, for an oscillating air flow with $U_o = 2$ mm s^{-1}. The electrophysiologial impulse responses (Barth and Höller, 1999) are divided by 10 for plotting. The vertical arrow shows that the maximum discharge rate of the sensory cell coincides with the mechanical resonance frequency of the hair ($f_{\mathrm{res}(\theta)}$) and the air flow frequency that maximizes the slope of $\dot{\theta}_{\max}(f_{(\mathrm{d}\dot{\theta}/\mathrm{d}\omega)\max})$.

velocity, $f_{(d\dot{\theta}/d\omega)\max}$. (For stimulus frequencies smaller and larger than $f_{res(\theta)}$ the action potentials curve drops to comparatively smaller values.) In Appendix A we show that $f_{(d\dot{\theta}/d\omega)\max} \cong 2/3 f_{res(\theta)}$ is a general property of flow-sensing hairs modelled as damped forced harmonic oscillators. Thus, in mechanically responding most optimally to its resonance frequency (pointing to an adaptation for selectivity) a spider hair automatically selects for the range of angular velocities, $\dot{\theta}_{max}$, most sensitive to variations in the flow oscillation frequency, f, (pointing to an adaptation for sensitivity).

4.2 SENSORY ECOLOGY

4.2.1 *Motion sensing in air and in water*

All the relations in Table 4 for hairs in water, and those for θ_{res} and $\dot{\theta}_{res}$ for hairs in air, show a dependence on the medium dynamic viscosity μ and, therefore, should be sensitive to changes in this quantity. The dynamic viscosities of air and water can, indeed, vary in the environment through changes in temperature. Variations of $\pm 15\,^{\circ}C$ about an average of $27\,^{\circ}C$ change μ by about $\pm 4\%$ in air and $\pm 34\%$ in water (see Section 3.2.1). Thus, the potential sensitivity to changes in μ is much larger for hairs in water than for hairs in air. For a 250 μm long hair in water, for which $\mu L^3 > R$, it can be shown that

$$\frac{(\theta_{res})_{wat(T_L)}}{(\theta_{res})_{wat(T_H)}} \approx \frac{\mu_{wat(T_L)}}{\mu_{wat(T_H)}}$$

and

$$\frac{(\omega_{res(\theta)})_{wat(T_L)}}{(\omega_{res(\theta)})_{wat(T_H)}} \approx \frac{\mu_{wat(T_H)}}{\mu_{wat(T_L)}}$$

where T_L and T_H denote low and high fluid medium temperatures, respectively. Taking $T_L = 15\,^{\circ}C$ and $T_H = 30^{\circ}C$ for which $\mu_{wat(T_L)} = 1.14 \times 10^{-3}$ (kg m^{-1} s^{-1}) and $\mu_{wat(T_H)} = 8.0 \times 10^{-4}$ (kg m s^{-1}), respectively, it follows that $(\theta_{res})_{wat(T_L)} \approx 1.43 \times (\theta_{res})_{wat(T_H)}$ and $(\omega_{res(\theta)})_{wat(T_L)} \approx 0.70 \times (\omega_{res(\theta)})_{wat(T_H)}$. Thus increasing (decreasing) water temperature decreases (increases) the maximum angular displacement at resonance frequency while it increases (decreases) the resonance frequency. This viscosity dependence in water appears to be significant, whereas that in air will hardly affect the mechanical response of the hair.

When exposed to the same far-field amplitude of velocity, equal length hairs operating in air and water show very different performance characteristics. For example, for hairs with $L = 250\,\mu m$ the relations

$(\theta_{res})_{wat} \approx 29(\theta_{res})_{air}$ and $(\omega_{res(\theta)})_{wat} \approx 0.06(\omega_{res(\theta)})_{air}$ apply (see Section 3.2.1). Consider what happens if a hair optimized to operate in one medium is required to operate in the other. For purposes of the discussion presented in Section 4.3, concerning evolution through selective pressures on different parameters, let us require a 'water-hair' to operate in air. Call $(\theta_{res}^{wat-hair})_{air}$ and $(\omega_{res(\theta)}^{wat-hair})_{air}$ the quantities of interest for the water-hair operating in air and $(\theta_{res}^{air-hair})_{air}$ and $(\omega_{res(\theta)}^{air-hair})_{air}$ the corresponding reference values for an 'air-hair' also operating in air. From the relations for θ_{res} and $\omega_{res(\theta)}$ in Table 4 for hairs in air the following maximum angular displacement and resonance frequency ratios are obtained

$$\Theta_{res} \equiv \frac{\left(\theta_{res}^{wat-hair}\right)_{air}}{\left(\theta_{res}^{air-hair}\right)_{air}} \approx \left(\frac{\rho_{h(wat)}}{\rho_{h(air)}}\right)^{1/2} \left(\frac{d_{wat}}{d_{air}}\right)\left(\frac{L_{wat}}{L_{air}}\right)^{7/2}\left(\frac{S_{air}}{S_{wat}}\right)^{1/2}\left(\frac{R_{air}+\mu_{air}L_{air}^3}{R_{wat}+\mu_{air}L_{wat}^3}\right) \tag{28a}$$

$$\Omega_{res(\theta)} \equiv \frac{\left(\omega_{res(\theta)}^{wat-hair}\right)_{air}}{\left(\omega_{res(\theta)}^{air-hair}\right)_{air}} \approx \left(\frac{\rho_{h(air)}}{\rho_{h(wat)}}\right)^{1/2}\left(\frac{d_{air}}{d_{wat}}\right)\left(\frac{L_{air}}{L_{wat}}\right)^{3/2}\left(\frac{S_{wat}}{S_{air}}\right)^{1/2}. \tag{28b}$$

In these relations the subscripts 'air' and 'wat' denote properties associated with the air-hair and water-hair, respectively. It is assumed that both hairs are exposed to the same far-field amplitude of velocity, U_o, of the air medium. To further simplify the analysis, it is also assumed that the densities and diameters of the two hairs are close enough to cancel out over the parameter ranges of interest so that

$$\Theta_{res} \equiv \frac{(\theta_{res}^{wat-hair})_{air}}{(\theta_{res}^{air-hair})_{air}} \approx \left(\frac{L_{wat}}{L_{air}}\right)^{7/2}\left(\frac{S_{air}}{S_{wat}}\right)^{1/2}\left(\frac{R_{air}+\mu_{air}L_{air}^3}{R_{wat}+\mu_{air}L_{air}^3}\right) \tag{29a}$$

$$\Omega_{res(\theta)} \equiv \frac{(\omega_{res(\theta)}^{wat-hair})_{air}}{(\omega_{res(\theta)}^{air-hair})_{air}} \approx \left(\frac{L_{air}}{L_{wat}}\right)^{3/2}\left(\frac{S_{wat}}{S_{air}}\right)^{1/2}. \tag{29b}$$

To illustrate the use of these relations, we fix $S_{air} = 10^{-13}$ and $S_{wat} = 10^{-12}$ (N m rad^{-1}), and $R_{air} = 10^{-16}$ and $R_{wat} = 10^{-15}$ (N m s rad^{-1}). These values correspond closely to those listed in Table 4 for air-hairs and water-hairs 250 μm long. We also take $\mu_{air} = 1.85 \times 10^{-5}$ (kg m^{-1} s^{-1}) from Table 2. Figure 24 shows the results of evaluating Θ_{res} and $\Omega_{res(\theta)}$ as a function of L_{wat}/L_{air} for three values of L_{air} corresponding to 250, 500, and 750 μm. (Note that because Θ_{res} depends independently on L_{air} and L_{wat} it gives rise to three different curves in the figure, whereas because $\Omega_{res(\theta)}$ depends on

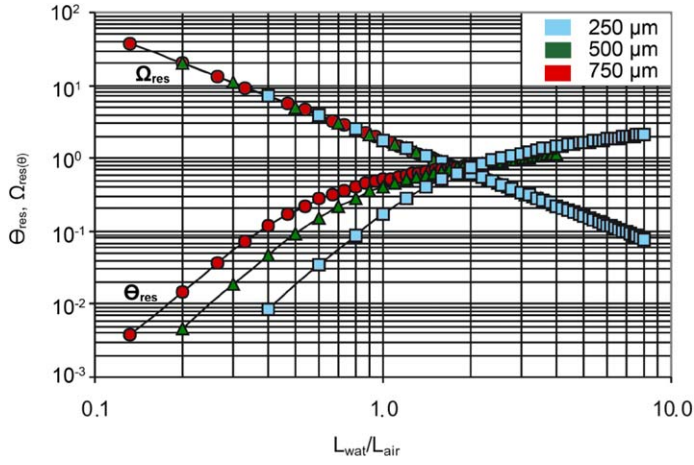

FIG. 24 PAM calculated variations of the dimensionless ratios Θ_{res} and $\Omega_{res(\theta)}$ (see text) characterizing the performance of a water-hair of length L_{wat} operating in air relative to an air-hair of length L_{air} also operating in air. The values of L_{air} used in the calculations are shown in the insert and the values of S, R, d, and U_o are given in the text.

the ratio L_{air}/L_{wat} there is only one curve.) The data reveal that for a water-hair in air to simulate the performance characteristics of an air-hair in air, meaning that $\Theta_{res} \approx 1$ and $\Omega_{res(\theta)} \approx 1$, the water-hair to air-hair length ratio should be $L_{wat}/L_{air} \approx 2$. Thus, for example, for a water-hair to perform in air like an air-hair of length 250 μm its length should be 500 μm, approximately. We have verified this PAM finding using the PEM approach. For this, we have used the above values of S and R for the water-hair and air-hair, and we have set $d = 5$ μm and $U_o = 0.05\ m\ s^{-1}$ in the calculations for both hairs. The results obtained are shown in Table 5 where they are compared with corresponding PAM estimates and it is seen that agreement is close between the two models. In fact, the more exact PEM results show that for the conditions explored a water-hair twice the length of an air-hair can achieve the resonance frequency of the air-hair while closely matching its maximum angular displacement at that resonance frequency. We have also checked the sensitivity of L_{wat}/L_{air} to changes in the values of S and R for the water-hair and find that increasing both by one order of magnitude to $S_{wat} = 10^{-11}$ $(N\ m\ rad^{-1})$ and $R_{wat} = 10^{-14}$ $(N\ m\ s\ rad^{-1})$ to simulate even stiffer hairs requires that $L_{wat}/L_{air} \approx 3.5$ to achieve values of $\Theta_{res} \approx 1$ and $\Omega_{res(\theta)} \approx 1$, respectively, in the range $250 \leq$ μm $L_{air} \leq 750$ μm. These are important findings since, as discussed in Section 4.3, they provide a possible evolutionary path for flow-sensing hairs in water to have adapted via natural selection pressures to operate in air.

TABLE 5 Comparisons between PAM estimates and PEM calculations of the maximum angular displacement ratio, Θ_{res}, and resonance frequency ratio, $\Omega_{res(\theta)}$, defined in the text for air-hair and water-hair pairs oscillating in air with far field velocity amplitude of $U_o = 0.05\,m/s$

	PAM Estimate		PEM Calculation	
$L_{wat}/L_{air} = 2$	Θ_{res}	$\Omega_{res(\theta)}$	Θ_{res}	$\Omega_{res(\theta)}$
$L_{air} = 250\,\mu m$	0.75	0.63	0.65	0.98
$L_{wat} = 500\,\mu m$				
$L_{air} = 500\,\mu m$	0.79	0.63	0.69	1.00
$L_{wat} = 1000\,\mu m$				

Note: In the calculations all hairs have: $d = 5\,\mu m$; $S_{air} = 10^{-13}$, and $S_{wat} = 10^{-12}$ ($N\,m\,rad^{-1}$); $R_{air} = 10^{-16}$ and $R_{wat} = 10^{-15}$ ($N\,m\,s\,rad^{-1}$).

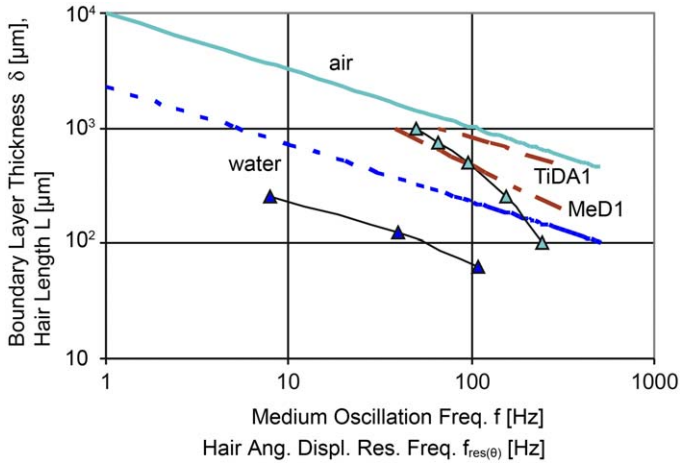

FIG. 25 Boundary layer thickness, δ, in air (light blue continuous line) and in water (dark blue dotted line) plotted as a function of medium oscillation frequency, f. Also shown are PEM calculated maximum angular displacement resonance frequency, $f_{res(\theta)}$, as a function of trichobothria length, L, for *C. salei* hairs in air (light blue triangles) and nominal hairs in water (dark blue triangles). Fits to the experimental data for $f_{res(\theta)} = f(L)$ in Barth *et al.* (1993) are plotted for MeD1 (brown dash-dot line) and TiDA1 (brown dashed line) trichobothria of *C. salei*.

Further evidence supporting the need for hairs of different length in air and water media is provided in Fig. 25. Earlier work (Barth *et al.*, 1993; Barth, 2004) and present findings pertaining to hairs stimulated by sinusoidally oscillating flow fields suggest that the length of a hair, L, scales with the thickness, δ, of the boundary layer flow whose frequency it is best matched to detect. By this we mean that a flow oscillating at frequency $\omega = 2\pi f$ over a surface generates a boundary layer of thickness $\delta \propto (\nu/\omega)^{1/2}$

($\delta = 6.34(\nu/\omega)^{1/2}$ for a flat surface) and that the filiform hair best tuned to match ω has length $L \leq \delta$. We suggest below why this scaling should arise.

Panton (1996) shows that the maximum amplitude of velocity in a boundary layer generated by a fluid medium oscillating over a flat surface occurs at $y/\delta \cong 0.5$, irrespective of the medium physical properties, oscillation amplitude, or frequency. Using the analysis in Panton (1996) it is also possible to show that a hair of length $L \approx \delta$ in such an oscillating flow experiences an approaching fluid velocity equal to or larger than the imposed far-field velocity over about 50% of its distal length. Thus, we suggest that: (i) Natural selection has led to arrays of hairs of different length such that at any biologically meaningful flow oscillation frequency there will be a match between the length of some hair in the array and the boundary layer thickness, thus guaranteeing that most of the length of that hair experiences the full amplitude of the oscillating flow. (ii) Natural selection has simultaneously led to hair geometries and densities (which determine a hair's moment of inertia, I), as well as cuticular hair suspension membrane material properties and structure (which determine a hair's torsional restoring and damping constants, S and R), so that the resonance frequency of a hair will match the frequency associated with the boundary layer thickness it scales with. (iii) With over about 50% of the length of a hair fully exposed to the far field velocity of an oscillating flow whose frequency it is best matched to detect, further lengthening of that hair by growth would not only be wasteful of energy and materials but would also alter the total moment of inertia of the hair and so detract from the frequency matching.

4.2.2 *Modelling filiform hair responses to natural flows*

The biological importance of transient flow effects on hair motion has been remarked on by Wiese (1976), Camhi (1984), Barth *et al.* (1995), Friedel and Barth (1997), Barth and Höller (1999), Dangles *et al.* (2006b), and Humphrey and Mellon (2007), and has been discussed in reviews by Barth (2000) and Barth (2002a). So far in this chapter we have considered motion-sensing filiform hairs immersed in sinusoidally oscillating flows with zero net mean velocity. This is a situation that is commonly set up in the laboratory for purposes of characterizing the behaviour and response characteristics of filiform hairs (Shimozawa and Kanou, 1984b; Barth *et al.*, 1993). We wish to know the extent to which the findings for such flows (for which boundary layer thickness is a function of frequency only) may be altered in the natural environment by transient flows consisting of a low frequency background motion with high frequency components of motion superimposed (Barth *et al.*, 1995; Barth and Höller, 1999). In this case the flow does not reverse direction but, instead, accelerates and decelerates in a pulsating manner in the direction of motion as a function

of time. Contrary to the strictly oscillating case, in such a flow the thickness of the boundary layer formed on a fixed surface entirely immersed in the flow will decrease with increasing velocity and vice versa. This is the situation that arises when, for example, an insect flies over a spider. Hot wire anemometer measurements of the air flow generated by a fly tethered upstream of a *Cupiennius* spider confirm that it consists of a fairly strong draft with oscillations superimposed (Barth *et al.*, 1995).

An analysis of the response of a filiform hair to a transient pulsating boundary layer flow is provided in Appendix B. Here we discuss the major results obtained for the flow developing from rest around a spider leg of diameter 2 mm. Using the data of Barth *et al.* (1995) for guidance, the background flow is fixed to 50 mm s^{-1} and the oscillating component to 10 mm s^{-1} with a frequency of 100 Hz. The flow acts on three hairs of different lengths (250, 500, and 1000 μm) immersed in the pulsating boundary layer.

Whereas the far-field velocity $U_o(t)$ and the boundary layer thickness δ_{BL} (Fig. 26a) acquire their steady periodic states in less than 50 ms, the effects of the periodic component of motion on the three hairs examined are noticeable within 15 ms. In this regard, values of V_f plotted at y locations corresponding to half a hair length are shown in the figure and, for reference, the length of a hair 1000 μm long is also shown. It is clear that all three hairs lie well within the pulsating boundary layer flow. As expected, because longer hairs extend further into the boundary layer they experience higher air velocities than shorter ones and, for the same reason, Fig. 26b shows significantly larger tip velocities for long hairs compared to short ones. Figures 26c and d show hair angular displacements and velocities, respectively. For the conditions examined, the 1000, 500, and 250 μm hairs experience maximum steady periodic angular displacements corresponding to about $\pm 0.40^\circ$, $\pm 0.18^\circ$, and $\pm 0.08^\circ$, respectively, about their average equilibrium values. However, within 5 ms of the start of motion each of these three hairs has been deflected by approximately 0.10°, 0.06°, and 0.03°; values large enough, in principle, to trigger action potentials from the sensory cells connected to the hairs.

Although the transient flow analysis has been applied to spider filiform hairs only, the findings suggest the following general conclusions: (i) Both in the laboratory and natural environment, filiform hairs exposed to pulsating boundary layer flows are well embedded in the boundary layers formed on the substrates that support the hairs. (ii) A hair immersed in a pulsating boundary layer flow in the natural environment oscillates around its average equilibrium angular location and, provided $Re \ll 1$, its resonance frequency is the same as that determined in the laboratory using a purely oscillatory flow. However, for the unusual condition that $Re \geq 1$, the non-linear dependence of the drag force on Re (see Eq. B5) will affect hair motion and it becomes necessary to reproduce the natural flow condition in the laboratory. (iii) Not surprisingly, in the natural

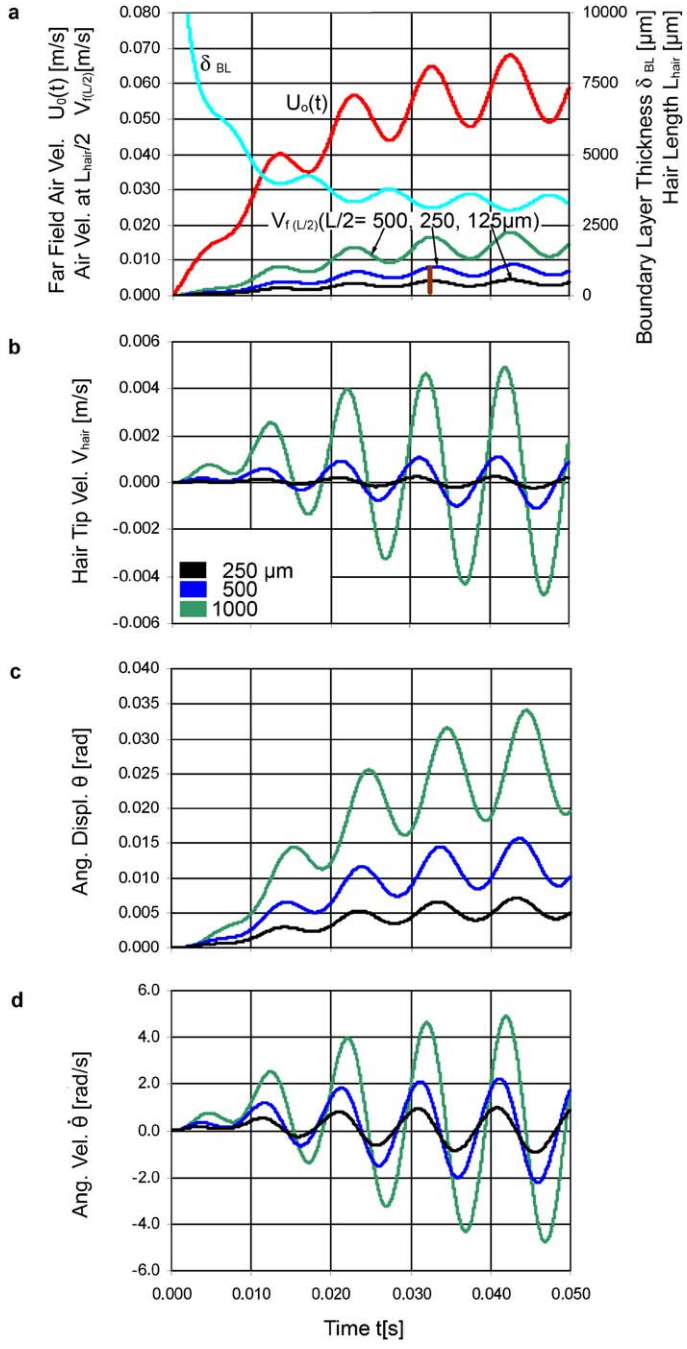
a
b
c
d
Far Field Air Vel. $U_o(t)$ [m/s]
Air Vel. at $L_{hair}/2$ $V_{f(L/2)}$[m/s]
δ_{BL}
$U_o(t)$
$V_{f\,(L/2)}$(L/2= 500, 250, 125μm)
Boundary Layer Thickness δ_{BL} [μm]
Hair Length L_{hair} [μm]
Hair Tip Vel. V_{hair} [m/s]
250 μm
500
1000
Ang. Displ. θ [rad]
Ang. Vel. $\dot{\theta}$ [rad/s]
Time t[s]

environment the medium flow can induce initial hair angular displacements and velocities potentially large enough to trigger sensory cell responses in a matter of a few milliseconds. The third conclusion points to the possible influence transient effects may have on the response characteristics of flow-sensing filiform hairs under natural conditions.

4.3 EVOLUTION THROUGH SELECTIVE PRESSURES ON DIFFERENT PARAMETERS

What can Physics say about the adaptive evolution of medium flow sensors? This fundamental question has been a focal point in an earlier study (Humphrey *et al.*, 2001). It seems reasonable to assume that over evolutionary time periods flow-sensing hairs have adapted to selective pressures in response to changes in the displacement, velocity, acceleration, and frequency characteristics of the medium signals detected. In this subsection we apply selected results from the PAM model to explain how physical pressures and constraints may have possibly influenced and guided the evolutionary adaptation of filiform hairs.

If we restrict attention to long hairs in air (1000 μm) and in water (250 μm), for which $\mu L^3 > R$, the relations in Table 1 yield

Hairs in air:

$$\theta_{\text{res}} \approx \frac{\rho_{\text{h}}^{1/2} d L^{1/2} U_{\text{o}}}{S^{1/2}} \quad \text{and} \quad \omega_{\text{res}(\theta)} \approx \frac{S^{1/2}}{\rho_{\text{h}}^{1/2} d L^{3/2}} \tag{30}$$

Hairs in water:

$$\theta_{\text{res}} \approx \frac{\mu L^2 U_{\text{o}}}{S} \quad \text{and} \quad \omega_{\text{res}(\theta)} \approx \frac{S}{\mu L^3} \tag{31}$$

Whereas θ_{res} and $\omega_{\text{res}(\theta)}$ are insensitive to the values of the medium physical properties for long hairs in air, they depend on the dynamic viscosity for

FIG. 26 Numerically calculated response characteristics of three MeD1 *C. salei* filiform hairs of length $L = 250$, 500, and 1000 μm exposed to a time-dependent flow of air generating a boundary layer around a spider leg of diameter $D = 2$ mm. The approaching flow is normal to the leg axis and the far-field air velocity is given by $U_{\text{o}}(t) = g(t)\ [U_1 + U_2\ (1 + \sin(2\pi f t))]$, where $g(t)$ is an exponential ramping function of time (see text) and $U_1 = 50\ \text{mm s}^{-1}$, $U_2 = 10\ \text{mm s}^{-1}$, $f = 100$ Hz. The results shown correspond to a 90° location around the leg circumference starting from the front stagnation point on the leg. Values of $S = S(L)$ and $R = R(L)$ are specified using the correlations for MeD1 hairs given in Table 1. (a) Far-field air velocity, $U_{\text{o}}(t)$; air velocities approaching the three hairs at their half-length location, $V_{\text{f}(L/2)}$; scaled filiform hair of length $L_{\text{hair}} = 1000$ μm; boundary layer thickness, δ_{BL}. (b) Hair tip velocity. (c) Hair angular displacement, θ. (d) Hair angular velocity, $\dot{\theta}$.

long hairs in water. This finding is in keeping with the temperature dependence of μ for water, which can significantly affect the performance of a hair (Section 3.2.1). The role of μ as a selective pressure for the adaptive evolution of hairs in water is compelling and has been discussed by Devarakonda *et al.* (1996). Such hairs have evolved combinations of lengths L and torsional restoring constants S that enable them to best displace and vibrate in water in tune with the hydrodynamic signals they must detect. In contrast, hair density and diameter emerge as important parameters for determining θ_{res} and $\omega_{\mathrm{res}(\theta)}$ for hairs in air, while they do not for hairs in water. This can be traced back to the dominant role played by the moment of inertia of a hair oscillating in air, which is $I \propto \rho_{\mathrm{h}} d^2 L^3$ (Eq. 2). Thus, for hairs in air selective pressures have worked to evolve optimal combinations of the parameters ρ_{h} and d in combination with S and L that favour aerodynamic signal detection.

Recent molecular evidence suggests that crustaceans may have successfully invaded land as insects (Glenner *et al.*, 2006). We ask the following two questions. How might the functional dependencies of θ_{res} and $\omega_{\mathrm{res}(\theta)}$ (and of $\dot{\theta}_{\mathrm{res}}$ and $\omega_{\mathrm{res}(\dot{\theta})}$) of flow-sensing filiform hairs have changed over evolutionary times to allow the move from water to air? In particular, since it would take many generations for sensory adaptation to occur via natural selection, how did the intervening generations of an evolving animal manage to bridge the change in habitats using water-adapted sensors in the new air medium?

From the discussions presented in Section 4.2.1 we learned two things: (i) Because of the complex dependencies of hair motion on μ, S, R, and L, hairs optimized to operate in one medium do not function ideally in the other. (ii) However, hair length emerged as a major variable that can offset differences in μ, S, and R between media and their hairs allowing, for example, long water-hairs to function in air similarly to the way short air-hairs do (see discussions of Fig. 24 and Table 5). Therefore, if a water-dwelling arthropod were to initially have a number of flow-sensing hairs of different lengths dispersed over its body, in principle some of the longer ones could also function in air. In this overlapping niches adaptation potential scenario, to effect a transition from water to air, the first intervening generations of this animal would rely on the longer hairs already available, while selective pressures in the new air environment would work to evolve more optimally performing hairs. Such a natural selection process would tinker with the values of d, L, S, R, ρ_{h} of the hairs to match their performance characteristics with the values of ρ, μ, U_{o}, and ω in air. The mechanoreceptive sensilla of some extant crustaceans such as lobsters and amphibious littoral crabs can, indeed, be quite long, reaching lengths of $\sim 2000\,\mu\mathrm{m}$ in the case of the smooth and squamous setae, and the serrate setae, of the lobster *Homarus americanus* (Derby, 1982).

5 Bio-inspired artificial motion sensors

The miniaturization and integration of many functions, ranging from stimulus transformation by the non-nervous sensillum apparatus to the generation of electro-chemical nervous signals are typical features of natural sensors such as flow-sensing filiform hairs. The sensitivity, selectivity, and efficient performance characteristics of these systems have been perfected over hundreds of millions of years by evolutionary advances under the influence and control of natural selective pressures. Only relatively recently, as the result of the development and application of new materials in parallel with major advances in Micro-Electro-Mechanical Systems (MEMS) fabrication technologies, has it been possible to build highly integrated artificial sensory systems at very small scales. By this we mean milliscale platforms with a number of compactly packaged and interdependent microscale electro-mechanical components capable of sensing. The motivation for doing this is clear, since artificial microsensors have the potential to revolutionize the way science, medicine, and engineering are practiced through the implantation of accurate, robust, multifunctional sensing devices, singly or in arrays, in the media or structures of interest. And although nature has for a long time undoubtedly been a source of inspiration to many an inquisitive and applied mind, it is even more recent that these new materials and advanced fabrication technologies have combined with in-depth biological insight and physical–mathematical modelling to make bio-inspired MEMS systems possible (Barth *et al.*, 2003). By bio-inspired we mean the conceptualization and development of an artificial device, such as a hair-like medium motion sensor, based on the understanding of biological principles and observations, as opposed to its imitation. Because the bio-inspired electro-mechanical hair-like medium motion sensors of interest here should function, ideally, like the organs of living animals, it is appropriate to refer to them as 'bionic'. In this subsection we elaborate on several of the above points.

5.1 MOTIVATION AND APPLICATIONS

There are a number of quantitatively accurate ways to measure the fluid mechanical characteristics of a flowing medium including pressure, velocity, and shear stress (Holman, 1978; Goldstein, 1983; Beckwith *et al.*, 1993). The methods may be mechanical (Pitot tube and Preston tube), thermal (hot wire and hot film), optical (laser-Doppler velocimetry, particle image velocimetry, photochromic, thermochromic), electromagnetic (magnetic resonance imaging), etc. Because of their non-invasive nature, the optically and electromagnetically based techniques are especially attractive but they require the presence of motion tracers in the flow. Some methods (Pitot tube, hot wire and film, laser-Doppler

velocimetry) provide point-measurements of velocity while others (particle image velocimetry and magnetic resonance imaging) provide field views. The spatial resolution of these methods varies, being in the order of a few millimeters for a fine Pitot tube, to tens of microns for a laser-Doppler velocimeter, to a few microns for a hot wire anemometer. The temporal resolution also varies, ranging from as high as 10^{-1} s for a Pitot tube in water to 2×10^{-6} s for a hot wire anemometer in air. Pitot tube and hot wire setups are both inexpensive and portable, whereas laser-Doppler and particle image velocimeters are neither. Because of the bulkiness of the equipment, one major disadvantage common to all these techniques is their inability to perform simultaneous velocity measurements at multiple points on or near the surfaces of bodies of arbitrary shape and orientation immersed in complex flows; and even if this were technically feasible, for any reasonable spatial resolution it would be extremely cumbersome and prohibitively expensive to do.

The motivation is strong, therefore, to develop arrays of artificial hair-like fluid motion-sensors that can be applied to surfaces exposed to fluid motion and from which pertinent flow field information can be derived. Of special interest is that the arrays be inexpensive and easily replaced, and that they should consist of relatively large numbers of rugged sensors. Such arrays could be used, for example, in the laboratory environment to explore the flow structures embedded in the viscous sublayer of a turbulent boundary layer flow, or in the field by an autonomous underwater vehicle tracking the wake of an extraneous object by means of the patterns of velocity information impressed on its hull.

5.2 ENABLING MATERIALS AND FABRICATION TECHNOLOGIES

Because hair-like motion sensor microfabrication technologies are so closely intertwined with the materials used they are discussed together. The construction of a flow measurement device consisting of an organized arrangement of artificial hair-like motion sensors has to overcome three challenges (Humphrey *et al.*, 2003): (i) fabricating an array of mechanical structures analogous to filiform hairs that will respond to the local fluid motion; (ii) implementing an appropriate transduction mechanism that will encode the mechanical motion of each sensor into a useful electrical signal; (iii) interfacing the signals from a large number of sensors to a logic processing unit by means of appropriate circuitry. Microfabrication processes employ lithographic pattern transfer tools and techniques especially well suited to the two-dimensional world of microelectronic circuits and devices having element heights out of the substrate plane of only a few microns (Meixner, 2003). In contrast, the fabrication of a hair-like microsensor array requires setting up individual, electrically wired, post-like structures of diameter 5–20 μm and length normal to the substrate

plane 100–2500 μm. The archetypal microfabrication materials are relatively stiff, consisting of silicon, silicon oxide (SiO_2), and some metals and glasses. Recently, however, plastics and soft elastomer materials such as Polydimethylsiloxane (PDMS) and polyurethane have been used. Possible mechanical-to-electrical sensor transduction technologies include piezoelectric thin films, porous membranes (in which stress modulates ionic conductivity), capacitors with moving electrodes, tunnelling current devices (in which mechanical deflection exponentially controls tip current), and micromirror devices (in which a probing light beam is deflected by induced strain). The integration of any of these with a hair-like sensor requires sensitive, low-noise, signal detection electronics, and each sensor in an array must be wired electrically to either a local or a centralized logic processing unit.

Significant strides have been made in the development and microfabrication of artificial hair-like motion sensor arrays. Using the cercal hairs of the cricket as their biological model, Dijkstra *et al.* (2005) and Krijnen *et al.* (2006) have applied MEMS technology to fabricate arrays of hairs up to 1000 μm in length made from SU-8, an epoxy-based polymer (Fig. 27a). The hairs are supported by Si_xN_y membranes of two designs leading to different stiffness and, therefore, different performance characteristics. The membranes have translational and rotational degrees of freedom normal to the substrate, and the movements of the hairs are detected capacitively via pairs of electrodes built onto the undersurfaces of their displaceable membranes and the facing substrate. A loudspeaker–tube combination is used to stimulate the sensor array in the ranges

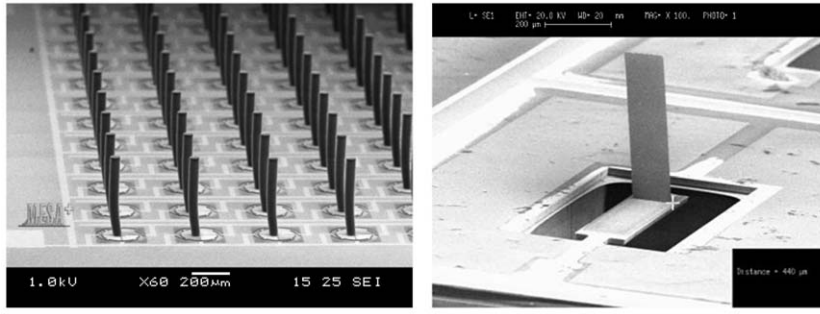

FIG. 27 Examples of bioinspired artificial motion sensing hairs: (a) Array of SU-8 epoxy-based polymer hairs 470 μm long supported by Si_xN_y membranes (Dijkstra *et al.*, 2005 and Krijnen *et al.*, 2006). (b) Single hair-like sensor consisting of a horizontal cantilever silicon beam with a vertical parallelepiped-shaped gold post with electroplated Permalloy attached to its free end. Cantilever length, width, and thickness are 1100, 180, and 17 μm, and post length (height), width, and thickness are 820, 100, and 10 μm (Fan *et al.*, 2002).

0.1–1.0 m s^{-1} and 20–100 Hz, approximately. Although these sensors are not as sensitive as cricket filiform hairs, measurements of capacitance versus voltage, frequency dependence, and directional sensitivity demonstrate their viability.

Using the neuromasts of the lateral line of fish as their model, Fan *et al.* (2002) have also applied MEMS technology followed by Plastic Deformation Magnetic Assembly (PDMA) to fabricate individual hair-like motion sensors capable of operating in water (Fig. 27b). The finished sensor unit consists of a horizontal cantilever beam made of silicon with doped piezoresistor at the base. Attached to the free end of the cantilever is a vertical parallelepiped-shaped post made of gold with electroplated Permalloy that is assembled using the PDMA technique. The length, width, and thickness of the cantilever beam are 1100, 180, and 17 μm, respectively. The length (height), width, and thickness of the post are 820, 100, and 10 μm, respectively. The entire unit is coated with a 300 nm thick Parylene film to provide the necessary electrical insulation for operating in water. Fluid forces acting on the two (length × width) surfaces of the post create a moment that bends the cantilever beam, and the deflection of the beam is detected by means of piezoresistive strain gauges located at its base. The strain gauges are integrated with the cantilever beam as part of the microfabrication process. Tests with a sensor mounted on a flat plate in laminar flow show that it can detect velocities ranging from 0.2 m s^{-1} to 0.9 m s^{-1}, approximately.

In a variation of the above microfabrication approach, Chen *et al.* (2007) replaced the motion-sensitive Permalloy post of rectangular cross-section with one of circular cross-section made of SU-8 epoxy polymer. The SU-8 post is of length 500 μm and diameter 80 μm. They also modified the construction of the cantilever beam to consist of two, parallel, narrow beams of length, width, and thickness equal to 100, 20, and 2 μm, respectively. The SU-8 post rests on a paddle-like extension of the beam that is 100 μm × 100 μm. Otherwise, the unit was similar in terms of its working principles to that described in Fan *et al.* (2002). The sensor was tested in air and water flows and showed significantly improved performance characteristics relative to the sensor of Fan *et al.* (2002). For steady flow in water (0–0.4 m s^{-1}) it yielded ~ 2.5 V m^{-1} s, and for steady flow in air (0–20 m s^{-1}) it yielded 0.06 V m^{-1} s. Additional tests performed using a sphere oscillating at 40 Hz in water yielded a sensitivity of about 1.6 mV mm^{-1} s. The sensor had strong directional sensitivity with an off-axis rejection ratio of approximately 17.5:1.

Similarly, inspired by biological medium motion sensors, Barbier *et al.* (2007) have fabricated and tested an array of hybrid-like sensors that embody favourable features taken from spider trichobothria (flexible membrane structure that supports the hair) and seal vibrissae (longer hair length). A picture of their 2 × 2 sensor array is shown in Fig. 28a, and a

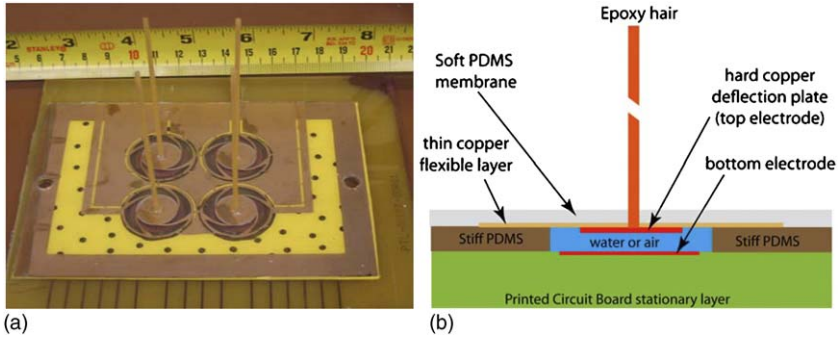

FIG. 28 Example of a bioinspired artificial motion sensing array of hybrid hairs: (a) 2×2 array of epoxy hairs, of length 65 mm and diameter 2 mm, embedded in a thin PDMS layer and bonded to a hard copper deflection plate. (b) Schematic of a single hybrid sensor showing the PDMS film holding the hard copper plate and its associated thin, flexible copper layer leads. (Barbier *et al.*, 2007).

schematic diagram of a single sensor is shown in Fig. 28b. Each sensor consists of an epoxy 'hair' embedded in a layer of PDMS(Dow Corning Silastic type M). The bottom stationary layer of each sensor consists of a printed circuit board with a 2×2 array of circular electrode plates divided into quadrants. Each quadrant is brought to a solder pad where wire leads are attached. A rigid substrate made of stiff PDMS with capacitor wells about 500 μm deep is added to allow an air or water gap between the top and bottom electrodes. The top electrode is composed of a hard copper plate of thickness 0.003 inches and a thin copper layer etched from 0.0005-inch thick copper foil to allow freedom of movement without damaging the copper conductor. The thin copper layer is embedded in a thin PDMS flexible membrane. A spiral pattern is used with four curved spokes to make electrical connection to the deflection plate while offering minimized resistance to movement. The hairs are fabricated by molding sections of 1.8 mm steel rod in PDMS. These are then cast using a two part epoxy (BJB Enterprises, TC-1614). The strength and density of this material works well for the design intent and it has the advantage of allowing hot bending after the sensor is complete. In this way, a variety of different hair shapes can be tested using the same array. The hairs are approximately 6.5 cm long and are bonded to the hard copper deflection plate.

Because of concerns that PDMS is water-permeable, the copper is insulated from water contact by means of an acrylic material made to conformal coat electronics from water and chemicals to seal the copper (Resinlab AR1018). The PDMS is then only used for mechanical suspension of the parts, and not for electrical insulation. With the copper insulated, the gap between the plates can be flooded with water through a pinhole in the PDMS membrane. This is desirable for operation in water as

it allows for a larger dielectric constant between the plates while avoiding sealed air pockets that would compress differently at different depths in a water-medium application.

Due to the rigid connection between each epoxy hair and its copper deflection plate, a deflection of a hair induces a deflection of its top electrode, which induces a change of capacitances in the sensor. All the capacitances of the sensors (4 per sensor) are measured using an electronic circuit with a current-to-voltage converter, the voltage being linearly related to the capacitance. Data acquisition is performed using a computer with a PCI card from National Instrument (NI PCI-6221).

One of the four hairs was selected for sensitivity characterization as a function of angular displacement. Experimental measurements of the torsional restoring constant and damping constant for this hair yielded $S = 2 \times 10^{-3}$ N m rad^{-1} ($\pm 9.4 \times 10^{-4}$ N m rad^{-1}), and $R = 1.8 \times 10^{-5}$ N m s rad^{-1}, approximately. In these experiments, the hair tip was deflected with a precision translation stage to find a non-linear response consisting, primarily, of two well-defined regimes corresponding to 2.9 mV/° for deflection angles ranging from 0° to 5°, and 52 mV/° for deflection angles ranging from 5° to 7°. While the dynamical performance characteristics of this sensor array were not determined, qualitative tests showed it could easily track the edge of the shear layer of a turbulent jet many diameters downstream from the nozzle.

5.3 SOME PRACTICAL CONSIDERATIONS

The earlier examples of bio-inspired fluid motion sensors are quite different from their respective biological models. The three most noteworthy differences are (i) the inorganic (versus organic) nature of the artificial sensor materials; (ii) the dry (versus wet, meaning electro-chemical) mechanical-to-electrical transduction of the artificial sensor stimulus signal; (iii) the relatively large (versus small) surface area occupied by the artificial sensors because of the electrical connections required. The artificial sensors also differ fundamentally from the biological in the way they are constructed. In the engineering world 'assembly', here taken to be the equivalent of 'growth' in biology, is still very much outside → in, whereas in the biological it is entirely inside → out guided by instructions at the molecular level. Thus, the engineering fabrication approach is in stark contrast with the biological which virtually offers a molecular-scale degree of refined assembly. Such refinement allows the creation of highly diverse organic materials assembled in intricate ways for the complex structural and neurobiological processes they are intended to serve. A fundamental engineering breakthrough is needed in the area of materials self-assembly at submicron scales to create highly integrated functional hair-like motion sensors and arrays comparable to those found in nature.

In contrast, for purposes of design, many of the considerations presented in this chapter, in particular the PEM approach to modelling flow-sensing hairs, can be applied to the improved design of artificial sensors and their arrays.

While the primary current challenge to success is the fabrication of robust, sensitive, and reliably working motion sensors and arrays, that to follow will be the processing of the large quantities of spatial and temporal information the arrays will provide. Here, mathematical, statistical, and graphical techniques can combine to create images of parameters derived from the array outputs, with conclusions and actuation decisions made in short times based on the patterns of information observed. On this issue biology has the upper hand because of the tremendous capacity of the nervous system to quickly process enormous amounts of information. An engineering solution to this problem may come in the form of the decentralized, autonomous, peripheral processing of information by interconnected subarray sensor units (Meixner, 2003). The questions remain concerning how many sensors to use and where to place them on a particular surface to achieve a measurement objective. If, for example, the surface corresponds to the hull of an autonomous underwater vehicle or the limbs of a terrestrial robot, and the purpose is for these units to follow another one in relative motion, how many sensors should be used and where should they be located? Again, biology may well provide valuable clues through what is known or can be learned concerning, for example, the number and distribution of filiform hairs on insects, arachnids, and crustaceans. But another major problem must also be solved, since there is no purpose for a robot to only sense motion. The robot also needs to generate instructions directed at actuators that will work to provide it with the correct 'behavioural' response to the stimulus detected.

In applications involving artificial fluid medium motion sensors practical problems arise due to sensor degradation through mechanical wear, debris or particulate contamination and, in water especially, the corrosion of sensor components and/or biofouling. The mechanical wear problem may be offset by implementing sensor redundancy, but the other problems are not so readily controlled in the field and require in-depth research.

Notation (dimensions in SI units)

d	diameter of a hair (m)
D	diameter of the substrate (leg or cercus) supporting a hair (m)
f	frequency of oscillating fluid medium ($f = \omega/2\pi$; Hz)
$f_{\mathrm{res}(\theta)}$	maximum angular displacement resonance frequency of a hair ($f_{\mathrm{res}(\theta)} = \omega_{\mathrm{res}(\theta)}/2\pi$; Hz)

$f_{(d\dot{\theta}/d\omega)\,\max}$	value of frequency that maximizes the slope of $d\dot{\theta}/d\omega$ for a hair (Hz)
F	total force per unit length acting on a hair (Eq. (5); $\mathrm{N\,m^{-1}}$)
F_{D}	empirically determined viscous drag force per unit length acting on a cylinder (Eq. B5; $\mathrm{N\,m^{-1}}$)
F_{AM}	added mass force per unit length acting on a cylinder (Eq. B6; $\mathrm{N\,m^{-1}}$)
$F(\mu, V_{\mathrm{r}})$	force per unit length acting on a hair associated with μ and V_{r} (Eq. 6a, $\mathrm{N\,m^{-1}}$)
$F(\mu, \dot{V}_{\mathrm{r}})$	force per unit length acting on a hair associated with μ and $\dot{V}_{\mathrm{r}}$ (Eq. 6b; $\mathrm{N\,m^{-1}}$)
$F(\rho, \dot{V}_{\mathrm{r}})$	force per unit length acting on a hair associated with ρ and $\dot{V}_{\mathrm{r}}$ (Eq. 6c; $\mathrm{N\,m^{-1}}$)
g	dimensionless parameter in Stokes' theory (Eq. 8)
$g(t)$	dimensionless ramping function for velocity in a transient flow (Eq. B2)
G	dimensionless parameter in Stokes' theory (Eq. 7)
I	moment of inertia of a hair (Eq. 2; $\mathrm{N\,m\,s^2\,rad^{-1}}$)
I_{t}	total moment of inertia of a hair (Eq. 17; $\mathrm{N\,m\,s^2\,rad^{-1}}$)
I_{μ}	fluid medium contribution to the moment of inertia of a hair associated with μ (Eq. 11; $\mathrm{N\,m\,s^2\,rad^{-1}}$)
I_{ρ}	fluid medium contribution to the moment of inertia of a hair associated with ρ (Eq. 10; $\mathrm{N\,m\,s^2\,rad^{-1}}$)
ℓ_{M}	maximum distance between any two points on a pair of adjacent hairs (m)
ℓ_{v}	characteristic viscous diffusion length scale ($=1/\beta$; m)
L	length of a hair (m)
L^*	dimensionless length of a hair $\left(L^* = (L/\delta)_{\omega_{\mathrm{res}(\theta)}}\right)$
R	damping constant of a hair ($\mathrm{N\,m\,s\,rad^{-1}}$)
R_{t}	total damping constant of a hair (Eq. 18; $\mathrm{N\,m\,s\,rad^{-1}}$)
R_{μ}	fluid medium contribution to the damping constant of a hair associated with μ (Eq. 12; $\mathrm{N\,m\,s\,rad^{-1}}$)
Re	characteristic Reynolds number of a cylindrically shaped hair based on $d/2$ ($Re \equiv \lvert V_{\mathrm{r}}\rvert\,(d/2)/\nu$)
Re_d	characteristic Reynolds number of a cylindrically shaped hair based on d ($Re_d \equiv \lvert V_r\rvert d/\nu$)
$Re_x(t)$	Reynolds number at location x for the flow along a surface with far-field velocity $U_{\mathrm{o}}(t)$ ($Re_x(t) = xU_{\mathrm{o}}(t)/\nu$)
s	dimensionless parameter related to Re in Stokes' theory (Eq. 4), also used to denote the spacing between a pair of hairs
S	torsional restoring constant of a hair ($\mathrm{N\,m\,rad^{-1}}$)
S^*	dimensionless parameter characterizing the sensitivity of a hair to the motion of an oscillating fluid medium (Eq. 27)

Δt_{BL}	time scale associated with the maximum change in thickness of a boundary layer with velocity $U_o(t)$ ($\Delta t_{BL} \approx (\Delta \delta_{BL})^2/\nu$)
T	torque acting on a hair (N m)
T_p	period of a flow oscillation cycle ($T_p = 1/f$; s^{-1})
U_o	far-field amplitude of velocity for a fluid medium oscillating over a flat surface ($m\,s^{-1}$)
$U_o(t)$	far-field velocity consisting of a mean value plus an oscillatory component (Eq. B1, $m\,s^{-1}$)
V_{air}	air medium velocity at the tip of a hair ($m\,s^{-1}$)
V_c	velocity of a cylindrically shaped hair at a distance y along its length ($V_c = y\dot{\theta}$; $m\,s^{-1}$)
$\lvert V_c \rvert$	absolute value of V_c ($m\,s^{-1}$)
V_f	velocity of a fluid approaching a hair at a distance y along its length ($m\,s^{-1}$)
$\dot{V}_f$	acceleration of a fluid approaching a hair at a distance y along its length ($m\,s^{-1}$)
V_{hair}	velocity of the tip of a hair ($m\,s^{-1}$)
V_r	relative velocity of a fluid approaching a hair at a distance y along its length ($V_r = V_f - V_c$; $m\,s^{-1}$)
V_r^*	dimensionless relative air medium velocity at the tip of a hair evaluated at the time corresponding to the maximum value of V_{air} in an oscillation cycle of period T_p ($V_r^* = (V_{air} - V_{hair})_{air\,max}/U_o$; $m\,s^{-1}$)
$\lvert V_r \rvert$	absolute value of V_r ($m\,s^{-1}$)
$\dot{V}_r$	relative acceleration of a fluid approaching a hair at a distance y along its length ($\dot{V}_r = \dot{V}_f - \dot{V}_c$; $m\,s^{-2}$)
x	distance along a surface in a boundary layer flow (m)
y	distance along a hair (m)
β	parameter related to δ ($\beta \equiv (\omega/2\nu)^{1/2} = 4.5/\delta$; m^{-1})
δ	thickness of a boundary layer for a fluid oscillating over a flat surface (Eq. 14; m)
δ_{BL}	thickness of a boundary layer at location x for a fluid flowing along a surface with velocity $U_o(t)$ (Eq. B3; m)
$\Delta \delta_{BL}$	maximum change in the thickness of a boundary layer with velocity $U_o(t)$
ϕ	dimensionless phase difference between V_{air} and V_{hair} evaluated at the time in an oscillation cycle corresponding to the maximum values of V_{air} and V_{hair} $\left(\phi = (t_{air}^{max} - t_{hair}^{max})/T_p\right)$
$\Delta\Phi$	phase difference between hair displacement and medium velocity (Eq. 24; rad)
κ_1	dimensionless coefficient characterizing the viscous coupling of one hair of a pair (Eq. 25)
μ	dynamic viscosity of fluid medium ($kg\,m^{-1}\,s^{-1}$)

ν	kinematic viscosity of fluid medium ($\nu \equiv \mu/\rho$; $m^2\,s^{-1}$)
θ	angular displacement of a hair (rad)
θ_{max}	maximum angular displacement of a hair (Eq. (21a); rad)
$\dot{\theta}$	angular velocity of a hair ($rad\,s^{-1}$)
$\dot{\theta}_{max}$	maximum angular velocity of a hair (Eq. (21b); $rad\,s^{-1}$)
$\ddot{\theta}$	angular acceleration of a hair ($rad\,s^{-2}$)
$\ddot{\theta}_{max}$	maximum angular acceleration of a hair (Eq. (21c); $rad\,s^{-2}$)
θ_{res}	maximum angular displacement at resonance frequency $\omega_{res(\theta)}$ of a hair (Eq. 22a; $rad\,s^{-1}$)
$\dot{\theta}_{res}$	maximum angular acceleration at resonance frequency $\omega_{res(\dot{\theta})}$ of a hair (Eq. 22b; $rad\,s^{-1}$)
θ_1	maximum angular displacement of a hair with viscous coupling (rad)
$\theta_{1(ref)}$	maximum angular displacement of a hair without viscous coupling (rad)
Θ_{res}	ratio of the maximum angular displacements at resonance frequency of a water-hair operating in air and an air-hair operating in air (Eq. 28a)
$\Omega_{res(\theta)}$	ratio of the maximum angular displacement resonance frequencies of a water-hair operating in air and an air-hair operating in air (Eq. 28b)
ρ	density of fluid medium ($kg\,m^{-3}$)
ρ_h	density of a hair ($kg\,m^{-3}$
τ	characteristic time (Eq. B2, s)
ω	oscillation frequency of medium flow ($\omega = 2\pi f$; $rad\,s^{-1}$)
$\omega_{res(\theta)}$	maximum angular displacement resonance frequency of a hair (Eq. 23a; $rad\,s^{-1}$)
$\omega_{res(\dot{\theta})}$	maximum angular velocity resonance frequency of a hair (Eq. 23b; $rad\,s^{-1}$)

Acknowledgements

The authors jointly acknowledge the financial support provided by DARPA BioSenSE AFOSR Grant # FA9550-05-1-0459 during the writing of this chapter. JACH expresses his sincere appreciation to the University of Virginia for a one year sabbatical leave, and to the University of Vienna for a most stimulating Guest Professorship in the Department of Neurobiology and Cognition Research, which allowed him the quality time needed to focus on this work. We thank Dr. Bree Cummins of Montana State University for providing and discussing with us the viscous coupling results for cricket hairs.

References

Anton, S. (1991). Zentrale Projektionen von Mechano- und Chemorezeptoren bei der Jagdspinne *Cupiennius salei* Keys. Dissertation, Universität Wien.

Barbier, C., Humphrey, J. A. C., Paulus, J. and Appleby, M. (2007). Design, fabrication and testing of a bioinspired hybrid hair-like fluid medium motion sensor array. Paper IMECE-2007-43006, *Proceedings of the Symposium on the Fundamentals and Applications of Sensors and Sensing in Engineering and Biology*, International Mechanical Engineering Congress & Exposition of the American Society of Mechanical Engineers, Seattle, Washington, November 12–15, 2007.

Barth, F. G. (2000). How to catch the wind: spider hairs specialized for sensing the movement of air. *Naturwissenschaften* **87**, 51–58.

Barth, F. G. (2002a). Spider senses – technical perfection and biology. Karl von Frisch-Lecture. *Zoology* **105**, 271–285.

Barth, F. G. (2002b). *A Spider's World. Senses and Behavior*. Berlin: Springer.

Barth, F. G. (2004). Spider mechanoreceptors. *Curr. Opin. Neurobiol.* **14**, 415–422.

Barth, F. G. and Dechant, H.-E. (2003). Arthropod cuticular hairs: tactile sensors and the refinement of stimulus transformation. In: *Sensors and Sensing in Biology and Engineering* (eds Barth, F. G., Humphrey, J. A. C. and Secomb, T. W.), pp. 159–171. Wien, New York: Springer..

Barth, F. G. and Höller, A. (1999). Dynamics of arthropod filiform hairs. V. The response of spider trichobothria to natural stimuli. *Phil. Trans. R. Soc. Lond. B* **354**, 183–192.

Barth, F. G., Humphrey, J. A. C. and Secomb, T. W. (2003). *Sensors and Sensing in Biology an Engineering*. Wien, New York: Springer.

Barth, F. G., Humphrey, J. A. C., Wastl, U., Halbritter, J. and Brittinger, W. (1995). Dynamics of arthropod filiform hairs. III. Flow patterns related to air movement detection in a spider (*Cupiennius salei* Keys.). *Phil. Trans. R. Soc. Lond. B* **347**, 397–412.

Barth, F. G., Wastl, U., Humphrey, J. A. C. and Devarakonda, R. (1993). Dynamics of arthropod filiform hairs. II. Mechanical properties of spider trichobothria (*Cupiennius salei* KEYS.). *Phil. Trans. R. Soc. Lond. B* **340**, 445–461.

Bathellier, B., Barth, F. G., Albert, J. T. and Humphrey, J. A. C. (2005). Viscosity-mediated motion coupling between pairs of trichobothria on the leg of the spider *Cupiennius salei*. *J. Comp. Physiol. A* **191**, 733–746.

Beckwith, T. G., Marangoni, R. D. and Lienhard, J. H. (1993). *Mechanical Measurements*. Reading, MAs: Addison-Wesley.

Bleckmann, H. (1994). Reception of hydrodynamic stimuli in aquatic and semiaquatic animals. In: *Progress in Zoology*, Vol. 41, pp. 1–115. Stuttgart: Fischer.

Brittinger, W. (1998). Trichobothrien, Medienströmung und das Verhalten von Jagdspinnen (*Cupiennius salei* , Keys.). Dissertation, Universität Wien, pp. 1–87.

Budelmann, B. U. (1989). Hydrodynamic receptor systems in invertebrates. In: *The Mechanosensory Lateral Line: Neurobiology and Evolution* (eds Coombs, S., Görner, P. and Münz, H.), pp. 607–631. New York: Springer.

Camhi, J. (1984). *Neuroethology: Nerve Cells and the Natural Behavior of Animals*. Sunderland, MA: Sinauer.

Cheer, A. Y. L. and Koehl, M. A. R. (1987). Paddles and rakes: fluid flow through bristled appendages of small organisms. *J. Theor. Biol.* **129**, 17–39.

Chen, N., Tucker, C., Engel, J. M., Yang, Y., Pandya, S. and Liu, C. (2007). Design and characterization of artificial haircell sensor for flow sensing with ultrahigh velocity and angular sensitivity. *J. Microelectromechanic. Syst.* **16**, 999–1014.

Christian, U. H. (1971). Zur Feinstruktur der Trichobothrien der Winkelspinne *Tegenaria derhami* (Scopoli), (Agelenidae, Araneae). *Cytobiology* **4**, 172–185.

Christian, U. H. (1972). Trichobothrien, ein Mechanoreceptor bei Spinnen. Elektronenmikroskopische Befunde bei der Winkelspinne *Tegenaria derhami* (Scopoli), (Agelenidae, Araneae). *Verh. Dtsch. Zool. Ges.* **66**, 31–36.

Cortez, R. (2001). The method of regularized stokeslets. *SIAM J. Sci. Comput.* **23**, 1204–1225.

Cummins, B., Gedeon, T., Klapper, I. and Cortez, R. (2007). Interaction between arthropod filiform hairs in a fluid environment. *J. Theor. Biol.* **247**, 266–280.

Dangles, O., Casas, J. and Coolen, I. (2006b). Textbook cricket goes to the field: the ecological scene of the neuroethological play. *J. Exp. Biol.* **209**, 393–398.

Dangles, O., Magal, C., Pierre, D., Olivier, A. and Casas, J. (2005). Variation in morphology and performance of predator-sensing system in wild cricket populations. *J. Exp. Biol.* **208**, 461–468.

Dangles, O., Pierre, D., Magal, C., Vannier, F. and Casas, J. (2006a). Ontogeny of air-motion sensing in cricket. *J. Exp. Biol.* **209**, 4363–4370.

Dangles, O., Steinmann, T., Pierre, D., Vannier, F. and Casas, J. (2007). Design of cricket's cercal system revealed by air flow velocimetry and spatial analyses of hair positioning. *Arthropod Struct. Dev.* (in press).

Dechant, H.-E., Hößl, B., Rammerstorfer, F. G. and Barth, F. G. (2006). Arthropod mechanoreceptive hairs: modelling the directionality of the joint. *J. Comp. Physiol. A* **192**, 1271–1278.

Dechant, H.-E., Rammerstorfer, F. G. and Barth, F. G. (2001). Arthropod touch reception: stimulus transformation and finite element model of spider tactile hairs. *J. Comp. Physiol. A* **187**, 313–322.; See also errata (2001). **187**, 851.

Denny, M. W. (1993). *Air and water: the biology and physics of life's media*. Princeton, NJ: Princeton University Press.

Den Otter, C. J. (1974). Setiform sensilla and prey detection in the bird-spider *Sericopelma rubronitens* Ausserer (Araneae, Theraphosidae). *Neth. J. Zool.* **24**, 219–235.

Derby, C. D. (1982). Structure and function of cuticular sensilla of the lobster *Homarus americanus*. *J. Crustacean Biol.* **2**, 1–21.

Devarakonda, R., Barth, F. G. and Humphrey, J. A. C. (1996). Dynamics of arthropod filiform hairs. IV. Hair motion in air and water. *Phil. Trans. R. Soc. Lond. B* **351**, 933–946.

Dijkstra, M., van Baar, J. J., Wiegerink, R. J., Lammerink, T. S. J., de Boer, J. H. and Krijnen, G. J. M. (2005). Artificial sensory hairs based on the flow sensitive receptor hairs of crickets. *J. Micromech. Microeng.* **15**, S132–S138.

Douglass, J. K., Wilkens, L., Pantazelou, E. and Moss, F. (1993). Noise enhancement of information transfer in crayfish mechanoreceptors by stochastic resonance. *Nature* **365**, 337–340.

Fan, Z., Chen, J., Zou, J., Bullen, D., Liu, C. and Delcomyn, F. (2002). Design and fabrication of artificial lateral line flow sensors. *J. Micromech. Microeng.* **12**, 655–661.

Fletcher, N. H. (1978). Acoustical response of hair receptors in insects. *J. Comp. Physiol.* **127**, 185–189.

Friedel, T. and Barth, F. G. (1997). Wind-sensitive interneurons in the spider CNS (*Cupiennius salei*). Directional information processing of sensory inputs from trichobothria on the walking legs. *J. Comp. Physiol. A* **180**, 223–233.

Gitter, A. H. and Klinke, R. (1989). Die Energieschwellen von Auge und Ohr in heutiger Sicht. *Naturwissenschaften* **76**, 160–164.

Glenner, H., Thomsen, P. F., Hebsgaard, M. B., Sorensen, M. V. and Willerslev, E. (2006). The origin of insects. *Science* **314**, 1883–1884.

Gnatzy, W. (1996). *Digger Wasp vs. Cricket: Neuroethology of a Predator–Prey Interaction*. Stuttgart: Fischer.

Gnatzy, W. and Schmidt, K. (1971). Die Feinstruktur der Sinneshaare auf den Cerci von *Gryllus bimaculatus* (Saltatoria, Gryllidae). *Z. Zellforsch.* **122**, 190–209.

Gnatzy, W. and Tautz, J. (1980). Ultrastructure and mechanical properties of an insect mechanoreceptor: stimulus-transmitting structures and sensory apparatus of the cercal filiform hairs of *Gryllus*. *Cell Tissue Res.* **213**, 441–463.

Goldstein, R. J. (1983). *Fluid Mechanics Measurements*. Washington: Hemisphere Publishing Corp.

Görner, P. (1965). A proposed transducing mechanism for a multiply-innervated mechanoreceptor (trichobothrium) in spiders. *Cold Spring Harbor Symp. Quant. Biol.* **30**, 69–73.

Görner, P. and Andrews, P. (1969). Trichobothrien, ein Ferntastsinnesorgan bei Webspinnen (Araneen). *Z. vergl. Physiol.* **64**, 301–317.

Henson, B. L. and Wilkens, L. A. (1979). A mathematical model for the motion of mechanoreceptor hairs in fluid environments. *Biophys. J.* **27**, 277–286.

Hoffmann, C. (1967). Bau und Funktion der Trichobothrien von *Euscorpius carpathicus* L. *Z. vergl. Physiol.* **54**, 290–352.

Holman, J. P. (1978). *Experimental Methods for Engineers*. New York: McGraw-Hill.

Holman, J. P. (1997). *Heat Transfer*. New York: McGraw-Hill.

Humphrey, J. A. C., Barth, F. G., Reed, M. and Spak, A. (2003). The physics of arthropod medium-flow sensitive hairs: biological models for artificial sensors. In: *Sensors and Sensing in Biology and Engineering* (eds Barth, F. G., Humphrey, J. A. C. and Secomb, T. W.), pp. 129–144. Wien, New York: Springer.

Humphrey, J. A. C., Barth, F. G. and Voss, K. (2001). The motion-sensing hairs of arthropods: using physics to understand sensory ecology and adaptive evolution. In: *Ecology of Sensing* (eds Barth, F. G. and Schmid, A.), pp. 105–125. Berlin: Springer.

Humphrey, J. A. C., Devarakonda, R., Iglesias, I. and Barth, F. G. (1993). Dynamics of arthropod filiform hairs. I. Mathematical modelling of the hair and air motions. *Phil. Trans. R. Soc. Lond. B* **340**, 423–444; See also Errata (1997). **352**, 1995 and Errata (1998). **353**, 2163.

Humphrey, J. A. C. and Mellon, De. F. (2007). Analytical and numerical investigation of the flow past the lateral antennular flagellum of the crayfish *Procambarus clarkii*. *J. Exp. Biol.* **210**, 2969–2978.

Klopsch, C., Barth, F. G. and Humphrey, J. A. C. (2007). The air flow generated by a flying prey insect around a wandering spider and its motion-sensing hair sensilla. *Proceedings of the 5th International Symposium on Turbulence and Shear Flow Phenomena*, pp. 1023–1028, TU Munich, August 27–29, 2007.

Kreyszig, E. (1988). *Advanced Engineering Mathematics*, 6th edn, pp. 1023–1028, New York: Wiley.

Krijnen, G. J. M., Dijkstra, M., van Baar, J. J., Shankar, S. S., Kuipers, W. J., de Boer, R. J. H., Altpeter, D., Lammerink, T. S. J. and Wiegerink, R. (2006). MEMS based hair flow-sensors as model system for acoustic perception studies. *Nanotechnology* **17**, S84–S89.

Kumagai, T., Shimozawa, T. and Baba, Y. (1998). Mobilities of the cercal wind-receptor hairs of the cricket, *Gryllus bimaculatus*. *J. Comp. Physiol. A* **183**, 7–21.

Landolfa, M. A. and Jacobs, G. A. (1995). Direction sensitivity of the filiform hair population of the cricket cercal system. *J. Comp. Physiol. A* **177**, 759–766.

Levin, J. E. and Miller, J. P. (1996). Broadband neural encoding in the cricket cercal sensory system enhanced by stochastic resonance. *Nature* **380**, 165–168.

Magal, C., Dangles, O., Caparroy, P. and Casas, J. (2006). Hair canopy of cricket sensory system tuned to predator signals. *J. Theor. Biol.* **241**, 459–466.

Mahnert, V. (1976). Etude comparative des trichobothries de pseudoscorpions au microscope électronique à balayage. *CR Séanc Soc. Phys. Hist. Nat.* **11**, 96–99.

Markl, H. and Tautz, J. (1975). The sensitivity of hair receptors in caterpillars of *Barathra brassicae* L. (Lepidoptera, Noctuidae) to particle movement in a sound field. *J. Comp. Physiol.* **99**, 79–87.

Meixner, H. (2003). Sensors and sensing: an engineer's view. In: *Sensors and Sensing in Biology and Engineering* (eds Barth, F. G., Humphrey, J. A. C. and Secomb, T. W.), pp. 17–34. Wien, New York: Springer.

Milne-Thomson, L. M. (1986). *Theoretical Hydrodynamics*, 5th edn (revised). London: McMillan Education Ltd.

Nicklaus, R. (1965). Die Erregung einzelner Fadenhaare von *Periplaneta americana* in Abhängigkeit von der Größe und Richtung der Auslenkung. *Z. vergl. Physiol.* **50**, 331–362.

Panton, R. L. (1996). *Incompressible Flow*. New York: Wiley.

Paydar, S., Doan, C. A. and Jacobs, G. A. (1999). Neural mapping of direction and frequency in the cricket cercal sensory system. *J. Neurosci.* **19**, 1771–1781.

Reißland, A. and Görner, P. (1978). Mechanics of trichobothria in orb-weaving spiders (Agelenidae; Araneae). *J. Comp. Physiol. A.* **123**, 59–69.

Reißland, A. and Görner, P. (1985). Trichobothria. In: *Neurobiology of Arachnids* (ed. Barth, F. G.), pp. 138–161. Berlin: Springer.

Schlichting, H. (1979). *Boundary Layer Theory*. New York: McGraw-Hill.

Shimozawa, T. and Kanou, M. (1984a). Varieties of filiform hairs: range fractionation by sensory afferents and cercal interneurons of a cricket. *J. Comp. Physiol. A* **155**, 485–493.

Shimozawa, T. and Kanou, M. (1984b). The aerodynamics and sensory physiology of range fractionation in the cercal filiform sensilla of the cricket *Gryllus bimaculatus*. *J. Comp. Physiol. A* **155**, 495–505.

Shimozawa, T., Kumagai, T. and Baba, Y. (1998). Structural scaling and functional design of the cercal wind-receptor hairs of a cricket. *J. Comp. Physiol. A* **183**, 171–186.

Shimozawa, T., Murakami, J. and Kumagai, T. (2003). Cricket wind receptors: thermal noise for the highest sensitivity known. In: *Sensors and Sensing in Biology and Engineering* (eds Barth, F. G., Humphrey, J. A. C. and Secomb, T. W.), pp. 145–159. Wien, New York: Springer..

Steinmann, T., Casas, J., Krijnen, G. and Dangles, O. (2006). Air-flow sensitive hairs: boundary layers in oscillatory flows around arthropod appendages. *J. Exp. Biol.* **209**, 4398–4408.

Stokes, G. G. (1851). On the effect of the internal friction of fluids on the motion of pendulums. *Trans. Camb. Phil. Soc.* **9**, 8ff. (Reprinted in: *Mathematical and Physical Papers*, Vol. III, pp. 1–141, Cambridge University Press, 1901.)

Tautz, J. and Markl, H. (1978). Caterpillars detect flying wasps by hairs sensitive to airborne vibration. *Behav. Ecol. Sociobiol.* **4**, 101–110.

Thurm, U. (1982a). Biophysik der Mechanoreception. In: *Biophysik* (eds Hoppe, W., Lohmann, W., Markl, H. and Ziegler, H.), 2nd edn, pp. 691–696. Berlin Heidelberg New York: Springer.

Thurm, U. (1982b). Grundzüge der Transduktionsmechanismen in Sinneszellen. Mechano-elektrische Transduktion. In: *Biophysik* (eds Hoppe, W., Lohmann, W., Markl, H. and Ziegler, H.), pp. 681–696. Berlin: Springer.

Vachon, M. (1973). Étude des caractères utilisées pour classer les familles et les genres de Scorpions (Arachnides). 1. La trichobothriotaxie en arachnologie. Sigles trichobothriaux et types de trichobothriotaxie chez les Scorpions. *Bull. Mus. Hist. Nat. 3 Ser.* **140**, 857–958.

White, F. M. (1991). *Viscous Fluid Flow*. New York: McGraw-Hill.

Wiese, K. (1976). Mechanoreceptors for near-field water displacements in crayfish. *J. Neurophysiol.* **39**, 816–833.

Appendix A Determination of the frequency corresponding to the maximum slope of the maximum angular velocity of an oscillating hair

In this appendix we prove a property revealed by the $\theta_{\max}$ and $\dot{\theta}_{\max}$ plots of oscillating hair motion that bears on the discussion on 'Sensitivity and selectivity' in Section 4.1. This is that for any hair, in air or water, the value of its resonance frequency $f_{\mathrm{res}(\theta)}$ in the plot for $\theta_{\max}$ closely matches the value of frequency that maximizes the slope of the corresponding plot for $\dot{\theta}_{\max}$, a quantity we denote by $f_{(\mathrm{d}\dot{\theta}/\mathrm{d}\omega)\max}$. Thus, with reference to Figs. 18a and b, we show below that the frequency corresponding to the maximum (or steepest) slope of the maximum angular velocity of a hair, $\dot{\theta}_{\max}$, plotted as a function of frequency, is given by $f_{(\mathrm{d}\dot{\theta}/\mathrm{d}\omega)\max} \cong C f_{\mathrm{res}(\theta)}$, where $f_{\mathrm{res}(\theta)}$ is the resonance frequency of the hair and C is a constant of order one. In principle, the exact relation between $f_{(\mathrm{d}\dot{\theta}/\mathrm{d}\omega)\max}$ and $f_{\mathrm{res}(\theta)}$ can be derived from analysis of Eq. (21b), by finding the value of ω ($\equiv 2\pi f$) that yields

$$\frac{\mathrm{d}^2\dot{\theta}_{\max}(\omega)}{\mathrm{d}\omega^2} = 0.$$

However, because this is algebraically involved to do, we pursue a less rigorous but much shorter proof.

We note that in the range $0 \leq f \leq f_{\mathrm{res}(\theta)}$ or, equivalently, $0 \leq \omega \leq \omega_{\mathrm{res}(\theta)}$ the maximum angular displacement of a hair is well approximated by a quadratic function

$$\theta_{\max} = -\frac{\theta_{\mathrm{res}}}{\omega^2_{\mathrm{res}(\theta)}}\omega^2 + \frac{2\theta_{\mathrm{res}}}{\omega_{\mathrm{res}(\theta)}}\omega. \tag{A1}$$

From this it follows that

$$\frac{\mathrm{d}\theta_{\max}}{\mathrm{d}\omega} = -\frac{2\omega\theta_{\mathrm{res}}}{\omega^2_{\mathrm{res}(\theta)}} + \frac{2\theta_{\mathrm{res}}}{\omega_{\mathrm{res}(\theta)}} \tag{A2}$$

and

$$\frac{\mathrm{d}^2\theta_{\max}}{\mathrm{d}\omega^2} = -\frac{2\theta_{\mathrm{res}}}{\omega^2_{\mathrm{res}(\theta)}}. \tag{A3}$$

Substitution of Eq. (21a) into Eq. (21b) yields

$$\dot{\theta}_{\max} = \omega\theta_{\max} \tag{A4}$$

and differentiating this expression twice with respect to ω gives

$$\frac{\mathrm{d}^2\dot{\theta}_{\max}}{\mathrm{d}\omega^2} = \omega\frac{\mathrm{d}^2\theta_{\max}}{\mathrm{d}\omega^2} + 2\frac{\mathrm{d}\theta_{\max}}{\mathrm{d}\omega}. \tag{A5}$$

Substitution of Eqs. (A2) and (A3) into Eq. (A5) and setting the result equal to zero yields an expression for the value of ω corresponding to the steepest slope of $\dot{\theta}_{\max}$. The result is $\omega_{(\mathrm{d}\dot{\theta}/\mathrm{d}\omega)\max} = 2/3\omega_{\mathrm{res}(\theta)}$ or, equivalently,

$$f_{(\mathrm{d}\dot{\theta}/\mathrm{d}\omega)\max} = \frac{2}{3}f_{\mathrm{res}(\theta)}. \tag{A6}$$

Appendix B Filiform hair response to a transient pulsating boundary layer flow[9]

We wish to model the response of a filiform hair to the flow in a pulsating boundary layer accelerating from rest. For purposes of analysis, the medium motion is modelled by the relatively simple function

$$U_{\mathrm{o}}(t) = g(t)[U_1 + U_2(1 + \sin(2\pi ft))] \tag{B1}$$

where

$$g(t) = \frac{2}{1 + \mathrm{e}^{-t/\tau}} - 1 \tag{B2}$$

[9]The authors thank Dr. J. Casas for drawing their attention to the theoretical analysis of Henson and Wilkens (1979) who investigated the same problem for the case of a filiform hair responding to the suddenly imposed motion of a fluid at constant acceleration. Being numerically based, the analysis in this appendix is more general in the form of the forcing function used, Eq. (B1), and in the retention of damping constant, R, and added mass, Eq. (B6), effects on hair motion. In addition, the boundary layer thickness, Eq. (B3), of the present study is a function of time whereas it seems to have been kept constant in the analysis of Henson and Wilkens (1979).

is an exponential function that ramps $U_o(t)$ from zero to its final steady periodic value in a characteristic time of order τ that is determined experimentally. Using the data of Barth *et al.* (1995) for guidance, in the analysis presented below we set $U_1 = 50\,\text{mm s}^{-1}$, $U_2 = 10\,\text{mm s}^{-1}$, $f = 100\,\text{Hz}$, and $\tau = 0.01\,\text{s}$ in Eqs. (B1) and (B2).

We now characterize the pulsating boundary layer that develops from rest around a spider leg of effective diameter $D = 2\,\text{mm}$ for the case of a uniform flow of air approaching the leg in a direction normal to it and with velocity given by Eq. (B1). The flow develops to either side of the front stagnation point on the leg, and we assume that a filiform hair of diameter d and length L projects normal to the leg at one of the two 90° locations circumferentially around it starting from the front stagnation point. The time-varying thickness, δ_{BL}, of the boundary layer is estimated from the relation

$$\frac{\delta_{BL}}{x} = 4.64(Re_x(t))^{-1/2} \tag{B3}$$

where $Re_x(t) = xU_o(t)/\nu$ is the time-dependent Reynolds number of the flow and $x = 2\pi(D/2)/4$ is the arc length around the leg from the front stagnation point to the 90° location of the filiform hair. With δ_{BL} known as a function of time, it is possible to estimate the time-dependent velocity, V_f, of the air approaching a location y along the length of the hair, starting from its base, from the relation

$$V_f = U_o(t)\left(\frac{3}{2}\frac{y}{\delta_{BL}} - \frac{1}{2}\left(\frac{y}{\delta_{BL}}\right)^3\right) \tag{B4}$$

with $y \le \delta_{BL}$.

In a strict sense, Eqs. (B3) and (B4) apply to steady, laminar, boundary layer flows (Holman, 1997). The laminar nature of the flow is not in question since the values of $Re_x(t)$ of biological interest are much smaller than the critical value for transition to turbulence ($\sim 5 \times 10^5$). However, the use of these equations implies that for the flows being considered changes in δ_{BL} and V_f due to the time dependence of $U_o(t)$ occur relatively quickly. The frequency range for which this assumption is reasonable can be estimated by noting that the mechanism accounting for changes in δ_{BL} is the diffusion of streamwise momentum in a direction normal to the boundary layer. It follows that the time scale associated with a maximum change in boundary layer thickness $\Delta\delta_{BL}$ (that is, over half an oscillation) is given by $\Delta t_{BL} \approx (\Delta\delta_{BL})^2/\nu$, approximately. We find from our calculations below that, typically, $\Delta\delta_{BL} \approx 3 \times 10^{-4}\,\text{m}$ from which it follows that $\Delta t_{BL} \approx 4.9 \times 10^{-3}\,\text{s}$. Thus, provided the frequency of the unsteady

component of motion in Eq. (B1) is $f \leq 1/(2\Delta t_{BL})$, ($f \leq 100$ Hz), Eqs. (B3) and (B4) should yield reasonable results.

Using a fourth-order Runge–Kutta technique, Eq. (1) in the main text is solved for the motion of the filiform hair at the 90° location around the spider leg as the result of the velocity V_f imposed along its length as given by Eq. (B4). For this, the moment of inertia I is calculated from Eq. (2) and the torque T from Eq. (3). For illustration purposes we assume an MeD1 *C. salei* hair for which $S = S(L)$ and $R = R(L)$ are given by the correlations in Table 1. The force per unit length, F, in Eq. (3) is the sum of the drag force F_D and a force F_{AM} due to the added mass of air that accelerates with the hair. The quantity F_D is obtained from an empirical correlation for the drag coefficient of a cylinder in crossflow (White, 1991), rewritten here in the form[10]

$$F_D = \frac{1}{2}\rho V_r |V_r| d\left(1.18 + \frac{6.8}{Re_d^{0.89}} + \frac{1.96}{Re_d^{0.50}} - \frac{4 \times 10^{-4} Re_d}{1 + 3.64 \times 10^{-7} Re_d^2}\right) \quad \text{(B5)}$$

which is valid with good accuracy[11] in the range $10^{-6} < Re_d < 2 \times 10^5$. In Eq. (B5) the Reynolds number is defined as $Re_d \equiv |V_r| d/v$, the quantity $V_r = V_f - y\dot{\theta}$ is the relative velocity of the approaching fluid with respect to the hair at a location y along its length, and the vertical bars denote absolute value. The force F_{AM} due to the added mass of accelerating air is given by (Milne-Thomson, 1986)

$$F_{AM} = \pi\left(\frac{d}{2}\right)^2 \rho \dot{V}_r. \quad \text{(B6)}$$

Plots of the calculated results obtained for the conditions set earlier are shown in Fig. 26 and discussed in Section 4.2.2 of the main text.

[10]Note that the last term of Eq. (B5) is misprinted in White (1991). The correct form is given here (White, personal communication).

[11]For a hair with $Re_d < 1$ a more accurate relation for F_D can be obtained from the Oseen solution for the drag force on a cylinder (White, 1991). However, the accuracy of the Oseen solution degrades exponentially for $Re_d \geq 1$ and we wish to retain the capability of calculating the drag-induced motion of a hair for such a condition. Equation (B5) applies with very good accuracy for $Re_d \geq 1$, and agrees to within 12% with the Oseen solution in the range $10^{-6} \leq Re \leq 10^{-2}$ and to within 7% in the range $10^{-2} \leq Re \leq 1$. For the calculation conditions of this appendix, the use of Eq. (B5) overpredicts the hair angular displacement amplitude by less than 15% and the hair angular velocity amplitude by less than 7.5%. In contrast, all temporal features of hair motion are accurately calculated using Eq. (B5).

Smooth Attachment Devices in Insects: Functional Morphology and Biomechanics

Stanislav N. Gorb

Evolutionary Biomaterials Group, Department of Thin Films and Biosystems, Max Planck Institute for Metals Research, Stuttgart, Germany

1 Two functional types of insect attachment pads 82
2 Diversity of smooth attachment devices of insects 83
  2.1 Evolution 83
  2.2 Ultrastructure 86
  2.3 Surface pattern 88
  2.4 Passive and active pads 89
3 Material properties 90
  3.1 Elasticity 90
  3.2 Viscoelasticity 92
  3.3 Spring model 93
4 Adhesive properties 95
  4.1 Adhesion forces measured in different animals 95
  4.2 Basic physical forces contributing to adhesion 95
  4.3 Roughness effects 96
  4.4 Dependence on material stiffness 96
  4.5 Size effects 98
5 Frictional properties 99
6 Fluid 102
  6.1 Chemical composition 102
  6.2 Role in adhesion 102
  6.3 Prevention of aquaplaning 104
7 Functional effects of smooth pads 104
  7.1 Adaptation to fractal surfaces due to hierarchical organisation 104
  7.2 Soft in compression – strong in tension 105
  7.3 Surface pattern: prevention of aquaplaning 106
  7.4 Anisotropy in fibre orientation 106
  7.5 Role of the thin surface layer 106
8 Comparison to other animal groups 107
9 Biomimetic implications 108
  9.1 "Sandwich" adhesives 108
  9.2 Surface pattern of tyres 109
  9.3 Surface wrinkles 109
  9.4 Anisotropy 110

ADVANCES IN INSECT PHYSIOLOGY VOL. 34
ISBN 978-0-12-373714-4
DOI: 10.1016/S0065-2806(07)34002-2

10 Outlook 110
Acknowledgements 110
References 111

Abstract

In this chapter, I summarise the data collected in the literature on structure and mechanics of smooth attachment pads of insects. The ultrastructure, surface pattern, origin of different smooth pads, and their evolution are described. Results of mechanical testing of their material properties (elasticity, viscoelasticity, adhesion, friction) and basic physical forces contributing to adhesion are discussed. The influence of different factors, such as substrate roughness and stiffness of the pad, on contact forces is shown. Chemical composition of pad fluid, which is an important component of an adhesive function, is reviewed. Such structural features of pads, as anisotropic fibre orientation, hierarchical organisation of the fibrous architecture of the pads, and their surface microstructure are discussed in relationship to their mechanical effects. Data from insects are compared to those obtained from representatives of other animal groups, such as Echinodermata, Arachnida, and Mammalia. Finally, biomimetic implications of the results are briefly presented.

1 Two functional types of insect attachment pads

To date, both the morphological and ultrastructural bases of the ability of animals to walk on vertical surfaces and ceilings have been studied in detail in many taxa, including insects (Orthoptera, Thysanoptera, Heteroptera, Auchenorrhyncha, Dermaptera, Strepsiptera, Hymenoptera, Diptera, Coleoptera) (Beutel and Gorb, 2001, 2006; Gorb, 2001; Gorb and Beutel, 2001), arachnids (Homann, 1957; Kesel *et al*., 2003; Gorb *et al*., 2006; Niederegger and Gorb, 2006), tree frogs (Hanna and Barnes, 1990; Ba-Omar *et al*., 2000), and lizards (Hiller, 1968; Autumn *et al*., 2000; Autumn and Peattie, 2002; Gao *et al*., 2005; Huber *et al*., 2005a,b; Autumn, 2006; Rizzo *et al*., 2006). These studies show that during the course of biological evolution, animals have developed two distinctly different types of structures to attach themselves to a variety of substrates: *hairy* (*setose*) *pads* and *smooth pads*.

Hairy pads are covered with *setae* or *acanthae* (Richards and Richards, 1979), fine surface outgrowths, which due to their flexibility can maximise the number of contacts with a wide range of microscopically rough substrate profiles (Fig. 1A, B) and, due to the low bending stiffness of their terminal plates, can even adapt to substrates with roughness on a sub-nanometer scale.

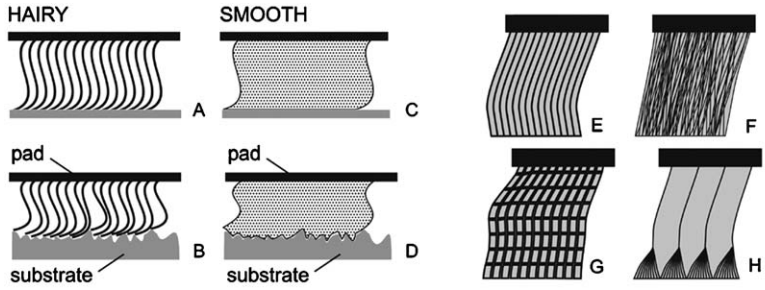

FIG. 1 Hairy and smooth attachment systems. (A–D) Diagram of the action of "hairy" (A, B) and "smooth" (C, D) pad attachment systems on the smooth (A, C), and structured (B, D) substrata (Gorb, 2001). Both systems are able to adapt to the surface profile. (E, F) Diagrams of the inner structure of the surface layer of smooth attachment pads in different animals (Schargott *et al.*, 2006). (E) Generic fibre-like type found in most pads. (F) Thin filamentous type of honeybee (Hymenoptera). (G) Foam-like type found in cicada (Auchenorrhyncha). (H) Hierarchical type found in some grasshoppers (Orthoptera).

Smooth pads can also maximise their contact areas with a variety of substrates due to their specialised material structure and properties (Fig. 1C, D).

In this chapter, I summarise the data collected in the literature on structure and mechanics of smooth attachment pads of insects; describe ultrastructure, surface patterns, origin of different smooth pads and their evolution; discuss the results of mechanical testing of material properties (elasticity, viscoelasticity, adhesion, friction) and basic physical forces contributing to adhesion of smooth pads; show the influence of different factors, such as substrate roughness and pad stiffness, on contact forces; and review the chemical composition of pad fluid, which is an important component of an adhesive function. Also, the structural features of pads, such as anisotropic fibre orientation, hierarchical organisation of the fibrous architecture of the pads, and their surface microstructure are discussed in relation to their mechanical effects. I also compare data obtained from insects to data obtained from representatives of other animal groups, such as Echinodermata, Arachnids, and Mammalia. Finally, the biomimetic implications of the results are briefly presented.

2 Diversity of smooth attachment devices of insects

2.1 EVOLUTION

Both types of attachment pads can be found in different groups of the same animal lineage. For example, within arachnids, representatives of Solifugae

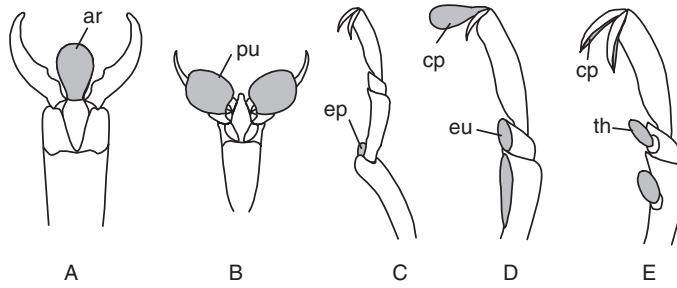

FIG. 2 Diversity of smooth leg attachment devices (grey-coloured areas) in hexapods (Beutel and Gorb, 2001). (A) Arolium, (B) pulvilli, (C) eversible structure between tibia and tarsus (ep), (D) euplantulae (eu) and claw pad (cp), and (E) tarsal thorns transformed into adhesive structures (th), claw pad (cp).

have smooth pads (Kästner, 1941; Cushing *et al.*, 2005), whereas Araneae are characterised by hairy ones (Foelix, 1982). Among reptiles, Gekkonidae and Anolinae have hairy pads, while some skinks possess smooth ones (Williams and Peterson, 1982). Numerous insect groups, such as ephemeropterans, orthopterans, plecopterans, and hymenopterans, rely on smooth pads, whereas others (e.g. dipterans, coleopterans, megalopterans) have developed hairy structures. Interestingly, these highly specialised structures are not restricted to one particular area of the insect leg. For example, they may be located on claws, derivatives of the pretarsus, tarsomeres, or tibia (Fig. 2) (Gorb, 2001). In some cases (Symphyta, Hymenoptera), tarsal spines on the ventral side of the tarsus are transformed into plantae, smooth attachment pads with movable socket-like connection to the tarsus (Schedl, 1991; Beutel and Gorb, 2001; Schulmeister, 2003). Such structural diversity of smooth pads correlates to differences in their origin. Indeed, recent phylogenetic analysis of hexapods based on the pad characters, processed together with characters of other organ systems, aided in resolving the question of attachment pad evolution in hexapods and showed that smooth pads have evolved several times, independently (Gorb and Beutel, 2001; Beutel and Gorb, 2001, 2006). The number of hexapod groups with smooth pads is much higher than those with hairy pads. This fact led us to suggest that smooth systems appeared earlier than hairy ones in insect evolution. A fibrous composite material such as hexapod cuticle (Neville, 1975) was presumably a preadaptation for local development of soft areas of integument, due only to a change in the fibre architecture and density. Such areas were able to form larger contact areas with different substrata, under the same load conditions.

Smooth attachment devices of insects are adaptive structures. Their construction and properties may correlate to the preferred substrata used by a particular species. That is why we do not see any clear evolutionary

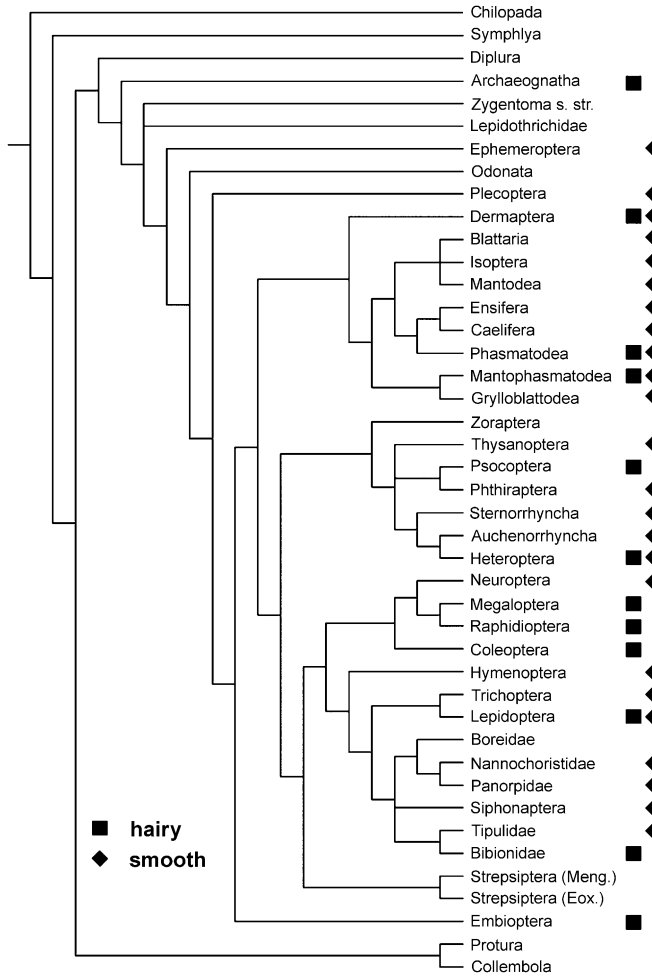

FIG. 3 Strict consensus cladogram of 48 minimal length trees with 180 steps (Beutel and Gorb, 2006). Adhesive pad characters are mapped on cladogram. Note that smooth attachment pads appeared several times independently in the hexapod evolution.

pattern in the distribution of lineages with smooth types of pads (Fig. 3). Smooth arolia and euplantulae have evolved independently in several lineages (Beutel and Gorb, 2001, 2006). It has been previously hypothesised that hexapod attachment pads probably evolved to facilitate walking on plant surfaces (Gorb, 2001; Gorb and Beutel, 2001). During their evolution, plants have not only developed structures attracting pollinators, but also a wide variety of structural and chemical attributes of their

surfaces related to defence against herbivores (Gorb and Gorb, 2002). Plant surfaces have a wide range of textures: they may be smooth, hairy, and covered with waxes or with moist secretions. As with any integument, plant cuticle is a functional organ reflecting response to a variety of environmental pressures. This results in the particular design, ultrastructure, and chemistry of the plant surface. The co-evolution of plant surfaces and pads in some hexapods presumably results from a competition between hexapod attachment systems and plant anti-attachment surfaces.

2.2 ULTRASTRUCTURE

Smooth pads consist of a fibrous material with a specific inner structure. In some orthopterans, tiny filaments are located just under the epicuticle of euplantulae. In *Tettigonia viridissima* (Ensifera), the exocuticle is 45–50 μm thick and consists of primary filaments (Fig. 4A) (Kendall, 1970; Henning, 1974). They are oriented at an angle to the surface. At relatively regular intervals (5–10 μm), cross-links interconnecting fibres are present. In the branching zone, at a depth of 10–22 μm, the primary filaments branch into secondary ones terminating at the epicuticle, a thin superficial layer (0.2–0.3 μm thick). A relatively thick resilin-containing layer (20 μm), fluorescing blue at UV wavelength, approximately corresponds to the layer of secondary rods (Fig. 4D). It has been shown that the filaments can change their shape under loads (Gorb and Scherge, 2000).

The organisation of the pad cuticle in *Locusta migratoria* (Caelifera) is rather different from that of *T. viridissima* (Perez Goodwyn *et al*., 2006). The exocuticle is approximately 60 μm thick, consisting of long, densely packed filaments. The filaments are composed of several fibres bundled together. Between the filaments, numerous interconnecting cross-links are present, so that the material resembles a foam-like structure. The filaments are 2.5–3.5 μm wide, extending through the entire exocuticle. The space between rods is comparable to their width (3–4 μm). The exocuticle can be subdivided into three zones according to its ultrastructural organisation. The deepest zone, starting from the endocuticle, is 35–40 μm thick, and represents the layer of filaments where single filaments are clearly visible. Fluorescent microscopy also reveals the presence of resilin, a rubber-like protein fluorescing blue at UV wavelength (Fig. 4E). The intermediate zone consists of a layer of branching filaments. In the vicinity of the surface, filaments divide into thinner fibre bundles. The branching is observed approximately at a depth of 20–25 μm. This layer shows fluorescence at all three wavelengths (Fig. 4E). The most superficial layer is 2–4 μm thick. Here the filaments are fused together forming a dense layer seen as an electron-dense structure in a transmission electron microscope (TEM) (Schwarz and Gorb, 2003).

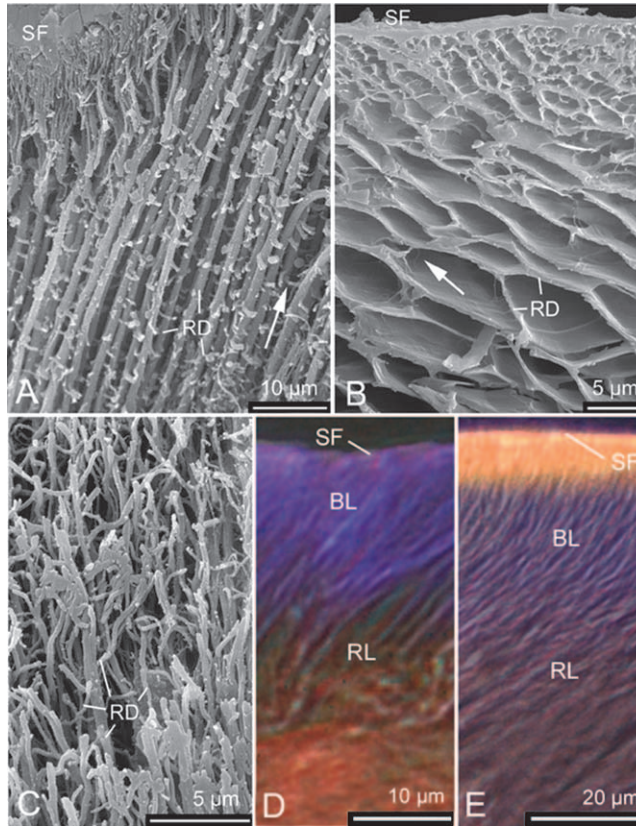

FIG. 4 Material structure of smooth pads. (A, D) *Tettigonia viridissima* (Ensifera), euplantula; (B) *Cercopis vulnerata* (Auchenorrhyncha), arolium; (C) *Apis mellifera* (Hymenoptera), arolium; and (E) *Locusta migratoria* (Caelifera), euplantula. (A–C) Scanning electron microscopy (SEM) (Gorb, 2001). Freezing-fractured, substituted, dehydrated, and critical point dried preparations. (D, E) Fluorescence microscopy (Perez Goodwyn *et al.*, 2006). *Note*: BL, layer of branching rods; SF, superficial layer; RD, rods or filaments; and RL, layer of primary rods.

The arolium of bees contains thinner and longer filaments (Fig. 4C), which may provide even higher flexibility of the material (Federle *et al.*, 2001; Gorb, 2001). Internal architecture of the arolium of cicadas resembles foam, consisting of fluid-filled cells surrounded by flexible cuticle (Scherge and Gorb, 2001) (Fig. 4B). The diameter of the cells increases in deeper layers of the material (integral foam).

Interestingly, because of a comparatively thin epicuticle of euplantulae, the tarsi of both orthopteran species mentioned earlier lose their water content much faster than the tibiae. However, the water-loss rate was

relatively higher for tarsi of *T. viridissima* inhabiting humid areas, compared with *L. migratoria* living in more arid habitats (Perez Goodwyn *et al.*, 2006). Thus, the rate of water loss correlates inversely with the thickness and density of the superficial layer of the attachment pad.

2.3 SURFACE PATTERN

The surface of smooth attachment pads appears smooth in a binocular microscope. In *L. migratoria*, the surface is smooth indeed, when observed in a scanning electron microscope (SEM) (Fig. 5B), with a white light interferometer or even with an atomic force microscope (Perez Goodwyn *et al.*, 2006). However, it may consist of a pattern of hexagonal structures as in representatives of Ensifera (Fig. 5A). The external hexagonal cell-like structures correspond to the pattern of the primary filaments observed in the inner architecture of the pad (Gorb and Scherge, 2000; Scherge and

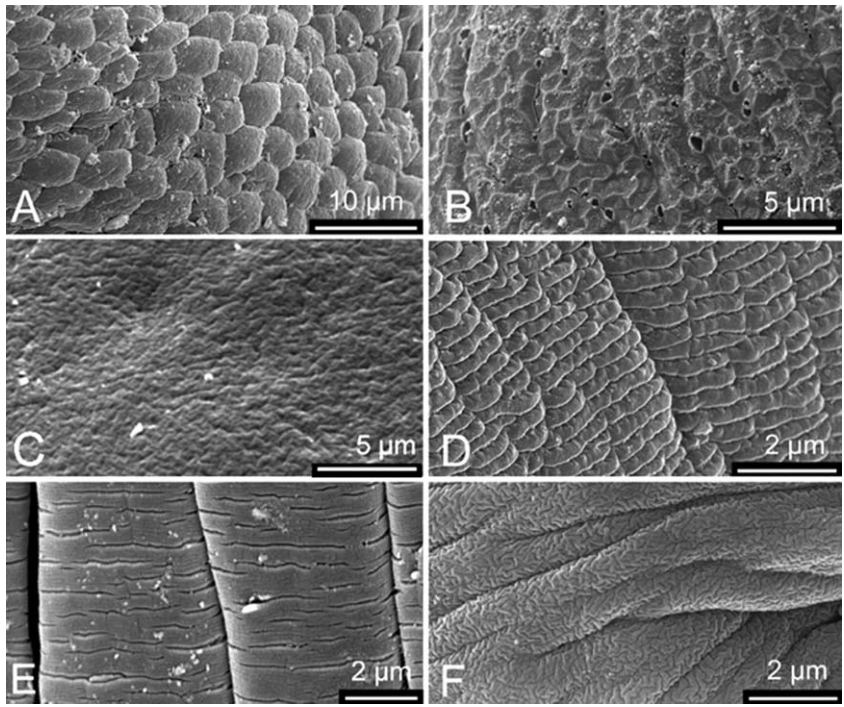

FIG. 5 Surface details of smooth systems of hexapod tarsi. (A) *Tettigonia viridissima* (Ensifera), euplantula; (B) *Apis mellifera* (Hymenoptera), arolium; (C) *Locusta migratoria* (Caelifera), euplantula; (D) *Panorpa communis* (Mecoptera), arolium; (E) *Vespa crabro* (Hymenoptera), arolium; and (F) *Tipula* sp. (Diptera), arolium. (A, B, D–F) Reproduced from Gorb (2001) and (C) from Perez Goodwyn *et al.* (2006).

Gorb, 2001; Perez Goodwyn *et al.*, 2006). The hymenopteran (Fig. 5B) and mecopteran (Fig. 5D, E) arolium may be patterned in lines running perpendicular to the longitudinal axis of the pretarsus. The surface of a tipulid arolium exhibits a complex pattern of microfolds (Fig. 5F) (Gorb, 2001).

2.4 PASSIVE AND ACTIVE PADS

It has been previously shown that the attachment ability of *T. viridissima* euplantulae strongly depends on the load applied by pressing the entire tarsus to the substrate (Jiao *et al.*, 2000). Such an action increases the contact perimeter due to the mechanical deformation of the pad. This seems to be a general principle involved in the function of most smooth attachment pads. The pad surface usually remains exposed to the substrate, and the animal controls the action of the pad only by tarsal movements.

On the other hand, there are smooth pads with rather complex kinematics, such as hymenopteran arolia (Fig. 6). These structures are composed of numerous mobile sclerites and a prestrained bow-like band called the arcus (Snodgrass, 1956). Such a mobile suspension of arolium parts enables unfolding of the arolium, when it contacts the substrate, and folding, when the contact breaks (Federle *et al.*, 2001; Frantsevich and Gorb, 2002, 2004). The spreading movement of the arolium results

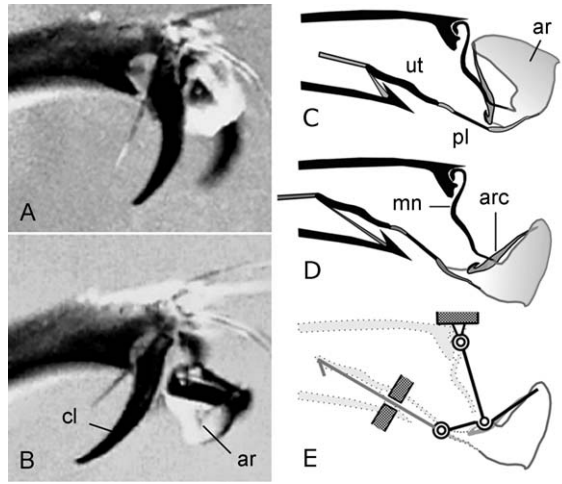

FIG. 6 Kinematics of the arolium in the hornet *Vespa crabro* (Frantsevich and Gorb, 2004). (A, B) Downward turn of the arolium on retraction of the pretarsus, individual video-frames. (C–E) Arolium kinematics. (C, D) Kinematic scheme of the arolium. (D) Diagram of the aroliar articulation. *Note*: ar, arolium; arc, arcus; cl, claws; mn, manubrium; pl, planta; and ut, unguitractor.

automatically from the pull of the claw flexor muscle, and the downward pressure of the tarsus on the base of the pretarsus, when claws fail to grasp the support (Snodgrass, 1956; Frantsevich and Gorb, 2004) (Fig. 6). The proximal pull of the arolium, which has initial contact with the substrate, also results in a complete spreading of the arolium ventral surface over the substrate (Federle *et al.*, 2001). The unfolding is presumably achieved by the action of resilin springs of the pretarsus and by the prestrained arcus.

During locomotion, folding and unfolding of the arolium take place in a very short time (30–40 ms). Action of the arolium during leg detachment was recorded using a high-speed video camera on bees walking on a glass plate under an optical microscope (Baur and Gorb, 2000; Federle *et al.*, 2001). It was revealed that the bee releases its arolium by changing the arolium contact area with the substrate. During this action, the soft part of the arolium is driven by the arcus, lateral parts of which press together. After the reduction of the contact area to 20 per cent of the fully spread condition, the leg jumps from contact. It seems that small hymenopteran insects, such as ants, use a hydraulic control mechanism of the arolium (Federle *et al.*, 2001), whereas large animals mainly rely on the combination of muscle control and action of elastic springs (Frantsevich and Gorb, 2002, 2004).

Arolium mechanics can work as a preflex, passively changing the contact area when carrying loads, as previously shown for some ants (Federle and Endlein, 2004). Hymenopterans and probably other insect groups with a retractable arolium are also able to passively control the contact area.

The presence of an active response has been previously discussed also for pads with less elaborate mechanics, such as grasshopper euplantulae. The presence of air sacks within the euplantula might be a possible structural basis for active control of contact formation. In indentation experiments on pads of living animals, the contact force under load slightly increases after an initial stage of viscoelastic relaxation (Gorb *et al.*, 2000). In contrast, the contact force of the pads of severed legs always decreases during the relaxation process. This difference in response between living and severed legs might be due to the active regulation of internal pressure within the pad. However, this hypothesis requires further experimental evidence.

3 Material properties

3.1 ELASTICITY

The material structure of adhesive pads suggests their high flexibility. To evaluate an effective elasticity module (EEM), microindentation experiments have been applied (Gorb *et al.*, 2000). For characterisation

of inhomogeneous materials (foams, composites, porous materials), the concept of EEM is used instead of elasticity modulus. By estimation of the EEM, it is assumed that the material is solid. The EEM is always lower than the elasticity modulus of the stiffest component of the composite. Since almost all biological materials are composites, the EEM is widely used for evaluation of their mechanical properties.

A typical force-versus-time curve measured on the pad of *T. viridissima* is shown in Fig. 7A. The dependence of indentation depth on the applied

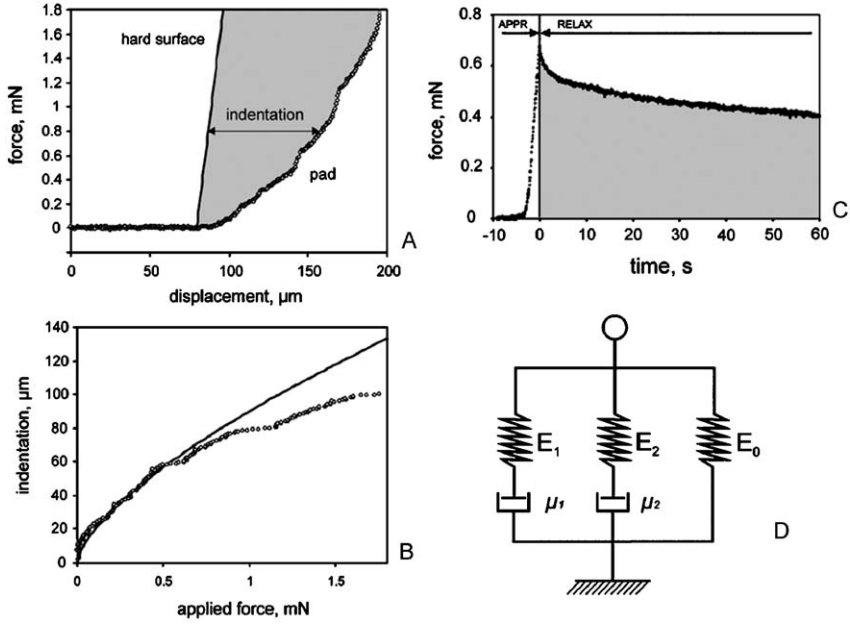

FIG. 7 Elasticity and viscoelasticity of pads in the great green bushcricket *Tettigonia viridissima* (Gorb *et al*., 2000). (A, B) The force–distance curves used for calculation of the elastic modulus of the pad. (A) The indentation (grey-marked section) of the pad obtained from the subtraction of force–distance curves of the pad (dotted line) and hard sample (solid line). (B) The indentation of the pad versus applied force (dotted line). The solid line indicates the indentation data fitted according to the Hertz theory. (C) A typical force curve for evaluation of viscoelastic properties of the pad. It includes two distinct parts: *approaching* (APPR) and *relaxation* (RELAX). In the approaching process, the pad was rapidly approached to the hard silicon surface to obtain an interacting force F (applied force). Generally, it took 46 s to reach an applied force of 0.6–0.7 mN. After that the pad was kept in contact with the silicon surface, the interacting force slowly relaxed (grey-marked section). (D) The Kelvin viscoelastic model applied to the relaxing part of the curve shown in C. It has two sets of dashpot and spring E_1, μ_1, E_2, μ_2, responsible for both rapid and slow relaxation processes. E_0 determines the stress at the equilibrium.

load force was obtained by comparison of the spring deflections caused by the pad, and a hard lower sample (Fig. 7B). Using spherical geometry of an indenter and treating the pad as part of a sphere, the indentation can be modelled by the Hertz theory (Hertz, 1881) (Fig. 7), Johnson–Kendall–Roberts (JKR) theory (Johnson *et al.*, 1971), or by the spring model (Schargott *et al.*, 2006) (see below).

Comparison of effective elasticity moduli (E_{eff}) for pads with different internal structures of the material (see above) reveals that the pads of *L. migratoria* have higher moduli compared to those of *T. viridissima* (Gorb *et al.*, 2000; Perez Goodwyn *et al.*, 2006). The E_{eff} ranges from 30–100 KPa (*T. viridissima*) to 250–500 KPa (*L. migratoria*) reflecting higher density of the pad material in the second species. Interestingly, at the shallower indentation depth (about 30–40 μm), the E_{eff} was considerably higher than at the deeper indentation depth, regardless of the indenter tip used. This effect can be explained by the stronger contribution of relatively stiffer epicuticle at a shallow indentation depth. E_{eff} values obtained in nano-indentation experiments at indentation depths in the range of a few micrometres, support this hypothesis (Perez Goodwyn *et al.*, 2006).

3.2 VISCOELASTICITY

As can be seen above, pad material is far from being solid. It can be defined as a fibrous composite filled with fluid. Additionally, some pads contain air sacs branching from the tracheal trunk (Henning, 1974). Spaces within the tarsus are filled with haemolymph. The air sacs surrounded by the fluid may provide an additional mechanism responsible for the flexibility of the pad material. For smooth systems, the viscoelastic properties of the pad material have been suggested previously (Brainerd, 1994) and recently demonstrated experimentally. Viscoelasticity is the general property of soft natural fibrous composites, such as biopolymer gels, cells, tissues, and muscles (Sanjeevi, 1982; Mak, 1986; Flaud and Quemada, 1988). It was shown that *T. viridissima* pads deform elastically under rapidly applied forces and behave viscoelastically under slowly increasing forces (Gorb *et al.*, 2000) (Fig. 7C). Since pads consist of several different subunits with presumably different viscous properties, two relaxation processes have been observed: the rapid one, and the slow one. That is why when modelling such processes, more than one set of parallel-connected dashpots and springs (Fig. 7D) are needed. Rapid relaxation is attributed to the structure of deeper layers of the cuticle underlying more externally located filaments. Filaments, in their interaction with fluid, are responsible for slow relaxation.

Viscoelasticity of pads leads to an increase of pull off forces. As was previously shown for *T. viridissima* pads, an increase in the time that

a pad remained in contact affects the stronger pull off force measured (Gorb *et al.*, 2000). Attachment forces were also higher in bugs *Coreus marginatus* tested on a centrifuge at higher angular acceleration (Gorb and Gorb, 2004). However, there is an additional function of viscoelasticity in such a dynamic system as the insect leg. When pads demonstrate only elastic properties, one would expect strong elastic energy storage during landing after a jump. In this case, an insect would be accelerated again just after landing, because elastic material would prevent contact to the surface in such a behavioural situation. On the contrary, viscoelastic material serves as a kind of damper in which relaxation response aids in surface replication and optimisation of real contact between pad and substrate. This behaviour should be comparable with the dynamics of viscoelastic polymers (Barquins and Maugis, 1981; Maugis, 1999).

3.3 SPRING MODEL

Experimental data on adhesion of smooth pads have demonstrated a strong dependence of pull off force on the applied force (Jiao *et al.*, 2000; Scherge and Gorb, 2001). The adhesion force increases at relatively low load forces and then reaches a certain level of saturation at higher loads. This effect is connected to the curved geometry of the pad as well as to the fibrillar structure of the material enabling large deformations. The dependence of the attachment force on the applied force might be part of the mechanism enabling control of the attachment and detachment processes. However, the classical JKR contact theory (Johnson *et al.*, 1971) is not able to describe such effects properly, since it considers perfectly elastic contact of two solid spherical bodies at low degrees of deformation. As shown above, pad material is viscoelastic and operates at large deformations.

Recently, it has been shown that the dependence of pad deformation and adhesive force on the applied load can be explained by considering contact between a flat substrate and curved pad surface to be subdivided into an array of elastic springs situated on a rigid supporting material (Fig. 8A) (Schargott *et al.*, 2006). Since pad material consists of discrete fibres, it can be considered as an array of springs able to act independently during contact formation and breakage (Fig. 8B–D). The present model is somewhat simplified in comparison to most real systems, because biological systems possess interconnected fibres, which work independently only at certain degrees of deformation. In spite of this structural feature, the proposed model well describes the load-adhesion behaviour of the smooth adhesive pad of the grasshopper *T. viridissima* (Jiao *et al.*, 2000; Scherge and Gorb, 2001) (Fig. 9B).

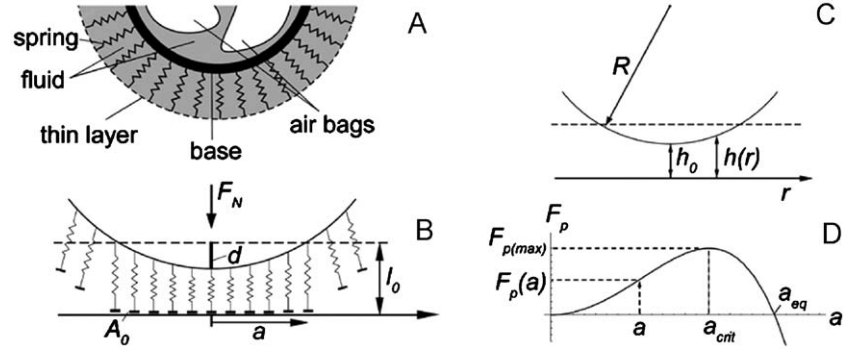

FIG. 8 Spring model of the smooth pad mechanics (Schargott *et al.*, 2006). (A) Diagram of the principal organisation of the bushcricket pad. (B) Elastic springs are used to model the soft flexible layer of the attachment pad. Small contact plates of the area A_0 are considered not to be connected to each other. If the normal force F_N is applied to the pad, the circular contact spot has the contact radius a. (C) Geometry of the spherical pad. (D) Dependence of the pulling force F_p on the contact radius a. *Note*: a_{crit}, critical contact radius at the maximum applied load and a_{eq}, contact radius at the equilibrium.

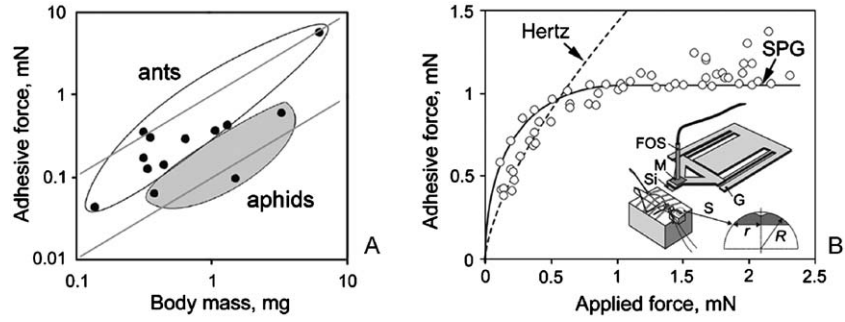

FIG. 9 Adhesion forces. (A) Adhesion forces of smooth pads generated by different insects (according to data of different authors: Lees and Hardie, 1988; Dixon *et al.*, 1990; Federle *et al.*, 2000). (B) Adhesion force measured at different loads in the pad of the great green bushcricket *T. viridissima.* Inset demonstrates experimental setup. The lower sample (S), the pad of a living insect, is fixed to the platform, and the upper sample (Si), a silicon chip, is attached to the spring. Driven by a motor, the platform moves the lower sample to make contact with, and retract from the upper sample. The deflection of the glass spring (G) is monitored by the fibre-optical sensor (FOS) through the mirror (M). Scheme of a cross-section of the pad is outlined by a semi-circle. *Note*: R, radius of pad curvature and r, pad width. Measurements and fit according to Hertz theory (dotted line) (Jiao *et al.*, 2000). Solid line (SPG) demonstrates fit of same data using the spring model (Schargott *et al.*, 2006).

4 Adhesive properties

4.1 ADHESION FORCES MEASURED IN DIFFERENT ANIMALS

Adhesion forces of smooth pads have been measured by a variety of methods ranging from strain gauges to a centrifugal device (Lees and Hardie, 1988; Dixon *et al*., 1990; Federle *et al*., 2000; Gorb and Gorb, 2004). The forces of the whole animals ranged from 0.05 to 10 mN, depending on the species and body mass of the insect (Fig. 9A). The comparison of two groups, such as ants and aphids, clearly shows that ants of the same body mass generate a relatively stronger adhesive force than aphids, which might be due to the different pad size, location, and material properties.

Adhesion forces measured at the level of single pads demonstrate strong dependence of the pull off force of smooth pads on the applied load (Fig. 9B). From the point of view of classical JKR contact theory (Johnson *et al*., 1971), which implies, for elastic material and dry contact, adhesion in spherical contact is not dependent on the applied load. That is why such an experimentally measured effect may be explained by viscoelastic material properties of the pad and presence of fluid in the contact area. Further dynamic measurements at different loading and unloading speeds as well as duration of contact are necessary to prove this argument.

4.2 BASIC PHYSICAL FORCES CONTRIBUTING TO ADHESION

It has been recently shown that hairy attachment devices of the fly *Calliphora vicina* strongly rely on capillary forces mediated by the fluid in the contact area, but intermolecular (van der Waals) forces are also involved in overall adhesion (Langer *et al*., 2004). Previous authors have demonstrated that the bug *Rhodnius prolixus* with pads treated with solvents had poorer attachment performance than non-treated pads (Edwards and Tarkanian, 1970). Aphids *Aphis fabae*, after some period of walking on silica gel, lost their ability to attach to smooth surfaces (Dixon *et al*., 1990). Experiments with a saphire bead in contact with a flat surface covered with footprint fluid of *T. viridissima* demonstrated higher pull off force than that measured on a clean, dry control surface (Jiao *et al*., 2000). These experiments demonstrate the importance of the fluid to the smooth pad adhesion mechanism.

Recent works on the smooth adhesive pads of tree frogs have demonstrated that the fluid layer in contact between the pad and substrate is so thin that molecular contact between two solid bodies might be possible (Federle *et al*., 2006). It is shown that tree frog attachment forces are significantly enhanced by close contact and boundary friction between the

pad epidermis and the substrate, facilitated by the highly regular pad microstructure. That is why the presence of fluid in contact might only be a complementary mechanism for optimisation of contact formation (covering nano-scale roughness), but not necessarily the driving force for strong adhesion due to capillary interaction. Similar arguments may possibly be used in relation to the smooth pads of insects.

4.3 ROUGHNESS EFFECTS

It has been previously demonstrated that insects with different pad structure have trouble attaching to plant surfaces covered by crystalline waxes (Stork, 1980; Eigenbrode and Espelie, 1995; Eigenbrode and Kabalo, 1999; Eigenbrode *et al.*, 2000; Federle *et al.*, 2000). We have proposed four different hypotheses explaining such a reduction in the adhesive ability on specialised surfaces of plants (Gorb and Gorb, 2002). The roughness hypothesis explains this effect by the reduction of the contact area between the pad surface and plant substrate (Gorb *et al.*, 2005). The roughness hypothesis has been recently tested experimentally for hairy attachment devices of beetles and flies (Peressadko and Gorb, 2004).

Our original unpublished data on the effect of substrate roughness on the adhesion of smooth locust pads show different behaviour of smooth pads compared to the behaviour of hairy pads (Fig. 10). Hairy pads show a clear-cut minimum of adhesion at certain ranges of substrate roughness. Such a critical range of roughness depends on the relationship between the diameter of single contact elements of the pad and the length scale of the roughness (Peressadko and Gorb, 2004). Since, in the case of *L. migratoria*, contact is not split up into many subcontacts, the adhesion force did not increase with an increasing substrate roughness after reaching the minimum (Fig. 10). This behaviour is similar to the adhesive behaviour of soft rubber previously experimentally studied by Fuller and Tabor (Kendall, 2001). In the case of the locust, this effect can be explained by the reduced capability of the interconnected fibres to act independently in response to the local substrate roughness.

4.4 DEPENDENCE ON MATERIAL STIFFNESS

As shown above, the higher density of rods and interconnecting filaments are responsible for the higher E_{eff} in the pad of *L. migratoria* in comparison to that of *T. viridissima* (Gorb *et al.*, 2000; Perez Goodwyn *et al.*, 2006). It has been recently demonstrated that a thin highly deformable band would better conform to substrate asperities compared to the bulk material with the same material properties (Persson and Gorb, 2003).

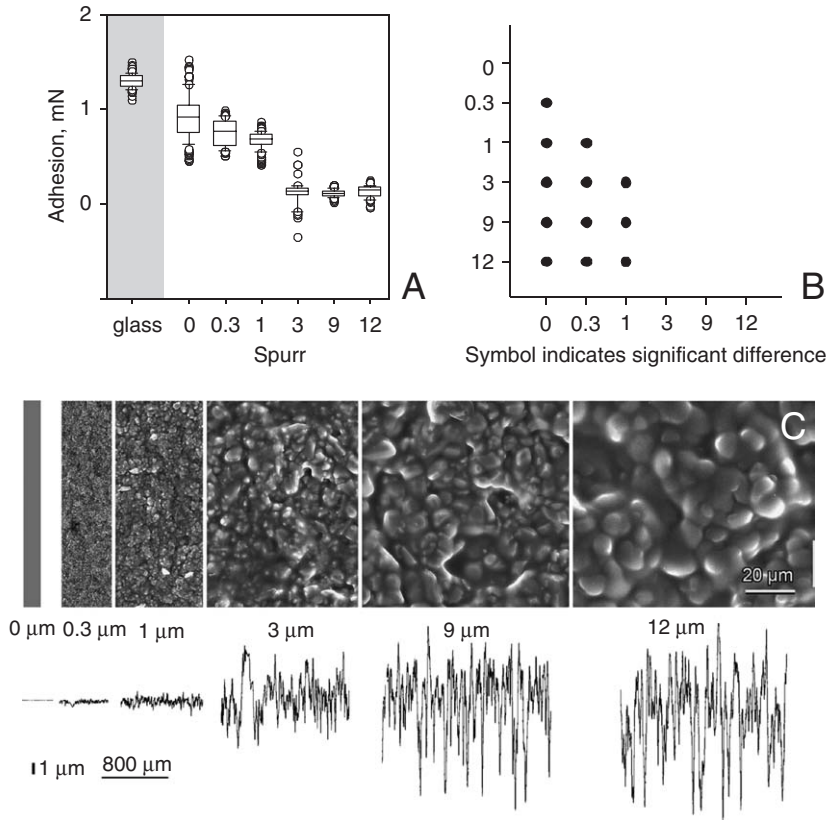

FIG. 10 Adhesion of the euplantula of *Locusta migratoria* on substrata with varied roughness (Gorb, original data). Roughness is dependent on the size of substrate asperities (A) Adhesion data obtained on polymerised epoxy resin surface with different roughness (clean glass was used as a control surface). (B) Comparison of statistical significance of adhesion on different substrata ($H = 566$, df = 6, $P < 0.001$, Kruskal–Wallis ANOVA on Ranks and Dunn's method). (C) SEM micrographs and profiles of substrata used in the experiment.

This is only true, however, as long as the wavelength of the surface roughness is greater than the layer thickness. The thickness of the stiffer surface layer (superficial layer plus branching layer) of *L. migratoria* is about 20 µm. The pad, consisting of a soft core covered by a stiffer layer, combines conformability to the surface unevenness and resistance to the environment. Comparison of these two species, having differences in the ultrastructure of the pad material and its stiffness, clearly demonstrates strong correlation between low stiffness of the material and high adhesive ability (Fig. 11).

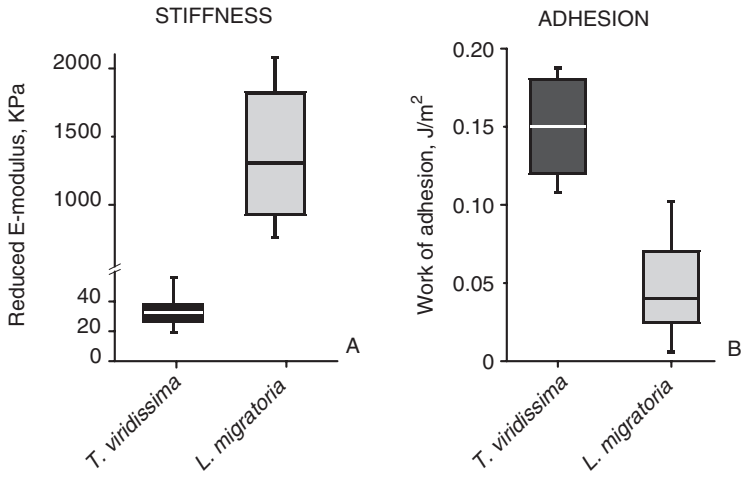

FIG. 11 Material stiffness of the pad and adhesion (Perez Goodwyn *et al*., 2006). (A) Effective elastic modulus (E_{eff}) obtained using a nano-indenter with the tip radius of 250 μm for attachment pads of *Tettigonia viridissima* and *Locusta migratoria*. (B) Work of adhesion calculated from the Johnson–Kendall–Roberts (JKR) model fitting of the unload curve for attachment pads of the same species (indentation with sapphire bead with the radius of 32 μm). The ends of the boxes define the 25th and 75th percentiles, with a line at the median and error bars defining the 10th and 90th percentiles.

4.5 SIZE EFFECTS

Centrifugal force measurements on the bug *C. marginatus* (Fig. 12A–C), having tarsi equipped with smooth pulvilli (Fig. 12D), have demonstrated that attachment properties of pulvilli do not change during ontogenesis (Gorb and Gorb, 2004). Thus, only the growth of pulvilli and, therefore, the increased contact area contribute to the increasing attachment ability in insects at later larval stages (Fig. 12E). In other insect groups with smooth pulvilli, the same scaling relationships have been shown (Lees and Hardie, 1988; Dixon *et al*., 1990; Federle *et al*., 2000; Scherge and Gorb, 2001) (Fig. 9A). Owing to different scaling of the body mass and area of attachment organs, smaller *C. marginatus* bugs attach relatively more strongly (Fig. 12F), which corresponds to the simple physical principle that smaller objects adhere relatively more strongly than larger objects (Kendall, 2001). Interestingly, in a living system, this principle has an important biological significance. Small (juvenile) animals are flightless and stronger attachment ability might be essential for them to stay attached to the host plant (Gorb and Gorb, 2004).

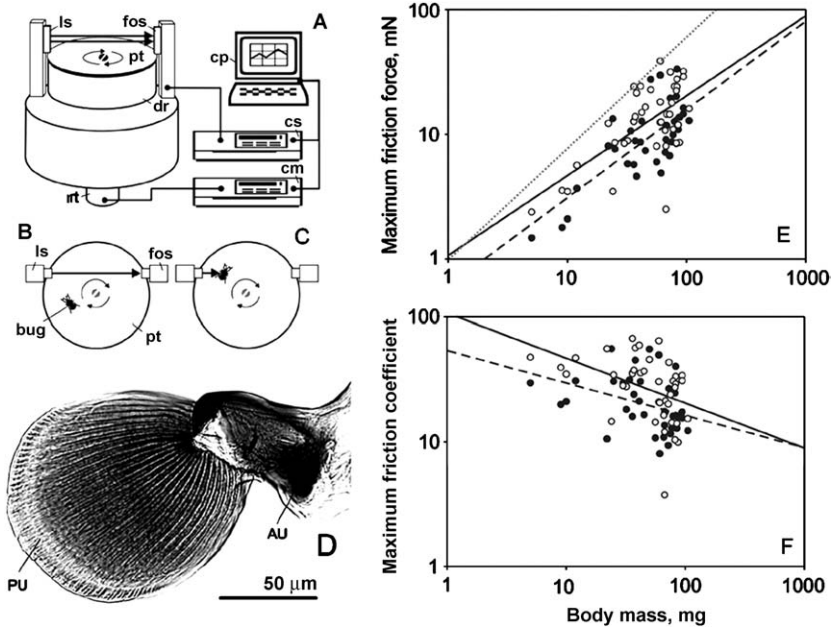

FIG. 12 Size effects on attachment force in the pulvilli of the coreid bug *Coreus marginatus* (Gorb and Gorb, 2004). (A–C) Computer-controlled centrifugal device equipped with a fibre-optical sensor. (A) Scheme of the device. (B, C) Position of the focused light source (ls, sender) and fibre-optical sensor (fos, receiver) relative to the drum centre with an insect rotating on the horizontal drum surface, viewed from above. Abbreviations: cm, motor control; cp, computer; cs, sensor control; dr, drum; pt, plexiglas plate; and rt, rotor of the motor. (D) Single pulvillus, light microscopy, phase contrast. Each tarsus bears two pulvilli (PU) attached to the auxiliar sclerite (AU). (E, F) Dependence of the friction force (E) and frictional coefficient ($\mu = F_{\text{friction}}/F_{\text{normal}}$) (F) on the body mass for individual insects ($N = 40$); average values for individual experimental insects. Data are fitted with a linear regression. Solid lines and open circles, results of experiments at high acceleration ($12.1\,\text{rev}\,\text{s}^{-2}$); broken lines and black circles, results of experiments at low acceleration ($1.21\,\text{rev}\,\text{s}^{-2}$). (E) Maximum friction force; dotted line shows predicted slope for regression line. (F) Maximum frictional coefficient.

5 Frictional properties

Friction forces of pads in ants (Federle *et al.*, 2002) and bugs (Gorb and Gorb, 2004) have been estimated using a centrifugal force tester. From this type of experiment, we know that the frictional component of attachment force in different insects is approximately 5–11 times higher than the adhesive force (Gorb *et al.*, 2002). To gain detailed tribological information about pad material, a tribotester Basalt-01 has been applied (Scherge and Gorb, 2000; Scherge and Gorb, 2001). Friction of the pad

surface was obtained by oscillating the sample over a certain distance along the *x*-axis (distal–proximal), in both directions (Fig. 13A). The friction force of the attachment pads was measured under different loads in euplantulae of living and dead *T. viridissima*. Two series of friction experiments have been carried out: (1) at different normal forces ranging from 50 to 650 μN, at a constant frequency of 0.5 Hz; (2) at

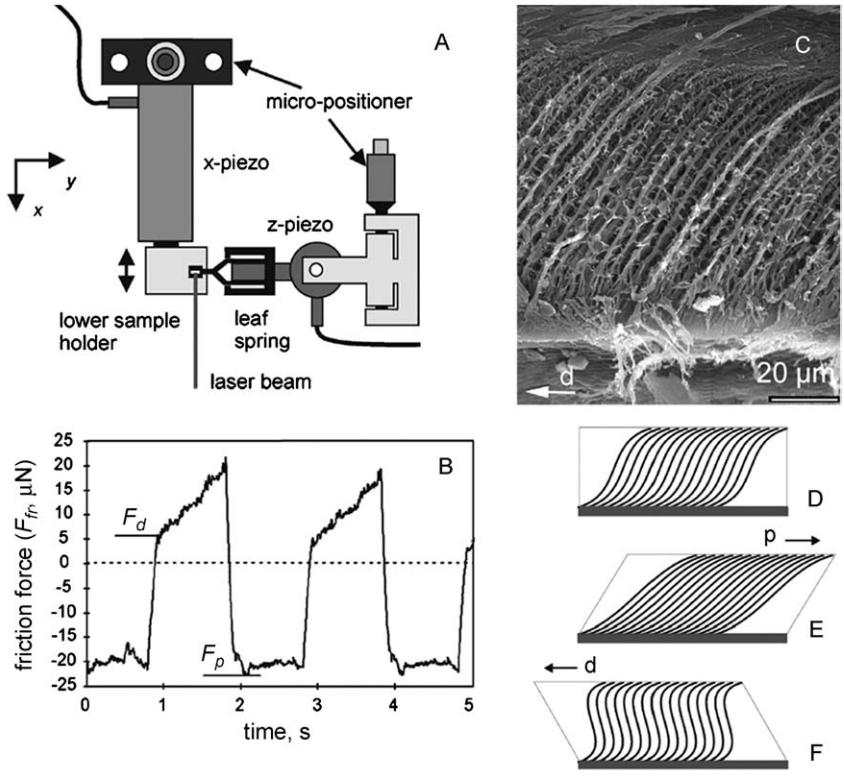

FIG. 13 Friction force measurements on the pad of the great green bushcricket *Tettigonia viridissima* (Gorb and Scherge, 2000). (A) Microforce-tester setup. The oscillatory motion is provided by an x-piezo. The pad is attached to the x-piezo. A silicon plate, attached to a glass spring, served as an upper sample. A laser beam reflected by a mirror, attached to the spring, was used to detect deflection of the spring. In the *z*-direction, a z-piezo is attached to adjust the normal force. (B) Friction behaviour of the pad in different directions. (C) Shock-frozen pad material after substitution and fracture. Note that rods are sloped in the distal direction at an angle of about 45°. (D–F) Hypothetical deformability of initially sloped rods (D) in the proximal direction (E), and in the distal direction (F). *Note*: d, distal direction; p, proximal direction; F_d, friction force to the distal direction of the pad; and F_p, friction force to the proximal direction of the pad.

different frequencies ranging from 0.05 to 2 Hz, at a constant normal force of 87 μN.

The experiments revealed that the static friction during proximal movement was larger and more stable compared to distal movement (Fig. 13B). During distal movement, friction slowly increases. This effect is reflected in the rising part of the curve. The anisotropy increased slightly with an increasing load. The ultrastructural study shows that the inner and outer architecture of pads provide stability and, simultaneously, extreme flexibility. This allows the pad material to adapt to different substrate roughness, unpredictable for mobile insects. Through particular orientation of stiff components in the composite material (Fig. 13C), the material is optimised for maximum friction in one direction (Fig. 13D–F). Another interesting feature of the system is that the differently sized hierarchical filaments of the pad seem to be adapted to different scales of roughness (micro- and meso-scale roughness). The friction behaviour of the pad changes with the velocity (Fig. 14). Minimum friction force occurred at 0.5 Hz (10 μm s^{-1}) and is higher at both slower and faster velocities (Scherge and Gorb, 2001). At low velocity, pad material has presumably enough time to optimise contact with the substrate and increase adhesion which, in this case, positively correlates with friction. At high velocity, the increase of friction may be explained by viscous effects of the fluid sheared in contact between the pad and substrate.

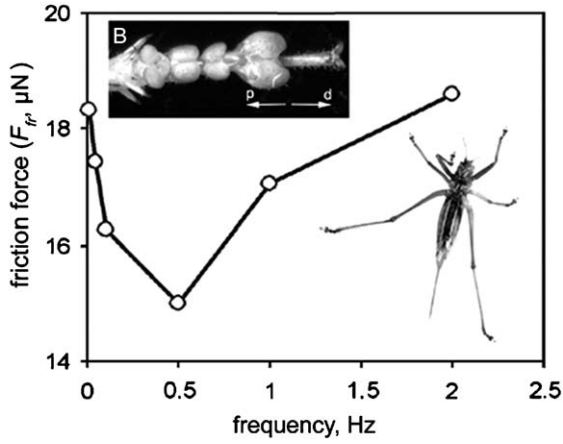

FIG. 14 Velocity effects on the friction force of the pad (B) of the great green bushcricket *Tettigonia viridissima* (A) (Gorb and Scherge, 2000). Friction force is plotted versus frequency of the sliding pad in proximal (p) and distal (d) directions at a normal force of 87 μN.

6 Fluid

6.1 CHEMICAL COMPOSITION

Fluid is well known from the smooth pads of cockroaches (Roth and Willis, 1952), grasshoppers (Jiao *et al*., 2000), aphids (Lees and Hardie, 1988; Dixon *et al*., 1990), and bugs (Hasenfuss, 1977, 1978; Ghasi-Bayat and Hasenfuss, 1980a,b). Footprints can be easily observed with the light microscope, especially under phase contrast. The hairy pad secretion was chemically studied mostly in representatives of Coleoptera. It contains a non-volatile, lipid-like substance that can be observed in footprints stained with Sudan Black. It has been shown that in ladybird beetles (Coccinellidae) pad adhesive secretion consists of hydrocarbons and true waxes (Ishii, 1987; Kosaki and Yamaoka, 1996), which correspond well to the composition of the cuticle coverage. Similar data have been obtained for the chrysomelid beetle *Hemisphaerota cyanea* (Chrysomelidae, Cassidinae) (Attygalle *et al*., 2000).

For smooth insect pads, there has been only one attempt to characterise the chemical composition of the pad secretion in the locust *L. migratoria* with gas chromatography and mass spectrometry (GC-MS) techniques (Vötsch *et al*., 2002). The pad secretion consists of a water-soluble and a lipid-soluble part. Data obtained from shock-freezing, carbon–platinum coating, and replica preparation show that the secretory droplets contain nano-droplets on their surfaces (Fig. 15A, inset). Chemical composition of the pad fluid (Fig. 15A) differs from the cuticle coverage, in particular, with respect to the fatty acid distribution: in the secretion, saturated and unsaturated fatty acids with chain lengths between C16 and C20 in both the free form and as glycerides predominate, whereas cuticle coverage contains waxes of long-chain fatty acids bound to long-chain primary alcohols (Fig. 15B). The second important difference is the significant amount of glucose and other saccharides found in methanolyzates of the pad fluid. A considerable amount of amino acids (up to 53%) was detected in the non-volatile portion of the fluid. These results led authors to suggest that the pad secretion is an emulsion consisting of lipoid nano-droplets dispersed in an aqueous liquid. The chemical composition of the secretion suggests a high viscosity of the fluid.

6.2 ROLE IN ADHESION

The fluid within the pad between the filaments contributes to the viscoelastic behaviour of the pad because the fluid is able to flow through the gaps between the rods when the pad deforms during contact formation and breakage (Gorb *et al*., 2000; Gorb and Scherge, 2000). Fluid, which is pressed out of the pad in the contact area, may serve several functions.

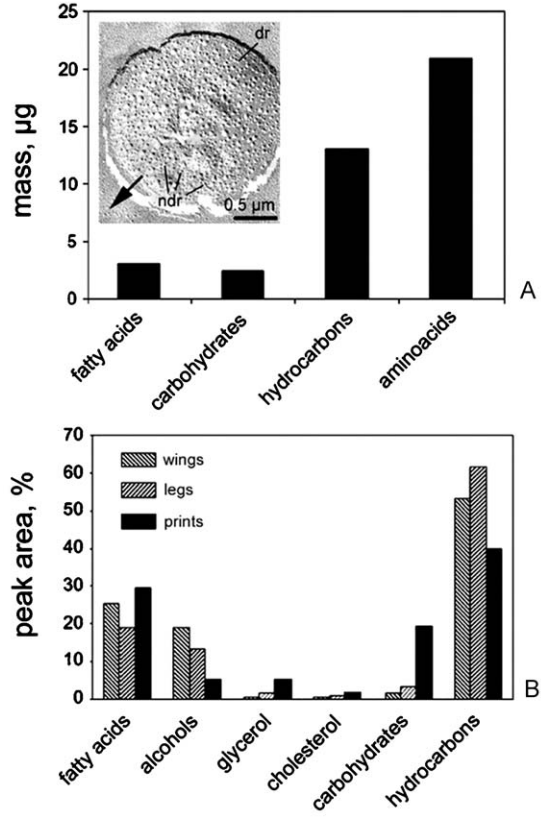

FIG. 15 Chemical composition of the pad secretion of the euplantulae of *Locusta migratoria* (Vötsch *et al.*, 2002). (A) Absolute concentration of substance groups in 5400 prints (290–400 µg) (hydrocarbons, fatty acids, and carbohydrates determined by FID-GC, amino acids by SIM-GC-MS). (B) Relative concentration of substance groups in footprints of euplantulae in comparison to that in control samples (leg and wing surfaces) (determined by FD-GC).

It can enhance the contact initialisation due to the capillary forces, which represent long-range interactions. The capillary forces themselves contribute to pad adhesion. Fluid can also fill nano-scale gaps on the surface and thus improve contact on non-smooth substrata. Since the fluid of smooth pads consists of two phases (water-soluble and lipid-soluble) (Vötsch *et al.*, 2002), it has higher affinity to substrata with various physico-chemical properties (hydrophilic, hydrophobic). In other words, the fluid may be a kind of coupling agent, promoting and strengthening adhesion between otherwise incompatible materials by providing the proximity of contact for intermolecular forces. At relatively high separation or sliding velocities, the contribution of viscous forces to

adhesion and friction will be enhanced due to the presence of a thin fluid layer in the contact area (Scherge and Gorb, 2001).

6.3 PREVENTION OF AQUAPLANING

Capillary adhesion is stronger when the fluid layer in contact is thinner. Patterned surface would aid in keeping the fluid layer as thin as possible under various environmental conditions (different air humidity, rain). Comparative analysis shows that with few exceptions, most surfaces of smooth attachment pads are not absolutely smooth. A most striking hexagonal pattern was found in grasshoppers from the family Tettigoniidae. The pattern strongly resembles that found in tree frogs (Ernst, 1973a,b; Hanna and Barnes, 1990; Ba-Omar *et al.*, 2000). In tree frogs, the regular structure of hexagonal cells results in guiding the fluid in all directions, thus wetting the whole pad in a regular manner and, presumably, optimising the use of the fluid (Ohler, 1995). The elongated cells of *Amolops* frogs guide the fluid in a disto-proximal direction. In this case, the fluid will be directed out of the pad, and the distance from the pad to the substrate will be minimised. In an extreme case, such an action will result in an increase of the pull off force due to the enhancement of van der Waals interactions at the interface between two solid bodies (pad and substrate).

An alternative explanation of the surface structures of smooth pads is contact subdivision. The hexagons of the *T. viridissima* surface can be considered as independent contact elements. Multiplication of the contact elements leads to an increase of an overall perimeter of contact, to the enhancement of the ability for replication of the uneven surface profile, and therefore to the enhancement of adhesion force (considering the JKR equation) (Scherge and Gorb, 2001; Autumn and Peattie, 2002; Arzt *et al.*, 2003; Persson, 2003).

7 Functional effects of smooth pads

7.1 ADAPTATION TO FRACTAL SURFACES DUE TO HIERARCHICAL ORGANISATION

Interconnecting filaments presumably prevent rod buckling, when these are bending during contact. The pad presumably works as a damper during jumping or landing, at high-speed deformation, as well as a means of replicating a complex substratum profile at slow deformation speeds. Also, the rod-like organisation of the pad architecture would allow an independent local load distribution over the area of contact between pad and substrate. This would aid in an enhancement of the adaptation of the pad to imperfections of natural substrata. Presumably, the pad structure of

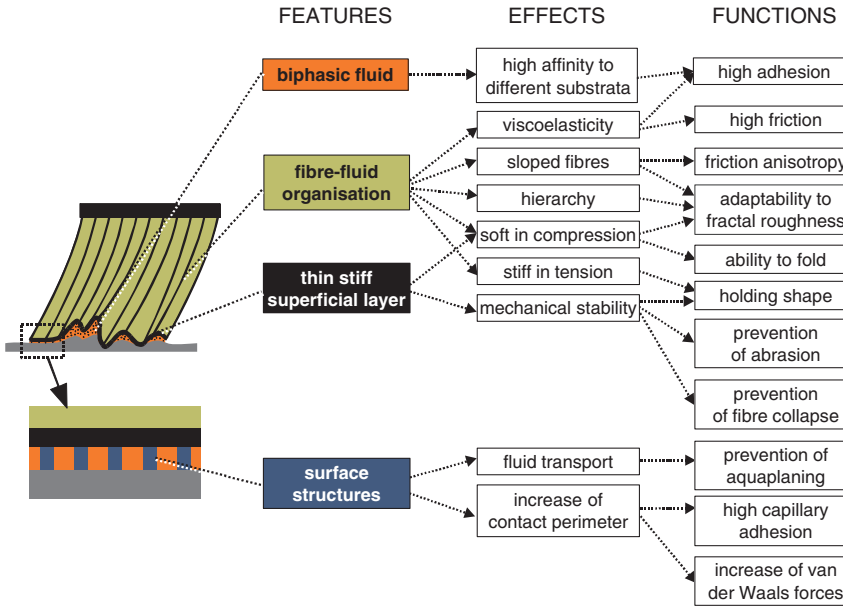

FIG. 16 Structural features of smooth attachment pads responsible for particular functional effects.

L. migratoria works in a similar way to that of *T. viridissima*. The foam-like organisation should have a similar ability to conform to the substrate profile during contact formation (Fig. 16).

This study shows that the same basic architecture of the pads can be tuned in the evolution of species to different needs and constraints. The structural principle, based on branching rods, contributes to holding the shape of the pad. This principle, combined with the presence of a relatively stiff superficial layer, provides the adaptability of the attachment pad to unevenness of natural substrata. In species living in arid environments, the superficial layer must protect animals from desiccation. However, at the same time, the adhesive properties will be reduced because of the reduced ability to form close contact with rough substrata.

7.2 SOFT IN COMPRESSION – STRONG IN TENSION

It is well known that an array of thin fibres is soft in compression, but exceptionally strong in tension (Neville, 1993). This is the key principle of smooth pad architecture (Fig. 16). The specific internal structure of pads is not only responsible for their softness in compression, but also for stiffness in tension. The specific arrangement of thin fibres in the direction of tensile forces, acting on the pad in contact, aids in resisting such forces when an

insect is hanging on the ceiling or wall, or sliding along the substrate. The relatively high tensile strength of a soft material would not otherwise be possible. Actually, fibrillar organisation of smooth pads represents their main functional similarity to hairy pads, which, due to the subdivision in multiple microscopical hairs, have a low effective elastic modulus in compression and have high tensile strength in tension (Jagota and Bennison, 2002; Persson, 2003).

7.3 SURFACE PATTERN: PREVENTION OF AQUAPLANING

Since most smooth pads are indeed not ideally smooth but rather wrinkled or in some cases even patterned at micron or submicron levels, one may assume possible functions of these structures (Fig. 16). Tops of surface patterns in contact with substrate may come very close to the counterpart. In this case, solid–solid interactions between pad material and substrate may occur. Under a certain load, fluid is pressed out of the contact into the gaps between outgrowths. The non-ideal smooth surface of the pad, similar to a tyre profile, prevents aquaplaning and enhances solid–solid interactions, which are important not only for adhesion enhancement due to van der Waals forces, but especially for enhancement of friction. Fluid trapped by gaps might be additionally used in the next step cycle. Prevention of aquaplaning is especially important for walking on wet surfaces in the environment of a rain forest or in temperate areas.

7.4 ANISOTROPY IN FIBRE ORIENTATION

Since fibres are normally oriented not perpendicularly to the pad surface but rather at some angle (45–60°) and sloped into the distal direction, they do not buckle but rather bend under load, which makes pad material much more flexible. Structural anisotropy of the pad material is also responsible for the frictional anisotropy. Friction is higher, while the pad is sliding in a proximal direction, because the fibres can be more easily recruited in this case. Such a mechanism may secure the stable position of an animal on a ceiling. Because shear forces in such a situation are directed proximally, towards the body, and because of stronger friction in this direction, pad sliding can be prevented. The fibre anisotropy may also be involved in the detachment mechanism of the pad.

7.5 ROLE OF THE THIN SURFACE LAYER

An important functional principle of operation in smooth attachment devices is the presence of thin superficial film (epicuticle) covering fibrous material of the pad. The film is responsible for proper contact formation with the substrate due to its low bending stiffness either with or without the

minimum of a normal load (Persson and Gorb, 2003). The film presumably functions in a way similar to the spatulae of geckos, spiders, beetles, and flies. It is able to adapt to the surface profile and to replicate surface irregularities of certain length scales. The range of length scales, to which adaptation is still possible, depends on the stiffness of the film. Previous structural data on the grasshopper *T. viridissima* and locust *L. migratoria* (Perez Goodwyn *et al.*, 2006) let us assume that the latter species has lower adaptability to surface roughness because of much thicker superficial film.

Furthermore, there are several other functions of the superficial film. Since it terminates fibres, which are sometimes of an extreme high aspect ratio, it prevents their lateral collapse (Jagota and Bennison, 2002; Spolenak *et al.*, 2005a,b). That is why, in smooth systems, such high aspect ratio of fibres is possible. They would otherwise condensate with each other and not work as separate springs. The film also delimits the pad as a reservoir filled with fluid and, as such, holds the pad as a stable unit. The superficial film also minimises water loss (Perez Goodwyn *et al.*, 2006) and presumably prevents fragile fibrous material from wearing out during walking. This design, combining fluid and individual fibres, terminated by a thin superficial film, allows extreme local deformations (Gorb *et al.*, 2000). This would be impossible even with rather soft bulk material.

8 Comparison to other animal groups

Representatives of Echinodermata bear tube feet or podia used to adhere under water to various substrata (Feder, 1955; Lavoie, 1956). The podia are external appendages of the hydraulic (ambulacral) system and are driven partly by muscles and partly by hydraulic pressure (Paine, 1929). There are six types of podia: descending, penicillate, knob ending, lamellate, ramified, and digitate (Flammang, 1996). In echinoids and holothuroids, the external connective layer may contain one or several kinds of embedded calcareous needles (spicules) (McKenzie, 1987; Flammang and Jangoux, 1993). Externally, the epidermis is covered by a multi-layered cuticle. The cuticle consists of fibrous and sometimes, granular material. There are 3–5 sublayers, the outermost of which is composed of numerous fibrils. Only the distal parts of the tube feet (knobs, discs, and digitation structures all functionally corresponding to insect pads discussed earlier) are involved in contact formation and attachment. These adhesive organs operate according to mechanical and chemical mechanisms. The mechanics of the extremely soft podial end plates may play an important role in an increase of the contact area (Santos *et al.*, 2005).

Within the amphibians, smooth pads are reported from both tree and torrent frogs. They belong to at least seven different frog families and, like insect adhesive structures, are another excellent example of convergent evolution (Barnes, 2007). Some external (hexagonal pattern) and internal (vertical fibres) features of tree frog pads are very similar to some insect smooth pads discussed earlier. The toe pad epithelium consists of an array of flat-topped cells separated by mucous-filled grooves (Welsch *et al*., 1974; Green, 1979; McAllister and Channing, 1983; Hanna and Barnes, 1990). In many species, the cell surface contains submicron knob-like structures located at the ends of filament bundles (Ernst, 1973a,b). Some species of arboreal salamanders from the genus *Bolitoglossa* bear toe pads with extensive digital webbing (Green and Alberch, 1981). The entire foot functions as a single smooth pad. In most species, the surfaces of the cells are smooth. Only *Bolitoglossa odonelli* possesses a pad surface covered by peg-like structures similar to those of tree frogs.

Smooth adhesive pads are also reported in arboreal possums (Marsupiala), which can climb vertical sheets of glass. A histological analysis of pads in the feather-tailed glider (*Acrobates pygmaeus*) shows that pads, which are present on the digits and ventral surfaces of hands and feet, consist of an epidermal layer of stratified squamous epithelium (Rosenberg and Rose, 1999). The pad material is soft and consists of a pattern of alternating ridges and grooves oriented parallel to the longitudinal axis of the digit. Sweat glands empty into the grooves, providing the fluid for wet adhesion.

Comparison of the material structure in smooth pads of insects with those of other animal groups demonstrates a striking similarity of such features as fibrous organisation, fibre orientation perpendicular or at some angle to the surface, presence of a thin superficial layer, presence of fluid of different chemical composition, extreme low elasticity modulus, and viscoelastic properties. Most of them are related to contact formation with non-smooth substrata and to withstanding high tensile forces while adhering.

9 Biomimetic implications

9.1 "SANDWICH" ADHESIVES

Glassmaker *et al*. (2006) have recently designed the sandwich-like foil consisting of small pillars covered with thin, spin-coated film of the same polymer. This material demonstrates an excellent adhesion (by a factor 2.0–3.5 higher compared to a flat substrate) and high tolerance against crack propagation. There are certain functional parallels between biological smooth pads and artificial material made of continuous film covering tips of numerous filaments (Fig. 17). The described material is dry inside. We believe that the adhesive properties might be additionally

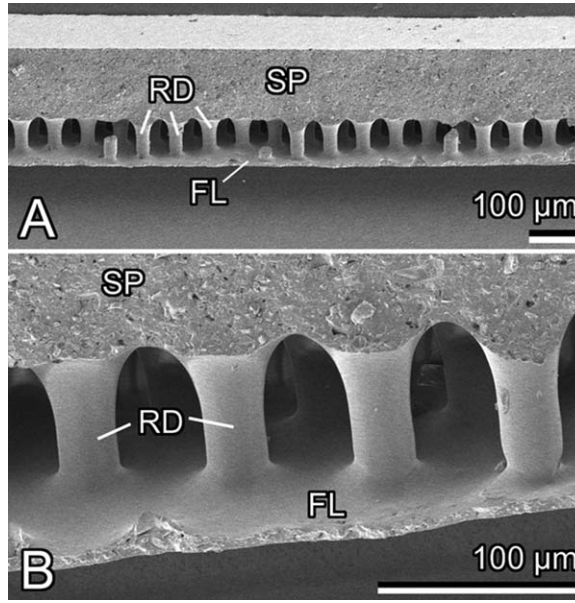

FIG. 17 Cross-section of the sandwich-like adhesive film made of the polymer polyvinylsiloxane (PVS), SEM micrograph. *Note*: FL, thin superficial film; RD, rods; and SP, supporting layer.

improved by filling the space between pillars with viscous fluid (oil, water-based protein gel, sugar solution), which will add a viscous component to the material. Such a design will certainly effect stronger energy dissipation during contact breakage and thus a stronger adhesion.

9.2 SURFACE PATTERN OF TYRES

Recently, the tyre company Continental has developed a winter tyre type with honeycomb profiles similar to those existing on the attachment pads of the grasshopper *T. viridissima* or tree frogs (Barnes, 1999; Barnes *et al.*, 2002). The company promises enhanced wear performance on dry roads, less aquaplaning and better braking on wet roads, substantially improved lateral guidance, better grip, and more traction on ice. The honeycomb spikes provide more gripping edges than conventional spikes, thus considerably improving track holding in curves.

9.3 SURFACE WRINKLES

Chan and Crosby (2007) recently showed that a soft polymer surface patterned with little wrinkles, even with low aspect ratio but high density,

as previously observed in various smooth adhesive pads (Gorb, 2001), can substantially improve adhesion. Such miniature structures on polymer surfaces might be optimised for particular applications according to specific patterns found in pads of insect species differing in their mode of locomotion, weight, environment, etc.

9.4 ANISOTROPY

Smooth materials with anisotropic friction properties similar to those previously described for the pads of *T. viridissima* might find numerous applications, from frictionally active bases for transporting purposes, coverage for robot grippers, and tyres to sporting and consumer goods. "Sandwich" adhesives mentioned earlier might represent a good starting point for further developments. Materials designed in a similar way, but with sloped pillars inside would already be a good proof of the principle.

10 Outlook

In spite of numerous publications on smooth type of attachment devices of insects, there are many questions that still remained unresolved. From our previous results of measurements on material properties in the pads and from knowledge on behaviour of artificial viscoelastic adhesives (Barquins and Maugis, 1981; Maugis, 1999; Kendall, 2001), one may suggest an important role of time effects related to viscoelastic properties of pads in generating strong adhesion, but there is no rigorous proof of this hypothesis. A number of important questions for further studies are related to the pad fluid. Its chemical composition is currently studied only in one species, but we know nothing about fluids from smooth pads which have convergently appeared in other insect lineages. It seems to be obvious that secreted fluid is involved in an enhancement of contact formation on rough surfaces, but this particular role and other possible roles of the fluid (especially on rough substrata) have still to be clarified. Other questions have to be answered by future research: (1) What is the relationship between mechanical properties of the pad and fluid thickness, composition, properties? (2) How do pad structure and mechanics scale with an increasing body size in different insect groups? (3) How strong is wear of pads having different structure and properties on various plant substrata?

Acknowledgements

The author thanks J. Casas (University of Tours, France) and two anonymous reviewers for valuable suggestions, and also S. J. Simpson

(University of Sydney, Australia) for linguistic corrections. This study was supported by the Federal Ministry of Education, Science, and Technology, Germany to SG (project InspiRat 01RI0633D).

References

Arzt, E., Gorb, S. and Spolenak, R. (2003). From micro to nano contacts in biological attachment devices. *Proc. Natl. Acad. Sci. USA* **100**, 10603–10606.

Attygalle, A. B., Aneshansley, D. J., Meinwald, J. and Eisner, T. (2000). Defence by foot adhesion in a chrysomelid beetle (*Hemisphaerota cyanea*): characterization of the adhesive oil. *Zoology* **103**, 1–6.

Autumn, K. (2006). How gecko toes stick. *Am. Sci.* **94**, 124–132.

Autumn, K., Liang, Y. A., Hsieh, S. T., Zesch, W., Chan, W. P., Kenny, T. W., Fearing, R. and Full, R. J. (2000). Adhesive force of a single gecko foot-hair. *Nature* **405**, 681–685.

Autumn, K. and Peattie, A. M. (2002). Mechanisms of adhesion in geckos. *Integr. Comp. Biol.* **42**, 1081–1090.

Ba-Omar, T. A., Downie, J. R. and Barnes, W. J. P. (2000). Development of adhesive toe-pads in the tree-frog (*Phyllomedusa trinitatis*). *J. Zool. Lond.* **250**, 267–282.

Barnes, W. J. P. (1999). Tree frogs and tire technology. *Tire Technol. Int.* (March), 42–47.

Barnes, W. J. P. (2007). Functional morphology and design constraints of smooth adhesive pads. *MRS Bull.* **32**, 479–485.

Barnes, W. J. P., Smith, J., Oines, C. and Mundl, R. (2002). Bionics and wet grip. *Tire Technol. Int.* (December), 56–61.

Barquins, M. and Maugis, D. (1981). Tackiness of elastomers. *J. Adhesion* **13**, 53–65.

Baur, F. and Gorb, S. N. (2000). How the bee releases its leg attachment devices. *Biona Rep.* **15**, 295–297.

Beutel, R. G. and Gorb, S. N. (2001). Ultrastructure of attachment specializations of hexapods (Arthropoda): evolutionary patterns inferred from a revised ordinal phylogeny. *J. Zool. Syst. Evol. Res.* **39**, 177–207.

Beutel, R. G. and Gorb, S. N. (2006). A revised interpretation of the evolution of attachment structures in Hexapoda with special emphasis on Mantophasmatodea. *Arthropod Syst. Phylogeny* **64** (1), 3–25.

Brainerd, E. L. (1994). Adhesion force of ants on smooth surfaces. *Am. Zool.* **34**, 128.

Chan, E. P. and Crosby, A. J. (2007). Wrinkled geckos: controlling polymer adhesion with fabricated surface wrinkles. *Proceedings 30th Annual Meeting of the Adhesion Society*, pp. 320–321, Inc. Tampa, Florida.

Cushing, P. E., Brookhart, J. O., Kleebe, H.-J., Zito, G. and Payne, P. (2005). The suctorial organ of the Solifugae (Aarchnida, Solifugae). *Arthropod Struct. Dev.* **34**, 397–406.

Dixon, A. F. G., Croghan, P. C. and Gowing, R. P. (1990). The mechanism by which aphids adhere to smooth surfaces. *J. Exp. Biol.* **152**, 243–253.

Edwards, J. S. and Tarkanian, M. (1970). The adhesive pads of Heteroptera: a re-examination. *Proc. R. Entomol. Soc. Lond.* **A45** (1–3), 1–5.

Eigenbrode, S. D. and Espelie, K. E. (1995). Effects of plant epicuticular lipids on insect herbivores. *Ann. Rev. Entomol.* **40**, 171–194.

Eigenbrode, S. D. and Kabalo, N. N. (1999). Effects of *Brassica oleracea* waxblooms on predation and attachment by *Hippodomia convergens*. *Entomol. Exp. Appl.* **91**, 125–130.
Eigenbrode, S. D., Rayor, L., Chow, J. and Latty, P. (2000). Effects of wax bloom variation in *Brassica oleracea* on foraging by a vespid wasp. *Entomol. Exp. Appl.* **97**, 161–166.
Ernst, V. V. (1973a). The digital pads of the tree frog, *Hyla cinerea*. I. The epidermis. *Tissue Cell* **5** (1), 83–96.
Ernst, V. V. (1973b). The digital pads of the tree frog, *Hyla cinerea*. II. The mucous glands. *Tissue Cell* **5** (1), 96–104.
Feder, H. M. (1955). On the method used by the starfish *Pisaster ochraceus* in opening three types of bivalve molluscs. *Ecology* **36** (4), 764–767.
Federle, W., Barnes, W. J. P., Baumgartner, W., Drechsler, P. and Smith, J. M. (2006). Wet but not slippery: boundary friction in tree frog adhesive toe pads. *J. R. Soc. Interface* **3**, 689–697.
Federle, W., Brainerd, E. L., McMahon, T. A. and Hölldobler, B. (2001). Biomechanics of the movable pretarsal adhesive organ in ant and bees. *Proc. Natl. Acad. Sci. USA* **98** (11), 6215–6220.
Federle, W. and Endlein, T. (2004). Locomotion and adhesion: dynamic control of adhesive surface contact in ants. *Arthropod Struct. Dev.* **33**, 67–75.
Federle, W., Riehle, M., Curtis, A. S. G. and Full, R. J. (2002). An integrative study of insect adhesion: mechanics and wet adhesion of pretarsal pads in ants. *Integr. Comp. Biol.* **42**, 1100–1106.
Federle, W., Rohrseitz, K. and Hölldobler, B. (2000). Attachment forces of ants measured with a centrifuge: better "wax-runners" have a poorer attachment to a smooth surface. *J. Exp. Biol.* **203**, 505–512.
Flammang, P. (1996). Adhesion in echinoderms. *Echinoderm Stud.* **5**, 1–60.
Flammang, P. and Jangoux, M. (1993). Functional morphology of coronal and peristomeal podia in *Sphaerechinus granularis* (Echinodermata, Echinoida). *Zoomorphology* **113**, 47–60.
Flaud, P. and Quemada, D. (1988). A structural viscoelastic model of soft tissues. *Biorheology* **25**, 95–105.
Foelix, R. (1982). *The Biology of Spiders*. Massachusetts: Harvard University Press.
Frantsevich, L. I. and Gorb, S. N. (2002). Arcus as a tensegrity structure in the arolium of wasps (Hymenoptera: Vespidae). *Zoology* **105**, 225–237.
Frantsevich, L. I. and Gorb, S. N. (2004). Structure and mechanics of the tarsal chain in the hornet, *Vespa crabro* (Hymenoptera: Vespidae): implications on the attachment mechanism. *Arthropod Struct. Dev.* **33**, 77–89.
Gao, H., Wang, X., Yao, H., Gorb, S. and Arzt, E. (2005). Mechanics of hierarchical adhesion structures of geckos. *Mech. Mater.* **37**, 275–285.
Ghasi-Bayat, A. and Hasenfuss, I. (1980a). Die Oberflächenstrukturen der Prätarsus von *Elasmucha ferrugata* (Fabricius) (Acanthosomatidae, Heteroptera). *Zool. Anz.* **205** (1/2), 76–80.
Ghasi-Bayat, A. and Hasenfuss, I. (1980b). Zur Herkunft der Adhäsionsflüssigkeit der Tarsalen Haftlappen bei den Pentatomidae (Heteroptera). *Zool. Anz.* **204** (1/2), 13–18.
Glassmaker, N. J., Jagota, A., Chaudhury, M. K. and Hui, C.-Y. (2006). Contact and adhesion mechanics of biomimetic fibrillar interfaces. *Proceedings 29th Annual Meeting of the Adhesion Society*, pp. 93–95, Inc. Jacksonville, Florida.
Gorb, E. V. and Gorb, S. N. (2002). Attachment ability of the beetle *Chrysolina fastuosa* on various plant surfaces. *Entomol. Exp. Appl.* **105**, 13–28.

Gorb, E. V., Haas, K., Henrich, A., Enders, S., Barbakadze, N. and Gorb, S. (2005). Composite structure of the crystalline epicuticular wax layer of the slippery zone in the pitchers of the carnivorous plant *Nepenthes alata* and its effect on insect attachment. *J. Exp. Biol.* **208**, 4651–4662.

Gorb, S. N. (2001). *Attachment Devices of Insect Cuticle*. Kluwer Academic Publishers: Dordrecht.

Gorb, S. N., Beutel, R., Gorb, E. V., Jiao, Y., Kastner, V., Niederegger, S., Popov, V. L., Scherge, M., Schwarz, U. and Vötsch, W. (2002). Structural design and biomechanics of friction-based releasable attachment devices in insects. *Integr. Comp. Biol.* **42** (6), 1127–1139.

Gorb, S. N. and Beutel, R. G. (2001). Evolution of locomotory attachment pads of hexapods. *Naturwissenschaften* **88**, 530–534.

Gorb, S. N. and Gorb, E. V. (2004). Ontogenesis of the attachment ability in the bug *Coreus marginatus* (Heteroptera, Insecta). *J. Exp. Biol.* **207**, 2917–2924.

Gorb, S. N., Niederegger, S., Hayashi, C. Y., Summers, A., Vötsch, W. and Walther, P. (2006). Silk-like secretion from tarantula feet. *Nature* **443**, 407.

Gorb, S. N. and Scherge, M. (2000). Biological microtribology: anisotropy in frictional forces of orthopteran attachment pads reflects the ultrastructure of a highly deformable material. *Proc. R. Soc. Lond. B* **267**, 1239–1244.

Gorb, S. N., Jiao, Y. and Scherge, M. (2000). Ultrastructural architecture and mechanical properties of attachment pads in *Tettigonia Viridissima* (Orthoptera Tettigoniidae). *J. Comp. Physiol. A* **186**, 821–831.

Green, D. M. (1979). Tree frog toe pads: comparative surface morphology using scanning electron microscopy. *Can. J. Zool.* **57**, 2033–2046.

Green, D. M. and Alberch, P. (1981). Interdigital webbing and skin morphology in the neotropical salamander genus *Bolitoglossa* (Amphibia; Plethodonitidae). *J. Morphol.* **170**, 273–282.

Hanna, G. and Barnes, W. J. P. (1990). Adhesion and detachment of the toe pads of tree frogs. *J. Exp. Biol.* **155**, 103–125.

Hasenfuss, I. (1977). Die Herkunft der Adhäsionsflüssigkeit bei Insekten. *Zoomorphology* **87**, 51–64.

Hasenfuss, I. (1978). Über das Haften von Insekten an glatten Flächen – Herkunft der Adhäsionsflüssigkeit. *Zool. Jb. Anat.* **99**, 115–116.

Henning, B. (1974). Morphologie und Histologie der Tarsen von *Tettigonia viridissima* L. (Orthoptera, Ensifera). *Z. Morphol. Tiere* **79**, 323–342.

Hertz, H. (1881). Über die Berührung fester elastischer Körper. *J. Reine Angew. Math.* **92**, 156–171.

Hiller, U. (1968). Untersuchungen zum Feinbau und zur Funktion der Haftborsten von Reptilien. *Z. Morphol. Tiere* **62**, 307–362.

Homann, H. (1957). Haften Spinnen an einer Wasserhaut?. *Naturwissenschaften* **44** (11), 318–319.

Huber, G., Gorb, S. N., Spolenak, R. and Arzt, E. (2005a). Resolving the nanoscale adhesion of individual gecko spatulae by atomic force microscopy. *Biol. Lett.* **1**, 2–4.

Huber, G., Mantz, H., Spolenak, R., Mecke, K., Jacobs, K., Gorb, S. N. and Arzt, E. (2005b). Evidence for capillarity contributions to gecko adhesion from single spatula nanomechanical measurements. *Proc. Natl. Acad. Sci. USA* **102** (45), 16293–16296.

Ishii, S. (1987). Adhesion of a leaf feeding ladybird *Epilachna vigintioctomaculata* (Coleoptera: Coccinellidae) on a vertically smooth surface. *Appl. Entomol. Zool.* **22** (2), 222–228.

Jagota, A. and Bennison, S. J. (2002). Mechanics of adhesion through a fibrillar microstructure. *Integr. Comp. Biol.* **42**, 1140–1145.

Jiao, Y., Gorb, S. N. and Scherge, M. (2000). Adhesion measured on the attachment pads of *Tettigonia viridissima* (Orthoptera, Insecta). *J. Exp. Biol.* **203** (12), 1887–1895.

Johnson, K. L., Kendall, K. and Roberts, A. D. (1971). Surface energy and the contact of elastic solids. *Proc. R. Soc. Lond. A* **324** (1558), 301–313.

Kästner, A. (1941). Ordnung der Arachnida: Solifugae. In: *Chelicerata* (ed. Krumbach, T.), pp. 204–215. Berlin: W. de Gruyter.

Kendall, K. (2001). *Molecular Adhesion and its Applications*. New York: Kluwer Academic Publishers.

Kendall, U. D. (1970). The anatomy of the tarsi of *Schistocerca gregaria* Forskål. *Z. Zellforsch.* **109**, 112–137.

Kesel, A. B., Martin, A. and Seidl, T. (2003). Adhesion measurements on the attachment devices of the jumping spider *Evarcha arcuata*. *J. Exp. Biol.* **206**, 2733–2738.

Kosaki, A. and Yamaoka, R. (1996). Chemical composition of footprints and cuticula lipids of three species of lady beetles. *Jpn. J. Appl. Entomol. Zool.* **40**, 47–53.

Langer, M. G., Ruppersberg, J. P. and Gorb, S. N. (2004). Adhesion forces measured at the level of a terminal plate of the fly's seta. *Proc. R. Soc. Lond. B* **271**, 2209–2215.

Lavoie, M. E. (1956). How sea stars open bivalves. *Biol. Bull.* **111**, 114–122.

Lees, A. M. and Hardie, J. (1988). The organs of adhesion in the aphid *Megoura viciae*. *J. Exp. Biol.* **136**, 209–228.

Mak, A. F. (1986). Unconfined compression of hydrated viscoelastic tissues: a biphasic poroviscoelastic analysis. *Biorheology* **23**, 371–383.

Maugis, D. (1999). *Contact, Adhesion and Rupture of Elastic Solids*. Berlin: Springer.

McAllister, W. and Channing, A. (1983). Comparison of toe pads of some southern African climbing frogs. *S. Afr. J. Zool.* **18** (2), 110–114.

McKenzie, J. D. (1987). The ultrastructure of the tentacles of eleven species of dendrochirote holothurians studied with special reference to the surface coats and papillae. *Cell Tissue Res.* **248** (1), 187–199.

Neville, A. C. (1975). *Biology of the Arthropod Cuticle*. Berlin: Springer.

Neville, A. C. (1993). *Biology of Fibrous Composites*. Cambridge: Cambridge University Press.

Niederegger, S. and Gorb, S. N. (2006). Friction and adhesion in the tarsal and metatarsal scopulae of spiders. *J. Comp. Physiol. A* **192**, 1223–1232.

Ohler, A. (1995). Digital pad morphology in torrent-living Ranid frogs. *Asiatic Herpetol. Res.* **6**, 85–96.

Paine, V. L. (1929). The tube feet of starfishes as autonomous organs. *Am. Nat.* **62**, 517–529.

Peressadko, A. and Gorb S. N. (2004). Surface profile and friction force generated by insects. In: *Fortschritt-Berichte VDI* (eds Boblan, I. and Bannasch, R.). Düsseldorf: VDI. **249**(15), 257–261.

Perez Goodwyn, P. P., Peressadko, A., Schwarz, H., Kastner, V. and Gorb, S. (2006). Material structure, stiffness, and adhesion: why attachment pads of the grasshopper (*Tettigonia viridissima*) adhere more strongly than those of the locust (*Locusta migratoria*) (Insecta: Orthoptera). *J. Comp. Physiol. A* **192**, 1233–1243.

Persson, B. N. J. (2003). On the mechanism of adhesion in biological systems. *J. Chem. Phys.* **118**, 7614–7621.

Persson, B. N. J. and Gorb, S. N. (2003). The effect of surface roughness on the adhesion of elastic plates with application to biological systems. *J. Chem. Phys.* **119**, 11437–11444.

Richards, A. G. and Richards, P. A. (1979). The cuticular protuberances of insects. *Int. J. Insect Morphol. Embryol.* **8**, 143–157.

Rizzo, N. W., Gardner, K. H., Walls, D. J., Keiper-Hrynko, N. M., Ganzke, T. S. and Hallahan, D. L. (2006). Characterization of the structure and composition of gecko adhesive setae. *J. R. Soc. Interface* **3**, 441–451.

Rosenberg, H. I. and Rose, R. (1999). Volar adhesive pads of the feathertail glider, *Acrobates pygmaeus* (Marsupialia; Acrobatidae). *Can. J. Zool.* **77**, 233–248.

Roth, L. M. and Willis, E. R. (1952). Tarsal structure and climbing ability of cockroaches. *J. Exp. Zool.* **119**, 483–517.

Sanjeevi, R. (1982). A viscoelastic model for the mechanical properties of biological materials. *J. Biomech.* **15**, 107–109.

Santos, R., Gorb, S., Jamar, V. and Flammang, P. (2005). Adhesion of echinoderm tube feet to rough surfaces. *J. Exp. Biol.* **208** (13), 2555–2567.

Schargott, M., Popov, V. L. and Gorb, S. N. (2006). Spring model of biological attachment pads. *J. Theor. Biol.* **243**, 48–53.

Schedl, W. (1991). Hymenoptera: Unterordnung Symphyta (Pflanzenwespen). In: *Handbuch der Zoologie* (ed. Fischer, M.), pp. 1–117. Berlin: W. de Gruyter

Scherge, M. and Gorb, S. N. (2000). Microtribology of biological materials. *Tribol. Lett.* **8** (1), 1–7.

Scherge, M. and Gorb, S. N. (2001). *Biological Micro- and Nanotribology: Nature's Solutions*. Berlin: Springer.

Schulmeister, S. (2003). Morphology and evolution of the tarsal plantulae in Hymenoptera (Insecta), focussing on the basal lineages. *Zool. Scr.* **32** (2), 153–172.

Schwarz, H. and Gorb, S. (2003). Method of platinum–carbon coating of ultrathin sections for transmission and scanning electron microscopy: an application for study of biological composites. *Microsc. Res. Tech.* **62**, 218–224.

Snodgrass, R. E. (1956). *Anatomy of the Honeybee*. New York: Comstock Publishing Associates.

Spolenak, R., Gorb, S., Gao, H. and Arzt, E. (2005a). Effects of contact shape on the scaling of biological attachments. *Proc. R. Soc. Lond. A* **461** (2054), 305–319.

Spolenak, R., Gorb, S. and Arzt, E. (2005b). Adhesion design maps for bio-inspired attachment systems. *Acta Biomater.* **1**, 5–13.

Stork, N. E. (1980). Role of wax blooms in preventing attachment to brassicas by the mustard beetle, *Phaedon cochleariae*. *Entomol. Exp. Appl.* **28**, 100–107.

Vötsch, W., Nicholson, G., Müller, R., Stierhof, Y.-D., Gorb, S. N. and Schwarz, U. (2002). Chemical composition of the attachment pad secretion of the locust *Locusta migratoria*. *Insect Biochem. Mol. Biol.* **32**, 1605–1613.

Welsch, U., Storch, V. and Fuchs, W. (1974). The fine structure of the digital pads of Rhacophorid tree frogs. *Cell Tissue Res.* **148**, 407–416.

Williams, E. E. and Peterson, J. A. (1982). Convergent and alternative designs in the digital adhesive pads of scincid lizards. *Science* **215**, 1509–1511.

The Integument of Water-walking Arthropods: Form and Function

John W.M. Bush[a], David L. Hu[b] and Manu Prakash[c]

[a]*Department of Mathematics, MIT, Cambridge, MA, USA*

[b]*The Courant Institute of Mathematical Sciences, NYU, New York, NY, USA*

[c]*Center for Bits and Atoms, MIT, Cambridge, MA, USA*

1 Introduction 118
2 Surface tension 120
  2.1 Weight support 124
  2.2 Capillary attraction 128
  2.3 Propulsion 130
3 Wetting 131
  3.1 The contact angle 132
  3.2 Surface roughening 133
  3.3 Contact angle hysteresis 139
  3.4 Water-repellency 142
4 Insect cuticle 144
  4.1 Composition 144
  4.2 Morphology 145
  4.3 Stability 153
5 Function 157
  5.1 Water- and rain-proofing 157
  5.2 Plastron respiration 161
  5.3 Clasping the free surface 165
  5.4 Drag reduction and thrust generation 167
6 Imaging techniques 169
  6.1 Scanning electron microscopy 170
  6.2 Optical microscopy 173
  6.3 Scanning probe microscopy 176
7 Discussion 177
  Acknowledgements 181
  References 181

ADVANCES IN INSECT PHYSIOLOGY VOL. 34
ISBN 978-0-12-373714-4
DOI: 10.1016/S0065-2806(07)34003-4

Abstract

We develop a coherent view of the form and function of the integument of water-walking insects and spiders by reviewing biological work on the subject in light of recent advances in surface science. Particular attention is given to understanding the complex nature of the interaction between water-walking arthropods and the air–water surface. We begin with a discussion of the fundamental principles of surface tension and the wetting of a solid by a fluid. These basic concepts are applied to rationalize the form of various body parts of water-walking arthropods according to their function. Particular attention is given to the influence of surface roughness on water-repellency, a critical feature of water-walkers that enables them to avoid entrapment at the interface, survive the impact of raindrops and breathe if submerged. The dynamic roles of specific surface features in thrust generation, drag reduction and anchoring on the free surface are considered. New imaging techniques that promise important insights into this class of problems are discussed. Finally, we highlight the interplay between the biology, physics and engineering communities responsible for the rapid recent advances in the biomimetic design of smart, water-repellent surfaces.

1 Introduction

Textured surfaces are known to play an important dynamical role for a number of swimmers and fliers (Bushnell and Moore, 1991; Fish, 1998, 2006); however, no creature depends more critically on its surface structure than do water-walking arthropods. Their surface roughness is critical in maintaining water-repellency, generating thrust as they strike the water surface, reducing drag as they glide across the surface and generating buoyancy and permitting respiration when they are submerged.

Water-repellency is generated in the same way in both plant and animal kingdoms (on plant leaves, animal fur and bird feathers) by presenting a textured waxy or oily surface that increases the energetic cost of wetting and so discourages fluid–solid contact. Lotus leaves are known to be both water-repellent and self-cleaning owing to their complex surface structure (Barthlott and Neinhuis, 1997; Neinhuis and Barthlott, 1997). Their surface is characterized by roughness on two scales (the smallest being sub-micron) and a waxy coating, which together render it superhydrophobic. When water drops strike it, instead of sticking, they roll off, taking with them any dust that might have collected on the plant. The rough piliferous integument of water-walking arthropods plays a similar role in maintaining water-repellency. Moreover, we shall see that it also plays a critical dynamic role in both thrust generation and drag reduction.

The interaction of fluid interfaces and solids arises in a wide range of problems in biology and industry. Much of the early work on fluid–solid interactions was motivated by the desire to optimize insecticides designed to coat their insect target while leaving the plant unharmed (Moore, 1921; English, 1928; Wilcoxon and Hartzell, 1931; O'Kane *et al.*, 1932; Hoskins, 1940; Pal, 1951), a task made all the more challenging by the fact that the two coverings are often virtually identical (e.g. Hadley, 1981; Farrell and Mitter, 1990; Barthlott *et al.*, 1994). Subsequently, the subject was reconsidered with a view to developing water-repellent textiles (Cassie, 1944; Cassie and Baxter, 1945; Bartell *et al.*, 1948). Most recently, the subtle water-proofing strategies of plants and insects have provided important guidance in the rapid advances in the development of superhydrophobic surfaces (Feng *et al.*, 2002; Wagner *et al.*, 2003; Callies and Quéré, 2005; Furstner *et al.*, 2005; Mock *et al.*, 2005; Liu *et al.*, 2006; Feng and Jiang, 2006). This new class of engineered biomimetic surfaces are finding a wealth of applications including self-cleaning, water-repellent windows (Blossey, 2003), corrosion protection (Kousik *et al.*, 2001), drag reduction (Ou *et al.*, 2004; Choi and Kim, 2006; Choi *et al.*, 2006), clean inkjet nozzle release (Yi and Kim, 2004) and devices for underwater breathing (Shirtcliffe *et al.*, 2006).

Water-walking arthropods have been evolving for over 100 million years, and so from a purely mechanical perspective represent a highly adapted, robust system. There are over 1200 species of water-walking insects and spiders (Andersen, 1982; Fig. 1) each of which depends critically on its ability to manipulate and control the air–water interface. Propulsive forces may be generated by striking or deforming the free

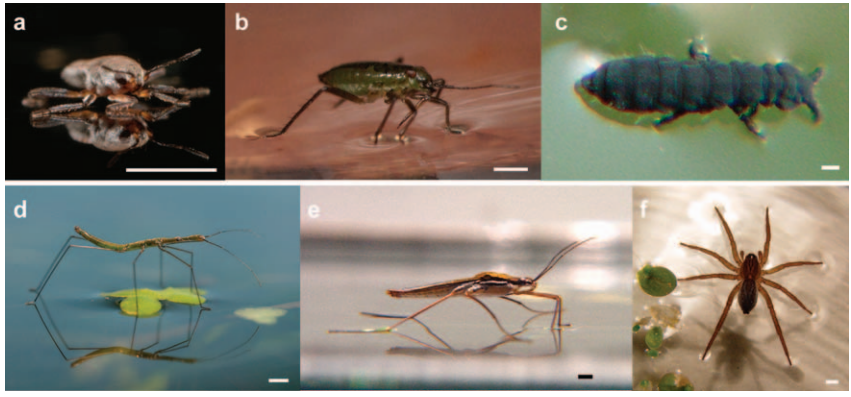

FIG. 1 Common water-walking arthropods, ordered roughly by size. (a) Broad-shouldered water strider *Microvelia*, (b) water treader *Mesovelia*, (c) springtail *Anurida maritima*, (d) water measurer *Hydrometra stagnorum*, (e) water strider *Gerris* and (f) fisher spider *Dolomedes triton*. Scale bars, 1 mm.

surface or by chemically altering the surface tension (Bush and Hu, 2006; see Section 3.3). The ability to manipulate the free surface depends critically on the creature's wetting properties; for example, without a water-repellent coating, insects cannot be sustained atop the interface by surface tension forces, but instead pass through it and sink. The vital role of the wetting properties of water-walking insects has long been recognized (Imms, 1906; Brocher, 1910; Hungerford, 1919; Baudoin, 1955, 1976). The goal of this review is to develop a coherent view of the form and function of the surface structure of water-walking arthropods by reviewing biological work on the subject in light of recent advances in surface science.

The arthropod integument has received attention from various fields of biology. Entomological material scientists have focused on the chemical structure of the surface layer, or cuticle (e.g. Vincent and Wegst, 2004); developmental entomologists have considered the changes prompted by growth of the cuticle (e.g. Wigglesworth, 1950, 1979) and comparative entomologists have contrasted the water-repellent properties of terrestrial, aquatic, and semi-aquatic arthropods (Heckman, 1983; Stratton *et al.*, 2004b; Perez-Goodwyn, 2007). This article is written from the perspective of a fluid mechanician rather than a biologist, but with a biological audience in mind. We shall thus devote considerable effort to reviewing the fundamental physical principles required to understand the static and dynamic interaction between water-walking arthropods and the free surface. Given our limited backgrounds in biology, we shall try to avoid the use (and probable misuse) of all but the most basic biological jargon, and to suppress any discussion of the ecology or philogeny of water-walkers. Instead, we take a purely mechanistic view of the subject of water-walking arthropods, and hope to highlight outstanding physical problems required to rationalize their existence and persistence at the interface.

In Section 2, we review fundamental concepts of surface tension and discuss its importance in both the statics and dynamics of water-walking arthropods. In Section 3, we discuss the fundamentals of wetting, giving particular attention to the impact of surface roughness on water-repellency. In Section 4, we review biological studies of the cuticle of water-walking arthropods. In Section 5, we attempt to understand the composition, morphology and stability of the cuticle on the basis of principles discussed in Sections 2 and 3. In Section 6, we review new imaging techniques that promise novel insights into the interaction between water-walking arthropods and the free surface.

2 Surface tension

We begin with a brief introduction to surface tension, then proceed to consider the capillary forces generated by objects residing at rest at an

air–water interface. In Section 2.1, we describe the role of surface tension in the weight support of small floating bodies. In Section 2.2, we describe the lateral forces that arise between two adjacent objects at a free surface. In Section 2.3, we demonstrate that the propulsive force of water-walking arthropods is typically the contact force generated by the driving leg striking the free surface.

Discussions of the molecular origins of surface tension may be found in Rowlinson and Widom (1982), Israelachvili (1992) and de Gennes *et al.* (2003). Molecules in a fluid feel a mutual attraction. Let us consider the free surface between air and water. A water molecule in the bulk is surrounded by attractive neighbours, while a molecule at the surface is attracted by a reduced number of neighbours and so in an energetically unfavourable state. The creation of new surface is thus energetically costly, and a fluid system will act to minimize its surface area. It is thus that small fluid bodies tend to evolve into spheres; for example, a thin water jet emerging from the kitchen tap will generally pinch off into spherical drops to minimize the total surface area (Plateau, 1873; Rayleigh, 1879).

If U is the total cohesive energy per molecule, then a molecule at a flat surface will lose $U/2$. Surface tension is a direct measure of this energy loss per unit area of surface. If the characteristic molecular dimension is R, its area scales as R^2; thus the surface tension $\sigma \sim U/(2R^2)$. Note that surface tension increases as the intermolecular attraction increases and the molecular size decreases. Surface tension σ has the units of force/length or equivalently energy/area. To create a surface of area A thus requires an energy σA. For a clean air–water interface, $\sigma = 72$ dynes cm^{-1}. Impurities will generally act to reduce the surface tension, so that in ponds or other standing bodies of water, $\sigma \sim 62 - 70$ dynes cm^{-1}. An exception to this rule is salt, which may act to increase surface tension slightly: at sea, surface tensions as high as $\sigma \sim 72$ dynes cm^{-1} have been reported (White, 1994).

Surface tension is a force per unit length acting everywhere tangent to the free surface. When an interface adjoins a solid, it applies a contact force per unit length σ along the contact line in a direction tangent to the interface. It is precisely these forces that enable water-walking arthropods to reside at rest on the free surface: by deforming the planar free surface, they generate contact forces that bear their weight (Fig. 2a). The influence of surface tension on an initially planar interface is two-fold. First, it resists the distortion of the interface and the associated increase in surface energy. This resistance may be expressed as a jump in normal stress (force/area) across an interface, termed the curvature pressure: $P_c = \sigma(R_1^{-1} + R_2^{-1})$, where R_1 and R_2 are the principle radii of curvature of the deformed interface (de Gennes *et al.*, 2003). Inside a spherical drop of radius R the pressure is higher than that outside by an amount $2\sigma/R$; hence the vigorous popping of surfacing champagne bubbles. Figure 3 illustrates a *Mesovelia*

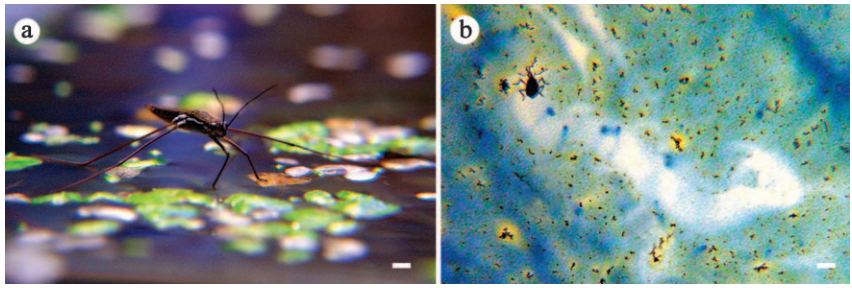

FIG. 2 Surface tension may be used by water-walkers for both weight support and propulsion. (a) A water strider's weight is supported by the curvature or contact forces generated by its deforming the free surface. (b) By releasing surfactants onto the free surface, *Microvelia* generates surface tension gradients that propel it forward. The surfactants reduce the surface tension, causing surface divergent motions that sweep the surface clear of the blue dye. Scale bars, 1 mm.

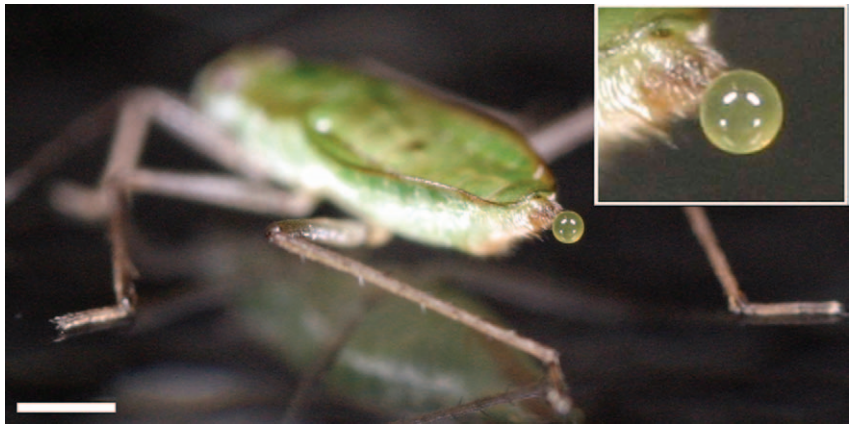

FIG. 3 Care must be taken by semi-aquatic insects to excrete liquid without compromising their water-repellency. Here, fluid is excreted from the anus of *Mesovelia*. A drop of size $R \sim 0.3$ mm requires an excess pressure of $P \sim 2\sigma/R = 0.004$ atm. Scale bar, 1 mm.

excreting liquid waste: the size of the droplet indicates excess extrusion pressures on the order of 0.004 atm.

Insofar as normal stresses are concerned, the surface tension makes the air–water interface behave like a trampoline. The second physical effect of surface tension accompanies gradients in surface tension, as may be generated by gradients in temperature or surface chemistry. Surface tension gradients correspond to tangential stresses at a free surface, and so necessarily drive flows known as Marangoni flows (Scriven and Sternling, 1970).

If an object floats on a free surface, and if the surface tension is diminished on one side relative to the other, the body will be propelled in the direction of increasing surface tension. This means of propulsion, termed Marangoni propulsion (Bush and Hu, 2006), is used as an escape mechanism by a number of water-walking insects, as well as beetles and terrestrial insects that accidentally fall onto the water surface (Fig. 2b). By releasing a lipid that reduces the surface tension, such creatures can propel themselves forward at peak speeds of order $20\,\mathrm{cm\,s^{-1}}$ (Schildknecht, 1976). When a pine needle falls into a lake or pond, it is similarly propelled across the surface since the resin at its base decreases the local surface tension.

While the world of humans is dominated by gravity, surface tension dominates that of water-walking arthropods. The relative magnitude of gravitational and capillary forces is made clear by considering a fluid drop of radius a placed on a substrate. Gravity acts to flatten the drop into a planar film, while surface tension acts to maintain its sphericity. The relative magnitudes of these two competing effects may be expressed as the ratio of the hydrostatic and curvature pressures, termed the Bond number: $Bo = \rho g a^2/\sigma$. These two pressures are comparable when $Bo = 1$, which arises at a length scale corresponding to the capillary length: $\ell_c = (\sigma/(\rho g))^{1/2}$. For an air–water surface, for example, $\sigma \sim 70$ dynes cm^{-1}, $\rho = 1\,\mathrm{g\,cc^{-1}}$ and $g = 980\,\mathrm{cm\,s^{-2}}$, so that $\ell_c \sim 2$ mm. Bodies of water in air are dominated by the influence of surface tension provided they are smaller than the capillary length. The capillary length prescribes the maximum size of raindrops, and of pendant drops that may hang from a ceiling. Note that as a fluid system becomes progressively smaller, surface tension becomes progressively more important relative to gravity.

Surfactants, or surface-active reagents, are molecules that have an affinity for interfaces; common examples include soaps and lipids. Owing to their molecular structure (often a hydrophylic head and hydrophobic tail), they find it energetically favourable to reside at the free surface. Their presence reduces the surface tension; consequently, gradients in surfactant concentration Γ result in surface tension gradients and concomitant Marangoni flows (Fig. 2b). There are many different types of surfactants, some of which are insoluble (and so remain at the interface), others of which are soluble in the suspending fluid and so diffuse into the bulk. Most organic materials are surface active; therefore, surfactants are ubiquitous in the natural aqueous environment. For a wide range of common surfactants, surface tension is a monotonically decreasing function of Γ until a critical concentration is achieved, beyond which σ remains constant (de Gennes *et al.*, 2003). Surfactants rarely reduce the surface tension of water to less than 30 dynes cm^{-1}, although superwetting agents have recently been introduced by Dow Corning that reduce it to 23 dynes cm^{-1}. It is noteworthy that the peril posed by surfactants to water-walking creatures does not result from the reduction in surface tension and so

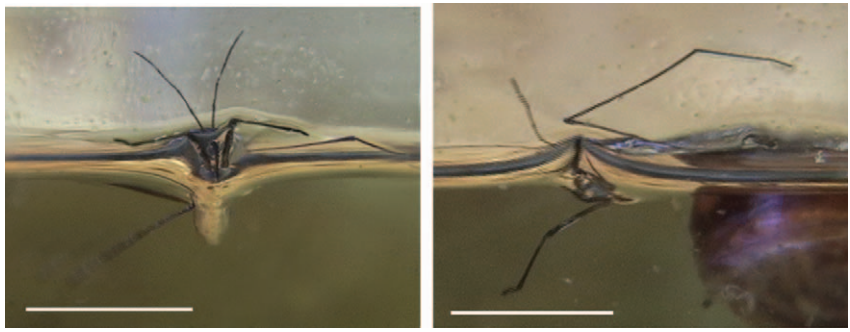

FIG. 4 Surface contamination presents a grave risk for water-walking arthropods. Here, a drop of soap on the water surface destroys the water-repellency of the water strider: water impregnates its hair layer, causing it to sink. Scale bars, 1 cm.

weight-bearing potential of the free surface: as we shall demonstrate in Section 2.1, the great majority of water-walking arthropods maintain a large margin of safety. Rather, surfactants such as soap or petroleum are a danger owing to their tendency to drastically alter the wetting properties of the insect cuticle (Sections 3 and 4), eliminating their water-repellency and so allowing them to pass through the interface. The perilous effect of a commercial soap on a water strider is evident in Fig. 4. Brown (1966) discusses the deleterious effects of surfactants on stream invertebrates.

2.1 WEIGHT SUPPORT

Archimedes principle states that the buoyancy force on a floating object is equal to the weight of fluid displaced by that object. It follows that bodies heavier than water sink, and bodies lighter than water float with a submerged volume prescribed by the relative magnitudes of the body and fluid densities. Water-walking arthropods are generally more dense than water, and so would sink unless sustained by surface tension forces. The statics of small floating bodies is well understood (Mansfield *et al.*, 1997; Keller, 1998; Vella *et al.*, 2006a) and may be applied directly to understand the vertical force balance on a creature residing at rest on the air–water surface.

Consider a body with density greater than that of water $\rho_b > \rho$ and mass M floating at the interface (Fig. 5a). Its borders will generally be adjoined by a meniscus, details of which will depend on the wetting properties of the solid, but whose lateral extent will correspond to the capillary length $\ell_c = (\sigma/(\rho g))^{1/2} \approx 2$ mm. The body weight must be supported by some combination of the buoyancy force, F_b, and contact force, F_c: $Mg = F_b + F_c$. The buoyancy force is deduced by integrating the hydrostatic pressure

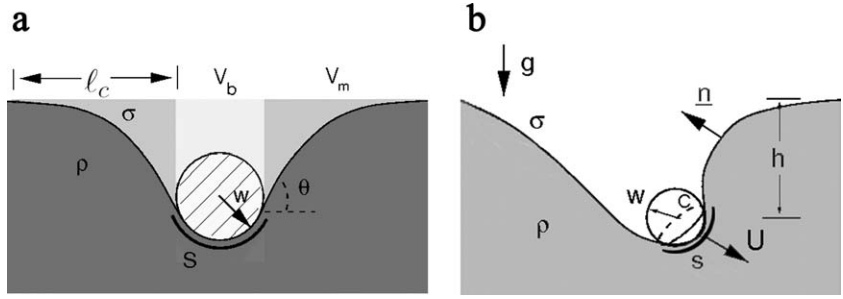

FIG. 5 Schematic illustrations of the leg of a water-walking creature in both static and dynamic states. n denotes the normal to the surface and σ the surface tension. (a) We consider the forces on a floating body of characteristic length w with a contact line C and wetted area S. Its weight is supported by a combination of buoyancy and curvature forces, whose magnitudes are prescribed by the weights of the fluid volumes displaced inside and outside the contact line, respectively V_b and V_m. (b) The body strikes the free surface obliquely at a speed U. Its motion is resisted by some combination of the forces enumerated in Eq. (2).

$p = \rho g z$ over the body surface S in contact with the water, and so is equal to the weight of fluid V_b displaced above the body and inside the contact line C. The contact force may be deduced by integrating the surface tension force along the contact line: for a two-dimensional (2D) body (Fig. 5a), the vertical contact force per unit length is $2\sigma \sin\theta$.

Mansfield *et al.* (1997) and Keller (1998) demonstrate that the contact force is precisely equal to the weight of fluid displaced outside the contact line, thereby generalizing Archimedes principle to the case where surface tension forces are important: the force acting on a floating body is equal to the total weight of the fluid displaced. The buoyancy and contact forces are equal to the weights of the fluid displaced by the meniscus, respectively, in- and outside the contact line. For long thin bodies such as insect legs, their relative magnitudes are thus prescribed by the ratio of the characteristic body size w to the capillary length ℓ_c.

$$\frac{F_b}{F_c} \sim \frac{V_b}{V_m} \sim \frac{w}{\ell_c} \tag{1}$$

Bodies small relative to the capillary length are supported primarily by surface tension and can be sustained even when they are more dense than the underlying fluid. As the leg diameter of most water-walking arthropods is $\sim 100\,\mu m \ll \ell_c$, one sees that they rely primarily on surface tension for their support: by deforming the free surface like a trampoline, they generate tensile forces that bear their weight.

The cuticle of water-walking arthopods significantly complicates the nature of their interaction with the free surface. In particular, the contact lines do not run smoothly along the tarsi in contact with the free surface;

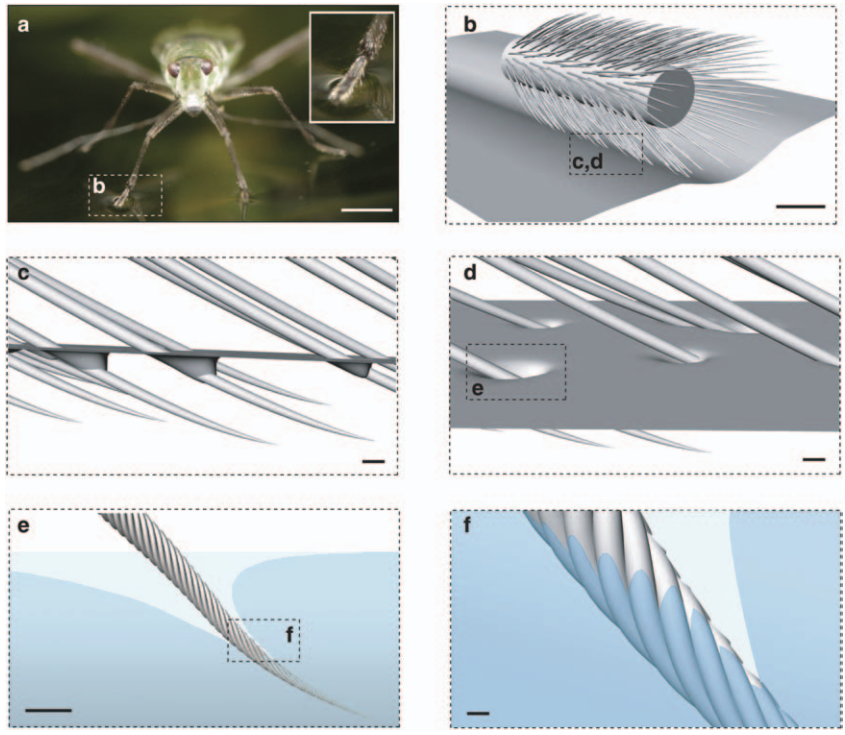

FIG. 6 The contact between the water treader *Mesovelia* and the free surface. (a) *Mesovelia* supports its weight by deforming the surface. Scale bar, 1 mm. (b) A schematic of a hairy leg. Scale bar, 100 μm. (c–d) Further zooms of individual hairs penetrating the surface. Scale bar, 1 μm. (e) A single hair penetrating the free surface. Scale bar, 1 μm. (f) The hairs are covered in nanogrooves that trap air when the hair is submerged. Scale bar, 0.1 μm.

rather, they correspond to loops along the individual hairs abutting the free surface (Fig. 6). Nevertheless, one can gain some insight by crudely thinking of their having contact with the free surface along the entire contact length P of their support legs. One can then define the maximum supporting curvature force available to such a creature as $F_s \sim \sigma P$. In Fig. 7, we plot the relation between F_s and the weight $F_g = Mg$ for various water-walking arthropods. Creatures above the line $\mathrm{Ba} = F_g/F_s = 1$ may be statically supported by surface tension; those below cannot. Assuming that the insects are isometric, with body proportions independent of their size (McMahon and Bonner, 1985), one anticipates that $M \sim L^3$ and $P \sim L$, so that $\mathrm{Ba} \sim L^2$ (Baudoin, 1955). The best fit for Fig. 7 is $F_s \sim F_g^{0.46}$, which indicates $\mathrm{Ba} = F_g/F_s \sim F_g^{0.5} \sim L^{3/2}$. This slightly weaker dependence of Ba on L may suggest that water-walker's legs grow proportionally longer

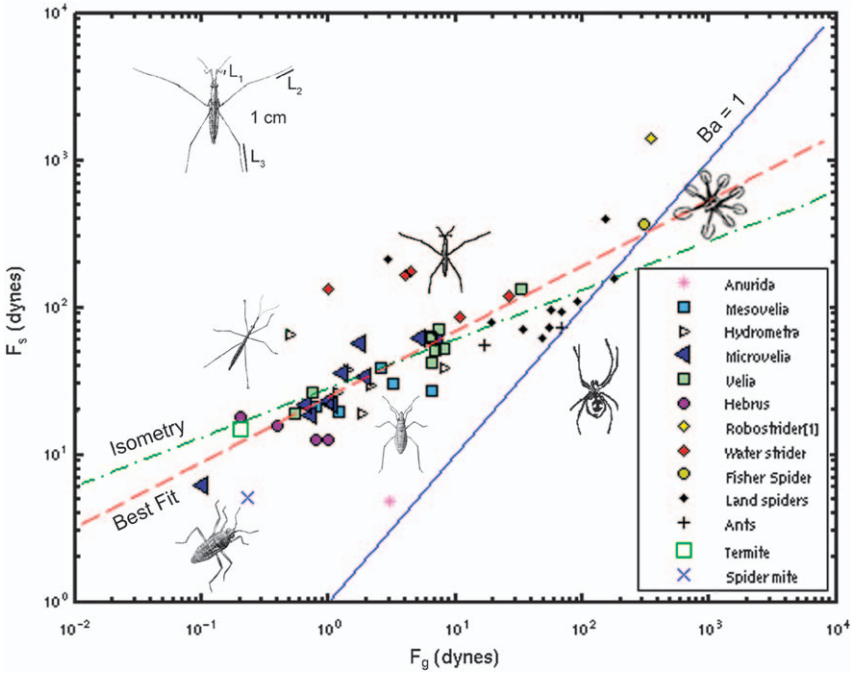

FIG. 7 The relation between the weight, $F_g = Mg$, and the maximum supporting surface tension force, $F_s = \sigma P$, for water-walking insects and spiders, where the contact perimeter $P = 4(L_1 + L_2 + L_3)$ (see inset top left). All water-walking arthropods fall above the line $Ba = 1$ and so may reside at rest on the water surface. Their margin of safety generally decreases with body size. Note that many terrestrial insects (such as the ants and spiders included here) can also be supported by surface tension if they are sufficiently water-repellent. Isometry would suggest $F_s \sim F_g^{1/3}$, a relation indicated by the dash-dotted line. The best fit to the data is given by $F_s \sim F_g^{0.46}$ (dashed line). Data reprinted from Hu and Bush (2008a) and Hu, Chan and Bush (2003).

with increasing body size; alternatively, it may indicate the significance of the microscale topology of the insect cuticle on weight support.

It is important to note that the surface deformation will in general depend on the surface structure of the floating object. For a smooth object, the curvature force will depend explicitly on the contact angle (see Section 3.1; Vella *et al.*, 2006a). Water-walking arthropods are covered in a complex layer of hair that traps air, thereby increasing the volume of fluid displaced and the concomitant force of buoyancy. As we shall see in Section 4, this trapped air layer may be a substantial fraction of the leg volume and so contribute significantly to the force of buoyancy (Fig. 6). Feng *et al.* (2007) examine the surface distortion generated by depressing a water strider leg. They found that, owing to its high contact angle, the leg was capable of

reaching depths as high as 4.8 mm before breaking through. Matsuda *et al.* (1985) used a shearing interferometer to measure the free surface deflections generated by stationary water striders, and found distortions of order 100 μm. The new imaging techniques discussed in Section 6 will provide new insight into the floatation of roughened bodies.

2.2 CAPILLARY ATTRACTION

An object floating at a free surface may be subject not only to vertical but also lateral forces. Fluid mechanicians (Nicolson, 1949; Gifford and Scriven, 1971; Chan *et al.*, 1981; Mansfield *et al.*, 1997; Kralchevsky and Denkov, 2001) have long known that lateral capillary forces exist between small floating objects, an effect responsible for the formation of bubble rafts in champagne and the clumping of Cheerios in a cereal bowl (Vella and Mahadevan, 2005). Recently, such capillary forces have been recognized as a means by which to promote self-assembly of microstructures at a free surface (Gryzbowski *et al.*, 2001; Whitesides and Grzybowski, 2002; Manoharan *et al.*, 2003; Lauga and Brenner, 2004; Zeng *et al.*, 2006). Understanding such forces is critical for rationalizing the ability of certain insects to propel themselves up menisci by surface deformation (Baudoin, 1955; Hu and Bush, 2005) and for assessing the stability of insect cuticle (Crisp, 1950).

Consider two objects floating on the free surface (Fig. 8). The total energy of the system as a function of distance of separation, x, can be expressed as the sum of the gravitational potential energy and the surface energy $\sigma A(x)$, where A is the difference in areas of the deformed and undeformed surfaces.

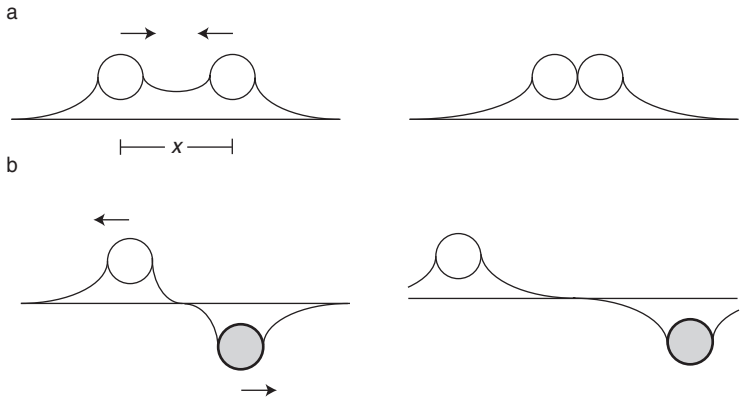

FIG. 8 Lateral capillary forces between small floating bodies initially separated by a distance x. (a) Two floating bubbles generate like-signed menisci and so are mutually attracted. (b) Two floating objects with opposite buoyancy generate opposite-signed menisci and so are mutually repelled. The range of these capillary forces is limited to the capillary length, $\ell_c \sim 3$ mm for an air–water interface.

If this total energy decreases with decreasing x, then the bodies will be subject to an attractive force. Such is the case when both bodies have the same density anomaly, that is, for a pair of bubbles (Fig. 8a) or for two relatively heavy particles. Conversely, if the total energy increases with decreasing x, a repulsive force is felt. Such is the case between two floating objects with opposite density anomaly (Fig. 8b). The range of such forces is prescribed by the lateral extent of the surface deformation, specifically, the capillary length. Their magnitude is prescribed by the rate of change of total energy (surface plus gravitational potential energy) with separation distance. Finally, we note that such forces also depend not only on the buoyancy of the objects, but on their wettability (Whitesides and Grzybowski, 2002), a matter to be discussed in Section 3.

Baudoin (1955) first reported that some insects may climb menisci without moving their limbs. Wetting creatures, such as the beetle larve, are circumscribed by a contact line; consequently, by arching their backs, they generate menisci at their nose and tail and an associated lateral capillary force that drives them up menisci (Fig. 9a). Their ascent is best understood in terms of energetics: if the surface energy they create through arching their backs exceeds the gravitational potential energy gained through their

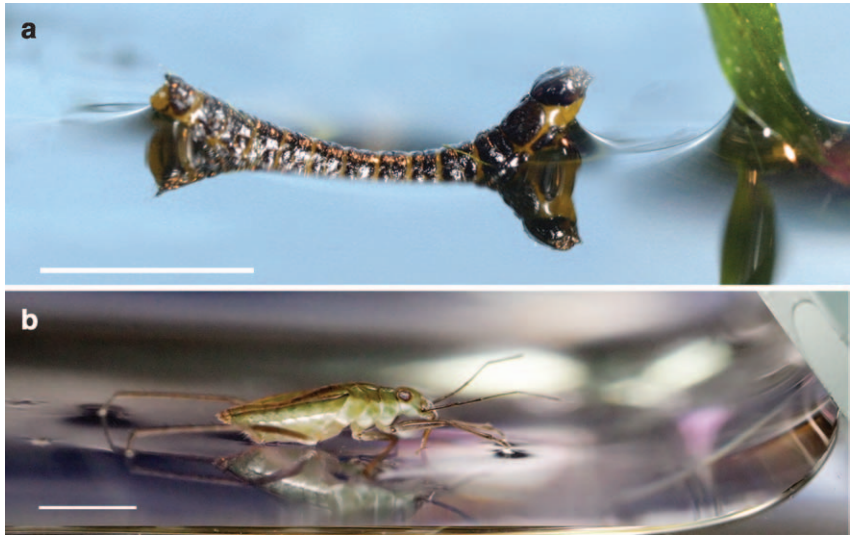

FIG. 9 Meniscus climbing by wetting and non-wetting insects. (a) The beetle larva *Pyrrhalta* is circumscribed by a contact line and so may generate menisci simply by arching its back. The resulting lateral capillary force (Fig. 8a) propels it towards the leaf. (b) The water treader *Mesovelia* has a water-repellent body, but uses the hydrophilic claws (or ungui) at its leg tips to clasp the free surface (see Figs. 22 and 35), and so generate the capillary force that drives it up the meniscus at right Hu and Bush (2005). Scale bars, 3 mm.

ascent, they will be drawn up the meniscus by capillary forces (Hu and Bush, 2005). Baudoin (1955) performed a simple experiment to demonstrate that floating metal rectangles, when arched slightly, will ascend menisci just as do wetting climbers. The manner in which water-walking insects, which are generally water-repellent, are able to clasp the free surface and so climb menisci will be discussed in Section 5.3.

The lateral capillary forces between bodies at an interface are also of critical importance in the maintenance of the water-repellency of water-walkers. As we shall see in Section 4.3, an air layer is maintained between the insect surface and the water by cuticle hairs lying roughly tangent to the interface. Provided these hairs deform the interface, there will be a capillary force acting between them. Crisp (1950) pointed out that such forces, if not matched by the hair's resistance to bending, may destabilize the hair layer: the clumping of hairs in one region will necessarily lead to bald patches into which water more readily intrudes. The elastocapillary stability of insect cuticle at an interface will be further considered in Section 4.3.

2.3 PROPULSION

The hydrodynamics of water-walking creatures were reviewed in Bush and Hu (2006), where the relevant equations are presented and discussed in greater detail. They present the first dynamic classification of all water-walking creatures by grouping them according to their primary source of thrust. Consider a smooth object of characteristic scale w striking the free surface above water (density ρ, dynamic viscosity μ, kinematic viscosity $\nu = \mu/\rho$, surface tension σ) at an impact speed U (Fig. 5b). Its motion will be resisted by some combination of hydrostatic, contact and hydrodynamic forces. The buoyancy force arises from the hydrostatic pressure (that increases with depth z as $\rho g z$) acting on the wall of the cavity against which the water-walker strokes (Glasheen and McMahon, 1996a,b). Contact forces act along the contact lines and have characteristic magnitude σw. The form drag results from the dynamic pressure generated by the impact, that scales as ρU^2. An estimate for the viscous drag is obtained by integrating a characteristic viscous stress $\mu U/w$ over the contact area $A \sim w^2$ of the body. Finally, an added mass force arises from the acceleration of fluid by the impacting body (Daniel, 1984; Glasheen and McMahon, 1996c).

The net force exerted on the impacting body may thus be roughly expressed as

$$|\mathrm{F}| \sim \underbrace{\rho U^2 w^2}_{\text{form drag}} + \underbrace{\rho g h w^2}_{\text{buoyancy}} + \underbrace{\rho V \frac{dU}{dt}}_{\text{added mass}} + \underbrace{\mu U w}_{\text{viscosity}} + \underbrace{\sigma w}_{\text{curvature}} - \underbrace{\nabla \sigma w^2}_{\text{Marangoni}} \tag{2}$$

The relative magnitudes of the six force components are prescribed by five dimensionless groups, the Reynolds *Re*, Weber *We*, Bond *Bo*, Strouhal *St* and Marangoni *Ma* numbers, defined, respectively, by

$$Re = \frac{Uw}{\nu} = \frac{\text{inertia}}{\text{viscous}} \qquad We = \frac{\rho U^2 w}{\sigma} = \frac{\text{inertia}}{\text{curvature}}$$

$$Bo = \frac{\rho g h}{\sigma / w} = \frac{\text{buoyancy}}{\text{curvature}} \qquad St = \frac{fw}{U} = \frac{\text{added mass}}{\text{inertia}}$$

$$Ma = \frac{\nabla \sigma}{\sigma / w} = \frac{\text{Marangoni}}{\text{curvature}}$$

The magnitudes of these dimensionless groups for representative water-walkers were assessed by Bush and Hu (2006), who show that the motion of the great majority of water-walking arthropods is characterized by $Re > 1$, $We < 1$ and $Bo < 1$. The principal force resisting their driving legs, and so the principal propulsive force, is thus the curvature force. By deforming the free surface, they generate contact forces that propel them forward.

We note that this macroscopic picture of the dynamics of water-walking creatures needs to be revised in light of the fact that the driving legs of arthropods are not smooth cylinders, but rather roughened hydrophobic surfaces. As will become clear in Section 3, each of the components of the hydrodynamic force listed in Eq. (2) is directly affected by the form of the surface roughness. These issues notwithstanding, the revised estimates for the relative magnitudes of these force components still indicate the dominance of contact forces in the propulsion of water-walking arthropods. The dynamic role of arthropod cuticle will be considered in Section 5.4.

3 Wetting

Wetting arises when a liquid–gas interface comes into contact with a solid (Dussan, 1979; Adamson, 1982; de Gennes, 1985). The degree of wetting is in general determined by both the material properties of the solid and fluid phases, and the topography of the solid surface. In Section 3.1, we consider the classic scenario of water wetting a flat solid surface, then in Section 3.2 proceed by describing the influence of surface roughness. The important concept of contact angle hysteresis is discussed in Section 3.3. The conditions required for a surface to be water-repellent are enumerated in Section 3.4. Our discussion follows that presented in de Gennes *et al.* (2003).

3.1 THE CONTACT ANGLE

Just as a fluid–fluid interface has an associated energy per unit area (or equivalently, a surface tension, σ), so do solid–fluid interfaces. For the case of a liquid–gas interface with tension σ in contact with a solid, the relevant surface energies are those of the solid–liquid and solid–gas interfaces, respectively, γ_{SL} and γ_{SG} (Fig. 10). The tendency of the liquid to wet the solid depends on the relative magnitudes of σ, γ_{SL} and γ_{SG} through the spreading parameter (Ross and Becher, 1992)

$$S = \gamma_{SG} - (\gamma_{SL} + \sigma) \tag{3}$$

If $S > 0$, the surface energy of the solid is lower wet than dry, so the liquid spreads completely into a thin film. Such is the case for oils spreading on most solids, including glass. Conversely, when $S<0$, it is energetically favourable for the solid to stay dry, so the fluid remains in the form of a droplet with a finite chemical (or equilibrium) contact angle θ_e. The fluid is then said to partially wet the solid. Given σ, γ_{SL} and γ_{SG}, one can calculate the contact angle θ_e by considering the horizontal force balance at the contact line or triple junction (Fig. 10)

$$\sigma \cos\theta_e = \gamma_{SG} - \gamma_{SL} \tag{4}$$

known as Young's relation (Young, 1805). This may alternatively be derived by considering the change in energy $\mathrm{d}W$ associated with the contact line moving a distance $\mathrm{d}x$

$$\mathrm{d}W = \mathrm{d}x(\gamma_{SG} - \gamma_{SL}) - \mathrm{d}x\ \ \sigma\cos\theta_e \tag{5}$$

At equilibrium, $\mathrm{d}W/\mathrm{d}x = 0$, and Young's relation (Eq. (4)) again emerges.

Consider the case of interest: an air–water interface in contact with a solid. Complete wetting arises only if $\theta_e = 0$; otherwise, the normal situation of partial wetting obtains. The solid is said to be hydrophilic if $\theta_e \leq 90^\circ$,

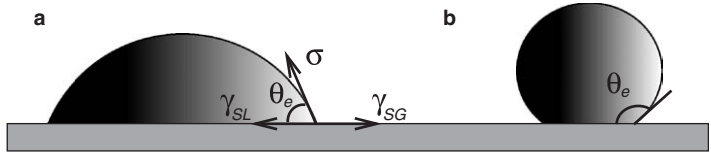

FIG. 10 The wetting of a solid by a liquid drop. The system is characterized by the surface energies per unit area of the liquid–gas interface, σ; solid–liquid interface, γ_{SL} and solid–gas interface, γ_{SG}. The horizontal force balance at the contact line yields the equilibrium contact angle θ_e in terms of σ, γ_{SL} and γ_{SG} via Young's relation (Eq. (4)). For a water drop, a surface is (a) hydrophilic if $\theta_e < 90^\circ$ and (b) hydrophobic if $\theta_e > 90^\circ$. Here, drops are assumed to be sufficiently small that gravity is negligible, so the drops assume the form of spherical caps.

hydrophobic if $\theta_e \geq 90^\circ$ and superhydrophobic if $\theta_e \geq 150^\circ$ (Fig. 10). Water is totally wetting on perfectly clean glass, but partially wetting on most solids. The equilibrium contact angles for water on a number of naturally occuring and manufactured substrates are listed in Table 1.

A liquid rises or falls in a vertical capillary tube piercing a horizontal interface according to whether θ_e is greater or less than 90°. The rise height is prescribed by a balance between curvature and hydrostatic pressures just beneath the interface. A fluid column of density ρ within a capillary tube of radius R will rise to a height h

$$h = \frac{2\sigma \cos\theta_e}{\rho g R} \tag{6}$$

provided $R \ll h$ (de Gennes *et al.*, 2003). The rise height increases with increasing surface tension and decreasing radius. Most notably, the sign of h changes with contact angle: hydrophilic tubes ($\theta_e < 90^\circ$) draw water upwards, while hydrophobic tubes ($\theta_e > 90^\circ$) oppose the impregnation of water. This simple model has important implications for the wetting of rough surfaces: fluid that is not predisposed to wetting ($\theta_e > 90^\circ$) is even less likely to enter pore-like intrusions. Finally, we note that if the tube is tilted by an angle α relative to the vertical, the rise height remains the same, but the intrusion distance along the tube increases by a factor of $1/\cos\alpha$.

3.2 SURFACE ROUGHENING

If a solid surface is not smooth, the chemical contact angle θ_e will generally differ from that observed on a macroscopic scale, specifically, the apparent contact angle θ^* (Fig. 11). Moreover, the energetic cost of wetting will depend not only on the surface chemistry (which prescribes γ_{SG} and γ_{SL}), but also the surface roughness. The influence of surface roughness may be incorporated by reconsidering Eq. (5). If we define the roughness r to be the real surface area per planar area of the surface, then the energetic cost of contact line motion becomes

$$dW = r\ dx(\gamma_{SG} - \gamma_{SL}) - dx\ \sigma\cos\theta^* \tag{7}$$

The equilibrium condition, $dW/dx = 0$, when taken in conjunction with the Young's relation Eq. (4) then yields the relationship between the apparent and microscopic contact angles

$$\cos\theta^* = r\cos\theta_e \tag{8}$$

a result known as Wenzel's (1936) relation. If a surface is hydrophilic ($\theta_e < 90^\circ$), roughening will generally make it more so: the additional surface area exposed through roughening will make the surface all the more

TABLE 1 Contact angles in nature and technology

Substrate	Contact Angle θ_e	Advancing Angle θ_A	Receding Angle θ_R	Reference
Natural materials				
Human skin	91 +/−4			Elkhyat *et al.* (2004)
Beeswax	97			Pal (1951)
Human hair		103 +/−4		Lodge and Bhushan (2006)
Chitin (composes the insect cuticle)	105			Holdgate (1955)
Plants				
Water lily *Nymphaea*		68		Fogg (1948)
Wax palm (carnuba wax, same wax as lotus)		74 +/−8		Cheng and Rodak (2005)
Surface of a common weed *Plantago lancelota*		74		Holloway (1970)
Cherry laurel evergreen shrub *Prunus laurocerasus*		75		Fogg (1948)
Pine needles	105–115			Cape (1983)
with wax removed	79			Cape (1983)
Various plant waxes (from uroslic acid to *n*-Alkanes C_{18}–C_{36})	89–109			Holloway (1970)
Wild mustard plant *Sinapis arvensis*		96		Fogg (1948)
Isolated wax of a common weed *Plantago lancelota*		102		Holloway (1970)
Eucalytpus leaf *Eucalyptus globulus*, isolated wax		105		Holloway (1970)
surface		170		Holloway (1970)
Wheat germ *Triticum vulgare*		141		Fogg (1948)
Lotus leaf	160			Cheng and Rodak (2005)
Indian cress	180			Otten and Herminghaus (2004)
Birds				
Duck feather material, smooth		90	65	Cassie and Baxter (1945)
with roughness included	150			Cassie and Baxter (1945)
Uropygial gland oil (in aquatic birds)		90	60	Rijke (1970)
Mallard, breast		137	121	Elowson (1984)
Reed cormorant, breast		133	130	Elowson (1984)
feather shaft		155	146	Elowson (1984)
Insects				
Aquatic				
Water boatman *Notonecta glauca*, adult, wings		30		Pal (1951)
dorsal		180		Pal (1951)

Water bug *Naucoris cimecoides*, prothorax		90	56	Holdgate (1955)
Great diving beetle *Dytiscus marginalis*, elytra		90	10	Holdgate (1955)
Water scavenger beetles *Hydrobius*		87	0–50	Holdgate (1955)
Water scorpion *Ranatra linearis*, elytra		62	0	Holdgate (1955)
Emperor dragonfly *Anax imperator*, aquatic nymph		45	0	Holdgate (1955)
Damselfly *Coenagrion puellam*, aquatic nymph		35	0	Holdgate (1955)
Water bug *Naucoris cimicoides*, larva	110			Pal (1951)
Terrestrial				
Tick *Ornithodorus moubata*, dorsal		43–95		Pal (1951)
Aphid *Aphis*	62			Pal (1951)
Orb weaving spider *Mangora placida*, legs	74			Stratton *et al.* (2004a,b)
Cockroach *Periplaneta americana*, legs		67		Pal (1951)
ventral		77		Pal (1951)
dorsal		83		Pal (1951)
wings		85		Pal (1951)
elytra		106	91	Holdgate (1955)
Mealworm *Tenebrio molitor*, adult, elytra		107	92	Holdgate (1955)
Potato aphid *Macrosiphum*	106			Pal (1951)
Grain weevil *Calandra granaria*, larva	107			Pal (1951)
Spitting spider *Scytodes*, legs	100–112			Stratton *et al.* (2004a,b)
Common jumping spider *Phidippus audax*, legs	145			Stratton *et al.* (2004a,b)
Flying				
Blowfly *Calliphora erthrocephala*		175	155	Holdgate (1955)
Variable damselfly *Coenagrion puellam*, adult		175	170	Holdgate (1955)
Locust *Locusta migratoria*, prothorax, flanks		128	104	Holdgate (1955)
forewings		107	89	Holdgate (1955)
Garden tiger moth *Arctia caja*, dorsal, single hair	97			Pal (1951)
array	180			Pal (1951)
Mediterranean flour moth *Ephestia kuhniella* Zell	85			Pal (1951)
House mosquito *Culex pipiens*, *larva*, dorsal		180		Pal (1951)
ventral		180		Pal (1951)
legs		75		Pal (1951)
wings		95		Pal (1951)
Semiaquatic				
Whirligig beetle *Gyrinus marinus*		105	90	Holdgate (1955)

TABLE 1 (*Continued*)

Substrate	Contact Angle θ_e	Advancing Angle θ_A	Receding Angle θ_R	Reference
Fisher spider *Dolomedes triton*, legs	147			Stratton *et al.* (2004a,b)
Water strider *Gerris lacustris*, legs	168			Gao and Jiang (2004)
Larvae				
Cutworm *Polia oleracea*	18			Pal (1951)
Housefly *Musca domestica*	48–65			Pal (1951)
Cabbage moth *Mamestra brassicae*	18			Pal (1951)
Man-made materials				
Plexiglass (Polymethyl methacrylate)		63	41	Taylor *et al.* (1998)
Glass	42 +/−4			Slodowska *et al.* (1999)
Candle wax (parrafin), smooth	105–110			Pike *et al.* (2002)
rough	110–140			Zisman 1964
Teflon		120	118	Sabbatovskii *et al.* (2004)
Alkylketene dimer, smooth	109			Onda *et al.* (1996)
rough	174			Onda *et al.* (1996)
Fluorosilanated silicon, smooth		118	100	Bico *et al.* (1999)
Fluorosilanated silicon, decorated with holes		138	75	Bico *et al.* (1999)
stripes (parallel to motion)		143	125	Bico *et al.* (1999)
stripes (perpendicular to motion)		165	132	Bico *et al.* (1999)
spikes		170	155	Bico *et al.* (1999)
Fluoroalkylsilanated silicon, smooth	114			Yoshimitsu *et al.* (2002)
rough	153			Yoshimitsu *et al.* (2002)
Methylchlorosilanated silicon (Lichau's surface)	180	180	180	Gao and McCarthy (2006)

Note: On rough surfaces, the values correspond to the apparent contact angle θ^*. Measurement techniques are detailed in the accompanying references. Contact angles in each category are listed in roughly increasing order. Among the insects, contact angles are highest for the semi-aquatic creatures, then in turn for their flying, terrestrial and aquatic counterparts. Note that contact angle generally varies with body region. Data reproduced from Elkhyat *et al.* (2004), Pal (1951), Lodge and Bhushan (2006), Cheng and Rodak (2005), Holloway (1970), Fogg (1948), Cape (1983), Otten and Herminghaus (2004), Cassie and Baxter (1945), Rijke (1970), Holdgate (1955), Stratton *et al.* (2004a), Gao and Jiang (2004), Taylor *et al.* (1998), Slodowska *et al.* (1999), Pike *et al.* (2002), Sabbatovskii *et al.* (2004), Onda *et al.* (1996), Bico *et al.* (1999), Yoshimitsu *et al.* (2002), Zisman (1964) and Gao and McCarthy (2006).

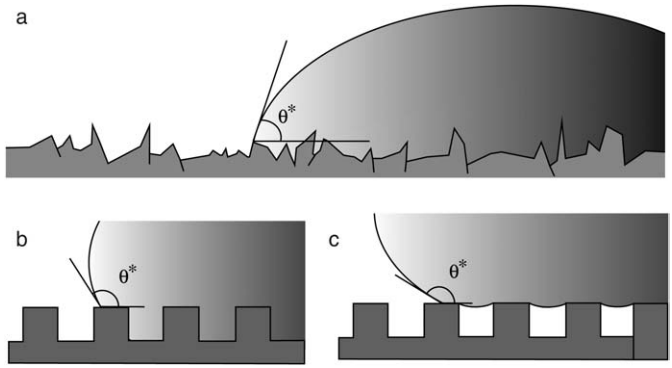

FIG. 11 Roughening a surface will amplify its wetting tendencies. In the randomly roughened surface in (a), the microscopic contact angle remains θ_e, but the observed contact angle on the macroscopic scale is θ^*. The two generic states of wetting, the Wenzel and Cassie states, are shown schematically in (b) and (c). In the Wenzel state (b), the pores are impregnated by fluid, increasing the fluid–solid contact. In the Cassie state (c), air pockets are trapped by the overlying fluid, reducing the fluid–solid contact.

attractive to the spreading liquid. Similarly, a hydrophobic surface ($\theta_e > 90^\circ$) will become all the more so when roughened (Cassie, 1948). This is a critical point when considered in the context of water-walking arthropods and their elaborate covering of micron scale hairs: if the surface of the insect cuticle had a contact angle $\theta_e < 90^\circ$, insects would be hydrophilic rather than hydrophobic. As we shall see in Section 4, their waxy surface coating generally ensures that $\theta_e > 90^\circ$ (Holdgate, 1955), so that their surface roughening encourages rather than discourages their water-repellency.

If the surface is sufficiently rough, air pockets are trapped between the liquid and solid and the Wenzel picture of wetting no longer applies. This scenario is described by the Cassie–Baxter model for a planar but chemically heterogeneous surface (Fig. 11c). We consider a planar surface tiled with two materials characterized by respective areal fractions f_1 and f_2 and contact angles θ_1 and θ_2. The motion of the contact line by an amount dx brings about a change in surface energy

$$dW = f_1(\gamma_{SG} - \gamma_{SL})_1\, dx + f_2(\gamma_{SG} - \gamma_{SL})_2\, dx - \sigma \cos\theta^* dx \qquad (9)$$

The equilibrium condition, in conjunction with Young's relation applied to both materials, yields the Cassie–Baxter relation

$$\cos\theta^* = f_1 \cos\theta_1 + f_2 \cos\theta_2 \qquad (10)$$

The apparent contact angle on such a surface is the mean of the contact angles in each region weighted by their areal fractions. If the tiled material

designated as 1 is air (contact angle $\theta_1 = 180^\circ$), the Cassie–Baxter relation yields

$$\cos\theta^* = -1 + f_S(1 + \cos\theta_e) \tag{11}$$

where f_S is the exposed area fraction of the solid substrate and θ_e is the contact angle of water on a planar solid substrate. The validity of this equation for fluid drops on a number of patterned surfaces was demonstrated by Bico *et al.* (1999). Note that as the area fraction of the solid $f_S \to 0$, the apparent contact angle approaches 180°. As we shall see in Sections 4 and 5, this Cassie–Baxter model is appropriate for describing the wetting by water of rough insect cuticle.

de Gennes *et al.* (2003) and Carbone and Mangialardi (2005) present criteria for the trapping of an air layer by a rough surface. In their 2D model, fluid contacting a rough surface characterized by sinusoidal undulations of amplitude a and wavelength $\lambda = 2\pi/k$ (Fig. 12) will remain in a Cassie–Baxter state provided

$$a > \frac{1}{2\pi}\lambda\tan\theta_e \tag{12}$$

where θ_e represents the equilibrium contact angle. In the limit of small amplitude roughness, $ka \ll 1$, the roughness is given by $r = 1 + \frac{1}{4}(ka)^2$, and the critical roughness beyond which trapping occurs is simply expressed

$$r_T = 1 + \frac{1}{4}\tan^2\theta_e \tag{13}$$

We note, however, the importance of three-dimensional (3D) effects on the wetting of corrugated surfaces in the presence of a gravitational field. Shuttleworth and Bailey (1948) considered the spreading of a liquid over a corrugated solid, specifically, a surface with a field of 2D grooves. By analogy with the case of a closed capillary tube, if $\theta_e < 90^\circ$, fluid will be drawn into the grooves with a force that increases inversely with the groove

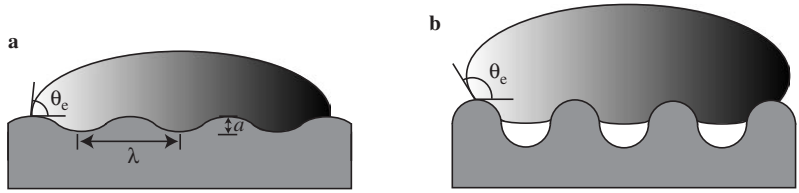

FIG. 12 Wetting on a sinusoidally varying surface with wavelength λ and amplitude a. (a) In the limit of small amplitude roughness, fluid fills the troughs of the sinusoid and a Wenzel state obtains. (b) If the roughness exceeds a critical amplitude defined by Eq. (13), air is trapped in the troughs, resulting in a Cassie–Baxter state.

width. Conversely, if $\theta_e > 90^\circ$, fluid will be expelled from the grooves, and complete wetting of the corrugated surface will be discouraged. A detailed investigation of rough wetting is presented by Bico *et al.* (2001).

The two different modes of wetting have been observed in both the plant and animal kingdoms. For reasons to be discussed in Section 3.4, the maintenance of a Cassie–Baxter rather than a Wenzel state (Fig. 11) is generally required for water-repellency. The water-repellent nature of the lotus leaf is attributed to its surface roughening (Barthlott and Neinhuis, 1997). Similar surface structures have been reported on a number of other plant leaves, including the rice plant (Feng *et al.*, 2002) and the lady's mantle (Mock *et al.*, 2005; Otten and Herminghaus, 2004) and in the animal kingdom on butterflies (Wagner *et al.*, 1996), beetles (Parker and Lawrence, 2001) and cicadae (Lee *et al.*, 2004). The common feature to most of these naturally occuring water-repellent surfaces is hierarchical roughness on two or more scales, the smallest being the sub-micron scale.

Bico *et al.* (1999) examine how surface roughening can be exploited to produce large contact angles on synthetic materials. Onda *et al.* (1996) produced a synthetic hydrophobic surface from an alkylketene dimer film that exhibited a static contact angle of 174°. The surface took a complex fractal-like form with several scales of roughness; owing to the heightened roughness of such surfaces, the cost of wetting can be enormous and the contact angle correspondingly high. The authors were able to rationalize the observed contact angles on the basis of the Cassie–Baxter relation (Eq. (11)) in conjunction with the theoretical predictions of Hazlett (1990) for the hydrophobicity of fractal surfaces. Herminghaus (2000) argues that roughness beyond a second scale is vital in the hydrophobicity of plant leaves. Indeed, he demonstrates theoretically that fractal roughness may generate water-repellency on solids with any finite contact angle, a conjecture demonstrated experimentally by Feng *et al.* (2003). de Gennes *et al.* (2003) note, however, that hydrophobic states generated by complex surface texturing of hydrophilic material are only metastable. It is worth noting that such engineered superhydrophobic surfaces generally rely on complex surface topography such as sharp corners (Oliver *et al.*, 1977; Carbone and Mangialardi, 2005) that are not typical of the piliferous cuticle of water-walking insects. Finally, the most water-repellent man-made surface is the recently developed 'Lichao's surface' (Gao and McCarthy, 2006), composed of a tangled network of 40 nm fibers that exhibits a static contact angle of 180°.

3.3 CONTACT ANGLE HYSTERESIS

While the concept of an equilibrium contact angle is useful conceptually, it is important to note that, for a given solid–fluid combination, a range of

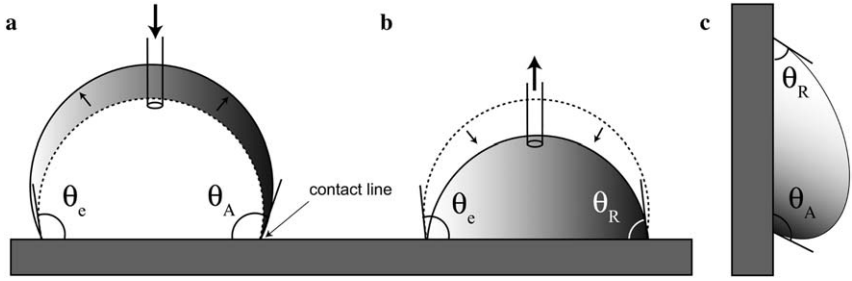

FIG. 13 Contact angle hysteresis. A drop of fluid at rest on a solid may exhibit a range of contact angles. (a) If a drop is filled with a pipette, it swells while remaining pinned at the contact line until the contact angle reaches a critical value, θ_A, at which the contact line advances. (b) If fluid is withdrawn from the drop, its contact angle decreases progressively until it reaches θ_R, after which the contact line recedes. The difference $\theta_A - \theta_R$ is known as the contact angle hysteresis. (c) Contact angle hysteresis is responsible for suspending drops on vertical windows. The largest drop that can be so supported is prescribed by Eq. (15).

static contact angles may be observed (Dettre and Johnson, 1964; Johnson and Dettre, 1964). Consider a drop of fluid emplaced on a solid. If the drop is filled, it will grow, and its contact angle increase progressively until reaching a critical value, θ_A, at which the contact line begins to advance (Fig. 13). If conversely, fluid is withdrawn from the drop, its contact angle will decrease progressively until reaching a critical value, θ_R, at which the contact line begins to recede. Observed static contact angles θ may thus lie anywhere within the range $\theta_A > \theta > \theta_R$, bounded above and below by the advancing and receding contact angles. This finite range is associated with microscopic surface imperfections that distort the advancing interface, thereby resisting contact line motion (Joanny and de Gennes, 1984; Nadkarni and Garoff, 1992).

The finite range of static values for a given three-phase system is referred to as the contact angle hysteresis

$$\Delta\theta = \theta_A - \theta_R \tag{14}$$

An important consequence of this hysteresis is that there is a concomitant force of retention F_r that causes droplets to adhere to surfaces: differences in the contact angle around the perimeter of a drop may result in a net contact force that resists its motion (Dussan, 1979; Extrand and Gent, 1990). For example, raindrops may stick to window panes because of the difference in the contact angles on their upper and lower edges (Fig. 13c; Dussan and Chow, 1983). For droplets with circular contact lines the retention force may be approximated by (Extrand and Kumagai, 1995).

$$F_r = \frac{\pi}{2} D \ \sigma (\cos\theta_R - \cos\theta_A) \tag{15}$$

where D is the diameter of the contact region. There is thus a maximum droplet size that can be supported by the retention force: drops bigger than a critical size (comparable to the capillary length) will roll down the windowpane under the influence of gravity. Values of $\Delta\theta$ for water on a number of naturally occuring and man-made substances may be computed from Table 1 via Eq. (14).

The dependence of contact angle hysteresis $\Delta\theta$ on surface roughness is subtle (Johnson and Dettre, 1964) and depends on whether a Wenzel or Cassie–Baxter state is obtained (Bico *et al.*, 1999, 2002; Lafuma and Quéré, 2003). In the Wenzel state arising at low surface roughness, surfaces exhibit high advancing contact angles and low receding angles relative to those on a flat surface; consequently, $\Delta\theta$ is greatly increased. On rougher surfaces in a Cassie–Baxter state, both advancing and receding contact angles are higher; the contact angle hysteresis is moderately reduced relative to that on a smooth surface, and greatly reduced relative to that in the Wenzel state. The maintenance of a Cassie–Baxter state is thus critical in reducing the force of adhesion, F_r, of water droplets on rough solids, and so is considered as important a criterion for water-repellency as a high contact angle.

Öner and McKarthy (2000), Extrand (2003) and Gao and McCarthy (2007) examine the influence of importance of surface architecture on the contact angle hysteresis. Extrand (2002) considers a uniform array of pillars of width d and spacing δ tilted at an angle ω relative to the surface normal (Fig. 14a), and argues that the contact angle hysteresis for such a surface may be simply expressed as the weighted mean

$$\Delta\theta = \frac{d}{\delta}(\Delta\theta_0 + \omega) \tag{16}$$

where $\Delta\theta_0$ is the contact angle hysteresis on a planar surface. Note that the contact angle hysteresis and so the force of retention may be decreased by

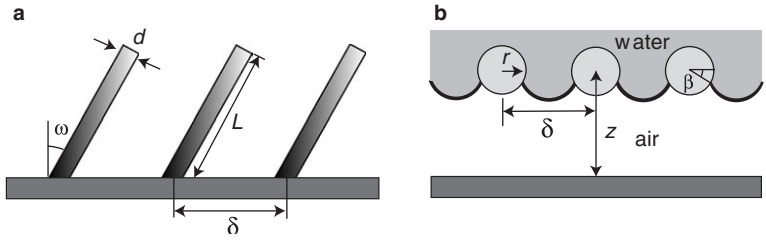

FIG. 14 Two geometries considered for the water-repellent hair pile. (a) A regular square array of cylindrical posts (either rectangular or cylindrical) of length L, width d and spacing δ are tilted at an angle ω relative to the vertical. (b) A regular array of horizontal cylinders of diameter r, spacing δ and height z above a horizontal substrate. The curved menisci, which intersect the hairs at a contact line lying at an angle β relative to the horizontal, protect the air layer from impregnation by the overlying water.

decreasing the size to spacing ratio of the pillars, and increased by increasing the tilt angle of the pillars. The dependence of the retention force on the topology of the substrate will be further discussed in the context of water-repellency in Section 3.4.

The contact angles of water on various plants and arthropods are listed in Table 1. The highest contact angles in the animal kingdom arise on water-walking arthropods, with θ ranges from 150° to 170°. The second group are the flying insects, whose survival depends on their ability to avoid or deflect raindrops; they exhibit contact angles between 90° and 170°. Third are terrestrial insects, with θ between 20° and 145°. Finally, aquatic insects prefer to remain wet when they surface and typically exhibit contact angles between 10° and 90°. We note that insect larvae do not generally have a waxy coating and so exhibit particularly low contact angles (Wigglesworth, 1950). In terms of contact angles, the integument of water-walking arthropods compares favourably with the most hydrophobic manufactured surfaces. Only Lichao's surface (Gao and McCarthy, 2006) achieves the ideal limit of perfect water-repellency $\theta_A = \theta_R = \theta^* = 180°$.

3.4 WATER-REPELLENCY

Water-repellency is a necessary adaptation for water-walkers. A creature of characteristic length L whose leg lies beneath the water surface can apply a maximum force that scales as L^2 (Alexander, 1985). If acting along its leg perimeter, the surface tension force that resists its leg crossing the interface scales as L, so the ratio of available muscular to curvature forces scales as L. Water striders are capable of penetrating the free surface (Perez-Goodwyn and Fujisaki, 2007). However, smaller creatures may be too weak to overcome curvature forces and it becomes a matter of survival that they do not wet, specifically, that they maintain a Cassie–Baxter state.

For a surface to be water-repellent, it must have two properties. First, it must resist impregnation of water. Second, it must exhibit minimal drop retention, so that when droplets strike the surface, they roll off rather than adhering. The wetting properties of rough solids have been shown to be hysteretic in a variety of settings. The hydrophobicity of certain plant leaves can be lost if the plant is submerged in water for an extended period (Herminghaus, 2000), and the same has been observed for a number of insects (e.g. Holdgate, 1955). Once the surface roughness has been impregnated with water, in the absence of evaporation it will remain so indefinitely unless subjected to high pressures. Owing to contact angle hysteresis, the required evacuation pressure generally exceeds the impregnation pressure (Adam, 1948). These observations make clear the importance of the insects remaining in a Cassie–Baxter rather than Wenzel state: the transition from one to the other is accompanied by a transition

from hydrophobic to hydrophilic states. Clear observational evidence of the air layer trapped in the integument of water-walking insects will be provided in Section 6.

For a rough solid to resist fluid impregnation, the curvature pressures generated by the interface that spans its roughness elements must be larger than any applied pressures. The magnitude of such curvature pressures depends critically on the geometry of the surface roughening (Lafuma and Quéré, 2003). A number of simple geometries have been considered experimentally. Patankar (2004) considers the influence of the weight of a dropet on its transition from a Cassie–Baxter to a Wenzel states when placed on a square array of rectangular posts. Journet *et al.* (2005) considered flow in the vicinity of a surface covered with a carbon nanotube forest, a regular array of vertical cylinders rolled from sheets of carbon atoms (Lau *et al.*, 2003). They demonstrate that the intrusion into a substrate with characteristic roughness scale δ by a surface with tension σ and equilibrium contact angle θ_e can be forced by a pressure of characteristic magnitude

$$\Delta P \sim \frac{2\sigma}{\delta}\cos\theta_e \tag{17}$$

with a slight correction required to account for the finite amplitude of the roughness. Note that this observation may be understood on the basis of Eq. (6) by viewing the space between the roughness elements as simple capillary tubes. Reyssat *et al.* (2006) and Bartolo *et al.* (2006) considered forced wetting of a surface decorated with pillars of height h spaced a distance δ apart, and demonstrated that when $h/\delta \ll 1$, the impregnation pressure is reduced by a factor of h/δ.

With the wetting of insect cuticle in mind, Thorpe and Crisp (1947a) and Crisp and Thorpe (1948) calculate the impregnation pressures required to force fluid through various arrangements of cylinders on a horizontal surface. They first considered a square array of vertical cylinders of diameter $d=2r$ and uniform spacing δ tilted at an angle ω relative to the vertical (Fig. 14a). Not surprisingly, they concluded that the impregnation pressure is maximized by decreasing the spacing of the array. Moreover, they found that impregnation pressures increases with ω: by reducing the free space between the cylinders, tilting the pillars serves to promote water-repellency. A similar conclusion was drawn by Extrand (2004) in his calculation of the impregnation pressure of a square array of square pillars: tilting the pillars enhances water-repellency. Thorpe and Crisp (1947a) and Crisp and Thorpe (1948) also considered a horizontal array of cylinders (Fig. 14b), and concluded that such an arrangement of may provide water-proofing for any $\theta_e > 0$. The horizontal arrangement of cylinders provides greater resistance than the tilted array: fluid impregnation between the horizontal cylinders requires the production of maximum surface area

and so maximum surface energy. For any such arrangement of cylinders (vertical, tilted or horizontal), the smaller the scale of the surface structure, the greater its effect on water-repellency: the impregnation pressure is generally inversely proportional to a characteristic length scale of the hair pile. Extrand (2006) notes that while tilting the pillars increase a rough surface's resistance to fluid impregnation, according to Eq. (16) it simultaneously increases the force of drop retention. Moreover, for a fixed spacing δ, while increasing the pillar size increases the surfaces resistance to impregnation, it increases the force of retention that acts along the drop perimeter.

4 Insect cuticle

As detailed in Section 3.2, the degree of wetting of a solid by a liquid is determined by both the material properties and the topography of the solid surface (de Gennes *et al.*, 2003). Surface roughening has long been used as a means of rendering a solid effectively non-wetting (Cassie, 1944, 1948; Adam, 1963): through increasing the contact area, one increases the energetic cost of wetting, and so encourages a non-wetting situation. We proceed by describing the form of insect integument to rationalize its water-repellent properties and elucidate its role in propulsion.

4.1 COMPOSITION

Wigglesworth (1979, 1984) and Hadley (1981) review studies of the form and function of insect cuticle, the outermost layer adjoining the epidermal cells. Insect cuticle is composed of a chitin–protein complex, and covered with a layer of epicuticular wax that serves to discourage the penetration of water. Insect cuticle consists of three layers, each with a distinct function. The bulk of the cuticle is the innermost endocuticle, which allows for the flexibility and extensibility required for movement, and the increases in bulk that accompany feeding. A hard exocuticle provides rigidity to some regions, such as the head. The outermost layer, the waxy epicuticle, is responsible for waterproofing and the prevention of dessication. Reviews of the chemistry of insect waxes are provided by Blomquist and Jackson (1979) and Howard (1993).

Holdgate (1955) reports the presence of a 0.25-μm-thick waxy or greasy layer (lipids such as hydrocarbons and esters) on the insect cuticle, and estimates its effect on the wetting of the cuticle by applying wax solvents that dissolve the layer. The presence of this waxy layer has long been known (Kühnelt, 1928; Wigglesworth, 1933) and Wigglesworth (1945) demonstrated its importance not only in water-proofing the insect, but in

water-retention: removing the wax layer of insects lead to their rapid dessication. The asymmetry of insect cuticle with respect to water permeability was considered by Hurst (1941, 1948), who concluded that the cuticle provides a greater impediment to outgoing than incoming water, a critical feature for desert beetles (Hadley, 1978, 1979). Beament (1945, 1948) reports that the wax layer thickness is remarkably constant, 0.2–0.3 μm for a great many insects, and suggests that this is the minimum thickness capable of providing maximum water-proofing. The wax layer can be removed by gently rubbing with an abrasive dust; if the insect is then exposed to dry air, it quickly dies; if exposed to moist air, the insect can secrete a fresh layer of wax and so restore its waterproofing. Wigglesworth (1984) reported that the wax layer of burrowing insects is so worn that they cannot survive in dry air.

The cuticle typically has numerous irregular structures such as hairs, scales and regions of varying curvature, all of which make the contact angle highly variable (Pal, 1951). Pal (1951) and Holdgate (1955) conducted comparative studies of the wetting properties of many terrestrial, semi-aquatic and aquatic insects, and concluded that terrestrial insects are generally hydrophobic and lipophilic (wetted by oil), while the aquatic species are often both hydrophilic and lipophilic. Key exceptions include plastron-bearing aquatic creatures such as the backswimmer *Notonecta* (Fig. 28) to be considered in Section 5.2. Contact angle hysteresis was documented; moreover, the contact angle was found to be a function of humidity, time after moulting and time after submergence in water. Pal (1951) noted the dependence of wetting properties on body part: generally, the legs and antennae are more wettable than the wings. Pal (1951) also measured the contact angles on individual insect hairs by spraying them with microdroplets generated by an atomizer. He demonstrates that the hairs of some terrestrial and aerial insects are sufficiently flexible to be drawn together by drops of water clinging to them. The flexibility of the cuticle of water-walking insects has only recently been confirmed experimentally (Bush and Prakash, 2007) and will be further discussed in Section 4.3. The contact angles of water on many terrestrial and aquatic insects are listed in Table 1.

4.2 MORPHOLOGY

Dufour (1833) was the first to note the importance of the microstructure of the leg-coating for water-walking insects: 'their legs are covered with a very fine velvet that is impermeable and gives these insects the ability to stand or run on water without getting wet.' The characteristics of the hair layer of many water-walking arthropods have been established using macrophotography and scanning electron microscopy. Some qualitative features of the

insect cuticle and its interaction with the free surface can be elucidated with macrophotography. The legs, bodies and antennae of the water-walkers are covered with hairs that reflect light to provide a colourful glossy sheen (Fig. 1; Gu *et al.*, 2003). The hair mats of *Mesovelia* and *Microvelia* are apparent in Fig. 15, while that of the fisher spider is evident in Fig. 16. Close-up images show that when a water-walking arthropod resides at rest on the free surface, its leg hairs appear as spokes whose tips abutt the free surface; therefore, a Cassie state is maintained.

Traditional microscopy techniques can be used to image the interaction between water droplets and the cuticle of water-walking arthropods. Stratton *et al.* (2004b) assessed the wetting properties of 25 species of terrestrial and semi-aquatic spiders by examining the contact angle of water microdroplets on individual hairs and on the hair pile. They found that the Fisher spider, which spends the bulk of its life on the water surface, exhibits substantially higher apparent contact angles θ^* than do its terrestrial counterparts, owing to its relatively large hair densities and chemical contact angles (Fig. 17). A number of their observations concerning the morphology of spider cuticle are reported in Tables 1 and 2.

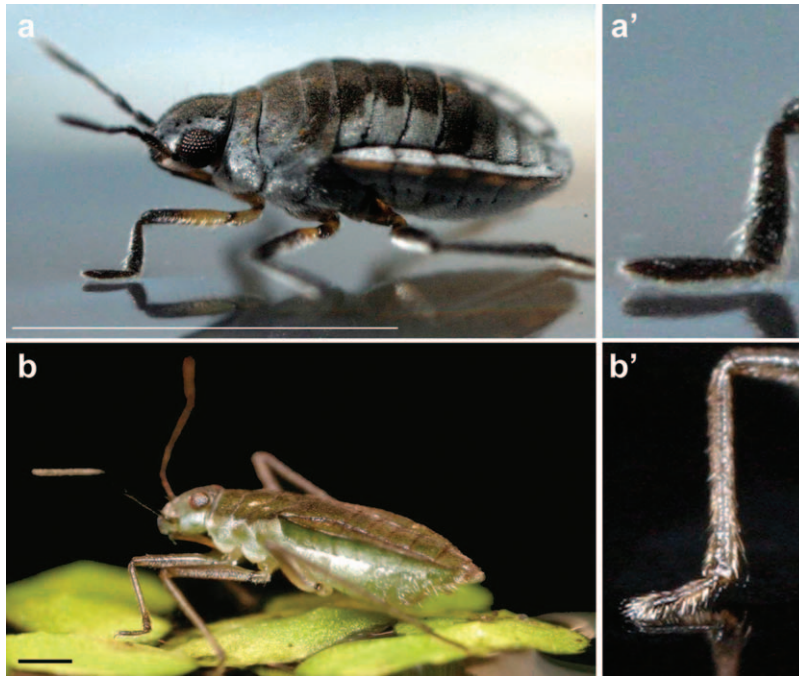

FIG. 15 The dense hair layer of two water-walkers: (a) *Microvelia* and (b) *Mesovelia*. Close-up images of their driving legs are given at right. Scale bars, 1 mm.

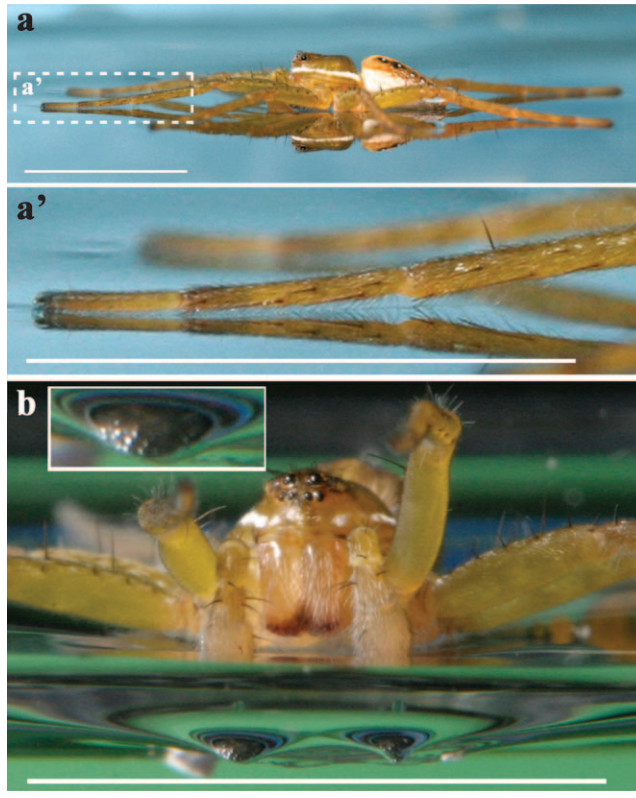

FIG. 16 The fisher spider on the free surface. (a) Hairs protrude from the leg and abut the free surface. In (b), the inset shows a magnified view of the dimpled surface deformation generated by the array of hairs. Scale bars, 1 cm.

Scanning Electron Microscopy (see Section 6.1) was first used to image the cuticle of water-walking insects by Cheng (1973), who considered freshwater and marine water striders. Subsequently, Andersen (1977, 1982) examined a wide range of semi-aquatic bugs under an electron microscope and provided detailed characterizations of their hair cover. Their studies provide fine detailed images of the hair pile, as well as the orientation and microstructure of the individual hairs. A hair map of the water strider is presented in Fig. 18; close-ups at locations numbered 1–6 are provided in Figs. 19–21. Fig. 19 depicts Scanning Electron Microscope (SEM) images of a water strider head, forelegs, flank and leg joint, virtually all of which are covered in hair.

Figure 20 indicates the form of the water strider's leg hair. The hairs are typically 30 μm long, tapering to a point from a 1-μm-diameter base,

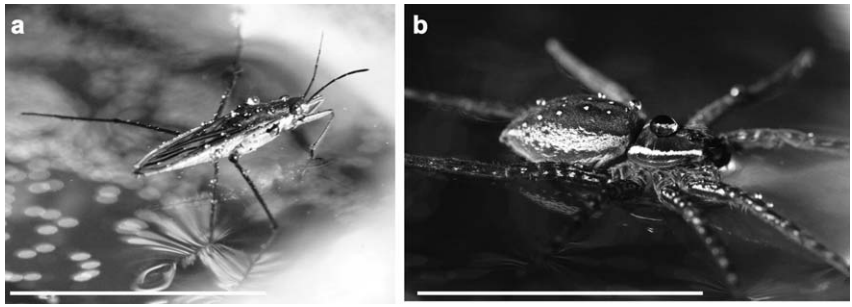

FIG. 17 Pearl drops generated by a fine water spray impinging on (a) the water strider and (b) the fisher spider. Their dense hair carpet is water repellent as indicated by the high contact angle of the droplets. Once wet, the water strider may dry itself by grooming or flipping over on its back: failing that, it can wait for the droplets to evaporate. Scale bars, 1 cm.

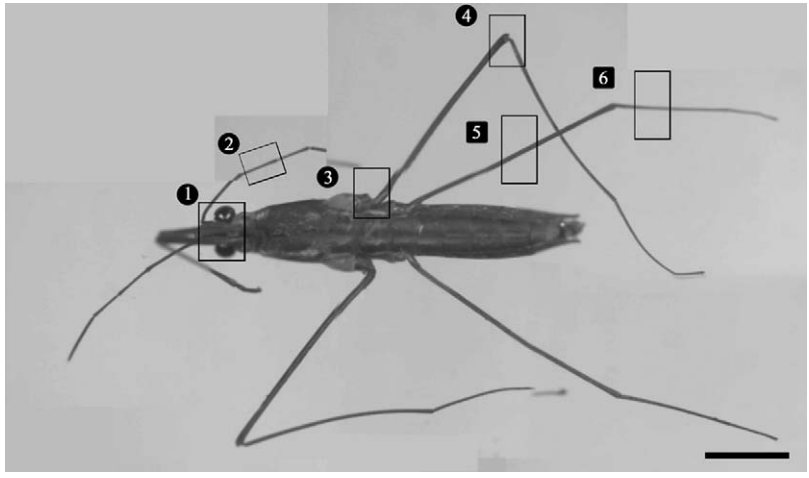

FIG. 18 A composite of photomicrographs of the adult water strider: a map indicating the origins of the SEM images presented in Figs. 19–21. Close-ups of regions 1–4 are displayed in Fig. 19 and of 5–6 in Fig. 20. Scale bar, 2 mm.

and inclined at an angle of $\sim 30^{\circ}$ to the underlying leg surface, forming a layer 10 μm thick. These hairs, termed macrotrichia, point in the direction of the leg tip, and bend inwards at their tips so as to lie roughly tangent to the leg and water surface. The hair density varies along the leg: the density is 4–6000 hairs mm^{-2} on the front tarsus, 12–16 000 mm^{-2} on the middle tarsus and 8–10 000 mm^{-2} on the hind tarsus (Andersen, 1977). The higher density on the middle tarsus might be anticipated on the grounds that it is

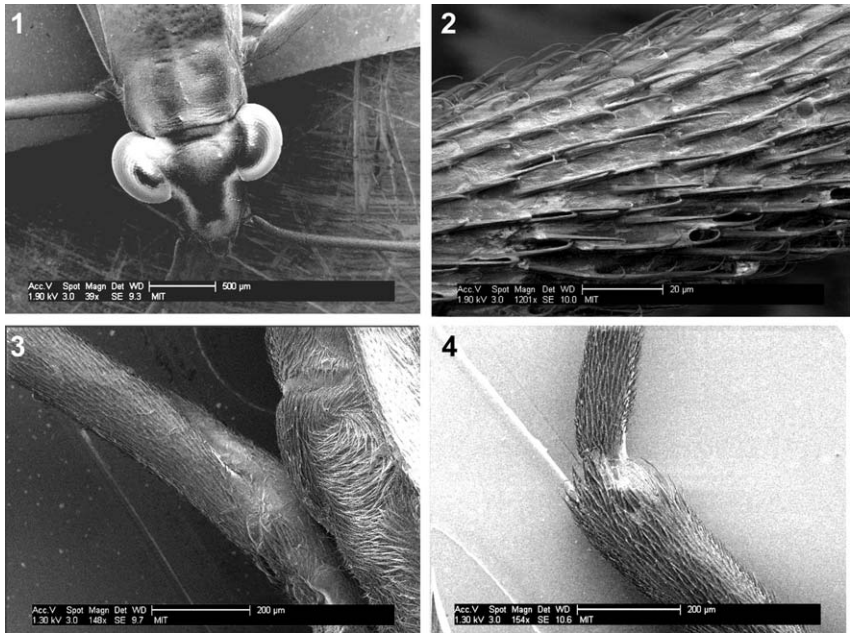

FIG. 19 Scanning electron microscope images of the water strider's (1) head, (2) antenna, (3) flank and (4) leg joint at locations indicated on Fig. 18. The great majority of the strider's body is covered with hair to repel water.

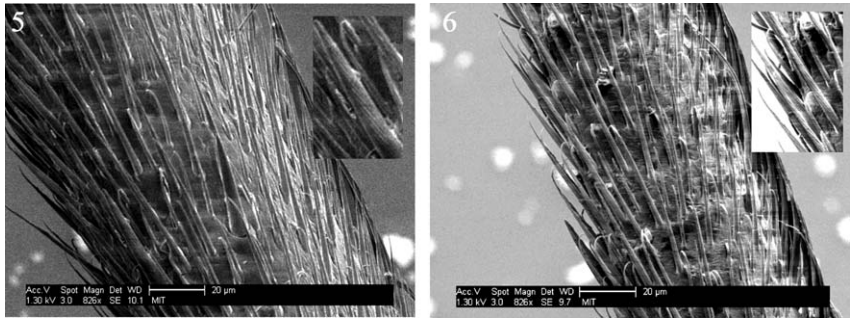

FIG. 20 Scanning electron microscope images of the strider's leg at locations (5) and (6) indicated on the hair map (Fig. 18). The insets reveal the nano-grooves on the hair surface (for a closer look, see Fig. 21). Note that the hair tips are bent inwards towards the leg, which discourages their piercing the water surface.

used for rowing and must therefore sustain higher dynamic pressures than the front and hind tarsi. Individual macrotrichia are covered in nano-grooves, roughly 400 nm wide and 200 nm deep, aligned with the direction of the hair (Andersen, 1977; Gao and Jiang, 2004; Fig. 21). On the thorax,

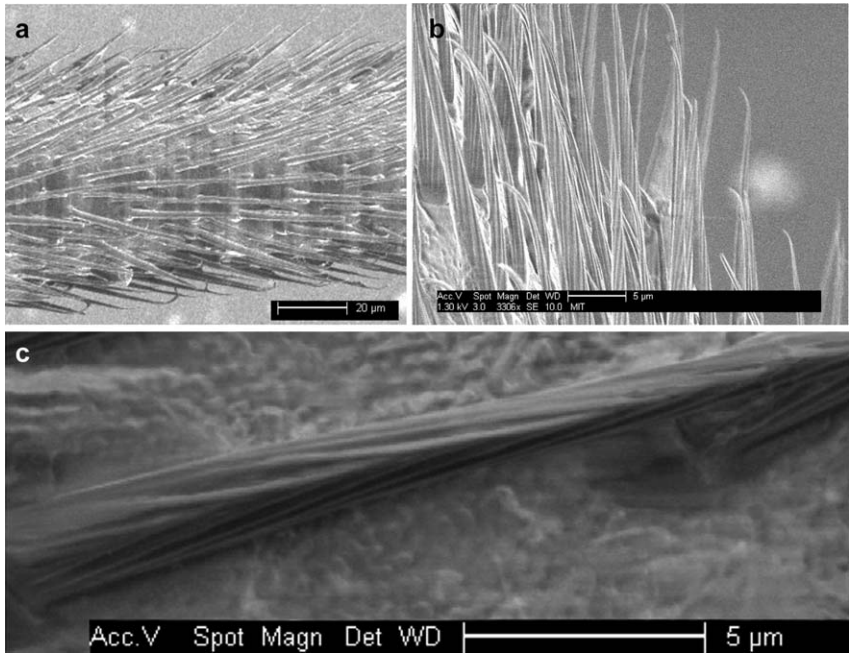

FIG. 21 SEM images of the hair layer of the water strider leg. (a) While the leg has thickness comparable to that of a human hair, it resembles a brush, whose thick carpet of hairs are tilted at $\sim 30^\circ$ relative to the leg surface. Hairs are typically 30 μm long, 1–3 μm thick at the base and tapered; their density is 12 000–16 000 hairs mm^{-2}. (b) A closer view of the hairs shows that their tips are bent inwards, towards the leg; moreover, each hair is patterned with grooves of characteristic width 400 nm that run its length, (c). Note that the leg surface at the roots of the hairs, evident in (c), is patterned with isotropic roughness reminiscent of plant cuticle.

in addition to the macrotrichia, there is an inner layer of microtrichia (Cheng, 1973; Andersen, 1977; Andersen and Cheng, 2004), whose purpose is to trap a layer of air and so permit respiration in case of submergence (see Section 5.2). While these are not as orderly as the macrotrichia, Cheng (1973) notes that for the sea-going Hemiptera, these hairs are also curved at their tips to lie tangent to the free surface. Andersen (1977) notes that their disorder and tangling may provide structural support against hydrostatic pressures during times of submergence. Finally, Fig. 22a depicts the smooth hydrophilic ungue present at the water strider leg tip.

Holdgate (1955) measured the static contact angle of water on cuticle wax, finding a value of $\theta_e = 105^\circ$. Gao and Jiang (2004) measured the static contact angle of water on a water strider leg, and report a value of $\theta^* = 167^\circ$. This large value was explained by considering the two scales of roughness on the strider leg; specifically, the 20-μm-scale roughness

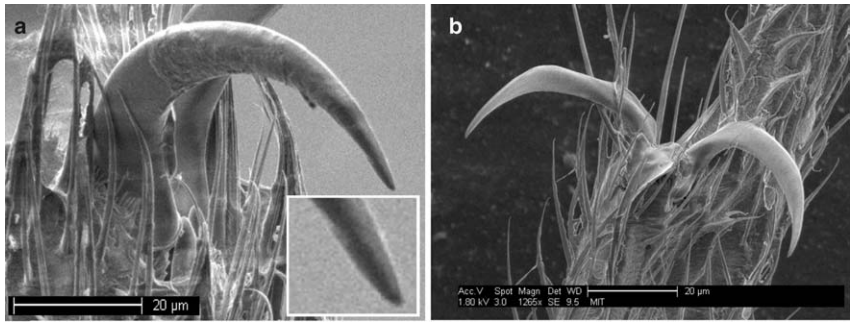

FIG. 22 The ungui at the leg tips of (a) the water strider and (b) *Microvelia*. Water striders may use their ungui to anchor themselves on the free surface against the wind. *Microvelia* use their ungues to grasp and lift the free surface to generate the lateral capillary forces used to climb menisci (Fig. 9b). The inset shows that, unlike the grooved hairs (Fig. 21), the ungui are smooth.

associated with microsetae, and the 100-nm-scale roughness associated with the nanogrooves on the microsetae. On the basis of the Cassie relation (Eq. (11)), the authors inferred that the solid fraction on the rough strider surface is merely $f = 3.14\%$. Feng *et al.* (2007) apply Cassie's Law to estimate 120° for the static contact angle required on smooth microsetae to rationalize the high apparent contact angle of $\theta^* = 167°$. Again using Cassie's relation, and the geometry of the nanogrooves (characteristic width and depth of, respectively, 400 and 200 nm), they find that the inferred 120° is consistent with the $\theta_e = 105°$ measured by Holdgate. They thus conclude that not only the microsetae but their nanogrooves are critical to achieving the high apparent contact angle on water strider legs.

We also conducted equivalent SEM imaging studies of *Microveia*, whose body hair is responsible for its sheen (Figs. 1a and 15b). The characteristic smooth, tapered horns of the two-pronged ungui are evident at the leg tip (Fig. 22b). The images in Fig. 23 depict the form of the body hair present on the tarsi and thorax. 20-μm-long hairs tilted at $\sim 45°$ are apparent on the tarsus (Fig. 23a). The hair density is significantly less than that on water strider legs. As on the strider, two distinct hair types are evident on the thorax: the relatively long and thick macrotrichia, and the inner layer of microtrichia (Fig. 23b). The macrotrichia are typically 20 μm long, 1 μm wide and curved so that their tips are roughly parallel to the body surface. The microtrichia are typically 2 μm long, 100 nm wide and more randomly oriented. Note the peg plates (that cover the spiracles through which the insect breathes) nestled in the microtrichia (Fig. 23c). Our scans also reveal the first evidence of nanogrooves on the macrotrichia of *Microvelia*, of characteristic width 200 nm and depth 50 nm (Fig. 23b). This new

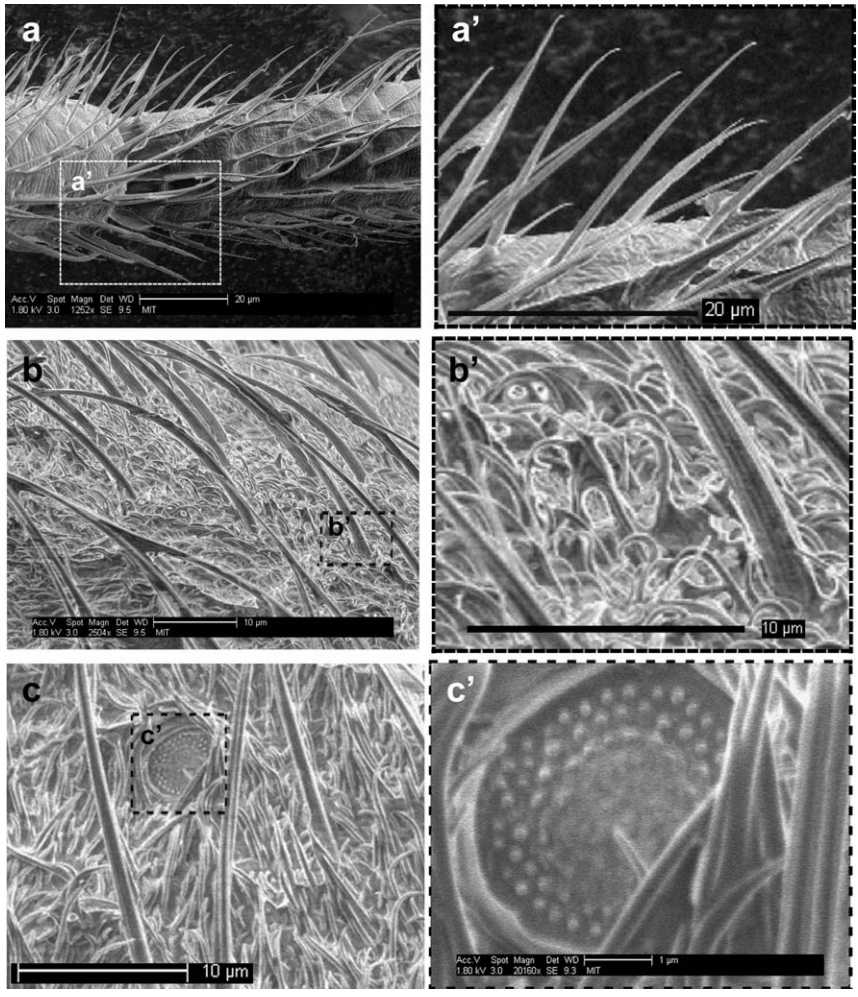

FIG. 23 SEM images of the hairy surface of the water treader *Microvelia*. (a) Leg hairs. In the magnified view (a′), the hair tips are bent inwards, which again discourages their penetrating the water surface. Evident in (a′) is the roughness of the leg surface to which the hairs adjoin, which may also play a role in water-repellency. (b) Body hairs: macrotrichia emerge from a tangle of microtrichia. (b′) Makes clear the grooves on the macrotrichia. The smaller-scale microtrichia twist and bend around one another for support (Andersen, 1977). (c) Among the microtrichia are the peg plates (c′) that cover the spiracles through which the insects breathe. Note that the surface of the peg plate has bumps reminiscent of the isotropic roughness on the lotus leaf.

observation indicates that these grooves are not peculiar to the water strider but may instead be a common feature on the macrotrichia of water-walking arthropods. Figure 6 is a cartoon depiction of the surface structure of *Mesovelia*.

The characteristics of the hair piles of other water-walking arthropods are reported in Table 2. The geometry of the hair layer is similar in nearly all water-walkers, but the hair density η varies among species, with the faster species generally having higher hair density. Included in Table 2 are estimates of the contact widths w_c along the tarsi of various water-walkers. The insect's weight is supported by the surface forces that act around the contact lines on its individual hairs. w_c corresponds to the width of the contact region required for the contact forces on the hairs to support the insect's weight: $w_c \sim 2\mathrm{Ba}/(\pi\eta d)$. Note that the contact width decreases with increasing hair density and tarsi length, but increases with insect weight. The extent of the observed contact widths of several water-walking arthropods will be rationalized in Section 6.2.

4.3 STABILITY

An important aspect of the insect cuticle is its stability (Crisp, 1950): if the hair is sufficiently flexible, it may bend or twist under the combined influence of curvature, van der Waals or electrostatic forces. Hair distortion will necessarily lead to gaps in the hair covering, which represent points of weakness in terms of fluid impregnation. Crisp (1950) studied the stability of an air layer bound by uniformly spaced horizontal hairs on a horizontal surface (Fig. 14b) and subjected to a uniform external pressure. He found that if the spacing is varied, hairs in regions with greater spacing may be deflected downwards by the pressure gradient. Moreover, he found that the force of capillary attraction between adjacent hairs (see Section 2.3) may lead to an instability characterized by the clumping of hairs. In the absence of a resistance to bending that maintains the positions of the hairs, the air layer would thus be intrinsically unstable. Thorpe and Crisp (1946, p. 262) considered the stiffness of the hairs, and so assessed their stability to buckling. For the case of *Alphelocheirus*, the air layer is observed to collapse through wetting when subjected to a pressure of 3 atm corresponding to a depth of 30 m. Thorpe and Crisp (1947a) suggest that this collapse results from the buckling of the hairs; however, Hinton (1976) calculates that the hairs should be stable to buckling at 40 atm, advocating the physical picture of effectively rigid cuticle hairs.

The maximum curvature force that can exist between two hairs will arise if they are spanned by a capillary bridge (Rabinovich *et al.*, 2005), in which case a capillary force per length 2σ will draw them together (Fig. 24). van der Waals forces are known to be responsible for strong dry adhesion of gecko setae to smooth surfaces (Autumn *et al.*, 2002) and bundling in carbon nanotube forests (Liew *et al.*, 2005). At nanometre length scales, van der Waals forces become relevant and can be responsible for the sticking of dust particles on the hair surface (Persson, 2003). Electrostatic forces arising from the development of friction-induced charges on the cuticle of honey

TABLE 2 Properties of common water-walking insects and their hair coats

				Strider		*Mesovelia*		*Hydrometra*	*Microvelia*	Fisher Spider
I Macroscopic properties	M	Mass	mg	4.5		3.2		1.8	0.1	350.0
	U	Leg speed	$\mathrm{cm\,s^{-1}}$	37.0		15.9		9.7	10.3	35.0
	w	Leg width	μm	102		68		52	41	1500
	h	Rowing leg length	cm	1.40		0.60		0.80	0.80	0.50
	P	Leg contact perimeter	cm	2.5		0.4		0.5	0.1	10.0
		Hair type		Macro	Micro	Macro	Micro	Macro	Macro	Macro
II Microscopic properties	η	Hair density	$\mathrm{hairs\,cm^{-2}} \times 10^5$	14.0	800.0	4.0	600.0	2.5	5.0	2.5
	d	Hair width	μm	1.5	0.6	5.0	0.5	5.0	1.5	6.5
	L	Hair length	μm	30	7.0	15	3.0	15	25	300
	ω	Tilt angle	degrees	30–50	NA	50	NA	90	50	NA
	δ	Hair spacing	μm	7.0	0.5	10.8	0.8	15.0	14.3	13.5
III Dimensionless groups	$Re_\delta = U\delta/v$	Reynolds		2.6	0.2	1.7	0.1	1.5	1.5	4.7
	$We_\delta = \rho U^2\delta/\sigma$	Weber	$\times 10^2$	1.3	0.1	0.4	0.03	0.2	0.2	2.3
	$Bo_\delta = \rho g h\delta/\sigma$	Bond	$\times 10^{-3}$	2.9	1.1	4.1	0.4	5.4	0.2	4.4

	$Ba = Mg/(\sigma P)$	Baudoin		0.02	NA	0.12	NA	0.05	0.02	0.49
	$r = (1+\eta\pi DL)$	Roughness		3.0	11.6	1.9	3.8	1.6	1.5	16.3
	$G = d^3/(32L^2L_e)$	Elasticity/curvature		12	14	1736	43	1736	NA	NA
IV Calculated values	$P^* = 1+\sigma/\delta$	Impregnation pressure	atm	1.10	2.37	1.07	1.90	1.05	1.05	1.05
	$U_w = (2\sigma \cos \theta_e/(\rho\delta))^{1/2}$	Wetting speed	cm s^{-1}	223	818	179	662	152	156	160
	$Z_w = \sigma\cos \theta_e/(\rho g\delta)$	Wetting depth	cm	25	342	16	224	12	12	13
	$w_c = 2Ba/(\eta\pi d)$	Predicted contact width	μm	0.76	0.03	3.67	0.24	2.39	1.34	19.26

Note: These measurements are gathered from our own SEM study, Hu and Bush (2008a,b), Andersen (1976, 1977, 1982) and Stratton *et al.* (2004a). In general, the fastest creatures have the highest hair density: the water strider has the highest hair density and is the most water-repellent. In II–IV, both types of body hair are considered, the macrotrichia present over the bulk of the body, and the microtrichia present on the thorax. The pressures, speeds and depths sustainable by the cuticle are reported for each of the insects, along with the inferred contact width required for their weight support. In these calculations, θ_e was taken as 105°.

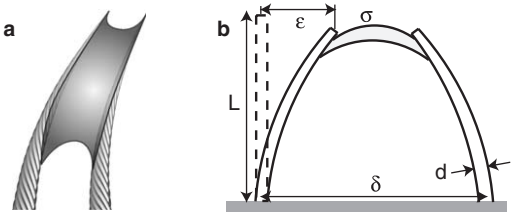

FIG. 24 (a) A schematic illustration of a capillary bridge between two flexible hairs. The resulting contact force will draw the hairs together, jeopardizing the water-repellency of the insect. (b) Definitions of the simple theoretical model of a capillary bridge between elastic rods. The cylindrical rods have diameter d, undeformed length L and are displaced a distance ε at their tips due to the capillary bridge.

bees have been shown to enhance transfer of pollen grains from the flower (Vaknin *et al.*, 2000). Grooming, as is commonly used by most water-walking insects to clean themselves, can generate static-electric charges on the insulating body surface of the insects, resulting in electrostatic repulsion or attraction between hairs.

The following relations provide the relative magnitude of characteristic van der Waals and electrostatic forces to capillary forces expected to arise on insect cuticle:

$$\frac{\text{van der Waals}}{\text{capillary}} \sim \frac{Hd}{\sigma\delta^3} \sim 10^{-12} \tag{18}$$

$$\frac{\text{electrostatic}}{\text{capillary}} \sim \frac{Kq_0^2 d^2 L^2}{\sigma\delta^3} \sim 10^{-13} \tag{19}$$

where d and L are the hair diameter and length, δ the average distance between hairs, $H = 10^{-20}$ J the Hamaker constant, $K = 9 \times 10^9$ Nm^2 C^{-2} the Coulomb force constant and q_0 the average electrostatic charge per unit area on the hair. Choosing typical values for the width, length, hair distance from Table 2 ($d \sim 1\,\mu$m, $L \sim 30\,\mu$m, $\delta \sim 10\,\mu$m) and a charge per unit area of $q_0 = 10^{-8}$ cm^{-2} (the maximum charge sustainable by a bumble bee in flight; Vaknin *et al.*, 2000), indicates that the leg hairs are dominated by curvature forces.

The greatest danger posed to the regular array of hairs comprising the insect cuticle are thus the curvature forces generated by capillary bridges spanning the hairs (Fig. 24). The stability of the hair layer will thus be determined by the relative magnitudes of the hair's resistance to bending and these destabilizing curvature forces.

$$G = \frac{\text{elastic resistance}}{\text{capillary}} \sim \frac{1}{32}\frac{d^3}{L^2\ell_e} \tag{20}$$

where $\ell_e = \sigma/E$ is the elastocapillary length and E the Young's modulus (Bico *et al.*, 2004). Substituting values for the width, length and Young's modulus ($E \sim 10^{11}$dynes cm^{-2}) of the insect hair (Hinton, 1976) suggests $G \sim 10$. The calculation of torsional stiffness is similar and has been examined by Dechant *et al.* (2001).

This crude scaling argument would seem to bring into question the conclusion of Hinton (1976) that the hairs are effectively rigid under the influence of capillary forces. If the hairs become sufficiently long and thin, capillary forces may pose an appreciable danger to the stability of the cuticle. Note that the hairs taper at the tip, where curvature forces are thus likely to cause appreciable deformation. Bico *et al.* (2004) and Kim and Mahadevan (2006) considered the capillary clumping of a series of elastic threads or sheets hanging through a horizontal free surface, and deduced criteria for the resulting elastocapillary instability. The authors define an elastocapillary length, $\ell_e = \sigma/E$ at which capillary forces become comparable to elastic forces. Using the value suggested by Hinton (1976) and Dechant *et al.* (2001) for the Young's modulus of insect cuticle, $E = 10^{11}$dynes cm^{-2}, indicates an elastocapillary length of 10^{-2} nm. While one thus does not expect the clumping of cuticle hairs poking through the surface, hair flexure may still arise. Figure 30 illustrates the interaction of the driving leg of a water strider and a 500 μm droplet moving along its length. Note that individual hairs are deflected by the contact forces associated with the advancing interface, then snap back into position once it has passed (Bush and Prakash, 2007). As we shall see in Section 7, the flexibility of the insect cuticle poses not only dangers but benefits to water-walking arthropods.

5 Function

We proceed by describing the principle functions of insect cuticle, in an attempt to rationalize its form. In Section 5.1, we consider the two types of body hairs discernible on water-walking creatures, respectively, macro- and microtrichia and their distinct roles in maintaining water-repellency. In Section 5.2, we consider the plastron, the air layer trapped on the body surface when an insect is submerged. In Section 5.3, we consider the ungui, the hydrophilic leg tips present on many water-walkers. Finally, in Section 5.4, we discuss the dynamic role of the insect cuticle in thrust generation and drag reduction.

5.1 WATER- AND RAIN-PROOFING

As we noted in Section 3.4, there are in general two criteria for water-repellency. The first is resistance to fluid impregnation while the second is

the resistance to adhesion by droplets. Thorpe and Crisp (1947c, 1949) distinguished between the two in the context of water-faring insects, and referred to them as, respectively, water- and rain-proofing.

To be waterproof, the insect cuticle must maintain a layer of trapped air, thereby retaining a Cassie–Baxter state. Doing so requires that the curvature pressures exceed all fluid pressures acting to cause impregnation. Of particular interest to water-walking arthropods are the hydrostatic pressures that they face if submerged and the dynamic pressures generated by their leg stroke or the impact of raindrops. The fluid pressure in a standing body of water in a static fluid increases with depth from the surface z as $P_0 + \rho g z$, where P_0 is atmospheric pressure, ρ the density of water and g the acceleration due to gravity. Roughly speaking, the hydrostatic pressure $\rho g z$ increases by 1 atm every 10 m. For a submerged hydrophobic body to stay in the Cassie–Baxter state, the curvature pressures generated along its surface must be sufficient to overcome the hydrostatic pressures. If the surface roughness is characterized by a single length scale δ (e.g. hairs of length and radius δ with a spacing δ), then, according to Eq. (17), the water-repellency may be preserved down to a critical depth, the wetting depth Z_w, defined by the balance: $\rho g Z_w \sim \sigma \cos\ \theta_e/\delta$. For $z > Z_w = \sigma \cos\theta_e/\rho g \delta$, an air layer trapped on the surface of an insect will collapse under the influence of hydrostatic pressures. For example, the wetting depth for cuticle with roughness $\delta \sim 1\,\mu m$ is $\sim 10\,m$.

When there is relative motion U between a solid and fluid, dynamic pressures within the fluid (of order $P_d \sim \frac{1}{2}\rho U^2$) may cause wetting. The transition from the Cassie–Baxter to Wenzel states will arise when the dynamic pressure exceeds the characteristic curvature pressure across the roughness, i.e. $P_d > \sigma \cos\theta_e/\delta$, that is for speeds $U > U_w = (2\sigma\cos\theta_e/\rho\delta)^{1/2}$. To avoid the transition to a Wenzel state, the insect must not exceed either the wetting speed U_w or the wetting depth Z_w. The criteria for the preservation of a Cassie–Baxter state for insect cuticle may thus be expressed in terms of surface Bond and Weber numbers

$$Bo_\delta = \frac{\text{buoyancy}}{\text{curvature}} = \frac{\rho g z \delta}{\sigma \cos\theta_e} < 1, \quad We_\delta = \frac{\text{inertia}}{\text{curvature}} = \frac{\rho U^2 \delta}{\sigma \cos\theta_e} < 1 \qquad (21)$$

Figure 25 is a regime diagram indicating the values of Bo_δ and We_δ for a number of semi-aquatic creatures. For all water-walking arthropods considered, $(Bo_\delta, We_\delta) \ll 1$: the curvature forces generated by fluid impregnation are more than sufficient to counter typical hydrostatic and hydrodynamic pressures generated by their leg strokes. Conversely, for large, diving creatures such as the otter, water-repellency is not critical: the air layer initially trapped in their fur is evacuated at depth by hydrostatic pressures.

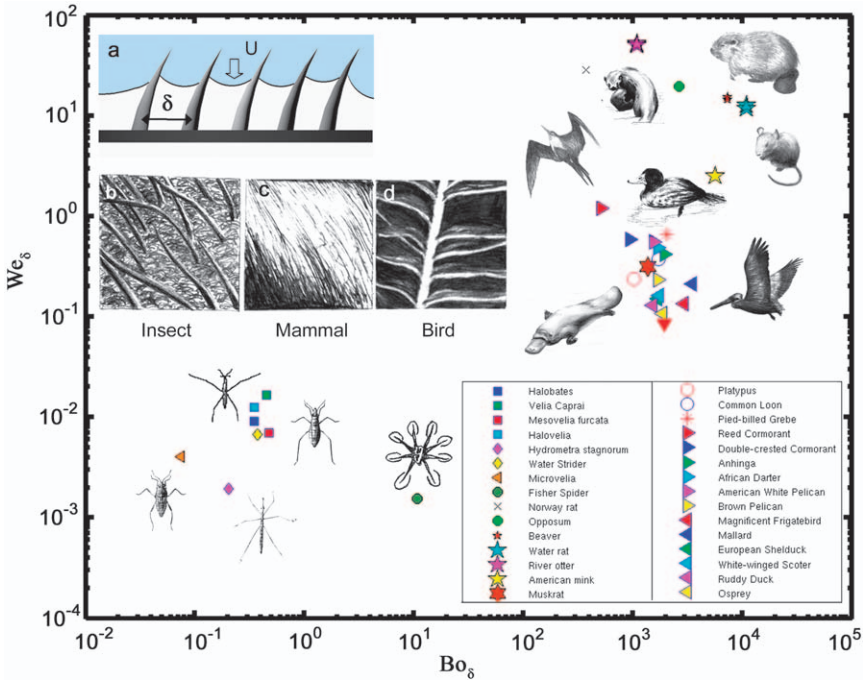

FIG. 25 Weber $We_\delta = \rho U^2 \delta/\sigma$ and Bond $Bo_\delta = \rho g h \delta/\sigma$ numbers characterizing the hair layers of 47 semi-aquatic creatures. (a) A schematic of the hair layer. Here U represents the peak leg speed, δ the inter-hair spacing and h the leg length. Definitions differ from Eq. (21) through omission of the contact angle dependence, owing to uncertainties in θ_e. (b–d) Sketches of water-repellent insect hairs, marine mammal fur and bird feathers (drawn from Dyck (p. 8, 1985) and Grant (p. 25, 1995)). Henceforth we shall refer to the barbs of the bird feather as their "hair". There is a clear division between two types of creatures. The first are water-walking arthropods for which maintenance of hydrophobicity is critical for their survival; the second are the semi-aquatic mammals and birds. The insects are characterized by low Weber number, indicating that their driving legs remain in a Cassie state as they propel themselves on the water surface (Fig. 11c). Conversely, semi-aquatic mammals and birds are characterized by high Bond and Weber numbers, indicating that air trapped in their hairs is forced out by dynamic pressures generated during their driving stroke or by hydrostatic pressures when they dive. Data is taken from Table 2 and collected from Mordvinov (1976), Andersen (1977), Elowson (1984), Fish (1984), Allers and Culik (1997), Fish *et al.* (1997, 2002), Fish and Baudinette (1999), Johansson and Norber (2001), Stratton *et al.* (2004b) and Ribak *et al.* (2005). Illustrations courtesy of Christina Sielert.

Wetting speeds and depths for a number of common water-walking arthropods are listed in Table 2. The impregnation pressure is greatest for the water striders, nearly 2.4 atm, indicating that they can dive to depths of 14 m before the air layer trapped by their microtrichia collapses. Insects

specialized for sub-surface breathing can typically ascend to greater depths (Vogel, 2006), and will be discussed in Section 5.2. The wetting speed for the strider is given by $U_w \sim 300\ \mathrm{cm\ s^{-1}}$, approximately three times the peak speed of its driving leg. We note that the arthropods most susceptible to wetting by hydrostatic or hydrodynamic pressures are generally the slowest moving.

Another fluid pressure that may cause impregnation of a rough solid is the curvature pressure inside small droplets adhering to the surface. McHale *et al.* (2005) studied the evaporation of water drops on superhydrophobic surfaces consisting of pillar-like structures fabricated using photolithography. Zhang *et al.* (2006) examined the so-called fakir transition from a Cassie–Baxter to a Wenzel state for water drops on the lotus leaf and biomimetic polymer surfaces. Contact line motion for evaporating drops in the Wenzel and Cassie–Baxter states differs drastically. A drop in the Wenzel state has a pinned contact line: evaporation occurs with no contact line movement. Conversely, for a drop in the Cassie–Baxter state, evaporation involves discrete de-pinning events at the contact line: the contact line recedes in discrete steps of a magnitude prescribed by the geometry of the surface roughness. Eventually, as evaporation proceeds, a fakir transition occurs, and the drop fluid impregnates the rough solid (Quéré, 2002). McHale *et al.* (2005) report that the transition occurs suddenly and is independent of drop size; however, a criterion for wetting in this situation is suggested by the study of Reyssat *et al.* (2006). In Section 6.1, we report experimental observations of this fakir transition on the legs of water striders.

As we saw in Section 3.4, while both water- and rain-proofing are encouraged by rigid, hydrophobic hairs, they benefit from qualitatively different hair morphologies. Water-proofing benefits from large amounts of solid–liquid contact, while rain-proofing benefits from minimizing this contact so that droplets can most easily escape the body (Extrand, 2006; Gao and McCarthy, 2007). Moreover, rain-proofing benefits from topologies that minimize the length of advancing or retreating contact lines (Joanny and de Gennes, 1984; Yoshimitsu *et al.*, 2002). Thorpe and Crisp (1947c, 1949) postulate different roles for the two hair layers on the thorax: the relatively long and stiff mesotrichia play the role of rain-proofing, while the inner layer of microtrichia play the role of water-proofing in the case of submergence. This two-tiered architecture has been reported in Hemiptera (Cheng, 1973; Andersen and Cheng, 2004), and various other semi-aquatic bugs (Andersen, 1977) including the water strider and *Microvelia* (Fig. 23), and so may be taken as a general feature of water-walking arthropods. According to the considerations of Section 3, the microtrichia's dense packing favours water-resistance. Moreover, they are often curved (Cheng, 1973) so as to arrive tangent to the free surface,

thus further enhancing resistance to fluid impregnation (Crisp and Thorpe, 1948; Section 3.4).

If the corrugations on the macrotrichia are in the vicinity of an interface, one expects on the basis of Eq. (6) that air will intrude to a considerable depth beneath the surface via the equivalent of capillary rise (Shuttleworth and Bailey, 1948). Such corrugations will thus necessarily trap air, thereby decreasing the force of retention of drops that come into contact with the insect cuticle. Moreover, one expects the grooves on the hairs to be beneficial in terms of structural rigidity, increasing the area moment of inertia of the hair without substantially increasing their weight (e.g. Crandall *et al.*, 1978). The dynamical role of the microgrooves will be considered in Section 5.4.

Rain-proofing is generally considered a measure of the ability of a surface to rid itself of small water droplets. For water-walking arthropods, however, the term must be taken more literally: the impact of a raindrop poses a potentially lethal threat. The impact of drops on a hydrophobic surface have been considered by Reyssat *et al.* (2006) and Bartolo *et al.* (2006), who deduced impalement criteria consistent with Eq. (21). Since the terminal velocity of a raindrop may be as large as $U_r \sim 10\ \mathrm{m\ s^{-1}}$, the associated impregnation pressures generated during impact, $\rho U_r^2 \sim 0.8$ atm, may exceed those generated during the leg stroke by two orders of magnitude. It is not entirely surprising that insects have been reported to seek refuge beneath overhanging vegetation, dive beneath the surface or leap vertically during rainstorms, presumably to reduce their exposed target area. Simply put, raindrops have terminal velocities that may exceed the wetting speed of insect cuticle (Table 2), and so pose a real threat to water-walking arthropods. As we shall see in Section 6, however, the wetting of their integument is not fatal: the cuticle dries via evaporation on the timescale of a minute.

The water-resistence of a hair pile will always be determined by its weakest point, for example, a gap in the hair pile. The maintenance of the order of the hairs of the insect cuticle is thus critical for ensuring their water-repellency. Kovac and Maschwitz (1999) discuss the role of grooming in maintaining the hydrophobic properties of various terrestrial beetles, while Stratton *et al.* (2004b) noted the same behaviour in terrestrial and semi-aquatic spiders. The grooming behaviour of a number of water-walking insects is apparent in Fig. 26.

5.2 PLASTRON RESPIRATION

A number of water-walking arthropods cross the surface during the course of their lives. Female water striders may submerge completely while laying

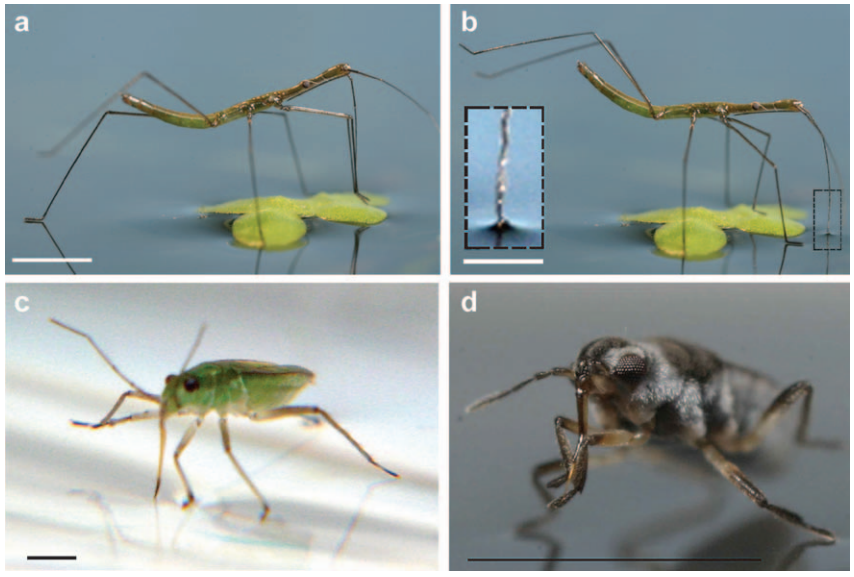

FIG. 26 Grooming of water-walking arthropods. (a) *Hydrometra* grooms its antenna with its forelegs. (b) *Hydrometra* grooms its hind legs by leaning forward, and anchoring with its antenna (see inset). (c) *Mesovelia* leans on its proboscis as it grooms its forelegs. (d) *Microvelia* grooms its proboscis. Scale bars, 1 mm.

eggs (Andersen, 1976) and the resulting strider nymphs hatch from eggs beneath the surface, swimming awkwardly to the surface before puncturing the interface (Fig. 27). Torre-Bueno (1907) reports that Veliidae can submerge completely, and Andersen and Polhemus (1976) report that sea-going water striders also dive to avoid pursuit. Spence *et al.* (1980) report several accounts of subsurface activity in the water strider. The water spider *Argyroneta aquatica* is known to submerge and fish beneath the surface with a bubble that serves as an air supply, periodically replenished from an underwater air-filled bell of silk (Lamoral, 1968). Finally, Kellen (1956) reports that certain intertidal species, such as *Halovelia*, remain submerged at high tide, enclosed in air pockets within porous volcanic rocks. It is also inevitable that water-walking arthropods be accidentally submerged, either by the impact of raindrops, crashing waves or attack from a predator. The hair layer is thus necessary not only in minimizing direct contact with the free surface, but in enabling these creatures to breath if accidentally submerged.

When submerged, many bugs and beetles appear to have shiny coatings owing to a thin layer of air trapped by their hair coating (Noble-Nesbitt, 1963; Rovner, 1986; Hebets and Chapman, 2000; Fig. 28). The term ‘plastron’ for this air layer was coined by Brocher (1909, 1912a,b,c, 1914),

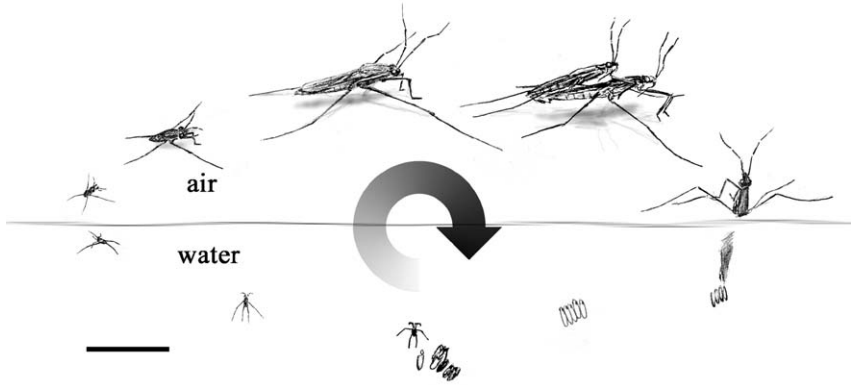

FIG. 27 The life cycle of the most common water-walker, the water strider. Other water-walking insects have a similar cycle involving underwater birth and several stages of growth. Gravid female water striders penetrate the free surface to lay their eggs underwater. The first-instar water striders that emerge from these eggs swim awkwardly towards then puncture the water surface, where their wet cuticle is dried via evaporation (see Fig. 32). Once atop the water surface, they moult several times before reaching adulthood. During mating, the larger female supports the weight of the male. Illustration courtesy of Brian Chan. Scale bar, 1 cm.

who recognized its importance in providing the buoyancy required for the insects to resurface. The importance of the plastron in respiration was first recognized by Straus-Durckheim (1828) and Dutrochet (1837). de Ruiter *et al*. (1951) provide an excellent review of studies of plastron respiration. The viability of plastron respiration was discussed in the context of various aquatic Hemiptera by Dogs (1908), Hagemann (1910) and Hoppe (1911); however, it was Ege (1915) who first provided the theoretical rationale for plastron respiration.

Plastron respiration was examined in a series of papers by Thorpe and Crisp (1947a,b,c, 1949) and Thorpe (1950), and found to be of critical importance to a number of semi-aquatic insects. The plastron is maintained by an array of hairs that lie roughly parallel to the body (Vogel, 2006; Fig. 14b). The ambient hydrostatic pressure is opposed by the curvature pressures generated as the water attempts to impregnate the gas film. The submerged insect breathes the air in the plastron through its spiracles (Fig. 23c), the orifices distributed regularly along its thorax. As the oxygen supply in the plastron is exhausted, oxygen is absorbed across the bubble surface from the ambient water. The plastron thus functions as an external gill: owing to the large surface area to volume ratio of the plastron, it presents an effective means of oxygen uptake from the water. The resulting plastron respiration is effective provided the bubble maintains a critical size, whose limiting value is prescribed by the initial volume of nitrogen

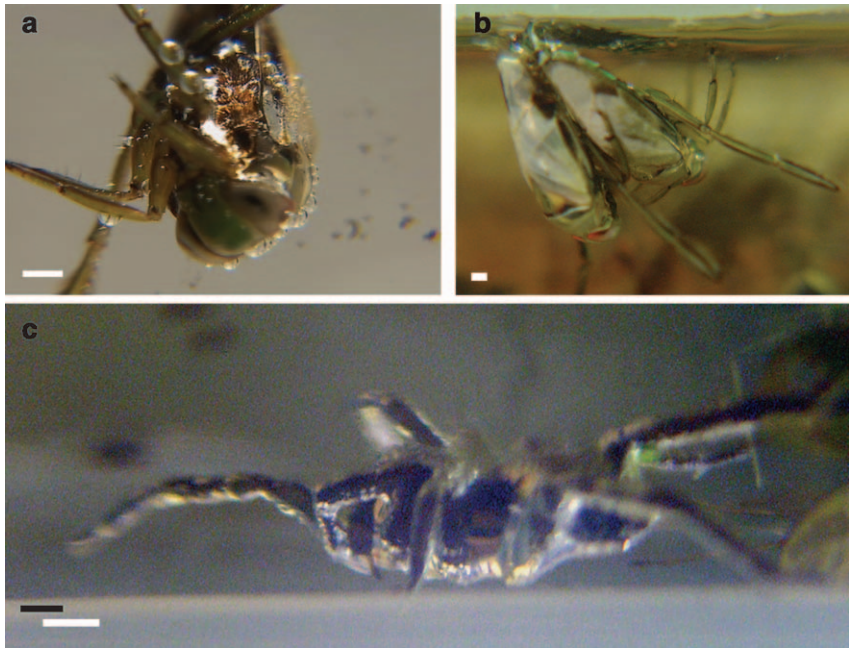

FIG. 28 Plastrons of (a–b) the backswimmer *Notonecta glauca* and (c) the fisher spider, visible as a silver envelope around the body and legs. Oxygen diffuses into these air layers, permitting underwater breathing. Formation of the plastron for the backswimmers begins as individual bubbles that are redistributed into a uniform sheet via vigorous grooming. The fisher spider generates a plastron simply by walking down emerging vegetation to cross the interface, a process documented by Brocher (1910). Scale bars, 1 cm.

in the bubble. Plastron respiration was considered by Vlasblom (1970), and models of gas exchange in a number of diving insects were developed by Rahn and Paganelli (1968), Gittelman (1975), Hinton and Jarman (1976) and Chaui-Berlinck *et al.* (2001). Philip *et al.* (2006) examined the plastron respiration of the backswimmer *Anisops*. By measuring the oxygen partial pressure within the beetle's captured bubble, they confirmed the conjecture of Miller (1964) that it maintains both oxygen levels and buoyancy via exchange with its haemoglobin. Experiments (Thorpe and Crisp, 1947a) indicate that for most insects, the collapse of the plastron typically arose at ambient pressures between 1 and 5 atm, corresponding to depths between 10 and 50 m.

Comstock (1887) and Harpster (1944) noted that certain diving insects actively drive flow over their trapped bubbles by flapping their limbs in 'respiration' movements. Stride (1955) noted that flow past the plastron may enhance the oxygen intake, a theory further discussed by Vogel (2006).

Brown (1987) describes plastron breathing in riffle beetles that live in aerated streams. While Ege (1915), Thorpe and Crisp (1947a) and Hinton (1976) assume that there is no substantial pressure jump across the interface, such will not generally be the case when flow speeds are high, or at great depth, where hydrostatic pressure will bow the plastron interface. Flynn and Bush (2008) note that while a closely packed hair lattice favours water-repellency, it reduces the area across which the insect breathes. By coupling the plastron chemistry and interfacial mechanics, they calculate the range of conditions over which plastrons can function. Shirtcliffe *et al.* (2006) created a biomimetic plastron consisting of a hydrophobic sol-gel foam material. The submerged chamber had a volume of 2.5 cm^3 and an external surface area of about 18 cm^2, and was supplied with oxygen from the water at a constant rate. They suggest that such a device, if scaled up to a sphere of 3 m diameter, might provide enough oxygen to support the oxygen requirements of a human.

Finally, we note the importance of plastron respiration in a number of terrestrial spiders, larvae (Krivosheina, 2005) and insect eggs (Hinton, 1969). During times of flooding, terrestrial insect eggs maintain a plastron via their textured hydrophobic surface, thereby surviving the deluge (Hinton, 1976). The silk nests of terrestrial spiders play a similar role, allowing their inhabitants to survive 10 times longer than in its absence (Rovner, 1986). Krantz and Baker (1982) examine the plastrons of certain species of mites that inhabit aquatic habitats.

5.3 CLASPING THE FREE SURFACE

While virtually all water-walkers have a rough surface coating to render them hydrophobic, many also have hydrophilic body parts that may be used to manipulate the free surface to various ends, including propelling themselves up menisci, launching themselves off the free surface, attracting mates, detecting prey, balancing and anchoring. Nutman (1941), Baudoin (1955) and Noble-Nesbitt (1963) pointed out that many water-walkers have hydrophilic claws or 'ungui' at the ends of their hydrophobic tarsal leg segments that they may use to penetrate or raise the free surface. The curved, conical ungui of the water strider and *Microvelia* are apparent in Fig. 22. Janssens (2005) (see also Thibaud, 1970) describes the ungui of *Anurida* as a three-sided prism, two sides being hydrophobic and the third hydrophylic, and argued the utility of this arrangement for their dynamic stability. The critical importance of ungui in meniscus-climbing by water-walking insects was first suggested by Baudoin (1955).

Figure 9b illustrates the posture assumed by *Mesovelia* during the ascent of a meniscus. The insect pulls up on the free surface with the ungui on its front legs, thus generating a lateral capillary force that draws it up the

meniscus (Section 2.2). The torque balance on the insect requires that it pull upwards with its hind legs. Finally, the vertical force balance requires that its central pair of legs bear its weight in addition to the vertical forces applied by its front and hind legs. Hu and Bush (2005) applied this simple physical picture to account for the ascent rates observed in their experimental study. Both Miyamoto (1955) and Andersen (1976) reported that certain species of insects assume laterally asymmetric, tilted body postures during their ascent. Hu and Bush (2005) rationalized this tilting behaviour by demonstrating that, depending on the relative leg lengths of the insect, tilting may be advantageous in maximizing the capillary propulsive force.

Wigglesworth (1950), Nutman (1941), Baudoin (1955) and Noble-Nesbitt (1963) report that certain surface-dwelling springtails, for example *Podura aquatica* and *Anurida maritima*, have a wetting ventral tube vessical that allows them to locally raise the free surface. Assuming the posture indicated in Fig. 29a allows the springtail to quickly escape aquatic predators: by releasing its grip on the free surface, it is propelled upwards by the curvature forces acting on its nose and tail. This posture also enables them to attract neighbours over a distance comparable to the capillary length (approximately their body length) and so provide capillary stabilization to their floating colony (Fig. 29b). Bounds on the maximum size of such colonies may be inferred from the study of Vella *et al.* (2006b), who develop equilibrium conditions for multiple floating bodies. We note that such capillary forces are presumably responsible for the novel crystal-like packings observed in floating mosquito larvae (Saliternik, 1942).

Many flying insects such as flies (West, 1982; Gorb, 1998) and mosquitoes (Wu and Kong, 2007) have specialized foot pads for anchoring themselves on solids using a variety of adhesion mechanisms (Gorb, 2008). Similarly, many water-walking insects, for example, Collembola (Janssens, 2005), are able to secure themselves to the free surface by way of hydrophilic ungui on their leg tips (Fig. 22). The ungui thus provide water-walking arthropods with a means of anchoring themselves to the surface.

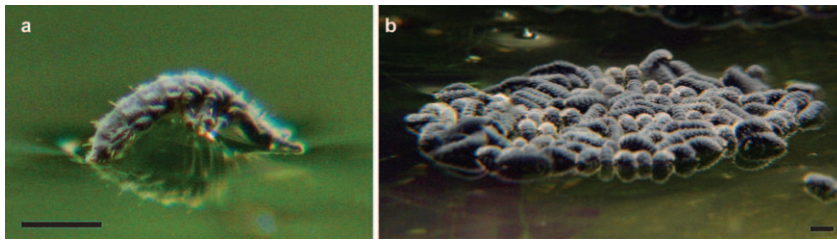

FIG. 29 Capillary attraction of Anuridae. (a) By arching its back and pulling up with its wetting ventral tube, Anurida forms a meniscus that will attract nearby partners. (b) Mutual capillary attraction facilitates the aggregation of an entire colony. Scale bars, 3mm.

The maximum capillary force that can be generated in such a fashion is $F_A \sim \pi D\sigma$, where D is the ungue diameter. For a water strider, $D \sim 30$ μm, so $F_A \sim 1$ dynes is comparable to its weight. It is noteworthy that a characteristic aerodynamic force on such a creature generated by a wind of magnitude $U \sim 1\ \mathrm{m\ s^{-1}}$, $F_a \sim \rho_a U^2 A \sim 1$ dyne (where A is the exposed area), has comparable order. Should a larger anchoring force be required, the creature may presumably wet some fraction of its leg cuticle to increase the contact forces acting thereon. In Fig. 26b, the antenna of *Hydrometra* is evidently being used as an anchor as it grooms its hind legs.

5.4 DRAG REDUCTION AND THRUST GENERATION

While the importance of the rough arthropod integument for water-repellency has been given considerable attention, its dynamical role has only recently been considered (Bush and Prakash, 2007). The role of superhydrophobocity in drag reduction is currently the subject of vigorous research (Cottin-Bizonne *et al.*, 2003; Choi and Kim, 2006; Choi *et al.*, 2006; Joseph *et al.*, 2006). When a rough surface advancing through a fluid is in its Cassie–Baxter state, that is, when much of its effective area is covered in air, the opposing viscous stresses are greatly diminished. Joseph *et al.* (2006) measured the velocity profiles of flow parallel to surfaces covered in carbon nanotube forests. For a surface in the Cassie–Baxter state, the net effect of the surface roughness is to reduce the tangential stresses felt at the boundary by an amount proportional to the ratio of the exposed solid area to the planar area. One thus expects that the rough surface of water-walking insects is important not only in maintaining their water-repellency, but in reducing their drag as they glide along the surface (Bush and Prakash, 2007).

The effects of anisotropic surface roughening on drag have also been considered. Patterning surfaces with microgrooves aligned with the flow may decrease drag by 5–10%, and is the basis of riblet technology (Walsh, 1990), which is finding applications in both aircraft and sailboat design (Choi *et al.*, 1996; Bechert *et al.*, 2000). For a surface with microchannels in the Wenzel state, Min and Kim (2004) demonstrate that the surface topography generally decreases hydrodynamic drag in the direction of the channels. Choi *et al.* (2006) examined the flow past superhydrophobic microchannels of characteristic width 200 nm in a Cassie–Baxter state. Drag was found to be reduced substantially in the direction of the grating owing to the air trapped in the grating. Conversely, the drag generated by flow perpendicular to the grating was enhanced relative to that on a smooth surface. We thus expect that both the orientation of the hairs and the presence of the nanogrooves on the macrotrichia will serve to reduce the drag on legs gliding along their length. Conversely, we expect these linear

features to enhance the resistance to the leg motion perpendicular to the direction of motion: the propulsive thrust generated in the driving stroke is thus maximized.

The water-repellency of a surface depends not only on a high contact angle, but on low drop adhesion (Gao and McCarthy, 2007). The force of retention depends not only on the contact angle hysteresis, but on the contact line geometry (Extrand, 2002, 2006). The influence of surface topography on the force of adhesion has been considered by Bico *et al.* (1999). Yoshimitsu *et al.* (2002) examined the force of adhesion that acts on water droplets suspended in a Cassie–Baxter state on surfaces decorated with grooves and pillars. They place a droplet on the surface and measure the critical tilt angle at which the force of gravity exceeds the force of adhesion, and the droplet rolls off the surface. Their experiments clearly demonstrate that drops roll with greatest ease in the direction of the grooves and with greatest difficulty perpendicular to the grooves; the case of square pillars being intermediate between the two. Their observations may be understood on the grounds that contact lines move with greatest difficulty in a direction normal to the line: imperfections existing even on a smooth surface cause the contact line to be caught, and the associated creation of surface area is energetically costly and so resists motion (Joanny and de Gennes, 1984; Nadkarni and Garoff, 1992). The experiments of Yoshimitsu *et al.* (2002) beautifully demonstrate the importance of the geometry of surface topography on adhesion; moreover, it allows us to rationalize the tilted hair orientation and grooved structures on the macrotrichia of water-walking insects.

For a water-walker on top of the free surface, the macrotrichia alone interact with the free surface. The nanogrooves on the macrotrichia reported on the water strider (Andersen, 1977; Gao and Jiang, 2004) and the *Microvelia* (Section 4) may be a generic feature of water-walking arthropods. When a hair slides in the direction of the grooves, the grooves minimize the extent of the advancing and retreating contact line (Yoshimitsu *et al.*, 2002), thereby reducing the contact force on the insect cuticle and associated drag on the insect. Conversely, when such a hair brushes the surface in a direction perpendicular to the grooves, relatively large contact forces will be generated. This would seem to be an important feature of the driving stroke: insects such as the water strider strike the surface perpendicular to the grooves, thereby generating large contact forces. Thereafter, they swing their legs through a 90° angle to align with the direction of motion, thereby reducing the contact force and allowing their legs to release from the free surface.

Water-walking arthropods rely on contact forces for both their weight support and propulsion; for both purposes, they benefit from maximum contact with the free surface. The maximum thrust is bounded by the total contact force sustainable by the cuticle during the driving stroke: if the

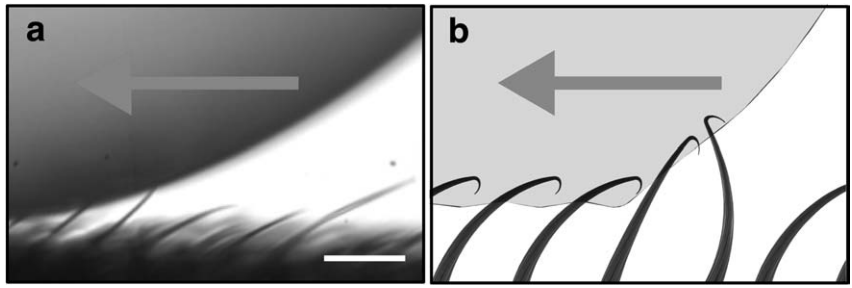

FIG. 30 Flexibility of insect cuticle caused by its interaction with a moving fluid interface. (a) The hairs on the driving leg of the water strider bend significantly when subjected to contact forces generated by a drop moving against the grain of the hairs. Once the drop has passed, the flexible hairs snap back into position. (b) A schematic illustration of the same.

applied force exceeds this value, the leg will detach from the free surface. By considering the geometry of the leg strike, one can thus rationalize the alignment of the leg hairs and nanogrooves on the macrotrichia, which both maximize the contact force felt by the driving leg. Contact forces are felt along each hair in contact with the free surface: moreover, they are amplified proportionally to every air-filled groove on the macrotrichia. To lift its legs following the driving stroke, the arthropod must detach from the free surface, and so overcome the contact forces acting on it (Fig. 30). This may be done most easily by withdrawing the leg along its length in a peeling motion, so that the contact force acts only across the wetted fraction of the hairs. Bush and Prakash (2007) thus argue that the variation in the contact force, as generated by the anisotropy of the insect cuticle in conjunction with the geometry of the leg stroke, is the basis for the propulsion of water-walking arthropods.

6 Imaging techniques

We proceed by reviewing microscopy techniques used in imaging solid–fluid interfaces, and highlighting the potential importance of these techniques in gaining insight into the dynamics of water-walking arthropods. In Section 6.1, we describe SEM imaging, giving particular attention to the advantages of wet-SEM over traditional SEM in imaging the interaction between insect cuticle and the free surface. In Section 6.2, we describe advances in optical imaging, including confocal imaging of 3D fluid interfaces, and interfacing with high-speed videography. We also describe a modified inverted confocal microscopy technique that enables one to study the dynamic interaction between live water-walking arthropods and the

free surface. In Section 6.3, we describe recent advances in scanning probe microscopy and its applications in imaging fluid interfaces at nanometric length scales. A discussion of recent advances in Particle Image Velocimetry (PIV) and micro-PIV techniques relevant to this class of problems is presented in Steinmann *et al.* (2006).

6.1 SCANNING ELECTRON MICROSCOPY

A huge advance in our understanding of the form of the insect cuticle accompanied the development of the SEM by Knoll (1935). The technique was improved upon until, by 1952, the instrument (built by Sir Charles Oatley) had achieved a resolution of 50 nm (Breton, 1999). Prior to the SEM, imaging small-scale objects relied on optical microscopy. An empirical limit, the Rayleigh criterion, yields the spatial resolution Δl (the minimum distance between two point objects that a microscope can clearly resolve) of a lens of diameter D and focal length f in terms of the wavelength λ of the light source: $\Delta l = 1.22 f\lambda/D$. This fundamental limitation was overcome by the invention of the SEM, which uses a beam of energized electrons instead of a light source. Modern SEMs yield resolutions of order 1–5 nm.

SEM is a scanning microscope, wherein a beam of electrons is focused at a narrow spot on the sample: electrons emitted from the sample are captured at the secondary electrodes. The main components of the microscope are the electron gun (for generating the high energy electron beam), electromagnetic lens assemblies (to focus and control the electron beam), low-pressure imaging chamber and a low-vibrational noise sample stage. The focused beam spot is scanned over an imaging area and the resulting intensity map (constructed from the current at the secondary electron electrode) is captured and stored as an image. Various parameters (e.g. pressure, gas composition, temperature and humidity) need to be precisely controlled inside the imaging chamber.

Most of the insights gained into the microstructure of the integument of water-walking arthropods reported in Section 4 were obtained via SEM. While traditional SEM provides very high-resolution images ($\sim 1-5$ nm resolution), the samples are subjected to extremely low vacuum pressures of order 10^{-9} atm. Such a vacuum is a harsh environment for biological samples, and may result in dehydration, crumpling and buckling of the sample. Moreover, only completely dry samples can be imaged effectively in this manner, thus precluding the possibility of studying the interaction between arthropod cuticle and fluid interfaces.

Various techniques have been developed to prepare biological samples for traditional SEM imaging. A common problem in SEM imaging of insulating surfaces (e.g. insect cuticle), charge build-up, may be averted by

coating the sample with a very thin layer (~ 1 nm) of a highly conducting surface, such as gold, platinum, graphite or tungsten (Reimer, 1998). A disadvantage of such coatings is that they modify the surface properties of the sample. Consequently, the sample cannot be used for studies where the surface chemistry is important, for example, to consider the interaction between water droplets and insect cuticle. Recent techniques for rapid freezing have made it possible to image fully hydrated biological samples using cryo-SEM (Walther and Muller, 1997; Craig and Beaton, 1996). While this method allows for imaging of delicate plant tissue and cells with no crumpling and buckling of the sample, its disadvantage is that ice crystals may form during cooling, damaging the sample and producing erroneous imaging artifacts.

A modification of traditional SEM techniques, wet or environmental SEM, provides a means of imaging samples with water vapour inside the imaging chamber (Donald, 2003). Jenkins and Donald (1999) and Stelmashenko *et al.* (2001) used wet SEM to directly measure contact angles and surface properties of partially wetting droplets on various substrates. In the context of insect cuticle, wet SEM allows for imaging without evaporation and dehydration of the sample. Moreover, it introduces the possibility of visualizing the interaction between the cuticle and the free surface in both static and dynamic settings. The technique relies on the exact control of three parameters inside the imaging chamber; temperature, pressure and water vapour pressure. Moreover, since no pre-treatment is required for imaging insulating substrates for wet-SEM, the surface properties are unmodified during the imaging procedure; this is crucial for studying the wetting properties of biological samples.

The principle difference between SEM and wet-SEM lies in the sample environment. In both cases, the electron gun is maintained at low pressure (1.3×10^{-9} atm). For the case of wet-SEM, the imaging chamber pressure can be as high as 10^{-2} atm. This is achieved by a differential pressure valve isolating the high- from the low-pressure regions. Thus the imaging chamber can be filled with various gases and water vapour, keeping the sample hydrated over an extended period. Since electrons colliding with gas molecules produce positive ions, no build-up of negative charge occurs on insulating samples. Moreover, a Peltier stage can be used to control condensation onto (or evaporation from) the sample. The resulting precise temperature, pressure and humidity control inside the imaging chamber is useful for studying structure-interface interactions in various experimental conditions.

The first biological application of wet-SEM was an examination of the interaction of droplets and the lotus leaf. Recent ESEM imaging demonstrates a fakir transition between Cassie–Baxter and Wenzel states for drops of a size comparable to the roughness scale (Cheng and Rodak, 2005). We here use wet-SEM techniques to image the interaction of the free

surface with the cuticle of water-walking insects; specifically, an XL30 ESEM from FEI Company was used to image wet samples of water strider legs. Legs from recently dead water striders were mounted on a silicon substrate and sprayed with a water mist to form a thin water film on the leg surface. Samples were then introduced into the imaging chamber, mounted inside the SEM on a three-axis stage. The chamber was carefully pumped up to 3×10^{-3} atm following the procedures of Stelmashenko *et al.* (2001) and Donald (2002), injecting water vapour from time to time to avoid complete dehydration of the sample. Figure 31 illustrates the fakir transition that accompanies the evaporation of an initially 10-μm-scale drop on a water strider leg using a conventional video microscope. Given the dangers inherent in such a transition, that transforms the cuticle from hydrophobic to hydrophilic, it bears further consideration in this biological context.

Figure 32 presents environmental SEM images of a thin water film that completely coats and wets the hairy surface of a water strider leg. Images of the film interface were taken at various beam energies as the water film evaporated. In the first image, the hairs are all coated with water, but are apparent as deformations of the free surface. In the second image, evaporation has reduced the mean film thickness and hairs have penetrated its surface. Note that the entire time taken for the wetted cuticle to dry via evaporation was ~ 30 s. This imaging technique is expected to yield valuable insight into the stability of the hair layer. We are currently performing a more extensive set of experiments to explore the nature of the interaction between insect cuticle and the air–water interface.

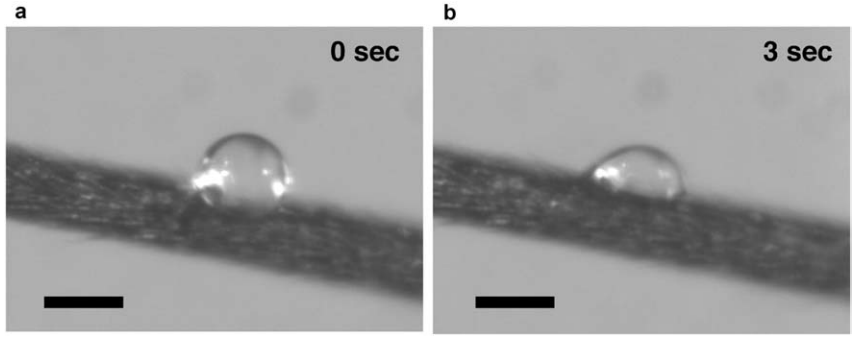

FIG. 31 The fakir transition of a water drop on a water strider leg. (a) A water drop initially deposited on the leg exhibits a high contact angle ($\sim 167^\circ$; Gao and Jiang, 2004), and is in a Cassie–Baxter state. (b) After evaporating for 3 s, its contact angle decreases dramatically to 60°, indicating a transition to a Wenzel state. Not shown: after 7 s, the drop has completely evaporated. Sequence photographed using a stereo microscope (STEMI Stereomicroscope by Zeiss). Scale bars, 200 μm.

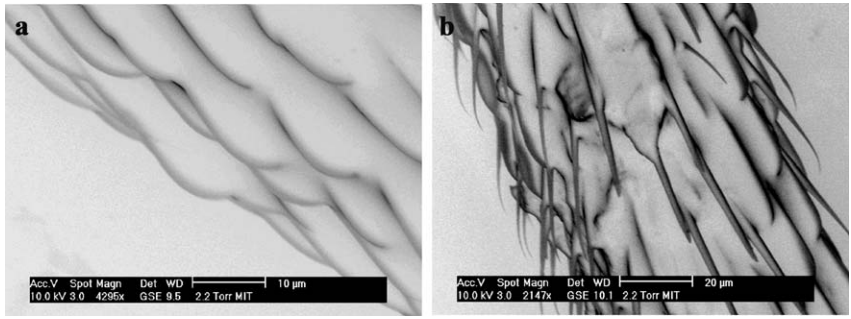

FIG. 32 The evolution of a thin film of water on the surface of a strider leg, as imaged via wet-SEM. (a) A fully wetted water strider leg: a water film covers the entire leg. The 10-μm-scale hairs generate indentations beneath the free surface. (b) After 10 s, the film has evaporated to the point that hairs poke through the free surface. Hairs are not visibly distorted by their interaction with the interface. The entire process of evaporative drying takes $\sim$30 s, and provides an important means of restoring the water-repellency of the cuticle following submergence.

6.2 OPTICAL MICROSCOPY

Even though SEM and wet-SEM imaging techniques provide unprecedented resolution and fine details of the interface-body interaction, the imaging environment is generally too harsh for live samples. This precludes the possibility of elucidating the dynamic interaction between a live insect leg and the free surface. We proceed by reviewing recent advances in optical imaging that make it possible to do so.

Laser-scanning-based confocal microscopy techniques provide a means to image dynamic 3D fluid interfaces with a resolution of order 1 μm. The underlying principles for confocal microscopy were first developed by Minsky (1953, 1988) to study the 3D structure of brain cells, and the technique was widely adopted in the biological community in the 1980s with the advent of commercial systems with multiple light sources and automated laser slicing. The technique uses an extremely thin focal plane and a laser as a light source. Images are taken through different slices, then later combined to construct a 3D map. Aarts *et al.* (2004) used confocal imaging to study the interfacial dynamics of a phase-separated colloid-polymer dispersion, observing thermal fluctuations on a fluid–fluid interface for the first time.

A conventional microscope configuration consists of an eyepiece and an objective above a sample holding stage with back or side illumination. An inverted microscope configures the light source on the top of a sample holding stage, while the objective and the eyepiece lie below the image sample plane. The inverted microscope is well suited to imaging the interface with live samples from below, yielding a resolution of order 2 μm.

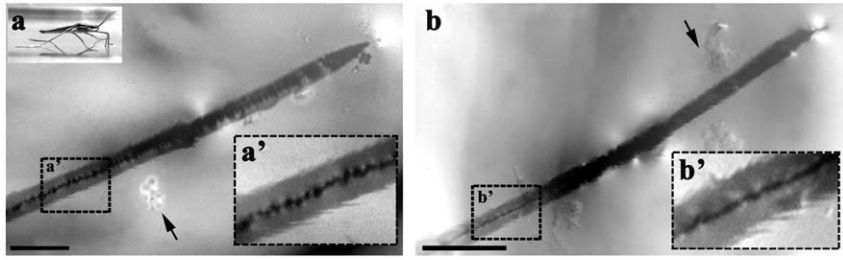

FIG. 33 Two views from below of the contact of a water strider leg with the underlying water. Only a single line of hairs intersects the free surface (rationalized in Table 2). The small white droplets of oil (indicated by the arrows) were shed by the leg. The photomicrographs were taken with an inverted microscope (Zeiss LSM Pascal) and a 20x and a 50x objective lense. Live insects were imaged as they moved freely on a water film above the microscope objective. Scale bars, 100 μm.

Bush and Prakash (2007) present a new inverted microscope technique that allows for both static and dynamic high-resolution imaging of the free surface and contact lines in water-walking arthropods. Our images yield new insight into the nature of the contact between water-walkers and the underlying fluid.

In Fig. 33, we present a series of inverted microscope images (Zeiss LSM Confocal microscope) of the contact of a live water strider leg with the free surface. The darker regions indicate the regions of contact with the surface. Note in Fig. 33 that only a small fraction of the leg, indicated by the thin dark line along the leg's centerline, is in contact with the surface: the weight-bearing section is narrow relative to the leg width. In Fig. 33a, the leg tip is marked by a bright white spot that results from the interaction of the hydrophilic ungue with the water surface. Small droplets of an oil-like substance released from the leg, perhaps cuticle wax, are apparent as white blobs floating on the surface.

Figure 34 is a series of inverted microscope images of a *Microvelia* standing on the water surface. The outline of the overlying insect body is clearly visible in the photomicrographs. The images depict *Microvelia* grooming; consequently, not all of its legs are in contact with the surface. The precise nature of the contact line on the insect cuticle may be observed by zooming in on the area of interest. Figure 34 depicts pinholes corresponding to individual hairs in contact with the water surface. The water strider needs only a single line of hairs to support its weight; conversely, since *Microvelia* has relatively shorter legs and a lower hair density, it requires a relatively broad swath of hairs to support its weight. The predicted values of w_c reported in Table 2 are thus consistent with those observed in Figs. 33 and 34. To the best of our knowledge, these images present the most detailed picture of the interaction between the

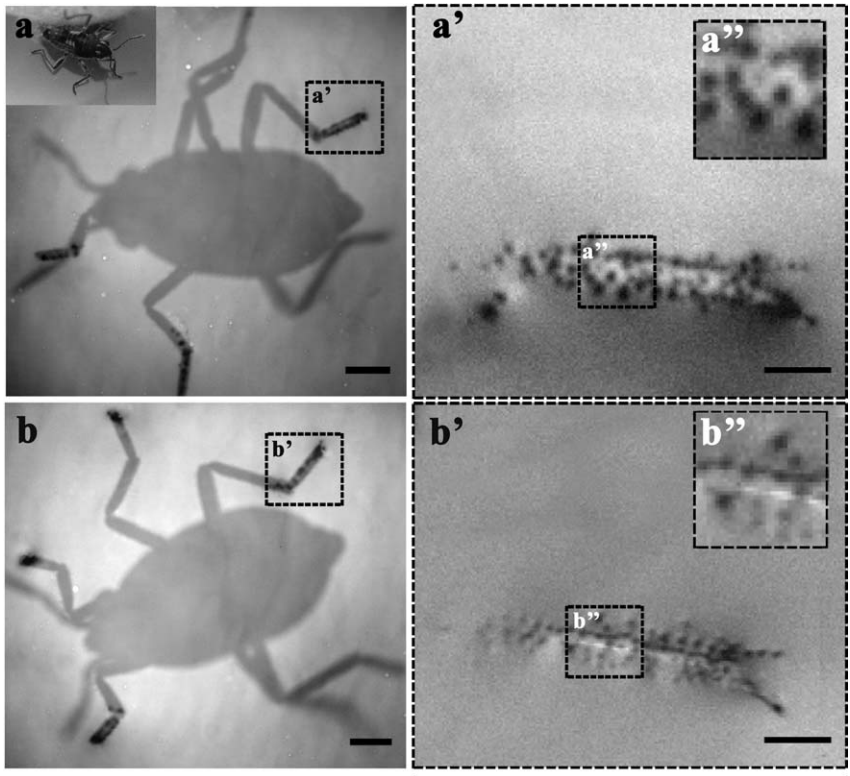

FIG. 34 The contact of *Microvelia*, as viewed from below. Its tarsi are shorter and less piliferous than those of the water strider leg, as can be seen by comparing Figs. 21a and 23a. Consequently, a contact region 5 hairs wide and 50 hairs long intersects the free surface, generating a pincushion-like deformation signature. The contact widths of various water-walking arthropods are rationalized in Table 2. The photomicrographs were taken as in Fig. 33. Scale bars, 20 μm.

interface and water-walking insects, and give clear evidence of the cuticle being in a Cassie–Baxter state.

Recent developments in high speed imaging provide insight into the fast interactions between solids and interfaces (e.g. Bergmann *et al.*, 2006). In Fig. 35, we show the interaction of a water strider leg tip with the free surface as imaged with a high-speed camera (Phantom V5, Vision Research). As we saw in Fig. 22, the ungui at the leg tips of water-walkers are smooth and hydrophilic. The leg of a dead water strider was mounted on a micro-positioner and brought down to the interface until its ungue just touched the interface. Thereafter, the leg was slowly extracted until the free surface was released by the ungue. The sequence of

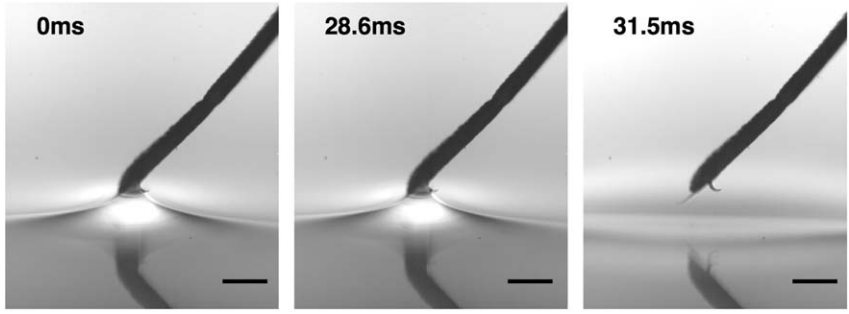

FIG. 35 A sequence of high-speed photomicrographs depicting the ungue of an adult water strider releasing the free surface. The initially wet ungue is slowly extracted from the water surface until the point of release. The sequence was taken using a high-speed video camera (Phantom V4). Scale bars, 100 μm.

images illustrates the rapid detachment of the free surface from the hydrophilic ungue.

Topographical imaging of fluid interfaces at such small length scales is a nascent field for which no quantitative high-speed imaging techniques have been developed. Techniques allowing reconstruction of the fast, microscopic distortions of fluid interfaces would greatly enhance our understanding of the dynamics of this class of problems.

6.3 SCANNING PROBE MICROSCOPY

In scanning probe microscopy, weak force interactions between a pointed tip and imaging substrate are utilized to image a sample. In essence, a mechanical, pointed probe (of diameter 10–100 nm) is scanned over the sample, and the deflection of the probe is measured optically or electronically. Since no light or particle source is used for illumination, this provides the highest resolution of any microscopic imaging technique, with resolutions on the order of molecular dimensions.

In Atomic Force Microscopy (AFM), a micro-scale cantilever is used to image a surface by scanning it over a given sample. Various interaction forces between the cantilever tip and the sample can be used, including contact, capillary, van der Waals, electrostatic and chemical forces. It is also possible to modify the tip geometry or chemistry to enhance the force being characterized. The deflection of the micro-scale cantilever during scanning operation is measured by an optical lever: by shining a laser beam onto the top surface of the cantilever.

Snyder *et al.* (1997) and Aston and Berg (2001) modified the AFM technique to image fluid interfaces at small length scales (a technique referred to as Fluid-Interface AFM). A polystyrene bead was attached to

the cantilever tip, and used to image an oil drop in water using a tapping mode. The capillary force of attraction between the bead attached to the cantilever tip and the oil–water interface was used to image the oil drop. Owing to the sensitivity of the AFM cantilevers, dynamic drop deformations due to particle–drop interactions can be imaged. Numerous authors (Lou *et al.*, 2000; Agrawal *et al.*, 2005; Agrawal and McKinley, 2005) have used AFM microscopy to image the spontaneous formation of nanometre-scale air pockets on hydrophobic surfaces. The ability to image dynamic interfaces on the nanometre scale using AFM will significantly enhance our understanding of fluid–structure interactions.

7 Discussion

It is ironic that workers in the subject water-repellency, first motivated by a desire to control the insect population, are now drawing their inspiration from this population. We have reviewed the modern theory of water-repellency and its relevance in understanding the integument of water-walking arthropods. We have seen that arthropod cuticle exhibits many of the characteristics of optimally hydrophobic surfaces. Moreover, we have noted the similarities and differences between the surface structure of plants and water-walking arthropods. The differences, in particular the anisotropic adhesive properties of the arthropod cuticle, have been rationalized in terms of their additional dynamical role.

The epicuticle of water-walking arthropods consists of a waxy substance that increases the contact angle beyond 90°; therefore, the addition of surface roughness renders the insect cuticle hydrophobic rather than hydrophilic, allowing the cuticle to remain in a Cassie–Baxter rather than a Wenzel state. Roughness arises in the form of an array of hairs, the form of which varies slightly from species to species and on different body parts of a given species. All water-walking insects and arthropods are covered in a layer of hairs that are tilted relative to the body surface so that they meet the free surface at an oblique angle, thus providing enhanced resistance to fluid impregnation (Crisp and Thorpe, 1948). This hair layer is most dense on the leg tips, where it precludes the impregnation of water under the influence of hydrodynamic pressures generated by the driving stroke. The outermost layer of macrotrichia is responsible not only for resisting impregnation pressures, but for channelling water droplets off the insect's surface (Thorpe and Crisp, 1949). On their thorax, most water-walking arthropods have a second relatively fine inner hair layer, microtrichia, that serves to preserve a plastron against hydrostatic pressures when the insect is submerged, thus enabling them to breathe underwater. In terms of wetting, the greatest risk to water-walking arthropods is the impact of raindrops.

In the case of fluid impregnation of the cuticle, recent experiments indicate that evaporation evacuates the cuticle in less than a minute.

The role of a second scale of roughness, specifically, grooves on the macrotrichia (as evident in our SEM images of the water strider and *Microvelia*), has only recently been considered. Gao and Jiang (2004) point out its importance in increasing the apparent contact angle of water on water strider cuticle; however, its dynamical significance has only recently been considered (Bush and Prakash, 2007). Feng *et al.* (2002) demonstrate that the anisotropic roughness on the hydrophobic rice leaf causes water droplets to roll parallel rather than perpendicular to the leaf edge. Yoshimitsu *et al.* (2002) clearly demonstrated that grooves of sufficient amplitude to maintain a Cassie–Baxter state act to dramatically reduce the force of adhesion in the direction of the grooves and to increase it in the perpendicular direction. This study suggests two dynamic roles of the nanogrooves. First, they reduce the force of retention parallel to the hairs, and so permit drops striking insects to more readily roll off them. Second, owing to the alignment of the hairs and the nanogrooves, the retention force experienced by a strider leg will be larger when the leg is aligned perpendicular than parallel to the flow. Bush and Prakash (2007) thus rationalize the form of the driving stroke of the water strider: the leg strike perpendicular to the direction of motion maximizes the propulsive contact force, while the alignment of the rear pair of legs with the direction of motion minimizes drag as they glide along the surface. The driving leg is extracted by lifting it along its length in a peeling motion; here again, the topology of the cuticle is beneficial, as the force of extraction is minimized by the grooved hairs. Finally, Bush and Prakash (2007) demonstrate that the leg cuticle exhibits unidirectional adhesion: fluid advances most easily towards the leg tip, and with greatest difficulty perpendicular to the leg. The implications of the unidirectionality of insect cuticle are currently under investigation.

Consideration of the flow on the scale of the insect cuticle requires that we revise the macroscopic view of both the statics and dynamics presented in Section 2. In terms of statics, the contact line is not the perimeter of the tarsus, but rather those around individual hairs (Fig. 6). Nevertheless, the total vertical curvature force available for weight-bearing is limited by the generalized Archimedes law: the total force on a floating body is precisely equal to the fluid displaced by the body. The air trapped in the cuticle displaces fluid, thereby enhancing the buoyancy force that bears the insect's weight. In considering the dynamics, the relevant length scale changes from the width of the driving leg to that of the hairs or perhaps even the nanogrooves on the hairs. Flows on this scale are characterized by $(Re, We) \ll 1$ and so dominated by fluid viscosity and surface tension. Moreover, we expect the surface roughness to affect all of the components of the propulsive force enumerated in Section 2.3. The physical picture that

emerges is thus one of a small-scale viscously dominated flow on the scale of the individual hairs combining to give rise to a bulk flow on the scale of the insect leg. Hu *et al.* (2003) and Hu and Bush (2008a) performed the first flow visualization studies of water-walking arthropods, and demonstrate that their wake is typically characterized by vortices that allow one to understand their propulsion in terms of momentum transfer. Consideration of the precise form of the contact between the arthropod and the water surface indicates that the vortices are generated by viscous interaction with the hairs on the driving legs.

A problem that has received very little attention is strategies of detachment from the free surface. Such strategies would seem all the more important given that the need to escape from an air–water surface is common to all insects: terrestrial insects must contend with capillary forces in times of heavy rain or flooding, and flying insects whenever they land on a body of water. While the contact perimeter may be reduced through the rough water-repellent cuticle, there are nevertheless contact forces that must be overcome to detach from the free surface, as arises with every step of a water-walker. The nanogrooves on the macrotrichia of the water strider and *Microvelia* suggest an interesting detachment mechanism. The grooves will tend to favour attachment through a single film of water whose thickness t is prescribed by the spacing between the nanogrooves. Tilting of the hair relative to the water surface will generate a film with a free edge that will necessarily retract under the influence of the surface tension force per length 2σ. Neglecting the effect of the body surface, one expects the sheet to retract at the Culick speed $U = (2\sigma/\rho t)^{1/2}$ that necessarily increases with decreasing sheet thickness t. Choosing $t = 500\,\text{nm}$ yields a retraction speed $U \sim 10\,\text{m}\,\text{s}^{-1}$. The details of this detachment mechanism are currently under investigation theoretically and experimentally.

One subject that certainly merits further investigation is the influence of elastic deformation of insect cuticle under the influence of capillary forces. While such deformation was proposed by Thorpe (1950) to set the maximum depth to which diving insects could descend, Hinton (1976) argued that the cuticle is effectively rigid at such pressures. Nevertheless, the recent study of Bush and Prakash (2007) indicates that the elastic deformation of arthropod cuticle is dynamically significant. Zheng *et al.* (2007) demonstrate that butterfly wings exhibit anisotropic adhesive properties: drops roll readily towards the wing's edge, but are pinned if they roll in the opposite direction. This directional adhesion was explained in terms of the wing's surface structure, which consists of a series of 50 μm scales themselves composed of a series of 500 nm bundles of tubes of diameter 100 nm aligned perpendicular to the wing's edge. From each of these bundles, one flexible tube protrudes. When drops roll towards the wing edge, the flexible tube is compressed and lies flush with its bundle. When they roll in the opposite direction, the tube tip is deflected away from its bundle, resisting drop

motion through the generation of surface energy. Bush and Prakash (2007) indicate that similar mechanisms arise on the cuticle of water-walking arthropods. The role of the flexibility of insect cuticle is currently being investigated both theoretically and experimentally.

Variable wetting properties are used by terrestrial insects to good effect. Certain bark-inhabiting bugs have hydrophilic body parts that are wetted by rain water so as to provide better camouflage against the backdrop of wet bark (Silberglied and Aiello, 1980). Just as water-walking insects maintain a thin layer of air with their hair layer, these creatures can preserve their camouflage by supporting a thin layer of water. The beetle *Stenorca* inhabits the Namib desert where it virtually never rains; thus, out of necessity, it has developed an ingenious means of condensing water from fog droplets in the 1–40 μm range (Parker and Lawrence, 2001). Its bumpy back consists of a series of hydrophilic peaks (of characteristic diameter 0.5 mm) in hydrophobic troughs: the fog drops thus stick to the peaks and grow by accretion until reaching a size that will allow them to be blown by the wind towards the insect's mouth. This technique is currently being investigated as a means of condensing water in inhospitable regions of the world.

Fundamental fluid mechanics problems are also suggested by this review. Recent studies have illustrated the importance of wetting properties on the form of the flow generated by bodies striking the free surface. Duez *et al.* (2007) examined a falling sphere impacting a free surface and found a surprising dependence on the sphere's wetting properties. In the high Re and We limits, where a smooth sphere makes no splash, a pronounced cavity and splash accompanied the roughened sphere. This study raises many interesting questions concerning the influence of water-repellency on water-walking arthropods. Through increasing the splash, hydrophobicity presumably increases the collapse time of the cavity, thereby granting the creature more time to withdraw its leg. The influence of water-repellency on impact in the small Bo limit of interest to water-walking arthropods is currently under investigation (Aristoff and Bush, 2008).

Finally, recent technological advances in microscopy, specifically, wet-SEM and inverted confocal microscopy, promise important insights into the interaction of insects and the water surface. Particular attention should be given to elucidating the detailed nature of the static and dynamic interactions between the interface and the micron-scale cuticle hairs. Coupling these microscopy techniques with high-speed videography is likely to yield unprecedented insights into dynamic wetting and optimal water-repellency. Providing the link between the micro- and macroscale dynamics will prove invaluable in rationalizing the locomotion of water-walking arthropods; moreover, it is likely to play a critical role in the engineering of smart surfaces, for example, those capable of self-cleaning, water-repellency and directional adhesion.

Acknowledgements

The authors thank David Quéré and two anonymous reviewers for their thoughtful comments on the manuscript; Mathilde Callies Reyssat for kindly forwarding an early version of her thesis; Robert Suter for generously sharing his data on the wetting properties of spiders and Lucy Mendel and Brian Chan for their assistance with illustrations. The authors gratefully acknowledge the financial support of the NSF: JB through grant CTS-0624830 and Career Grant CTS-0130465; DH through a Mathematical Sciences Postdoctoral Research Fellowship and MP through grant CCR-0122419. MP also acknowledges the microscopy resources at Center for Bits and Atoms, and thanks Jaebum Joo for assistance with the wet SEM.

References

Aarts, D. G., Schmidt, M. and Lekkerkerker, H. N. W. (2004). Direct visual observation of thermal capillary waves. *Science* **304**, 847–850.

Adam, N. K. (1948). Principles of penetration of liquids into solids. *Discuss Faraday Soc.* **3**, 5–11.

Adam, N. K. (1963). Principles of water repellency. In: *Waterproofing and Water-repellency* (ed. Moilliet, J. L.), pp. 1–23. New York: Elsevier.

Adamson, A. W. (1982). *Physical Chemistry of Surfaces*. New York: Wiley.

Agrawal, A. and McKinley, G. H. (2005). Nanobubble formation at the solid–liquid interface studied by atomic force microscopy. *Mater. Res. Soc. Symp. Proc.* **899**, 146–151.

Agrawal, A., Park, J., Ryu, D., Hammond, P., Russell, T. and McKinley, G. (2005). Controlling the location and spatial extent of nanobubbles using hydrophobically nanopatterned surfaces. *Nano Lett.* **5**, 1751–1756.

Alexander, R. M. (1985). The maximum forces exerted by animals. *J. Exp. Biol.* **115**, 138–231.

Allers, D. and Culik, B. M. (1997). Energy requirements of beavers (*Castor canadensis*) swimming underwater. *Physiol. Zool.* **70**, 456–463.

Andersen, N. M. (1976). A comparative study of locomotion on the water surface in semiaquatic bugs (Insects, Hemiptera, Gerromorpha). *Vidensk. Meddr. Dansk. Naturh. Foren.* **139**, 337–396.

Andersen, N. M. (1977). Fine structure of the body hair layers and morphology of the spiracles of semiaquatic bugs in relation to life on the water surface. *Vidensk. Meddr. Dansk. Naturh. Foren.* **140**, 7–37.

Andersen, N. M. (1982). *The Semiaquatic Bugs (Hemiptera, Gerromorpha): Phylogeny, Adaptations, Biogeography and Classification*. Klampenborg, Denmark: Scandinavian Science Press Ltd.

Andersen, N. M. and Cheng, L. (2004). Marine insect halobates (heteroptera: Gerridae): biology, adaptations, distribution, and phylogeny. *Oceanog. Mar. Biol. Annu. Rev.* **42**, 119–180.

Andersen, N. M. and Polhemus, J. T. (1976). Water-striders (Hemiptera: Gerridae, Veliidae, etc.). In: *Marine Insects* (ed. Cheng, L.), pp. 187–224. Amsterdam: North Holland Publication Co.

Aristoff, J. and Bush, J. W. M. (2008). Water entry of small hydrophobic bodies. *J. Fluid Mech*. submitted.
Aston, D. E. and Berg, J. C. (2001). Quantitative analysis of fluid-interface-atomic force microscopy (FI-AFM). *J. Coll. Interf. Sci.* **235**, 162–169.
Autumn, K., Sitti, M., Liang, Y. A., Peattie, A. M., Hansen, W. R., Sponberg, S., Kenny, T. W., Fearing, R., Israelachvili, J. N. and Full, R. J. (2002). Evidence for van der Waals adhesion in gecko setae. *Proc. Natl. Acad. Sci. USA* **99**, 12252–12256.
Bartell, F. E., Purcell, W. R. and Dodd, C. G. (1948). The measurement of effective pore size and of the water-repellency of tightly woven textiles. *Discuss Faraday Soc.* **3**, 257–264.
Barthlott, W. and Neinhuis, C. (1997). Purity of the sacred lotus, or escape from contamination in biological surfaces. *Planta* **202**, 1–8.
Barthlott, W., Riede, K. and Wolter, M. (1994). Mimicry and ultrastructural analogy between the semi-aquatic grasshopper *Paulina acuminata* (Arthropoda; Pauliniidae) and its foodplant, the water-fern *Salvinia auriculata* (Filicatae; Salviniaceae). *Amazoniana*, 47–58.
Bartolo, D., Bouamrirene, F., Verneuil, E., Beguin, A., Silberzan, P. and Moulinet, S. (2006). Bouncing or sticky droplets: impalement transitions on super-hydrophobic micropatterned surfaces. *Europhys. Lett.* **74**, 299–305.
Baudoin, R. (1955). La physico-chimie des surfaces dans la vie des Arthropodes aeriens des miroirs d'eau, des rivages marins et lacustres et de la zone intercotidale. *Bull. Biol. Fr. Belg.* **89**, 16–164.
Baudoin, R. (1976). Les insectes vivant a la surface et au sein des eaux. *Grassé Trait'e de Zool.* **8**, 843–926.
Beament, J. W. L. (1945). The cuticular lipoids of insects. *J. Exp. Biol.* **21**, 115–131.
Beament, J. W. L. (1948). The role of wax layers in the waterproofing of insect cuticle and egg-shell. *Discuss Faraday Soc.* **3**, 177–182.
Bechert, D. W., Bruse, M., Hage, W. and Meyer, R. (2000). Fluid mechanics of biological surfaces and their technological application. *Naturwissenschaften* **87**, 157–171.
Bergmann, R., van der Meer, D., Stijnman, M., Sandtke, M., Prosperetti, A. and Lohse, D. (2006). Giant bubble pinch-off. *Phys. Rev. Lett.* **96**, 154505 (4 pages).
Bico, J., Marzolin, C. and Quèrè, D. (1999). Pearl drops. *Europhys. Lett.* **47**, 220–226.
Bico, J., Roman, B., Moulin, L. and Boudaoud, A. (2004). Elastocapillary coalescence in wet hair. *Nature* **432**, 690.
Bico, J., Thiele, U. and Quere, D. (2002). Wetting of textured surfaces. *Colloids Surf. A* **206**, 41–46.
Bico, J., Tordeux, C. and Quère, D. (2001). Rough wetting. *Europhys. Lett.* **55**, 214–220.
Blomquist, G. J. and Jackson, L. L. (1979). Chemistry and biochemistry of insect waxes. *Prog. Lipid Res.* **17**, 319–345.
Blossey, R. (2003). Self-cleaning surfaces – virtual realities. *Nat. Mater.* **2**, 301–306.
Breton, P. (1999). From microns to nanometers: early landmarks in the science of scanning electron microscope imaging. *Scanning Microsc.* **13**, 1–6.
Brocher, F. (1909). Recherches sur la respiration des insectes aquatiques adultes. Les Dyticidés. *Ann. Biol. Lacustre* **4**, 383–398.
Brocher, F. (1910). Les phénomènes capillaires, leur importance dans la biologie aquatique. *Ann. Biol. Lacustre* **4**, 89–139.
Brocher, F. (1912a). Recherches sur la respiration des insectes aquatiques adultes. Les Elmides. *Ann. Biol. Lacustre* **5**, 136–179.

Brocher, F. (1912b). Recherches sur la respiration des insectes aquatiques adultes. Les Haemonia. *Ann. Biol. Lacustre* **5**, 5–26.
Brocher, F. (1912c). Recherches sur la respiration des insectes aquatiques adultes. L'Hydrophile. *Ann. Biol. Lacustre* **5**, 220–258.
Brocher, F. (1914). Recherches sur la respiration des insectes aquatiques adultes. Les Dyticidés (2me article), suivi d'une notice sur les mouvements respiratoires de l'Hydrophile. *Ann. Biol. Lacustre* **7**, 5–39.
Brown, H. P. (1966). Effects of soap pollution upon stream invertebrates. *Trans. Am. Microsc. Soc.* **85**, 167.
Brown, H. P. (1987). Biology of riffle beetles. *Annu. Rev. Entomol.* **32**, 253–273.
Bush, J. W. M. and Hu, D. L. (2006). Walking on water: Biolocomotion at the interface. *Ann. Rev. Fluid Mech.* **38**, 339–369.
Bush, J. W. M. and Prakash, M. (2007). Propulsion by directional adhesion. Submitted for publication.
Bushnell, D. M. and Moore, K. J. (1991). Drag reduction in nature. *Annu. Rev. Fluid Mech.* **23**, 65–79.
Callies, M. and Quéré, D. (2005). On water repellency. *Soft matter* **1**, 55–61.
Cape, J. N. (1983). Contact angles of water droplets on needles of Scots pine (*Pinus sylvestris*) growing in polluted atmospheres. *New Phytol.* **93**, 293–299.
Carbone, G. and Mangialardi, L. (2005). Hydrophobic properties of a wavy rough substrate. *Eur. Phys. J. E* **16**, 67–76.
Cassie, A. B. D. (1944). Physics and textiles. *Rep. Prog. Phys.* **10**, 141–171.
Cassie, A. B. D. (1948). Contact angles. *Discuss Faraday Soc.* **3**, 11–16.
Cassie, A. B. D. and Baxter, S. (1945). Large contact angles of plant and animal surfaces. *Nature* **155**, 21–22.
Chan, D. Y. C., Henry, J. D. J. and White, L. R. (1981). The interaction of colloidal particles collected at fluid interfaces. *J. Coll. Interf. Sci.* **79** (2), 410–418.
Chaui-Berlinck, J. G., Bicudo, J. E. and Monteiro, L. H. (2001). The oxygen gain of diving insects. *Respir. Physiol.* **128**, 229–233.
Cheng, L. (1973). Marine and freshwater skaters: differences in surface fine structures. *Nature* **42**, 119–180.
Cheng, Y.-T. and Rodak, D. E. (2005). Is the lotus leaf superhydrophobic? *Appl. Phys. Lett.* **86**, 144101–144103.
Choi, C.-H. and Kim, C.-J. (2006). Large slip of aqueous liquid flow over a nanoengineered superhydrophobic surface. *Phys. Rev. Lett.* **96**, 066001.
Choi, C.-H., Ulmanella, U., Kim, J., Ho, C.-M. and Kim, C.-J. (2006). Effective slip and friction reduction in nanograted superhydrophobic microchannels. *Phys. Fluids* **18**, 087105.
Choi, K. S., Prasad, K. K. and Truong, T. V. (1996). *Emerging Techniques in Drag Reduction*. London: Mechanical Engineering Publication Ltd.
Comstock, J. H. (1887). Note on the respiration of aquatic bugs. *Amer. Nat.* **21**, 577–578.
Cottin-Bizonne, C., Barrat, J. L., Bocquet, L. and Charlaix, E. (2003). Low-friction flows of liquid at nanopatterned interfaces. *Nat. Mater.* **2**, 237–240.
Craig, S. and Beaton, C. D. (1996). A simple cryo-SEM method for delicate plant tissues. *J. Microsc.* **182**, 102–105.
Crandall, S. H., Dahl, N. C. and Lardner, T. J. (1978). *An Introduction to the Mechanics of Solids*. New York: McGraw-Hill, Inc.
Crisp, D. J. (1950). The stability of structures at a fluid interface. *Trans. Faraday Soc.* **46**, 228–235.
Crisp, D. J. and Thorpe, W. H. (1948). The water-protecting properties of insect hairs. *Discuss Faraday Soc.* **3**, 210–220.
Daniel, T. L. (1984). Unsteady aspects of aquatic locomotion. *Am. Zool.* **24**, 121–134.

Dechant, H. E., Rammerstorfer, F. and Barth, F. (2001). Arthropod touch reception: stimulus transformation and finite element model of spider tactile hairs. *J. Comp. Physiol. A* **187**, 313–322.
De Gennes, P. G. (1985). Wetting: statics and dynamics. *Rev. Mod. Phys.* **57**, 827–863.
De Gennes, P. G., Brochard-Wyart, F. and Quéré, D. (2003). *Capillarity and Wetting Phenomena: Drops, Bubbles, Pearls and Waves*. Berlin: Springer.
Dettre, R. H. and Johnson, R. E. (1964). Contact angle hysteresis II. Contact angle measurements on rough surfaces. In: *Contact Angle, Wettability, and Adhesion* (ed. Fowkes, F. M.) Advances in Chemistry Series, Vol. 43, pp. 136–144. Washington, DC: American Chemical Society.
Dogs, W. (1908). Metamorphose der respirationsorgane bein *Nepa cinera*. *Mitth. Natur. Ver Neuv.* **40**, 1–55.
Donald, A. M. (2002). No need to dry – environmental scanning electron microscopy of hydrated system. *Mater. Res. Soc. Symp. Proc* **711**, 93–100.
Donald, A. M. (2003). The use of environmental scanning electron microscopy for imaging wet and insulating materials. *Nat. Mater.* **2**, 511–516.
Duez, C., Ybert, C., Clanet, C. and Bocquet, L. (2007). Making a splash with water repellency. *Nat. Phys.* **3**, 180–183.
Dufour, L. (1833). *Recherches Anatomiques et Physiologiques sur les Hémiptères, Accompagnées de Considèrations Relatives à l'Histoire Naturelle et à la Classification de ces Insectes*, pp. 68–74. Paris: Impr. de Bachelier, extrait des Mémoires des savans étrangers, tome IV.
Dussan, E. B. (1979). On the spreading of liquids on solid surfaces: static and dynamic contact lines. *Annu. Rev. Fluid Mech.* **11**, 371–400.
Dussan, E. B. and Chow, R. T. (1983). On the ability of drops or bubbles to stick to non-horizontal surfaces of solids. *J. Fluid Mech.* **137**, 1–29.
Dutrochet, M. H. (1837). *Memoires pour Servir à l'Histoire Anatomique et Physiologique des Végétaux et des Animaux: Du Mécanisme de la Respiration des Insectes*, pp. 486–491. Paris: Chez J.-B. Bailliére.
Dyck, J. (1985). The evolution of feathers. *Zool. Scripta* **14**, 137–154.
Ege, R. (1915). On the respiratory function of the air stores carried by some aquatic insects. *Z. Allg. Physiol.* **17**, 81.
Elkhyat, A., Courderot-Masuyer, C., Gharbi, T. and Humbert, P. (2004). Influence of the hydrophobic and hydrophilic characteristics of sliding and slider surfaces on friction coefficient: *in vivo* human skin friction comparison. *Skin Res. Tech.* **10**, 215221.
Elowson, A. M. (1984). Spread-wing postures and the water repellency of feathers: a test of Rijke's hypothesis. *Auk* **101**, 371–383.
English, L. L. (1928). Some properties of oil emulsions influencing insecticidal efficiency. *Bull. Ill. Nat. Hist. Surv.* **17**, 233–259.
Extrand, C. W. (2002). Model for contact angles and hysteresis on rough and ultraphobic surfaces. *Langmuir* **18**, 7991–7999.
Extrand, C. W. (2003). Contact angles and hysteresis on surfaces with chemically heterogeneous islands. *Langmuir* **19**, 3793–3796.
Extrand, C. W. (2004). Criteria for ultralyophobic surfaces. *Langmuir* **20**, 5013–5018.
Extrand, C. W. (2006). Designing for optimum liquid repellency. *Langmuir* **22**, 1711–1714.
Extrand, C. W. and Gent, A. (1990). Retention of liquid drops by solid surfaces. *J. Coll. Interf. Sci.* **138**, 431–442.
Extrand, C. W. and Kumagai, Y. (1995). Liquid drop on an inclined plane: the relation between contact angles, drop shape, and retentive force. *J. Coll. Interf. Sci.* **170**, 515–521.

Farrell, B. and Mitter, C. (1990). Phylogenesis of insect/plant interactions: have Phyllobrotica leaf beetles (Chrysomelidae) and the Lamiales diversified in parallel? *Evolution* **44**, 1389–1403.

Feng, L., Song, Y., Zhai, J., Liu, B., Xu, J., Jiang, L. and Zhu, D. (2003). Creation of a superhydrophobic surface from an amphiphilic polymer. *Adv. Mater.* **42**, 42–44.

Feng, X., Li, S., Li, Y., Li, H., Zhang, L., Zhai, J., Song, Y., Liu, B., Jiang, L. and Zhu, D. (2002). Super-hydrophobic surfaces: from natural to artificial. *Adv. Mater.* **14**, 1857–1860.

Feng, X.-Q., Gao, X., Wu, Z., Jiang, L. and Zheng, Q.-S. (2007). Superior water repellency of water strider legs with hierarchical structures: experiments and analysis. *Langmuir* **23** (9), 4892–4896.

Feng, X.-Q. and Jiang, L. (2006). Design and creation of superwetting/antiwetting surfaces. *Adv. Mater.* **18**, 3063–3078.

Fish, F. E. (1984). Mechanics, power output and efficiency of the swimming muskrat (*Ondatra zibethicus*). *J. Exp. Biol.* **110**, 183–201.

Fish, F. E. (1998). Imaginative solutions by marine organisms for drag reduction. In: *Proceedings of the International Symposium On Seawater Drag Reduction* (ed. Meng, J. C. S.), pp. 443–450. Arlington, VA: Office of Naval Research, Newport, Rhode Island.

Fish, F. E. (2006). The myth and reality of Gray's paradox: implication of dolphin drag reduction for technology. *Bioinsp. Biomim.* **1**, R17–R25.

Fish, F. E. and Baudinette, R. V. (1999). Energetics of locomotion by the Australian water rat (*Hydromys chrysogaster*): a comparison of swimming and running in a semi-aquatic mammal. *J. Exp. Biol.* **202**, 353–363.

Fish, F. E., Baudinette, R. V., Frappel, P. B. and Sarre, M. P. (1997). Energetics of swimming by the platypus *Ornithorhynchus*: metabolic effort associated with rowing. *J. Exp. Biol.* **200**, 2647–2652.

Fish, F. E., Smelstoys, J., Baudinette, R. V. and Reynolds, P. S. (2002). Fur does not fly, it floats: buoyancy of pelage in semi-aquatic mammals. *Aquat. Mamm.* **28**, 103–112.

Flynn, M. R. and Bush, J. W. M. (2008). Underwater breathing. *J. Fluid Mech.* Submitted.

Fogg, G. E. (1948). Adhesion of water to the external surfaces of leaves. *Faraday Disc. Chem. Soc.* **3**, 162–166.

Furstner, R., Barthlott, W., Neinhuis, C. and Walzel, P. (2005). Wetting and self-cleaning properties of artificial superhydrophobic surfaces. *Langmuir* **21**, 956–961.

Gao, L. and McCarthy, T. J. (2006). A perfectly hydrophobic surface ($\theta_a/\theta_r = 180^\circ/180^\circ$). *J. Am. Chem. Soc.* **128**, 9052–9053.

Gao, L. and McCarthy, T. J. (2007). How Wenzel and Cassie were wrong. *Langmuir* **23**, 3762–3765.

Gao, X. and Jiang, L. (2004). Water-repellent legs of water striders. *Nature* **432**, 36.

Gifford, W. A. and Scriven, L. E. (1971). On the attraction of floating particles. *Chem. Eng. Sci.* **26**, 287–297.

Gittelman, S. H. (1975). Physical gill efficiency and winter dormancy in pigmy backswimmer, *Neoplea striola* (Hemiptera: Pleidae). *Ann. Entomol. Soc. Amer.* **68**, 1011–1017.

Glasheen, J. W. and McMahon, T. A. (1996a). A hydrodynamic model of locomotion in the basilisk lizard. *Nature* **380**, 340–342.

Glasheen, J. W. and McMahon, T. A. (1996b). Size dependence of water-running ability in basilisk lizards *Basiliscus basiliscus*. *J. Exp. Biol.* **199**, 2611–2618.

Glasheen, J. W. and McMahon, T. A. (1996c). Vertical water entry of disks at low Froude numbers. *Phys. Fluids* **8**, 2078–2083.
Gorb, N. S. (1998). The design of the fly adhesive pad: distal tenent setae are adapted to the delivery of an adhesive secretion. *Proc. R. Soc. Lond. B* **265**, 747–752.
Gorb, N. S. (2008). Chapter in this issue. *Adv. Insect Physiol.*
Grant T. (1995). *The platypus: a unique mammal*. Sidney: University of New SouthWales Press Ltd.
Gryzbowski, B. A., Bowden, N., Arias, F., Yang, H. and Whitesides, G. M. (2001). Modeling of menisci and capillary forces from the millimeter to the micrometer size. *J. Phys. Chem. B* **105**, 404–412.
Gu, Z. Z., Uetsuka, H., Takahashi, K., Nakajima, R., Onishi, H., Fujishima, A. and Sato, O. (2003). Structural color and the lotus effect. *Angew. Chem. Int. Ed.* **42**, 894–899.
Hadley, N. F. (1978). Cuticular permeability of desert tenebrionid beetles: correlations with epicuticular hydrocarbon composition. *Insect Biochem.* **8**, 17–22.
Hadley, N. F. (1979). Wax secretion and color phases of the desert tenebrionid beetle *Cryptoglossa verrucosa* (LeConte). *Science* **293**, 367–369.
Hadley, N. F. (1981). Cuticular lipids of terrestrial plants and arthropods: a comparison of their structure, composition, and waterproofing function. *Biol. Rev.* **56**, 23–47.
Hagemann, J. (1910). Beitrige zur kenntnis von corixa. *Zool. Jahrb. Abt. Anat. Ontog. Tiere.* **30**, 373–2685.
Harpster, H. T. (1944). The gaseous plastron as a respiratory mechanism in *Stenelmis quadrimaculata* Horn (Dryopidae). *Trans. Amer. Micro. Soc.* **63**, 1–26.
Hazlett, R. D. (1990). Fractal applications: wettability and contact angle. *J. Coll. Interf. Sci.* **137**, 527–533.
Hebets, E. A. and Chapman, R. F. (2000). Surviving the flood: plastron respiration in the nontracheate arthropod *Phrynus marginemaculatus* (Amblypygi; Arachnida). *J. Insect Physiol.* **46**, 13–19.
Heckman, C. W. (1983). Comparative morphology of arthropod exterior surfaces with the capability of binding a film of air underwater. *Int. Revue. Ges. Hydrobiol.* **68**, 715–736.
Herminghaus, S. (2000). Roughness-induced non-wetting. *Europhys. Lett.* **52**, 165–170.
Hinton, H. E. (1969). Respiratory systems of insect egg shells. *Annu. Rev. Entomol.* **14**, 343–368.
Hinton, H. E. (1976). Plastron respiration in bugs and beetles. *J. Insect Physiol.* **22**, 1529–1550.
Hinton, H. E. and Jarman, G. M. (1976). A diffusion equation for tapered plastrons. *J. Insect Physiol.* **22**, 1263–1265.
Holdgate, M. W. (1955). The wetting of insect cuticle by water. *J. Exp. Biol.* **32**, 591–617.
Holloway, P. J. (1970). Surface factors affecting the wetting of leaves. *Pestic. Sci.* **1**, 156–163.
Hoppe, J. (1911). Die atmung von Notoencta glauca. *Zool. Jb. Abt. Allg. Zoo.* **31**, 189–244.
Hoskins, W. M. (1940). Recent contributions of insect physiology to insect toxicology and control. *Hilgardia* **13**, 307–386.
Howard, R. W. (1993). Cuticular hydrocarbons and chemical communication in insect lipids. In: *Insect Lipids: Chemistry, Biochemistry, and Biology* (eds Stanley-Samuelson, D. W. and Nelson, D. R.), pp. 179–226. Lincoln, NE: University of Nebraska Press.

Hu, D. L. and Bush, J. W. M. (2005). Meniscus-climbing insects. *Nature* **437**, 733–736.
Hu, D. L. and Bush, J. W. M. (2008a). The hydrodynamics of water-walking arthropods: Part 1. Experiments. *J. Fluid Mech.* To be submitted.
Hu, D. L. and Bush, J. W. M. (2008b). The hydrodynamics of water-walking arthropods: Part 2. Theory. *J. Fluid Mech*. To be submitted.
Hu, D. L., Chan, B. and Bush, J. W. M. (2003). The hydrodynamics of water strider locomotion. *Nature* **424**, 663–666.
Hungerford, H. B. (1919). The biology and ecology of aquatic and semiaquatic Hemiptera. *Kans. Univ. Sci. Bull.* **11**, 1–328.
Hurst, H. (1941). Insect cuticle as an asymmetrical membrane. *Nature* **147**, 388.
Hurst, H. (1948). Asymmetrical behaviour of insect cuticle in relation to water permeability. *Disc. Faraday. Soc.* **3**, 193–210.
Imms, A. D. (1906). *Anurida (a springtail). LMBC Mem. XIII Typical British Marine Plants and Animals*. London: Williams & Norgate.
Israelachvili, J. (1992). *Intermolecular and Surface Forces*, 2nd edn New York: Academic Press.
Janssens, F. (2005). Checklist of the Collembola of the world: Note on the morphology and origin of the foot of the Collembola. http://www.Collembola.org/publicat/unguis.htm
Jenkins, L. and Donald, A. (1999). Condensation of water droplets onto individual fibres for contact angle measurement in the ESEM. *Langmuir* **15**, 7829–7835.
Joanny, J. F. and de Gennes, P. G. (1984). A model for contact angle hysteresis. *J. Chem. Phys.* **81**, 552–562.
Johansson, L. C. and Norber, U. M. L. (2001). Lift-based paddling in diving grebe. *J. Exp. Biol.* **240**, 1687–1696.
Johnson, R. E. and Dettre, R. H. (1964). Contact angle hysteresis I. Study of an idealized rough surface. In: *Contact Angle, Wettability, and Adhesion* (ed. Fowkes, F. M.), Advances in Chemistry Series, Vol. 43, pp. 112–135. Washington, DC: American Chemical Society.
Joseph, P., Cottin-Bizonne, C., Benoît, J. M., Ybert, C., Journet, C., Tabeling, P. and Bocquet, L. (2006). Slippage of water past superhydrophobic carbon nanotube forests in microchannels. *Phys. Rev. Lett.* **97**, 156104.
Journet, C., Moulinet, S., Ybert, C., Purcell, S. T. and Bocquet, L. (2005). Contact angle measurements on superhydrophobic carbon nanotube forests: effect of fluid pressure. *Europhys. Lett.* **71**, 104–109.
Kellen, W. R. (1956). Notes on the biology of *Halovelia marianarum* Usinger in Samoa (Veliidae: Heteroptera). *Ann. Entomol. Soc. Am.* **52**, 53–62.
Keller, J. B. (1998). Surface tension force on a partly submerged body. *Phys. Fluids* **10**, 3009–3010.
Kim, H.-Y. and Mahadevan, L. (2006). Capillary rise between elastic sheets. *J. Fluid Mech.* **548**, 141–150.
Knoll, M. (1935). Aufladepotentiel und sekundäremission elektronenbestrahlter körper. *Z. Tech. Phys.* **16**, 467–475.
Kousik, G., Pitchumani, S. and Renganathan, N. G. (2001). Electrochemical characterization of polythiophene-coated steel. *Prog. Org. Coat.* **43**, 286.
Kovac, D. and Maschwitz, U. (1999). Protection of hydrofuge respiratory structures against detrimental microbiotic growth by terrestrial grooming in water beetles. *Entomol. Gen.* **24**, 277–292.
Kralchevsky, P. A. and Denkov, N. D. (2001). Capillary forces and structuring in layers of colloid particles. *Curr. Opin. Coll. Interf. Sci.* **6**, 383–401.

Krantz, G. W. and Baker, G. T. (1982). Observations on the plastron mechanism of *Hydrozetes* sp. (Acari: Oribatida: Hydrozetidae). *Acarologia* **23**, 273–277.
Krivosheina, M. G. (2005). The plastron is a universal structure that ensures breathing of dipteran larvae both in the water and in the air. *Doklady Bio. Sci.* **401**, 112–115.
Kühnelt, W. (1928). Über den bau des insektenskelettes. *Zool. Jb. (Anat.)* **50**, 219–278.
Lafuma, A. and Quéré, D. (2003). Superhydrophobic states. *Nat. Mater.* **2**, 457–460.
Lamoral, B. H. (1968). On the ecology and habitat adaptations of two intertidal spiders, *Desis formidabilis* and *Amaurobioides africanus* Hewitt at 'The Island' (Kommetjie, Cape Peninsula), with notes on the occurrence of two other spiders. *Ann. Natal. Mus.* **20**, 151–193.
Lau, K., Bico, J., Teo, K., Milne, W., McKinley, G. and Gleason, K. (2003). Superhydrophobic carbon nanotube forest. *Nano Lett.* **3**, 1701–1705.
Lauga, E. and Brenner, M. P. (2004). Evaporation-driven assembly of colloidal particles. *Phys. Rev. Lett.* **93**, 238–301.
Lee, W., Jin, M. K., Yoo, W. C. and Lee, J. K. (2004). Nanostructuring of a polymeric substrate with well-defined nanometer-scale topography and tailored surface wettability. *Langmuir* **20**, 7665–7669.
Liew, K. M., Wong, C. H. and Tan, M. J. (2005). Buckling properties of carbon nanotube bundles. *Appl. Phys. Lett.* **87**, 041901.
Liu, H., Zhai, J. and Jiang, L. (2006). Wetting and anti-wetting on aligned carbon nanotube films. *Soft Matter.* **2**, 811–821.
Lodge, R. A. and Bhushan, B. (2006). Wetting properties of human hair by means of dynamic contact angle measurement. *J. Appl. Polymer Sci.* **102**, 5255–5265.
Lou, S.-T., Ouyang, Z.-Q., Zhang, Y., Li, X.-J., Hu, J., Li, M.-Q. and Yang, F.-J. (2000). Nanobubbles on solid surface imaged by atomic force microscopy. *J. Vac. Sci. Technol. B* **18**, 2573–2575.
Manoharan, V. N., Elsesser, M. T. and Pine, D. J. (2003). Dense packing and symmetry in small clusters of microspheres. *Science* **301**, 483–487.
Mansfield, E. H., Sepangi, H. R. and Eastwood, E. A. (1997). Equilibrium and mutual attraction or repulsion of objects supported by surface tension. *Philos. Trans. R. Soc. Lond. Ser. A* **355**, 869–919.
Matsuda, K., Watanabe, S. and Eiju, T. (1985). Real-time measurement of large liquid surface deformation using a holographic shearing interferometer. *Appl. Optics.* **24** (24), 4443–4447.
McHale, G., Aqil, S., Shirtcliffe, N. J., Newton, M. I. and Erbil, H. Y. (2005). Analysis of droplet evaporation on a superhydrophobic surface. *Langmuir* **21**, 11053–11060.
McMahon, T. A. and Bonner, J. T. (1985). *On Size and Life*, p. 211. New York: Scientific American Library.
Miller, P. L. (1964). Possible function of haemoglobin in *Anisops*. *Nature* **201**, 1052.
Min, T. and Kim, J. (2004). Effects of hydrophobic surfaces on skin-friction drag. *Phys. Fluids* **16**, 55–58.
Minsky, M. (1953). Neural-analog networks and the brain-model problem. Ph.D. thesis, Princeton University Press, Princeton, NJ.
Minsky, M. (1988). Memoir on inventing the confocal scanning microscope. *Scanning* **10**, 128–138.
Miyamoto, S. (1955). On a special mode of locomotion utilizing surface tension at the water-edge in some semiaquatic insects. *Kontyû* **23**, 45–52.

Mock, U., Förster, R., Menz, W. and Rühe, J. (2005). Towards ultrahydrophobic surfaces: a biomimetic approach. *J. Phys.: Condens. Mat.* **17**, S639–S648.
Moore, W. (1921). Spreading and adherence of arsenical sprays. *Minnesota Agric. Exp. Sta. Tech. Bull.* **2**, 1–50.
Mordvinov, Y. E. (1976). Locomotion in water and the indices of effectiveness of propelling systems for some aquatic mammals. *Zool. Zh.* **55**, 1375–1382. (in Russian).
Nadkarni, G. and Garoff, S. (1992). An investigation of microscopic aspects of contact angle hysteresis: pinning of the contact line on a single defect. *Europhys. Lett.* **20**, 523.
Neinhuis, C. and Barthlott, W. (1997). Characterization and distribution of water-repellent, self-cleaning plant surfaces. *Ann. Bot.* **79**, 667–677.
Nicolson, M. M. (1949). The interaction between floating particles. *Proc. Camb. Phil. Soc.* **45**, 288–295.
Noble-Nesbitt, J. (1963). Transpiration in *Podura aquatica* L. (Collembola, Isotomidae) and the wetting properties of its cuticle. *J. Exp. Biol.* **40**, 681–700.
Nutman, S. (1941). The function of the ventral tube in *Onychiurus armatus* (Collembola). *Nature* **148**, 168–169.
O'Kane, W. C., Westgate, W. A., Glover, L. C. and Lowry, P. R. (1932). Studies of contact insecticides. V. The performance of certain contact agents on various insects. *Tech. Bull. NH Agric. Exp. Sta.* **51**, 1–20.
Oliver, J. F., Huh, C. and Mason, S. G. (1977). Resistance to spreading of liquids by sharp edges. *J. Colloid Interf. Sci.* **59**, 568–581.
Onda, T., Shibuichi, S., Satoh, N. and Tsujii, K. (1996). Super-water-repellent fractal surfaces. *Langmuir* **12**, 2125–2127.
Öner, D. and McKarthy, T. J. (2000). Ultrahydrophobic surfaces. Effects of topography length scales on wettability. *Langmuir* **16**, 7777–7782.
Otten, A. and Herminghaus, S. (2004). How plants keep dry: a physicist's point of view. *Langmuir* **20**, 2405–2408.
Ou, J., Perot, B. and Rothstein, J. P. (2004). Laminar drag reduction in micro-channels using ultrahydrophobic surfaces. *Phys. Fluids* **16**, 4635–4643.
Pal, R. (1951). The wetting of insect cuticle. *Bull. Ent. Res.* **51**, 121–139.
Parker, A. R. and Lawrence, C. R. (2001). Water capture by a desert beetle. *Nature* **414**, 33–34.
Patankar, N. A. (2004). Transition between superhydrophobic states on rough surfaces. *Langmuir* **20**, 7097–7102.
Perez-Goodwyn, P. and Fujisaki, K. (2007). Sexual conflicts, loss of flight, and fitness gains in locomotion of polymorphic water striders (*Gerridae*). *Entomol. Exper. Appli.* In press.
Perez-Goodwyn, P. J. (2007). *Functional surfaces in biology,* chap. Anti-wetting surfaces in Heteroptera (Insecta): Hairy solutions to any problem. Dordrecht: Springer. In press.
Persson, B. (2003). On the mechanism of adhesion in biological systems. *J. Chem. Phys.* **118**, 7614–7621.
Philip, G. D., Matthews, D. and Seymour, R. S. (2006). Diving insects boost their buoyancy bubbles. *Nature* **441**, 171.
Pike, N., Richard, D., Foster, W. A. and Mahadevan, L. (2002). How aphids lose their marbles. *Proc. R. Soc. Lond. B* **269**, 1211–1215.
Plateau, J. (1873). *Statique Expérimentale et Théorique des Liquides Soumis aux Seules Forces Moléculaires*. Paris: Gauthier-Villars.
Quéré, D. (2002). Fakir droplets. *Nat. Mater.* **1**, 1415.

Rabinovich, Y. I., Esayanur, M. S. and Moudgil, B. M. (2005). Capillary forces between two spheres with a fixed volume liquid bridge: theory and experiment. *Langmuir* **21**, 10992–10997.
Rahn, H. and Paganelli, C. V. (1968). Gas exchange in gas gills of diving insects. *Respir. Physiol.* **5**, 145–164.
Rayleigh, L. (1879). On the instability of jets. *Proc. Lond. Math. Soc.* **10**, 413.
Reimer, L. (1998). *Scanning Electron Microscopy: Physics of Image Formation and Microanalysis*. Berlin: Springer.
Reyssat, M., Pépin, A., Marty, F., Chen, Y. and Quéré, D. (2006). Bouncing transitions in microtextured materials. *Europhys. Lett.* **74**, 306–312.
Ribak, G., Weihs, D. and Arad, Z. (2005). Water retention in the plumage of diving great cormorants *Phalacrocorax carbo sinensis*. *J. Avian Biol.* **36**, 89–95.
Rijke, A. M. (1970). Wettability and phylogenetic development of feather structure in water birds. *J. Exp. Biol.* **52**, 469–479.
Ross, S. and Becher, P. (1992). The history of the spreading coefficient. *J. Colloid Int. Sci.* **149**, 575–579.
Rovner, J. S. (1986). Spider hairiness: air stores and low activity enhance flooding survival in inland terrestrial species. In: *Acta X International Congress of Arachnology Jaca/Espana*, 123–129.
Rowlinson, J. S. and Widom, B. (1982). *Molecular Theory of Capillarity*. Mineola, New York: Dover Publications, Inc.
de Ruiter, L., Wolvekamp, H. P. and van Tooren, A. J. (1951). Experiments on the respiration of some aquatic insects (*Hydrous piceus* L., *Naucoris cimicoides* L., and *Notonecta glauca* L.). *Acta Physiol. et Pharmacol. Neerl.* **1**, 657–659.
Sabbatovskii, K. G., Dutschk, V., Nitschke, M. and Grundke, F. S. K. (2004). Properties of the teflon AF1601S surface treated with the low-pressure argon plasma. *Colloid J.* **66**, 208–215.
Saliternik, Z. (1942). The macroscopic differentiation of anopheline eggs according to their pattern on the surface of the water. *Bull. Entomol. Res.* **33**, 221.
Schildknecht, H. (1976). Chemical ecology — a chapter of modern natural products chemistry. *Angew. Chem. Int. Ed. Engl.* **15**, 214–222.
Scriven, L. E. and Sternling, C. V. (1970). The Marangoni effects. *Nature* **187**, 186–188.
Shirtcliffe, N. J., McHale, G., Newton, M. I., Perry, C. C. and Pyatt, F. B. (2006). Plastron properties of a superhydrophobic surface. *Appl. Phys. Lett.* **89**, 104–106 (2 pages).
Shuttleworth, R. and Bailey, G. L. (1948). Spreading of a liquid over a rough solid. *Disc. Faraday Soc.* **3**, 16–22.
Silberglied, R. and Aiello, A. (1980). Camouflage by integumentary wetting in bark bugs. *Science* **207**, 773–775.
Slodowska, A., Woźnak, M. and Matlakowska, R. (1999). The method of contact angle measurements and estimation of work of adhesion in bioleaching of metals. *Biol. Proc. Online* **1** (3), 114–121.
Snyder, B. A., Aston, D. E. and Berg, J. C. (1997). Particle-drop interactions examined with an atomic-force microscope. *Langmuir* **13**, 590–593.
Spence, J. R., Spence, D. H. and Scudder, G. G. (1980). Submergence behavior in *Gerris*: underwater basking. *Am. Midl. Nat.* **103**, 385–391.
Steinmann, T., Casas, J., Krijnen, G. and Dangles, O. (2006). Air-flow sensitive hairs: boundary layers in oscillatory flows around arthropods appendages. *J. Exp. Biol.* **209**, 4398–4408.
Stelmashenko, N. A., Craven, J. P., Donald, A. M., Terentjev, E. M. and Thiel, B. L. (2001). Topographic contrast of partially wetting water droplets in environmental scanning electron microscopy. *J. Microsc.* **204**, 172–183.

Stratton, G. E., Suter, R. B. and Miller, P. R. (2004a). Evolution of water surface locomotion by spiders: a comparative approach. *Biol. J. Linn. Soc.* **81** (1), 63–78.

Stratton, G. E., Suter, R. B. and Miller, P. R. (2004b). Taxonomic variation among spiders in the ability to repel water: surface adhesion and hair density. *J. Arachnol.* **32**, 11–21.

Straus-Durckheim, H. (1828). *Considérations générales sur l'anatomie comparée des animaux articulés, auxquels on a joint anatomie descriptive du Hanneton vulgaire (Melolontha vulgaris)*, p. 435. Paris, Strasbourg, Bruxelles: F.G. Levrault.

Stride, G. O. (1955). On the respiration of an aquatic African beetle, *Piotamodytes tuberosus* Hinton. *Ann. Entomol. Soc. Am.* **48**, 344–351.

Taylor, R. L., Verran, J., Lees, G. C. and Ward, A. J. (1998). The influence of substratum topography on bacterial adhesion to polymethyl methacrylate. *J. Mater. Sci. Mater. Med.* **9**, 17–22.

Thibaud, J. M. (1970). Biologie et écologie des Collemboles, Hypogastruidae, édaphiques et Cavernicoles. *Mém. Mus. Natl. Hist. Nat. Nouvelle Sér. A* **61**, 83201.

Thorpe, W. H. (1950). Plastron respiration in aquatic insects. *Biol. Rev.* **25**, 344–390.

Thorpe, W. H. and Crisp, D. J. (1947a). Studies on plastron respiration I. The biology of *Apelocheirus* [Hemiptera, Aphelocheiridae (Naucoridae)] and the mechanism of plastron rentention. *J. Exp. Biol.* **24**, 227–269.

Thorpe, W. H. and Crisp, D. J. (1947b). Studies on plastron respiration II. The respiratory efficiency of the plastron in *Apelocheirus*. *J. Exp. Biol.* **24**, 270–303.

Thorpe, W. H. and Crisp, D. J. (1947c). Studies on plastron respiration III. The orientation responses of *Apelocheirus* [Hemiptera, Aphelocheiridae (Naucoridae)] in relation to plastron respiration; together with an account of specialized pressure receptors in aquatic insects. *J. Exp. Biol.* **24**, 310–328.

Thorpe, W. H. and Crisp, D. J. (1949). Studies on plastron respiration IV: plastron respiration in the Coleoptera. *J. Exp. Biol.* **25** (3), 219–261.

Torre-Bueno, J. R. (1907). On *Rhagovelia obesa* Uhler. *Can. Entomol.* **39**, 61–64.

Vaknin, Y., Gan-Mor, S., Bechar, A., Ronen, B. and Eisikowitch, D. (2000). The role of electrostatic forces in pollination. *Plant Syst. Evol.* **222**, 133–142.

Vella, D., Lee, D.-G. and Kim, H.-Y. (2006a). Sinking of a horizontal cylinder. *Langmuir* **22**, 2972–2974.

Vella, D. and Mahadevan, L. (2005). The "Cheerios effect". *Am. J. Phys.* **73**, 817–825.

Vella, D., Metcalfe, P. D. and Whittaker, R. J. (2006b). Equilibrium conditions for the floating of multiple interfacial objects. *J. Fluid Mech.* **549**, 215–224.

Vincent, J. F. V. and Wegst, U. G. K. (2004). Design and mechanical properties of insect cuticle. *Arthrop. Struct. Dev.* **33**, 187–199.

Vlasblom, G. V. (1970). Respiratory significance of physical gill in some adult insects. *Comp. Biochem. Physiol.* **36**, 377–385.

Vogel, S. (2006). Living in a physical world. VIII. Gravity and life in water. *J. Biosci.* **30** (3), 309–322.

Wagner, P., Furstner, R., Barthlott, W. and Neinhuis, C. (2003). Quantitative assessment to the structural basis of water repellency in natural and technical surfaces. *J. Exp. Bot.* **54**, 1295–1303.

Wagner, P., Neinhuis, C. and Barthlott, W. (1996). Wettability and contaminability of insect wings as a function of their surface sculpture. *Acta Zool.* **77**, 213–225.

Walsh, M. J. (1990). Riblets. In: *Viscous Drag Reduction in Boundary Layers* (eds Bushnell, D. M. and Hefner, J. N.), Progress in Astronautics and Aeronautics,

Vol. 123, pp. 203–261. Washington, DC: American Institute of Aeronautics and Astronautics, Inc.
Walther, P. and Muller, M. (1997). Double-layer coating for field-emission cryo-scanning electron microscopy-present state and applications. *Scanning* **19**, 343–3488.
Wenzel, R. N. (1936). Resistance of solid surfaces to wetting by water. *Ind. Eng. Chem.* **28**, 988–994.
West, T. (1982). The foot of the fly; its structure and action: elucidated by comparison with the feet of other insects. *Trans. Linn. Soc. Lond.* **23**, 393–421.
White, F. M. (1994). *Fluid Mechanics*. New York: McGraw-Hill, Inc.
Whitesides, G. and Grzybowski, B. (2002). Self-assembly at all scales. *Science* **295**, 2418–2421.
Wigglesworth, V. B. (1933). The physiology of the cuticle and of ecdysis in *Rhodnius prolixus* (Triatomidae, Hemiptera); with special reference to the function of the oenocytes and of the dermal glands. *Q. J. Microsc. Sci.* **76**, 269–318.
Wigglesworth, V. B. (1945). Transpiration through the cuticle of insects. *J. Exp. Biol.* **21**, 97–114.
Wigglesworth, V. B. (1950). *The Principles of Insect Physiology*. London: Methuen.
Wigglesworth, V. B. (1979). The physiology of insect cuticle. *Annu. Rev. Entomol.* **2**, 37–54.
Wigglesworth, V. B. (1984). *Insect Physiology*, pp. 1–17. London: Chapman and Hall.
Wilcoxon, F. and Hartzell, A. (1931). Some factors affecting the efficiency of contact pesticides. I. Surface forces as related to wetting and tracheal pentration. *Contr. Boyce. Thompson Inst.* **3**, 1–12.
Wu, C. W., Kong, X. Q. and Wu, D. (2007). Micronanostructures of the scales on a mosquito's legs and their role in weight support. *Phys. Rev. E.* **76**, 017301 (4 pages).
Yi, U.-C. and Kim, C.-J. (2004). Soft printing of droplets pre-metered by electrowetting. *Sens. Actuat. A* **114**, 347354.
Yoshimitsu, Z., Nakajima, A., Watanabe, T. and Hashimoto, K. (2002). Effects of surface structure on the hydrophobicity and sliding behavior of water droplets. *Langmuir* **3**, 5818–5822.
Young, T. (1805). An essay on the cohesion of fluids. *Phil. Trans. Roy. Soc. Lond. A* **95**, 65–87.
Zeng, C., Bissig, H. and Dinsmore, A. D. (2006). Particles on droplets: from fundamental physics to novel materials. *Solid State Comm.* **139**, 547–556.
Zhang, X., Tan, S., Zhao, N., Guo, X., Zhang, X., Zhang, Y. and Xu, J. (2006). Evaporation of sessile water droplets on superhydrophobic natural lotus and biomimetic polymer surfaces. *Chem. Phys. Chem.* **7**, 2067–2070.
Zheng, Y., Gao, X. and Jiang, L. (2007). Directional adhesion of superhydrophobic buttery wings. *Soft Mater.* **3**, 178–182.
Zisman, W. A. (1964). Relation of equilibrium contact angle to liquid and solid constitution. In: *Contact Angle, Wettability and Adhesion; The Kendall Award Symposium Honoring William A. Zisman* (ed. Fowkes, F. M.), Advances in Chemistry Series, Vol. 43, p. 6. Washington, DC: American Chemical Society.

Mechanosensory Feedback in Walking: From Joint Control to Locomotor Patterns

Ansgar Büschges and Matthias Gruhn

Department of Animal Physiology, Zoological Institute, University of Cologne, Cologne, Germany

1 Introduction 194
2 Mechanosensory feedback signals 195
3 The control of posture 199
4 Mechanosensory control of walking 201
5 Organization of neural networks controlling single-leg stepping 204
6 Specificity of sensory–motor influences 209
7 Mechanosensory signals in inter-leg coordination 211
8 Neural mechanisms underlying modifications in the locomotor output 213
  8.1 Changing walking speed 213
  8.2 Changing walking direction 216
  8.3 Turning 218
9 Conclusions 221
  Acknowledgements 222
  References 222

Abstract

The generation of a functional motor output for walking is the result of the activity of central pattern generating networks, local feedback from sensory neurons about movements and forces generated in the locomotor organs and through interaction with coordinating signals from neighbouring segments or appendages. This chapter addresses the current knowledge about the role and processing of mechanosensory feedback for walking in insects. Special focus will be given to (i) the mechanosensory signals that are utilized for the generation and control of walking, and the state-dependent modification in their processing, (ii) the organization of neural networks controlling single-leg stepping, (iii) the role of mechanosensory signals in intersegmental coordination and, finally, (iv) modifications in the walking motor output that are associated with changing walking speed and walking direction. We will place the current knowledge and new results

ADVANCES IN INSECT PHYSIOLOGY VOL. 34
ISBN 978-0-12-373714-4
DOI: 10.1016/S0065-2806(07)34004-6

into the broader context of motor pattern generation for other locomotor behaviours and in other organisms.

1 Introduction

Walking is one of the most common means of terrestrial locomotion. An organism moving this way needs to be equipped with limbs and it is required to generate a cyclic two-phase stepping pattern consisting of a stance and a swing phase. Stance phase is the power stroke in walking during which the leg has ground contact and serves propulsion of the body. It is followed by a swing phase, a return stroke during which the leg is lifted off the ground and moved to the starting position for the next stance phase.

Although the walking pattern only has these two phases, its neuronal control can be considered very complex. First, because intra-leg coordination has to be achieved between the single segments of the multi-segmented legs; coordinating up to five parts of an insect leg demands appropriate activation of more than a dozen muscles, and the coordination may change according to the behavioural task or situation. Second, because the movements of the various legs of the animal have to be coordinated to keep the animal off the ground and generate propulsion. This requires posture control and inter-leg coordination. Both of these coordinating functions require considerable interaction between sensory structures associated with the legs and elements within the central nervous system, to match leg movements to the requirements of different behaviours and conditions within the animal and its environment.

In the last two decades, substantial information has been gathered from a variety of walking animals on how functional walking motor outputs are generated. Among the best investigated animals are vertebrates such as the cat, mouse, mudpuppy and rat, as well as some arthropods, like crayfish, cockroach and stick insect (for reviews see Pearson, 1993; Orlovsky *et al.*, 1999; Büschges, 2005). Recently, this knowledge has allowed the formulation of a basic controller architecture for single-joint and single-leg control in stepping for the three thoracic leg pairs of the stick insect (Ekeberg *et al.*, 2004) and the cat hind leg (Ekeberg and Pearson, 2005; Pearson *et al.*, 2006). In both cases, the role of mechanosensory signals in this complex control task is emphasized.

This chapter will address four main topics. First, we will review different kinds of mechanosensory signals and their roles in posture control and walking pattern generation for the insect leg muscle control system. Second, we will summarize today's knowledge on the organization of the neural networks generating a basic locomotor output for the stick insect

leg. Third, we will address the role of mechanosensory signals in intersegmental coordination, and, finally, we will report on mechanisms that allow changes in the motor output for walking with respect to changes in speed and walking direction. This chapter is not intended to give an introduction to insect sensory–motor processing or motor control in general. Instead, the results presented were selected exclusively for to their novelty and relevance for walking pattern generation.

2 Mechanosensory feedback signals

The legs of all orthopteran insects are externally and internally equipped with a large number of mechanosensory sense organs. Externally, there are hundreds of tactile hairs on the cuticle of the leg segments, which report contact with obstacles. At various locations, mostly close to the joints, these hair sensilla form fields, the so-called hair plates, or rows that are stimulated by movements of the joint membranes during leg movements. Pulvilli receptors at the ventral surface of the tarsus report touch to the ground and campaniform sensilla (CS) report strain in the cuticle of the leg (Fig. 1A). Internally, there are at least three different kinds of mechanosensory receptors. On the one hand, there are muscle receptors organs and strand receptors, and on the other, there are chordotonal organs (COs). Whereas the former two are single-cell sense organs that respond to length changes of their apodemes, the COs consist of a multitude of sensory neurons that code specific movement parameters, such as position, velocity and acceleration.

This chapter will focus on the structure and physiology of those sense organs that have been shown to contribute to the control of the locomotor output for insect stepping. A more general summary on the different receptor types on the insect leg can be found elsewhere, e.g. in Bässler (1983), Burrows (1996), Field and Matheson (1998) or Graham (1985).

Today, it is clear that two kinds of sensory signals from the insect leg (Fig. 1) play a key role in the generation and control of the stance and swing phases of a stepping leg: These are, first, movement and position signals from the leg joints, and, second, force or strain signals from the cuticle of the leg segments (for summary see Prochazka, 1996; Bässler and Büschges, 1998; Zill *et al.*, 2004; Büschges, 2005).

As mentioned before, movements of the leg segments are reported by hair plates located at the leg joints (Fig. 1A, B). These consist of groups of hair sensilla that are bent by the joint cuticle during flexion of a leg joint. The ventral coxal hair plate (vcxHP) of the stick insect leg, for example, is located on the ventral coxa, proximal to the joint pivot of the thorax-coxa (ThC-) joint. It consists of two groups of hairs, groups G1 and G2 (Büschges and Schmitz, 1991; Dean and Schmitz, 1992) that report

position and movements of the coxa relative to the thorax. Upon protraction of the leg, the joint cuticle is deformed and causes bending and activation of the G1 and G2 hair sensilla (arrows, Fig. 1B). Upon retraction of the leg, the hair sensilla are released, which is the appropriate stimulus for some of the sensory hairs in the hair plate. Three of the four hair plates on the stick insect leg are located on the coxa and one on the trochanter (Tartar, 1976; Schmitz, 1986a). Additional hair rows are located on the posterior coxa and are stimulated by the joint membrane upon

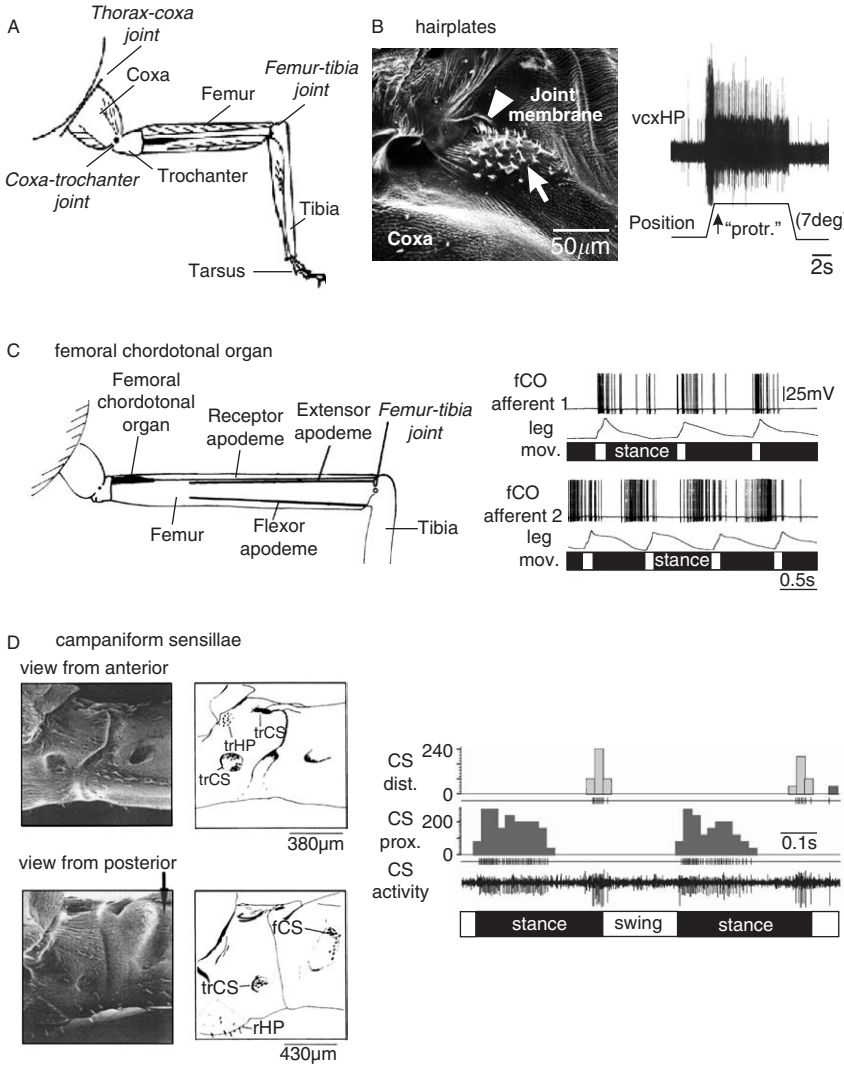

retraction and protraction of the coxa (Tartar, 1976; Dean and Schmitz, 1992). In addition to the sensory hairs, movements and position of the trochanter are also reported by an internal sense organ, the levator receptor organ, which is located parallel to the levator trochanteris muscle in the coxa (Schmitz and Schöwerling, 1992).

Movements and position of the tibia are monitored by the internal femoral chordotonal organ (fCO; Bässler, 1965, 1977), common to all insects (Field and Matheson, 1998). The fCO is bipartite, with a dorsal and a ventral strand, inside the femur (Fig. 1C). Its sensory cells are located at the proximal end of the femur and are connected to the dorsal rim of the tibia by a long tendon. Flexion of the tibia elongates the fCO and extension relaxes it. The sensory cells in the fCO respond to position, velocity and acceleration of tibial movements (Hofmann and Koch, 1985; Hofmann *et al.*, 1985), but only the 80 sensory neurons in its ventral strand – out of approximately 400 total sensory neurons (Füller and Ernst, 1974) – contribute to joint control of the femur-tibia (FTi-) joint in orthopteran insects (Field and Pflüger, 1989; Kittmann and Schmitz, 1992; Büschges, 1994).

As stated above, force and strain signals play a decisive role in the leg muscle control system of arthropods by reporting increased, decreased and/or maintained strain from the cuticle (cockroach: e.g. Zill *et al.*, 1999; Noah *et al.*, 2004; Quimby *et al.*, 2006; stick insect: Hofmann and Bässler, 1982; Delcomyn, 1991; review in Zill *et al.*, 2004). These are reported by CS, which are sensory hairs, each under a small cap protruding from the cuticle, located in groups of up to 30 cells at specific locations on each leg (Fig. 1D). For the stick insect leg, four fields of CS are known to exist on

FIG. 1 Mechanosensory sense organs of the insect leg contributing to generation and control of locomotor activity. (A) Schematic representation of an insect leg, emphasizing the main leg segments and joints. (B) Hair plates. *Left:* Scanning Electron Micrograph (SEM) picture of the ventral coxal hair plate (vcxHP) in the stick insect *Carausius morosus* (adapted from Bässler and Büschges, 1998). The arrowhead points to subgroup G1 and the arrow indicates subgroup G2. *Right:* Extracellular recording of activity of sensory neurons from the vcxHP during stimulation of its hair sensilla by means of moving the joint membrane of the thorax-coxa (ThC-) joint mimicking protraction (upward deflection of the stimulus trace) and retraction of the leg. Note that bending of the hair sensilla results in phasic and tonic activation of sensory neurons (adapted from Schmitz, 1986c). (C) Femoral Chordotonal Organ (fCO). *Left:* Morphological arrangement of the fCO in the stick insect middle leg. *Right:* Recording from two sensory neurons of the fCO during middle-leg walking in the locust (courtesy of H. Wolf; for methods of recording see Wolf and Burrows, 1995). (D) Campaniform sensilla (CS). *Left:* SEM and corresponding drawings from anterior and posterior views of the four CS fields on the trochanter and femur of the stick insect leg (adapted from Akay *et al.*, 2001). *Right:* Extracellularly recorded activity of two CS on the distal and proximal tibia of the cockroach middle leg during stepping (courtesy of S.N. Zill; taken from Zill *et al.*, 2006).

the leg (Hofmann and Bässler, 1982). One is located on the posterior side of the femur, close to the edge of the trochanter, two others on the posterior side of the dorsal coxa and a fourth one is situated on the anterior side of the ventral coxa (Akay *et al.*, 2001). It is important to note that strain in the cuticle can result from both, load onto the leg, or self-generated forces by leg muscles (Pringle, 1938; Hofmann and Bässler, 1982; Delcomyn, 1991).

What role do all these leg sense organs serve? We will address this issue with a special focus on the stick insect, for which the most complete set of data is available. In a stick insect leg, three main leg joints are involved in generating coordinated stepping movements. These are the ThC-joint, the coxa-trochanter (CTr-) joint and the FTi-joint. They serve pro- and retraction as well as levation and depression of the whole leg, and flexion and extension of the tibia, in that order (Fig. 1A). First indications about the role of movement and load feedback in the control of leg stepping arose from behavioural experiments, when sense organs on the legs were manipulated surgically (e.g. Wendler, 1964; Bässler, 1977; Cruse, 1985a,b). When the vcxHP, which monitors position and movement of the ThC-joint, was manipulated in a way that it continuously signalled a protracted leg regardless of its actual position, this leg was moved backward as far as possible and often remained in a continuous stance phase (Bässler, 1977).

Stepping movements were similarly disturbed when the fCO was surgically manipulated so that it signalled reversed information about movement and position of the FTi-joint. In this case, the fCO signalled flexion of the joint when the tibia was extended, and vice versa (Graham and Bässler, 1981). As a consequence, the leg most often could not terminate the swing phase and was held in a fully extended position above ground, as if it needed to be extended further (“saluting”, see Graham and Bässler, 1981).

A third drastic effect on stepping activity was observed when the load measuring CS on the trochanter was continuously stimulated (Bässler, 1977). This resulted in the generation of a sustained stance phase. All these experiments clearly demonstrated that movement and load feedback are important factors in controlling leg stepping, and in particular the step phase transitions.

On a side note, there are other external sensory organs on the leg, like hair sensilla that cover the surface of the leg segments, which produce resistance or avoidance reflexes upon their activation, both, when the animal is standing and when it is walking (e.g. Laurent and Hustert, 1988; Wolf, 1992). These, however, do not play a prime role for generating basic stepping movements. A lack of knowledge concerning the potential role for walking pattern generation of other sensors in and on the insect leg does not mean that these other signals are not important.

3 The control of posture

How does mechanosensory feedback contribute to the control of the walking motor output for a single leg? To understand this we need to take a closer look at how the walking system works. There are two tasks that have to be fulfilled in a walking animal: the control of posture and equilibrium, and the control of active leg movements underlying locomotion. Some complexity arises from the fact that both control tasks have to be executed at the same time, and they exert their influences at the same output level.

The situation is relatively simple in the standing insect. In this case, movement feedback from sense organs on the limbs exclusively serves posture control. This function becomes obvious in the generation of the so-called resistance reflexes (Fig. 2A). Resistance reflexes aim at keeping a desired posture against external forces like gravity or movements of the environment such as moving twigs on which the leg is placed. So, when for example, the tibia of an insect leg is passively flexed, the extensor tibiae motoneurons will be activated or increase their activity. This in turn increases the extensor muscle force to resist the imposed change in FTi-angle. The sense organs providing the necessary feedback from the leg are the hair plates at the joints and the fCO (e.g. Bässler, 1983; Burrows, 1996). Likewise, strain signals from the legs serve to control the motor output at rest to stabilize the current resting posture of the animal (e.g. Schmitz, 1993). Strain signals, however, are also utilized to generate avoidance reflexes. When, for example, load on one limb is increased by imposed forces, this limb will be moved away from the source of the load stimulus (reviews e.g. in Bässler, 1983, 1993a; Burrows, 1996).

Today, we know that postural reflexes in insect legs result from processing of movement signals in distributed neural networks within the thoracic ganglia (summary in Bässler, 1993a; Bässler and Büschges, 1998; Stein and Schmitz, 1999). In addition to monosynaptic pathways between sensory neurons and motoneurons (review in Burrows, 1996), polysynaptic pathways have been shown to be involved in the generation of the reflex motor output (reviews in Burrows, 1996; Büschges *et al.*, 2000). Within these polysynaptic pathways, identified nonspiking local interneurons form important gateways for processing movement feedback in insect joint control (recent reviews in Burrows, 1996; Bässler and Büschges, 1998; Field and Matheson, 1998; Fig. 2B). These usually act in an antagonistic manner, always causing the actual motor neuron activity to reflect the sum of the antagonistic parallel pathways that process specific sensory signals (Bässler, 1993a; Fig. 2B–D, for simplicity reasons, only supporting pathways are shown).

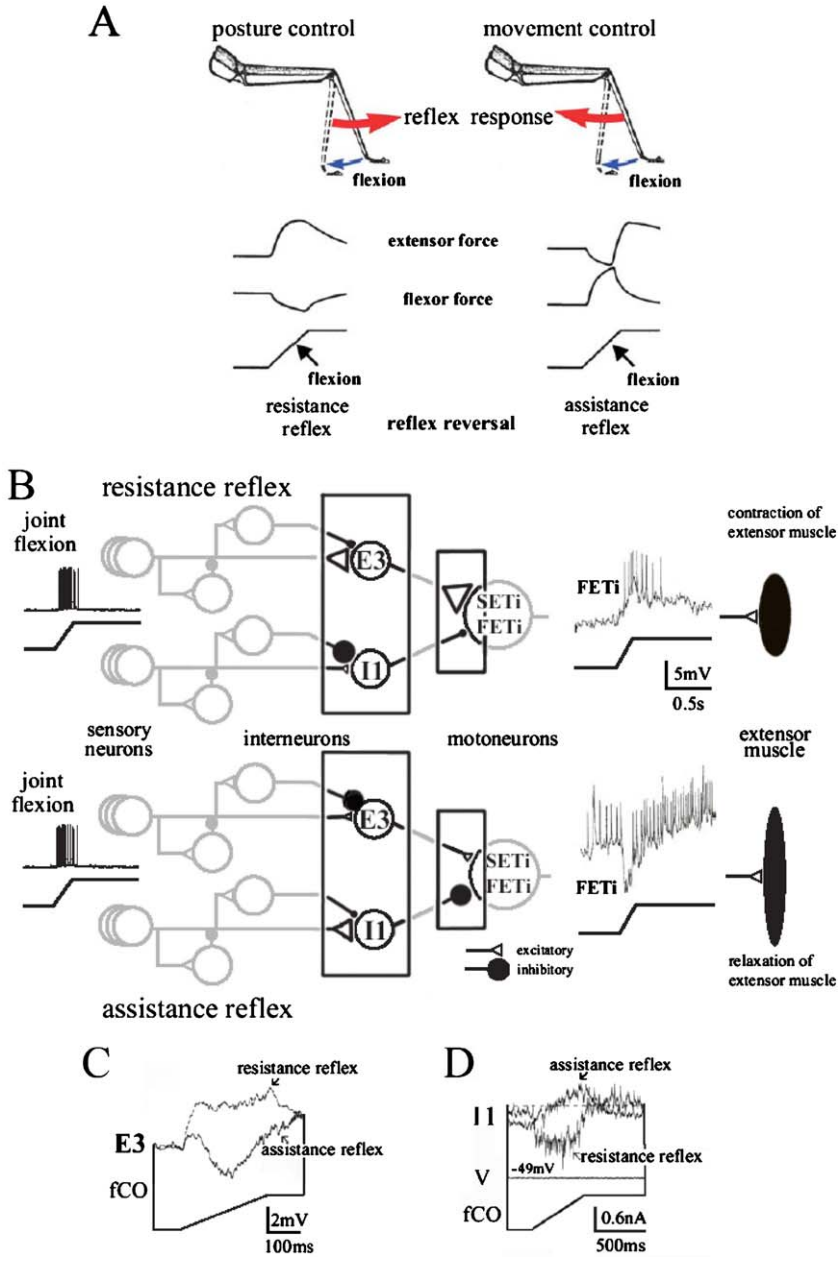
A
posture control
movement control
reflex response
flexion
flexion
extensor force
flexor force
flexion
flexion
resistance reflex
reflex reversal
assistance reflex
B
resistance reflex
joint flexion
E3
I1
SETi
FETi
contraction of extensor muscle
FETi
5mV
0.5s
sensory neurons
interneurons
motoneurons
extensor muscle
joint flexion
E3
I1
SETi
FETi
FETi
excitatory
inhibitory
relaxation of extensor muscle
assistance reflex
C
resistance reflex
E3
assistance reflex
fCO
2mV
100ms
D
assistance reflex
I1
-49mV
resistance reflex
V
fCO
0.6nA
500ms

4 Mechanosensory control of walking

The role and processing of mechanosensory feedback have to change as soon as active leg movements such as stepping are generated. While sensory signals are exclusively used for posture control in standing, they have to be used to serve both, the control of posture and movement during locomotion. It has been shown that sensory feedback in the locomoting animal takes part in shaping the actual motor output by influencing two different factors: the magnitude of the rhythmic motor activity and its timing (Fig. 3).

Assisting and resisting are the two modes in which sensory feedback affects the magnitude of motor activity in the walking animal. In the stick insect or the cockroach, for example, load signals during stance assist in a stronger activation of stance phase motor neurons (Wendler, 1964; Schmitz, 1993; Zill *et al.*, 1999).

FIG. 2 (A) Schematic drawing depicting the role of proprioceptive signals in controlling motor activity during standing and walking. The scheme is based on the situation in the stick insect leg muscle control system of the femur-tibia (FTi-) (knee) joint (Bässler and Büschges, 1998), but also reflects the situation in other walking systems, in which proprioceptive signals have been shown to be used to control motor output by reinforcing movement (Pearson, 1993; Prochazka, 1996). When standing (posture control; left), sensory information signalling knee flexion (small arrow) elicits resistance reflex action in motoneurons and muscles of the FTi-joint (large arrow) opposing flexion of the appendage. The time course of activity in knee extensor and flexor muscles is given schematically. During walking (movement control, right), the same sensory signals (flexion, small arrow) are used to control movements of the joint and reinforce the ongoing movement (large arrow). This is most obvious from the generation of an assistance reflex response. (B) Diagram summarizing state-dependent alterations in the processing of signals from the fCO in polysynaptic pathways of the stick insect FTi-control network, comparing the processing of flexion signals from the fCO during the generation of a resistance reflex (top) and an assistance reflex (bottom). Alterations of inhibitory and excitatory synaptic inputs (see differing scaling of synaptic connections) to local nonspiking interneurons (E3, I1, large box) and motoneurons (small box) mediate the different motor output of the FTi-network. For simplicity, changes are only depicted for two polysynaptic pathways, involving identified nonspiking interneurons E3 and I1 (for details see Bässler and Büschges, 1998). Sensory signals from the fCO are exemplified by an intracellular recording of a flexion sensitive fCO-afferent (left). Motoneuronal activity upon flexion signals from the fCO in both situations is shown by intracellular recordings from the FETi motoneuron (right). (C) Modulation of nonspiking interneuron E3 upon flexion signals from the fCO at rest (resistance reflex, solid line) and during walking (assistance reflex, broken line). Note the reversal of the synaptic drive onto interneuron E3 (data taken from Driesang and Büschges, 1996). (D) Modulation of nonspiking interneuron I1 upon flexion signals from the fCO at rest (resistance reflex) and during walking (assistance reflex) shown by the net membrane current recorded under dSEVC conditions. Note the reversal of the net membrane current in the two motor responses (stippled line – 0 nA; data taken from Driesang and Büschges, 1996) (see color plate section at the end of this book).

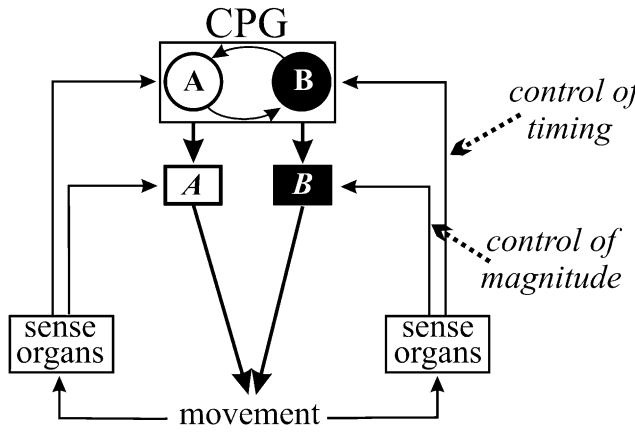

FIG. 3 Schematic drawing of the organization of the principal sensory–central interactions in locomotor pattern generation. A Central Pattern Generating network (CPG, square box with two neurons A and B interacting with each other) generates a basic rhythmic output that drives sets of antagonistic motoneurons pools and muscles (combined in square boxes and marked with *A*, *B* in *italics*). Feedback about the resulting limb movement is provided by sense organs, contributing either to the *control of magnitude* or *of timing* of motor output.

Interestingly, in exerting an assisting influence, sensory feedback was also found to invert its sign of action on motoneuron activity, different from when the animal is at rest (reviews in Büschges and El Manira, 1998; Clarac *et al.*, 2000). This phenomenon is called reflex reversal. An example is the flexion signal from the FTi-joint (Fig. 2A, B), which will reinforce flexor activation and inhibit extensor motoneuron activity when the locomotor system of the stick insect is active (Bässler, 1983). Thereby flexion of the tibia is reinforced, but only up to a given flexed position of the FTi-joint (Bässler, 1976, 1986, 1988). When this position is reached, flexor activity is terminated and extensor activity is initiated (Bässler, 1986).

Bässler, who first described this phenomenon for the stick insect front leg, coined the term "active reaction" for this two-state motor response, the first of which is an assistance reflex for flexion signals (Bässler, 1986, 1988, 1993b). The active reaction was subsequently also described for the middle (Bässler and Büschges, 1990; Driesang and Büschges, 1996) and hind legs (Nothof and Bässler, 1990). Bässler and coworkers provided evidence that the role of this motor response in walking pattern generation is (i) to assist an ongoing stance phase motor output and to (ii) terminate stance phase activity and initiate swing phase of the leg at a specific FTi-joint position (review in Bässler and Büschges, 1998).

This reflex reversal in the active animal is generated through the contribution of the same premotor neurons that also generate the resistance

reflex in the FTi-joint of the resting animal. Its execution is again based on distributed processing, and is caused by a reversal of the net synaptic drive to the tibial motoneurons upon flexion movements of the tibia as soon as the locomotor system becomes active (Sauer *et al.*, 1995, 1996; Driesang and Büschges, 1996; review in Bässler and Büschges, 1998). Similar modifications in reflex pathways are known in all well-investigated walking systems, from crayfish (DiCaprio and Clarac, 1981) and locust (Bässler, 1992) to mammals (for reviews see Büschges and El Manira, 1998; Pearson, 2000; for a comparative review see Clarac *et al.*, 2000). The exact underlying neural mechanism is presently not fully understood.

Besides influencing its magnitude, the second way through which sensory feedback takes part in the generation and control of the actual motor output is by influencing the timing of motor activity. Thereby it can determine the step phase transitions during walking. In this case, it is clear that the influence of sensory feedback is mediated by its access to the central neural networks generating a basic rhythmic motor activity, the so-called *Central Pattern Generators* (CPGs) (for reviews see Bässler and Büschges, 1998; Clarac *et al.*, 1998).

In insects as well as in crustaceans, CPGs in the central nervous system contribute to the generation of rhythmic and alternating activity in antagonistic motoneuron pools that control the leg joints (Pearson and Iles, 1970; Zill, 1986; Chrachri and Clarac, 1987; Ryckebusch and Laurent, 1993; Büschges *et al.*, 1995; Johnston and Levine, 1996; Le Ray *et al.*, 1997a,b). Data from the locust walking system suggest that CPGs that generate alternating activity in tibial motoneurons during locomotion may also be involved in reflex reversal (Knop *et al.*, 2001).

Two sets of experiments have demonstrated the contribution of CPGs to leg motor control in stick insects. In the first, tactile stimulation to the head or abdomen evoked bouts of alternating burst activity in antagonistic motoneuron pools of a leg joint (Bässler and Wegener, 1983; Büschges *et al.*, 2004). In the second, application of the muscarinic agonist pilocarpine onto deafferented thoracic ganglia evoked long-lasting alternating activity in antagonistic motoneuron pools of the individual leg joints (Fig. 4; Büschges, 1995; Büschges *et al.*, 1995). In such rhythmic preparations, it was shown that stimulation of movement and load sensors was able to reset and entrain the activity of the CPGs in the leg muscle control system (e.g. Hess and Büschges, 1999; Akay *et al.*, 2001, 2004; Bucher *et al.*, 2003). It was shown, for example, that movement signals from the FTi-joint are able to cause a transition in the activity of motoneurons that supply the CTr-joint (Fig. 4B and see below; Hess and Büschges, 1999).

How can such timing influence be differentiated from influences that modify the magnitude of actual motor activity? First, a timing influence is able to reset an ongoing motor activity and restart its rhythmicity (Fig. 4C) (see above). Second, there is no dependence of timing influence on the

magnitude of the sensory signal itself. This means that the probability to induce a transition in motor activity does not depend on the magnitude of the sensory signal, but only on its sign (Fig. 4D).

5 Organization of neural networks controlling single-leg stepping

As stated above, evidence strongly suggests that in insects as well as in vertebrates, CPGs in the central nervous system are responsible for the generation of rhythmic and alternating activity in the motoneuron pools

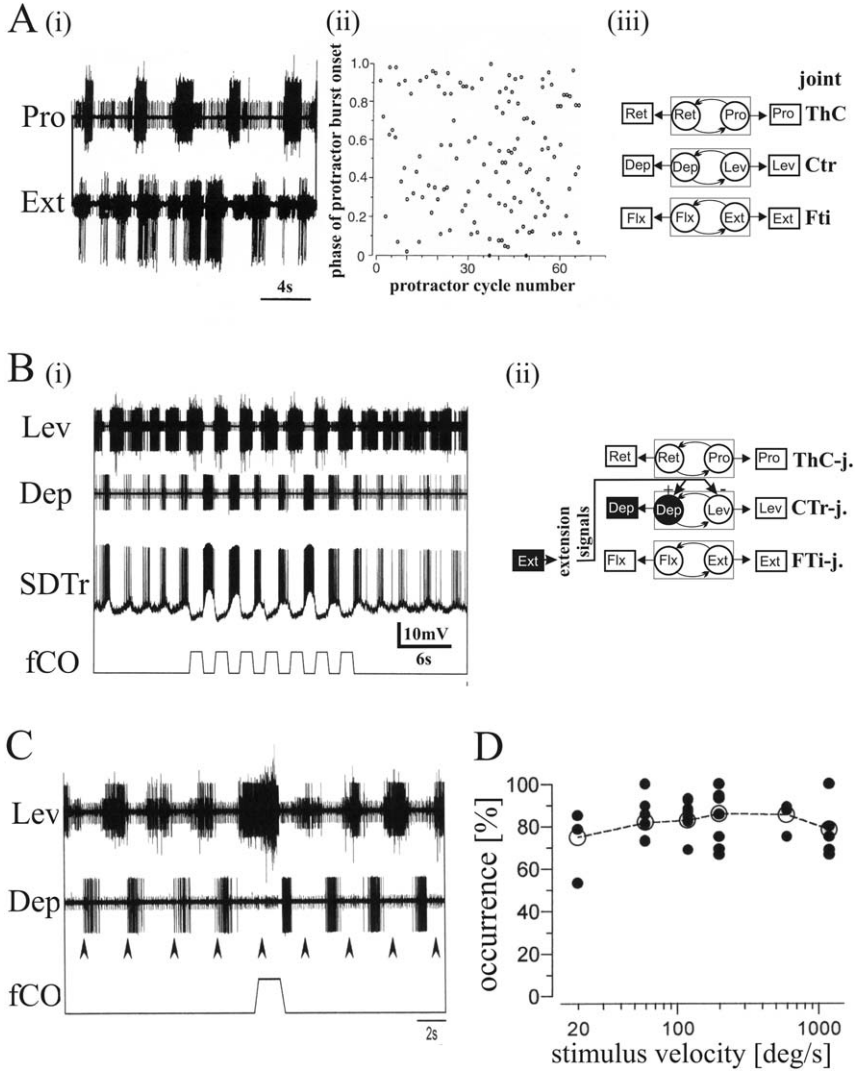

appropriate for the control of the leg joints (Grillner, 2003; Büschges, 2005). The generation of a well-coordinated motor output for a multi-segmented insect leg, however, is a much more complex task than controlling one leg joint alone. As stated earlier, coordinating up to five parts of an insect leg demands appropriate activation of more than a dozen muscles. An example for the timing of leg motoneuron activity during stepping in two extremely different situations is given in Fig. 5. This figure shows the activity of the six motoneuron pools that control the three main leg joints during middle-leg stepping on the treadwheel in the intact walking animal (e.g. Bässler, 1993b; Büschges *et al.*, 1994), and in the single-leg preparation in which pro- and retraction of the leg is prevented (Fischer *et al.*, 2001).

Two ways to coordinate this motor activity are conceivable. On the one hand, coupling of activity in the different sets of leg motoneuron pools could arise from the activity of one central network producing the timing

FIG. 4 Rhythmic motor activity induced by the muscarinic agonist pilocarpine in the isolated mesothoracic ganglion of the stick insect and its modulation by mechanosensory signals. (A) (i) Extracellular recordings from protractor coxae (Pro) supplying the ThC-joint and tibial extensor motoneurons (Ext) supplying the FTi-joint in the mesothoracic segment following application of 3×10^{-3} m pilocarpine. (ii) Plot of the phase of the onset of extensor bursts in the protractor cycle as a function of the protractor cycle number. There is neither absolute nor relative coordination detectable between rhythmic activities in both motoneuron pools. (iii) Schematic drawing of the central organization of the stick insect walking pattern generating system, composed out of individual joint CPGs. The CPGs are each symbolized by two interacting neurons in a box according to the motoneuron pools driven, e.g. the retractor (Ret) and protractor (Pro) motoneurons in case of the inner hip joint (TC-joint). Each CPG is connected to two antagonistic sets of motoneurons and muscles they innervate (depicted by boxes; Pro, Ret, Dep, Lev, Flx, Ext; see text). (B) (i) One example for the sensory modulation of pilocarpine induced centrally generated rhythmic motor activity by movement signals from the leg. Entrainment of the rhythmic activity in the motoneuron pools of the coxa-trochanter (CTr-) joint by signals from the fCO. Intracellular recordings from the Slow Depressor Trochanteris Motoneuron (SDTr) during entrainment of the rhythmic activity. Note that movement signals from the fCO induce transitions in activity between Dep and Lev motoneurons. (ii) Schematic of the influence described by the recording shown in (i). Movement and position signals of the knee joint (FTi-joint) have access to the CPG of the adjacent CTr-joint. Extension signals from the FTi-joint provided by the fCO switch the CTr-CPG from levator ("−") to depressor ("+") activity, and vice versa (see Hess and Büschges, 1999 for details). (C) Resetting rhythmicity in CTr-joint motoneurons through flexion signals from the fCO. Arrows denote the time and expected time of occurrence of depressor bursts before and after fCO stimulation, respectively. (D) Probability of occurrence for the occurrence of transition in activity between depressor and levator motoneurons versus fCO elongation stimulus velocity (filled circles – data from individual animals (*N* between 3 and 7); step *n* between 4 and 55 per animal; open circles – mean of the pooled data) (adapted from Hess and Büschges, 1999).

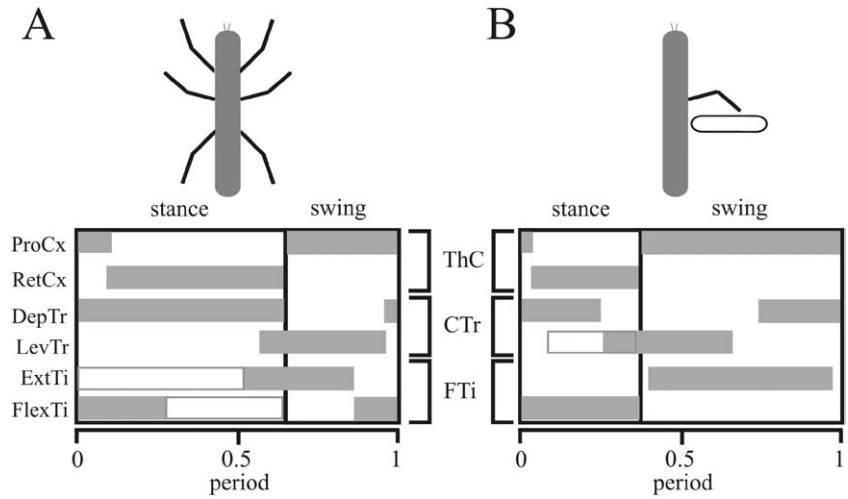

FIG. 5 Activity pattern of mesothoracic muscles and motoneurons driving the three proximal leg joints during middle-leg stepping as a function of phase in the leg stepping cycle, (A) from the six-legged animal walking on a double treadwheel (summarizing data from Graham, 1985; Büschges *et al.*, 1994) and (B) from the single-middle-leg preparation stepping on a treadband in which pro- and retraction of the leg were prevented (Fischer *et al.*, 2001). *Note:* ProCx – protractor coxae; RetCx – retractor coxae; LevTr – levator trochanteris; DepTr – depressor trochanteris; ExtTi – extensor tibiae; FlxTi – flexor tibiae. Filled grey bars denote phase of activity, open bars denote subtle slow motoneuron activity.

to ensure proper phasing of motoneuron activity. This has been shown for locomotor networks in the vertebrate spinal cord (Grillner and Zangger, 1979, 1984; Jordan *et al.*, 1979; Matsushima and Grillner, 1992). On the other, sensory feedback from the legs could serve to establish proper intra-limb coordination.

It appears that both mechanisms are realized to coordinate the stepping movements of a single insect leg, albeit to varying degrees for different species (Bässler and Büschges, 1998; Büschges, 2005). In locusts, for example, upon pharmacological activation and in the absence of sensory feedback from the limbs, CPGs driving leg motoneurons have been reported to generate a coordinated motor output for all motoneuron pools of a leg (e.g. Ryckebusch and Laurent, 1993). On top of this, in the sphinx moth *Manduca sexta*, intersegmental coordination appears to result from the activity of the walking CPGs as well (Johnston and Levine, 2002). In contrast, in the stick insect a well-coordinated motor output for stepping is not generated without sensory feedback. We will focus on this in more detail in the upcoming paragraphs.

When we activate CPGs in the stick insect walking system either pharmacologically or by tactile stimulation, no reliable cycle-to-cycle

coupling is present between the activities of the motoneurons controlling different leg joints of an individual leg (Büschges *et al.*, 1995; Fig. 4A). These findings have led to the conclusion that there are individual joint CPGs for the ThC-, CTr- and FTi-joints that operate in parallel and rather independently from each other. The CPGs contribute to patterning leg motoneuron activity by an inhibitory phasic synaptic output. This inhibitory synaptic drive sculpts a tonic background depolarization which is elicited upon activation of the locomotor system in leg motoneurons into a phasic activity pattern (Büschges, 1998; Büschges *et al.*, 2004; Ludwar *et al.*, 2005b). However, although some premotor interneurons capable of resetting the rhythm within the CPGs have been identified (Büschges, 1995), the detailed network topology is currently unknown.

For the stick insect, the influence of sensory signals on the activity of joint CPGs has been studied in quite some detail. Signals from leg proprioceptors that report the movement of a leg segment and load or strain on the cuticle affect the timing of the three main leg joint CPGs. As such, sensory signals can induce transitions in the activity of the individual CPGs (e.g. Hess and Büschges, 1999; Akay *et al.*, 2001). One example has been introduced in Fig. 4B, where each joint CPG is symbolized as a box with two mutually interacting interneurons that drive two antagonistic motoneuron pools. Movement and position signals from the fCO, the transducer of the knee (FTi) joint reporting extension of the tibia, can induce a transition in the CTr-joint CPG from levation into depression phase (Hess and Büschges, 1999; Bucher *et al.*, 2003). The reverse transition can be induced by flexion signals from the FTi-joint (Fig. 4B). While movement signals from the fCO induce phase transitions, position signals affect the cycle period of the CTr-CPG and can even ''lock'' the CTr-CPG in a specific activity phase, e.g. levator activity with a flexed FTi-joint (Bucher *et al.*, 2003). The phase transitions in activity of joint-CPGs induced by movement signals from the fCO may be mediated through two parallel neural pathways: one that elicits the transition, and the other that determines the direction of transition (Bässler *et al.*, 2003).

Figure 6A summarizes the known sensory-to-CPG influences identified in the stick insect mesothoracic segment by arranging them in the appropriate sequence for generating the stepping motor pattern typical for the single-middle-leg preparation as given in Fischer *et al.* (2001). The diagram covers the events and interactions from the second half of a swing phase to the first half of the next swing phase, and it divides the step into a sequence of four states (1–4). It is important to note that the scheme only contains those sensory influences that affect the timing of motor activity. It does not cover the control of motor activity magnitude through sensory feedback (see also Büschges, 2005).

The full sequence of events has been described elsewhere in detail (Büschges, 2005; Ritzmann and Büschges, 2007), and therefore we will only

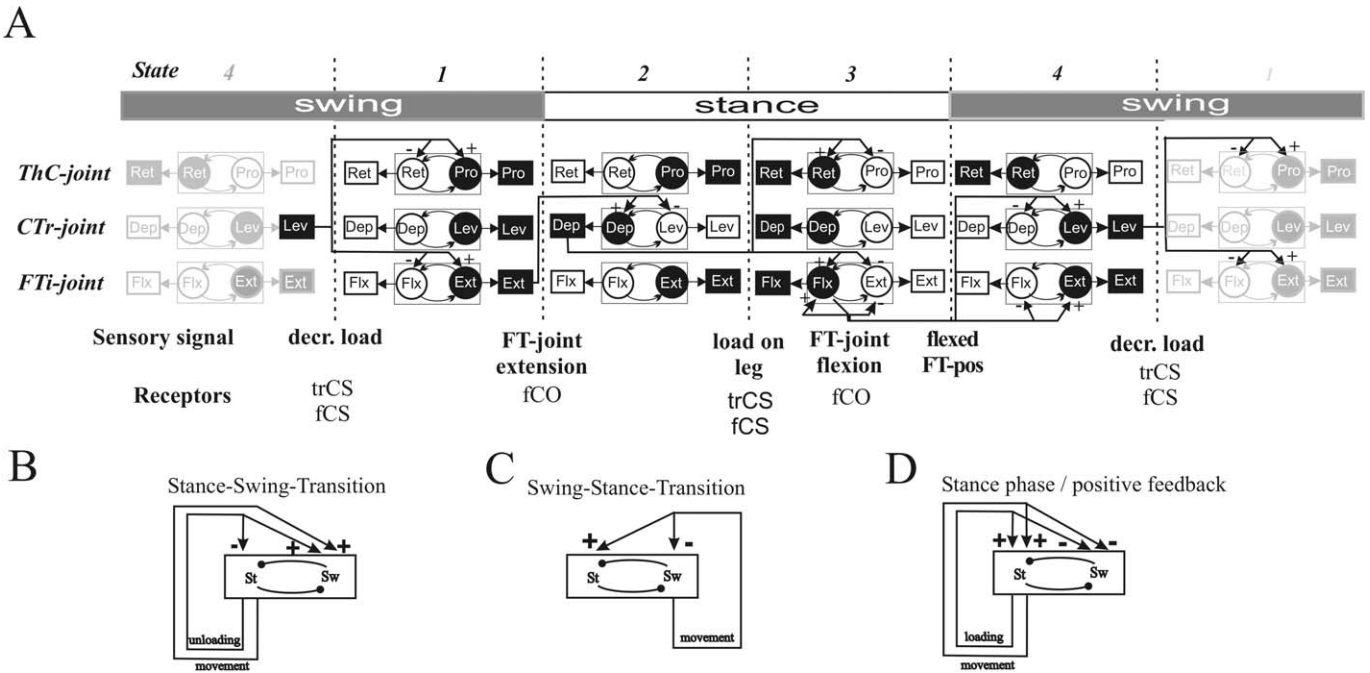

FIG. 6 (A) Diagram summarizing all known sensory influences on the timing of motor activity in intra- and inter-joint coordination for single-middle-leg stepping (for a detailed description see Ekeberg *et al.*, 2004 or Büschges, 2005). Filled symbols denote active elements/neurons, open symbols denote inactive elements/neurons. Sensory influences on the CPGs are either excitatory ("+") or inhibitory ("−"). The description of the sequence of events is organized in a state-like fashion moving from the *state 1* (second row on the left) to *state 4* (second to last row), after which state 1 follows again. To exemplify the continuing succession of events, states 4 and 1 are repeated at the left and right margin of the scheme. Along the arrows, the kinds of sensory signals, e.g. decreased load, and the sense organ providing the signals, e.g. trCS, are given. (B–D) Diagrams summarizing all known sensory influences on the timing of motor activity for intra- and inter-joint coordination in leg stepping; the schematic holds for stick insect. (B, C) Sensory signals responsible for stance-to-swing transition (B) and for swing-to-stance transition (C); (D) sensory signals for stance control. In these schemes, the central neural networks generating stance and swing phases motor activity are simplified and grouped together to form two states, i.e. stance (st) and swing (sw). Sensory influences are indicated and identified by arrows that either initiate (+) or terminate (−) one of the two phases of motor output.

briefly concentrate on the transition from state 1 to 2. During the second phase of swing of a stick insect middle leg (*state 1*), levator trochanteris (Lev) and extensor motoneurons (Ext) are active together with protractor coxae motoneurons (Pro). Sensory feedback about extension of the FTi-joint initiates depressor trochanteris (Dep) and terminates Lev motoneuron activity, and is thus the first event initiating stance phase. This causes the leg to be set down (Hess and Büschges, 1999; Bucher *et al.*, 2003). Ground contact and the subsequent increase in load induce a transition in activity in the CPG that controls the ThC-joint and thereby terminates activity in Pro and initiate activity in retractor coxae (Ret) motoneurons (*state 2*; Akay *et al.*, 2004, 2007). This would cause a backward movement of the ThC-joint in a freely moving leg. The same load signals affect knee joint motoneurons by exciting flexor tibiae (Flx) and inhibiting extensor tibiae (Ext) motoneurons (Akay *et al.*, 2001, 2004). Consecutive events are triggered by sensory feedback from the leg and this generates a motor output appropriate for forward walking in the stick insect middle leg.

There are still unknowns, like the nature of sensory control of the swing–stance transition which includes targeting of a leg's tarsus towards the position of the anterior legs' tarsus (Cruse, 1985b). Therefore, it should be noted that the outline of the sequence of events shown in Fig. 6A does not claim to contain the complete set of sensory influences determining the timing of motor activity in the stepping cycle, although the ones shown have been proven to be sufficient for this task (e.g. Ekeberg *et al.*, 2004).

6 Specificity of sensory–motor influences

In each of the three main leg joints, movement signals are utilized for intra-joint control, e.g. signals from the fCO in FTi-joint control (Bässler, 1986, 1988), from the trHP in CTr-joint control (Schmitz, 1986a,b) and signals from the cxHP in ThC-joint control (Cruse, 1985a; Büschges and Schmitz, 1991). Inter-joint coordination, caused by movement signals in one joint, as mentioned above, has only been found between two of the three major leg joints and in one direction only, namely, from the FTi-joint to the CTr-joint (Hess and Büschges, 1999). No influence of movement signals was found for the opposite direction (Akay *et al.*, 2001) or the control of inter-joint timing between any of the leg joints (Akay *et al.*, 2001).

The situation is similar for load signals from the leg. As stated above, load signals are detected by CS that are arranged in four fields close to the CTr-joint, one field located on the proximal femur (fCS) and three others located on the trochanter (trCS). Motoneurons of the FTi-joint are exclusively affected by signals from the fCS. On the other hand, motoneurons of the ThC-joint are affected by both, signals from trCS, and,

to a lesser extend from the fCS (Akay *et al.*, 2004, 2007; see also Fig. 9D(i)).

It is interesting to note that load and movement signals are not processed independently from each other, but interact within the premotor network. First, indications for this arose from experiments by Cruse (1985a), in which he showed that the posterior leg position and a decrease in load can trigger leg swing at the end of leg stance. A recent study has shown that load, signalled by the fCS, facilitates the influence of movement signals on FTi-motoneuron activity (Akay and Büschges, 2006).

The sufficiency of the identified sensory–motor pathways to generate a basic stepping pattern has been assessed by a computer simulation with a 3D neuro-mechanical model, a tool in physiological research that has proven important for the study of locomotor systems (e.g. Ekeberg and Grillner, 1999; reviewed in Pearson *et al.*, 2006). This simulation verified that a leg controller in which the identified sensory–motor pathways are implemented is indeed able to generate coordinated stepping movements for a middle leg. With only minor modifications front leg stepping could be generated as well (Ekeberg *et al.*, 2004).

The results from these studies, based on stick insect data, show that the leg muscle control system primarily uses a fairly small number of the possible sensory-to-CPG influences (Ekeberg *et al.*, 2004; Büschges, 2005). Although, for example, each leg joint is associated with a sense organ that monitors movements of that joint (Bässler, 1983), only movement signals from the FTi-joint affect the CPG controlling the CTr-joint. Such a selective use of specific sensory signals may indicate that the stick insect walking system operates through a reduction in the degrees of freedom in the control task for generating a stepping motor output for its multi-jointed legs. Owing to the obvious computing advantages, such a control regime is attractive to researchers developing controllers for walking robots (Lewinger *et al.*, 2006; Rutter *et al.*, 2007).

How do the results on stick insect walking pattern generation compare to other locomotor systems? Unfortunately, in most of the other insects studied, information on the neural control of single-leg stepping is not as advanced as in the stick insect, with partial exception of the cockroach. The situation is similar for the cat being currently the best studied walking vertebrate. Thus, at present, a sufficient knowledge-based comparison between walking systems has to be limited to those two.

Interestingly, with respect to the role of sensory feedback there is a striking similarity between stick insect and cat (Büschges, 2005). Both, movement and load signals serve the same purpose in stick insect and cat step-cycle control (e.g. Grillner and Rossignol, 1978; Hiebert *et al.*, 1996; Hiebert and Pearson, 1999; Fig. 6B). In both systems, (i) swing-to-stance transition is initiated by movement and position signals, (ii) stance-to-swing transition is initiated by a combination of a decrease in load and

position signals from the leg and (iii) during stance, sensory signals from movement and load sensors assist the generation of the motor activity by reinforcing the ongoing motor output. This means that, given the evolutionary distance between insects and mammals, these mechanisms may turn out to be general principles in step-cycle control (see Fig. 6B). Our current idea about the central organization of the insect locomotor system is very similar to the *Unit-Burst-Generator* (*UBG*) concept formulated by Grillner and Zangger about 25 years ago, which is derived from observations in the cat (Grillner and Zangger, 1979). This concept suggests that each group of motoneurons may be controlled by its own pattern generating network which can be coordinated in various ways depending on the behavioural task at hand.

7 Mechanosensory signals in inter-leg coordination

The movements of the legs in a walking animal are coordinated to achieve stable propulsion in addition to posture and equilibrium. This way, specific gaits can be established. The first typical gait in the insect is the tripod gait, in which three legs serve stance at a given moment while the other three legs generate a swing phase. The second is the tetrapod gait, during which four legs are in stance simultaneously. The use of either of these two gaits is related to stepping frequency and the load acting on the insect (Graham, 1985): when insects walk at high frequencies, like the cockroach, the tripod gait is used (Delcomyn, 1971; Pearson and Iles, 1973), when insects walk at low speed or under loaded conditions, like the adult stick insect, the tetrapod gait is generated (Graham, 1981; summary in Graham, 1985). It should, however, be noted that these two gaits represent ideal forms of coordination. In most situations, the walking animals do not produce these two gaits in a separable manner (Wendler, 1965).

Wendler, Bässler and most notably Cruse and colleagues, in recent years have identified a set of six different rules for establishing inter-leg coordination, the so-called "coordination rules" (Cruse, 1990; Dürr *et al.*, 2004; recent review in Cruse *et al.*, 2007). This was done by behavioural experiments, in which the influence of perturbations of the stepping movement of one leg onto its own and onto the walking movements of the other legs was investigated. For example, when one leg is starting a swing phase, this prevents a swing phase in the anterior, ipsilateral neighbouring leg. Six such influences have been described (Fig. 7).

Presently, the neural basis of these coordination rules is not known. The alterations observed in response to perturbations can only be explained when we assume that mechanosensory feedback from the stimulated leg is involved, be it movement or load feedback. This applies specifically for

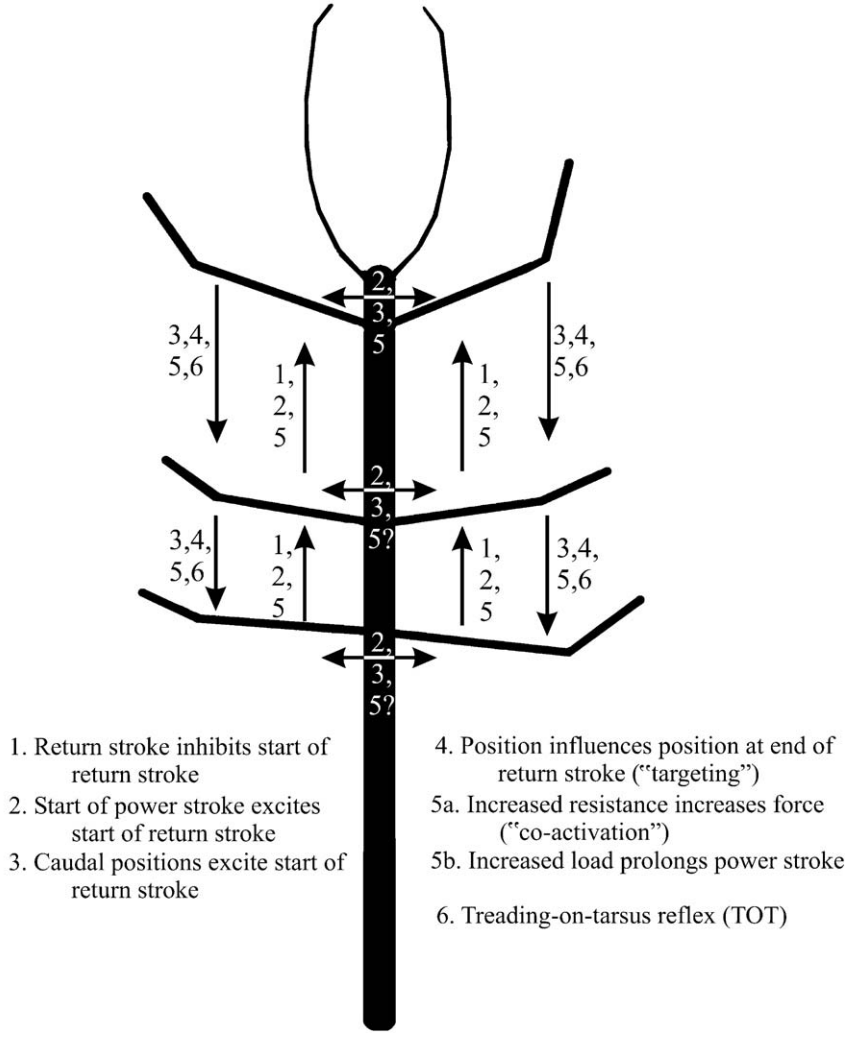

FIG. 7 Coordinating influences contributing to the coordination of stepping movements between the legs of a walking stick insect according to Dürr *et al.* (2004). Arrows give the direction of the influences. Numbers 1–6 relate to the "coordination rules" listed in the figure. In all cases the coordinating influence of rule 5 is valid for 5a and 5b.

coordination rule six, the treading-on-tarsus reflex, which is elicited, when a posterior leg is set down on the tarsus of its anterior neighbour at the swing-to-stance transition. In this case, the posterior leg is immediately lifted off again and set down a bit more posteriorly (Graham, 1985; Schmitz and Hassfeld, 1989).

As indicated above, however, we know little about the identity of the leg sensors involved in inter-leg coordination. When perturbing leg movements during walking by stopping the whole leg, or by touching a leg segment, it is not clear which sensors are likely to be affected. These could be exteroceptors, like tactile hairs, movement sensors like hair plates and/or load measuring sense organs, like the CS. Available information on the influence of individual sense organs between legs is almost exclusively restricted to influences generated in the resting animal (e.g. Graham and Wendler, 1981; Büschges, 1989; Laurent and Burrows, 1989; Brunn and Dean, 1994).

Three recent studies have addressed this issue to identify sense organs involved in inter-leg coordination. In these studies, the influences of movement (fCO) in the active stick insect locomotor system were studied by stimulating each sense organ selectively. In all cases, the sensory signals affected the activity of motoneuron pools in the neighbouring legs when the locomotor system of the stick insect was active (Ludwar *et al.*, 2005a; Stein *et al.*, 2006; Borgmann *et al.*, 2007). As an example, flexion signals from the fCO in the front leg facilitated retractor activity in the mesothoracic segment (Ludwar *et al.*, 2005a). It should be noted though, that in none of the studies signals from any one particular leg sensor were sufficient to affect motor activity in an adjacent leg in a manner that could totally account for one of the known coordination rules.

These findings suggest that, indeed, for a given sensory signal to produce the proper effect on the sender and/or on the receiver segment/leg according to the relevant coordination rules, additional information is needed. This information most likely consists of signals that define the state of the receiving leg as stance or swing. Subsequent investigations will need to address these issues to unravel the neural mechanisms underlying coordinating information transfer between legs in the stick insect walking system.

It can be speculated that such a mechanosensory influence is likely to vary between species and to depend on the speed of locomotion. Strain signals from the tarsi of locusts have been reported to reach the CNS within a millisecond through an activation of the CS (Höltje and Hustert, 2003), and are therefore a potential source for relevant cycle-by-cycle sensory input even in a cockroach running at 20 Hz (Graham, 1985). These proximally located load sensors should be prime targets to investigate mechanosensory influence on coordination in this species.

8 Neural mechanisms underlying modifications in the locomotor output

8.1 CHANGING WALKING SPEED

Walking is only one element of a variety of complex behavioural tasks and can involve adaptive changes in speed and the generation of turns and

complex climbing movements. In all animals, changes in the speed of walking are a result of changes in the organization of motor activity in the movement cycle of a single leg and the intersegmental coordination of leg movements. At higher speeds, animals decrease the number of legs that synchronously touch the ground. Quadrupeds, for example, change their gait from walk, to trot, to gallop when the speed increases (summary in Orlovsky *et al.*, 1999). The stick insect, which moves slowly in dense leaves and twigs, needs a high adaptability in the way the legs are coordinated. Usually, it uses a highly variable tetrapod gait unless it walks quickly on a smooth surface, when it may switch to the tripod gait (Graham, 1972, 1985). The cockroach, which often walks or runs over smooth surfaces, even at low speeds uses a tripod gait. Nevertheless, it is capable of slow, adaptive walking with the ipsilateral legs moving in a slow metachronal wave, for example when walking on an air-cushioned ball or on a slope (Delcomyn, 1971; Spirito and Mushrush, 1979).

Apart from these changes in coordination, changes in walking speed in insects result primarily from changes in cycle period (Wendler, 1964; Wilson, 1966; Graham, 1972; Graham and Cruse, 1981; Halbertsma, 1983; Yakovenko *et al.*, 2005; review in Orlovsky *et al.*, 1999), as it is also the case for crustaceans (Clarac and Chasserat, 1986). A faster speed is the result of a decrease in cycle period. This decrease is generally achieved by a decrease in stance phase duration, while swing duration changes only little (Wendler, 1964; Burns, 1973; Halbertsma, 1983; reviewed in Orlovsky *et al.*, 1999). It has been suggested for insect walking that descending drive, mainly from the suboesophageal ganglion, provides tonic excitation, the strength of which could influence walking speed (Roeder, 1937; Ridgel and Ritzmann, 2005; Gal and Libersat, 2006).

How the activity pattern of motoneurons in the thoracic ganglia of a walking animal is altered during changes in walking speed was recently the focus of a study in the stick insect (Gabriel and Büschges, 2006). In single-middle-leg stepping, an increase in stepping velocity is the result of changes in stance phase activity of the flexor motoneurons, while duration and activation of swing phase (extensor) motoneurons are not modified (Fig. 8A–D). The depolarization of flexor motoneurons shows two components (Fig. 8B, C). One is a stereotypic initial depolarization at the beginning of stance, which is similar in shape at all stepping velocities. The other is a subsequent larger depolarization that determines suprathreshold activation of the flexor motoneurons, and which changes with stepping velocity (Fig. 8B, C; Gabriel and Büschges, 2006). During fast steps, this second component develops faster and shows larger amplitudes as compared to slow steps. The independence of the first and the dependence of the second component on stance phase velocity indicate that mechanisms for altering stepping velocity become effective only during an already ongoing stance phase motor output.

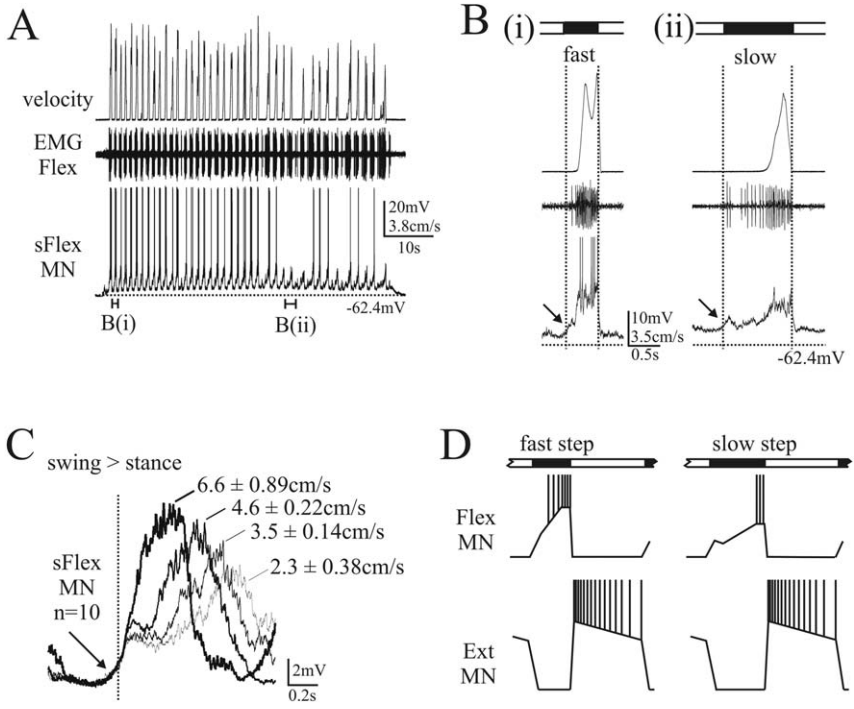

FIG. 8 Modifications in the activation pattern of leg motoneurons with changing stepping velocity. (A) Intracellular recording of a slow flexor (sFlex) MN during a stepping sequence in which stepping velocity changed between individual steps, indicated by changes in the belt velocity of the tread band (top trace). The stippled line in the bottom trace marks the resting membrane potential, "B(i)" and "B(ii)" below the trace mark the two steps shown in (B). (B) Steps from (A) with fast (i) and slow step (ii). (C) Superimposed selection of the average membrane potential recorded during 10 steps at 4 varying stepping speeds from the same neuron. The membrane potential was averaged and aligned to the beginning of stance phase after spike elimination. Note the similar initial depolarization at the swing–stance transition in all averaged traces. During the slowest steps, the initial depolarization had the smallest amplitude. At around 100–200 ms after the initiation of stance, another slow depolarization can be observed. At faster steps, the amplitude of the late depolarization is greater and occurs sooner (and more rapidly) than at slow steps. (D) Schematic of membrane potential modulations in flexor and extensor MNs during fast and slow steps. Flexor and extensor MNs show antagonistic activity in both cases, but flexor MN activity is dependent, extensor MN activity is independent of stepping speed (adapted from Gabriel and Büschges, 2006).

Currently, the changes in premotor network activity underlying these observations are not known. Alterations in the state-dependent tonic background excitation present during locomotor movements (Büschges *et al.*, 2004; Ludwar *et al.*, 2005b) appear not to play a role in controlling motoneuron activity for changes in stepping velocity (Fig. 8A). There are

indications of an influence of sensory feedback which arise from the fact that flexor motoneurons are excited by movement and load feedback during the stance phase when the locomotor system is active (e.g. Bässler, 1993a,b; Akay *et al.*, 2001).

Given that some of the depolarizing synaptic drive onto the flexor motoneurons arises from sense organs on the leg, it is conceivable that changes in the effectiveness or gain of the underlying sensory–motor pathways – perhaps arising from descending inputs – may alter rate and amplitude of their activation (Bässler, 1986, 1988; Akay *et al.*, 2001). A similar solution to explain changes in the cycle period during walking through modifications of the gain of sensory feedback from the limb has recently been discussed for the cat (Yakovenko *et al.*, 2005).

8.2 CHANGING WALKING DIRECTION

Similar modifications in the motor output are not sufficient when it comes to changes in the direction of walking, for example from forward to backward. Here, motor output and leg movements differ significantly under the two conditions (crayfish: Ayers and Davis, 1977; cat: Buford and Smith, 1990; Carpenter *et al.*, 1997; human: Grasso *et al.*, 1998). In a forward walking stick insect, for example, the stance phase of a middle leg is the result of the retraction of the coxa at the ThC-joint together with a depression of the trochanterofemur at the CTr-joint. The coordination is reversed during backward walking, when stance phase is the outcome of a depression of the trochanterofemur during protraction of the coxa, while retraction of the coxa contributes to swing phase generation (e.g. Graham and Epstein, 1985).

One could argue that such differences in the coordination of leg segments go along with changes in the processing of mechanosensory feedback. This has been shown to be the case in a recent study in which modifications in the sensory-to-central influence of load signals underlying the generation of a forward and backward motor pattern have been demonstrated (Fig. 9; Akay *et al.*, 2007).

During forward walking, signals from trochanteral CS affect the activity in the motoneuron pools of the ThC-joint (Fig. 9A(i), B top histogram). They promote retractor coxae motoneuron activity during leg stance in a forward walking leg through accessing the CPG of the ThC-joint (see above and Fig. 6; Akay *et al.*, 2004, 2007). This influence is reversed during backward walking, when signals from the same trochanteral CS promote protractor coxae motoneuron activity during leg stance. This was demonstrated through selectively stimulating the trochanteral CS in the restrained middle or hind leg of an animal that was otherwise walking forward and backward with the remaining five legs (Fig. 9A, B).

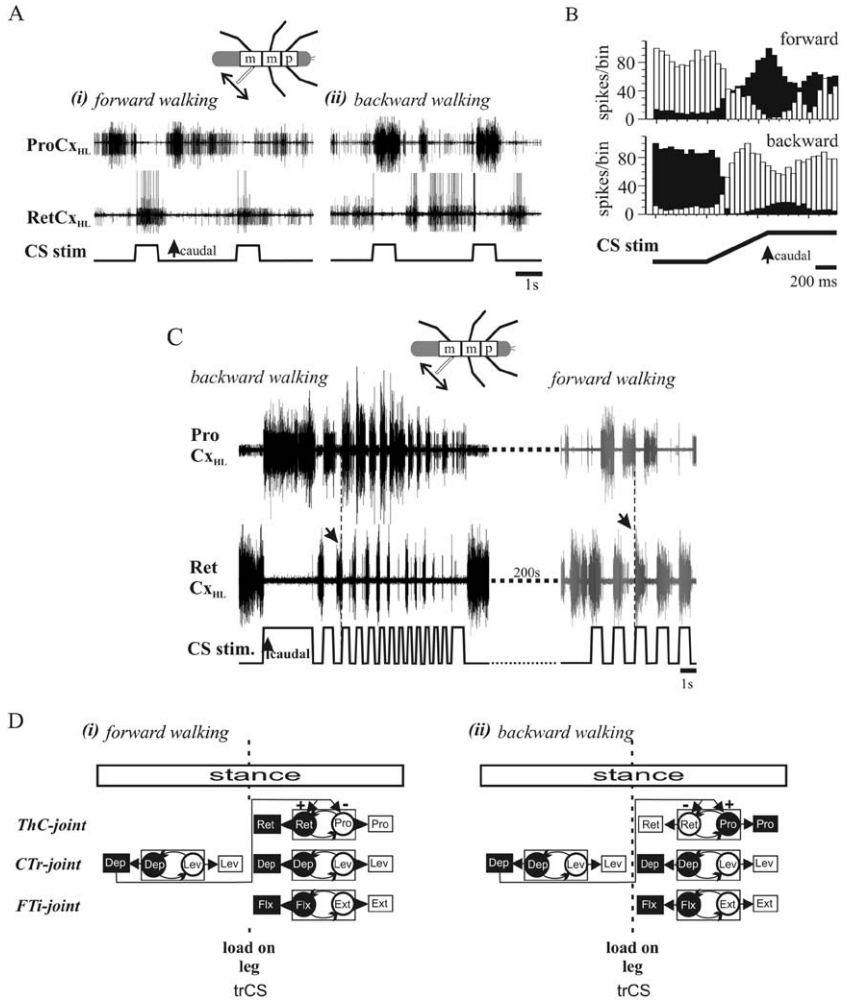

FIG. 9 Effect of load signals on ThC-joint motoneuron activity during forward and backward walking in the hind leg with all other legs walking on a slippery surface. (A) Extracellular nerve recordings from ProCx of the hind leg ($ProCx_{HL}$ top trace) and RetCx of the hind leg ($RetCx_{HL}$, middle trace) during stimulation of load sensors (bottom traces) in the hind leg during forward walking (A) (i) and backward walking (A) (ii). (B) Stimulus time histogram (bin width 50 ms) showing mean activity profile of PrCx (white bars) and RetCx (black bars) during CS stimulation during forward (top) and backward walking (bottom). (C) Extracellular $ProCx_{HL}$ and $RetCx_{HL}$ nerve recordings during stimulation of load sensors in the hind leg during backward and forward walking (same animal and traces as in (A)). (D) Schematic representation of the influence of load signals on the CPG of the ThC-joint in forward (i) and backward (ii) walking. Note that upon increased load, motoneuron activity switches from ProCx to RetCx during forward and from RetCx to ProCx during backward walking. Figures A–C adapted from Akay *et al.* (2007).

The stimulation even allowed resetting and entraining the coxal CPG with the load stimulus regime in both walking directions (Fig. 9C).

This study showed for the first time that walking direction-dependent reversal in the sign of sensory to CPG feedback contributes to the generation of forward versus backward walking in an insect (Fig. 9D). The observed changes are reminiscent of the reflex reversal that is observed in tibial motoneurons and which occurs when a stick insect switches from an inactive to an active state (see above; Bässler, 1986, 1988).

Two questions arise now: (i) what are the mechanisms underlying such changes and (ii) does such a reversal also occur in movement-related feedback. Experimental data suggest at least two potential mechanisms that could mediate the observed changes.

First, afferent fibres from load sensors in insects are subject to presynaptic inhibition (Stein and Schmitz, 1999). In the present case, presynaptic inhibition could modify the gain of CS afferent synapses onto neurons of the ThC-joint CPG in a phase-dependent manner. As a consequence, this could switch the influence of CS signals on ThC-motoneurons.

Second, in a number of motor systems, distributed pathways involved in sensory–motor processing have been shown to be subject to extensive modulation (Kristan and Shaw, 1997; summary in Büschges and El Manira, 1998; Clarac *et al.*, 2000). In the present context, similar parallel distributed pathways, which transmit CS signals, could be shifted in their weights and thereby mediate the feedback reversal in the stick insect (see also Büschges *et al.*, 2000).

8.3 TURNING

Much less is presently known about the neural basis for turning, and specifically on the potential role of sensory feedback in the generation of related leg movements. It has been observed that intra- and inter-limb coordination changes drastically between straight walks and turns (Jander, 1982; Dürr and Ebeling, 2005). The inside front and middle legs of stick insects performing narrow turns, for example, can reverse the normal stepping pattern, in that protraction of the leg often occurs during stance and retraction during swing (Jander, 1985). In the cockroach, where the middle leg usually extends during stance, this pattern is switched for the inside leg to an extension during swing (Mu and Ritzmann, 2005). Essentially, in these cases the inside legs often walk sideways or even backwards, while the outside legs perform wider steps in the front to back direction (bee: Zolotov *et al.*, 1975; beetle: Frantsevich and Mokrushov, 1980; stick insect: Jander, 1985).

An alternative strategy for turning can be an alteration in the tripod gait and a change in walking speed of the inside leg, which then slows down

significantly as compared to the outside leg (bee: Zolotov *et al.*, 1975; cockroach: Franklin *et al.*, 1981; stick insect: Jander, 1985; ants: Zollikofer, 1994). In most cases, a combination of both is likely to cause the turning movement. Most of our current knowledge on the operation of an insect's walking system in these situations is based on observations from kinematic studies and the analysis of inter-leg coordination. From these, the action of the contributing neural networks was inferred (e.g. Wendler, 1964; Zolotov *et al.*, 1975; Cruse, 1976; Strauß and Heisenberg, 1990; Jindrich and Full, 1999; Watson *et al.*, 2002; Bläsing and Cruse, 2004; Dürr and Ebeling, 2005; Schumm and Cruse, 2006).

The exact neural basis of generating turns in insect walking, as in walking of all other animals, however, is still unknown. It is clear that descending signals from the brain as well as the local locomotor networks are participating. The nature of the descending signals involved is unknown, except for the fact that the central body complex obviously plays an important role in organizing translational behaviours during locomotion (Strauß and Heisenberg, 1993; Ridgel *et al.*, 2007; reviewed in Strauß, 2002). Mutations as well as lesions in the CBC and the protocerebral bridge caused severe impairment in correct turning behaviour. Other studies have shown that cockroaches are still capable of escaping turning behaviour after lesions of the connectives anteriorly to the prothoracic ganglion, but that the movement pattern of the front and middle legs is changed (Schaefer and Ritzmann, 2001). So, while higher centres in the brain seem to be responsible for certain aspects of posture and turning commands, it remains unclear how much of the generation of turning is dependent on the descending inputs from higher brain centres or on the specific action of local networks.

To understand how the leg muscle control systems in the thoracic ganglia and local sensory feedback contribute to a given behaviour, it is necessary to discriminate between descending, intersegmental and local interactions within the walking system.

One important limitation to understanding the sensory–motor influence on adaptive locomotor behaviours such as turning arises from the fact that, for many electrophysiological studies, the animal has to be either completely restrained, or the locomotor movements of the legs are restricted to a single plane or even to a single joint (Bässler, 1986, 1988). This is, for example, the case in the single-leg preparation of the stick insect, where the leg is generating "stepping-like" sideways movements in a plane perpendicular to the thorax of the animal, but not in the horizontal plane, that is, forwards or backwards (for discussion see Fischer *et al.*, 2001; Gabriel *et al.*, 2003). This experimental setup prevents studying the neural basis of leg stepping under more natural conditions and studying it during adaptive walking behaviours like turning, obstacle crossing, climbing, etc.

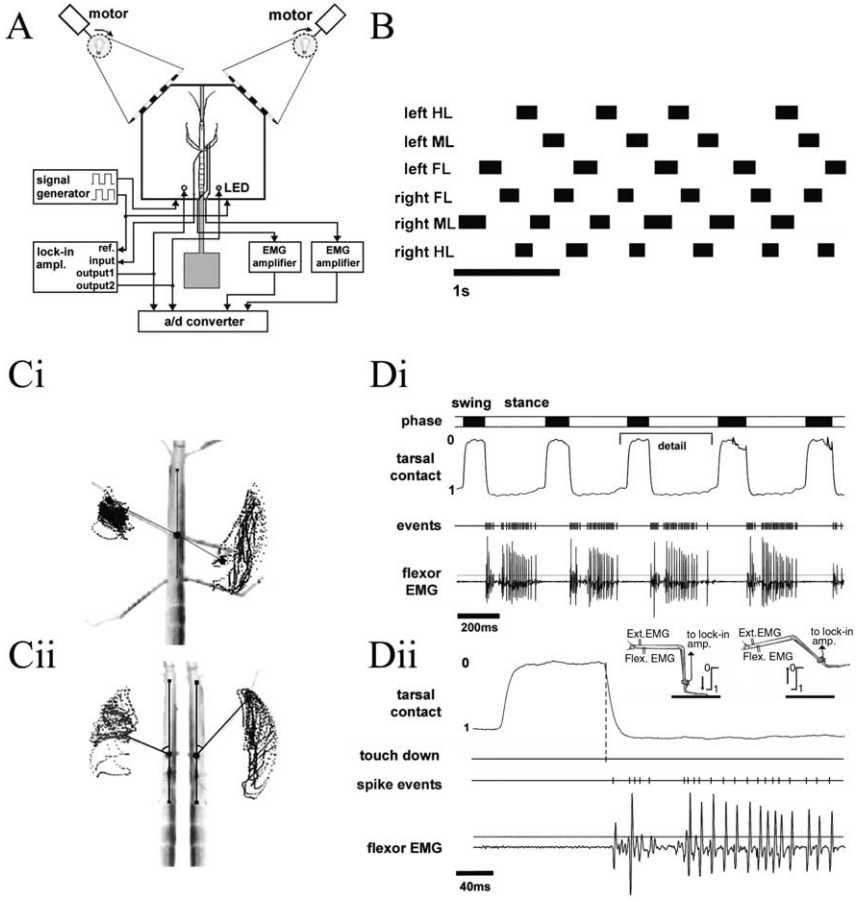

FIG. 10 (A) Wiring diagram for the simultaneous recording of tarsal contact and the correlation with EMG recordings during optically induced straight walking and turning for a single leg on each side of the animal. The stick insect is mounted on a balsa stick over the slippery surface in front of the striped pattern on the ground glass screens for optomotor stimulation. ''ref.'' means reference signal. (B) Walking pattern of a stick insect walking on the slippery surface. The black bars mark the swing phases of the leg marked on the left side of the figure. (C) (i) Compound picture of all leg positions taken by the middle legs during one turning sequence in the intact animal. (C) (ii) Compound picture with all leg positions taken by a single-middle-leg preparation during the function as an inside leg (left) and outside leg (right) while performing turning sequences. The right animal is the same as in the left half, but digitally mirrored for easier visualization. (D) (i) EMG traces in the flexor of a straight walking middle leg with the corresponding tarsal contact trace in the intact animal. Swing and stance phases are marked in black and white bars above the sequence, based on times of tarsal contact. The tarsal contact trace switches between states 1 (tarsus on the ground) and 0 (tarsus in the air, inset). (D) (ii) Detailed view from (D) (i) at a higher time resolution showing the beginning of flexor activity with a very short latency to touchdown. The broken line in the tarsal contact trace marks the threshold set for the event channel to mark touchdown (adapted from Gruhn *et al.*, 2006).

What is needed are experimental approaches in which the nervous system of the animal is accessible to physiological investigations upon generation of adaptive locomotor behaviours. Recent results suggest that this is indeed possible (Mu and Ritzmann, 2005; Gruhn *et al.*, 2006).

A setup that allows the study of intersegmental coordination under mechanical uncoupling of the legs was originally introduced by Camhi and Nolen (1981) and Epstein and Graham (1983), using a stationary animal walking on a moveable or a slippery ground ("slippery surface"). By combining the "slippery surface" with an optomotor stimulus (Gruhn *et al.*, 2006; Fig. 10A, B), it is now possible to study the stick insect physiologically under varying situations, i.e. with six, two or only one leg generating stepping movements in wide or narrow turns (Fig. 10C).

Initial results from this preparation suggest that generating a basic motor and movement pattern for turning in any given single leg does not rely on the presence of neighbouring legs or a mechanical coupling, but can be generated by each single leg (Fig. 10C; Gruhn *et al.*, 2006). Interestingly, intact, six-legged stick insects occasionally show an increase in stepping frequency for the inside legs when walking on the slippery surface (Fig. 10B, Gruhn *et al.*, in preparation).

First, experiments on muscle timing of the flexor tibiae muscle in straight walking and optically induced turning stick insects yielded another interesting finding (Fig. 10D(i, ii)). The combination of monitoring tarsal contact electrically, kinematics with high-speed video and muscle activity with electromyogram (EMG) electrodes, demonstrated that latencies for activation of this particular muscle are as short as 4 ms and do not vary depending on the behavioural context (Gruhn *et al.*, 2006).

These results show that the initiation of flexor muscle activity at the beginning of stance follows touchdown of the leg extremely quickly. Contact signals from tarsal hair receptors to the neuromuscular synapses are unlikely to be the source for relevant sensory input in the stick insect, because they take between 5 and 7 ms in locusts, which have shorter legs (Höltje and Hustert, 2003). These new findings raise the interesting possibility of load and strain signals from the trochanteral cuticle having exclusive responsibility for flexor muscle activation (see above).

9 Conclusions

Several conclusions can be drawn from our current understanding of the role of mechanosensory signals in the control of the walking motor output in insects: (i) Mechanosensory signals from the legs report movement and load. This input plays an important role in determining not only the magnitude of the actual motor output, but also the timing of stance and swing phases. In the stick insect, these signals directly affect the activity of

central rhythm generating networks of the individual leg joints, and thereby contribute to inter-joint coordination during stepping of each single leg. (ii) Together with very similar data from walking or swimming vertebrates this supports the notion that central neural networks contain multiple CPGs corresponding to and responsible for the segmental structure of the locomotor system (see also Ijspeert *et al.*, 2007). This allows the modelling of a generally applicable control sequence for a basic stepping pattern which is based on neurophysiological data. (iii) Task-specific modifications in the processing of mechanosensory feedback are important for generating adaptive locomotor movements such as changes in speed or direction. To understand the underlying neural mechanisms responsible, we need to identify and analyse the central pattern generating machinery responsible for the task-specific flexibility of locomotor outputs.

Acknowledgements

We thank Dr. J. Schmidt, Marcus Blümel and Dr. Bruce Johnson for their comments on earlier versions of the manuscript. We also thank Sharon Meyen-Southard for her editorial help. Work reported on insect walking by AB, MG and collaborators was supported by various DFG grants (Bu857; Schm1084), the Institute for Advanced Study Berlin and the Boehringer Ingelheim Foundation.

References

Akay, T., Bässler, U., Gerharz, P. and Büschges, A. (2001). The role of sensory signals from the insect coxa-trochanteral joint in controlling motor activity of the femur-tibia joint. *J. Neurophysiol.* **85**, 594–604.

Akay, T. and Büschges, A. (2006). Load signals assist the generation of movement dependent reflex reversal in the femur-tibia joint of stick insects. *J. Neurophysiol.* **96**, 3532–3537.

Akay, T., Haehn, S., Schmitz, J. and Büschges, A. (2004). Signals from load sensors underlie interjoint coordination during stepping movements of the stick insect leg. *J. Neurophysiol.* **92**, 42–51.

Akay, T., Ludwar, B. Ch., Göritz, M. L., Schmitz, J. and Büschges, A. (2007). Segment specificity of load signal processing depends on walking direction in the stick insect leg muscle control system. *J. Neurosci.* **27** (12), 3285–3294.

Ayers, J. L. and Davis, W. J. (1977). Neuronal control of locomotion in the lobster *Homarus americanus*. *J. Comp. Physiol.* **115**, 29–46.

Bässler, U. (1965). Propriorezeptoren am Subcoxal- und Femur-Tibia-Gelenk der Stabheuschrecke *Carausius morosus* und ihre Rolle bei der Wahrnehmung der Schwerkraftrichtung. *Kybernetik* **2**, 168–193.

Bässler, U. (1976). Reversal of a reflex to a single motoneuron in the stick insect *Carausius morosus*. *Biol. Cybern.* **24**, 47–49.

Bässler, U. (1977). Sensory control of leg movement in the stick insect *Carausius morosus*. *Biol. Cybern.* **25**, 61–72.
Bässler, U. (1983). *Neural Basis of Elementary Behavior in Stick Insects*. Berlin: Springer.
Bässler, U. (1986). Afferent control of walking movements in the stick insect *Cuniculina impigra*. II. Reflex reversal and the release of swing phase in the restrained foreleg. *J. Comp. Physiol. A* **158**, 351–362.
Bässler, U. (1988). Functional principles of pattern generation for walking movements of stick insect forelegs: the role of the femoral chordotonal organ afferences. *J. Exp. Biol.* **136**, 125–147.
Bässler, U. (1992). Variability of femoral chordotonal organ reflexes in the locust, *Locusta migratoria*. *Physiol. Entomol.* **17**, 208–212.
Bässler, U. (1993a). The femur-tibia control system of stick insects – a model system for the study of the neural basis of joint control. *Brain Res. Rev.* **18**, 207–226.
Bässler, U. (1993b). The walking- (and searching-) pattern generator of stick insects, a modular system composed of reflex chains and endogenous oscillators. *Biol. Cybern.* **69**, 305–317.
Bässler, U. and Büschges, A. (1990). Interneurones participating in the "active reaction" in stick insects. *Biol. Cybern.* **62**, 529–538.
Bässler, U. and Büschges, A. (1998). Pattern generation for stick insect walking movements-multisensory control of a locomotor program. *Brain Res. Rev.* **27**, 65–88.
Bässler, U., Sauer, A. E. and Büschges, A. (2003). Vibration signals from the FT-joint can induce phase-transitions in motoneuron pools of the stick insect walking system. *J. Neurobiol.* **56**, 125–138.
Bässler, U. and Wegener, U. (1983). Motor output of the denervated thoracic ventral nerve cord in the stick insect *Carausius morosus*. *J. Exp. Biol.* **105**, 127–145.
Bläsing, B. and Cruse, H. (2004). Mechanisms of stick insect locomotion in a gap-crossing paradigm. *J. Comp. Physiol. A* **190**, 173–183.
Borgmann, A., Scharstein, H. and Büschges, A. (2007). Intersegmental coordination: the influence of a single walking leg on the neighbouring segments in the stick insect walking system. *J. Neurophysiol.* **98**, 1685–1696.
Brunn, D. E. and Dean, J. (1994). Intersegmental and local interneurons in the metathorax of the stick insect *Carausius morosus* that monitor leg position. *J. Neurophysiol.* **72**, 1208–1219.
Bucher, D., Akay, T., DiCaprio, R. A. and Büschges, A. (2003). Interjoint coordination in the stick insect leg-control system: the role of positional signaling. *J. Neurophysiol.* **89**, 1245–1255.
Buford, J. A. and Smith, J. L. (1990). Adaptive control for backward quadrupedal walking. II. Hindlimb muscle synergies. *J. Neurophysiol.* **64**, 756–765.
Burns, M. D. (1973). The control of walking in Orthoptera. I. Leg movements in normal walking. *J. Exp. Biol.* **58**, 45–58.
Burrows, M. (1996). *The Neurobiology of an Insect Brain*. Oxford: Oxford University Press.
Büschges, A. (1989). Processing of sensory input from the femoral chordotonal organ by spiking interneurones of stick insects. *J. Exp. Biol.* **144**, 81–111.
Büschges, A. (1994). The physiology of sensory cells in the ventral scoloparium of the stick insect femoral chordotonal organ. *J. Exp. Biol.* **189**, 285–292.
Büschges, A. (1995). Role of local nonspiking interneurons in the generation of rhythmic motor activity in the stick insect. *J. Neurobiol.* **27** (4), 488–512.

Büschges, A. (1998). Inhibitory synaptic drive patterns motoneuronal activity in rhythmic preparations of isolated thoracic ganglia in the stick insect. *Brain Res.* **783**, 262–271.

Büschges, A. (2005). Sensory control and organization of neural networks mediating coordination of multisegmental organs for locomotion. *J. Neurophysiol.* **93**, 1127–1135.

Büschges, A. and El Manira, A. (1998). Sensory pathways and their modulation in the control of locomotion. *Curr. Opin. Neurobiol.* **8**, 733–739.

Büschges, A., Kittmann, R. and Schmitz, J. (1994). An identified nonspiking interneuron in an insect involved in the control of proximal leg joints in local and intersegmental reflexes and during walking. *J. Comp. Physiol. A* **174**, 685–700.

Büschges, A., Ludwar, B. C., Bucher, D., Schmidt, J. and DiCaprio, R. A. (2004). Synaptic drive contributing to rhythmic activation of motoneurons in the deafferented stick insect walking system. *Eur. J. Neurosci.* **19**, 1856–1862.

Büschges, A., Sauer, A. E. and Bässler, U. (2000). Flexibility of a proprioceptive feedback system results from its "parliamentary" (distributed) organisation. In: *Prerational Intelligence: Adaptive Behavior and Intelligent Systems without Symbols and Logic* (eds Cruse, H., Dean, J. and Ritter, H.), pp. 267–286. Dordrecht, Boston, London: Kluwer Academic Publishers.

Büschges, A. and Schmitz, J. (1991). Nonspiking pathways antagonize the resistance reflex in the thoraco-coxal joint of stick insects. *J. Neurobiol.* **22** (3), 224–237.

Büschges, A., Schmitz, J. and Bässler, U. (1995). Rhythmic patterns in the thoracic nerve cord of the stick insect induced by pilocarpine. *J. Exp. Biol.* **198**, 435–456.

Camhi, J. M. and Nolen, T. G. (1981). Properties of the escape system of cockroaches during walking. *J. Comp. Physiol. A* **142**, 339–346.

Carpenter, M. G., Bellos, A. and Patla, A. E. (1997). Is backward stepping over obstacles achieved through a simple temporal reversal of forward stepping? *Int. J. Neurosci.* **93**, 189–196.

Chrachri, A. and Clarac, F. (1987). Induction of rhythmic activity in motoneurons of crayfish thoracic ganglia by cholinergic agonists. *Neurosci. Lett.* **77**, 49–54.

Clarac, F., Cattaert, D. and Le Ray, D. (2000). Central control components of a 'simple' stretch reflex. *TINS* **23**, 199–208.

Clarac, F. and Chasserat, C. (1986). Basic processes of locomotor coordination in the rock lobster. I. Statistical analysis of walking parameters. *Biol. Cybern.* **55**, 159–170.

Clarac, F., Vinay, L., Cazalets, J.-R., Fady, J.-C. and Jamon, M. (1998). Role of gravity in the development of posture and locomotion in the neonatal rat. *Brain. Res. Rev.* **28**, 35–43.

Cruse, H. (1976). The function of the legs in the free walking stick insect, *Carausius morosus*. *J. Comp. Physiol. A* **112**, 235–262.

Cruse, H. (1985a). Which parameters control the leg movement of a walking insect? I. Velocity control during the stance phase. *J. Exp. Biol.* **116**, 343–355.

Cruse, H. (1985b). Which parameters control the leg movement of a walking insect? II. The start of swing phase. *J. Exp. Biol.* **116**, 357–362.

Cruse, H. (1990). Which mechanisms coordinate leg movement in walking arthropods? *TINS* **13**, 15–21.

Cruse, H., Dürr, V. and Schmitz, J. (2007). Insect walking on a decentralized architecture revealing a simple and robust controller. *Phil. Trans. R. Soc. A* **365**, 221–250.

Dean, J. and Schmitz, J. (1992). The two groups of sensilla in the ventral coxal hairplate of *Carausius morosus* have different roles during walking. *Physiol. Entomol.* **17**, 331–341.
Delcomyn, F. (1971). The locomotion of the cockroach *Periplaneta americana*. *J. Exp. Biol.* **54**, 443–452.
Delcomyn, F. (1991). Activity and directional sensitivity of leg campaniform sensilla in a stick insect. *J. Comp. Physiol. A* **168**, 113–119.
DiCaprio, R. A. and Clarac, F. (1981). Reversal of a walking leg reflex elicited by a muscle receptor. *J. Exp. Biol.* **90**, 197–203.
Driesang, R. B. and Büschges, A. (1996). Physiological changes in central neuronal pathways contributing to the generation of a reflex reversal. *J. Comp. Physiol.* **179**, 45–57.
Dürr, V. and Ebeling, W. (2005). The behavioural transition from straight to curve walking: kinetics of leg movement parameters and the initiation of turning. *J. Exp. Biol.* **208**, 2237–2252.
Dürr, V., Schmitz, J. and Cruse, H. (2004). Behavior-based modelling of hexapod locomotion: linking biology and technical application. *Arthropod Struct. Dev.* **33**, 237–250.
Ekeberg, Ö., Blümel, M. and Büschges, A. (2004). Dynamic simulation of insect walking. *Arthropod Struct. Dev.* **33**, 287–300.
Ekeberg, Ö. and Grillner, S. (1999). Simulations of neuromuscular control in lamprey swimming. *Phil. Trans. R. Soc. Lond. B* **354**, 895–902.
Ekeberg, Ö. and Pearson, K. G. (2005). Computer simulation of stepping in the hind legs of the cat: an examination of mechanisms regulating the stance-to-swing transition. *J. Neurophysiol.* **94**, 4256–4268.
Epstein, S. and Graham, D. (1983). Behavior and motor output for an insect walking on a slippery surface. 1. Forward walking. *J. Exp. Biol.* **105**, 215–229.
Field, L. H. and Matheson, T. (1998). Chordotonal organs of insects. *Adv. Insect Physiol.* **27**, 1–228.
Field, L. H. and Pflüger, H. J. (1989). The femoral chordotonal organ: a bifunctional orthopteran (*Locusta migratoria*) sense organ? *Comp. Biochem. Physiol. A* **93**, 729–743.
Fischer, H., Schmidt, J., Haas, R. and Büschges, A. (2001). Pattern generation for walking and searching movements of a stick insect leg: 1. Intra- and interjoint coordination of motor activity in a single middle leg preparation. *J. Neurophysiol.* **85**, 341–353.
Franklin, R., Bell, W. and Jander, R. (1981). Rotational locomotion by the cockroach *Blatella germanica*. *J. Insect Physiol.* **27**, 249–255.
Frantsevich, L. I. and Mokrushov, P. A. (1980). Turning and righting in Geotrupes (Coleoptera, Scarabaeidae). *J. Comp. Physiol.* **136**, 279–289.
Füller, H. and Ernst, A. (1974). Die Ultrastruktur der femoralen Chordotonalorgane von *Carausius morosus* (*BR.*). *Zool. Jb. Anat.* **91**, 574–601.
Gabriel, J. P. and Büschges, A. (2006). Generation and control of stepping velocity in the single leg of a stick insect walking on a treadmill. *Phil. Trans. R. Soc. B* **365**, 251–271.
Gabriel, J. P., Scharstein, H., Schmidt, J. and Büschges, A. (2003). Control of flexor motoneuron activity during single leg walking of the stick insect on an electronically controlled treadwheel. *J. Neurobiol.* **56**, 237–251.
Gal, R. and Libersat, F. (2006). New vistas on the initiation and maintenance of insect motor behaviors revealed by specific lesions of the head ganglia. *J. Comp. Physiol. A* **192** (9), 1003–1020.

Graham, D. (1972). A behavioural analysis of the temporal organization of walking movements in the 1st instar and adult stick insect (*Carausius morosus*). *J. Comp. Physiol.* **81**, 23–52.
Graham, D. (1981). Walking kinetics of the stick insect using a low inertia, counter-balanced pair of independent treadwheels. *Biol. Cybern.* **40**, 49–58.
Graham, D. (1985). Pattern and control of walking in insects. *Adv. Insect Physiol.* **18**, 31–140.
Graham, D. and Bässler, U. (1981). Effects of afference sign reversal on motor activity in walking stick insects. *J. Exp. Biol.* **91**, 179–193.
Graham, D. and Cruse, H. (1981). Coordinated walking of stick insects on a mercury surface. *J. Exp. Biol.* **92**, 229–241.
Graham, D. and Epstein, D. (1985). Behaviour and motor output for an insect walking on a slippery surface. II. Backward walking. *J. Exp. Biol.* **118**, 287–296.
Graham, D. and Wendler, G. (1981). The reflex behaviour and innervation of the tergo-coxal retractor muscles of the stick insect *Carausius morosus*. *J. Comp. Physiol.* **143**, 81–91.
Grasso, R., Bianchi, L. and Lacquaniti, F. (1998). Motor patterns for human gait: backward versus forward locomotion. *J. Neurophysiol.* **80**, 1868–1885.
Grillner, S. (2003). The motor infrastructure: from ion channels to neuronal networks. *Nat. Rev.* **4**, 573–586.
Grillner, S. and Rossignol, S. (1978). On the initiation of the swing phase of locomotion in chronic spinal cats. *Brain Res.* **146**, 269–277.
Grillner, S. and Zangger, P. (1979). On the central generation of locomotion in the low spinal cat. *Exp. Brain Res.* **34**, 241–261.
Grillner, S. and Zangger, P. (1984). The effect of dorsal root transection on the afferent motor pattern in the cat's hindlimb during locomotion. *Acta Physiol. Scand.* **120**, 393–405.
Gruhn, M., Hofmann, O., Dübbert, M., Scharstein, H. and Büschges, A. (2006). Tethered stick insect walking: a modified slippery surface setup with optomotor stimulation and electrical monitoring of tarsal contact. *J. Neurosci. Methods* **158**, 195–206.
Halbertsma, J. M. (1983). The stride cycle of the cat: the modeling of locomotion by computerized analysis of automatic recordings. *Acta Physiol. Scand.* **521** (Suppl), 1–75.
Hess, D. and Büschges, A. (1999). Role of proprioceptive signals from an insect femur-tibia joint in patterning motoneuronal activity of an adjacent leg joint. *J. Neurophysiol.* **81**, 1856–1865.
Hiebert, G. and Pearson, K. G. (1999). The contribution of sensory feedback to the generation of extensor activity during walking in decerebrate cats. *J. Neurophysiol.* **81**, 758–770.
Hiebert, G., Whelan, P. J., Prochazka, A. and Pearson, K. G. (1996). Contributions of hindlimb flexor muscle afferents to the timing of phase transitions in the cat step cycle. *J. Neurophyisol.* **75**, 1126–1137.
Hofmann, T. and Bässler, U. (1982). Anatomy and physiology of trochanteral campaniform sensilla in the stick insect *Cuniculina impigra*. *Physiol. Entomol.* **7**, 413–426.
Hofmann, T. and Koch, U. T. (1985). Acceleration receptors in the femoral chordotonal organ in the stick insect *Cuniculina impigra*. *J. Exp. Biol.* **114**, 225–237.
Hofmann, T., Koch, U. T. and Bässler, U. (1985). Physiology of the femoral chordotonal organ in the stick insect *Cuniculina impigra*. *J. Exp. Biol.* **114**, 207–223.

Höltje, M. and Hustert, R. (2003). Rapid mechano-sensory pathways code leg impact and elicit very rapid reflexes in insects. *J. Exp. Biol.* **206**, 2715–2724.
Ijspeert, A. J., Crespi, A., Ryczko, D. and Cabelguen, J. M. (2007). From swimming to walking with a salamander robot driven by a spinal cord model. *Science* **315**, 1416–1420.
Jander, J. P. (1982). Untersuchungen zum Mechanismus und zur zentralnervösen Steuerung des Kurvenlaufs bei Stabheuschrecken (*Carausius morosus*). Ph.D. thesis, University of Cologne, Cologne, Germany.
Jander, J. P. (1985). Mechanical stability in stick insects when walking straight and around curves. In: *Insect Locomotion* (eds Gewecke, M. and Wendler, G.), pp. 33–42. Berlin: Paul Parey.
Jindrich, D. L. and Full, R. J. (1999). Many-legged manoeuvrability: dynamics of turning in hexapods. *J. Exp. Biol.* **202** (Pt 12), 1603–1623.
Johnston, R. M. and Levine, R. B. (1996). Crawling motor patterns induced by pilocarpine in isolated larval nerve cords of *Manduca sexta*. *J. Neurophysiol.* **76** (5), 3178–3195.
Johnston, R. M. and Levine, R. B. (2002). Thoracic leg motoneurons in the isolated CNS of adult *Manduca* produce patterned activity in response to pilocarpine, which is distinct from that produced in larvae. *Invert. Neurosci.* **4** (4), 175–192.
Jordan, L. M., Pratt, C. A. and Menzies, J. E. (1979). Locomotion evoked by brain stem stimulation: occurrence without phasic segmental afferent input. *Brain Res.* **177**, 204–207.
Kittmann, R. and Schmitz, J. (1992). Functional specialization of the scoloparia of the femoral chordotonal organ in stick insects. *J. Exp. Biol.* **173**, 91–108.
Knop, G., Denzer, L. and Büschges, A. (2001). A central pattern-generating network contributes to ''reflex-reversal''-like leg motoneuron activity in the locust. *J. Neurophysiol.* **86**, 3065–3068.
Kristan, W. B., Jr and Shaw, B. K. (1997). Population coding and behavioural choice. *Curr. Opin. Neurobiol.* **7**, 826–831.
Laurent, G. and Burrows, M. (1989). Distribution of intersegmental inputs to nonspiking local interneurons and motor neurons in the locust. *J. Neurosci.* **9**, 3019–3029.
Laurent, G. and Hustert, R. (1988). Motor neuronal receptive fields delimit patterns of motor activity during locomotion of the locust. *J. Neurosci.* **8**, 4349–4366.
Le Ray, D., Clarac, F. and Cattaert, D. (1997a). Functional analysis of the sensory motor pathway of resistance reflex in crayfish. I. Multisensory coding and motor neuron monosynaptic responses. *J. Neurophysiol.* **78**, 3133–3143.
Le Ray, D., Clarac, F. and Cattaert, D. (1997b). Functional analysis of the sensory motor pathway of resistance reflex in crayfish. II. Integration of sensory inputs in motor neurons. *J. Neurophysiol.* **78**, 3144–3153.
Lewinger, W. A., Rutter, B. L., Blümel, M., Büschges, A. and Quinn, R. D. (2006). Sensory coupled action switching modules generate robust, adaptive stepping in legged robots. *International Conference on Climbing and Walking Robots* (*CLAWAR'06*), September 12–14, Brussels, Belgium.
Ludwar, B. C., Göritz, M. L. and Schmidt, J. (2005a). Intersegmental coordination of walking movements in stick insects. *J. Neurophysiol.* **93**, 1255–1265.
Ludwar, B. C., Westmark, S., Büschges, A. and Schmidt, J. (2005b). Modulation of membrane potential in mesothoracic moto- and interneurons during stick insect front leg walking. *J. Neurophysiol.* **94**, 2772–2784.

Matsushima, T. and Grillner, S. (1992). Neural mechanisms of intersegmental coordination in lamprey: local excitability changes modify the phase coupling along the spinal cord. *J. Neurophysiol.* **67** (2), 373–388.

Mu, L. and Ritzmann, R. E. (2005). Kinematics and motor activity during tethered walking and turning in the cockroach, *Blaberus discoidalis*. *J. Comp. Physiol. A* **191**, 1037–1054.

Noah, J. A., Quimby, L., Frazier, S. F. and Zill, S. N. (2004). Walking on a 'peg leg': extensor muscle activities and sensory feedback after distal leg denervation in cockroaches. *J. Comp. Physiol. A* **190**, 217–231.

Nothof, U. and Bässler, U. (1990). The network producing the ''active reaction'' of stick insects is a functional element of different pattern generating systems. *Biol. Cybern.* **62**, 453–462.

Orlovsky, G. N., Deliagina, T. G. and Grillner, S. (1999). *Neuronal Control of Locomotion*. Oxford: Oxford University Press.

Pearson, K. G. (1993). Common principles of motor control in vertebrates and invertebrates. *Annu. Rev. Neurosci.* **16**, 265–297.

Pearson, K. G. (2000). Neural adaptation in the generation of rhythmic behavior. *Annu. Rev. Physiol.* **62**, 723–753.

Pearson, K. G., Ekeberg, Ö. and Büschges, A. (2006). Assessing sensory function in locomotor systems using neuro-mechanical simulations. *TINS* **29** (11), 625–631.

Pearson, K. G. and Iles, J. F. (1970). Discharge patterns of coxal levator and depressor motoneurones of cockroach, *Periplaneta americana*. *J. Exp. Biol.* **52**, 139–165.

Pearson, K. G. and Iles, J. F. (1973). Nervous mechanisms underlying intersegmental co-ordination of leg movements during walking in the cockroach. *J. Exp. Biol.* **58**, 725–744.

Pringle, J. W. S. (1938). Proprioception in insects. II. The action of the campaniform sensilla on the legs. *J. Exp. Biol.* **15**, 114–131.

Prochazka, A. (1996). Proprioceptive feedback and movement regulation. In: *Handbook of Physiology. Section 12. Exercise: Regulation and Integration of Multiple Systems* (eds Rowell, L. and Sheperd, J. T.), pp. 89–127. New York: American Physiological Society.

Quimby, L. A., Amer, A. S. and Zill, S. N. (2006). Common motor mechanisms support body load in serially homologous legs of cockroaches in posture and walking. *J. Comp. Physiol. A* **192**, 247–266.

Ridgel, A. L., Alexander, B. E. and Ritzmann, R. E. (2007). Descending control of turning behavior in the cockroach, *Blaberus discoidalis*. *J. Comp. Physiol. A* **170**, 443–462.

Ridgel, A. L. and Ritzmann, R. E. (2005). Effects of neck and circumoesophageal connective lesions on posture and locomotion in the cockroach. *J. Comp. Physiol. A* **191**, 559–573.

Ritzmann, R. E. and Büschges, A. (2007). Invertebrate neurobiology. In: *Chapter: Walking* (eds North, G. and Greenspan, R.). New York: Cold Spring Harbor Laboratory Press.

Roeder, K. (1937). The control of tonus and locomotor activity in the praying mantis (*Mantis religiosa* L.). *J. Exp. Biol.* **76**, 353–374.

Rutter, B. L., Lewinger, W. A., Blümel, M., Büschges, A. and Quinn, R. D. (2007). Simple muscle models regularize motion in a robotic leg with neurally-based step generation. *Proceedings of ICRA 2007*, Rome.

Ryckebusch, S. and Laurent, G. (1993). Rhythmic patterns evoked in locust leg motor neurons by the muscarinic agonist pilocarpine. *J. Neurophysiol.* **69** (5), 1583–1595.

Sauer, A., Driesang, R. B., Büschges, A. and Bässler, U. (1995). Information processing in the femur-tibia control loop of stick insects. 1. The response characteristics of two nonspiking interneurons result from parallel excitatory and inhibitory inputs. *J. Comp. Physiol. A* **177**, 145–158.

Sauer, A., Driesang, R. B., Büschges, A. and Bässler, U. (1996). Distributed processing on the basis of parallel and antagonistic pathways: simulation of the femur-tibia control system in the stick insect. *J. Comput. Neurosci.* **3**, 179–198.

Schaefer, P. L. and Ritzmann, R. E. (2001). Descending influences on escape behavior and motor pattern in the cockroach. *J. Neurobiol.* **49**, 9–28.

Schmitz, J. (1986a). The depressor trochanteris motoneurones and their role in the coxo-trochanteral feedback loop in the stick insect *Carausius morosus*. *Biol. Cybern.* **55**, 25–34.

Schmitz, J. (1986b). Properties of the feedback system controlling the coxa-trochanter joint in the stick insect *Carausius morosus*. *Biol. Cybern.* **55**, 35–42.

Schmitz, J. (1986c). Was messen die Borstenfelder von Carausius morosus? *Proceedings of the 14th Göttingen Neurobiology Conference*, Göttingen, Germany.

Schmitz, J. (1993). Load-compensating reactions in the proximal leg joints of stick insects during standing and walking. *J. Exp. Biol.* **183**, 15–33.

Schmitz, J. and Hassfeld, G. (1989). The treading-on-tarsus reflex in stick insects phase-dependence and modifications of the motor output during walking. *J. Exp. Biol.* **143**, 373–388.

Schmitz, J. and Schöwerling, H. (1992). No effects of coxo-trochanteral proprioceptors on extensor tibiae motor neurons in posture control. *Proceedings of the 20th Göttingen Neurobiology Conference*, p. 118.

Schumm, M. and Cruse, H. (2006). Control of swing movement: influences of differently shaped substrate. *J. Comp. Physiol. A* **192**, 1147–1164.

Spirito, C. P. and Mushrush, D. L. (1979). Interlimb coordination during slow walking in the cockroach. I. Effects of substrate alterations. *J. Exp. Biol.* **78**, 233–243.

Stein, W., Bässler, U. and Büschges, A. (2006). Intersegmental transfer of sensory signals in the stick insect leg muscle control system. *J. Neurobiol.* **66**, 1253–1269.

Stein, W. and Schmitz, J. (1999). Multimodal convergence of presynaptic afferent inhibition in insect proprioceptors. *J. Neurophysiol.* **82**, 512–514.

Strauß, R. (2002). The central complex and the genetic dissection of locomotor behaviour. *Curr. Opin. Neurobiol.* **12** (6), 633–638.

Strauß, R. and Heisenberg, M. (1990). Coordination of legs during straight walking and turning in *Drosophila melanogaster*. *J. Comp. Physiol. A* **167**, 403–412.

Strauß, R. and Heisenberg, M. (1993). A higher control center of locomotor behavior in the *Drosophila* brain. *J. Neurosci.* **13**, 1852–1861.

Tartar, G. (1976). Mechanische Sinnesorgane an den Beinen der Stabheuschrecke *Carausius morosus*. Ph.D. thesis, Universität Köln, Cologne, Germany.

Watson, J. T., Ritzmann, R. E. and Pollack, A. J. (2002). Control of climbing behavior in the cockroach, *Blaberus discoidalis*. II. Motor activities associated with joint movement. *J. Comp. Physiol. A* **188**, 55–69.

Wendler, G. (1964). Laufen und Stehen der Stabheuschrecke *Carausius morosus*: Sinnesborstenfelder in den Beingelenken als Glieder von Regelkreisen. *Z. Vergl. Physiol.* **48**, 198–250.

Wendler, G. (1965). The co-ordination of walking movements in arthropods. *Symp. Soc. Exp. Biol.* **20**, 229–249.

Wilson, D. M. (1966). Insect walking. *Ann. Rev. Entomol.* **11**, 103–122.

Wolf, H. (1992). Reflex modulation in locusts walking on a treadwheel intracellular recordings from motoneurons. *J. Comp. Physiol. A* **170**, 443–462.
Wolf, H. and Burrows, M. (1995). Proprioceptive sensory neurons of a locust leg receive rhythmic presynaptic inhibition during walking. *J. Neurosci.* **15**, 5623–5636.
Yakovenko, S., McCrea, D. A., Stecina, K. and Prochazka, A. (2005). Control of locomotor cycle durations. *J. Neurophysiol.* **94**, 1057–1065.
Zill, S. N. (1986). A model for walking pattern generation for cockroach reconsidered. *J. Neurobiol.* **17**, 317–328.
Zill, S. N., Duke, E. R. and Keller, B. R. (2006). Discrete sensory signals of load decreases in the legs of freely moving cockroaches. *Proceedings of the Meeting of the Society for Neuroscience 2006*, poster 449.9/V8.
Zill, S. N., Ridgel, A. L., DiCaprio, R. A. and Frazier, S. F. (1999). Load signalling by cockroach trochanteral campaniform sensilla. *Brain Res.* **822** (1–2), 271–275.
Zill, S. N., Schmitz, J. and Büschges, A. (2004). Leg sensors and sensory–motor interactions. *Arthropod Struct. Dev.* **33**, 273–286.
Zollikofer, C. P. E. (1994). Stepping patterns in ants. I. Influence of speed and curvature. *J. Exp. Biol.* **192**, 95–106.
Zolotov, V., Frantsevich, L. and Falck, E. M. (1975). Kinematik der phototaktischen Drehung bei der Honigbiene *Apis mellifera*. *J. Comp. Physiol.* **97**, 339–353.

Sensory Systems and Flight Stability: What do Insects Measure and Why?

Graham K. Taylor[a] and Holger G. Krapp[b]

[a]*Department of Zoology, University of Oxford, Tinbergen Building, South Parks Road, Oxford, OX1 3PS, UK*

[b]*Department of Bioengineering, Imperial College London, South Kensington Campus, London, SW7 2AZ, UK*

1 Introduction 232
2 Background 234
  2.1 Mechanics of flight 234
  2.2 Feedback control 235
3 Visual sensors 237
  3.1 Significance of visual sensing 237
  3.2 Visual sensing of directional motion 239
  3.3 Compound eyes 245
  3.4 Ocelli 256
  3.5 Fusion of inputs from the compound eyes and ocelli 259
4 Airflow sensors 260
  4.1 Significance of airflow sensing 260
  4.2 Antennae 260
  4.3 Wind-sensitive hairs 272
5 Inertial sensors 278
  5.1 Significance of inertial sensing 278
  5.2 Halteres 279
  5.3 Other inertial sensors 285
6 Wing-load sensors 286
  6.1 Significance of load sensing 286
  6.2 Wing campaniform sensilla 287
7 Conclusions 289
  7.1 Insects sense disturbances, not absolutes 289
  7.2 Insect sensory systems are tuned to specific directions of motion 292
  7.3 Insects sense composite, multi-modal quantities 295
  7.4 The natural-mode sensing hypothesis 297
  Acknowledgements 301
  References 302

ADVANCES IN INSECT PHYSIOLOGY VOL. 34
ISBN 978-0-12-373714-4
DOI: 10.1016/S0065-2806(07)34005-8

Abstract

In the absence of much passive stability, flying insects rely upon active stabilisation, necessitating the provision of rich sensory feedback across a range of modalities. Here we consider from a sensory perspective what quantities flying insects measure, in order to ask from a mechanical perspective why they should want to do so. We consider each of the sensory modalities separately and uncover three general principles. Firstly, we find that insects have evolved to measure changes in kinematic state, rather than absolute state. For example, although the antennae may be loosely thought of as airspeed sensors, we show that they are configured as a sophisticated adaptive sensing system which is much more appropriate for measuring changes in airspeed than absolute airspeed. Secondly, we find that insect sensory systems are tuned to sense self-motion components in specific directions. For example, certain visual interneurons of flies operate as matched filters that are tuned to detect the optic flow fields induced specifically by rotation about one particular axis. Thirdly, we find that insects commonly combine sensory input from across modalities to form composite, multi-modal quantities which they use as feedback to the control system. For example, certain individually identified descending interneurons combine input from the compound eyes, ocelli, antennae, and cephalic wind-sensitive hairs into one composite signal which is then used in flight control. We infer from these three general organisational principles that insects are configured to sense excitation of their natural modes of motion. This natural-mode sensing hypothesis: (1) explains why insects should want to sense changes in state rather than absolute state; (2) predicts what specific directions of motion they should sense, and (3) specifies how sensory input from different modalities should be combined.

1 Introduction

Insects bristle with sensors, many of which are intimately involved in the processes of flight control. Insects for the most part lack stabilising surfaces, and the feedback which these sensors provide is therefore a key part of the active stabilisation upon which insects rely for flight. Insect sensors are remarkably well studied, and their obvious necessity in providing feedback to the flight control system makes it tempting to assume that they are well understood. In physiological detail they are, but it is our contention that at a broader functional level, we understand much less than we think we do about insect sensory systems. We may think we have a good knowledge of what the individual sensory systems measure, but do we have a good understanding of why they have evolved to measure what they do? Can we

yet claim to understand, let alone predict, why feedback from different sensory modalities is combined in the specific ways that it is? In summary, how are insect sensory systems integrated into the higher level functioning of the dynamical systems they control?

Most insect sensors function as components of larger sensory systems, and only make sense when viewed as such. Thus it is that the thousands of photoreceptors in the compound eye of a fly, or the hundreds of wind-sensitive hairs on the head of a locust, do not directly supply input to the flight control system, but rather do so only after their input has been collectively processed by sensory interneurons. The bewildering complexity of sensory inputs at the periphery of the nervous system is thereby channelled into a smaller number of interneuronal inputs at the centre, which constitute the signals upon which the control system acts. Flying insects may indeed be 'sensor-rich' in comparison with aircraft (Żbikowski, 2004), but they are less so than might appear from a simple head-count of their sensors. Nevertheless, the observation that almost every one of an insect's sensory systems contains many separate transducers is reflective of the fact that the quantities they sense are far richer in information than the quantities measured by the sensors of a conventional aircraft. An aircraft's sensors may be complex in design, but typically there will still be only one transducer per sensor, providing a single point measurement of some tangible physical quantity. This begs the important question of what the rich – and in some respects unfamiliar – information content of insect sensory systems is really for.

In this chapter, we propose that the adaptive significance of insect sensory systems can only be properly understood in the light of the dynamics of the mechanical systems they control. Specifically, we will argue that the composite, and often multi-modal, quantities which insects sense are matched to the natural dynamics of their flight. To presage the conclusion but a little, insect sensors appear to sense specific combinations of motion which are less kinematically tangible, but more dynamically meaningful, than the absolute physical quantities measured by aircraft sensors. Rather than measuring straightforward kinematic quantities such as airspeed or angle of attack, insect sensors seem to be tuned to sense excitation of the insect's natural modes of motion. This is very much in the spirit of the now-classical description of invertebrate and vertebrate sensory systems as feature detectors, but builds upon this concept by giving a physical basis for the composite quantities which these sensory systems are tuned to detect. Thus, an understanding of flight mechanics opens the door to an adaptationist understanding of flight physiology.

In answering why insects sense certain quantities, we must first consider what these quantities are. This is not as trivial as it might sound, because the signals upon which the control system acts reside in the response properties of the sensory interneurons, and are not necessarily obvious from

the properties of the sensors themselves. Considerable progress has been made over the past thirty years in determining the response properties of identified interneurons for some sensory systems – notably the compound eyes. However, there remain many other important sensory systems, such as the antennae, for which the interneuronal response characteristics remain unknown. In the case of the visual system, we are therefore in the happy position of being able to infer what quantities are ultimately measured from their known interneuronal responses. In the case of the mechanosensory systems involved in flight control, the interneuronal responses are often less well known. In those cases, we shall therefore be obliged to make inferences about the quantities that are measured from the anatomy, physiology, and behaviours associated with the transduction apparatus and its sensory neurons.

We begin with a brief review of some foundational concepts in flight mechanics and control (Section 2). We then move to consider what quantities are really measured by each of the different sensory systems involved in insect flight stabilisation, dealing in turn with visual sensors (Section 3), airflow sensors (Section 4), inertial sensors (Section 5), and wing-load sensors (Section 6). We introduce each sensory system with a brief discussion of its role in flight control, before considering in greater detail its anatomy, physiology, and function, concluding by discussing precisely what each system measures. Finally, we synthesise these results to elaborate three general principles of sensing in insect flight control (Section 7), and propose a general hypothesis of function to explain why, in relation to flight mechanics, flying insects sense what they do.

2 Background

2.1 MECHANICS OF FLIGHT

Any rigid flying body has six degrees of freedom: three in rotation and three in translation. Insects are not rigid bodies, and have many additional postural and elastic degrees of freedom. Postural control is subsidiary, however, to control the insect's gross velocity, position, and orientation in space. For our purposes, we will therefore consider only the six rigid-body degrees of freedom, except in the case of vision, when it is necessary also to consider head movements stabilising gaze. For analytical simplicity, an orthogonal axis system is usually chosen to describe these six rigid-body degrees of freedom. In classical aircraft design, this reflects the reality of the control system, which generates control moments about the lateral pitch axis using the elevators, about the longitudinal roll axis using the ailerons, and about the downward-pointing yaw axis using the rudder. Reasonably

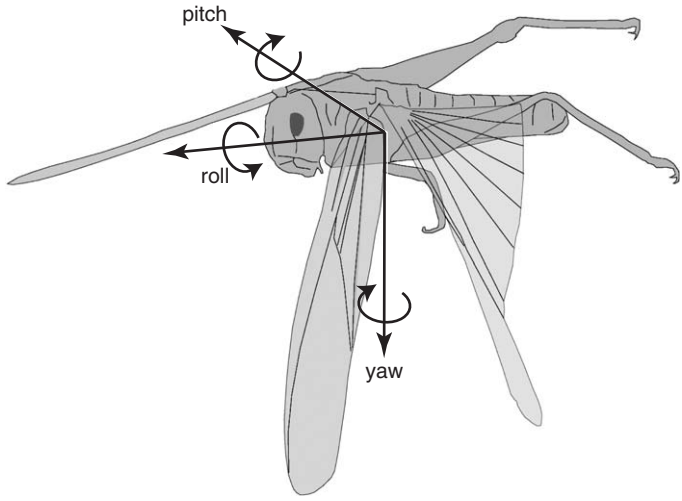

FIG. 1 Any rigid flying body has six degrees of freedom, which are usually resolved in a system of orthogonal pitch, roll, and yaw axes. Insects are not rigid bodies and have highly non-orthogonal control systems, but the same notation is nevertheless convenient for describing their gross motions in flight (outline of locust drawn from a photograph by John Brackenbury).

enough, the same terminology has been carried across to studies of insect flight (Fig. 1), but it is important to note that insect flight control systems are actuated in a highly non-orthogonal fashion (Taylor, 2001). Thus, whereas aircraft classically generate pitch, roll and yaw moments independently using orthogonally arranged control surfaces, a flying insect generates turning moments about variously directed axes using changes in wing kinematics driven by variously disposed muscles with variously aligned firing phase. Hence, while it is natural to distinguish symmetric from asymmetric motions, we must keep in mind that any further discretisation, such as the separation of roll and yaw, is usually of our own making and may not reflect any physiological reality. An obvious corollary is that whereas aircraft sensor systems are usually arranged orthogonally like the actuator systems they provide feedback to, insect sensory systems need not be arranged orthogonally. Any such non-orthogonality then begs the question of why those particular axes have been selected over any others.

2.2 FEEDBACK CONTROL

We have already touched upon the role of sensory feedback, and now need to clarify a few concepts in relation to feedback control. In aircraft flight control systems, feedback is provided by measuring the instantaneous state

of the vehicle, and then comparing this measured state to the vehicle's intended state. The measured difference between the actual and intended state is then used to form an actuating signal, which determines the commanded behaviour of the actuators according to some appropriate control law. This is known as state feedback (Stevens and Lewis, 2003). What is meant by state in this context is the kinematic state of the vehicle. For a rigid body in a quiescent atmosphere, 'state' usually means the velocity, angular velocity and orientation of the body with respect to an inertial frame of reference. In the presence of atmospheric disturbance, the same kinematic states with respect to the airflow will be relevant separately too. Depending upon which of the system's motions are unstable or require stability augmentation to improve handling, it will often be sufficient to measure a subset of these kinematic states in order to provide all of the necessary state feedback to the control system. Sometimes it may not be possible to measure all of the necessary kinematic states, and in that case these may need to be estimated using a dynamic observer or Kalman filter based upon measurements of those kinematic states which can be measured (Stevens and Lewis, 2003). State feedback also lies at the heart of insect-control systems, although as we will argue later, it is of a different kind to that used in aircraft.

Besides the state feedback loops associated with flight control, there may be numerous other control loops regulating the internal running of different components of the system. In an aircraft, the feedback in these systems is usually quite separate from the kinematic state feedback used to control the vehicle with respect to its external environment, and might include, for example, temperature sensors in the engines, or gauges monitoring the flow rate of the fuel lines. Similarly discrete feedback loops are undoubtedly present in insects too, but insects also use many of the same sensors to provide feedback regulating both the running of their flight motor and their kinematic state with respect to the external environment. We will distinguish between these two kinds of feedback by referring to them as peripheral feedback to the flight motor, and state feedback to the flight control system. Whereas peripheral feedback is used only to shape the pattern of the flight motor, state feedback is used to alter the wing kinematics so as to alter the insect's motion with respect to its external environment. The two are conceptually distinct because whereas peripheral feedback is self-generated and necessary even at equilibrium, state feedback can be generated by external perturbation and is needed only during disturbances from equilibrium. Mechanistically, however, they will often be linked, which poses problems for the experimentalist because it is never really possible to switch off the insect's 'autopilot' without also affecting its flight motor. Here we are primarily concerned with the role of state feedback in flight control, and shall deal with peripheral feedback loops only insofar as this aids in elucidating the state feedback loops.

In particular, we will only briefly mention sensory systems that are known to provide peripheral feedback to the flight motor, but have not been shown to provide state feedback to the flight control system. We will now consider each of the various sensory systems in turn.

3 Visual sensors

3.1 SIGNIFICANCE OF VISUAL SENSING

An enormous number of different insect behaviours involve visual information processing (for reviews, see Wehner, 1981; Land and Nilsson, 2002). Visual cues are essential in triggering escape or landing, controlling thrust and altitude, chasing mates and prey, as well as stabilising flight and gaze, to name but a few (for reviews, see Collett *et al.*, 1993; Egelhaaf and Borst, 1993; Heisenberg and Wolf, 1993; Hengstenberg, 1993; Krapp, 2000; Srinivasan and Zhang, 2000). Accordingly, in flies such as *Musca* and *Calliphora*, approximately two-thirds of the 360 000 or so neurons in the brain contribute to visual information processing (Strausfeld, 1976). What makes vision such a significant modality?

One key reason is that individual photoreceptors indicate light level changes over an extended distance range. Unlike mechanoreceptor-based systems, which require the action of local physical forces, visual information can be used for long-range identification of potential threats or targets, as well as to solve short-range feature extraction. Another reason why vision is such a key modality lies in the fact that, depending on how the signals of the photoreceptors are processed, different visual qualities emerge. Local light intensity changes are processed and integrated in different task-specific ways by separate parallel pathways: some pathways provide information about a potential target's retinal position, while others compute derived quantities such as the direction and magnitude of retinal motion. Other pathways establish colour vision, or allow some insects to analyse the polarisation pattern of a blue sky for navigation (for review, see Wehner, 1981). Yet, however complex the visual processing in each of these task-specific pathways might be, their outputs must finally be combined with information from other sensory modalities, and must converge on the final common pathway – the motoneurons controlling the muscles which eventually produce the behaviour. In the following sections, we will concentrate on the visual information processing used in the task of flight stabilisation.

Visual stabilisation reflexes are commonly subsumed under the term 'optomotor responses'. These are observed not only in flying insects, but across all visually oriented species including humans (for review, see Miles and Wallman, 1993). Optomotor responses have been investigated in many

insect species. Here we must necessarily confine ourselves to a few particularly well-studied model systems, in which quantitative behavioural, neuroanatomical, and electrophysiological studies have accumulated a vast body of data on the neural pathways and circuits underlying visual stabilisation reflexes (for reviews, see Wehner, 1981; Götz, 1983; Heisenberg and Wolf, 1984, 1993; Collett *et al.*, 1993; Hausen, 1993; Egelhaaf and Borst, 1993; Hengstenberg, 1993).

3.1.1 *Reflexes for gaze stabilisation*

Gaze stabilisation is a *sine qua non* for efficient visual processing in general. Relative to the transduction mechanisms of mechanosensory systems, the biochemical cascades in photoreceptors take a comparatively long time to convert the energy of photons into changes in membrane potential (for review, see Hardie, 1986). Relative motion between the eyes and the objects in the environment may therefore induce motion blur, which complicates the analysis of visual scenes if the retinal image is not stabilised. Another reason why gaze stabilisation is so important is that visual processing is considerably simplified if the eyes are maintained in a default orientation relative to the external world (for review, see Hengstenberg, 1993). For example, we usually require more time to read a text if the page is turned upside down. Maintaining a default image orientation becomes particularly important when visual information is used to estimate self-motion in space (Section 3.2.1). In order to achieve this task, changes in attitude are immediately compensated for by gaze stabilisation reflexes. In insects, this means using compensatory head movements and changes in body attitude, because the eyes of insects are firmly attached to the head (for review, see Hengstenberg, 1993).

Compensatory head and body movements have been especially well investigated in flight for Diptera (e.g. Land, 1973; Geiger and Poggio, 1977; Hengstenberg *et al.*, 1986; Hengstenberg, 1988, 1995), Orthoptera (e.g. Hensler and Robert, 1990; Miall, 1990) and Odonata (e.g. Mittelstaedt, 1950). Although such compensatory head and body movements are under multi-modal sensory control (Section 5.2), only the visual system is able to inform the insect whether or not these have actually been successful in stabilising gaze. For example, if no rotational image motion is added to the visual input, then this implies that the orientation of the head relative to the external environment remains in its default orientation. If there are any additional rotational components, then these can be corrected using visual feedback. In cases where both head and body movements contribute together to stabilising gaze, their eventual realignment is supported by proprioceptive systems measuring the angular position of the head relative to the thorax (for review, see Hengstenberg, 1993). The visual input to the neck motor system is particularly well known in *Calliphora*, in which 21 pairs

of neck muscles control the three degrees of freedom of head rotation and also control head retraction (Milde *et al*., 1987; Strausfeld *et al*., 1987). The muscles are arranged in blocks and usually only receive input from one motoneuron each. Altogether the system is capable of performing compensatory head movements in pitch and yaw over an angular range of $\pm 20^{\circ}$, and in roll over an angular range of $\pm 90^{\circ}$ (for review, see Hengstenberg, 1993). We discuss briefly below how visual information might be transformed into motor commands for gaze stabilisation in *Calliphora*.

3.1.2 *Reflexes for flight stabilisation*

Like gaze stabilisation, the visual stabilisation of flight has been particularly well investigated in flies and locusts. Although the flight motors of locusts and flies are organised quite differently, the way in which vision modifies their output is broadly similar, relying upon changes in the phase and intensity of muscle activation. For example, visual wide-field stimuli have an immediate impact on the activation pattern of the direct steering muscles in flies (for review, see Heide, 1983) and of the direct power muscles in locusts (e.g. Rowell, 1988). In each case, the output of the flight motor is modified appropriately to compensate for the kind of deviation from steady flight that the visual input signals. For instance, in tethered flies, visual stimulation contributes to thrust and altitude control, as well as to yaw, pitch and roll stabilisation (e.g. Götz, 1975; Srinivasan, 1977; Götz and Buchner, 1978; Götz and Wandel, 1984; Götz and Wehrhahn, 1984; Dickinson *et al*., 1993; Heide and Götz, 1996; Lehmann and Gotz, 1996; Tu and Dickinson, 1996). Locusts have also been shown to control both speed and attitude using visual wide-field motion cues (e.g. Taylor, 1981a; Eggers *et al*., 1991; Baader *et al*., 1992; Preiss, 1992; Preiss and Spork, 1993; Spork and Preiss, 1993). Hence, although flight stabilisation in general is under multisensory control and requires peripheral mechanosensory feedback (Diptera: e.g. Heide, 1983; Sherman and Dickinson, 2003, 2004; Frye and Dickinson, 2004; Orthoptera: e.g. Reichert and Rowell, 1986; Rowell, 1988), the analysis of visual motion assumes a key role in flight stabilisation.

3.2 VISUAL SENSING OF DIRECTIONAL MOTION

3.2.1 *Optic flow and self-motion*

Directional motion is processed in all visually oriented animals, including humans (for reviews, see Miles and Wallman, 1993; Lappe, 2000). While moving through an otherwise stationary environment, insects experience panoramic retinal image shifts, or optic flow, due to the introduction of relative motion between the eyes and objects in the environment.

The structure of the instantaneous optic flow field is governed by the insect's self-motion parameters – specifically the translational and rotational components of its movements in space. Analysing the optic flow field therefore allows the animal to assess its self-motion and to use this information to control its gaze, posture, and motion.

Gibson (1950) first proposed that optic flow provides a rich source of self-motion and distance information. Later, Nakayama and Loomis (1974) and subsequently Koenderink and van Doorn introduced a formal description of optic flow in vector notation that has proved to be extremely useful in studying the relationship between visual input and self-motion. Optic flow fields induced by translation have a fundamentally different global structure than those induced by rotation. Figure 2C, D compare optic flow fields occurring during upwards translation and left-handed roll, respectively. Both the flow fields were calculated using the mathematical formalism of Koenderink and van Doorn (1987), but assuming the same distance to all visual contrasts in the environment. Such unit distance distribution, though unrealistic, best emphasises the structural differences between rotational and translational flow fields.

The optic flow fields may be projected onto a 2-dimensional map to visualise better its complete structure across both hemispheres (Fig. 2C, D: right panels). This reduction to a cylindrical projection overemphasises the dorsal and ventral parts of the visual field where each position is determined by two angles: the horizontal azimuth and the vertical elevation. An azimuth and elevation of 0° defines the point directly in front of the animal (denoted f in Fig. 2C, D). Azimuths $<0^\circ$ and $>0^\circ$ indicate positions in the left and right visual hemisphere, respectively. Elevations $<0^\circ$ and $>0^\circ$ refer to positions below and above the horizon. On a sphere, the dorsal and ventral poles obviously consist only of a point, whereas in a cylindrical projection they form a line.

The orientation and length of each individual vector in Fig. 2C, D indicates the direction and relative velocity of retinal image shifts occurring at different positions in the visual field. Pure translational and rotational optic flow fields have in common that the direction of translation and the axis of rotation are both defined by the points in the flow field where no relative motion takes place and where the vectors therefore disappear. From these flow field singularities, the relative motion gradually increases to become maximal at the flow field equator. During most flight manoeuvres, translation and rotation occur together. In such cases, the translational and rotational optic flow fields are linearly combined, so that the flow field singularity no longer coincides with the direction of translation or the axis of rotation.

Despite these similarities, there are two important structural differences between translational and rotational optic flow. Firstly, in translational flow fields, the local velocity vectors are aligned along great circles

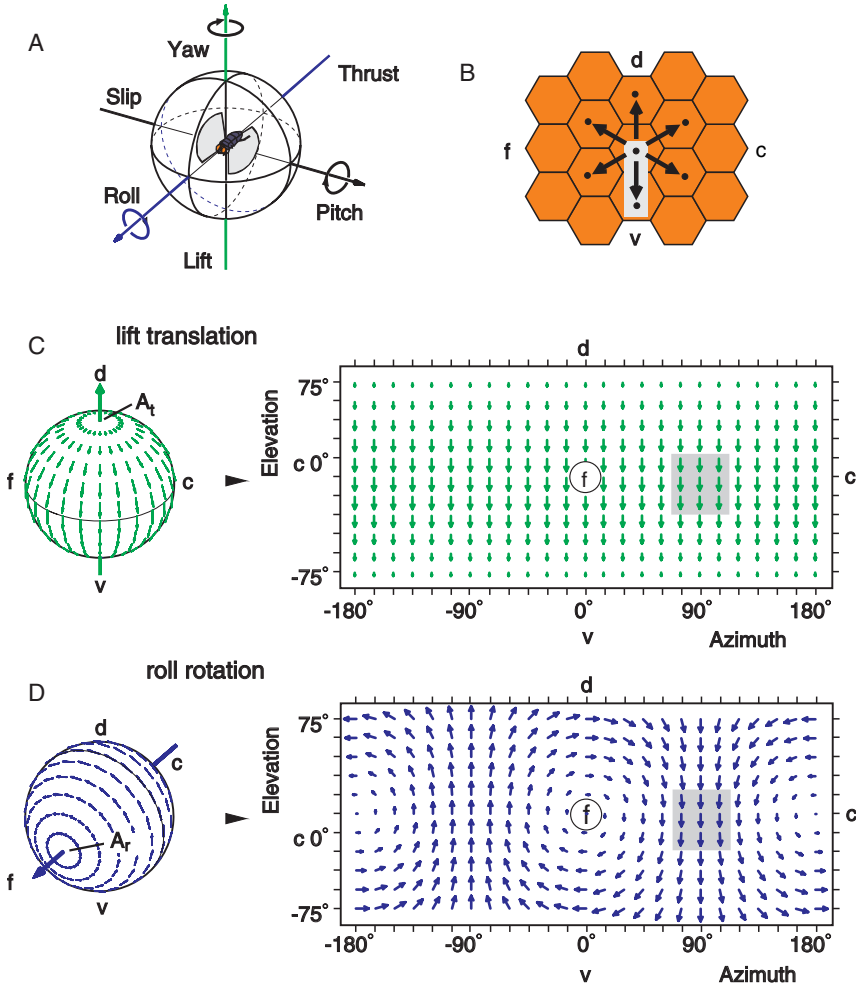

FIG. 2 Self-motion and optic flow. (A) Self-motion can be described in terms of translational and rotational components along and around the cardinal body axes, respectively. (B) Small section of a compound eye sampling information in the lateral visual field of the right eye. In a first approximation, the direction of local retinal image shifts is analysed along ommatidial rows within the hexagonal eye lattice (black arrows, f = frontal, c = caudal, d = dorsal, v = ventral). (C and D) Structural features of global optic flow generated during upward translation (C) and left-handed roll-rotation (D) is presented on the surface of the visual unit-sphere (left) and in a cylindrical projection (right), where f denotes the position directly in front of the animal. The axes of translation and rotation are denoted by A_t in (C) and A_r in (D), respectively. Note, the marked differences between translational and rotational optic flow at the global scale. At the local scale, however, the direction of flow vectors is ambiguous. In the right visual field, grey area, during upward-translation and roll-rotation, local flow vectors have the same orientation (adapted from Krapp and Hengstenberg, 1996; Krapp *et al.*, 1998) (see color plate section at the end of this book).

connecting the two flow field singularities, whereas in a rotational field, the vectors are aligned along parallel circles centred on the axis of rotation (Fig. 2C, D, spherical projection). Secondly, in translational optic flow fields, the magnitudes of the local vectors depend on the distance to the objects in the environment, whereas in rotational fields, the magnitudes of the local vectors are independent of distance.

We are all familiar with the distance dependence of translational optic flow from our everyday experience: when sitting on a train, bushes close by rush past very quickly, while trees and hills in the far distance hardly appear to move. This difference between translational and rotational optic flow is significant: translational optic flow provides relative distance information, which is important in the context of collision avoidance, whereas rotational optic flow does not. In fact, if superimposed on translational optic flow, rotational optic flow has a rather detrimental effect on distance estimation. This is yet another reason why compensatory head rotations are so important: they reduce the rotational component and therefore benefit distance estimation based upon translational optic flow.

3.2.2 *Analysis of directional motion information*

A necessary prerequisite for exploiting global optic flow information is the ability to sense the local direction of visual motion. Hassenstein and Reichardt (1953) carried out a number of behavioural experiments in a beetle, *Chlorophanus viridis* (Curculionidae), and derived a phenomenological model of an Elementary Movement Detector (EMD) used to detect local motion. The EMD model satisfied the necessary and sufficient conditions required for analysis of directional motion. These conditions are: (i) two spatially separated inputs, which are provided by nearby ommatidia, (ii) asymmetric processing of the two input signals, which is achieved by delaying one signal, and (iii) a non-linear operation on the delayed and undelayed signal, which is realised by a multiplication (for reviews, see Reichardt, 1961, 1987; Borst and Egelhaaf, 1989; Franceschini *et al*., 1989). The EMD generates a positive output in response to motion in its preferred direction, while motion in the opposite null-direction results in hardly any response (Fig. 3, upper panels). A fully directionally selective EMD is established by summing the outputs of two mirror-symmetrical EMDs with opposite signs. The summing unit then delivers a positive response to motion in the detector's preferred direction and a negative response to motion in the opposite direction (Fig. 3, lower panels). This EMD model is called a 'correlation-type motion detector' since it performs a spatio-temporal correlation of light intensities sampled at adjacent positions on the retina. Most of the directionally selective motion detectors found across phyla can be derived from the EMD. Borst and Egelhaaf (1993) discuss various motion detector schemes based on

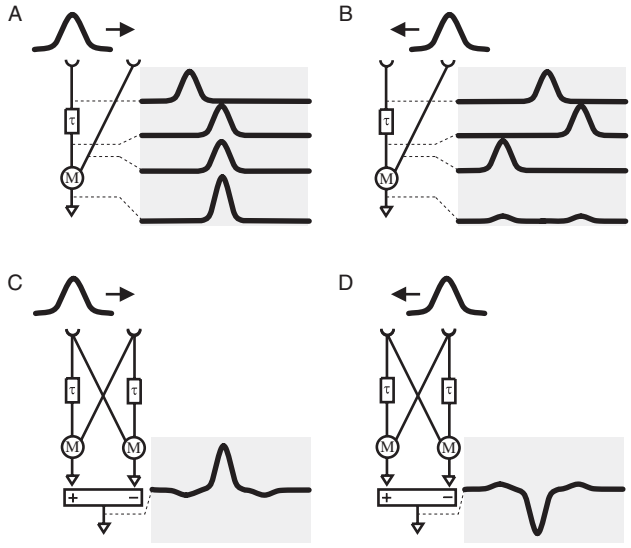

FIG. 3 Elementary movement detectors, EMDs, analyse directional motion by means of a spatio-temporal correlatation of local light intensities at neighbouring ommatidia in the compound eye. (A) Half-detector: a light stimulus (Gaussian function, upper left of each panel) moving from left-to-right in the detector's preferred direction is sensed by the left input channel first. Propagation of the signal in this channel is delayed by a certain period of time, τ, caused by the delay time constant of the EMD. If the time it takes the light stimulus to travel to the right input channel and the delay time constant of the EMD are equal, the signals from both channels simultaneously arrive at the multiplication stage (M) and yield a strong output. (B) Motion in the opposite, null-direction, results in de-correlating the two input signals in time. Consequently, the detector produces only a weak output. (C and D) If the outputs of two mirror-symmetrical half-detectors are subtracted from each other, the integrating stage gains the properties of a fully directional-selective EMD (redrawn from Borst and Egelhaaf, 1989).

experimental evidence obtained in different animal systems or from computer vision.

An inherent property of the EMD is that its response depends not only on the direction and velocity of visual motion, but also on parameters such as the contrast and spatial frequency content of the visual scene (for reviews, see Buchner, 1984; Borst and Egelhaaf, 1993). For example, the response of an EMD to a sinusoidally modulated grating of light intensity depends in a bell-shaped manner on the ratio between the velocity at which the grating moves and the spatial wavelength of the light intensity modulation. Such contrast frequency dependence, or temporal frequency dependence, is fundamentally different from the output of a gradient detector – a hypothetical movement detector originally adapted from computer vision (e.g. Srinivasan, 1990). Gradient detectors also fulfil the

three necessary and sufficient conditions required for directional-selective motion analysis, but their output signals are linear in the velocity domain. Although there is good evidence suggesting that flies employ correlation-type motion detectors (for review, see Buchner, 1984), bees have been found to use velocity information to solve many visually controlled tasks (e.g. Srinivasan and Zhang, 2000). It is not yet clear, however, whether this is because bees use gradient detectors: they might, for example, combine the outputs of correlation detectors tuned to different temporal frequencies, as has been found in Crustacea (Decapoda: Nalbach, 1989).

Combined experimental and theoretical studies have led to refinements of the basic functional EMD structure (e.g. Clifford *et al.*, 1997; Harris *et al.*, 1999; Borst *et al.*, 2003) and have explored the potential of EMDs, or any derivatives, to estimate velocity information (e.g. Reichardt *et al.*, 1988; Zanker *et al.*, 1999). Recently, EMD networks have been presented including more realistic assumptions about the properties of the peripheral visual system and gain control mechanisms. Such models are able to reduce significantly the pattern-dependent response component in simulated lobula plate tangential cells (LPTCs; see Section 3.3.3) and to increase the range over which the responses indicate image velocity (e.g. Dror *et al.*, 2001). The power to predict the responses of LPTCs has been further increased by using wide-field optic flow sequences composed of naturalistic spatial frequency distributions (van der Schaaf and van Hateren, 1996) as the input to the model networks (Heitwerth *et al.*, 2005; Lindemann *et al.*, 2005; Shoemaker *et al.*, 2005).

3.2.3 *Ambiguity of local motion information*

Besides the question of what information biological movement detectors actually encode, there is another problem which all animals face when analysing directional motion in the context of self-motion estimation. Any movement detector scheme, be it biological or technical, operates on a local scale (e.g. Bulthoff *et al.*, 1989; Borst and Egelhaaf, 1993; Barron *et al.*, 1994), whereas the distinction between different optic flow fields, and thus the estimation of particular self-motion parameters, is only possible on a global scale. This becomes obvious when revisiting Fig. 2C, D. Consider a set of local EMDs, each of which analyses directional motion along the three cardinal ommatidial rows of the hexagonal eye lattice (Fig. 2B). In the right lateral visual field, local velocity vectors in both flow fields have the same orientation around the eye equator (Fig. 2C, D, shaded area). An EMD analysing vertical downward motion in this region would therefore be activated during both upward translation and left-handed roll. Hence, based on the signal in this EMD alone, the fly would not be able to decide which of the two self-motion components led to the EMD's activation. We will see later how selective spatial integration of local motion information

provides a strategy to overcome the problem of local ambiguities when estimating self-motion from optic flow (Section 3.3.5).

3.3 COMPOUND EYES

3.3.1 *Significance of the compound eyes*

It is clear from Section 3.2.3 that an extended visual field is beneficial to the estimation of self-motion. Panoramic vision is a conspicuous feature of most insect visual systems, and in this respect, flying insects are very well equipped for the task of visually estimating self-motion. Depending upon size and species, the hexagonal eye lattice of the compound eyes contains between hundreds and tens of thousands of ommatidia supporting the analysis of directional motion and other visual cues necessary for the control of goal-directed behaviour (for review, see Land and Nilsson, 2002). Although we will focus on central processing stages of sensory input from the compound eyes, we first give a brief introduction to the general organisation of those parts of the visual system involved in motion vision which receive input from the compound eye. Within insects, the most comprehensive body of behavioural, anatomical, and physiological data on the processing of directional motion is available for Diptera (for reviews, see Götz, 1983; Buchner, 1984; Hausen, 1984; Hausen and Egelhaaf, 1989; Egelhaaf and Borst, 1993; Hausen, 1993;Krapp, 2000; Egelhaaf *et al.*, 2002; Haag and Borst, 2002). In the following sections on compound eyes we will therefore focus almost exclusively on flies, in order to illustrate principles of directional motion analysis by insect visual systems in general.

3.3.2 *Organisation of the motion–vision pathways*

The functional organisation of the fly visual system has been described by Strausfeld in several comprehensive accounts (e.g. Strausfeld, 1976, 1984; see Fig. 4 for schematic). The fly visual system consists of three visual neuropiles and the retina, which is connected to the hexagonal eye lattice of the compound eye. The lamina with the most neurons receiving input from the retinal photoreceptors is the first neuropile. Visual information is then transmitted on to the second neuropile, the medulla, via axons forming the external chiasm. From the medulla, connections are then made to the lobula complex, which in dipteran flies consists of the anterior lobula and the posterior lobula plate. Between the medulla and the lobula complex, the visual fibres build a second, internal chiasm. The whole system is retinotopically organised, and visual processing mostly takes place in separated columns. This means that information derived from neighbouring points in the visual field is processed in adjacent columns throughout the

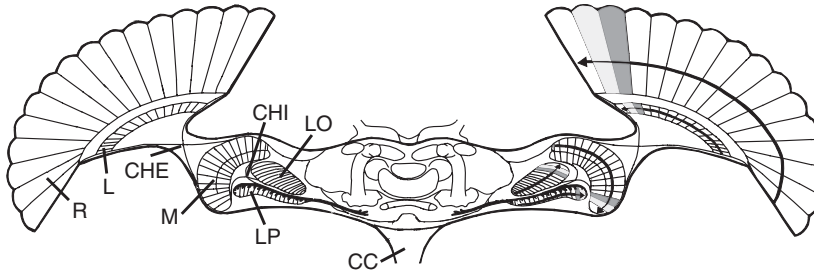

FIG. 4 Horizontal section through the fly visual system. The schematic shows the retina (R) and the visual neuropiles. The lamina (L) is connected to the medulla (M) via the external optic chiasm (CHE). Medulla output connections form the internal optic chiasm (CHI) before invading the lobula complex consisting of the anterior lobula (LO) and the posterior lobula plate (LP). Output fibres of the lobula terminate in the lateral protocerebrum. Arrowheads and grey shaded areas in the right half of the visual system indicate the retinotopic organisation throughout the neuropiles. CC: cervical connective (redrawn from Hausen, 1982).

visual system, up to the neuropiles in which local signals are spatially integrated. Owing to the two chiasms, the retinal image is inverted twice along the pathway. Signals obtained from the frontal and caudal visual field are delivered to distal and proximal locations, respectively, when arriving at the lobula and lobula plate, which both provide information to the various motor centres. No inversion of the visual image takes place along the dorso–ventral axis.

3.3.3 *Directionally selective lobula plate tangential cells (LPTCs)*

The lobula plate is one of the major centres for the integration of directional motion information (Fig. 4). In flies, this neuropile accommodates a population of about 60 visual interneurons – the lobula plate tangential cells (LPTCs, for review, see Hausen, 1993). Most LPTCs are characterised by extended dendritic input fields ramifying within distinct and conserved parts of the neuropile (for reviews, see Hausen, 1984, 1993). On their dendrites, LPTCs integrate the signals of hundreds – or in blowflies, even thousands – of directionally selective small-field elements (Strausfeld, 1976; Bausenwein and Fischbach, 1992). The responses of LPTCs when challenged with local motion stimuli directly reflect the properties of EMDs (e.g. Hausen, 1984; see Fig. 3). Four different functional groups of LPTCs have been anatomically identified and electrophysiologically characterised: (i) heterolateral LPTCs receive input from extended parts of the visual field and convey the integrated motion information by means of spike rate modulations to the lobula plate in the contralateral part of the brain (e.g. Hausen, 1993); (ii) output LPTCs receive retinotopic input from directionally selective

small-field elements and, in some cases, from heterolateral LPTCs (e.g. Hausen, 1993); (iii) centrifugal LPTCs, or CH-cells, receive directional motion inputs from various sources and establish intrinsic lobula plate circuits involved in figure detection (e.g. Hausen and Egelhaaf, 1989; Hausen, 1993); (iv) figure detection, or FD-cells (Egelhaaf, 1985a,b,c; for review, see Hausen and Egelhaaf, 1989), receive retinotopic input from directionally selective small-field elements and receive inhibitory input from CH-cells which results in a preference for small-field over wide-field motion (Warzecha *et al.*, 1993). Of these interneurons, the output LPTCs play a significant role in the control of stabilisation reflexes. We outline the properties of the output LPTCs in greater detail in the next section.

3.3.4 *Horizontal system (HS) and vertical system (VS) output LPTCs*

Among the output LPTCs of *Calliphora* there are two distinctly different sub-populations: three horizontal system cells (HS-cells: Hausen, 1982) and ten vertical system cells (VS-cells: Pierantoni, 1976; Hengstenberg, 1982; Hengstenberg *et al.*, 1982). Corresponding to the retinotopic organisation of the visual system, the three HS-cells – north (HSN), equatorial (HSE), and south (HSS) – integrate visual inputs from the dorsal, equatorial, and ventral parts of the ipsilateral visual field, respectively (Fig. 6; Hausen, 1982). HSN and HSE receive additional, rotation-specific signals from the contralateral visual field mediated by heterolateral LPTCs (e.g. Hausen, 1993). In terms of their morphology, the VS-cells are distinctly different from the HS-cells in that their main dendrites are not horizontally, but vertically, oriented (cf. cell reconstructions in Figs. 5 and 6). The VS1 main dendrite arborises in the distal lobula plate resulting in maximal sensitivity for vertical downward motion in the frontal visual field. The VS10 main dendrite arborises in the proximal lobula plate, responding best to vertical downward motion in the caudal visual field (Krapp *et al.*, 1998). VS- and HS-cell dendrites mainly arborise in four distinct directional input layers of the lobula plate. These layers convey information about vertical and horizontal motion presented in the equatorial visual field (Buchner *et al.*, 1979). The dendrites of some VS-cells, however, ramify in two input layers: VS1, for instance, has a second dendritic field located in the most anterior directional input layer which mediates back-to-front motion sensitivity (Hengstenberg, 1982; Hausen, unpublished). Furthermore, the proximal VS-cells, VS7–VS10, possess dendritic fields integrating input from the second most anterior input layer that provides information about front-to-back motion. The HS-cell dendrites ramify in the same directional layer (Hengstenberg, 1982; Hausen, 1982, Hausen, unpublished data).

The signals which the output LPTCs generate are distinctly different from those of the spiking heterolateral LPTCs from which they may receive

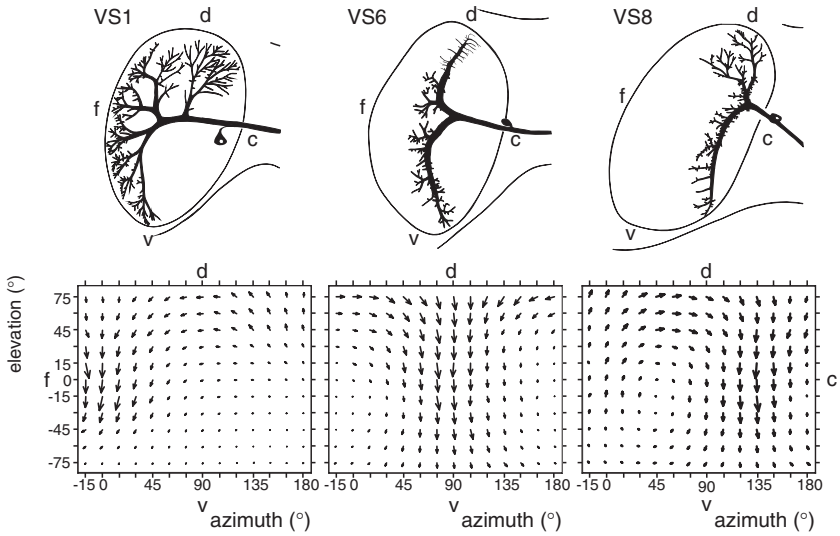

FIG. 5 Vertical system cells of *Calliphora* detect rotations about various near-horizontal axes. Upper row of panels: The reconstructions from intracellular stains of individually identified tangential cells VS1, VS6, and VS8 drawn in the contour of the lobula plate. Lower row of panels: The visual receptive fields averaged across results obtained from at least 5 different flies per cell type. The organisation of the receptive fields shows a smooth transition of local motion preference reminiscent of the directional gradient of velocity vectors in parts of, or entire, monocular rotation flow fields. The location of the main vertical dendrite within the lobula plate corresponds to the positions in the visual field where the respective VS-cell is most sensitive to vertical downward motion. In the case of the VS1-cell, the extent of its dendritic arborisation within the lobula plate is in agreement with the size and location of the cells receptive field, reflecting the retinotopic input organisation of the visual system (adapted from Krapp and Hengstenberg, 1996; Krapp *et al.*, 1998).

input. Motion in the neurons' preferred direction depolarises the cell, while motion in the opposite null-direction results in hyperpolarisation. Pharmacological studies have shown that VS- and HS-cells are equipped with ACh- and GABA receptors suggesting that they receive input from the two mirror-symmetrical subunits of an EMD: one excitatory, and the other inhibitory (Brotz and Borst, 1996; Section 3.2.2). Other studies provide tentative evidence, though, that local elements presynaptic to the LPTCs are already fully directionally selective (Douglass and Strausfeld, 1995, 1996). On top of the graded response to preferred direction motion, some VS- and HS-cells produce 'spikelets' of irregular amplitude (Hengstenberg, 1977). The application of channel blockers shows that spikelets are in fact regular sodium spikes (Haag and Borst, 1996). Their small and irregular amplitudes are the result of a comparatively shallow resting potential,

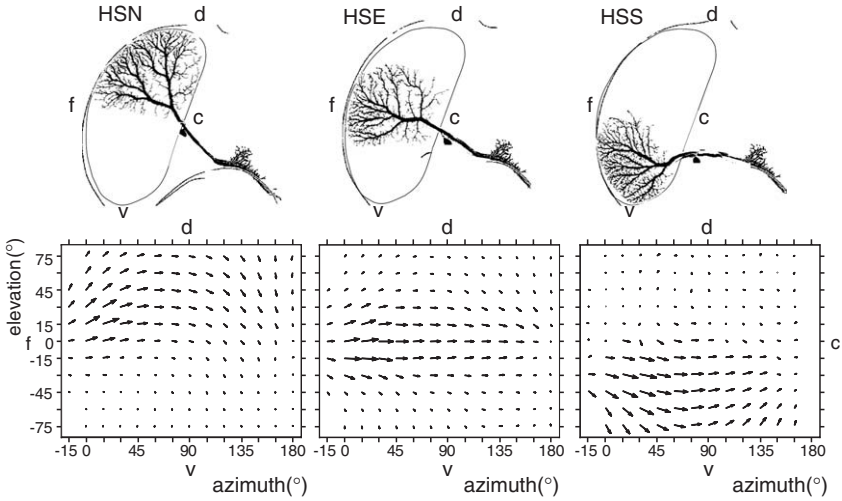

FIG. 6 Horizontal system cells of *Calliphora* indicate rotations around differently inclined but near-vertical axes, and specific translation-related parameters. Upper row of panels: reconstructions from intracellular stains of individually identified tangential cells HSN, HSE, and HSS drawn in the contour of the lobula plate. The main orientation of the HS-cell dendrites is horizontal. Lower row of panels: visual receptive fields averaged across results obtained from at least 5 different flies for HSN and HSE and 2 different flies for HSS. On average these cells prefer horizontal front-to-back motion but show a gradual change in their directional preferences reminiscent of translational optic flow. The distribution of sensitivity of the HS cells is correlated with the extent of their dendritic arborisation and thus reflects the retinotopic organisation of the visual system (redrawn from Krapp, 2000, Krapp unpublished results, and Hausen, 1993. Reconstructions of HS-cells courtesy of Klaus Hausen).

which reduces the number of sodium channels contributing to the spikes generated. The comparatively low input resistance causing the shallow resting potential shortens the cells' time constant and thus increases the bandwidth of VS- and HS-neurons (Haag and Borst, 1996). The resulting faster responses benefit the detection of rapid changes in attitude, but come at the cost of higher energy consumption (Laughlin, 2001). The fact that output LPTCs spend comparatively high amounts of energy to improve their coding efficiency reflects the vital role of these cells in flight stabilisation tasks which require high bandwidth and short response latencies.

The axon terminals of the VS- and HS-cells ramify in the ventrolateral protocerebrum of the ipsilateral half of the brain, where they connect to target neurons via mixed chemical-electrical synapses (Strausfeld, 1976; Strausfeld and Bassemir, 1983; Gauck *et al.*, 1997). Cells postsynaptic to the LPTCs are mostly descending neurons (Gronenberg and Strausfeld, 1990; Strausfeld and Gronenberg, 1990) projecting to various motor

neuropiles in the thoracic ganglia, as well as some motoneurons involved in gaze stabilisation (Gilbert *et al.*, 1995; Gronenberg *et al.*, 1995; Huston and Krapp, 2003). The area in which the LPTC terminals are located marks a multi-modal integration stage. It contains output arborisations of afferent fibres from other sensory systems (Strausfeld and Seyan, 1985), such as the ocelli (Section 3.4) and the antennae (Section 4.2), as well as from ascending neurons, which convey information from the halteres (Section 5.2).

The functional significance of HS- and VS-cells for visual stabilisation reflexes has been shown conclusively by a number of lesion experiments. In *Drosophila*, the neurogenetic mutant ombH31 produces flies that do not develop HS- and VS-cells (Heisenberg *et al.*, 1978). These mutants fail course and gaze stabilisation tasks (Blondeau and Heisenberg, 1982; Hengstenberg, 1995), but can still distinguish between object motion and background motion. This indicates that a separate neural pathway supporting goal-directed tasks such as chasing flights is preserved. Laser-ablation of HS and VS precursor cells in the larvae of *Calliphora* (Geiger and Nässel, 1981) and microsurgical lesions of the cells' axons in the adults (Hausen and Wehrhahn, 1983) lead to similar flight control deficiencies. Associated with their role in flight stabilisation, the number of VS-cells varies across flies in a fashion that broadly reflects the complexity of their flight patterns. Whereas *Calliphora* and *Musca* possess 10 and 8 VS-cells respectively, *Drosophila* have only 6 (Buschbeck and Strausfeld, 1997).

3.3.5 *HS- and VS-cells estimate optic flow parameters*

Originally, most LPTCs were distinguished on the basis of their predominant directional preferences for either horizontal or vertical motion. In the case of the HS- and VS-cells, the overall orientation of their main dendritic branches within the lobula plate also justified such basis distinction. Furthermore, retrieving the exact direction of local motion requires only a little additional computation if both the horizontal and vertical motion component at any location in the visual field is known. Krapp and Hengstenberg (1996) put forward an alternative idea that would considerably simplify the extraction of self-motion parameters from optic flow fields. To retrieve, for instance, the roll component of self-motion, the local motion preferences within the receptive field of a VS-cell should match the orientation of local velocity vectors in a roll-induced optic flow field. Such a matched filter for particular self-motion components would get around the problem that local motion information is insufficient to infer what self-motion had caused it (Fig. 2). This matched filter hypothesis requires the distribution of local motion preferences to change gradually in a position-dependent way altogether approximating the directional distribution of local velocity vectors within particular optic flow fields.

A detailed receptive field characterisation using a local motion stimulus procedure (Krapp and Hengstenberg, 1997) revealed that none of the LPTC receptive fields shows only horizontal or vertical motion preferences. Intracellular and extracellular recordings from many LPTCs indeed support the hypothesis that each individual interneuron is tuned to sense a specific self-motion component (Krapp and Hengstenberg, 1996; Krapp *et al*., 1998, 2001; review: Krapp, 2000). Not only does the distribution of local directional preferences match certain optic flow fields, but the local motion sensitivities within the receptive fields of some LPTCs seem to be optimised to distinguish between rotation-induced and translation-induced optic flow (Fig. 2). Modelling the optimal weighting of local motion measurements suggests that the decreased motion sensitivity in the ventral receptive field of VS-cells is an optimal strategy to produce a response that is largely independent of any superimposed translational flow (Franz and Krapp, 2000). This makes perfect sense for a matched filter indicating roll-rotation, since optic flow in the ventral visual field, where the distance to the visual structures is small, would be dominated by translation-induced flow distorting the roll-specific flow vectors. In the dorsal visual field, however, the distances to visual structures are far greater, resulting in smaller translation-induced optic flow components to interfere with the detection of roll. Conversely, LPTCs estimating translation components show higher motion sensitivities in the ventral visual field (Franz and Krapp, 2000). The known anisotropic distribution of motion sensitivities within LPTC receptive fields therefore suggests that the fly visual system has been selected to make intrinsic assumptions about the average distance distribution encountered in the environment. This is a powerful means of increasing the reliability with which specific self-motion parameters can be extracted from optic flow (Dahmen *et al*., 2001).

The receptive field organisation of the VS-cells suggests that each individual cell is matched to an optic flow field generated during a particular rotation around an axis roughly aligned with the horizontal plane (Krapp *et al*., 1998). A VS-cell, such as VS1, whose main vertical dendrite is located in the distal lobula plate, is perfectly well suited to indicate nose-up pitch (Fig. 5, left). The receptive field organisation of VS10, with its vertical dendrite arborising in the proximal lobula plate, is matched to an optic flow field generated during nose-down pitch in combination with a subtle roll component (Fig. 5, right). The other VS-cells analyse rotations around intermediate horizontal axes, with VS6 being tuned to pure roll-rotation (Fig. 5, middle). We discuss the mechanical significance of the specific axes to which the VS-cells are tuned in Section 7.2. The HSE-cell (Fig. 6, middle) has a binocular receptive field reminiscent of an optic flow field generated during a yaw rotation around the vertical body axis, while the HSN-cell (Fig. 6, left) is tuned to an intermediate axis between yaw and nose-down pitch (Krapp, 2000; Krapp *et al*., 2001). The HSS-cell does not receive input

from the contralateral eye, and is therefore monocular. Since this cell is highly sensitive to directional motion only in the ventral visual field, it has been suggested to be involved in sensing translational optic flow (Fig. 6, right). This interpretation is strongly supported by the HSS receptive field organisation, which is highly reminiscent of the velocity vector distribution in a flow field generated during forward translation with a small sideslip component.

The individual receptive field organisation of the HS- and VS-cells suggests that these neurons extract particular self-motion parameters. The specificity with which the cells sense rotational or translational parameters, however, also depends on the nature of any heterolateral connections. Most output LPTCs receive only weak contralateral input or none at all. Whenever contralateral input is provided via heterolateral LPTCs, the resulting receptive field properties become more specifically tuned to indicate rotations (Krapp *et al.*, 2001). Such heterolateral network interactions have been studied particularly well in HS-cells (for review, see Haag and Borst, 2002). The HSE- and HSN-cells, for instance, receive input from two heterolateral LPTCs, both of which mainly respond to horizontal back-to-front motion along the eye equator. During forward or nearly forward translation, this contralateral input is entirely inhibited and the graded depolarization of the HSE- and HSN-cell may also signal translational information. This possibility is supported by the monocular receptive field organisation of these cells, which is reminiscent of a translational optic flow field (Fig. 6, middle and left).

Recent studies indeed suggest a potential dual function of the HSE-cell (Kern *et al.*, 2005). Wide-field optic flow sequences reconstructed from self-motion parameters observed in semi-free flight (Schilstra and Van Hateren, 1999) and the activity difference of the left and right HSE-cells showed two peaks in a coherence analysis: one for sideslip-translation in the low dynamic range and another for rapid yaw rotations in a higher dynamic range (Kern *et al.*, 2005). While the coherence between HSE-cell activity and sideslip decreased with increased distance to the visual surroundings in the simulated stimulus sequences, the coherence with yaw rotations was distance-invariant (*loc. cit.*). The final distinction between rotation- and translation-induced HS-cell activity may involve a combination of specific signal decoding, information from other sensory modalities, and/or the use of efference copy.

Although the specificity of the VS-cells to horizontal rotations is very well supported by visual wide-field stimulation experiments (Karmeier *et al.*, 2005), they could – at least theoretically – also signal vertical translation (Karmeier *et al.*, 2006). However, as in the case of the HS-cells, all known binocular interactions mediated by identified heterolateral LPTCs are rotation-specific (Krapp *et al.*, 2001, Krapp *et al.*, unpublished). Information on lift-translation, therefore, could only be retrieved at the

processing stage, where the outputs of the VS-cells can be appropriately combined.

In the context of stabilisation reflexes, the rotational rather than translational degrees of freedom are the most important. Given that any rotation can be decomposed into its components around the three cardinal body axes (Figs. 1, 2A), the number of LPTCs dealing with rotations in *Calliphora* is far greater than is minimally required to determine the axis of rotation. Ten VS-cells and at least two HS-cells in each side of the brain seem to establish a highly redundant measuring system. A combined experimental and theoretical study suggests, however, that any arbitrary horizontal rotation can be detected considerably quicker and more reliably if the responses of all ten VS-cells are considered (Karmeier *et al.*, 2005). This holds true even if the intrinsic neuronal noise is correlated between the cells (Karmeier *et al.*, 2005) due to common local inputs and electrical coupling among neighbouring VS-cells (Haag and Borst, 2004; Farrow *et al.*, 2006).

3.3.6 *Adaptation and gain control in LPTCs*

A common problem in sensory processing that also concerns the visual system is dynamic range matching: the amplitude range of sensory stimuli may span several orders of magnitude, whereas the dynamic response range of any neuron is drastically limited. A simple solution, such as scaling the input range, would only work in an ideal noise-free system that codes information by means of analogue signals. Neural systems, however, are subject to intrinsic neural noise. Also, discretisation takes place at processing stages such as sensory transduction, synaptic transmission and signal propagation. Even for image processing in semiconductor circuits, dynamic range compression is a serious issue. How do biological systems, which operate under permanent energy constraints (Laughlin, 2001) and are built from proteins, fat, ions, and water, deal with this problem? The visual system, like most other senses, partly solves the problem by adapting its operating range in a way that emphasises changes in stimulus space. Adaptation reduces the responses to constant stimuli and maintains the sensitivity within those dynamic stimulus ranges where changes are most likely to occur. An example would be highpass filtering sensory signals to remove any DC component and to keep a high gain on signal changes. Such strategies have been demonstrated at several stages of the peripheral visual system in the context of light intensity and dynamic range adaptation (for reviews, see Laughlin and Hardie, 1978; Laughlin, 1989; Weckstrom *et al.*, 1991; Land, 1997).

Several mechanisms have been proposed to be involved in controlling the output range of the LPTCs. For instance, above a certain stimulus size, the local excitatory and inhibitory inputs are balanced in such a way that

the LPTC signal range is limited to a plateau value that depends on pattern velocity (Borst *et al.*, 1995). This dendritic gain control mechanism, which acts at the neuronal level, also explains the size- and velocity-dependent behavioural yaw-torque responses obtained in earlier studies on *Musca* (Reichardt *et al.*, 1983). Dendritic gain control has two functional consequences for the estimation of self-motion parameters in LPTCs: it prevents output saturation and renders the cells' responses independent of pattern size, while increasing their response to pattern velocity up to a certain range. Size-invariant responses of LPTCs are particularly important as the spatial distribution of visual contrasts may differ depending on the respective environment.

Prolonged motion in the preferred direction of the LPTCs drastically reduces the cells' responses to a subsequent test stimulus (e.g. Maddess and Laughlin, 1985; Harris *et al.*, 1999). Such adaptation phenomena are a common feature of directional motion pathways across phyla. This is reflected in the waterfall-effect: if we continue watching out of the window from a train that has just stopped in a station, we perceive motion in the opposite direction. The underlying neural mechanism is directionally selective, which means that only motion in the preferred direction of a cell processing optic flow elicits the waterfall-effect. Motion adaptation affects the velocity-dependent responses of LPTCs not only directly, but also through their contrast sensitivity. Harris *et al.* (2000) report two additional motion adaptation effects which reduce the contrast sensitivity in LPTCs in a non-directionally selective way. These contrast gain control mechanisms prevent the LPTC output from saturating and also keep all cells of the population in the same adaptational state, irrespective of their main preferred directions. The latter aspect is important for accurate self-motion estimation in cases where the outputs of two or more LPTCs are combined. Another recent study shows that the adaptational state at given locations on the LPTC dendrites affects the processing at neighbouring locations (Neri and Laughlin, 2005). This effect may overcome the problem that visual scenes sometimes consist of patchy contrast distributions, which could cause anisotropic adaptational states across the cell's dendritic input arborisation.

Only some of the physiological mechanisms underlying the spectrum of motion adaptation and gain control phenomena are so far understood. Nonetheless, they all potentially contribute to a robust estimation of self-motion parameters by the LPTCs. Within a certain range, adaptation mechanisms prevent output saturation and retain the cells' sensitivity to changes in stimulus velocity. However, it is obvious that this adaptation will make any absolute measure of the current self-motion parameters difficult to obtain, given that the EMD signals depend on several stimulus parameters and are only linear in the velocity domain over a limited dynamic range (for review, see Borst and Egelhaaf, 1993).

3.3.7 *What information do output LPTCs provide?*

All the evidence accumulated from behavioural, physiological, and modelling studies clearly suggest that output LPTCs, such as the HS- and VS-cells, are involved in processing optic flow induced by the insect's self-motion. They are vital in the control of stabilisation reflexes and, depending on how their outputs are combined, also provide information about translation-induced optic flow in the context of collision avoidance (Kern *et al.*, 2005; Lindemann *et al.*, 2005). HS- and VS-neurons connect either directly or indirectly, via descending neurons, to the various motor systems controlling locomotion and gaze. Loss of their function abolishes gaze stabilisation and wide-field optomotor responses (Hengstenberg, 1995; review: Hausen, 1993). But precisely what parameters related to stabilisation reflexes do HS- and VS-cells encode?

Ideally, the LPTC signal should be proportional to the angular velocity of a rotation around a specific axis. We have shown that the condition of directional specificity is met, because the tuning of VS-cells to wide-field rotation shows a robust maximum at an orientation that is readily predicted from the cells local receptive field properties (Karmeier *et al.*, 2003, 2005). Hence, the preferred rotation axes of the HS- and VS-cells set up a multi-dimensional non-orthogonal coordinate system of unit vectors, where each cell defines an individual dimension. Linear scaling of the individual coordinate with angular velocity is a problem, however, for two main reasons. Firstly, adaptation mechanisms such as dendritic gain control and contrast gain control, necessary to avoid output saturation, prevent the cells' signals from being linear in the velocity domain. Secondly, as mentioned earlier, the outputs of the EMDs depend on both angular velocity and the spatial frequency content of the pattern rather than on the pattern's angular velocity alone (for reviews, see Reichardt, 1987; Borst and Egelhaaf, 1993).

In conclusion, HS- and VS-cell signals indicate self-rotations around specific axes. Their response amplitude depends on the cells' adaptational state and may only be linearly related to angular velocity within a limited dynamic range. The major functional role of the HS- and VS-cells in the context of stabilisation reflexes is therefore seemingly to sense only differences or changes in image velocities rather than absolute image velocities (Maddess and Laughlin, 1985; Jian and Horridge, 1991). A second function of the LPTCs may be to set up a coordinate system that provides a common frame of reference for self-motion parameters obtained by visual and other sensory modalities. This coordinate system, if carried on to the next integration stage along the sensorimotor pathway, is likely to be designed according to the requirements of the various motor systems. For example, the contributions of the HS- and VS-cells may be combined with, or scaled by, self-motion parameter estimates obtained by the ocelli or

mechanosensors within this common frame of reference. Combining their input with that of other sensory systems could allow insects to encode angular velocity information, for instance, over an extended dynamic range. We now move to consider these other sensory systems.

3.4 OCELLI

3.4.1 *Significance of the ocelli*

Many flying insects employ a second visual system in flight control – the ocelli. It was noted long ago that there is a strong correlation between insects bearing wings and possessing 1–3 dorsal ocelli (Kalmus, 1945). Owing to the optical design, signal integration, and conductance properties of the ocellar afferent fibres, the system works faster than the compound eye and thus covers a higher dynamic range of light intensity changes. Goodman (1981) has provided a comprehensive review that compares ocellar structure and function among several insect species.

3.4.2 *Organisation of the ocellar pathways*

Although detailed differences have been found among species with regard to the position of the ocelli on the head, the optical properties of the lenses, and the neural equipment of the ocelli, it appears that the general anatomical organisation of the system is fairly conserved amongst flies, dragonflies, and locusts (for reviews, see Goodman, 1981; Mizunami, 1995). In this section, we introduce the neuroanatomy of the fly ocellar system, which has been described in some detail by Strausfeld (1976) and Nässel and Hagberg (1985). Attached to the retinae of the ocelli is a fused 1st order neuropile. From here, three different classes of interneurons project through the ocellar nerve to various areas in the brain and to the thoracic ganglia. The blowfly *Calliphora* employs 12 large interneurons, or L-neurons, which are particularly conspicuous because of their enormous axon diameter. The second class of interneuron comprises the 10 M-neurons with intermediate axon diameters, while the third class consists of a greater number of S-neurons having small axon diameters. L-neurons project to the posterior slope of the lateral protocerebrum – the same area where axons of the output LPTCs terminate (Section 3.3.2). M-neurons dispatch information to many parts of the nervous system, including the pro- and mesothoracic ganglia, the lateral protocerebrum, the lobula, and the ventral medulla. The latter projection is especially interesting, as columnar elements of the ventral medulla mediate information from the ventral visual field, where brightness levels are lower compared to those seen by the dorsally oriented ocelli. S-neurons

project to regions in the posterior slope also receiving input from antennal mechanosensory fibres (Nässel *et al.*, 1984) sensitive to airspeed (Section 4.2).

3.4.3 *Ocellar neurons spatially integrate changes in light intensity*

The single lenses of individual ocelli cast an underfocussed image on the retina that is unlikely to retain any detailed spatial information on the visual scene. This prevents the ocelli from contributing to the control of any behavioural task, which requires detailed positional information about light changes in the visual field. Although the species-specific optics of the ocellar lenses allow for a general estimate of the system's spatial resolution (e.g. Wilson, 1978b; for review, see Goodman, 1981), characterising the receptive fields of ocellar interneurons has further clarified its functional organisation. The huge diameter of the L-neuron axons – amongst the largest in insect nervous systems (Nässel and Hagberg, 1985; Simmons *et al.*, 1993) – has made these the main target of electrophysiological studies on ocellar interneurons (Simmons, 1999). This enormous axon diameter enables the L-neurons to propagate information at particularly high speed to the next processing stage.

L-neurons encode light level changes by means of graded membrane potential shifts, where increasing light intensity results in stronger hyperpolarisation (Orthoptera: Wilson, 1978b; Diptera: Simmons *et al.*, 1993). A common feature of L-neurons is the phasic-tonic nature of the neurons' light responses, which emphasises changes in light intensity (*loc. cit.*). In locusts, L-neurons possess extended receptive fields, which in the lateral ocelli integrate light from a visual angle of up to 140° (Wilson, 1978b). This massive spatial integration increases the light sensitivity of the L-neurons by an estimated factor of 5000 compared to the sensitivity of a single lamina neuron in the compound eye (*loc. cit.*). The receptive fields of dragonfly L-neurons are significantly smaller, which means that they retain at least some spatial information about where in the visual field light level changes occur (e.g. Berry *et al.*, 2006, see below). The spectral sensitivity of ocellar interneurons peaks in the UV range and has a variable second maximum around 500 nm (e.g. Wilson, 1978b; Mobbs *et al.*, 1981; van Kleef *et al.*, 2005). An intensity-dependent sensitivity shift from UV to the green range was suggested to facilitate the neurons efficiency to sense light level changes at different diurnal illumination conditions (Mobbs *et al.*, 1981). Taken together, these functional properties of the L-neurons suggest that the ocellar system is involved in mediating fast motor responses induced by sudden changes in light intensity. Indeed, stimulation of the ocelli requires considerably less time to elicit compensatory head movements than compound eye stimulation (Hengstenberg, 1993).

3.4.4 *What information do the ocelli provide?*

Although the ocelli were always seen as sense organs involved in flight and gaze control (e.g. Mittelstaedt, 1950) it was long unclear what parameters they would actually encode. Although present in many flying insects (Kalmus, 1945), ocellar systems turned out to be quite heterogeneous across species and the degree of their diversification seems to correlate with the manoeuvrability of the respective species. Early behavioural studies suggested that the locust ocellar system was involved in the control of flight speed (Bayramoglu-Ergene, 1964). This conclusion, however, may have been based on the observation of second-order effects resulting from interactions between compound eyes, mechanoreceptive systems, and the ocellar system, which were later shown to exist in dragonflies (Kondo, 1978). Other studies in flies and orthopterans strongly support the idea that the ocelli mainly serve as fast and ultra-sensitive horizon detectors, and the triangular orientation of the three ocelli present in these species in principle permits detection of horizon tilt about two axes. In all of the species investigated so far, the ocelli appear to contribute to the phasic dorsal-light response which compensates for imposed attitude changes by fast head and body movements (Orthoptera: Wilson, 1978a,b; Taylor, 1981a,b; Odonata: Stange and Howard, 1979; Stange, 1981; Diptera: e.g. Schuppe and Hengstenberg, 1993). The dynamic range of the phasic dorsal light response clearly exceeds, and thus complements, that of the compound eyes (review: Hengstenberg, 1991, 1993).

A comparison of dragonfly and locust ocellar systems reveals one interesting difference. Sophisticated fliers such as dragonflies have evolved a much more elaborate functional design than locusts which show less impressive manoeuvring flight performance. L-neurons in the locust ocellar system seem to measure attitude changes only around the roll- and pitch-axes (Wilson, 1978b). In dragonflies, however, lateral ocelli possess a considerably higher number of different L-neuron receptive fields analysing light intensity changes at several neighbouring locations along the external horizon (Berry *et al*., 2006, 2007a). Furthermore, optical and physiological adaptations in the dragonfly ocellar system still allow for a distinction between the dorsal and ventral halves of the visual field (Berry *et al*., 2007b). Accompanied by enhanced UV-green contrast (van Kleef *et al*., 2005) these features result in a remarkably sensitive, non-orthogonal detection mechanism of changes in attitude. Altogether, the functional organisation of the dragonfly ocellar system is reminiscent of the rather sophisticated fly vertical system sensing optic flow induced by rotations around horizontal axes (c.f. Section 3.3.5). Whether the fly ocellar system matches such complex organisation is currently unknown, but given its elaborate flight envelope one is tempted to expect that it does.

3.5 FUSION OF INPUTS FROM THE COMPOUND EYES AND OCELLI

Although our understanding of the functional organisation of the ocellar system is rather incomplete, the combination of ocellar input with sensory input from other modalities offers a perfect opportunity to study general principles of multi-sensory integration in the context of flight and gaze stabilisation. Recent electrophysiological studies in flies have shown that the spiking activity in the heterolateral LPTC V1, a postsynaptic target neuron of the VS-cells 1–4, is modulated by ocellar input (Parsons *et al*., 2006). This modulation is likely to be a consequence of both VS-cells and ocellar L-neurons connecting to the same descending neuron via mixed chemical and electrical synapses (Strausfeld, 1976). Ocellar inputs to the descending neuron may change, via the electrical synapses, the membrane potential in the VS-cells, which in turn modulate the activity in their postsynaptic target, the V1-cell (Parsons *et al*., 2006).

This unusual pathway establishes an early convergence of compound eye and ocellar signals at the level of the LPTCs. From a functional point of view, such early convergence makes perfect sense: recordings from neck motoneurons supplying the fly gaze stabilisation system suggest that LPTCs encode visual information in coordinates already adapted to the needs of the motor system (Huston and Krapp, 2003; Huston, 2005). Ocellar signals could thereby perform a scaling of LPTC activity based on independent information about one and the same rotation parameter – in the case of the V1-cell, a rotation about an axis intermediate between pitch and roll. This possibility is supported by recent studies showing that the ocellar-induced activity modulation follows a similar course to the preferred axis tuning of the V1-cell upon compound eye mediated wide-field rotation (Parsons, pers. comm.).

Behavioural experiments on the fly gaze stabilisation system conclusively show that compound eyes, ocelli, and halteres each contribute to compensatory head movements (for reviews, see Hengstenberg, 1991, 1993). Hengstenberg's studies suggest that the outputs of these sensory systems may be scaled and linearly combined to support gaze stabilisation (*loc. cit.*). As far as the ocellar input is concerned, conclusions were recently supported by electrophysiological studies on the integration properties of an individually identified descending neuron: simultaneous double recordings show that the descending neuron indeed combines ocellar and LPTC signals in a linear way (Haag *et al*., 2007). We will return to the question of multimodal sensory integration later, providing an explanation based on flight mechanics of why insects might want to combine input from different sensory modalities in a linear fashion (Section 7.3). In the meantime, we must move from the visual system to consider the various sensory modalities mediated by mechanoreceptors.

4 Airflow sensors

4.1 SIGNIFICANCE OF AIRFLOW SENSING

Airflow sensors play an especially important role in insect flight control. This is because the aerodynamic forces and moments that an insect produces depend upon its motion with respect to the surrounding air mass, which differs from its motion with respect to an inertial or visual frame of reference in the presence of a wind. The antennae are pre-eminent among the airflow sensors involved in insect flight control, and we shall focus most of our attention on them. In addition, insects are covered in numerous trichoid sensillae, at least some of which play a role as airflow sensors in flight. As will become apparent, the two systems complement each other – the antennae providing information on airspeed, and the trichoid sensilla providing information on flow direction.

4.2 ANTENNAE

4.2.1 *Role of the antennae*

All winged insects possess a single pair of antennae, which perform various roles in mechanoreception, chemoreception, hygroreception, and thermoreception (Schneider, 1964). Antennae have so far been implicated as mechanoceptors in the flight control of Diptera (Hollick, 1940), Hymenoptera (Heran, 1957), Orthoptera (Gewecke, 1971), Odonata (Gewecke *et al*., 1974), and Lepidoptera (Niehaus, 1981), in which they are thought to play an important role in the regulation of flight speed. Given this wide taxonomic distribution, it seems likely that the use of the antennae in flight control is primitive to all the living orders of Pterygota. Amputating the antennae of free-flying insects provides direct, but crude, evidence that they are involved in flight control. The speed of free-flying insects is usually found to decrease with antennal amputation (*Drosophila*: Campan, 1964; *Apis*: Neese, 1966; *Aglais*: Niehaus, 1981), but it is not clear whether this reflects a specific effect on the regulation of airspeed, or a general degradation of flight performance. Consistent with the latter interpretation, Lepidoptera do seem to lose flight stability following antennal amputation (*Aglais*: Niehaus, 1981; *Manduca*: Sane *et al*., 2007). Moreover, whereas free-flying *Aglais* fly slower after antennal amputation, the same insects actually fly faster when tethered to a flight mill on which stability is not an issue (Niehaus, 1981). Free-flight speed has been found to increase with antennal amputation in at least one species (*Aedes*: Bässler, 1958), and tethered *Locusta* have also been found to fly faster following antennal amputation if the airflow is regulated to balance the insect's thrust

and drag (Gewecke, 1971, 1975). However, while experiments in which speed is free to vary do clearly indicate that the antennae are involved in flight control, they cannot easily distinguish between the effects of peripheral feedback to the flight motor, and state feedback to the flight control system. For this reason, studies in which airspeed is set by the experimenter have proven more informative of antennal function.

The earliest experiments of this kind were by Hollick (1940), who showed that amputating the antennae of tethered Diptera (*Muscina* and *Musca*) altered the wingtip trajectory, whereas covering the antennae suppressed the wing beat altogether. These results are consistent with a role in providing peripheral feedback to the flight motor, but subsequent studies have demonstrated that the antennae also provide state feedback to the flight control system. Tethered insects typically decrease stroke amplitude in response to increases in the imposed airspeed. However, amputating both antennae makes stroke amplitude almost insensitive to airspeed in Hymenoptera (*Apis*: Heran, 1959), Diptera (*Aedes*: Bässler, 1958; *Calliphora*: Burkhardt and Gewecke, 1965; Gewecke, 1967b), Orthoptera (*Locusta*: Gewecke, 1970, 1972a), Odonata (*Orthetrum*: Gewecke *et al.*, 1974), and Lepidoptera (*Aglais*: Gewecke and Niehaus, 1981). Although stroke amplitude is only one of many kinematic parameters involved in flight control (Taylor, 2001), the consistency of this effect across orders is remarkable, and hints at a highly conserved function of the antennae in regulating airspeed. The results of unilateral antennal amputation differ among species: in *Locusta* this has no effect on the stroke amplitude of either wing (Gewecke, 1972a; Gewecke and Philippen, 1978), while in *Calliphora* only the stroke amplitude of the ipsilateral wing is affected (Burkhardt and Gewecke, 1965; Gewecke, 1967b). It is therefore possible that, in addition to regulating airspeed, the antennae might play some role in yaw control in *Calliphora* – though not apparently in *Locusta*.

4.2.2 *Antennal anatomy*

Antennae vary greatly in form across pterygotes, but the primitive form (shared with Thysanura) comprises two differentiated basal segments and a distal whip-like flagellum composed of many similarly shaped elements (Fig. 7B: Schneider, 1964). The proximal segment of the antenna is called the scape, and articulates with the head capsule under the actuation of two to five muscles originating on the tentorium: a skeletal structure formed by invaginations of the cephalic cuticle. Variation in the number of tentorio-scapal muscles reported from different insect orders seems to reflect as much on how authors classify functional sub-units of the same muscle, as on genuine anatomical differences. In general, however, the head–scape joint is hinge-like and actuated by fewer functional units in the more primitive orders such as Odonata

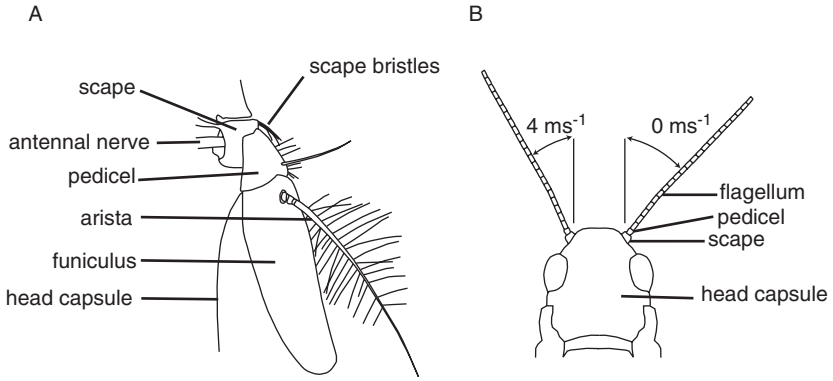

FIG. 7 Antennal anatomy of *Calliphora* (A) and *Schistocerca* (B). (A) The antenna of brachyceran Diptera is highly modified from the primitive flagellar form. The proximal segment, known as the scape, is rather rigidly attached to the head capsule. The second segment, called the pedicel, is free to rotate about a horizontal and a vertical axis. The first segment of the flagellum is enlarged to form a robust prolate structure called the funiculus, from which the remaining flagellar segments emerge laterally in a fine-feathered structure called the arista (redrawn after Gewecke, 1967b). (B) The antenna of a locust is typical of the primitive flagellar form, with the scape free to rotate about a hinge-like joint with the head capsule. The pedicel is free to rotate about another hinge-like joint, and articulates with the flagellum, which consists of many undifferentiated segments. In flight the antennae are rotated forward about the scape–pedicel joint in the so-called antennal positioning reaction (compare left antenna, shown as it would be positioned at $4\,ms^{-1}$ with right antenna, shown as it would be positioned at $0\,ms^{-1}$, redrawn after Gewecke and Heinzel, 1980).

(*Orthetrum*: Gewecke and Odendahl, 2004) and Orthoptera (*Locusta*: Gewecke, 1972b; Bauer and Gewecke, 1991; *Gryllus*: Honegger *et al.*, 1990), but socket-like and actuated by a greater number of functional units in the more derived orders such as Hymenoptera (*Apis*: Snodgrass, 1956) and Lepidoptera (*Aglais*: Niehaus and Gewecke, 1978; *Manduca*: Kloppenburg *et al.*, 1997). In brachyceran Diptera (Fig. 7A), the head–scape joint has become rather rigid – indeed, in *Calliphora* the tentorio-scapal muscles are actually reabsorbed after the imago's emergence from the pupa (Gewecke, 1967a). In most insects, the position of the head–scape joint may be monitored by sensory bristles on the scape. Internal mechanosensors associated with the tentorio-scapal muscles have almost certainly been underreported, but include a stretch-sensitive scolopalial organ known from Hymenoptera (*Apis*: Janet, 1911), and a stretch-sensitive strand receptor found in Orthoptera (*Schistocerca*: Braünig, 1985).

The second basal segment of the antenna is called the pedicel, and articulates with the scape under the actuation of two to four muscles originating within the scape (Snodgrass, 1956; Gewecke, 1967a, 1972b;

Niehaus and Gewecke, 1978; Kloppenburg *et al*., 1997; Gewecke and Odendahl, 2004). Variation in the number of scape muscles reported from different orders is likely to be incidental, because the scape–pedicel joint is always hinge-like, such that the muscles are constrained to act as two antagonistic units. The only exception reported so far is in the brachyceran Diptera, whose scape–pedicel joints have separate vertical and horizontal axes (*Calliphora*: Gewecke, 1967a; *Drosophila*: Göpfert and Robert, 2001b), which effectively replace the degrees of freedom that have been lost in the head–scape joint. Sensory bristles are ubiquitous on the pedicel, but vary greatly in number, distribution – and presumably importance – across orders. In Lepidoptera, their fields are especially well-defined, and are known as Böhm's bristles: in *Aglais*, the two dense pedicellar fields are located exactly above the insertion of the scape muscles, so are well-placed to sense pedicel movements (Niehaus and Gewecke, 1978). In *Calliphora*, it is likely that a loosely defined field of 8–13 bristles projecting from the dorsal surface of the scape sense pedicel elevation (Fig. 7A), but it is less clear how its angle about the vertical joint axis is sensed: possibly, an interlocking subset of the bristles on the scape and pedicel might together achieve this (Gewecke, 1967a). Once again, internal mechanosensors associated with the scape muscles have probably been underreported: those definitely known seem only to include a pair of stretch-sensitive scolopalial organs in *Locusta* (Gewecke, 1972b).

The remainder of the antenna is known as the flagellum (Fig. 7), and its segments may be variously modified to produce a variety of forms ranging from the long whip-like structures typical of crickets to the pectinate structures typical of many moths. The flagellum is especially highly modified in brachyceran Diptera, in which the first flagellar segment is enlarged to form a robust prolate structure called the funiculus, from which the remaining flagellar segments emerge laterally in a fine feathered structure called the arista (Fig. 7A). The articulation of the flagellum with the pedicel is always passive, and the flagellum itself also lacks its own muscles (Schneider, 1964). The rotational freedom and stiffness of the pedicel–flagellum joint are rather variable, but the same classes of mechanosensor are conserved across orders. Campaniform sensilla are usually present on the distal rim of the pedicel, although these can vary enormously in number and distribution, from the single large pedicellar campaniform sensillum of *Calliphora* (Gewecke, 1967a; Nässel *et al*., 1984; Gnatzy *et al*., 1987) and *Orthetrum* (Gewecke and Odendahl, 2004), to the field of seventy or so campaniform sensilla distributed evenly around the pedicel in *Locusta* (Gewecke, 1972b; Heinzel and Gewecke, 1979). Despite detailed anatomical study (Niehaus and Gewecke, 1978; Kloppenburg *et al*., 1997), campaniform sensilla have not been reported from the pedicel of *Manduca* or *Aglais*, but these may simply have been overlooked, as they are known from other Lepidoptera (*Bombyx mori*: Schneider and Kaißling, 1957).

A stretch-sensitive scolopalial receptor called the Johnston's organ inserts on the pedicel–flagellar joint in most insects. Its degree of development is also highly varied, with some 670 separate scolopidial units in *Manduca* (Vande Berg, 1971), as compared to the 12 or so in *Locusta* (Gewecke, 1972b). A separate stretch-sensitive scolopalial organ has also been found running centrally to the base of the flagellum in some species including *Bombyx* (Schneider and Kaißling, 1957) and *Locusta* (Gewecke, 1972b). The flagellum itself is also rich in sensory cells, but its own mechanosensors have not been implicated in flight control.

Two general points emerge from this comparative analysis of antennal anatomy. Firstly, whereas the head–scape joint is rather variable in terms of its freedom of movement and actuation, the scape–pedicel joint is always hinge-like and always actuated by a pair of functional units acting antagonistically. Secondly, whereas the mechanosensors of the head-scape and scape–pedicel joints do not appear to be especially refined, the mechanosensors of the pedicel–flagellum joint certainly are. This suggests that it will be necessary, though perhaps not sufficient, for any model of the antennal flight control system to include the scape muscles, the pedicellar campaniform sensilla and the Johnston's organ. Finally, it is worth cautioning that whereas locust antennae are representative of the primitive flagellar form, the antennae of *Calliphora* and other brachyceran Diptera are highly modified. Since the vast majority of existing physiological and behavioural studies have been conducted on one or other of these model animals, it is worth noting that the conclusions we draw for *Calliphora* will not necessarily extend to insects of other orders, or even to other dipteran sub-orders.

4.2.3 *The antennal positioning reaction*

In all of the species studied to date, the antennae are actively protracted in preparation for flight. This feedforward response is usually effected by the tentorio-scapal levator muscles, and almost certainly functions to expose the antennae to the oncoming flow. In Diptera, however, the scape muscles have assumed this function (Burkhardt and Gewecke, 1965). In most species, the angle of the protracted antennae is further adjusted during flight, in the so-called antennal positioning reaction. This feedback response is always effected by the scape muscles, and is normally interpreted as providing range adjustment for the pedicellar sensors (Burkhardt and Gewecke, 1965; Gewecke *et al.*, 1974). An antennal positioning reaction has so far been found in Hymenoptera (*Apis*: Heran, 1957, 1959; *Bombus*: Brandstätter, 1989), Diptera (*Calliphora*: Burkhardt and Gewecke, 1965; Gewecke, 1967b), and *Locusta* (Gewecke, 1972a; Gewecke and Heinzel, 1980; Saager and Gewecke, 1989). As airspeed is increased in tethered flight, the antenna rotates forward about the scape–pedicel joint (Fig. 7B), in

opposition to the rearward deflection about the pedicel–flagellum joint caused by drag on the flagellum (Burkhardt and Gewecke, 1965; Gewecke, 1967b, 1972a; Gewecke and Heinzel, 1980). This clearly demonstrates that antennal angle is under active adjustment in these species, although no relationship has been found between the angle of the scape–pedicel joint and airspeed in some Hymenoptera (*Paravespula*: Brandstätter, 1990) and Lepidoptera (*Aglais*: Gewecke and Niehaus, 1981), so the reaction may not be universal. The effect of the antennal positioning reaction is always to reduce the drag on the flagellum, because rotating the antennae forward reduces the projected area of the flagellum with respect to the oncoming flow. This presumably allows the mechanosensors of the pedicel–flagellum joint to operate over a wider range of airspeeds than would otherwise be possible without stiffening the joint. Furthermore, in *Calliphora* and *Locusta*, the antennal positioning reaction not only reduces the range of passive flagellar deflection, but also renders its relationship with airspeed approximately linear (Gewecke, 1967b; Gewecke and Heinzel, 1980).

Behavioural studies have provided insight into the physiology of the antennal positioning reaction. Amputating the appendages of the pterothorax, painting over the compound eyes and head capsule, and varying translational optic flow, have no effect upon the antennal positioning reaction in *Apis*, indicating that the reaction is self-contained with respect to the antennae (Heran, 1959). Immobilising the pedicel–flagellum joint is, however, sufficient to block the reaction, indicating that feedback from the mechanosensors of the pedicel–flagellum joint is essential (*Apis*: Heran, 1957, 1959; *Calliphora*: Burkhardt and Gewecke, 1965; Gewecke, 1967b). This feedback must be unilateral, since destroying one antenna does not affect the positioning reaction of the other (*Apis*: Heran, 1959; *Calliphora*: Burkhardt and Gewecke, 1965; Gewecke, 1967b; *Locusta*: Gewecke, 1972a). This unilaterality is reflected in the neuroanatomy of the antennae. The dendritic fields of the scape muscle motoneurons fall only within the ipsilateral part of the posterior deutocerebrum (*Locusta*: Bauer and Gewecke, 1991; *Gryllus*: Honegger *et al*., 1990; *Apis*: Kloppenburg, 1995; *Manduca*: Kloppenburg *et al*., 1997). There they overlap with ipsilateral projections of the antennal mechanosensors, including the scape bristles, pedicellar campaniform sensilla, Johnston's organ, and strand receptor (*Locusta*: Gewecke, 1979; Braünig *et al*., 1983; Braünig, 1985; *Gryllus*: Honegger *et al*., 1990; *Manduca*: Sane *et al*., 2007). This region of overlap is known as the antennal mechanosensory and motor centre, or AMMC (Homberg *et al*., 1989), and is presumably where the ipsilateral feedback involved in the antennal positioning reaction occurs. Contralateral projections of the pedicellar campaniform sensilla have been reported in *Calliphora* (Nässel *et al*., 1984), but it is not yet clear what function these might serve.

Although all of the main antennal mechanosensors have central projections in the AMMC, there is good evidence to suggest that only the pedicellar campaniform sensilla are essential to the antennal positioning reaction. The most direct evidence comes from *Calliphora*, in which the reaction persists even after the scape bristles and large parts of the Johnston's organ are obliterated, but disappears if the single campaniform sensillum is destroyed (Burkhardt and Gewecke, 1965; Gewecke, 1967b). Interestingly, the same manipulation does not block the stroke amplitude response, suggesting that the campaniform sensillum is not essential to that reaction (Burkhardt and Gewecke, 1965; Gewecke, 1967b). Behavioural experiments with *Calliphora* also show that while immobilising the pedicel–flagellum joint blocks the normal antennal positioning reaction, the angle at which the pedicel–flagellum joint is fixed controls the degree to which the antennae are brought forward at the onset of flight (Burkhardt and Gewecke, 1965; Gewecke, 1967b). This implies the involvement of a pedicellar receptor with directional, tonic response properties. Extracellular recordings from the pedicellar campaniform sensilla confirm that they have a phasic-tonic response (*Calliphora*: Schlegel, 1967, 1968, 1970; *Locusta*: Heinzel and Gewecke, 1979), in contrast to the strictly phasic response usually ascribed to Johnston's organ (*Apis*: Heran, 1959; *Calliphora*: Burkhardt and Schneider, 1957; Burkhardt, 1960; Burkhardt and Gewecke, 1965; Gewecke and Schlegel, 1970; *Locusta*: Uchiyama and Katsuki, 1956; *Manduca*: Sane *et al*., 2007). The specific response properties of the campaniform sensilla make them especially well suited to provide feedback to a static positioning reaction, as their tonic discharge frequency is approximately linear in the static deflection of the antenna (*Calliphora*: Schlegel, 1970; *Locusta*: Gewecke, 1979), while their phasic discharge frequency increases exponentially with the speed of deflection (*Calliphora*: Schlegel, 1970). Hence, it appears that feedback on the position of the pedicel–flagellum joint from the pedicellar campaniform sensilla is used to control the position of the scape–pedicel joint, presumably to keep the pedicel–flagellum joint within the preferred operating range of the Johnston's organ.

4.2.4 *Antennal oscillations*

Superimposed upon the steady passive deflections of the pedicel–flagellum joint are small forced oscillations ($\varphi 1^\circ$ amplitude) which occur at wing beat frequency. Antennal oscillations have so far been confirmed to occur during flight in Diptera (*Calliphora*: Gewecke and Schlegel, 1970), Orthoptera (*Locusta*: Heinzel and Gewecke, 1987), and Lepidoptera (*Manduca*: Sane *et al*., 2007), but they are likely to be universal given the cantilevered structure of the antennae. Antennal oscillations may be driven mechanically by transmission of thoracic vibrations, aerodynamically by periodic

induced flow, or acoustically by the flight tone. In most cases, the natural frequency of the flagellum has been shown to be somewhat higher than the wing beat frequency (Gewecke and Schlegel, 1968; Heinzel and Gewecke, 1987), which should allow its oscillations to track the wing beat faithfully without exciting resonance. In principle, antennal oscillations might also be excited by the periodic shedding of von Kármán vortices which occurs naturally behind cylinders and other bluff bodies at a frequency governed by the size of the body and the speed of the flow. However, vortex shedding occurs at frequencies on the order of 10^3 Hz for the scales associated with insect antennae, which is too high to excite mechanical resonance. Contrary to earlier suggestions (Heran, 1957, 1959), the frequency of von Kármán shedding cannot therefore be used by the antennae to measure airspeed (Heinzel and Gewecke, 1987).

Antennal oscillations appear to be below threshold for the pedicellar campaniform sensilla in *Calliphora* (Schlegel, 1967, 1968, 1970), but may be above threshold in *Locusta* (Heinzel and Gewecke, 1987). In any case, it seems likely that they form a sufficient stimulus for the phasic response of the Johnston's organ, as can be shown by electrophysiological experiments in which the flagellum is oscillated artificially. The most direct demonstration that antennal oscillations form a sufficient stimulus for the Johnston's organ is provided by a recent study in which intracellular recordings were made from its individual scolopidia, while oscillating the flagellum using constant-amplitude frequency sweeps (*Manduca*: Sane *et al.*, 2007). Less direct evidence is provided by a series of older studies which made extracellular recordings of the afferent discharge in the antennal nerve while oscillating the flagellum at approximately the wing beat frequency (*Calliphora*: Burkhardt and Schneider, 1957; Burkhardt, 1960; Burkhardt and Gewecke, 1965; Gewecke and Schlegel, 1970; *Apis*: Heran, 1959). This afferent discharge is generally assumed to represent the compound activity of the scolopidia of the Johnston's organ (Schneider, 1964; Burkhardt and Gewecke, 1965), although the occasional tonic responses recorded from the antennal nerve (Burkhardt, 1960) seem most likely to represent activity of the pedicellar campaniform sensillum. In *Calliphora*, this compound discharge is tightly phase-locked to stimuli at wing beat frequency, and is sensitive to oscillatory stimuli with amplitudes as low as 0.1°. Its response is typically biphasic, which is probably because the individual scolopidia are directionally sensitive (Burkhardt, 1960) and therefore fire either exactly in-phase or 180° out-of-phase during sinusoidal oscillation (Gewecke *et al.*, 1974). This interpretation is consistent with the results of intracellular recordings from *Manduca*, which show that individually the scolopidia have a monophasic response (Sane *et al.*, 2007).

The phasic response of Johnston's organ makes it especially sensitive to changes in airspeed (Gewecke *et al.*, 1974). For example, ramping up the airflow applied in electrophysiological experiments on *Calliphora* maximally

stimulates one phase of the biphasic compound response, while transiently suppressing the other; ramping down the airspeed stimulates both phases similarly (Gewecke and Schlegel, 1970). Perhaps less expectedly, the phasic response of the Johnston's organ is also affected by static airspeed in *Calliphora* (Gewecke and Schlegel, 1970). This appears to be the result of two separate mechanisms. Firstly, the amplitude of antennal oscillation is a decreasing function of mean flagellar deflection – probably as a result of the mechanical properties of the pedicel–flagellum joint. Hence, the peak amplitude of the compound discharge is a decreasing function of static airspeed (Gewecke and Schlegel, 1970). Secondly, because the individual scolopidia are directionally sensitive, the relative amplitude of the two phases of the compound discharge depends on the mean flagellar deflection, and is also a function of airspeed (Gewecke and Schlegel, 1970). Somewhat counterintuitively, the phasic response of the Johnston's organ may therefore be able to provide feedback in respect of the mean deflection of the flagellum. It is important to note, however, that the antennal positioning reaction does not normally operate in electrophysiological experiments because of the manner in which the insect is constrained. Hence, for reasons that will become clear later, the physiological potential of the Johnston's organ to sense mean antennal deflection need not necessarily imply a functional ability to sense static airspeed in flight.

The sensitivity of the Johnston's organ to minute vibrations is extraordinary, and is most highly developed in those insects in which it plays an auditory role. This is true especially of the smaller Diptera, in which the neuronal transduction machinery of the Johnston's organ has recently been shown to be capable of generating vibrations autonomously (*Toxorhynchites brevipalpis*: Göpfert and Robert, 2001a; *Drosophila*: Göpfert and Robert, 2001b, 2003). Although the amplitude of spontaneously produced oscillations is tiny, this ability of the Johnston's organ to produce – as well as to sense – motion, appears to enhance its response to external vibration. This is achieved by a positive feedback mechanism, in which the motility of the sense cells amplifies the external vibrations that they transduce (Göpfert and Robert, 2001a,b, 2003). Since the wing beat frequency falls within the bandwidth of active amplification by the Johnston's organ in both species, it is reasonable to suppose that active amplification of antennal oscillations by the mechanosensors may have consequences for flight control. This is an important area for future study, not least because it is possible that active amplification of antennal oscillations now used for hearing may have originated in respect of flight control.

4.2.5 *A hypothesis of antennal function*

Although aspects of the antennal system have been studied in several species, only in *Calliphora* have all of its key components been elucidated.

The model of the antennal flight control system that we present in this section is therefore formulated around the results we have described from *Calliphora*. However, as the model is consistent in most respects with the results from other species reviewed above, it may also serve as a more general hypothesis of antennal function. The model is structured as a pair of control loops: an inner one controlling the antennal positioning reaction, and an outer one controlling the kinematic response of the wings (Fig. 8). Since the left and right antennae are physiologically separate, the ipsilateral pair of control loops shown in the figure is doubled-up contralaterally in the real physiological system. We follow Burkhardt and

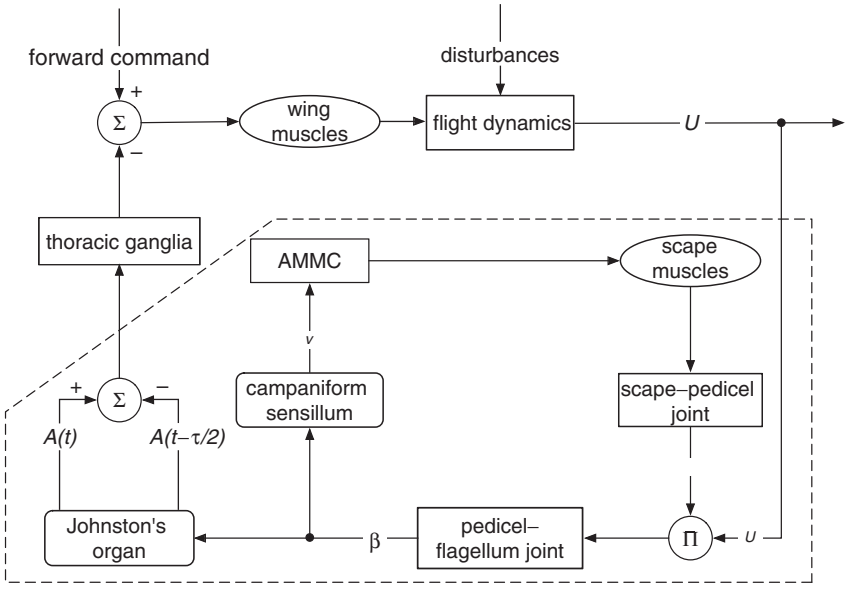

FIG. 8 Proposed model of the antennal flight control system in *Calliphora*. The inner loop is regulated by the antennal mechanosensory and motor centre (AMMC). The AMMC uses the average firing rate of the pedicellar campaniform sensillum (v) as its feedback signal, and slowly attempts to drive this receptor below threshold by adjusting the angle of scape–pedicel joint (α) so as to minimise the passive flagellar deflection (β). This re-centres the pedicel–flagellum joint so as to keep the faster and more sensitive Johnston's organ within its operating range. The outer loop uses the relative population activity of the two phases of the Johnston's organ ($A(t)$ and $A(t-\tau/2)$, where τ is the wingbeat period) as its feedback signal, and sums the resulting actuating signal with the forward command to the wing muscles so as to adjust airspeed (U). This corrects for external disturbances to the airspeed specified by the forward command. Overall, the system is therefore hypothesised to function as an airspeed regulator with adaptive sensing. The dashed line delimits the adaptive sensory system. Ovals designate actuators; rounded rectangles designate sensors; rectangles designate other dynamical systems; summation ($\sum$) and product ($\prod$) signs indicate whether quantities combine additively or multiplicatively.

Gewecke (1965) in assuming that the pedicellar campaniform sensilla provide slow feedback to the antennal positioning reaction and that the Johnston's organ provides fast feedback to the wing kinematic response: on this view, feedback from the slower and less-sensitive pedicellar campaniform sensilla is used to adapt the mechanical properties of the antennae so as to keep the faster and more-sensitive Johnston's organ within working range. We emphasise that this has the status of a hypothesis of function, although it is consistent with what is known of the sensory physiology of the pedicellar campaniform sensilla and the Johnston's organ as outlined in the previous sections. Overall, we propose that the system functions as an airspeed regulator using adaptive sensing to optimise the bandwidth of its sensor system.

Although they are assumed to use different receptors, both the antennal positioning reaction and wing kinematic response use the angle of the pedicel–flagellum joint (β) in feedback. However, whereas the antennal positioning reaction operates on β by adjusting the angle of the scape–pedicel joint (α), the wing kinematic response operates on β by adjusting airspeed (U). Hence, since β is a function of both U and α, it follows that the two reactions will be in competition unless they operate on distinct timescales. Given that U is the variable ultimately controlled by the antennal system, it follows that adjustments to α will have to be made more slowly than adjustments to U in order to prevent α from adapting to unintended changes in U before they can be corrected. This is consistent with what we know of the response properties of the receptors. Whereas each pedicellar campaniform sensillum signals β by its firing rate, the Johnston's organ signals β by the relative activity of the two populations of neurons contributing to its biphasic response. The former can only be measured accurately by averaging over some reasonable time interval, and probably many wing beats, while the latter can be measured accurately within a single wing beat. Hence, if the general structure of the model is correct, then competition between the two feedback loops might be avoided by having the inner loop operate more slowly than the outer one.

Since the antennal positioning reaction is used to re-centre the pedicel–flagellum joint and its sensors, it is reasonable to suppose that the reaction would attempt to drive the response of the pedicellar campaniform sensillum below threshold. This would make sense energetically, because the tonic response properties of the pedicellar campaniform sensilla would make them costly if they fired continuously in flight. It would also make sense functionally, because driving the pedicellar campaniform sensilla below threshold would help prevent adaptation of their tonic response. The inner loop could consequently be extremely simple because the feedback signal from the pedicellar campaniform sensillum could already form the actuating signal to the scape muscles, without needing first to be compared with a reference input. Assuming that the antennal positioning

reaction simply attempts to drive the pedicellar campaniform sensillum below threshold avoids the need to postulate any explicit reference signal with which the output of the pedicellar campaniform sensilla is compared. This is consistent with the apparently monosynaptic nature of the connections between the sensory neurons and motoneurons in the AMMC (Burkhardt and Gewecke, 1965). The main problem raised by this scheme is that the scape muscles need to be continuously activated in order to centre the pedicel–flagellum joint in flight. This implies either that the AMMC must have memory, such that the motoneurons continue to spike appropriately even after the pedicellar campaniform sensillum is driven below threshold, or that a forward command must be sent directly to the scape muscles to set them at a speed appropriate to the intended speed of flight. This forward pathway is not shown in Fig. 8 because there is no physiological evidence for it, but hypothetically, a forward command sent to the scape muscles might be used to up-regulate or down-regulate the flight motor via the resulting feedback to the outer loop. This would be instead of the forward command shown as being sent directly to the flight muscles in Fig. 8.

The occurrence of antennal oscillations at an amplitude above the threshold of the Johnston's organ ensures that it will always be active in flight. Since it is the relative, rather than combined, activity of its two neuronal populations that appears to form the feedback signal (Gewecke and Schlegel, 1970), it is reasonable to assume that the system compares the population activity of the two phases and then sums the resulting actuating signal with the forward command to the flight motor. The problem that this poses is the usual one faced by closed-loop control systems: that is, to ensure that the system tracks, rather than opposes, forward commands. This might be avoided by using an efferent copy of the forward command to cancel the feedback signal from the Johnston's organ during voluntary changes in airspeed. Alternatively, efferent copy might be used to modify the actuating signal sent to the scape muscles so as to re-centre the Johnston's organ during voluntary changes in airspeed. A third possibility is that the dynamics of the antennal positioning reaction allow the inner loop to re-centre the Johnston's organ in response to sustained changes in airspeed induced voluntarily, but not in response to transient changes in airspeed caused by external disturbances. Yet another possibility is the scheme mentioned above, in which a forward command is sent to the scape muscles, which consequentially causes an actuating signal to be sent to the flight motor via the feedback of the outer loop. Although we find this fourth possibility attractive, the third possibility is the most parsimonious, because it avoids the need to invoke unproven efferent copy or an unproven forward command to the scape muscles. The hypothetical model structure proposed in Fig. 8 invokes no physiological pathways that have not already been proven, and while the detailed structure of the real physiological system is

likely to be more complex, we are reasonably confident that the general structure of the model is correct for *Calliphora*. It remains to be seen whether the same model will hold for other insects as a more general hypothesis of antennal function.

4.2.6 *What do the antennae measure?*

A corollary of the model we have proposed for *Calliphora* is that although the antennae are used to regulate airspeed, they do not measure airspeed *per se*. Instead, because the antennal positioning reaction acts like a high-pass filter, the Johnston's organ senses changes in airspeed. This conclusion circumvents a problem that has not been properly addressed since it was first noted by Heran (1959) – namely, that any absolute measurement of airspeed by the sensors of the pedicel–flagellum joint can only ever be as good as the estimate of the angle of the scape–pedicel joint by its sensors. The fact that the bristles of the scape–pedicel joint seem so poorly adapted to measure position when compared to the mechanoreceptors of the pedicel–flagellum joint therefore argues strongly against the existence of an absolute sense of airspeed in insects in general. Based on the model we have proposed for *Calliphora*, however, it appears that they may be able to regulate their airspeed perfectly well without – simply by measuring changes in airspeed in a more or less linear manner. This same conclusion would apply to any insect with an antennal positioning reaction, the occurrence of which would always tend to make sensing absolute airspeed harder, but which would always enhance the sensing of changes in airspeed.

4.3 WIND-SENSITIVE HAIRS

4.3.1 *Role of wind-sensitive hairs*

In addition to the sophisticated adaptive wind-sensing system of the antennae, insects are richly covered in trichoid sensilla – at least some of which are sensitive to wind stimuli. Some of the most sensitive hairs are found on the anal cerci (Haskell, 1960; Shimozawa *et al*., 2003), but these have not been implicated in flight control. In fact, the only wind-sensitive hairs that have so far been proven to play a clear role in flight control are located on the head capsule. Those which have been the subject of almost all the relevant study to date are the 430 or so trichoid sensilla located in 5 indistinctly defined fields on each side of the frons and vertex in locusts (Weis-Fogh, 1949, 1956; Smola, 1970b). Weis-Fogh (1949) first demonstrated their involvement in the stimulation, maintenance, and control of flight by directing an airflow at the head of tethered *Schistocerca*, and observing their behavioural responses as the jet of air was rotated and as

fields of hairs were selectively covered. There is also limited behavioural evidence to suggest that trichoid sensilla on the compound eyes may play a role in correcting for wind drift in Hymenoptera. Honeybees (*Apis*: Neese, 1965) take less direct routes back to the hive from foraging sites if their interommatidial bristles are removed – especially when flying over water, which provides little optic flow as an alternative to aerodynamic cues. Interommatidial bristles are present in many other insects (Neese, 1965), including locusts (Bacon and Tyrer, 1979), and clearly warrant further investigation from the perspective of flight control. Certainly, the involvement of hairs on the head makes functional sense because the aerodynamic signal to noise ratio should be highest there, ahead of the wake, and it is likely that such hairs will prove important in the flight control of other orders of insect beyond the two already studied.

Other trichoid sensilla elsewhere on the body might also play a role in flight control, although there is no direct evidence for their involvement. A field of hairs on the prosternum of locusts has been shown to respond very sensitively to wind stimuli and might be involved in flight control (Pflüger and Tautz, 1982; Burrows and Pflüger, 1992). In addition, the pronotum, mesonotum, and metanotum of locusts are covered in strikingly long trichoid sensilla, which seem to be in an appropriate location to provide peripheral feedback to the flight motor (Knyazeva, 1970). The numerous innervated hairs on the wings of insects have also been widely assumed to play some role in flight control (Burrows, 1996), but while there are good theoretical reasons why insects might have evolved to sense airflow over the wings – specifically because it would circumvent some of the complexities associated with controlling unsteady aerodynamics (Taylor, 2007) – there is as yet no direct evidence that they do so (Page and Matheson, 2004). Altman *et al.* (1978) assumed that the 85 largest ($>1\,\mu m$) sensory afferents in the hind wing nerve of *Locusta* innervated the hind wing's 70 or so campaniform sensilla rather than its trichoid sensilla, but this would still leave a further 15 afferents of comparable diameter to those which innervate the cephalic trichoid sensilla (Bacon and Tyrer, 1979) to innervate some of the longer trichoid sensilla on the hind wings. Hence, Pringle's (1957) oft-repeated assertion that the axon and cell body size of the receptor cells of the wing hairs is too small for them to play a phasic role in flight control does not seem to have been backed up by any hard physiological data. In any case, the longer trichoid sensilla on the wings of insects certainly warrant study, even if only to settle the question of whether or not they are involved in flight control.

4.3.2 *Anatomy and physiology of the cephalic wind-sensitive hairs*

The cephalic trichoid sensilla of locusts have curved shafts ranging from 30 to 350 μm in length, some 25% of which are longer than 150 μm and hence

especially sensitive to wind stimuli (Smola, 1970b). The angular deflection of the hairs is a function of their length, wind speed and wind direction (Smola, 1970b), and is greatest when the air current is directed opposite to the shaft's curvature. Experiments isolating different components of the system show that this directional response is structured by the mechanical properties of the socket and the aerodynamic properties of the shaft (Camhi, 1969a). For a given angular deflection, extracellular recordings from individual sensilla show that their firing rate is also maximal in response to deflections against the shaft's curvature (Camhi, 1969a; Smola, 1970a). This directional physiological response appears to be due to the eccentric attachment of the dendrite (Guthrie, 1964, 1966; Camhi, 1969a). Thus, the physical and physiological tuning of each sensillum combines to give it a sharply directional response to wind stimuli. Since this response is maximal in the direction opposite to the shaft's curvature, the local directional properties of the hair fields can be easily mapped (Camhi, 1969a; Smola, 1970b), and while the precise number and location of the trichoid sensilla varies, the directional properties of each field are consistent across individuals Fig. 9.

Although the firing rate of a given trichoid sensillum is a function of wind direction, it is also a function of air speed (Camhi, 1969a) and temperature (Smola, 1970a). The individual response of a trichoid sensillum is therefore ambiguous in respect of wind direction, so it would make little sense for individual sensory cells to connect directly to the motoneurons. It is therefore unsurprising that the central projections of the trichoid sensilla mostly terminate in the suboesophageal ganglia, with only some 20% continuing on to the thoracic ganglia (Guthrie, 1964; Bacon and Tyrer, 1979): none appear to project to regions of the dorsal neuropile occupied by motoneurons (Tyrer *et al.*, 1979). Hence, it is the combined population response of the sensilla within the hair fields and not their individual response which matters (Bacon and Tyrer, 1979). Given appropriate signal processing by the descending interneurons (DNs), the fields of wind-sensitive hairs could therefore be used to indicate both the strength and direction of the airflow over the head. As we now discuss, this is used to provide non-directional peripheral feedback to the flight motor and directional state feedback to the flight control system.

4.3.3 *Function of the cephalic hairs*

By directing a jet of air onto the head capsule of tethered *Schistocerca*, Weis-Fogh (1949) was first able to show that an airflow over the cephalic hairs was sufficient to stimulate and maintain flight in locusts. Similar observations have been made in various other Acrididae (Boyd and Ewer, 1949). Covering the hair fields suppressed this reaction in *Schistocerca*, although the insects would still fly when thrown into the air, indicating that

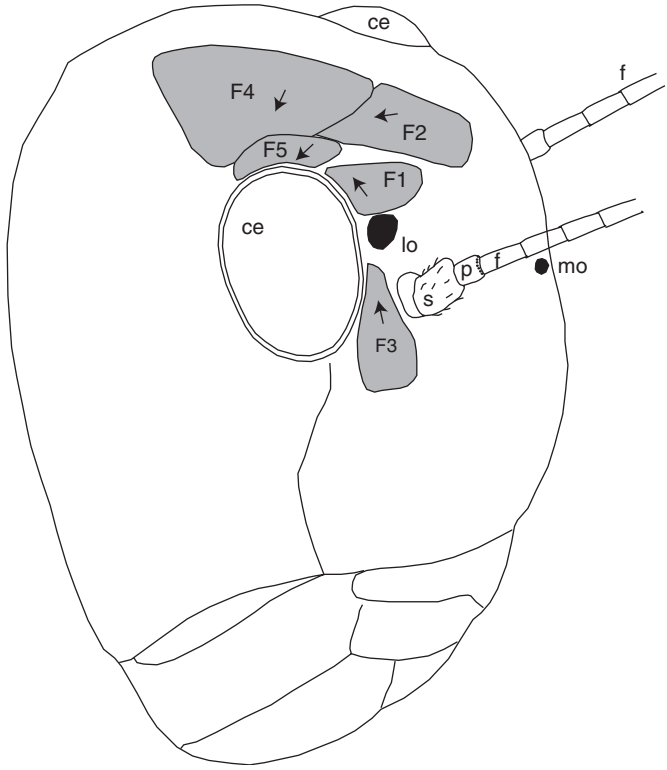

FIG. 9 Sensory apparatus of a locust's head. ce: compound eye; mo: median ocellus; lo: lateral ocellus; s: scape; p: pedicel; f: flagellum; F1–F5 fields of wind-sensitive hairs (numbering after Weis-Fogh, 1956). Arrows denote approximate directional sensitivity of hair fields after Camhi (1969a) and Smola (1970b), but are intended to be indicative only of average sensitivity since the directional sensitivity of the individual hairs varies somewhat across a field.

airflow over the cephalic hairs was not a necessary trigger for flight (Weis-Fogh, 1956). Importantly, static mechanical deflection of the hairs, as opposed to dynamic deflection due to a turbulent airflow, was insufficient to trigger flight (Boyd and Ewer, 1949; Weis-Fogh, 1956). This is because the hairs provide phasic rather than tonic input, as evidenced by muscle recordings from *Locusta* showing that the flight muscles become phase-locked to sinusoidal wind stimuli of a similar frequency to the wing beat (Horsmann *et al.*, 1983). This peripheral feedback seems to influence most strongly the firing of the wing elevator muscles, as waxing over the cephalic hairs increases the latency between firing of the depressors and elevators, but has little effect on elevator to depressor latency (Bacon and Möhl, 1983). Hence, when the cephalic hairs are waxed over, the consequent delay in the firing of the wing elevators leads to a reduction in wing beat

frequency (Gewecke, 1975; Bacon and Möhl, 1983). A possibly incidental consequence of this peripheral feedback mechanism is that a tethered locust will phase-lock its wing beat to that of another locust flying a short distance ahead in a wind tunnel, provided the cephalic hair fields are intact (Kutsch *et al*., 1994). While this might confer some energetic benefit to the tailing insect (Camhi *et al*., 1995), it seems more likely that this coupling behaviour is simply an epiphenomenon of the way in which the flight motor pattern is produced.

In addition to providing peripheral feedback to the flight motor, the cephalic wind-sensitive hairs also provide state feedback to the flight control system. Several studies have attempted to assign specific functions to the individual hair fields, so it is important to note that there has been some confusion in their naming. This arises from the contradictory terminology of the original papers by Weis-Fogh (1949, 1956) and as other authors except Camhi (1970b) have followed the later terminology of Weis-Fogh (1956), this is the convention we follow here, numbering the fields F1–F5 as shown in Fig. 9. Weis-Fogh (1949) found that an asymmetric airflow on the head caused tethered *Schistocerca* to turn into the airflow when mounted in an apparatus permitting rotation about the yaw axis: covering the F3 fields eliminated this yaw-stabilising reaction. Gewecke and Philippen (1978) measured the yaw torque involved in this reaction in *Locusta* and found that while covering any of the hair fields reduced the magnitude of the response, some response remained provided the F1 field was left intact; covering the F1 field alone suppressed the reaction as strongly as covering all five fields. This need not, however, contradict Weis-Fogh (1949)'s finding that covering the F3 field eliminated the yaw-stabilising reaction, as it is likely that his apparatus was less sensitive than that of Gewecke and Philippen (1978). Camhi (1970b) considered a further aspect of the flight-stabilising reactions of *Schistocerca* by observing movements of the abdomen, and found that while covering the F1 and F3 fields reduced abdominal ruddering, it did so to a much lesser degree than covering the F2 fields. In a companion study, Camhi (1970a) also found that symmetric movements of the abdomen could be induced by changes in airspeed, but only if the F2 field was left uncovered. Again, these results need not conflict with those already discussed, because in the absence of any airflow over the abdomen, the yaw torques registered by Weis-Fogh (1949) and Gewecke and Philippen (1978) must have been due to asymmetric wing kinematics, so that they would have been measuring a different reaction.

With hindsight, it is probably naive to attempt to assign a specific reaction to any one field – not least because at least one of the wind-sensitive interneurons known to be involved in flight control (the TCG: see Section 4.3.4 below) receives input from all five hair fields (Bacon and Tyrer, 1978; Bacon and Möhl, 1983; Möhl and Bacon, 1983). Moreover, the five spatially distinct fields distinguished by Weis-Fogh (1956) form only

three physiologically distinct groups (F3, F1 + F2, and F4 + F5) when classified according to their central neuronal projections (Tyrer *et al.*, 1979), rendering much of the past controversy moot. Nevertheless, the directional tuning of the hairs is relatively consistent within a field, but varies markedly between fields. This almost certainly reflects the directions in which air flows naturally over the different parts of the head capsule, but it is also likely that the placement of the fields reflects the quantities that they have evolved to sense. Hence, since the various hair fields will be deflected differently according to whether the insect is pitched or yawed, this opens the important question of whether the cephalic hairs might together sense aerodynamic angle of attack and sideslip angle, analogous to the angle of attack and sideslip vanes in aircraft (Taylor, 2007).

4.3.4 *What do the cephalic hairs measure?*

Although the firing rate of individual trichoid sensilla is a function of wind speed and direction, the apparent lack of any monosynaptic connections to the motoneurons indicates that it is the responses of the DNs which reveal what the wind-sensitive hairs really measure. Earlier work classified wind-sensitive DNs in the cervical connective according to their response properties (Svidersky, 1967; Svidersky and Knyazeva, 1968; Camhi, 1969b; Varanka and Svidersky, 1974a,b), but more recently it has become possible to measure the response properties and effects on the flight motor of individually identified DNs (Bacon and Tyrer, 1978; Bacon and Möhl, 1979; Simmons, 1980; Tyrer, 1981; Bacon and Möhl, 1983; Möhl and Bacon, 1983; Griss and Rowell, 1986; Rowell and Reichert, 1986; Tyrer *et al.*, 1988; Rowell, 1989). The picture that emerges is extremely complicated, not least because all the DNs which definitely receive input from the cephalic hairs also receive visual input from the compound eyes and/or ocelli, which substantially modulates their response to wind stimuli (TCG: Bacon and Tyrer, 1978; Bacon and Möhl, 1983; TCD: Tyrer *et al.*, 1988; DNI: Rowell and Reichert, 1986; DNC: Rowell and Reichert, 1986; DNM: Simmons, 1980; Rowell and Reichert, 1986). Rowell and Reichert (1986) have therefore argued that the DNs function as feature detectors matched to specific course deviations in a single 'emergent modality' combining visual and aerodynamic stimuli. A corollary is that normal responses will only be elicited if the stimuli presented are consistent across modalities, which rather undermines the results of many earlier experiments presenting stimuli in only one sensory modality. It therefore appears that it would be an oversimplification to regard the wind-sensitive hairs as simply measuring sideslip, angle of attack, or indeed any other purely aerodynamic state, as there is no neurophysiological evidence to suggest that any of these quantities is explicitly coded anywhere in the nervous system. Rather, as

descending sensory input from the wind-sensitive hairs appears to be fused with input from the visual system at the earliest possible stage of processing, the measurements that they make must be viewed as one component part of the multi-modal DN responses to which they contribute. This raises the important and so far unanswered question of what physical meaning this 'emergent modality' has for the insect, beyond the rather unsatisfying statement that it represents specific deviations from course (Rowell and Reichert, 1986). As we will show in Section 7.4, a possible answer to this question is provided by an understanding of the flight dynamics.

5 Inertial sensors

5.1 SIGNIFICANCE OF INERTIAL SENSING

Inertial sensors form an essential part of all modern aircraft flight control systems (Stevens and Lewis, 2003). On the whole, they are rather less important to most insects, which may reflect the fact that the forces transduced by any inertial sensor are proportional to the size of the proof mass whose inertia reacts to the applied accelerations. While this is not a significant constraint in large aircraft, it may be a significant constraint for small insects, in which weight reduction is a major concern. Hence, few insects seem to use inertial sensors that rely on a static proof mass. Dragonflies are a rare example, in which the mass of the head is sufficiently large because of the massive compound eyes and jaw apparatus that the head passively lags the body during angular rotations, thereby allowing the neck proprioceptors to detect angular accelerations (Mittelstaedt, 1950). As the proof mass in this case is the head itself, this is not a costly mechanism. By the same virtue, most walking insects sense gravity by measuring the load taken by their legs. In this case the proof mass is the body itself, but such a mechanism is obviously precluded in flight. Although there is evidence that the antennae (Horn and Kessler, 1975), cerci (Horn and Bischof, 1983) and even the halteres (Brauns, 1939) act as independent gravitational sensors during walking, there is no indication that any insect makes use of a static sense of gravity in flight (Hengstenberg, 1988). This makes functional sense, because the high accelerations experienced during flight would make any sense of gravity highly ambiguous (Burrows, 1996). In summary, flying insects do not for the most part seem to use static proof masses in order to measure accelerations. Instead, those which do measure inertial forces in flight make use of moving proof masses on which the inertial forces are larger and of a different sort. Of such sensors, much the best known are the halteres of dipteran flies (Fig. 10).

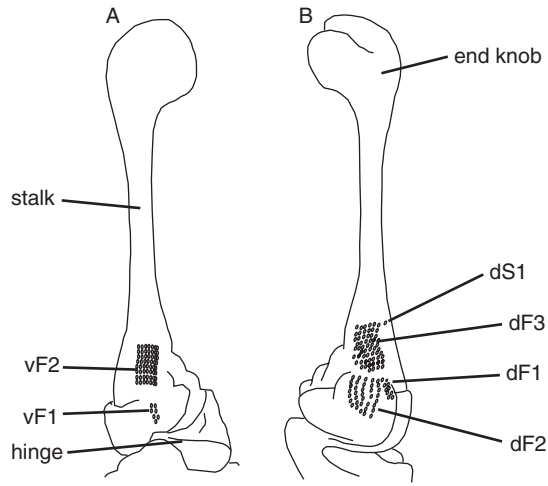

FIG. 10 Gross anatomy of a haltere showing the arrangement of the campaniform sensilla in ventral (A) and dorsal (B) views. The haltere's muscles cause it to oscillate through almost 180° about its hinge in antiphase to the wingbeat in a near-vertical plane. Coriolis forces acting on the end-knob normal to the plane of oscillation cause cuticular strain at the base of the stalk, which is detected by the campaniform sensilla. dF1–dF3: dorsal fields of campaniform sensilla; vF1–vF2: ventral fields of campaniform sensilla; dS1: single dorsal campaniform sensillum. The distribution of the campaniform sensilla within each field is approximate and diagrammatic (redrawn after Pringle, 1948 for the blowfly *Lucilia*; notation after Chan and Dickinson, 1996).

5.2 HALTERES

5.2.1 *Role of the halteres*

Halteres are unique to Diptera, although analogous structures are found in certain other insect orders and are discussed separately below (Section 5.3). Phylogenetically, halteres are highly modified hind wings; functionally, they are highly specialised inertial sensing systems. Halteres function according to the same principle as a vibratory gyroscope, used to measure angular velocity. Indeed, *Time* magazine records that engineers developing vibratory gyroscopes drew inspiration from halteres as long ago as 1946 (Anon., 1946), although it is only with the advent of Micro-Electro-Mechanical Systems (MEMS) technology that these have become practical. Vibratory gyroscopes now find use in a wide range of applications including image stabilisation in cameras and flight stabilisation in unmanned aircraft. Image stabilisation and gaze stabilisation are the two main roles played by the halteres in flies, offering a remarkable parallel between biology and engineering.

The significance of the halteres was first noted in the Boyle Lecture of 1711 by Derham, who observed that cutting off the halteres upset a fly's balance in flight. In fact, the degree to which amputating the halteres impairs flight varies across the families of Diptera (Brauns, 1939; Faust, 1952), but it is certainly significant in the Cyclorrhapa, or 'higher flies'. Derham (1714) himself considered that the halteres acted like the balancing pole of a tightrope walker, but as the halteres constitute on the order of 0.01% of the total body mass (Pringle, 1948), they cannot possibly influence flight in this way. This and a host of other often fantastical ideas (reviewed in Fraenkel, 1939) circulated the literature until a landmark paper by Fraenkel and Pringle (1938) correctly concluded that halteres operate as 'gyroscopic' sensors involved in flight stabilisation. In support was cited the classic result that a 10–15 cm long cotton thread attached to a fly's abdomen restores flight stability following amputation of the halteres (Fraenkel, 1939). This is generally attributed to the thread providing passive stability, which replaces the active stabilisation otherwise provided using feedback from the halteres. It seems most likely that this operates by damping the motions of the fly sufficiently that the slower response of its compound eyes becomes sufficient to stabilise its flight. Elegant as this experiment is, subsequent behavioural studies have provided much more direct demonstrations of the halteres' role in providing feedback to responses compensating for imposed rotations in flight.

Behavioural studies have shown that at least two distinct kinds of response are mediated by the halteres: (1) compensatory changes in stroke amplitude and other wing kinematic parameters (*Calliphora*: Faust and von Buddenbrock, 1951; Faust, 1952; Schneider, 1953; *Drosophila*: Dickinson, 1999; Sherman and Dickinson, 2003, 2004), and (2) compensatory head movements (*Musca*: Tracey, 1975; *Lucilia*: Sandeman, 1980; *Calliphora*: Hengstenberg, 1984; Hengstenberg *et al.*, 1986; Hengstenberg, 1988; Nalbach and Hengstenberg, 1994; Nalbach, 1994). These compensatory wing and head movements are observed in response to imposed mechanical pitch, roll, and yaw rotations in tethered flight, although head movements are not always coaxial with the stimulus that induces them (Nalbach and Hengstenberg, 1994). Concurrent asymmetric movements of the legs and abdomen have also been observed in *Calliphora* (Nalbach and Hengstenberg, 1994). In most of these studies, the involvement of the halteres was demonstrated by elimination experiments showing that these responses were lost or altered following manipulation of the halteres. Despite being driven by separate physiological pathways, wing and head movements are closely linked, because feedback from the cervical proprioceptors sensing head position drives changes in wing kinematics in flies (Liske, 1977). It is therefore likely that compensatory head movements serve indirectly to stabilise flight as well as directly to stabilise gaze. Both responses appear to be important in stabilising the fast saccadic motions

which characterise the flight of higher flies (*Drosophila*: Bender and Dickinson, 2006).

5.2.2 *Anatomy and physiology of the halteres*

A haltere is a dumbbell-shaped structure, comprising a distal end-knob and a basal stalk emerging from the metathorax (Fig. 10). In calyptrate flies, the halteres are housed within small pits, presumably to minimise aerodynamic interference. Each haltere is oscillated through an arc of almost 180° in antiphase to the forewings, and is driven at resonance by a single pair of indirect muscles in the metathorax (Pringle, 1948). A further 3 indirect and 8 direct muscles modulate the motion of each haltere (Chan *et al*., 1998). Each haltere's plane of oscillation is approximately vertical, but is angled back through about 30° so that the two halteres together form a highly non-orthogonal sensing system (Nalbach, 1994; Dickinson, 1999). The haemolymph-filled end-knob serves like the bob of a pendulum, and is sufficiently massive in comparison with the rest of the haltere that all of the inertial forces may be considered to act upon it (Pringle, 1948; Nalbach, 1993). The stalk is a laterally stiffened structure which articulates with the thorax about a longitudinal hinge joint, but also has some freedom of movement about a more distal secondary articulation with an axis at right angles to the primary axis of rotation. This additional freedom of movement is thought to ensure that the end-knob oscillates in a planar arc when the insect is in straight flight, but is sufficiently heavily damped that it does not interfere with the sensing of oscillatory forces (Pringle, 1948). Forces acting on the haltere end-knob generate strains at the base of the stalk, which are sensed by numerous campaniform sensilla and a single scolopalial organ.

The number of campaniform sensilla is closely correlated with the flight ability of the species concerned (Brauns, 1939), but in *Calliphora vicina* there are approximately 340 campaniform sensilla of various shapes, sizes, and orientations – all but one of which are grouped together in 5 distinct fields (Pringle, 1948; Gnatzy *et al*., 1987; Grünert and Gnatzy, 1987; Chan and Dickinson, 1996). Pringle (1948) has suggested on morphological grounds that each field is arranged to sense a specific direction of cuticular deformation. For example, the dF2 field, or 'basal plate', is appropriately arranged to sense deflections of the stalk normal to its plane of oscillation (Fig. 10). Sensory afferents from the halteres project to the prothoracic and mesothoracic neuropiles, where they overlap with the dendritic fields of the wing and neck motoneurons (*Calliphora*: Sandeman and Markl, 1980; Strausfeld and Seyan, 1985). Most of the afferent projections are ipsilateral, although weak contralateral afferent projections are probably present, and strong contralateral interneuronal connections certainly exist (Sandeman and Markl, 1980; Strausfeld and Seyan, 1985; Chan and Dickinson, 1996).

Extracellular recordings from the wing and neck motoneurons of *Calliphora* indicate ipsilateral and bilateral responses, respectively, to mechanical stimulation of the halteres. These electrophysiological responses have latencies of approximately 2 ms, suggesting that the motoneurons connect monosynaptically to the haltere afferents (Sandeman and Markl, 1980). Intracellular recordings from the motoneuron of the first basalar muscle of the flight apparatus confirm that it connects monosynaptically with the sensory afferents from the dF2 field of campaniform sensilla (Fayyazuddin and Dickinson, 1996, 1999). A fast electrical synapse with a latency < 1 ms dominates the response (Fayyazuddin and Dickinson, 1999), which seems likely to advance the once-per-cycle firing of the first basalar, so as to produce ipsilateral changes in stroke amplitude (Fayyazuddin and Dickinson, 1996).

5.2.3 *Function of the halteres*

The physical basis of the halteres' sense of rotation was elaborated more or less correctly by Pringle (1948), who inferred that the halteres must sense forces acting normal to the plane of oscillation, and derived a simplified expression for the force component in this direction. Several behavioural studies confirm that haltere-mediated responses are sensitive only to forces normal to the haltere's plane of oscillation. Pressing the haltere is effective in eliciting head movements only if the haltere is pushed forwards at right angles to the plane of oscillation (Sandeman and Markl, 1980), while linear vibrations of a fly with one haltere removed only elicit head movements if they involve a component normal to the remaining haltere's plane of oscillation (Nalbach, 1994). Extracellular recordings from the haltere nerve also show a much stronger response to deflections of the haltere normal to its plane of oscillation than in any other direction (Pringle, 1948). Normal components of force are generated in several different ways during turns, but are absent during straight flight, making them especially easy to detect. Rather like the model proposed for the antennae (Section 4.2.5), we think it likely, therefore, that the haltere-mediated stabilisation system simply acts to drive below threshold the dF2 field of campaniform sensilla that detects these normal components of force.

A complete expression of the forces acting on the end-knob has been given by (Nalbach, 1993). The largest normal force components are the Coriolis forces due to the angular velocity of turn (Nalbach, 1993). Coriolis forces appear when the inertial motion of a mass is measured in a rotating frame of reference. Because a moving mass tends to maintain its trajectory in an inertial frame of reference, its direction of motion with respect to a rotating frame of reference appears to change through time. This implies the action of a force normal to the axis of rotation, which is called the Coriolis force. It follows that the normal components of force sensed by

the haltere can only be caused by rotations about axes within the haltere's plane of oscillation. The Coriolis force depends multiplicatively upon the angular speed of rotation, the speed of the end-knob, and the sine of the angle between the velocity of the end-knob and the axis of rotation (i.e. the vector product of the angular velocity of the fly and the velocity of the end-knob). Even for a simple harmonic oscillation of the haltere this leads to a complicated phase modulation of the Coriolis forces, which is uniquely defined by the axis of rotation. This can be intuited by considering when the Coriolis forces vanish. This occurs when either the speed of the end-knob is zero, or its velocity vector is collinear with the axis of rotation. Hence, assuming a vertical plane of oscillation, the Coriolis forces associated with rotations about a horizontal axis will vanish twice-per-cycle, because the velocity of the end-knob becomes horizontal at the same time as it vanishes at the turning points of the oscillation. However, the Coriolis forces associated with rotations about a vertical axis will vanish four times per cycle, because the velocity of the end-knob becomes vertical 90° out of phase with the times at which it vanishes at the turning points of the oscillation. It follows that a single haltere could use the phase modulation of the normal component of force to distinguish nominal pitch and yaw rotations (Pringle, 1948; Nalbach, 1993, 1994). This discrimination will require sufficient bandwidth to sense forces modulated at twice the frequency of oscillation.

Three-axis sensitivity to rotations could be achieved in three ways. Firstly, a single haltere could achieve three-axis sensitivity by measuring radial as well as normal components of the Coriolis force (Nalbach, 1993). This does not appear to happen, because the radial component of the Coriolis force is overwhelmed by the much larger centrifugal force due to the haltere's own oscillation (Nalbach, 1993). Secondly, a single haltere could achieve three-axis sensitivity by driving its end-knob through an orbital trajectory. This has been proposed in the design of MEMS vibratory gyroscopes (John and Vinay, 2006), but is not borne out by the planar oscillation of the halteres. Thirdly, bilateral processing of haltere input should allow flies to distinguish rotations about all the three axes, provided that their oscillations are not co-planar (Pringle, 1948; Nalbach, 1994). Bilateral summation and inhibition of haltere input in respect of compensatory head movements has been proven by unilateral elimination experiments (Nalbach, 1994), consistent with the bilateral response of the neck motoneurons (Sandeman and Markl, 1980). However, the lack of any bilateral response in the wing motoneurons (Sandeman and Markl, 1980), and the absence of any change in contralateral stroke amplitude following unilateral haltere manipulation (Dickinson, 1999) suggest that bilateral processing might not be used to provide three-axis sensitivity in respect of compensatory wing movements. Instead, it seems likely that the differing wing kinematic responses to pitch, roll, and yaw result from symmetric

versus asymmetric stimulation of two separate two-axis control systems which are non-orthogonal with respect to each other.

5.2.4 *What do the halteres measure?*

The straightforward and correct answer to the question of what the halteres measure is that they measure forces normal to their plane of oscillation that are generated during turns. A correct answer in terms of state feedback is less straightforward. Proof that the halteres sense Coriolis forces is supplied by behavioural studies in which a tethered fly is mechanically rotated at constant angular velocity in the absence of visual stimuli (Hengstenberg, 1984; Hengstenberg *et al*., 1986; Hengstenberg, 1988). Compensatory head deflections have been shown to persist under these conditions for periods of 8 min, albeit with fatigue (Hengstenberg *et al*., 1986). It has proven harder to confirm whether the halteres might also sense acceleration, as angular velocity and angular acceleration are both present during rotational oscillations: merely correlating the fly's instantaneous state with its instantaneous velocity or angular velocity (Sandeman, 1980; Dickinson, 1999) is insufficient to distinguish rigorously between them, because it ignores the dynamics of the system being observed. Perversely, direct proof that the halteres are indeed capable of sensing acceleration is provided by a series of studies simulating Coriolis forces by applying linear accelerations phase-locked to the wing beat (Nalbach, 1993, 1994; Nalbach and Hengstenberg, 1994). The take-home message is that inertial forces are inertial forces no matter how they are produced, and it should not be so much a question of whether halteres do detect acceleration, as whether their inevitable sensitivity to acceleration interferes in any way with their measurement of Coriolis forces.

Given that the halteres do primarily sense Coriolis forces, it follows that they must in some sense measure angular velocity. In *Calliphora* the amplitude and speed of head deflection in roll is approximately linear in the angular velocity of rotation up to about $1000^\circ\,s^{-1}$ (Tracey, 1975; Hengstenberg *et al*., 1986; Hengstenberg, 1988; Nalbach and Hengstenberg, 1994), while changes in stroke amplitude are also approximately linear in the angular velocity of rotation up to at least $800^\circ\,s^{-1}$, and probably higher given that this was a limit imposed by the experiment (Dickinson, 1999; Sherman and Dickinson, 2003). This linear dependence on angular velocity is interesting, because the phase modulation of the Coriolis force means that the instantaneous activity of the campaniform sensilla of the dF2 field does not encode angular velocity directly. It is of course possible that the activity of other fields sensing the oscillation of the haltere could provide the time-varying reference needed to decode the signal. However, what we know of the monosynaptic connection between the dF2 field and the first basalar muscle's motoneuron does not suggest that any such sensory processing

occurs in the wing kinematic reflex. Rather, it appears that the population activity of the campaniform sensilla has different effects on the firing of the wing muscles according to its phase (Fayyazuddin and Dickinson, 1996, 1999). Hence, it is the interaction of the sensors and actuators which in effect encodes angular velocity: when the control system is treated as a black box, linear relationships between angular velocity and output states emerge, even though there is no nervous signal directly encoding angular velocity. It appears that halteres do measure angular velocity, but as an emergent property of the control system of which they are a part.

5.3 OTHER INERTIAL SENSORS

5.3.1 *Haltere analogues*

Several morphologically and phylogenetically distinct kinds of sensor have been proposed to function in other orders as analogues of the Dipteran halteres. Of these, much the best-substantiated are the reduced club-shaped forewings of male Strepsiptera (Pix *et al.*, 1993). Functionally, these are very similar to the halteres of flies, beating through a near-vertical plane of almost 160° in antiphase to the hind wings. Compensatory head movements of male *Xenos vesparum* in response to imposed rotations about the pitch and yaw axes in tethered flight are observed at angular speeds up to at least $1000^\circ s^{-1}$, but vanish when the reduced forewings are eliminated or stop beating (Pix *et al.*, 1993). Given the many functional similarities, it seems highly likely that the reduced forewings of male Strepsiptera do indeed sense Coriolis forces. Less well substantiated as inertial sensors are the reduced elytra of certain Coleoptera. The beetles *Sisyrphus schaefferi* (Wigglesworth, 1946) and *Atractocerus brevicornis* (Miller, 1971) have both been singled out as vibrating their reduced elytra in flight, but evidence of a role in flight stabilisation has only been put forward for the latter. *Atractocerus* is incapable of steady flight after removal of the elytra, which beat through an arc of 120° in flight. However, like Fraenkel (1939)'s flies, they recover this ability when a long thread is tied to the abdomen (Miller, 1971). This evidence is indicative, rather than compelling, but it hints that the evolution of sensitivity to Coriolis forces by a reduced wing pair may be widespread among functionally two-winged insects.

Most recently, Sane *et al.* (2007) have proposed that the antennae of the hawkmoth *Manduca* – and presumably many other insects – might also sense Coriolis forces during turns. For reasons now discussed, this is unlikely. In support of their hypothesis, Sane *et al.* (2007) show that *Manduca* lose the ability to perform stable flight in conditions of darkness after the flagella are removed and recover this ability when the flagella are restored. Sane *et al.* (2007) also estimate that the torque due to the Coriolis

force is of the same order of magnitude as aerodynamic drag, which the antennae can certainly sense. Finally, they show using intracellular recordings from individual scolopidia of the Johnston's organ that the antennae are tightly tuned to sense torques generated at twice the frequency of antennal oscillation, and suggest that this is indicative of a sensitivity to phase modulation of the Coriolis forces. The problem with this is that the absolute magnitude of the Coriolis forces generated at twice the frequency of oscillation will be negligible in comparison with those at the fundamental frequency. This is because the angular amplitude of antennal oscillation is, at $<1^\circ$, some two orders of magnitude smaller than the oscillations of dipteran halteres – or indeed of strepsipteran or coleopteran forewings. Recall that the higher harmonics experienced by halteres arise because the speed of the end-knob changes out of phase with its direction through an oscillation cycle. With a 1° amplitude oscillation, the antenna will scarcely change direction in the course of its oscillation, and hence the only significant force components will be at the fundamental frequency. Furthermore, the antenna will only be sensitive to rotations about one axis. Hence, it seems most unlikely that the tuning of the antennae of *Manduca* reflects a role in sensing Coriolis forces: perhaps a more likely candidate is the rapid acceleration of the antenna experienced twice-per-cycle in reaction to the rapidly changing forces at the top and bottom of the wing stroke. These inertial forces might be expected to induce peak cuticular stresses twice-per-cycle at the base of the antenna.

6 Wing-load sensors

6.1 SIGNIFICANCE OF LOAD SENSING

Insect wings are instrumented with an array of mechanosensors besides the trichoid sensilla already mentioned. Most of these seem to operate either as load sensors or proprioceptors. In locusts, which are much the best-studied group in this respect, the wing mechanosensors include stretch receptors, scolopidia, campaniform sensilla, and a complex organ called the tegula (reviewed in Burrows, 1996). In addition, there are some curious free-ending multipolar neurons distributed throughout the wing cuticle, whose function is unknown. These have axons large enough, at 2–3 μm diameter in some cases, to play some role in providing feedback for flight control (Knyazeva, 1970). Most of these sensors appear to provide peripheral feedback to the flight motor, and all except the campaniform sensilla have been studied only from this perspective. For this reason, we will not review them further here, except to note that some might also be involved in providing state feedback to the flight control

system. The remainder of this section deals exclusively with the campaniform sensilla.

6.2 WING CAMPANIFORM SENSILLA

6.2.1 *Role of the wing campaniform sensilla*

Several lines of evidence confirm that the wing campaniform sensilla are involved in the precise regulation of wing kinematics in Orthoptera and Diptera. This is presumably true of other insects too, since the number of campaniform sensilla is broadly correlated with the flight ability of the group concerned (Gettrup, 1966). In locusts, cauterising the campaniform sensilla or applying an anodic block eliminates the normal regulation of forewing twist in response to changes in aerodynamic angle of attack (*Schistocerca*: Gettrup and Wilson, 1964; Gettrup, 1965, 1966). Moreover, individuals which have their proximal group of forewing campaniform sensilla cauterized lose the ability to maintain stable free-flight (Gettrup, 1966). Evidence for a role of the campaniform sensilla in the flight control of Diptera is provided by behavioural experiments showing that asymmetric loading of the wings, due either to unilateral manipulation of the wings or asymmetric airflow, leads to compensatory head movements qualitatively similar to those elicited by the halteres (*Calliphora*: Hengstenberg, 1988).

6.2.2 *Anatomy of the wing campaniform sensilla*

We will not concern ourselves here with the fine structure of the campaniform sensilla, but rather with their distribution and orientation. In locusts and other Acrididae, all the campaniform sensilla are located proximally on the ventral surface of the wings, forming two distinct groups on the forewing and one group on the hind wing (*Stauroderus*: Zaćwilichowski, 1934; *Schistocerca*: Gettrup, 1966; *Locusta*: Knyazeva, 1970). In Diptera, the campaniform sensilla are mainly located on the dorsal wing surfaces, with a smaller number located ventrally. In *Calliphora* the campaniform sensilla form 8 distinct groups, with a number of other sensilla found singly and a separate field located on the tegula (*Calliphora*: Gnatzy *et al*., 1987). Almost all of the sensilla in *Calliphora* are elliptical (Grünert and Gnatzy, 1987) and in most cases all of the sensilla within a group share the same orientation (Gnatzy *et al*., 1987). The location and orientation of the single campaniform sensilla appears to be highly stereotyped within a species, and is remarkably conserved across genera (*Drosophila*, *Musca*, *Calliphora*, *Sarcophaga*: Dickinson and Palka, 1987). While this might simply reflect phylogenetic inertia, it seems more likely that it represents the effects of stabilising selection related to the function of the campaniform sensilla in sensing specific wing deformations.

6.2.3 *Function of the wing campaniform sensilla*

Extracellular recordings have been made from individually identified campaniform sensilla (*Drosophila*: Dickinson and Palka, 1987; *Calliphora*: Dickinson, 1990a,b) and from sensory nerves carrying their afferents at the wing base (*Schistocerca*: Gettrup, 1965, 1966; Elson, 1987a). Other studies have recorded the responses of individually identified interneurons (*Schistocerca*: Elson, 1987b,c) or flight muscles (*Schistocerca*: (Waldron, 1967; Elson, 1987a); *Locusta*: Wendler, 1974, 1978) to stimulation of the campaniform sensilla. Together, these studies demonstrate that the campaniform sensilla respond to particular deformations of the wing cuticle, and specifically to those associated with twisting of the wings. For example, Elson (1987a) found that the forewing campaniform sensilla of *Schistocerca* are excited by supination (nose-up rotation of the wings at the end of the downstroke) but inhibited by pronation (nose-down rotation of the wings at the end of the upstroke). In *Schistocerca*, the spike rate of the campaniform sensilla additionally reflects the magnitude of deformation (Elson, 1987a). In *Calliphora* and *Drosophila*, the spike rates of the single campaniform sensilla also depend on the magnitude of deformation, but saturate too quickly for this to be relevant (Dickinson and Palka, 1987; Dickinson, 1990a,b). Furthermore, the high wing beat frequency of flies means that each campaniform sensillum is only able to fire one phase-locked action potential per wing beat, and hence it is their phase and perhaps population activity which must encode the salient information (Dickinson, 1990a,b). Specifically, the distribution of the single sensilla along the wing should allow them collectively to encode information about the travel of torsional waves along the wing (Dickinson, 1990a). In any case, it appears that the campaniform sensilla of both flies and locusts may be able to provide the fast state feedback required for flight control (Elson, 1987a,b,c; Dickinson, 1990a).

6.2.4 *What do the wing campaniform sensilla measure?*

It is difficult to be sure of what the wing campaniform sensilla measure. The key conceptual difficulty arises because they form part of a peripheral feedback loop to the flight motor, which remains complete even in tethered flight. For example, we know that the firing of the campaniform sensilla in tethered locusts changes as the angle of attack of the insect is varied (*Schistocerca*: Gettrup, 1966), but this does not allow us to distinguish whether the firing of the campaniform sensilla changes because they sense changes in wing loading caused directly by changes in angle of attack, or changes in wing kinematics mediated by feedback from other sensors detecting changes in angle of attack. In any case, it appears that the campaniform sensilla provide a rather different kind of feedback from the

kinds of state feedback we have discussed so far – or indeed from anything that is used by aircraft (Weis-Fogh, 1956). Although all the mechanosensors we have discussed sense forces of one sort or another, most of these can be viewed as giving information on the kinematic state of the insect. This is true also for the campaniform sensilla, but the forces that they measure are of immediate relevance to the insect, because they provide a direct measure of the wing loading. Unlike the other mechanosensors we have discussed, they therefore feed back the forces which actually produce the flight dynamics. The closest analogue to this in aircraft design appears to be the use of accelerometer feedback to maintain a constant *g*-load in fighter aircraft manoeuvres (Stevens and Lewis, 2003). In insects, measuring the wing loading directly would have particular advantages, because the unsteadiness of the aerodynamics makes it unlikely otherwise that the control system would have a good estimate of the instantaneous wing loading (Taylor, 2007). To further complicate the picture, intracellular recordings from individually identified thoracic interneurons in *Schistocerca* demonstrate that monosynaptic input from the wing campaniform sensilla is combined with input from the contralateral and medial ocelli (Elson, 1987b). It therefore appears that state feedback and force feedback are combined to form a single signal to the flight motor encoding specific wing deformations associated with specific patterns of motion of the insect with respect to its environment. The campaniform sensilla are nothing if not complicated, and it is clear that further work will be required to elucidate their true role in providing feedback to the flight control system.

7 Conclusions

Several general principles emerge from our review of what the different sensory systems of flying insects measure. Our aim in this section is to elucidate these general principles in order finally to answer the question posed at the beginning of this chapter of why insect sensors measure what they do. We elaborate three general principles (Sections 7.1–7.3) before drawing these together to propose a novel hypothesis for the adaptive significance of insect sensory systems based on flight mechanics (Section 7.4).

7.1 INSECTS SENSE DISTURBANCES, NOT ABSOLUTES

Anyone who drives a car will be familiar with the observation that it is reasonably easy to maintain a steady speed with reference only to the road, but that an occasional glance at the speedometer is necessary to avoid slow drift. This drift usually causes us to speed up rather than slow down, and we will all be familiar with the sensation that intermediate driving speeds

seem much slower if we have just left a fast piece of road on which we have been driving for some time. Hence, while we are fairly good at using translational optic flow cues to stabilise our speed about some set point, we are much less good at using it to measure absolute speed. This is probably a reasonable analogy for the sensors of flying insects, which unlike the speedometer of a car, or the airspeed indicator of an aircraft, appear to sense changes and not to measure absolutes. We have already suggested specific reasons why this is the case for the sensory systems discussed above, and in this section aim to draw these together under two categories of explanation: extrinsic and intrinsic.

Extrinsic explanations of why insect sensors do not measure absolute quantities relate to the kind of sensory information that they use. For example, insects apparently lack an unambiguous sense of gravity or a magnetic sense of orientation in flight (Section 5) and therefore rely on horizon detection by the visual system in order to measure static orientation (Section 3). However, this can only ever provide an approximate sense of static orientation because there is no absolute visual reference for either the vertical or the horizontal: the approximately vertical direction of the brightness gradient will depend upon the ambient lighting conditions, while the approximately horizontal direction of the horizon will depend upon the structure of the environment. It follows that neither the compound eyes nor the ocelli can measure static orientation in an absolute sense unless initialised by reference to gravity prior to take-off. Nevertheless, both should be able to sense changes in static orientation. As we have discussed, visual systems can also be ambiguous in respect of self-motion (Section 3.2.3). In particular, the rate of translational optic flow is a function of the distance of the visual environment as well as its speed of relative motion (Section 3.2.1). Although it is possible that insects might estimate the distance of the visual environment to compensate, it is perhaps more likely that they follow simpler rules and respond to changes in the rate of optic flow. For example, free-flying honeybees adjust their flight speed to compensate for changes in the image velocity of their surroundings, but are only sensitive to stationary deviations in image velocity from their preferred setpoint when these exceed a certain threshold (Srinivasan and Zhang, 2000; Baird *et al.*, 2005).

Intrinsic explanations of why insect sensors do not measure absolute quantities relate to the way in which their sensory systems are configured and constructed. We have already discussed one specific example in relation to the EMDs of the compound eye, which may be sensitive to the contrast and spatial frequency of the visual environment, as well as to its distance and speed of relative motion (Section 3.2.2). However, there are several more general intrinsic reasons why insect sensors may be unable to measure absolutes, all of which relate to the time-variance of their gain functions. Firstly, neuronal adaptation means that the gain of any insect

sensor is liable to adapt through time if it is subject to a continuous stimulus. Secondly, several of the sensory systems we have discussed are configured to operate as adaptive sensing systems. Thirdly, several of them are strongly dependent on temperature. Unless some record is kept of these changing gain functions and used to compensate the output of the sensor, it follows that they cannot be used to measure absolute quantities, although transient disturbances will be sensed readily enough.

Neuronal adaptation is a universal and unavoidable property of biological sensors, but because it can enhance energetic efficiency and dynamic range, the rate of adaptation is also subject to natural selection. Hence, while some of the sensors we have discussed, such as the pedicellar campaniform sensilla of the antennae (Section 4.2) adapt slowly and therefore display a phasic-tonic response, others such as the Johnston's organ of the antennae (Section 4.2) and the cephalic wind-sensitive hairs of locusts (Section 4.3), adapt more quickly and have a strictly phasic response. Paradoxically, however, neuronal adaptation is probably more significant in preventing phasic-tonic sensors from measuring absolutes than in preventing phasic sensors from doing so. This is because phasic sensors are stimulated in an on–off fashion by the periodic stimulus of the wing beat, and therefore continue to fire periodically without ever having the chance to adapt. Hence, although they are only on for brief periods, their gain may be essentially time-invariant during those periods. Tonic sensors, however, adapt slowly but appreciably in flight, and are therefore bound to have a time-variant gain function. Both kinds of sensor are well-placed, however, to sense transient disturbances.

The clearest example of an adaptive sensing system that we have discussed is provided by the antennae (Section 4.2). The gain of the pedicellar campaniform sensilla and the Johnston's organ is modified mechanically by the antennal positioning reaction, which effectively adjusts the drag coefficient of the flagellum by varying the angle of the scape–pedicel joint. As we have already discussed (Section 4.2.6), this will hinder any measurement of absolute airspeed. Nevertheless, the consequence of the antennal positioning reaction is that the response of the antennal sensors to changes in airspeed is approximately linear and the system is therefore well-placed to sense transient disturbances. At a higher hierarchical level, head movements affect the responses of numerous different sensory systems. This is an exceedingly complex topic, and the details are not well worked out – indeed, many recent experimental studies continue the dubious physiological tradition of fixing the head during experiments. Nevertheless, it is clear that the static orientation of the head with respect to the body and its relative motion during compensatory movements will govern the gain and reference frame of any measurements made by the cephalic sensors.

Sensitivity to temperature is a common enough problem in manmade transducers as well as biological ones. Nevertheless, it is striking that

temperature should so strongly affect the spiking rates of certain key sensors such as the cephalic wind-sensitive hairs of locusts discussed in Section 4.3, and the wing-hinge stretch receptors (Pfau *et al.*, 1989) mentioned briefly in Section 6. Once again, it would be possible to compensate this with an independent measurement of temperature – perhaps even made by the free-ending neurons in the wing (Section 6) – but there is no clear evidence that insects do this and it seems likely that this is just yet another factor conspiring to make it difficult for insects to measure absolutes. Fortunately, since temperature drifts slowly compared to variables of interest in flight dynamics, such sensors are still able to sense transient disturbances quite adequately.

In summary, it seems to be a reasonably general principle that the sensors involved in insect flight control are better adapted to sense changes in state than to measure absolute state. Even the halteres, which arguably come the closest of any insect sensor to measuring an absolute kinematic state of the system, sense quantities that are non-zero only during disturbances. It is therefore misleading to think of most insect sensors as analogues of aircraft sensors such as Pitot tubes, sideslip vanes, and so on, which measure the absolute kinematic state of the system. Instead, we need to think of them as sensing changes in state – particularly disturbances from equilibrium. This is intuitively appealing, because whereas a signal representing an absolute measurement of kinematic state typically needs to have a signal representing the intended kinematic state subtracted from it before it can be used as an actuating signal in a feedback loop (Section 2.2), a measurement of a change in state can already be used as an actuating signal. Hence, it is not surprising to find that the feedback signal from the halteres connects monosynaptically to the motoneurons of the flight motor, without the need for any further processing (Section 5.2.2). We offer a more general functional explanation of why insects may benefit from sensing changes in state in Section 7.4.

7.2 INSECT SENSORY SYSTEMS ARE TUNED TO SPECIFIC DIRECTIONS OF MOTION

The arrangement of the axes along or about which insects sense disturbances is relevant both within and between different sensory systems. Some systems, such as the antennae, are not especially directionally sensitive, so we will concern ourselves here only with those which are. Of these, the best-studied examples are the tangential cells of the compound eyes (Section 3.3), the halteres of flies (Section 5.2), and the cephalic wind-sensitive hairs of locusts (Section 4.3). Each of these systems has a strong directional sensitivity, whether in respect of rotation, as for the halteres and tangential cells of the compound eyes, or in respect of wind direction,

as for the wind-sensitive cephalic hairs. We will now consider how the axes of sensitivity of each of these systems are arranged.

Concerning the compound eyes, we have already discussed in Section 3.3 how each VS-cells acts as a matched filter tuned to detect rotations of the visual field about a specific axis. Figure 11 plots the arrangement of these axes, which is highly non-orthogonal. This non-orthogonality is not in itself surprising, given the number of axes, but perhaps more surprising is the high degree of structure in their arrangement: natural selection has

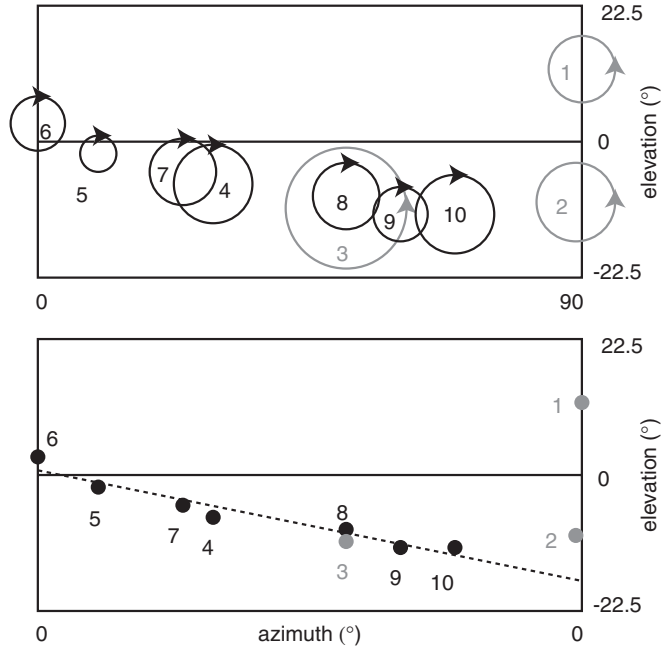

FIG. 11 Preferred rotational axes of the vertical system cells (VS1–VS10) of the visual system of *Calliphora* in a cylindrical projection of the right visual hemisphere. Upper panel shows the preferred axis and sense of rotation of each numbered cell, averaged over several different individuals. Cells in grey are excited by left-handed rotation about the axis shown; cells shown in black are excited by right-handed rotation. The opposite sense of rotation about these same axes inhibits the cells. The diameter of the circular arrows in the upper panel is proportional to the standard deviation of the preferred axis of rotation across individuals. Lower panel shows the cells' mean preferred axes of rotation, together with a linear regression ($p<0.05$, $R^2=0.93$) fitted to the preferred axes of VS4–VS10, which are all stimulated by the same sense of rotation and will therefore be stimulated sequentially in flight if the instantaneous axis of rotation moves along the line. This could occur during certain flight manoeuvres: for further explanation see Section 7.4 (drawn using original data from Krapp *et al.*, 1998).

clearly tuned them to operate in a highly specific fashion. Indeed, when their axes of sensitivity are plotted on a cylindrical projection of the visual field, the axes of eight of the ten VS-cells (VS3–VS10) fall along a straight line with a slope of about 12° with respect to the horizontal (linear regression: $p < 0.05$, $R^2 = 0.93$). Hence, while the neuron at the start of this line (VS6) is sensitive to pure roll motions, the remaining neurons along the line are sensitive to combinations of roll, pitch, and yaw. The other two VS-cells (VS1–VS2) are each sensitive to rotations about transverse axes tilted slightly with respect to the horizontal, so are sensitive to a combination of pitch, and to a lesser extent, yaw. The structure of this arrangement is striking: rather than being spread out across the visual field so as to sample as wide a range of rotations as possible, the ten VS-neurons are concentrated in a very specific manner. We propose a detailed explanation of this intriguing observation in Section 7.4, but for the time being will move on to consider how the axes of the other sensory systems are arranged.

Concerning the halteres, we have already said that each haltere is sensitive only to rotations within its plane of oscillation, but is able to distinguish the axis of rotation within this plane from the phase modulation of the forces (Section 5.2). Since the approximately vertical beating plane of each haltere is angled back through about 30° from a transverse axis, this means that a pair of halteres has four axes of sensitivity: two approximately collinear and therefore redundant vertical axes, and two horizontal axes making an angle of roughly 120°. This is confirmed by behavioural studies showing that the compensatory head movements and ipsilateral wing kinematic responses mediated by the halteres are maximal in respect of rotations about these same axes, varying in magnitude for other axes of rotation as the sine of the angle between the axis of rotation and the axis of maximal sensitivity (Nalbach, 1994; Dickinson, 1999). Nalbach (1994) has discussed some of the theoretical implications of this non-orthogonal sensing arrangement, but the key point to note from our perspective is that the directions of the two horizontal measuring axes do not coincide with either the morphological pitch or roll axes of the insect. Instead, they sense a combination of the two, and thereby display a mixed sensitivity to both symmetric and asymmetric motions. Hence, while the halteres together enable the fly to sense rotations about any axis, they are maximally sensitive to pure yaw rotations about a vertical axis, and to rotations about two horizontal axes combining both pitch and roll.

Concerning the cephalic wind-sensitive hairs of locusts, it is clear from the directional arrangement of the trichoid sensilla that their fields are disposed in a highly non-orthogonal fashion (Fig. 9). Although it is unknown how these dispositions correspond to patterns of flow over the head capsule, it is reasonable to assume that each hair field will be maximally stimulated by disturbances in a specific direction. Unfortunately, it remains largely unknown how this directional sensitivity is reflected in the

responses of the wind-sensitive interneurons: while certain interneurons are known to have a highly directional response, details have so far been published for only one unidentified interneuron (Camhi, 1969b). This interneuron was found to respond maximally to wind stimuli at a sideslip angle of approximately 10° to the right, and is presumably paired with a contralateral interneuron sensitive to the same degree of sideslip to the left. Incomplete as this evidence is, it is sufficient to conclude that the wind-sensitive hairs, like the halteres and the tangential cells of the compound eyes, also form a non-orthogonal sensing system. Unfortunately, we do not know whether these unidentified interneurons are unimodal or whether they, like other wind-sensitive interneurons, receive inputs from other sensory modalities. Further research mapping the directional response properties of the wind-sensitive interneurons is clearly required.

In summary, it seems to be a general principle that the sensors involved in insect flight are selected to be non-orthogonal. In contrast, manmade sensor systems have classically been designed to be orthogonal, which is partly because this simplifies the signal processing, but mainly because it ensures that the resulting system is equally sensitive to motions in any direction. For this reason, an orthogonal sensor system cannot be said to be tuned to any particular motion. Any non-orthogonality will, however, make the system more sensitive, and hence more accurate (Karmeier *et al.*, 2005), in respect of motions in some directions than in others. This is why we have talked above of the non-orthogonal sensory systems of insects being tuned to specific motions. This directional tuning is advantageous if particular motions are more important than others, because it can enhance the system's sensitivity to those motions. Non-orthogonality can also confer resilience, because the partial redundancy of the axes means that the loss of one need not render the sensory system inoperable. This is why flies are able to fly tolerably well after losing one, but not both, of their halteres (Nalbach, 1994). In contrast, manmade systems typically achieve resilience by having multiple completely redundant sensors. Doubtless, both advantages of non-orthogonality are important in explaining why the sensors involved in insect flight control have been selected for non-orthogonality.

7.3 INSECTS SENSE COMPOSITE, MULTI-MODAL QUANTITIES

We have not said much so far about the integration of sensory input from different modalities, or from different sensors within the same modality. This remains one of the least well-known aspects of the sensory systems involved in insect flight control. As we have seen, most earlier studies tended to focus upon just one modality, often eliminating sensory input in other modalities in order to demonstrate the involvement of the modality of interest. Furthermore, providing realistic multi-modal stimulation is

challenging, and it is only in recent years that the experimental apparatus to do this has become available (e.g. Dickinson, 1999). For this reason, we will not review in detail existing results on multi-modal integration, and will instead briefly discuss the ways in which this is known to occur. Multi-modal integration of sensory input appears to happen on two levels: interneuronal and sensorimotor.

It seems likely that integration of input from multiple sensory modalities will turn out to be a ubiquitous property of sensory interneurons – at least at the later stages of processing. Certainly, most of the higher order thoracic interneurons known from locusts are multi-modal (Rowell and Reichert, 1991), but we have also said that many of the descending sensory interneurons receive input from several modalities, including the compound eyes, ocelli, and cephalic wind-sensitive hairs (Section 4.3.4). Multi-sensory integration at the neuronal level has also been shown to occur in flies, in which inputs from the compound eyes combine with inputs from the ocelli (Parsons *et al.*, 2006; Haag *et al.*, 2007). Unfortunately, we know little about the quantitative aspects of this interneuronal integration, and while earlier studies pointed to a simple role in which input from one sensory system merely gated input from another (Simmons, 1980; Heide, 1983), subsequent work has suggested that the picture may be more complicated, with quantitatively different responses observed according to whether or not the stimuli are consistent across modalities (Rowell and Reichert, 1986). Elucidating the quantitative properties of multi-modal and multi-sensory integration by individually identified interneurons poses a significant experimental challenge, but will undoubtedly be a productive avenue of future research.

Perhaps less expectedly, integration of sensory input from multiple modalities can happen at the level of the sensors themselves, by virtue of adaptive sensing of the sort we have described in Section 7.1. We have already mentioned that feedback from the cervical proprioceptors sensing head position can drive changes in wing kinematics (Liske, 1977), and it is well known that input from several different sensory systems converges on the head–neck motor system (Strausfeld and Seyan, 1985). It follows that the head–neck system can act as a sensorimotor integrator of input from different sensory modalities. Moreover, since forward commands may also be sent to the head–neck motor system, this additionally provides a means of integrating and potentially de-conflicting forward and stabilising control inputs (Rowell, 1989). A similar mechanism has been proposed for the halteres of flies, the control muscles of which receive strong descending visual input (Chan *et al.*, 1998). It follows that the deflections measured by the basal fields of campaniform sensilla may be not only due to inertial forces, but also to active deflections mediated by input from the compound eyes, offering a means of integrating the two (Chan *et al.*, 1998). Such sensorimotor integration may turn out to be a general principle of insect

sensory systems, as any adaptive sensing system has the potential to operate in this way. It would certainly be worthwhile to re-examine the antennal positioning reaction to see whether this is also driven partly by input from other sensory systems beside the antennae or by forward commands, as we have suggested in Section 4.2.5.

In some cases, such as the model of haltere function proposed by Chan *et al.* (1998), the different sensory modalities that are combined measure similar quantities. In this case, it is well established that the halteres and compound eyes are both sensitive to angular velocity, but have very different bandwidths. Whereas the compound eyes are most sensitive to angular velocities on the order of $100^\circ\,s^{-1}$, the halteres display a linearly increasing response to angular velocity up to about $1000^\circ\,s^{-1}$, and respond with a significantly shorter latency (Hengstenberg, 1984). The response properties of the two systems therefore complement each other, and it is natural to expect that their responses should be combined. Indeed, for physically consistent combinations of visual and mechanical input, the wing kinematic response of *Drosophila* appears simply to represent the linear sum of the responses of the halteres and the compound eyes (Sherman and Dickinson, 2004). In other cases, such as the DNs of locusts, the different sensory modalities that are combined measure different physical quantities, which may however be induced by the same directional deviation. The spiking of the DNC, for example, is a function of both the aerodynamic stimuli transduced by the cephalic wind-sensitive hairs and the visual stimuli transduced by the compound eyes and ocelli (Rowell and Reichert, 1986). An obvious benefit of multi-modal sensor fusion is the enhancement of the signal to noise ratio across a wider bandwidth. This is well established for the gaze stabilisation system in flies (Hengstenberg, 1991, 1993) and presumably applies in respect of flight control as well. As we show in the next section, this may, however, be only part of the story.

7.4 THE NATURAL-MODE SENSING HYPOTHESIS

The general principles we have elucidated in the previous three sections all point to one final conclusion. We have seen that flying insects sense changes in state; that they are sensitive to changes with specific directional and temporal properties; and, that changes in different motion components and modalities are often combined into one signal. It is difficult to escape the conclusion, therefore, that natural selection has tuned flying insects to sense excitation of the natural modes of motion which characterise their flight dynamics. All mechanical systems which are free to move have natural modes of motion corresponding to the paths through state space that the system will naturally follow if disturbed from equilibrium. For example, left to its own devices, a simple pendulum will always follow the

most direct circular path back to its nadir, but will typically overshoot, leading to a harmonic oscillation of predictable frequency. In the same way, flying bodies, be they insects or aircraft, also have physically predictable modes which are excited whenever the body is disturbed from equilibrium. An excellent and detailed description of the physical basis of the modes of motion of aircraft can be found in Cook (1997). Here we provide only the briefest of introductions, firstly to illustrate what is meant by a natural mode of motion in flight, and secondly to offer an indication of what modes might be expected to arise naturally in flying insects. This is not to say that the natural modes of motion of flying insects will be the same as those of aircraft: they almost certainly will not be. Nevertheless, in the absence of much empirical data on the natural modes of insect flight, those of aircraft provide the closest intuition available into what a natural mode might look like in insect flight.

In a symmetrical aircraft, symmetric disturbances can induce no asymmetric forces, and therefore lead to pure longitudinal motions with no lateral component. Aircraft typically display two longitudinal modes: a fast pitching oscillation known as the short-period mode, and a slower oscillation in forward speed and altitude known as the phugoid mode. The short-period mode arises when the restoring pitching moments that provide pitch stability are strong enough to cause the system to overcorrect a pitch disturbance. In contrast, the phugoid mode arises as a consequence of the interchange of kinetic and potential energy which occurs as a result of the changes in lift which accompany changes in airspeed. Most aircraft also display three modes involving lateral motions: a complicated oscillation involving roll, yaw, and sideslip motions known as the Dutch roll mode, a motion involving steadily changing roll, yaw, and sideslip known as the spiral mode, and a motion involving steadily decreasing roll rate known as the roll subsidence mode. The Dutch roll mode arises when the restoring yawing moments that provide yaw stability are strong enough to cause the system to overcorrect a yaw disturbance, causing it to couple in to a roll oscillation lagging the yaw oscillation by approximately 90°. The spiral mode arises when the aircraft is already banked, which causes a sideslipping motion into which the restoring yawing moments that provide yaw stability cause the aircraft to turn. The roll subsidence mode arises during fast rolling motions as a result of the increased angle of attack of the leading wing and decreased angle of attack of the trailing wing. Qualitatively, most aircraft display all five of these natural modes of motion, although quantitatively they do of course differ.

Should we expect insects to display similar modes? The interchange of kinetic and potential energy which underpins the phugoid mode is an inevitable consequence of the general physical principle of conservation of energy, while the asymmetric change in angle of attack which leads to the roll subsidence mode applies as much to insects as to aircraft. It is therefore

reasonable to expect that insects will also display both the phugoid and roll subsidence modes. The other three modes arise as a result of features conferring pitch or yaw stability, and although the physical bases of these are very different in insects and aircraft, it makes no difference to the rigid-body motions how the restoring yawing and pitching moments are generated. It is therefore reasonable to expect that natural modes of motion similar to the short-period mode, Dutch roll mode, and spiral mode will also be displayed by flying insects, although the details are likely to differ. In any case, it is inevitable that flying insects will have natural modes of motion of some sort. For the time being, we may therefore take as our null hypothesis that the natural modes of motion displayed by flying insects are qualitatively similar to those displayed by aircraft. In support of this, the few studies which have derived equations of motion for flying insects have found at least some of the same modes: Taylor and Thomas (2003) working with *Schistocerca* and Sun and Xiong (2005) modelling *Bombus* both found a fast pitching mode closely resembling the short-period mode of aircraft among the longitudinal flight dynamics. Nevertheless, we expect that the details of the natural modes of motion of insects will be shown to differ from those of aircraft in various ways, as the dynamics of insect flight become better known. For example, the natural pitch dynamics of *Schistocerca* appear to be entrained by the periodic forcing of the wing beat (Taylor and Żbikowski, 2005).

The reason why natural modes of motion are so important is that they dictate the trajectories which a mechanical system will naturally follow – indeed, all the free motions of a linear system can be represented as a linear sum of its natural modes of motion and its equilibrium state. What is usually meant by a free motion in an aircraft is one in which the control system is turned off, but it is equally valid to define a free motion as one with the automatic control system operating in closed loop but with no pilot input. By analogy, we may consider as free motions those which an insect displays in response to external perturbations when it is not trying voluntarily to manoeuvre, as distinct from those forced motions which an insect may display during voluntary manoeuvres. This is important, because a mechanical system can be forced to move along any trajectory if it is forced appropriately. Nevertheless, we may expect that insects will have been selected to manoeuvre in a manner consistent with their natural modes of motion, as these offer the paths of least resistance for turning. By way of illustration, it is possible to keep a damped pendulum, such as a child's swing, oscillating indefinitely with very little effort, provided that it is forced at the same frequency as its natural motion and in an appropriate phase. In the same way, the banked turns which commercial aircraft use to manoeuvre are closely related to the spiral mode, with the difference that in a correctly coordinated banked turn the sideslip is kept at zero. Hence, in addition to dictating the trajectories which an insect will follow after an

external perturbation, an insect's natural modes of motion are also likely to be reflected in the ways in which it voluntarily manoeuvres.

Against this backdrop, it should be clear that it is important for the natural modes of motion to be observable by the control system. This can be guaranteed by having an orthogonal sensing system measuring all of the kinematic variables, but can also be achieved by having a non-orthogonal sensing system tuned to the specific combinations of motion that are experienced when each of the natural modes is excited. For example, the directional sensitivity of the VS4–VS10-cells of *Calliphora* (Fig. 11) is such that they should be able to sense Dutch roll oscillations. Since the Dutch roll mode involves coupled yaw and roll oscillations that are approximately 90° out of phase, the instantaneous axis of rotation will scan harmonically around the eye equator provided that the azimuth of the head either (a) leads the azimuth of the body, or (b) is stabilised in response to changes in the azimuth of the body. Kern *et al.* (2006) have shown that the azimuth of the head indeed leads the azimuth of the body during voluntary manoeuvres, and in this case, the combination of head azimuth and roll-rotation during a Dutch roll would tend to excite the VS4–VS10-cells sequentially. Conversely, the gaze stabilisation reflexes discussed in Section 3.1.1 should ensure that the azimuth of the head is stabilized against changes in body azimuth during involuntary motions, and in this case, the combination of head azimuth and roll-rotation during a Dutch roll would tend to inhibit the VS4–VS10-cells sequentially. By the same token, the directional sensitivity of the VS1–VS2-cells appears to be appropriate for detecting a spiral mode or banked turn, while that of VS3 appears to be appropriate for detecting the onset or recovery from such motions. The VS-neurons should therefore ensure that the Dutch roll mode and spiral mode are observable in *Calliphora*.

The hypothesis that the sensors of flying insects are tuned to sense their natural modes of motion therefore makes explicit and testable predictions about how the sensory axes should be arranged if the modes are to be observable. To formalise this for a linear system, the directions of its sensory axes should be arranged to coincide with the eigenvectors characterising its natural modes, although the general hypothesis does not assume or require linearity. The natural-mode sensing hypothesis also allows us to predict how sensory input from different modalities should be combined. The modes of motion that we have discussed combine changes in some or all of the different kinematic state variables. It follows that measurements of these should be combined by the sensory system in the same way as the kinematic states themselves are combined in the natural modes of motion in order to enhance the observability of the different modes. Unfortunately, we know too little about the quantitative details of multi-modal integration in insect flight control to permit us to make even a tentative test of this prediction. Nevertheless, the hypothesis makes sense of why insects might want to combine multi-modal sensory input in the first place.

To formalise this hypothesis for a linear system, we propose that the multi-modal integration of sensory input by the nervous system of insects effects a transformation from a coordinate system in state space to a coordinate system defined by its eigenvectors. This is known in the engineering literature as a modal coordinate system, although the terminology is unfortunate in a biological context, because 'modal' in this case refer to dynamic modes, rather than to sensory modalities. In aircraft flight dynamics analyses, transformations to modal coordinates are often used to aid in the analysis of a problem, because they make it particularly clear how to observe and control each mode (Bryson, 1994; Stevens and Lewis, 2003). This is because each modal coordinate represents one of the natural modes of motion, such that a measurement in any one modal coordinate provides all the feedback needed to observe and control the corresponding mode of motion.

Our hypothesis that flying insects are tuned to sense excitation of their natural modes of motion is consistent with what we know empirically about the anatomy, physiology, and behaviour of insect sensory systems. It also seems in principle to be a very natural route along which selection would have caused such systems to evolve. Based on physiological observation alone, Rowell and Reichert (1986) proposed that the sensory interneurons of insects had an 'emergent modality' resulting from the combination of input from different sensory modalities, which was matched to specific patterns of disturbance. Our hypothesis that insects are tuned to sense their natural modes of motion offers a physical basis for this physiological intuition, and shows that instead of being an abstract emergent property, the modality of the sensory interneurons may in fact be rooted deeply in physical reality. Far from being separate domains, the physics and physiology of insect flight are indeed tightly linked. Together they hold the key to understanding the adaptive significance of the rich array of sensors that enable insects to control their flight with such finesse.

Acknowledgements

We are grateful to Steve Simpson and Jerome Casas for their invitation to contribute this chapter, and thank Rafał Żbikowski, Simon Laughlin, Adrian Thomas, Richard Bomphrey, Johnny Evers, Gregg Abate, and Ric Wehling for many helpful discussions. GKT is a Royal Society University Research Fellow and RCUK Academic Fellow. This research is sponsored by the BBSRC under grant numbers BB/C518573/1 and BB/C007336/2, and by the Air Force Office of Scientific Research, Air Force Material Command, USAF, under grant number FW8655-05-1-3066. The U.S. Government is authorised to reproduce and distribute reprints for Governmental purpose notwithstanding any copyright notation thereon.

References

Altman, J. S., Anselment, E. and Kutsch, W. (1978). Postembryonic development of an insect sensory system: ingrowth of axons from hindwing sense organs in locusta migratoria. *Proc. Roy. Soc. Lond. B* **202**, 497–516.

Anon. (1946). Nature's gyroscopes. *Time*.

Baader, A., Schafer, M. and Rowell, C. H. F. (1992). The perception of the visual flow field by flying locusts-a behavioral and neuronal analysis. *J. Exp. Biol.* **165**, 137–160.

Bacon, J. and Möhl, B. (1979). Activity of an identified wind interneurone in a flying locust. *Nature* **278**, 638–640.

Bacon, J. and Möhl, B. (1983). The tritocerebral commissure giant (TCG) wind-sensitive interneurone in the locust. I. Its activity in straight flight. *J. Comp. Physiol. A* **150**, 439–452.

Bacon, J. and Tyrer, M. (1978). The tritocerebral commissure giant (TCG): a bimodal interneurone in the locustt, *Schistocerca gregaria*. *J. Comp. Physiol. A* **126**, 317–325.

Bacon, J. and Tyrer, M. (1979). The innervation of the wind-sensitive head hairs of the locust, *Schistocerca gregaria*. *Physiol. Entomol.* **4**, 301–309.

Baird, E., Srinivasan, M. V., Zhang, S. and Cowling, A. (2005). Visual control of flight speed in honeybees. *J. Exp. Biol.* **208**, 3895–3905.

Barron, J. L., Fleet, D. J. and Beauchemin, S. S. (1994). Performance of optical flow techniques. *Intern. J. Comp. Vis.* **12**, 43–77.

Bässler, U. (1958). Versuche zur Orientierung der Stechmücken: die Schwarmbildung und die Bedeutung des Johnstonschen Organs. *Z. Vergl. Physiol.* **41**, 300–330.

Bauer, C. K. and Gewecke, M. (1991). Motoneural control of antennal muscles in *Locusta migratoria*. *J. Insect Physiol.* **37**, 551–562.

Bausenwein, B. and Fischbach, K. F. (1992). Activity labeling patterns in the medulla of *Drosophila melanogaster* caused by motion stimuli. *Cell Tissue Res.* **270**, 25–35.

Bayramoglu-Ergene, S. (1964). Untersuchung ueber den Einfluss der Ocellen auf die Fluggeschwindigkeit der Wanderheuschrecke *Schistocerca gregaria*. *Z. Vergl. Physiol.* **48**, 467–480.

Bender, J. A. and Dickinson, M. H. (2006). A comparison of visual and haltere-mediated feedback in the control of body saccades in *Drosophila melanogaster*. *J. Exp. Biol.* **209**, 4597–4606.

Berry, R., van Kleef, J. and Stange, G. (2007a). The mapping of visual space by dragonfly lateral ocelli. *J. Comp. Physiol. A*.

Berry, R., Stange, G., Olberg, R. and van Kleef, J. (2006). The mapping of visual space by identified large second-order neurons in the dragonfly median ocellus. *J. Comp. Physiol. A* **192**, 1105–1123.

Berry, R. P., Stange, G. and Warrant, E. J. (2007b). Form vision in the insect dorsal ocelli: an anatomical and optical analysis of the dragonfly median ocellus. *Vision Res.* **47**, 1394–1409.

Blondeau, J. and Heisenberg, M. (1982). The three-dimensional optomotor torque system of *Drosophila melanogaster*. Studies on wildtype and the mutant optomotor-blind H31. *J. Comp. Physiol. A* **145**, 321–331.

Borst, A. and Egelhaaf, M. (1989). Principles of visual motion detection. *Trends Neurosci.* **12**, 297–306.

Borst, A. and Egelhaaf, M. (1993). Detecting visual motion: theory and models. *Rev. Oculomot. Res.* **5**, 3–27.

Borst, A., Egelhaaf, M. and Haag, J. (1995). Mechanisms of dendritic integration underlying gain control in fly motion-sensitive interneurons. *J. Comput. Neurosci.* **2**, 5–18.

Borst, A., Reisenman, C. and Haag, J. (2003). Adaptation of response transients in fly motion vision. II. Model studies. *Vision Res.* **43**, 1309–1322.

Boyd, K. and Ewer, D. W. (1949). Flight responses in grasshoppers. *S. African Sci.* **2**, 168–169.

Brandstätter, J. H. (1989). Untersuchungen zur Flugsteuerung und Antenneneinstellreaktion von Hummeln. *Zool. Jahrb.* **93**, 203–213.

Brandstätter, J. H. (1990). Some aspects of the significance of the antennae as air-current sense organs in the measurement of flight speed in wasps. *Zool. Jahrb. Physiol.* **94**, 323–331.

Braünig, P. (1985). Mechanoreceptive neurons in an insect brain. *J. Comp. Neurol.* **236**, 234–240.

Braünig, P., Pflüger, H. J. and Hustert, R. (1983). The specificity of central nervous projections of locust mechanoreceptors. *J. Comp. Neurol.* **218**, 197–207.

Brauns, A. (1939). Morphologische und physiologische Untersuchungen zum Halterenproblem unter besonderer Berücksichtigung brachypterer Arten. *Zool. Jahrb. Physiol.* **59**, 245–386.

Brotz, T. M. and Borst, A. (1996). Cholinergic and gabaergic receptors on fly tangential cells and their role in visual motion detection. *J. Neurophysiol.* **76**, 1786–1799.

Bryson, A. E. (1994). *Control of Spacecraft and Aircraft*. Princeton: Princeton University Press.

Buchner, E. (1984). Behavioural analysis of spatial vision in insects. In: *Photoreception and Vision in Invertebrates* (ed. Ali, M. A.), pp. 561–621. New York: Plenum Press.

Buchner, E., Buchner, S. and Hengstenberg, R. (1979). 2-deoxy-d-glucose maps movement-specific nervous activity in the second visual ganglion of *Drosophila*. *Science* **205**, 687–688.

Bulthoff, H., Little, J. and Poggio, T. (1989). A parallel algorithm for real-time computation of optical flow. *Nature* **337**, 549–555.

Burkhardt, D. (1960). Action potentials in the antennae of the blowfly (*Calliphora erythrocephala*) during mechanical stimulation. *J. Insect Physiol.* **4**, 138–145.

Burkhardt, D. and Gewecke, M. (1965). Mechanoreception in Arthropoda: the chain from stimulus to behavioral pattern. *Cold Spring Harb. Symp.* **30**, 601–614.

Burkhardt, D. and Schneider, G. (1957). Die Antennen von *Calliphora* als Anzeiger der Fluggeschwindigkeit. *Z. Naturforsch. B* **12**, 139–143.

Burrows, M. (1996). *The Neurobiology of an Insect Brain*. Oxford: Oxford University Press.

Burrows, M. and Pflüger, H. J. (1992). Output connections of a wind sensitive interneurone with motor neurones innervating flight steering muscles in the locust. *J. Comp. Physiol. A* **171**, 437–446.

Buschbeck, E. K. and Strausfeld, N. J. (1997). The relevance of neural architecture to visual performance: phylogenetic conservation and variation in dipteran visual systems. *J. Comp. Neurol.* **383**, 282–304.

Camhi, J. M. (1969a). Locust wind receptors I. Transducer mechanics and sensory response. *J. Exp. Biol.* **50**, 335–348.

Camhi, J. M. (1969b). Locust wind receptors II. Interneurones in the cervical connective. *J. Exp. Biol.* **50**, 349–362.

Camhi, J. M. (1970a). Sensory control of abdomen posture in flying locusts. *J. Exp. Biol.* **52**, 533–537.
Camhi, J. M. (1970b). Yaw-correcting postural changes in locusts. *J. Exp. Biol.* **52**, 519–531.
Camhi, J. M., Sumbre, G. and Wendler, G. (1995). Wing-beat coupling between flying locust pairs: preferred phase and lift enhancement. *J. Exp. Biol.* **198**, 1051–1063.
Campan, M. (1964). Recherches sur la fonction dynamogène de l'antenne des Insectes. Expériences sur la géotaxie ascensionnelle et la phototaxie positive de *Drosophila melanogaster* Meigen. *Comptes Rendus Séances Soc. Biol. Paris* **158**, 2189–2194.
Chan, W. P. and Dickinson, M. H. (1996). Position-specific central projections of mechanosensory neurons on the haltere of the blow fly, *Calliphora vicina*. *J. Comp. Neurol.* **369**, 405–418.
Chan, W. P., Prete, F. and Dickinson, M. H. (1998). Visual input to the efferent control system of a fly's 'gyroscope'. *Science* **280**, 281–294.
Clifford, C. W., Ibbotson, M. R. and Langley, K. (1997). An adaptive Reichardt detector model of motion adaptation in insects and mammals. *Vis. Neurosci.* **14**, 741–749.
Collett, T., Nalbach, H. O. and Wagner, H. (1993). Visual stabilization in arthropods. *Rev. Oculomot. Res.* **5**, 239–263.
Cook, M. V. (1997). *Flight Dynamics: Principles*. London: Arnold.
Dahmen, H., Franz, M. O. and Krapp, H. G. (2001). Extracting egomotion from optic flow: limits of accuracy and neural matched filters. In: *Motion Vision. Computational, Neural, and Ecological Constraints* (eds Zanker, J. M. and Zeil, J.), pp. 143–168. Berlin: Springer.
Derham, W. (1714). *Physico-theology*. 3rd edn. London: W. Innys.
Dickinson, M. H. (1990a). Comparison of encoding properties of campaniform sensilla on the fly wing. *J. Exp. Biol.* **151**, 245–261.
Dickinson, M. H. (1990b). Linear and nonlinear encoding properties of an identified mechanoreceptor on the fly wing measured with mechanical noise stimuli. *J. Exp. Biol.* **151**, 219–244.
Dickinson, M. H. (1999). Haltere-mediated equilibrium reflexes of the fruit fly, *Drosophila melanogaster*. *Phil. Trans. R. Soc. Lond. B* **354**, 973–980.
Dickinson, M. H., Lehmann, F.-O. and Götz, K. G. (1993). The active control of wing rotation by *Drosophila*. *J. Exp. Biol.* **182**, 185–190.
Dickinson, M. H. and Palka, J. (1987). Physiological properties, time of development, and central projection are correlated in the wing mechanoreceptors of *Drosophila*. *J. Neurosci.* **7**, 4201–4208.
Douglass, J. K. and Strausfeld, N. J. (1995). Visual motion detection circuits in flies: peripheral motion computation by identified small-field retinotopic neurons. *J. Neurosci.* **15**, 5596–5611.
Douglass, J. K. and Strausfeld, N. J. (1996). Visual motion-detection circuits in flies: parallel direction- and non-direction-sensitive pathways between the medulla and lobula plate. *J. Neurosci.* **16**, 4551–4562.
Dror, R. O., O'Carroll, D. C. and Laughlin, S. B. (2001). Accuracy of velocity estimation by Reichardt correlators. *J. Opt. Soc. Am. A* **18**, 241–252.
Egelhaaf, M. (1985a). On the neuronal basis of figure-ground discrimination by relative motion in the visual-system of the fly 1. Behavioral constraints imposed on the neuronal network and the role of the optomotor system. *Biol. Cybern.* **52**, 123–140.
Egelhaaf, M. (1985b). On the neuronal basis of figure-ground discrimination by relative motion in the visual-system of the fly 2. Figure-detection cells, a new class of visual interneurones. *Biol. Cybern.* **52**, 195–209.

Egelhaaf, M. (1985c). On the neuronal basis of figure-ground discrimination by relative motion in the visual-system of the fly 3. Possible input circuitries and behavioral significance of the FD-cells. *Biol. Cybern.* **52**, 267–280.
Egelhaaf, M. and Borst, A. (1993). Movement detection in arthropods. *Rev. Oculomot. Res.* **5**, 53–77.
Egelhaaf, M., Kern, R., Krapp, H. G., Kretzberg, J., Kurtz, R. and Warzecha, A.-K. (2002). Neural encoding of behaviourally relevant visual-motion in the fly. *Trends Neurosci.* **25**, 89–104.
Eggers, A., Preiss, R. and Gewecke, M. (1991). The optomotor yaw response of the desert locust, *Schistocerca gregaria*. *Physiol. Entomol.* **16**, 411–421.
Elson, R. C. (1987a). Flight motor neurone reflexes driven by strain-sensitive wing mechanoreceptors in the locust. *J. Comp. Physiol. A* **161**, 747–760.
Elson, R. C. (1987b). Integration of wing proprioceptive and descending exteroceptive sensory inputs by thoracic interneurones of the locust. *J. Exp. Biol.* **128**, 193–217.
Elson, R. C. (1987c). Interneuronal processing of inputs from the campaniform sensilla of the locust hindwing. *J. Comp. Physiol. A* **161**, 761–776.
Farrow, K., Haag, J. and Borst, A. (2006). Nonlinear, binocular interactions underlying flow field selectivity of a motion-sensitive neuron. *Nat. Neurosci.* **9**, 1312–1320.
Faust, R. (1952). Unterschungen zum Halterenproblem. *Zool. Jahr.* **63**, 325–366.
Faust, R. and von Buddenbrock, W. (1951). Die Regulierung des Gleichgewichtes der höheren Dipteren durch die Halteren. *Experientia* **7**, 265–266.
Fayyazuddin, A. and Dickinson, M. H. (1996). Haltere afferents provide direct, electrotonic input to a steering motor neuron in the blowfly, *Calliphora*. *J. Neurosci.* **16**, 5225–5232.
Fayyazuddin, A. and Dickinson, M. H. (1999). Convergent mechanosensory input structures the firing phase of a steering motor neuron in the blowfly, *Calliphora*. *J. Neurophysiol.* **82**, 1916–1926.
Fraenkel, G. (1939). The function of the halteres of flies (Diptera). *Proc. Zool. Soc. Lond. A* **109**, 69–78.
Fraenkel, G. and Pringle, J. W. S. (1938). Halteres as gyroscopic organs of equilibrium. *Nature* **141**, 919–920.
Franceschini, N., Riehle, A. and Le Nestour, A. (1989). Directional selective motion detection by insect neurons. In: *Facets of Vision* (eds Stavenga, D. G. and Hardie, R.), pp. 360–390. Heidelberg, Berlin: Springer.
Franz, M. O. and Krapp, H. G. (2000). Wide-field, motion-sensitive neurons and matched filters. *Biol. Cybern.* **83**, 185–199.
Frye, M. A. and Dickinson, M. H. (2004). Motor output reflects the linear superposition of visual and olfactory inputs in *Drosophila*. *J. Exp. Biol.* **207**, 123–131.
Gauck, V., Egelhaaf, M. and Borst, A. (1997). Synapse distribution on vch, an inhibitory, motion-sensitive interneuron in the fly visual system. *J. Comp. Neurol.* **381**, 489–499.
Geiger, G. and Nässel, D. R. (1981). Visual orientation behaviour of flies after selective laser beam ablation of interneurones. *Nature* **293**, 398–399.
Geiger, G. and Poggio, T. (1977). On head and body movements of flies. *Biol. Cybern.* **25**, 177–180.
Gettrup, E. (1965). Sensory mechanisms in locomotion: the campaniform sensilla of the insect wing and their function during flight. *Cold Spring Harb. Symp.* **30**, 615–622.
Gettrup, E. (1966). Sensory regulation of wing twisting in locusts. *J. Exp. Biol.* **44**, 6–17.

Gettrup, E. and Wilson, D. M. (1964). The lift control reaction of flying locusts. *J. Exp. Biol.* **41**, 173–191.
Gewecke, M. (1967a). Der Bewegungsapparat der Antennen von *Calliphora erythrocephala*. *Z. Morph. Ökol. Tiere.* **59**, 95–133.
Gewecke, M. (1967b). Die Wirkung von Luftströmung auf die Antennen und das Flugverhalten der blauen Schmeissfliege *Calliphora erythrocephala*. *Z. Vergl. Physiol.* **54**, 121–164.
Gewecke, M. (1970). Antennae: another wind-sensitive receptor in locusts. *Nature* **225**, 1281–1296.
Gewecke, M. (1971). Der unterschiedliche Einfluss der Antennen und Stirnhaare von *Locusta migratoria* auf die Fluggeschwindigkeit. *Naturwissenschaften* **58**, 101.
Gewecke, M. (1972a). Antennen und Stirn-Scheitelhaare von *Locusta migratoria* als Luftströmungs-Sinnesorgane bei der Flugsteuerung. *J. Comp. Physiol.* **80**, 57–94.
Gewecke, M. (1972b). Bewegungsmechanismus und Gelenkrezeptoren der Antennen von *Locusta migratoria* L. (Insecta, Orthoptera). *Z. Morp. Tiere* **71**, 128–149.
Gewecke, M. (1975). The influence of the air current sense organs on the flight behaviour of *Locusta migratoria*. *J. Comp. Physiol.* **103**, 93–97.
Gewecke, M. (1979). Central projection of antennal afferents for the flight motor in *Locusta migratoria* (Orthoptera: Acrididae). *Entomol. Gener.* **5**, 317–320.
Gewecke, M. and Heinzel, H.-G. (1980). Aerodynamic and mechanical properties of the antennae as air-current sense organs in *Locusta migratoria* I. Static characteristics. *J. Comp. Physiol. A* **139**, 357–366.
Gewecke, M., Heinzel, H.-G. and Philippen, J. (1974). Role of antennae of the dragonfly *Orthetrum cancellatum* in flight control. *Nature* **249**, 579–592.
Gewecke, M. and Niehaus, M. (1981). Flight and flight control by the antennae in the small tortoiseshell (*Aglais urticae* L., Lepidoptera) I. Flight balance experiments. *J. Comp. Physiol. A* **145**, 231–258.
Gewecke, M. and Odendahl, A. (2004). Der Bewegungensapparat der Antennen der Großen Blaupfeils *Orthetrum cancellatum* (Odonata: Libellulidae). *Entomol. Gener.* **27**, 73–85.
Gewecke, M. and Philippen, J. (1978). Control of the horizontal flight-course by air-current sense organs in *Locusta migratoria*. *Physiol. Entomol.* **3**, 35–53.
Gewecke, M. and Schlegel, P. (1968). Der Mechanismus der Antennenschwingungen von *Calliphora*. *Verh. d. Dtsch. Zool. Ges.* **62**, 399–404.
Gewecke, M. and Schlegel, P. (1970). Die Schwingungen der Antenne und ihre Bedeutung für die Flugsteuerung bei *Calliphora erythrocephala*. *Z. Vergl. Physiol.* **67**, 325–362.
Gibson, J. J. (1950). *The Perception of the Visual World*. Boston: Houghton Mifflin.
Gilbert, C., Gronenberg, W. and Strausfeld, N. J. (1995). Oculomotor control in calliphorid flies: head movements during activation and inhibition of neck motor neurons corroborate neuroanatomical predictions. *J. Comp. Neurol.* **361**, 285–297.
Gnatzy, W., Grünert, U. and Bender, M. (1987). Campaniform sensilla of *Calliphora vicina* (Insecta, Diptera). I. Topography. *Zoomorphology* **106**, 312–319.
Goodman, L. J. (1981). The organization and physiology of the insect ocellar system. In: *Handbook of Sensory Physiology* (ed. Autrum, H.), pp. 201–286. Berlin: Springer.
Göpfert, M. C. and Robert, D. (2001a). Active auditory mechanics in mosquitoes. *Proc. Roy. Soc. Lond. B* **268**, 333–339.
Göpfert, M. C. and Robert, D. (2001b). Turning the key on *Drosophila* audition. *Nature* **411**, 908.

Göpfert, M. C. and Robert, D. (2003). Motion generation by *Drosophila* mechanosensory neurons. *Proc. Nat. Acad. Sci. USA* **100**, 5514–5519.
Götz, K. G. (1975). The optomotor equilibrium of the *Drosophila* navigation system. *J. Comp. Physiol. A* **99**, 187–210.
Götz, K. G. (1983). Genetic defects of visual orientation in *Drosophila*. *Verh. Dtsch. zool. Ges.* **76**, 83–99.
Götz, K. G. and Buchner, E. (1978). Evidence for one-way movement detection in the visual system of *Drosophila*. *Biol. Cybern.* **31**, 243–248.
Götz, K. G. and Wandel, U. (1984). Optomotor control of the force of flight in *Drosophila* and *Musca* II. Covariance of lift and thrust in still air. *Biol. Cybern.* **51**, 113–143.
Götz, K. G. and Wehrhahn, C. (1984). Optomotor control of the force of flight in *Drosophila* and *Musca* I. Homology of wingbeat-inhibiting movement detectors. *Biol. Cybern.* **51**, 129–134.
Griss, C. and Rowell, C. H. F. (1986). Three descending interneurons reporting deviation from course in the locust. I. Anatomy. *J. Comp. Physiol. A* **158**, 765–774.
Gronenberg, W., Milde, J. J. and Strausfeld, N. J. (1995). Oculomotor control in calliphorid flies: organization of descending neurons to neck motor neurons responding to visual stimuli. *J. Comp. Neurol.* **361**, 267–284.
Gronenberg, W. and Strausfeld, N. J. (1990). Descending neurons supplying the neck and flight motor of diptera: physiological and anatomical characteristics. *J. Comp. Neurol.* **302**, 973–991.
Grünert, U. and Gnatzy, W. (1987). Campaniform sensilla of *Calliphora vicina* (Insecta, Diptera). II. Typology. *Zoomorphology* **106**, 320–328.
Guthrie, D. M. (1964). Observations on the nervous system of the flight apparatus in the locust *Schistocerca gregaria*. *Q. J. Micr. Sci.* **105**, 183–201.
Guthrie, D. M. (1966). The function and fine structure of the cephalic airflow receptor in *Schistocerca gregaria*. *J. Cell Sci.* **1**, 463–470.
Haag, J. and Borst, A. (1996). Amplification of high-frequency synaptic inputs by active dendritic membrane processes. *Nature* **379**, 639–641.
Haag, J. and Borst, A. (2002). Dendro-dendritic interactions between motion-sensitive large-field neurons in the fly. *J. Neurosci.* **22**, 3227–3233.
Haag, J. and Borst, A. (2004). Neural mechanism underlying complex receptive field properties of motion-sensitive interneurons. *Nat. Neurosci.* **7**, 628–634.
Haag, J., Wertz, A. and Borst, A. (2007). Integration of lobula plate output signals by DNOVS1, an identified premotor descending neuron. *J. Neurosci.* **27**, 1992–2000.
Hardie, R. C. (1986). The photoreceptor array of the dipteran retina. *Trends Neurosci.* **9**, 419–423.
Harris, R. A., O'Carroll, D. C. and Laughlin, S. B. (1999). Adaptation and the temporal delay filter of fly motion detectors. *Vision Res.* **39**, 2603–2613.
Harris, R. A., O'Carroll, D. C. and Laughlin, S. B. (2000). Contrast gain reduction in fly motion adaptation. *Neuron* **28**, 595–606.
Haskell, P. T. (1960). The sensory equipment of the migratory locust. *Symp. Zool. Soc. Lond.* **3**, 1–23.
Hassenstein, B. and Reichardt, W. (1953). Der Schluss von Reiz-Reaktions-Funktionen auf System-Strukturen. *Z. Naturforsch. B* **8**, 518–524.
Hausen, K. (1982). Motion sensitive interneurons in the optomotor system of the fly I. The horizontal cells – structure and signals. *Biol. Cybern.* **45**, 143–156.
Hausen, K. (1984). The lobula-complex of the fly: structure, function and significance in visual behaviour. In: *Photoreception and Vision in Invertebrates* (ed. Ali, M. A.), pp. 523–559. New York: Plenum Press.

Hausen, K. (1993). Decoding of retinal image flow in insects. *Rev. Oculomot. Res.* **5**, 203–235.

Hausen, K. and Egelhaaf, M. (1989). Neural mechanisms of visual course control in insects. In: *Facets of Vision* (eds Stavenga, D. G. and Hardie, R.), pp. 391–424. Heidelberg: Springer.

Hausen, K. and Wehrhahn, C. (1983). Microsurgical lesion of horizontal cells changes optomotor yaw responses in the blowfly *Calliphora erythrocephala*. *Proc. Roy. Soc. Lond. B* **219**, 211–216.

Heide, G. (1983). Neural mechanism of flight control in Diptera. In: *BIONA Report*, Vol. 2 (ed. Nachtigall, W.), pp. 35–52. Mainz: Gustav Fischer Akad. Wiss.

Heide, G. and Götz, K. G. (1996). Optomotor control of course and altitude in *Drosophila melanogaster* is correlated with distinct activities of at least three pairs of flight steering muscles. *J. Exp. Biol.* **199**, 1728–1732.

Heinzel, H.-G. and Gewecke, M. (1979). Directional sensitivity of the antennal campaniform sensilla in locusts. *Naturwissenschaften* **66**, 212–213.

Heinzel, H.-G. and Gewecke, M. (1987). Aerodynamic and mechanical properties of the antennae as air-current sense organs in *Locusta migratoria* I. Dynamic characteristics. *J. Comp. Physiol. A* **161**, 671–680.

Heisenberg, M. and Wolf, R. (1984). *Vision in Drosophila*. Genetics of Microbehaviour. Berlin: Springer.

Heisenberg, M. and Wolf, R. (1993). The sensory-motor link in motion-dependent flight control of flies. In: *Visual Motion and Its Role in the Stabilization of Gaze*, Ch. 12 (eds Miles, F. A. and Wallman, J.), pp. 258–286. London: Elsevier Science.

Heisenberg, M., Wonneberger, R. and Wolf, R. (1978). Optomotor-blind H31 – *Drosophila* mutant of lobula plate giant neurons. *J. Comp. Physiol.* **124**, 287–296.

Heitwerth, J., Kern, R., van Hateren, J. H. and Egelhaaf, M. (2005). Motion adaptation leads to parsimonious encoding of natural optic flow by blowfly motion vision system. *J. Neurophysiol.* **94**, 1761–1769.

Hengstenberg, R. (1977). Spike responses of 'non-spiking' visual interneurone. *Nature* **270**, 338–340.

Hengstenberg, R. (1982). Common visual response properties of giant vertical cells in the lobula plate of the blowfly *Calliphora*. *J. Comp. Physiol.* **149**, 179–193.

Hengstenberg, R. (1984). Roll-stabilization during flight of the blowfly's head and body by mechanical and visual cues. In: *Localization and Orientation in Biology and Engineering* (eds Varjú, D. and Schnitzler, H. U.), pp. 121–134. Heidelberg: Springer.

Hengstenberg, R. (1988). Mechanosensory control of compensatory head roll during flight in the blowfly *Calliphora erythrocephala* Meig. *J. Comp. Physiol. A* **163**, 159–168.

Hengstenberg, R. (1991). Gaze control in the blowfly *Calliphora*: a multisensory two-stage integration process. *The Neurosciences* **3**, 19–29.

Hengstenberg, R. (1993). Multisensory control in insect oculomotor systems. *Rev. Oculomot. Res.* **5**, 285–298.

Hengstenberg, R. (1995). Gain differences of gaze-stabilizing head movements, elicited by wide-field pattern motion, demonstrate in wildtype and mutant *Drosophila*, the importance of HS-and VS-neurons in the third visual neuropil for the control of turning behaviour. *Proceedings of the 4th International Congress Neuroethology*, p. 264, Stuttgart, New York: Thieme.

Hengstenberg, R., Hausen, K. and Hengstenberg, B. (1982). The number and structure of giant vertical cells (VS) in the lobula plate of the blowfly *Calliphora erythrocephala*. *J. Comp. Physiol.* **149**, 163–177.

Hengstenberg, R., Sandeman, D. C. and Hengstenberg, B. (1986). Compensatory head roll in the blowfly *Calliphora* during flight. *Proc. Roy. Soc. Lond. B* **227**, 455–482.

Hensler, K. and Robert, D. (1990). Compensatory head rolling during corrective flight steering in locusts. *J. Comp. Physiol. A* **166**, 685–693.

Heran, H. (1957). Die Bienenantenne als Messorgan der Flugeigengeschwindigkeit. *Naturwissenschaften* **44**, 475.

Heran, H. (1959). Wahrnehmung und Regelung der Flugeigengeschwindigkeit bei *Apis mellifica* L. *Z. Vergl. Physiol.* **42**, 103–163.

Hollick, F. S. J. (1940). The flight of the dipterous fly *Muscina stabulans* Fallén. *Phil. Trans. R. Soc. Lond. B* **230**, 383–392.

Homberg, U., Christensen, T. A. and Hildebrand, J. G. (1989). Structure and function of the deutocerebrum in insects. *Annu. Rev. Entomol.* **34**, 477–501.

Honegger, H.-W., Allgäuer, C., Klepsch, U. and Welker, J. (1990). Morphology of antennal motoneurons in the brains of two crickets, *Gryllus bimaculatus* and *Gryllus campestris*. *J. Comp. Neurol.* **291**, 256–268.

Horn, E. and Bischof, H.-J. (1983). Gravity reception in crickets: the influence of cercal and antennal afferences on the head position. *J. Comp. Physiol. A* **150**, 93–98.

Horn, E. and Kessler, W. (1975). The control of antennae lift movements and its importance on the gravity reception in the walking blowfly, *Calliphora erythrocephala*. *J. Comp. Physiol.* **97**, 189–203.

Horsmann, U., Heinzel, H.-G. and Wendler, G. (1983). The phasic influence of self-generated air current modulations on the locust flight motor. *J. Comp. Physiol. A* **150**, 427–438.

Huston, S. J. (2005). Neural basis of a visuo-motor transformation in the fly. Ph.D. thesis, Cambridge University, Cambridge, UK.

Huston, S. J. and Krapp, H. G. (2003). The visual receptive field of a fly motor neuron. In: *Göttingen Neurobiology Report 2003*, pp. 483–483. Stuttgart: Thieme.

Janet, C. (1911). Sur l'existence d'un organe chordotonal et d'une vésicule pulsatile antennaires chez l'abeille et sur la morphologie de la tête de cette espèce. *C. R. Acad. Sci.* **152**, 110–112.

Jian, S. and Horridge, G. A. (1991). The H1 neuron measures changes in velocity irrespective of contrast frequency, mean velocity or velocity modulation frequency. *Phil. Trans. R. Soc. Lond. B* **331**, 205–211.

John, J. D. and Vinay, T. (2006). Novel concept of a single-mass adaptively controlled triaxial angular rate sensor. *IEEE Sens. J.* **6**, 588–595.

Kalmus, H. (1945). Correlations between flight and vision, and particularly between wings and ocelli in insects. *Proc. Roy. Entomol. Soc. Lond. A* **20**, 84–96.

Karmeier, K., van Hateren, J. H., Kern, R. and Egelhaaf, M. (2006). Encoding of naturalistic optic flow by a population of blowfly motion-sensitive neurons. *J. Neurophysiol.* **96**, 1602–1614.

Karmeier, K., Krapp, H. G. and Egelhaaf, M. (2003). Robustness of the tuning of fly visual interneurons to rotatory optic flow. *J. Neurophysiol.* **90**, 1626–1634.

Karmeier, K., Krapp, H. G. and Egelhaaf, M. (2005). Population coding of self-motion: applying Bayesian analysis to a population of visual interneurons in the fly. *J. Neurophysiol.* **94**, 2182–2194.

Kern, R., van Hateren, J. H. and Egelhaaf, M. (2006). Representation of behaviourally relevant information by blowfly motion-sensitive visual interneurons requires precise compensatory head movements. *J. Exp. Biol.* **209**, 1251–1260.

Kern, R., van Hateren, J. H., Michaelis, C., Lindemann, J. P. and Egelhaaf, M. (2005). Function of a fly motion-sensitive neuron mateches eye movements during free flight. *PLoS Biol.* **3**, 1130–1138.

van Kleef, J., James, A. C. and Stange, G. (2005). A spatiotemporal white noise analysis of photoreceptor responses to UV and green light in the dragonfly median ocellus. *J. Gen. Physiol.* **126**, 481–497.

Kloppenburg, P. (1995). Anatomy of the antennal motoneurons in the brain of the honeybee (*Apis mellifera*). *J. Comp. Neurol.* **363**, 333–343.

Kloppenburg, P., Camazine, S. M., Sun, X. J., Randolph, P. and Hildebrand, J. G. (1997). Organization of the antennal motor system in the sphinx moth *Manduca sexta*. *Cell Tissue Res.* **287**, 425–433.

Knyazeva, N. I. (1970). Receptors of the wing apparatus regulating the flight of the migratory locust, *Locusta migratoria* L. (Orthoptera, Acrididae). *Entomol. Rev.* **49**, 311–317.

Koenderink, J. J. and van Doorn, A. J. (1987). Facts on optic flow. *Biol. Cybern.* **56**, 247–254.

Kondo, H. (1978). Efferent system of the lateral ocellus in the dragonfly: its relationship with the ocellar afferent units, the compound eyes, and the wing sensory system. *J. Comp. Physiol. A* **125**, 341–349.

Krapp, H. G. (2000). Neuronal matched filters for optic flow processing in flying insects. *Int. Rev. Neurobiol.* **44**, 93–120.

Krapp, H. G., Hengstenberg, B. and Henstenberg, R. (1998). Dendritic structure and receptive-field organization of optic flow processing interneurons in the fly. *J. Neurophysiol.* **79**, 1902–1917.

Krapp, H. G. and Hengstenberg, R. (1996). Estimation of self-motion by optic flow processing in single visual interneurons. *Nature* **384**, 447–468.

Krapp, H. G. and Hengstenberg, R. (1997). A fast stimulus procedure to determine local receptive field properties of motion-sensitive visual interneurons. *Vision Res.* **37**, 233–235.

Krapp, H. G., Hengstenberg, R. and Egelhaaf, M. (2001). Binocular contributions to optic flow processing in the fly visual system. *J. Neurophysiol.* **85**, 733–740.

Kutsch, W., Camhi, J. and Sumbre, G. (1994). Close encounters among flying locusts produce wing-beat coupling. *J. Comp. Physiol. A* **174**, 643–649.

Land, M. F. (1973). Head movements of flies during visually guided flight. *Nature* **243**, 299–300.

Land, M. F. (1997). Visual acuity in insects. *Annu. Rev. Entomol.* **42**, 147–177.

Land, M. F. and Nilsson, D. E. (2002). *Animal Eyes*. Oxford: Oxford University Press.

Lappe, M. (2000). Computational mechanisms for optic flow analysis in primate cortex. *Int. Rev. Neurobiol.* **44**, 235–268.

Laughlin, S. B. (1989). The role of sensory adaptation in the retina. *J. Exp. Biol.* **146**, 39–62.

Laughlin, S. B. (2001). Efficiency and complexity in neural coding. *Novartis Found. Symp.* **239**, 177–187.

Laughlin, S. B. and Hardie, R. C. (1978). Common strategies for light adaptation in the peripheral visual systems of fly and dragonfly. *J. Comp. Physiol. A* **128**, 319–340.

Lehmann, F. O. and Gotz, K. G. (1996). Activation phase ensures kinematic efficacy in flight-steering muscles of *Drosophila melanogaster*. *J. Comp. Physiol. A* **179**, 311–322.

Lindemann, J. P., Kern, R., van Hateren, J. H., Ritter, H. and Egelhaaf, M. (2005). On the computations analyzing natural optic flow: quantitative model analysis of the blowfly motion vision pathway. *J. Neurosci.* **25**, 6435–6448.

Liske, E. (1977). The influence of head position on the flight behaviour of the fly, *Calliphora erythrocephala*. *J. Insect Physiol.* **23**, 375–379.
Maddess, T. and Laughlin, S. B. (1985). Adaptation of the motion-sensitive neuron H-1 is generated locally and governed by contrast frequency. *Proc. Roy. Soc. Lond. B* **225**, 251–275.
Miall, R. C. (1990). Visual control of steering in locust flight – the effects of head movement on responses to roll stimuli. *J. Comp. Physiol. A* **166**, 735–744.
Milde, J. J., Seyan, H. S. and Strausfeld, N. J. (1987). The neck motor system of the fly *Calliphora erythrocephala* 2. Sensory organization. *J. Comp. Physiol. A* **160**, 225–238.
Miles, F. A. and Wallman, J. (1993). *Visual motion and its role in the stabilization of gaze*. Amsterdam: Elsevier.
Miller, P. L. (1971). The possible stabilising function of the elytra of *Atractocerus brevicornis* (L.) (Lymexylidae: Coleoptera) in flight. *Entomologist* **104**, 105–110.
Mittelstaedt, H. (1950). Physiologie des Gleichgewichtssines bei fliegenden Libellen. *Z. Vergl. Physiol.* **32**, 422–463.
Mizunami, M. (1995). Functional diversity of neural organization in insect ocellar systems. *Vision Res.* **35**, 445–453.
Mobbs, P. G., Guy, R. G., Goodman, L. J. and Chappell, R. L. (1981). Relative spectral sensitivity and reverse Purkinje shift in identified L neurons of the ocellar retina. *J. Comp. Physiol.* **144**, 91–97.
Möhl, B. and Bacon, J. (1983). The tritocerebral commissure giant (TCG) wind-sensitive interneurone in the locust. II. Directional sensitivity and role in flight stabilisation. *J. Comp. Physiol. A* **150**, 453–465.
Nakayama, K. and Loomis, J. M. (1974). Optical velocity patterns, velocity-sensitive neurons, and space perception: a hypothesis. *Perception* **3**, 63–80.
Nalbach, G. (1993). The halteres of the blowfly *Calliphora*. I. Kinematics and dynamics. *J. Comp. Physiol.* **173**, 299–304.
Nalbach, G. (1994). Extremely non-orthogonal axes in a sense organ for rotation: behavioural analysis of the dipteran haltere system. *Neuroscience* **61**, 155–163.
Nalbach, G. and Hengstenberg, R. (1994). The halteres of the blowfly *Calliphora*. II. Three-dimensional organization of compensatory reactions to real and simulated rotations. *J. Comp. Physiol. A* **175**, 708–709.
Nalbach, H. O. (1989). Three temporal frequency channels constitute the dynamics of the optokinetic system of the crab, carcinus-maenas (L.). *Biol. Cybern.* **61**, 59–70.
Nässel, D., Högmo, O. and Hallberg, E. (1984). Antennal receptors in the blowfly *Calliphora erythrocephala*. I. The gigantic central projection of the pedicellar campaniform sensillum. *J. Morphol.* **180**, 159–169.
Nässel, D. R. and Hagberg, M. (1985). Ocellar interneurones in the blowfly *Calliphora erythrocephala* – morphology and central projections. *Cell. Tissue Res.* **242**, 417–426.
Neese, V. (1965). Zur Funktion der Augenborsten bei der Honigbiene. *Z. Vergl. Physiol.* **49**, 543–585.
Neese, V. (1966). Zur Bedeutung der Augenborsten bei der Fluggeschwindigkeits-regulation der Bienen. *Z. Vergl. Physiol.* **52**, 149–154.
Neri, P. and Laughlin, S. B. (2005). Global versus local adaptation in fly motion-sensitive neurons. *Proc. Roy. Soc. Lond. B* **272**, 2243–2249.
Niehaus, M. (1981). Flight and flight control by the antennae in the small tortoiseshell (*Aglais urticae* L., Lepidoptera) II. Flight mill and free flight experiments. *J. Comp. Physiol. A* **145**, 262–266.

Niehaus, M. and Gewecke, M. (1978). The antennal movement apparatus in the small tortoiseshell (*Aglais urticae* L., Insecta, Lepidoptera). *Zoomorphologie* **91**, 19–36.

Page, K. L. and Matheson, T. (2004). Wing hair sensilla underlying aimed hindleg scratching of the locust. *J. Exp. Biol.* **207**, 2691–2703.

Parsons, M. M., Krapp, H. G. and Laughlin, S. B. (2006). A motion-sensitive neurone responds to signals from the two visual systems of the blowfly, the compound eyes and ocelli. *J. Exp. Biol.* **209**, 4464–4474.

Pfau, H. K., Koch, U. T. and Möhl, B. (1989). Temperature dependence and response characteristics of the isolated wing hinge stretch receptor in the locust. *J. Comp. Physiol. A* **165**, 247–252.

Pflüger, H.-J. and Tautz, J. (1982). Air movement sensitive hairs and interneurons in *Locusta migratoria*. *J. Comp. Physiol. A* **145**, 369–380.

Pierantoni, R. (1976). A look into the cockpit of a fly. *Cell Tissue Res.* **171**, 101–122.

Pix, W., Nalbach, G. and Zeil, J. (1993). Strepsipteran forewings are haltere-like organs of equilibrium. *Naturwissenschaften* **80**, 379–381.

Preiss, R. (1992). Set point of retinal velocity of ground images in the control of swarming flight of desert locusts. *J. Comp. Physiol. A* **171**, 251–256.

Preiss, R. and Spork, P. (1993). Flight-phase and visual-field related optomotor yaw responses in gregarious desert locusts during tethered flight. *J. Comp. Physiol. A* **172**, 727–742.

Pringle, J. W. S. (1948). The gyroscopic mechanism of the halteres of Diptera. *Phil. Trans. R. Soc. Lond. B* **233**, 347–384.

Pringle, J. W. S. (1957). *Insect Flight*. Cambridge: Cambridge University Press.

Reichardt, W. (1961). Autocorrelation, a principle for the evaluation of sensory information by the central nervous system. In: *Principles of Sensory Communications* (ed. Rosenblith, W. A.), pp. 303–317. New York: Wiley.

Reichardt, W. (1987). Evaluation of optical motion information by movement detectors. *J. Comp. Physiol. A* **161**, 533–547.

Reichardt, W., Egelhaaf, M. and Schlogl, R. W. (1988). Movement detectors provide sufficient information for local computation of 2-D velocity field. *Naturwissenschaften* **75**, 313–315.

Reichardt, W., Poggio, T. and Hausen, K. (1983). Figure-ground discrimination by relative movement in the visual-system of the fly 2. Towards the neural circuitry. *Biol. Cybern.* **46**, 1–30.

Reichert, H. and Rowell, C. H. F. (1986). Neuronal circuits controlling flight in the locust – how sensory information is processed for motor control. *Trends Neurosci.* **9**, 281–283.

Rowell, C. H. F. (1988). Mechanisms of flight steering in locusts. *Experientia* **44**, 369–401.

Rowell, C. H. F. (1989). Descending interneurones of the locust reporting deviation from flight course: what is their role in steering? *J. Exp. Biol.* **146**, 177–194.

Rowell, C. H. F. and Reichert, H. (1986). Three descending interneurons reporting deviation from course in the locust. II. Physiology. *J. Comp. Physiol. A* **158**, 775–794.

Rowell, C. H. F. and Reichert, H. (1991). Mesothoracic interneurons involved in flight steeing in the locust. *Tissue Cell* **23**, 75–139.

Saager, F. and Gewecke, M. (1989). Antennal reflexes in the desert locust *Schistocerca gregaria*. *J. Exp. Biol.* **147**, 519–532.

Sandeman, D. C. (1980). Angular acceleration, compensatory head movements and the halteres of flies (*Lucilia serricata*). *J. Comp. Physiol. A* **136**, 367–373.
Sandeman, D. C. and Markl, H. (1980). Head movements in flies (*Calliphora*) produced by deflexion of the halteres. *J. Exp. Biol.* **85**, 43–60.
Sane, S. P., Dieudonné, A., Willis, M. A. and Daniel, T. L. (2007). Antennal mechanosensors mediate flight control in moths. *Science* **315**, 863–866.
van der Schaaf, A. and van Hateren, J. H. (1996). Modelling the power spectra of natural images: statistics and information. *Vision Res.* **36**, 2759–2770.
Schilstra, C. and van Hateren, J. H. (1999). Blowfly flight and optic flow. I. Thorax kinematics and flight dynamics. *J. Exp. Biol.* **202**, 1481–1490.
Schlegel, P. (1967). Einzelableitungen von einem Stellungsrezeptor im Pedicellus-Funiculus-Gelenk des blauen Brummers (*Calliphora vicina* Rob. Desv., *erythrocephala* Auct.). *Z. Vergl. Physiol.* **55**, 278–285.
Schlegel, P. (1968). Untersuchungen an Mechanorezeptoren der Fliegenantenne. *Verh. d. Dtsch. Zool. Ges.* **1968**, 405–410.
Schlegel, P. (1970). Die Leistungen eines Gelenkrezeptors der Antenne von *Calliphora* für die Perzeption von Luftströmungen. Elektrophysiologie Untersuchungen. *Z. Vergl. Physiol.* **66**, 45–77.
Schneider, D. (1964). Insect antennae. *Annu. Rev. Entomol.* **9**, 103–122.
Schneider, D. and Kaißling, K.-E. (1957). Der Bau der Antenne des Seidenspinners *Bombyx mori* L. II. Sensillen, cuticulare Bildungen und inneren Bau. *Zool. Jahrb. Anat.* **76**, 223–250.
Schneider, G. (1953). Die Halteren der Schmeissfliege (*Calliphora*) als Sinnesorgane und als mechanische Flugstabilisatoren. *Z. Vergl. Physiol.* **35**, 416–458.
Schuppe, H. and Hengstenberg, R. (1993). Optical-properties of the ocelli of *Calliphora erythrocephala* and their role in the dorsal light response. *J. Comp. Physiol. A* **173**, 143–149.
Sherman, A. and Dickinson, M. H. (2003). A comparison of visual and haltere-mediated equilibrium reflexes in the fruit fly *Drosophila melanogaster*. *J. Exp. Biol.* **206**, 271–307.
Sherman, A. and Dickinson, M. H. (2004). Summation of visual and mechanosensory feedback in *Drosophila* flight control. *J. Exp. Biol.* **207**, 133–142.
Shimozawa, T., Murakami, J. and Kumagai, T. (2003). Cricket wind receptors: thermal noise for the highest sensitivity known. In: *Sensors and Sensing in Biology and Engineering* (eds Barth, F. G., Humphrey, J. A. C. and Secomb, T. W.), pp. 145–157. Wien: Springer.
Shoemaker, P. A., O'Carroll, D. C. and Straw, A. D. (2005). Velocity constancy and models for wide-field visual motion detection in insects. *Biol. Cybern.* **93**, 275–287.
Simmons, P. (1980). A locust wind and ocellar brain neurone. *J. Exp. Biol.* **85**, 281–294.
Simmons, P. J. (1999). The performance of synapses that convey discrete graded potentials in an insect visual pathway. *J. Neurosci.* **19**, 10584–10594.
Simmons, P. J., Jian, S. and Rind, F. C. (1993). Responses *in vivo* to light signals by large, 2nd-order ocellar neurons of the blowfly, *Calliphora erythrocephala*. *J. Physiol. Lond.* **473**, 244.
Smola, U. (1970a). Rezeptor- und Aktionspotentiale der Sinneshaare auf dem Kopf der Wanderheuschrecke *Locusta migratoria*. *Z. Vergl. Physiol.* **70**, 335–348.
Smola, U. (1970b). Untersuchung zur Topographie, Mechanik und Strömungsmechanik der Sinneshaare auf dem Kopf der Wanderheuschreke *Locusta migratoria*. *Z. Vergl. Physiol.* **67**, 382–402.
Snodgrass, R. E. (1956). *Anatomy of the Honeybee*. London: Constable.

Spork, P. and Preiss, R. (1993). Control of flight by means of lateral visual stimuli in gregarious desert locusts, *Schistocerca gregaria*. *Physiol. Entomol.* **18**, 188–204.
Srinivasan, M. V. (1977). A visually-evoked roll response in the housefly. Open-loop and closed-loop studies. *J. Comp. Physiol.* **119**, 1–15.
Srinivasan, M. V. (1990). Generalized gradient schemes for the measurement of two-dimensional image motion. *Biol. Cybern.* **63**, 421–431.
Srinivasan, M. V. and Zhang, S. W. (2000). Visual navigation in flying insects. *Int. Rev. Neurobiol.* **44**, 67–92.
Stange, G. (1981). The ocellar component of flight equilibrium control in dragonflies. *J. Comp. Physiol.* **141**, 335–347.
Stange, G. and Howard, J. (1979). An ocellar dorsal light response in a dragonfly. *J. Exp. Biol.* **83**, 353–359.
Stevens, B. L. and Lewis, F. L. (2003). *Aircraft Control and Simulation*, 2nd edn. New Jersey: Wiley.
Strausfeld, N. J. (1976). *Atlas of an Insect Brain*. Berlin: Springer.
Strausfeld, N. J. (1984). Functional neuroanatomy of the blowfly's visual system. In: *Photoreception and Vision in Invertebrates* (ed. Ali, M. A.), pp. 483–522. New York: Plenum Press.
Strausfeld, N. J. and Bassemir, U. K. (1983). Cobalt-coupled neurons of a giant fibre system in diptera. *J. Neurocytol.* **12**, 971–991.
Strausfeld, N. J. and Gronenberg, W. (1990). Descending neurons supplying the neck and flight motor of Diptera: organization and neuroanatomical relationships with visual pathways. *J. Comp. Neurol.* **302**, 954–972.
Strausfeld, N. J. and Seyan, H. S. (1985). Convergence of visual, haltere, and prosternal inputs at neck motor neurons of *Calliphora erythrocephala*. *Cell Tissue Res.* **240**, 601–615.
Strausfeld, N. J., Seyan, H. S. and Milde, J. J. (1987). The neck motor system of the fly *Calliphora erythrocephala* 1. Muscles and motor neurons. *J. Comp. Physiol. A* **160**, 205–224.
Sun, M. and Xiong, Y. (2005). Dynamic flight stability of a hovering bumblebee. *J. Exp. Biol.* **208**, 447–459.
Svidersky, V. L. (1967). Electrical activity in receptors concerned with maintenance of flight in locusts (In Russian). *Dokl. Akad. Nauk. Sci. SSSR* **172**, 1230–1233.
Svidersky, V. L. and Knyazeva, N. I. (1968). Central transformation of impulses sent by the head receptors to the neurons of wing muscles in the locust. (In Russian). *Dokl. Akad. Nauk. Sci. SSSR* **183**, 486–489.
Taylor, C. P. (1981a). Contribution of compound eyes and ocelli to steering of locusts in flight. I. Behavioural analysis. *J. Exp. Biol.* **93**, 1–18.
Taylor, C. P. (1981b). Contribution of compound eyes and ocelli to steering of locusts in flight. II. Timing changes in flight motor units. *J. Exp. Biol.* **93**, 27–32.
Taylor, G. K. (2001). Mechanics and aerodynamics of insect flight control. *Biol. Rev.* **76**, 449–471.
Taylor G. K. (2007). Modelling the effects of unsteady flow phenomena on flapping flight dynamics – stability and control. In: *Flow Phenomena in Nature: A Challenge to Engineering Design*, Vol. 1 (ed. Liebe, R.), pp. 155–166, Ch. 2. Southampton: WIT Press.
Taylor, G. K. and Thomas, A. L. R. (2003). Dynamic flight stability in the desert locust *Schistocerca gregaria*. *J. Exp. Biol.* **206**, 2803–2829.
Taylor, G. K. and Żbikowski, R. W. (2005). Nonlinear time-periodic models of the longitudinal flight dynamics of desert locusts. *J. Roy. Soc. Interface*, 197–221.

Tracey, D. (1975). Head movements mediated by halteres in the fly, *Musca domestica*. *Experientia* **31**, 44–45.

Tu, M. S. and Dickinson, M. H. (1996). The control of wing kinematics by two steering muscles of the blowfly (*Calliphora vicina*). *J. Comp. Physiol.* **178**, 833–845.

Tyrer, N. M. (1981). Transmission of wind information on the head of the locust to flight motor neurons. In: *Neurobiology of Invertebrates Advances in physiological sciences*, Vol. 25 (ed. Salánki, J.), pp. 557–571. New York: Pergamon.

Tyrer, N. M., Bacon, J. P. and Davies, C. A. (1979). Sensory projections from the wind-sensitive head hairs of the locust *Schistocerca gregaria*. Distribution in the central nervous system. *Cell Tissue Res.* **203**, 79–92.

Tyrer, N. M., Pozza, M. F., Humbel, U., Peters, B. H. and Bacon, J. P. (1988). The tritocerebral commissure 'dwarf' (TCD): a major GABA-immunoreactive descending interneuron in the locust. *J. Comp. Physiol. A* **164**, 141–150.

Uchiyama, H. and Katsuki, Y. (1956). Recording of action potentials from the antennal nerve of locusts by means of microelectrodes. *Physiol. Comp. Oecolog.* **4**, 154–163.

Vande Berg, J. S. (1971). Fine structural studies of Johnston's organ in the tobacco hornworm moth, *Manduca sexta* (Johannson). *J. Morphol.* **133**, 439–455.

Varanka, I. and Svidersky, V. L. (1974a). Functional characteristics of the interneurons of wind-sensitive hair receptors on the head in *Locusta migratoria* L. – I. Interneurons with excitatory responses. *Comp. Biochem. Physiol. A* **48**, 411–426.

Varanka, I. and Svidersky, V. L. (1974b). Functional characteristics of the interneurons of wind-sensitive hair receptors on the head in *Locusta migratoria* L. – II. Interneurons with inhibitory responses. *Comp. Biochem. Physiol. A* **48**, 427–438.

Waldron, I. (1967). Neural mechanism by which controlling inputs influence motor outputs in the flying locust. *J. Exp. Biol.* **47**, 225–230.

Warzecha, A. K., Egelhaaf, M. and Borst, A. (1993). Neural circuit tuning fly visual interneurons to motion of small objects. I. Dissection of the circuit by pharmacological and photoinactivation techniques. *J. Neurophysiol.* **69**, 329–339.

Weckstrom, M., Hardie, R. C. and Laughlin, S. B. (1991). Voltage-activated potassium channels in blowfly photoreceptors and their role in light adaptation. *J. Physiol.* **440**, 635–657.

Wehner, R. (1981). Spatial vision in arthropods. In: *Handbook of Sensory Physiology*, Vol. VII/6C (ed. Autrum, H.), pp. 287–616. Berlin: Springer.

Weis-Fogh, T. (1949). An aerodynamic sense organ stimulating and regulating flight in locusts. *Nature* **164**, 873–874.

Weis-Fogh, T. (1956). Biology and physics of locust flight. iv. Notes on sensory mechanisms in locust flight. *Phil. Trans. R. Soc. Lond. B* **239**, 553–584.

Wendler, G. (1974). The influence of proprioceptive feedback on locust flight co-ordination. *J. Comp. Physiol.* **88**, 173–200.

Wendler, G. (1978). The possible role of fast wing reflexes in locust flight. *Naturwissenschaften* **65**, 65–66.

Wigglesworth, V. B. (1946). Organs of equilibrium in flying insects. *Nature* **157**, 655.

Wilson, M. (1978a). Functional organization of locust ocelli. *J. Comp. Physiol.* **124**, 297–316.

Wilson, M. (1978b). Generation of graded potential signals in 2nd order cells of locust ocellus. *J. Comp. Physiol.* **124**, 317–331.

Zaćwilichowski, J. (1934). Über die Innervierung und die Sinnesorgane der Flügel der Feldheuschrecke *Stauroderus biguttulus* (L.). *Bull. Int. Acad. Pol. Sci. Lett. B* **11**, 187–196.

Zanker, J. M., Srinivasan, M. V. and Egelhaaf, M. (1999). Speed tuning in elementary motion detectors of the correlation type. *Biol. Cybern.* **80**, 109–116.

Żbikowski, R. (2004). Sensor-rich feedback control. *IEEE Instrum. Meas. Mag.* **7**, 19–26.

The Biomechanics of Chewing and Plant Fracture: Mechanisms and Implications

Fiona J. Clissold

Behaviour, Physiology and Ecology Research Group, School of Biological Sciences, The University of Sydney, Australia

1 Introduction 318
2 Accessing nutrients in plants 320
3 The mechanics of fracture 324
  3.1 Terminology 324
  3.2 Morphology and fracture 328
4 Morphology of mandibles and associated musculature 330
  4.1 Mandible morphology and its relation to host plant anatomy 330
  4.2 Mandible morphology, particle size and nutrient assimilation 334
  4.3 Phenotypic plasticity 336
5 The kinetics of mandible movement 337
  5.1 Mandible movement 337
  5.2 Integration of mandibular movement during feeding 341
  5.3 Changes in feeding behaviour with ontogeny 346
6 Neural control of mandibular movements 350
  6.1 Relationship between chewing rate and meal size 352
  6.2 Behavioural plasticity 353
7 Costs of consuming tough diets 354
  7.1 Metabolic cost of chewing 354
  7.2 Costs of nutrient dilution and imbalance 355
  7.3 Mandible wear 355
8 Conclusions 357
  Acknowledgements 361
  References 361

Abstract

Herbivores that chew on the leaves of flowering plants have had to evolve mechanisms to propagate fractures through structures that are chemically and physically heterogeneous. Associations exist between mandibular morphology and associated musculature and the nature of the plant diet, with species that feed on grasses sharing a suite of characteristics that differ from the features found in dicot-feeders. This pattern is evident in two

ADVANCES IN INSECT PHYSIOLOGY VOL. 34
ISBN 978-0-12-373714-4
DOI: 10.1186/1741-7007-5-6

major groups of chewing insects, larval Lepidoptera and Acrididae, and reflects differences in the biomechanical properties of leaves, mostly driven by the pattern of leaf venation. To what extent cell walls provide a physical barrier to the extraction of nutrients by acridids and lepidopterans has been the subject of debate. The degree to which a leaf is fragmented influences the rate and amount of nutrients assimilated from the cytoplasm of a plant cell. The mechanisms that influence the fractionation of leaf material by acridids and lepidopterans are complex. Mandible morphology and associated musculature determine first, if fractures can be initiated, second, the maximum size of the 'bites' taken, and third, the degree of post-bite processing (chewing). It is predicted that the degree of fractionation will be inversely related to meal size. On a single food type, large meals are eaten at a faster rate and less time is spent chewing than in smaller meals. The physical characteristics of the food also modify chewing behaviour. I argue that a full understanding of insect nutrition requires consideration of the biomechanics of food processing. Similarly, an understanding of the biomechanics of mandibles must take account of the ultimate function of feeding behaviour; the acquisition of nutrients.

1 Introduction

Terrestrial ecosystems are dominated by plants and insects (Hairston *et al.*, 1960; Strong *et al.*, 1984; Abe and Higashi, 1991; Schoonhoven *et al.*, 1998). Variations in the temporal and spatial quality and quantity of host plants have been used to explain patterns of herbivory and consequences on insect populations (Murdoch, 1966; Coley, 1980; Joern and Gaines, 1990; Tscharntke and Greiler, 1995; Ylioja *et al.*, 1999; Price and Hunter, 2005). To maximize evolutionary fitness an organism needs to meet its nutritional requirements from the surrounding environment (e.g. Joern and Behmer, 1997; Lee *et al.*, 2003; Simpson *et al.*, 2004). Insects attempt to match nutrient supply with demand, via mechanisms that can be separated into three groups: food choice and acquisition, nutrient acquisition from ingested food and post-ingestive balancing (e.g. selective absorption and egestion) (e.g. Zanotto *et al.*, 1993; Simpson *et al.*, 1995; Raubenheimer and Simpson, 1997; Raubenheimer and Jones, 2006). The behavioural and physiological mechanisms that herbivorous insects employ to regulate the intake of multiple nutrients are well understood (e.g. Simpson and Raubenheimer, 2000; Thompson and Redak, 2000; Behmer *et al.*, 2001; Behmer *et al.*, 2003). This knowledge has come from extensive research using artificial diets where all nutrients ingested are available for assimilation. In the 'real world', nutrient assimilation is rarely as indicated by plant chemistry. Leaf anatomical structure is one of the

prominent factors affecting nutrient assimilation. It follows that a major determinant of the availability of nutrients to chewing insects is the 'tools' they possess to process their food and the control they have of these tools.

Patterns of herbivore attack on plant leaves and insect performance often correlate better with leaf anatomical traits than their chemical composition (Feeny, 1970; Coley, 1983; Lowman and Box, 1983; Ohmart *et al.*, 1987; Larsson and Ohmart, 1988; Nichols-Orians and Schultz, 1990; Ohmart and Edwards, 1991; Stevenson *et al.*, 1993; Casher, 1996; Choong, 1996; Peeters *et al.*, 2007). From these studies, overcoming plant structural traits has been inferred to pose a significant problem for insects. However, the influence of leaf anatomical traits has been difficult to ascertain due to the multiplicity of these structural traits and their correlations with plant chemistry (primary and secondary metabolites) (e.g. Peeters, 2002a; Peeters, 2002b; Wright *et al.*, 2004).

Leaf-chewing insects are most prominent amongst the Orthoptera, Lepidoptera, Coleoptera and Hymenoptera. Discussion in this chapter will focus primarily on information gained from studies on acridids and lepidopterans, due to the comparative wealth and scope of information on these two groups. An excellent understanding of the mechanisms regulating feeding behaviour of these two groups has been gained by the use of chemically defined diets (e.g. Simpson, 1995; Simpson *et al.*, 1995; Simpson and Raubenheimer, 2000; Thompson and Redak, 2000; Raubenheimer and Simpson, 2003; Simpson *et al.*, 2004). Such mechanisms have also been related to performance consequences when the optimal amount and blend of nutrients cannot be obtained (e.g. Raubenheimer and Simpson, 1993; Simpson and Raubenheimer, 1993b; Simpson *et al.*, 2004). However, despite the apparent relationship between mandible morphology and plant type eaten, there is almost no knowledge regarding the advantages these morphological differences confer in providing the gut with leaf material and the outcome of this on absolute nutrient gain, i.e. nutrients available for growth and development net of those used to fuel metabolism. The majority of studies of nutrient assimilation by chewing insects on plants have been correlative or descriptive (e.g. Isely, 1944; Bernays, 1991; Slansky, 1993; Chapman, 1995). Studies of this nature have generated numerous hypotheses, many that have become paradigms despite either not having been tested, or if they have been tested, the variables used to infer fitness advantages of a particular morphological trait are questionable. For example, increased intake rate has been used numerous times to claim a particular morphological trait improved fitness (e.g. Bernays 1986; Thompson, 1992). However, intake rate is affected by numerous factors and its link to fitness consequences has not been established.

This chapter will discuss how chewing insects gain nutrients from leaves. Leaves need to be reduced in size to enable them to be ingested. The degree of fragmentation influences not only the amount of nutrients assimilated but

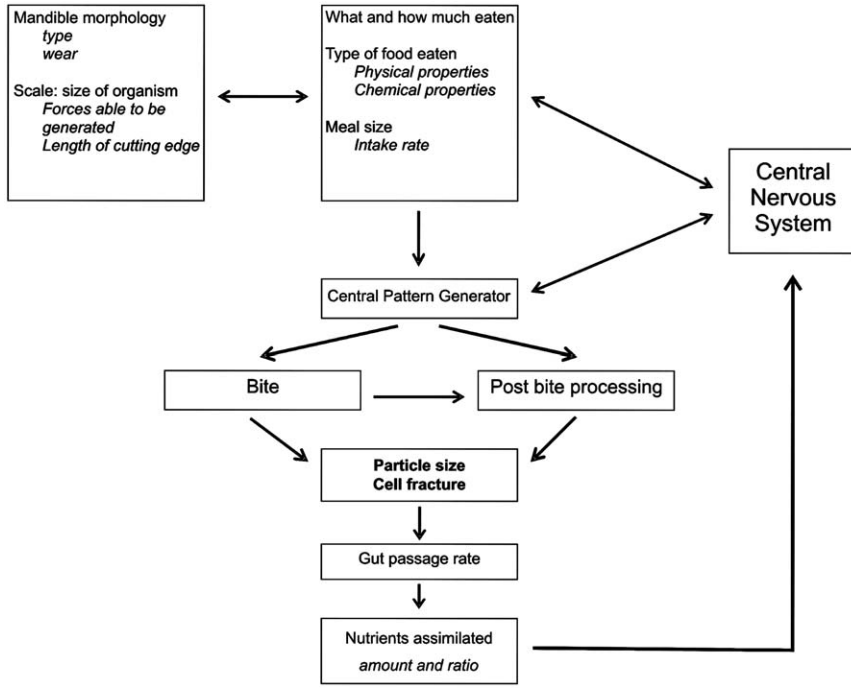

FIG. 1 Flow chart showing the factors that affect the final nutrient gain by a chewing phytophagous insect. The fractures created in leaf material are influenced by the size of the insect, the morphology of its mandibles and the physical and chemical properties of the leaf tissue being ingested. The rate of biting and chewing will be influenced by the interaction between the current nutrition state of the insect and the properties of the diet. See text for explanation.

also the rate at which they are assimilated. The factors that influence the amount of processing (chewing) a leaf undergoes before ingestion include the morphology of the mandibles and associated musculature and the neural control of mandibular movements (Fig. 1). The central nervous system controls what, how much and how quickly an insect eats. The size of the insect determines not only the forces it is able to generate but also the length of the cutting edges of the mandibles. I will demonstrate how each of these factors influences the final size of particles entering the gut, which in turn affects the rate of nutrient assimilation and the ratio of nutrients assimilated.

2 Accessing nutrients in plants

Plants consist of cells, the constituents of which can be divided into two main categories, the cell wall and the cell contents. The cell contents are

usually easily digested by the enzymes found in the saliva and gut of most animals, whilst the majority of the cell wall is not (Bacic *et al.*, 1988; Martin, 1991). Plant cell walls consist of cellulose fibres embedded in a matrix of polysaccharides, proteins and phenolics (Wilson, 1993; Brett and Waldron, 1996), and if utilized would be an abundant source of energy. Very few insects have the ability to degrade plant cell wall (Scrivener *et al.*, 1989; Martin, 1991; Slaytor, 1992; Cazemier *et al.*, 1997) and most of these insects are not leaf chewers (McGinnis and Kasting, 1969; Martin, 1983, 1991; Peterson *et al.*, 1988; Hochuli *et al.*, 1993; Clissold *et al.*, 2004). It has been argued that leaf-chewing insects have no need to utilize the abundant energy contained within the cell wall, because they obtain sufficient energy when they exploit the more easily digestible cell contents to obtain nitrogen (Martin, 1991). Acridids have an abundant gut bacterial flora (Stevenson, 1966; Hunt and Charnley, 1981), but little or no activity of enzymes that degrade cell wall has been found (Evans and Payne, 1964; Morgan, 1975, 1976). Nor is it likely that the cell wall would contribute to their nutritional requirements as acridids are unable to utilize cellulose or the pentoses (Dadd, 1960), which constitute the majority of the hemicellulose (Wilkie, 1979). The extremely short time food is resident in the gut (Uvarov, 1966; Baines *et al.*, 1973; Yang and Joern, 1994; Clissold *et al.*, 2006) may explain why the gut flora appears to play no role in nutrition in acridids (Charnley *et al.*, 1985).

Release of the cytoplasm from within cells can occur due to mechanical fracture of the cell walls, chemical degradation or leakage via pores in the cell wall. Barbehenn (1992, 2005) has argued that fracture of the cell wall is not necessary for leaf-chewing Orthoptera or Lepidoptera to utilize nutrients within the cytoplasm. It is thought that conditions within caterpillar guts facilitate rapid diffusion through cell walls: namely, high pH (Barbehenn, 1992), the presence of surfactants (Martin and Martin, 1984) and efficient phospholipases that degrade cell membranes (Barbehenn, 1989). The presence of surfactants has also been recorded for Orthoptera (Martin and Martin, 1984), but the neutral pH conditions in an acridid digestive tract (Evans and Payne, 1964; Ferreira *et al.*, 1990; Uvarov, 1966) would seem likely to make the dissociation of proteins difficult.

Molecules can pass into and out of plant cells through pores in the cell wall (plasmodesmata). For some molecules, movement can occur very rapidly (less than 10 min). The rate of diffusion is correlated with the radius of the molecule and is highly dependent on the size of the molecules and conditions surrounding the cells (Baron-Epel *et al.*, 1988; Read and Bacic, 1996; Zemke-White *et al.*, 2000; Roberts and Oparka, 2003). Proteins tend to be smaller and more tightly folded than polysaccharides with the same molecular mass, and thus are able to pass through the pores more rapidly. Molecules of starch and amylase can have larger radii (21–75 nm and 7–22 nm, respectively) (Parker and Ring, 2001) than the diameter of

plasmodesmata (*c.* 3.5–8.6 nm) (Read and Bacic, 1996). While polysaccharides may not be able to move out of cells, digestive enzymes can pass into the cells. However, the direction of flow, i.e. molecules out of cells or enzymes into cells, is also influenced by the osmolarity of the surroundings (Carpita *et al.*, 1979; Tepfer and Taylor, 1981). Plasmodesmata differ in their architecture within and between different plant tissue types and their number and pore size decline as leaves develop (reviewed by Roberts and Oparka, 2003). In living plant material, plasmodesmata have considerable control over the passage of molecules (reviewed by Roberts and Oparka, 2003) but it is unknown if facilitated transport occurs within an animal's gut or whether the conditions within the gut reduce plasmodesmata to static pores, which reduces the ability of molecules to pass through them. How particle size or the degree of fracture within leaf tissue affects diffusion through plasmodesmata is unknown.

While nutrients may be able to be obtained without the cell wall being chemically or physically degraded, when cell walls were mechanically fractured before ingestion, nutrient assimilation for an acridid was increased (Clissold *et al.*, 2006), and a caterpillar grew and developed faster (Feeny, 1970). Also, caterpillars that comminuted their food to smaller particles grew faster (Bernays and Janzen, 1988). In a study on the Australian plague locust, *Chortoicetes terminifera* (Clissold *et al.*, 2006), chemical analysis of the diet indicated that the concentration of non-structural carbohydrate was more than double that of protein, suggesting that dietary carbohydrate should have been in excess for an acridid (Raubenheimer and Simpson, 1993; Simpson and Raubenheimer, 1993b; Chambers *et al.*, 1995). When the cell wall was mechanically fractured before ingestion this was indeed the case for locusts, feeding on this diet. However, when feeding on the whole intact leaf blade, due to differential rates of assimilation, protein appeared to be the limiting nutrient, not because of its deficiency but rather its relative excess relative to carbohydrate (Fig. 2) (Clissold *et al.*, 2006). Thus, the degree to which the diet is fragmented appears to be the primary determinant not only of the rate at which nutrients move from the environment to the insect, but also the ratio of the primary macronutrients, protein and carbohydrate which are assimilated.

For the majority of herbivorous animals (mammals and insects) fractionating plant material with the mandibles or teeth is the sole mechanism by which food is processed, and generally the key factor affecting the nutrient assimilation efficiency (e.g. Perez-Barberia and Gordon, 1998; Sanson, 2006). Although the foreguts of most acridids are characterized by a lining of sclerotized spines (Williams, 1954; Uvarov, 1966; Hochuli *et al.*, 1992, 1994), these are thought to be involved in the peristaltic movement of food through the gut and holding the food particles against the influx of digestive enzymes from the midgut

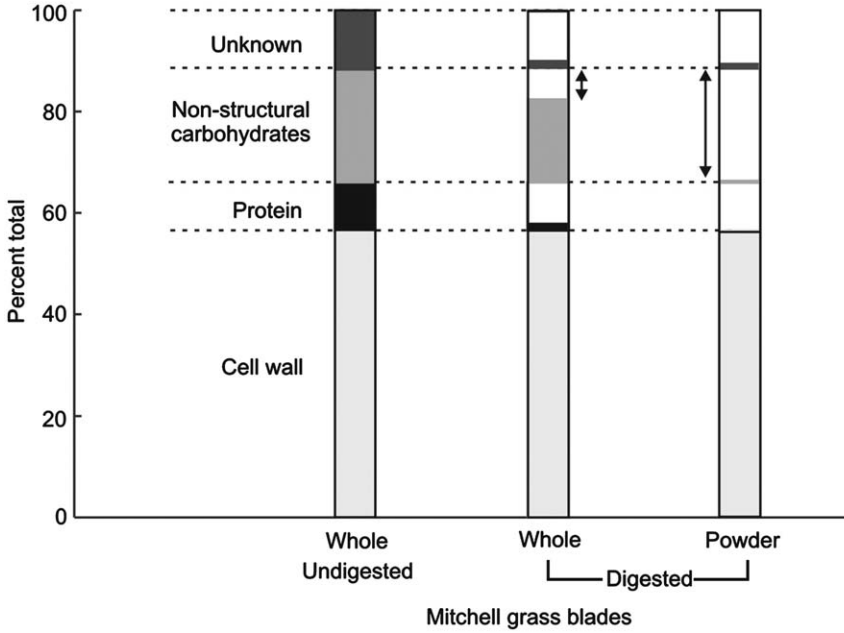

FIG. 2 Relationship between the chemical composition of Mitchell grass blades and the amounts digested by fifth instar Australian plague locusts, *Chortoicetes terminifera*, when feeding on whole leaf blades and when the barrier effects of the cell wall were removed by milling to a powder. Solid colours represent the nutrient component found in the frass. Unshaded areas are the nutrients assimilated by the locust. Cell wall, protein and non-structural carbohydrates were determined directly, the remainder was derived from total dry weights of the plant and frass. The amount of non-structural carbohydrates assimilated was most affected by mechanically fractionating the cell wall (as demonstrated by the length of the arrows).

(Hochuli *et al.*, 1994). For insects, the degree to which cells are fractured during a meal is the result of interactions between the chemical and physical properties of the host plant, the morphological features of the mandibles and chewing behaviour (Fig. 1). An insect is 'stuck' with a set of morphological tools: how much behavioural flexibility it has, may determine the nutritive consequences.

Observations reveal correlations between mandible morphology of chewing insects and the nature of the diet (reviewed by Bernays, 1991; Chapman, 1995). The key morphological features that determine a tooth's effectiveness when consuming a particular food, and the relationship between tooth morphology and chewing behaviour for mammals are still poorly understood, despite having received considerable attention (reviewed by Perez-Barberia and Gordon, 1998; Gordon, 2003). Terms

such as 'grinding', 'shearing' and 'snipping' are regularly encountered in the literature to describe the action of different mandible morphologies when ingesting food. The use of these terms is misleading and, it has been argued, limits understanding of the action of teeth (Lucas, 2004; Sanson, 2006). How teeth interact with each other or the type of fractures generated are not known and is still the subject of much debate (reviewed by Lucas, 2004; Griffiths, 2006). One problem is that the loading of force can be controlled in laboratory tests, when force is applied by the teeth to a food the resulting force is not homogeneous; often one part of the structure is in compression whilst the other is in tension (e.g. bending). Lucas (2004) has provided a comprehensive framework in which to study tooth morphology in relation to the fracture properties of the diet. He argues that to understand mammalian tooth morphology the factors that prevent the initiation and propagation of fractures in foods needs to be understood, rather than the way teeth apply loads (Lucas, 2004). A similar argument will likely apply to insects.

3 The mechanics of fracture

3.1 TERMINOLOGY

In many studies of insect–plant interactions, variations in the textural properties of plants have been invoked as an explanation of host choice or effects on insect performance. The terms hard, soft, strong or tough are often used ambiguously to describe mechanical properties of leaves with little regard for the fracture property that was actually determined or the underlying mechanism(s) that produced that response (Vincent, 1990, 1992c; Wright and Vincent, 1996; Lucas *et al.*, 2000; Sanson *et al.*, 2001).

The principles of mechanical fracture are relatively simple and the various methods used to assess fracture properties are fairly easy to perform (Vincent, 1992a,b,c; Aranwela *et al.*, 1999; Sanson *et al.*, 2001; Lucas, 2004). However, as plant leaves are complex composite structures made from many different materials, there is a lack of consensus on the appropriate way to characterize their fracture properties (Lucas *et al.*, 1995; Choong, 1996; Lucas *et al.*, 2000; Lucas, 2004; Sanson, 2006) and the appropriate techniques to use (Choong, 1996; Read and Sanson, 2003; Lucas, 2004; Read and Stokes, 2006). Each of the various materials that make up a leaf has its own fracture properties and when combined into a structure, the fracture properties of the whole leaf are often very different from that of the individual components (Lucas, 2004; Geitmann, 2006). Each method of assessing the fracture properties of materials and structures has limitations (reviewed by Vincent, 1992c; Aranwela *et al.*, 1999; Sanson *et al.*, 2001; Lucas, 2004). There is no one test that directly

mimics the way that teeth fracture material, as the way the teeth load strain and the resultant fractures are poorly understood (Lucas, 2004; Sanson, 2006). Thus the approach taken needs to be given careful consideration (Sanson *et al.*, 2001; Lucas, 2004).

The mechanics of fracture will be briefly described here as numerous texts have been devoted to this subject (e.g. Lucas and Pereira, 1990; Wright and Vincent, 1996; Sanson *et al.*, 2001; Lucas, 2004; Farquhar and Zhao, 2006). Fragmentation of a material first requires the initiation of a fracture and then its propagation through the material. The action of a *stress* on a material produces displacement which causes it to deform (Fig. 3a). Resistance to this stress is the *stiffness* of the material (or what biologists sometimes call *brittleness*, measured as Young's modulus, *E*). At some point, this deformation in the material changes from being elastic (the material will return to its original shape if the force is removed) to plastic (permanent deformation). This point is known as the *yield strength*. If force continues to be applied, at some point the material will 'fail'

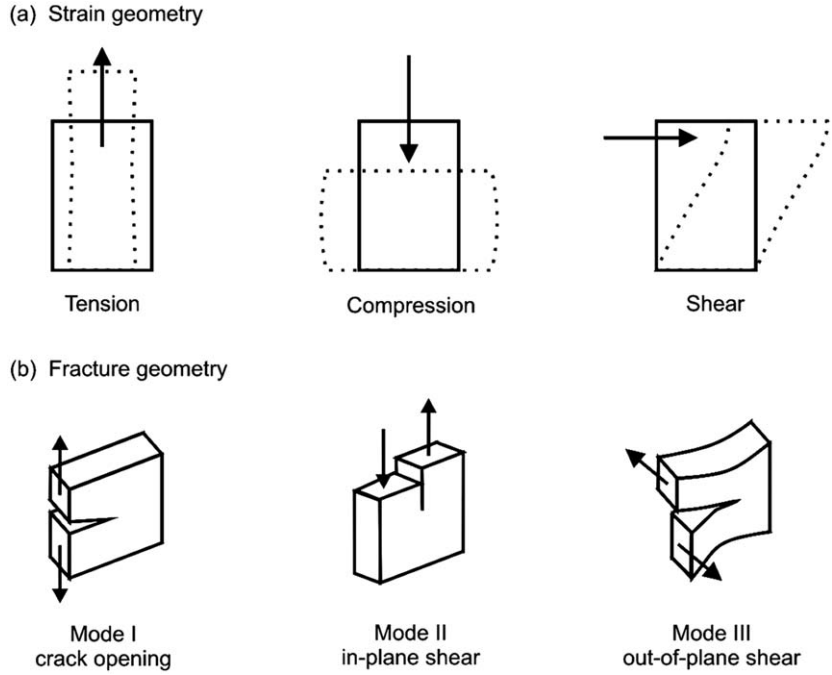

FIG. 3 (a) The three basic ways strain can be loaded onto a material (b) which may promote fracture in one of three ways as described by Atkins and Mai (1985) (adapted from Vincent, 1992c; Wright and Vincent, 1996; Lucas, 2004). The arrows show the direction of displacement. The relationship between loading geometry and fracture geometry will depend on the material.

i.e. cracks will occur. While fracture has been described as occurring in three ways (*Modes*) (Atkins and Mai, 1985; Vincent, 1992c) (Fig. 3b), the relationship between loading geometry and fracture geometry depends on the material (Lucas, 2004). The resistance to crack initiation is termed the *fracture stress* (one measure of strength) of the material, whereas *toughness* is a measure of the resistance to the propagation of that fracture (Atkins and Mai, 1985; Lucas *et al.*, 2000; Sanson *et al.*, 2001). Fracture is controlled by energy. Stresses are the means to provide energy to a particle while the nature of the particle will determine what happens to this energy, i.e. whether or not it will produce fracture (Lucas, 2004). In anisotropic (heterogeneous) materials, such as leaves, applying a stress will result in some tissues fracturing, some tissues reaching their yield strength (plastically deformed), while other tissues may only suffer elastic deformation (Sanson, 2006). Therefore, to fracture composite materials will require the continued initiation of cracks. For herbivores to fragment leaves, Sanson (2006) argues that the primary factor driving tooth shape is one that will promote elastic fracture over plastic deformation as this will maximize damage to the cell wall most energetically efficiently.

Structures fail because either sufficient stress is applied and/or they are displaced sufficiently. Thus, Lucas *et al.* (2000) based on Ashby (1999) proposed that there are two basic strategies plants can employ to prevent herbivores from fracturing leaf tissue and thus prevent its ingestion and subsequent fragmentation:

- *Stress-limited defence*: the prevention of crack initiation due to high-*yield stress* (*stiffness*). 'This occurs when a structural component is organized in such a way that it breaks at a force higher than an animal can achieve without its own structure failing' (Lucas *et al.*, 2000). Lucas proposed that this is achieved by the combination of food properties that increase the square root of toughness multiplied by Young's modulus $(ER)^{0.5}$ (Fig. 4a), or
- *Displacement-limited defence*: making a structural component fail at such a large displacement that it limits the degree of detachment that an herbivore could achieve in a given time. This is achieved with high *toughness* alone if the material is very thin (less than approximately 0.8 mm for plant tissues (Choong, 1996)) or for thicker materials, the square root of the ratio of toughness to Young's modulus $(R/E)^{0.5}$ (Fig. 4b) (Lucas, 2004). Biologists tend to term leaves that have high toughness as being ductile, as when stressed the material bends rather than breaking.

An example of these two mechanisms is a mast and sail on a yacht. The mast (stiff) will snap with very little displacement if stressed by sufficient force, whereas the same stress applied to the sail will cause it to bend without

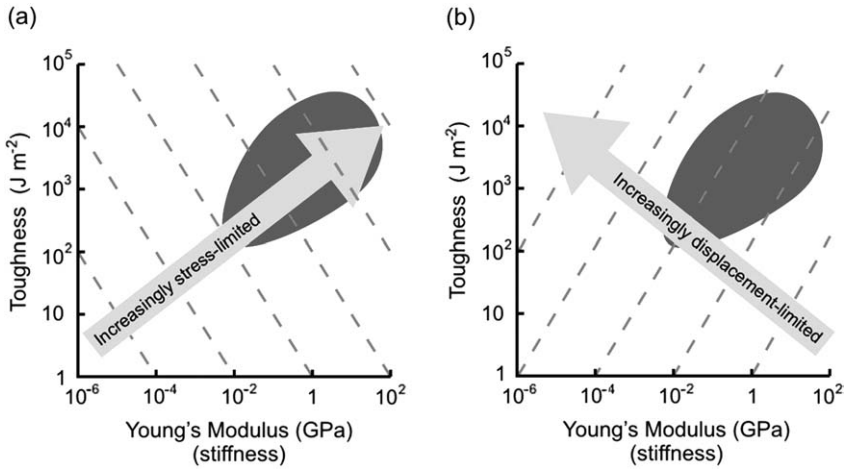

FIG. 4 Plots of toughness (R) versus Young's modulus (E) and the hypothesized relationship of these two factors in preventing the (a) initiation and (b) propagation of fracture (Lucas, 2004). The dashed lines give values of (a) equal $(ER)^{0.5}$ the properties of foods that are thought to prevent the initiation of fracture (stress-limited) and (b) values of equal $(R/E)^{0.5}$ the property of foods that affect resistance to fracture propagation (displacement-limited). The limited data to date, suggests plant leaves fall somewhat randomly within the shaded oval region as toughness and stiffness in leaves are obtained in different ways. Diagram adapted from Lucas (2004).

fracturing (tough). When plotting toughness against stiffness as determined by Young's modulus, plant leaves fall somewhat randomly on the graph as toughness and stiffness are obtained in different ways (Fig. 4) (Lucas, 1994).

Because leaf tissue is physically heterogeneous, the various components will fracture under different conditions, which will vary with the shape of the tool applying the force and the nature of that force (Jeronimidis, 1991; Wright and Vincent, 1996; Lucas, 2004; Sanson, 2006). The properties of leaf tissue that prevent the initiation of cracks are different from those that prevent crack propagation (Lucas *et al.*, 2000). Plant tissues such as spines, thorns, prickles and stiff hairs prevent organisms initiating cracks in them by being extremely dense; the result of not having cellular contents (Lucas *et al.*, 2000). Toughness is influenced by many factors; the amount, composition and organization of cell wall and the tissues it forms, the orientation of the vascular bundles as well as the thickness of the leaf and its cuticle (Lucas *et al.*, 1991; Wright and Illius, 1995; Choong, 1996; Wright and Vincent, 1996).

Stiffness may appear the better strategy for plant leaves to prevent attack from herbivores. However, if sufficient force can be applied to fracture stiff leaves, catastrophic or brittle failure often results

(e.g. shattering of glass) generating many small highly digestible particles. Once a fracture has been initiated in a leaf, its propagation will depend on the toughness of the material, i.e. whether it encounters energy-absorbing materials (crack stoppers) such as vascular bundles or silica deposits. In fact, the leaves of flowering plants seem to have sacrificed stiffness for toughness at many levels of organization; from orienting the cellulose fibres in the S2 layer of the cell wall around rather than parallel to the cellular axis (Choong, 1996), to varying the layout of the vascular bundles. Properties of plants that obstruct crack growth may alter the rate and ratio of nutrient assimilation and thus affect feeding behaviour. Therefore, it is has been hypothesized that, although toughness may be easier to overcome, it may influence patterns of herbivory more than stiffness (Lucas, 2004).

3.2 MORPHOLOGY AND FRACTURE

A major influence on mandible/teeth morphology of insect and mammal herbivores appears to have been the differences in fracture properties conferred by the pattern of leaf venation in different types of plants. The leaves of the two main groups of terrestrial flowering plants exhibit different organization of the veins; reticulate in the dicotyledons (woody plants, herbs and forbs) versus parallel in the monocotyledons (grasses, palms and sedges). This together with the cell wall composition (e.g. the degree of lignification), the ratio of cell wall to cell contents (cell wall volume), and the amount of silica, influences fracture properties and the shape of the tools best suited to fracture them (Wright and Vincent, 1996). The vascular bundles are a major impediment to crack initiation and propagation. It is more difficult to fracture across the parallel venation of grasses than in the same direction, and grass blades with their parallel vascular bundles are relatively insensitive to lateral notches as compared to the leaves of legumes with reticulate veins (Vincent, 1991). Thus for tough materials such as grasses, the more controlled the fracture path, the less energy is lost through deflection of the fracture (energy) into crack stoppers. Blades achieve this best. In less tough plant material, where cell wall volume is low and cracks once initiated will run more freely, cusped teeth that act like a mortar and pestle or 'multiple pestle' may be better at maximizing fracture (Lucas, 2004; Sanson, 2006) (Fig. 5). Cusps do not need to contact each other as they produce fractures ahead of their path (Mode I). For blades, sharpness and the amount of contact will influence the type of fracture produced. Blunt blades that loosely contact each other will produce fractures in Mode I, the direction of these fractures are less controlled than those that occur with sharper blades (Lucas, 2004; Sanson, 2006).

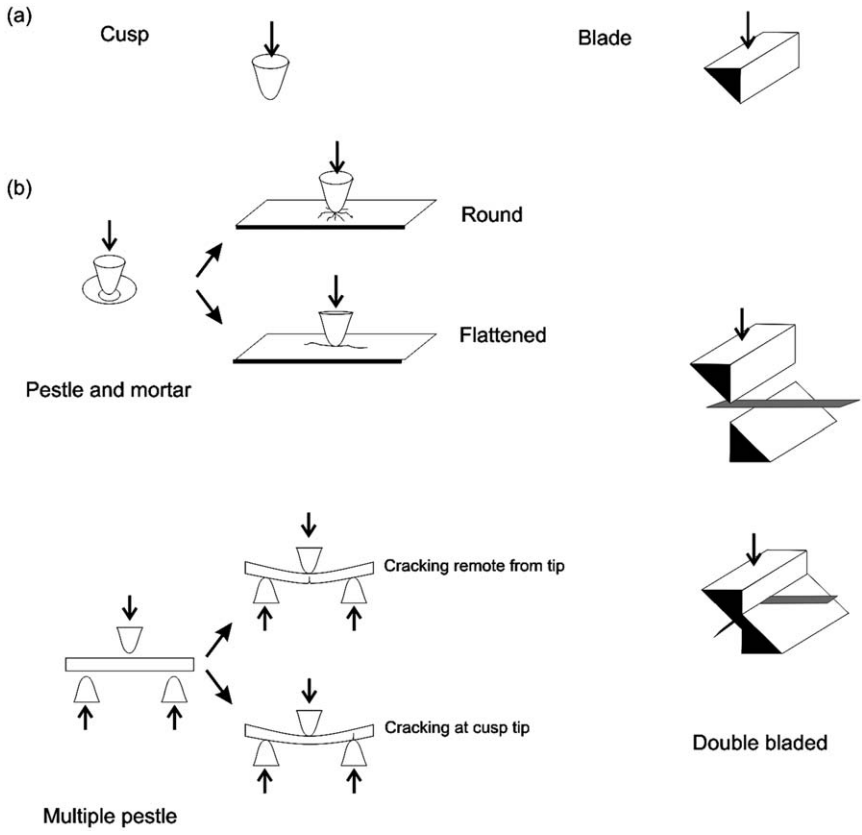

FIG. 5 (a) The hypothesized two basic surfaces of 'tools' (teeth or mandibles) required to fracture plant material; cusps and blades. (b) Cusps can act either singly in a 'pestle and mortar' type design or as 'multiple pestles'. Blades need to act in tandem to be effective. The type of fracture cusps will generate will depend on the shape of the cusp and the material. Double blades are able to control where the fracture occurs. (Diagram adapted from Lucas, 2004).

The size of the structure itself also influences the ability to propagate a fracture through it, although this is poorly understood (Sanson, 2006). Large structures tend to fracture in a more brittle way than smaller ones (Atkins and Mai, 1985). Since neither toughness nor stiffness scale geometrically, as the material is fractured into smaller particles its mechanical properties change (Lucas, 2004; Sanson, 2006). This combined with the discrepancy in size between insects and mammals, means that it is unknown whether the same combination of plant morphological characters that limit fragmentation in mammals will also apply to insects (Sanson, 2006). Compared to mammals, insects produce less force (stress)

and smaller displacement is available. Lucas (2004) argues that for mammals, ingestion will most likely be influenced by properties of the meal that make it stiff (stress-limited), whereas mastication will be limited by toughness (displacement-limited). Hence, mammalian incisors and molars differ in their morphology (Chapman, 1995). As discussed next, insect mandibles show a similar pattern, with the mandibles of caterpillars and acridids often having two distinct regions.

4 Morphology of mandibles and associated musculature

4.1 MANDIBLE MORPHOLOGY AND ITS RELATION TO HOST PLANT ANATOMY

The gnathobasic hexapod mouthparts (Popadic *et al.*, 1998) of phytophagous-chewing insects have been modified to form a pair of sclerotized, toothed structures, the mandibles. These mandibles are analogous to the mammalian tooth and jaw. A typical mandible from a dicondyl insect (all insect orders except the Archaeognatha) consists of two distinct regions; (i) a distal incisor region and (ii) a proximal molar region (Fig. 6). These regions are assumed to be for biting and chewing, arguably comparable to the incisors and molar teeth of mammalian herbivores. The molar region is well developed in acridid but not caterpillar mandibles, although various projections (dentes) are often found on the inner face of a caterpillar mandible (Bernays, 1991).

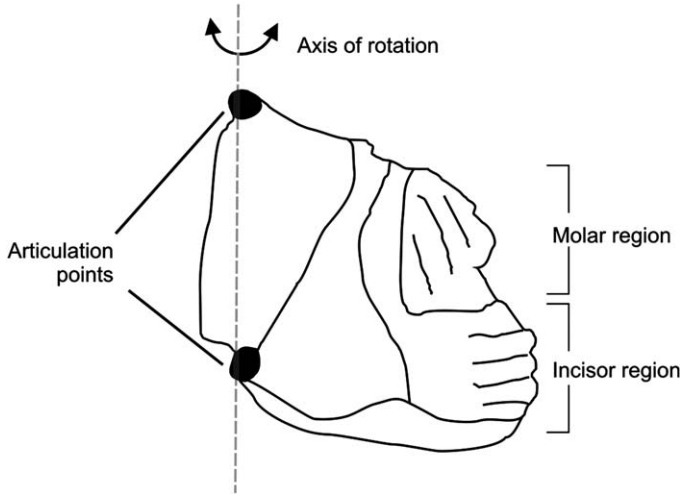

FIG. 6 Morphology of the left mandible from a generalized insect with dicondylar mandibles (all insect Orders except for Archaeognatha), showing the incisor and molar regions, the articulation points and the axis of rotation.

For species of acridids and caterpillars, grass-feeders tend to share convergent features that differ from those of non-grass feeders; these being differences in relative head and mandible size and mandible morphology (Fig. 7). Grass-feeding specialists have a larger head relative to body size compared to non-grass feeders (Patterson, 1984; Bernays, 1986; Bernays and Hamai, 1987). Larger heads appear to result from differences in the cross-sectional area of the mandibular muscle (Bernays and Hamai, 1987) and mandible size (Thompson, 1992). These appear to be functional adaptations to deal with the force needed to fracture grasses versus non-grasses (Patterson, 1984; Bernays, 1991). Bernays (1986; 1991) argued that the relatively larger mandibles and increased muscle mass are adaptations to dealing with hard diets, as C4 grasses are six times harder and C3 grasses three times harder than herbaceous dicots (Bernays and Hamai, 1987). However, the leaves from many woody plants are as hard as C4 grasses (Bernays and Hamai, 1987) and to date there is no information on whether species that feed on woody plants compared to forbs show differences in relative allocation to head size.

There also appears to be a relationship between the relative proportions of incisor length and hinge length, dependent on the hardness of food consumed (Patterson, 1984; Bernays, 1991). Tree-feeding and grass-feeding caterpillars tend to have 'stouter' mandibles than those that consume 'softer' herbaceous forbs (Bernays, 1991); this trend has also been recorded in acridids (Patterson, 1984). In stouter mandibles, the occlusial surface is closer to the hinge, which is thought to provide a mechanical advantage in initiating fracture and/or provide strength to the mandible. Both factors may be critical to the continued initiation of fracture in stiff leaves. Biomechanical modelling of the mandibles as levers (Fig. 8) confirms that 'stouter' mandibles should provide greater mechanical advantage, whereas more velocity can be generated with longer mandibles. This is discussed further in Section 5.

Acridid mandibles are asymmetrical, with the left hand mandible having four incisor cusps overlapping the three cusps of the right mandible. Both mandibles have a median molar cusp and obliquely transverse molar ridges. The right mandible generally has more molar ridges and the left mandible has extra cusps on the inside of the median molar, the inner median molar and the marginal molars. Acridid mandibles have been grouped into three classes based on similarity of morphological characteristics: 'graminivorous' (grass–feeding types), 'forbivorous' (herbaceous forb-feeding types) and 'mixed-feeding' (referred to sometimes as 'herbivorous') types (feed on both grass and herbaceous forbs) (Fig. 7) (Isely, 1944; Patterson, 1984). These categories transcend phylogenetic relationships and appear to be the result of convergent evolution (e.g. Isely, 1944; Chapman, 1964; Patterson, 1983, 1984; Smith and Capinera, 2005). 'Graminivorous' type mandibles are characterized by having very long and

Graminivorous mandibles

Forbivorous mandibles

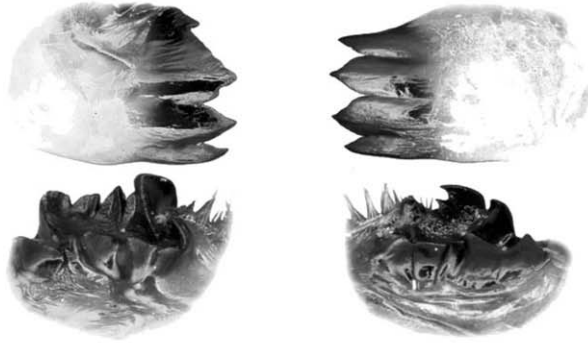

Mixed-feeder mandibles

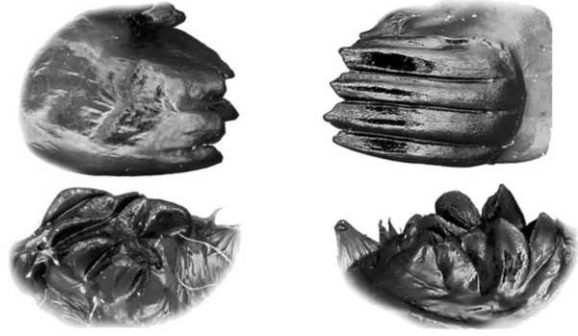

Right Left

relatively blunt left incisor cusps, while the right incisor cusps have chisel-like edges. The molar ridges are well developed on both mandibles, and the left marginal molar cusps are more equally developed. 'Forbivorous' type mandibles have incisors that are shorter with sharply pointed cusps and, instead of parallel molar ridges, various cusps project from the molar region. 'Mixed-feeding' type mandibles tend to have short incisor cusps similar to non-grass feeders but with the molar ridges of a grass-feeder (Fig. 7) (refer Isely, 1944; Chapman, 1964 for a complete description). The increased length of the incisors in grass–feeding species appears to mirror that seen in grass-feeding mammals (hypsodonty).

The association of mandible morphology with diet has not been defined as clearly for lepidopterans, and appears to be more closely aligned with taxonomic relationships than is the case in acridids (Bernays, 1991). Whereas the majority of acridids feed on grasses and/or herbaceous forbs, few lepidopteran species feed on grasses: most feed on plants with reticulated veins such as trees and forbs (Bernays and Barbehenn, 1987; Bernays, 1991); plants whose leaves have significantly different fracture properties to grasses. The mandibles of lepidopterans are not as complex as those of acridids. Typically, they consist of a simple row of incisor cusps with some projections on the oral surface (molar region) (Bernays, 1991). However, there appears to be some morphological similarities in mandible structure in Lepidoptera based on diet venation and fracture properties. Mandibles of lepidopteran larvae that feed on grasses, have blades and those that feed on forbs are toothed, analogous to that seen in orthopterans (Brown and Dewhurst, 1975; Hochuli, 1994). The mandibles of species that feed on plants with reticulated veins that are more succulent are long, toothed and have more complex ridges than those that feed on 'old tough tannin leaves' (Bernays and Janzen, 1988). This may reflect the differences in 'tools' that best fracture tough (succulent) versus hard (old) leaves. Unlike the mandibles of acridids that always close left over right, for mandibles of lepidopterans, even within a species, there is no consistent overlap and the mandibles tend to be more symmetrical (Hillerton, 1986) suggesting that the mandibles of acridids and caterpillars may act quite differently.

To fracture a material, the material doing the fracturing must be harder than that being fractured. In locusts with 'graminivorous' mandibles, the outer surfaces of the mandible incisors and the ridges in the molar region

FIG. 7 Image showing the incisor (top) and molar (bottom) regions from mandibles from *Amblytropidia mysteca*, *Schistocerca ceratiola* and *Spharagemon cristatum* to illustrate the differences in morphologies between the three basic mandible types, 'graminivorous', 'forbivorous' and 'mixed-feeders', respectively. The incisors are shown above the molars for each morphology type. Images from Smith and Capinera (2005).

are harder than the surrounding cuticle (Hillerton *et al.*, 1982). This increased hardness is believed to be predominantly due to the presence of zinc (Hillerton and Vincent, 1982) as well as having cuticle that is structurally different (Gardiner and Khan, 1979). Although cuticle is generally significantly softer than enamel, the impregnation of metals (Hillerton *et al.*, 1984) in the cutting edges of the incisors gives them comparable hardness to enamel (Vincent and Wegst (2004) but see Schoberl and Jager (2006)). The hardness of the mandibles appears to be important for leaf-snipping ants. These ants rarely harvest leaves until zinc has accumulated in the mandible incisors, resulting in a nearly threefold increase in hardness (Schofield *et al.*, 2002).

4.2 MANDIBLE MORPHOLOGY, PARTICLE SIZE AND NUTRIENT ASSIMILATION

To maximize nutrient gain, the optimal size of particles entering the gut may depend on factors other than the degree to which the cell wall is fractured. Biomechanical properties of materials change with size of the material. Fractionating a meal to overly fine particles may not allow the efficient absorption of nutrients or enzyme infiltration into the bolus within the gut (Lentle *et al.*, 2006) at least in mammals. A bolus of small particles has very little elasticity so that when it is compressed by peristaltic action of muscles surrounding the gut, permeation of fluid containing enzymes or digested nutrients occurs more slowly than with larger or more elastic particles (Lentle *et al.*, 2005).

The two factors that will determine the degree to which chewing mandibulate insect herbivores can fractionate their diet are (1) the morphology of their mandibles and (2) the degree to which they can process a leaf fragment once detached. This is likely to be dependent on the size of the insect and the fracture properties of the leaf material being ingested. Small insects may not need to 'chew', as the particles that are created when detaching a fragment may be of a sufficiently small size, or, due to the nature of the leaf material, the action of detaching the leaves may generate fractures within the particles.

The size and complexity of the mandibles appear to influence the degree to which plant material is fragmented. For an acridid, increases in mandible size with instar (age) correlated with reduced nutrient assimilation from a common plant diet (Clissold, 2003). However, not only did nutrient assimilation efficiency decrease with increasing body size, proportionately less carbohydrate compared with protein was assimilated. Particle size would appear to be the main factor determining this, since relative meal size and absolute retention time within the gut did not change with age and instar (Clissold, 2003). A correlation with increased mandible size and particle size was also recorded for saturniid caterpillars (Bernays and Janzen, 1988). These caterpillars appear to fragment leaves only with

the incisors (i.e. the molar region is undifferentiated), and the particles created are fairly uniform in size and scale with the size of the mandibles. By comparison, the mandibles of sphingid caterpillars have a complex array of ridges and dentes on the oral surface (Bernays and Janzen, 1988). The fragments created by sphingids are independent of mandible size and much smaller in size but their shape is more varied than that found for saturniids. Although these two groups of caterpillars consume quite different food types, 'hard' old leaves in the case of saturniids versus 'soft' young leaves in sphingids, it is thought that the differences in the complexity of the mandible surface resulted in differences in leaf fragmentation rather than differences in fracture properties of the two food types (Bernays and Janzen, 1988).

While there appears to be a correlation between mandible morphology and diet, very little is known about how differing mandible morphologies might optimize cell rupture and hence nutrient assimilation. When fed a variety of C3 and C4 grasses and forbs, higher assimilation efficiencies were recorded for acridids with 'mixed-feeding' type mandibles compared to those with 'forbivorous' mandibles (Bennack, 1981). In Bennack's experiment, six grasses (parallel venation) and eight plants with reticulated venation were fed to acridids with contrasting mandible morphologies. Of the available calories, acridids with 'mixed-feeder' type mandibles assimilated 65% while acridids with 'forbivorous' mandibles only assimilated 45%. Only the overall means were reported, not the values for each grass or plant with reticulated venation (Bennack, 1981). Thus, what drove the difference in assimilation efficiency was not determined. Grasshoppers with 'mixed-feeder' type mandibles may have processed both plant types more efficiently or the grasshoppers with 'forbivorous' type mandibles may have been unable to extract nutrients from the grasses. The finding by Boys (1981) that the 'graminivorous' mandibles of acridids were able to 'shear' the adaxial and abaxial surfaces of a grass leaf, exposing the parenchyma, whereas an acridid with 'forbivorous' mandibles could not, suggests that mandible morphology may significantly affect fragmentation of plants and subsequent nutrient assimilation. However, the link between particle size and the number of cells with their walls fractured is not straightforward (Barbehenn, 2005). An acridid with 'mixed-feeder' type mandibles, *Camnula pellucida*, produced on average larger particles than a species with 'forbivorous' type mandibles, *Melanoplus sanguinipes*, when feeding on a common grass. It was found that more cells were crushed by *C. pellucida* than by *M. sanguinipes* (Barbehenn, 2005). However, again utilization efficiency was not determined so the functional significance of the number of crushed cells and particle size is unknown.

Acridids with 'mixed-feeder' type mandibles are host plant generalists, i.e. their diet encompasses many different food types. As such, a food generalists may experience a wide range of nutritional environments which

could make them either nutrient specialists, as they can select between many plants and thus regulate intake within a limited region of nutrient space, or alternatively, they may be nutrient generalists, able to cope with diets that vary considerably in their nutrient ratios (Raubenheimer and Simpson, 1999, 2003). *Locusta migratoria*, the African migratory locust is a specialist grass-feeder with 'graminivorous' mandibles, whereas *Schistocerca gregaria*, the desert locust, feeds on both grasses and forbs and has 'mixed-feeder' type mandibles. When allowed to select their intake of the primary macronutrients found in plants, the mixed-feeder *S. gregaria*, selected both more protein over the last nymphal instar and a diet with more protein relative to carbohydrate compared to the grass-feeding *L. migratoria.* When restricted to a diet high in protein *S. gregaria* was able to tolerate overingestion of protein better than *Locusta*, and was able to use protein-derived carbon as an energy source (Raubenheimer and Simpson, 2003). The higher nitrogen (protein) requirements of *S. gregaria* could reflect the host-plant environment or the limitations of nutrient extraction posed by their mandibles (Bennack, 1981). Herbs and forbs often contain slightly more nitrogen than grasses (Wright *et al.*, 2004) and this may explain the differences in the total amount of protein ingested when the locusts were allowed to select the amount and ratio of protein:carbohydrate ingested (Raubenheimer and Simpson, 2003). However, the efficiency with which nutrients can be assimilated when consuming plant material is directly linked to the degree of leaf fragmentation (Clissold *et al.*, 2006). For the Australian plague locust, *C. terminifera,* relatively less carbohydrate was assimilated compared to protein when factors reduced the efficiency with which total nutrients were assimilated (Clissold, 2003; Clissold *et al.*, 2006). This may be the result of proteins being able to leak through plasmodesmata better than large carbohydrates in non-fragmented cells, coupled with the physiological mechanisms that control gut emptying (Abisgold and Simpson, 1987). Therefore, an insect with 'all-purpose tools', ('mixed-feeder' type mandibles) compared to those with 'specialized tools', ('graminivorous' mandibles), may assimilate different amounts and proportions of protein and carbohydrate while feeding on a plant. The higher protein:carbohydrate intake target of the generalist feeder (*S. gregaria*) may reflect the difficulty in assimilating the available carbohydrate compared to protein from grasses, forbs and herbs.

4.3 PHENOTYPIC PLASTICITY

Differences in head size of newly emerged lepidopteran and coleopteran larvae have been associated with host plant. Larvae from host plants with tough/stiff leaves often have bigger heads (Greene, 1989; Braby, 1994; Pappers *et al.*, 2001). When reared on 'tougher' plant leaves, survival of first instar larvae from three tropical butterfly species from the genus

Mycalesis, correlated positively with head size (Braby, 1994). Having a larger head could be advantageous for two reasons. First, larvae with bigger heads have a bigger gape and for some developing insects, the leaf tissue especially at the leaf margin is wider than their gape (Boys, 1981). Second, insects with larger heads appear to be able to generate more force and thus able to initiate fracture in stiff, tough plant tissues. However, bigger particles are often produced by bigger mandibles (Bernays and Janzen, 1988; Chapman, 1995), which can limit assimilation efficiency. Therefore, it would be predicted that having a relatively larger head may not be as advantageous for older instars (Clissold, 2003; Clissold *et al.*, 2006).

Relative differences in head size can arise through developmental plasticity. Developmental plasticity is thought to be an important component of adaptation to variable environments (West-Eberhard, 2003; Jablonka and Lamb, 2005). Caterpillars and acridids reared on 'hard' diets allocated relatively more resources to their heads than those reared on 'soft' diets (Bernays, 1986; Thompson, 1992), and this appeared to allow them to increase rates of consumption (Bernays, 1986; Thompson, 1992). This is not surprising as bigger insects are able to consume food at a faster rate (Clissold, 2003). However, a very thorough morphometric investigation revealed that while a grasshopper (*Melanoplus femurrubrum*) when reared on 'hard' diet had a relatively larger head than a full-sib reared on a 'soft' diet, there was no difference in the absolute head size between treatments (Thompson, 1999). It appeared that head size was maintained at the expense of other body parts when diets were hard/tough and low in nutrients: the relative head size had increased not because the head had got bigger but because the body was smaller. Perhaps an additional factor for the lack of difference in absolute head size between diet treatments was because feeding on the 'soft' diet may have required more chewing effort than was assumed from the textural properties of the diet (Thompson, 1999).

5 The kinetics of mandible movement

5.1 MANDIBLE MOVEMENT

The mandibles of caterpillars and acridids move in one plane around an axis of rotation occurring between the two condyles (Fig. 6). A pair of muscles inserted into apodemes located on the lateral margin of the mandible base either side of the axis of rotation produce the opening and closing movements of the mandibles. The adductor muscle located on the inner side closes the mandibles and they are opened by the abductor muscle on the outer edge (Chapman, 1995). These two muscles are attached to the

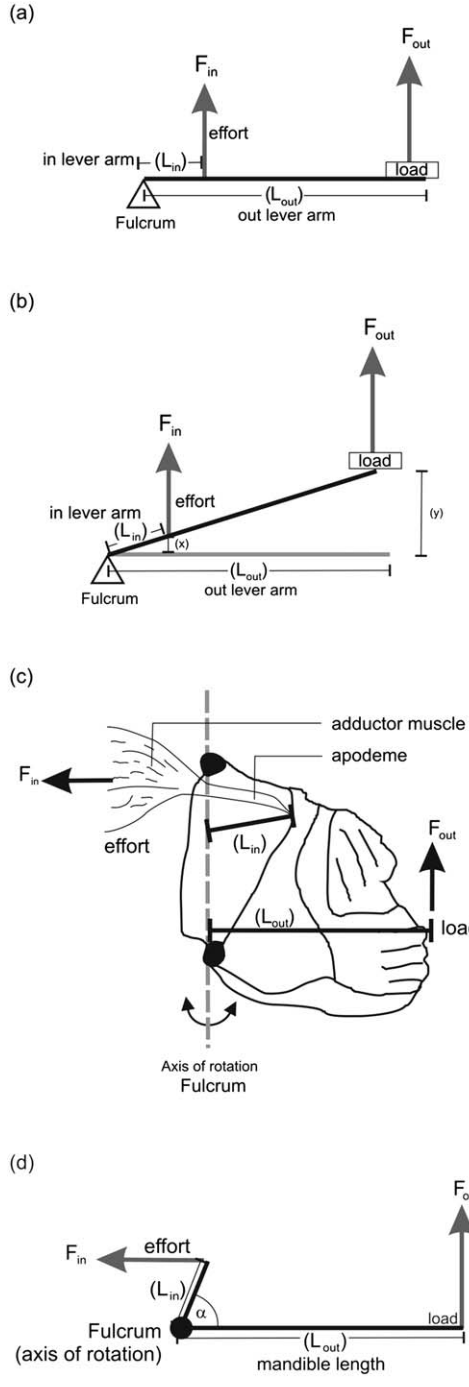
(a)
F_{out}
F_{in}
effort
in lever arm
(L_{in})
load
(L_{out})
out lever arm
Fulcrum
(b)
F_{out}
F_{in}
load
effort
in lever arm
(L_{in})
(x)
(y)
(L_{out})
out lever arm
Fulcrum
(c)
adductor muscle
apodeme
F_{in}
effort
(L_{in})
F_{out}
(L_{out})
load
Axis of rotation
Fulcrum
(d)
F_{out}
F_{in}
effort
(L_{in})
α
load
Fulcrum
(axis of rotation)
(L_{out})
mandible length

upper part of the head capsule and the adductor muscle is considerably larger than the abductor muscle. In all insects except for the Acrididae there are also ventral adductor muscles to assist in controlling mandibular movements (Snodgrass, 1935). Therefore, the mandibles and associated musculature are a kinetic system and, as such, can be modelled to examine their force and motion properties.

Modelling the mandibles and associated musculature as a lever system illustrates that, as the muscles are attached between the axis of rotation and the tip of the mandible, they operate as third-order levers (Fig. 8a). Unlike first-order levers (e.g. seesaws), third-order levers do not have good mechanical advantage, because the effort (muscle) is closer to the fulcrum (condyle) than the load (tip of mandibles). The advantage of such levers is that the distance moved by the load (tip of mandible) is greater than the distance moved by the effort (muscle contraction) (Fig. 8b), giving a velocity advantage (Westneat, 2003). When in equilibrium, the components of such a lever system transfers force from one place (effort) to another (load), and have the following relationship:

$$F_{\text{in}} L_{\text{in}} = F_{\text{out}} L_{\text{out}} \tag{1}$$

where F_{in} is the in force provided by the effort, F_{out} the out force delivered to the load at the tip of the out-lever and L_{out} and L_{in} the length of the out and in-lever, respectively (Fig. 8b). For acridids and caterpillars, F_{in} is provided by the adductor (or abductor) muscle, L_{in} is the distance between the axis of rotation and where the muscle is attached to the mandible and L_{out} is the distance from the axis of rotation to the tip of the incisors (Fig. 8c).

Because $F_{\text{out}} = F_{\text{in}}\, L_{\text{in}}/L_{\text{out}}$, differences in the force generated at the tip of the mandible will depend on the relative lengths of the levers and the force the muscles can generate. The ratio of the length of the in-lever to the length of the out-lever ($L_{\text{in}}/L_{\text{out}}$) gives the mechanical advantage. The

FIG. 8 Modelling mandibles as lever. (a) Diagram showing a third-order lever, the effort is between the fulcrum and the load with the out-lever (L_{out}) being the distance between the fulcrum and the load, and the in-lever (L_{in}) being the distance between the fulcrum and the effort. (b) With such a lever the distance the tip moves through (y) is much greater than the distance provided by the effort (x). (c) For insects with dicondyl mandibles the fulcrum is the axis of rotation between the two condyles, the out-lever is the length of the mandible and effort is provided by the adductor muscle. (d) Using a vector diagram to illustrate the mandibles as levers, the closing mechanical advantage is the ratio between the distance from the mandible adductor muscle attachment to the fulcrum (L_{in}) and the length of the mandible (L_{out}), i.e. $L_{\text{in}}/L_{\text{out}}$. The force that can be generated at the tip of the mandible is a function of the force the muscle can provide, the mechanical advantage and the angle of both muscle attachment and between the two lever arms. Adapted from Westneat (2003, 2004).

greater the length of L_{in} relative to L_{out}, the greater the mechanical advantage and the larger the force that can be generated at the mandible tip. Therefore, it is not surprising the in-lever to open the mandibles is shorter than the in-lever to close the mandibles, i.e. the mandible is asymmetrical around the axis of rotation. For equal F_{in} the mandibles should open faster than they close, which is what occurs in the locust, *S. gregaria,* even though the adductor muscle is very much larger than the abductor muscle (Seath, 1977b).

Levers provide mechanical advantage, but the force generated at the tip of the mandible is also a function of the physiology and size of muscle providing the effort and the angle of attachment (α) (Fig. 8c, d). As the adductor muscle contracts, this angle (α) will change, therefore, the force at the mandible tip will also change during closing (Westneat, 2004). However, calculating this is complex and elegant studies on the muscle fibre attachments of ant adductor muscles to the apodeme demonstrated that the force generated depends not only on the angle of attachment but also on the fibre diameter, its mode of attachment to the apodeme and the size of the apodeme itself (Gronenberg *et al.*, 1997; Paul and Gronenberg, 1999).

Force output would be optimized if the adductor muscle were attached to the apodeme in the direction of pull (0^{o}, i.e. the top of the head). This is never found, because if such a muscle were to contract, the resultant swelling would not fit within the head capsule (Paul and Gronenberg, 1999). The force a single muscle fibre contributes to the total force the adductor muscle can output is influenced by the angle of attachment of that muscle fibres with respect to the muscle's overall direction of pull. Modelling the angle of attachment of the adductor muscle fibres to the apodeme showed that force output is optimized when the angle is between 41°–45° (where 0° is if the muscle was attached to the top of the head) and more speed is generated at lower angles (Paul and Gronenberg, 1999).

The relationship between the force generated by the adductor muscle and the force at the mandible–food interface will be a product of the area over which that force is being applied and the physiological properties of the muscle itself. The force generated at the mandible tips of predaceous beetles is loosely correlated with the cross-sectional area of the adductor muscle, multiplied by its mechanical advantage (calculated as the width of the mandible at its base, divided by the length of the mandible) (Wheater and Evans, 1989). It was argued that beetle species producing less force than predicted from the apparent mechanical advantage, might be applying similar pressures to their prey through differences in mandible tip area (i.e. area over which force is applied). However, this was not determined (Wheater and Evans, 1989).

The cross-sectional area of the adductor muscle correlates with head size, and chewing insects that feed on 'harder' diets have relatively larger

heads than those feeding on 'softer' diets (Bernays, 1986; Bernays and Hamai, 1987). It has been claimed that a larger adductor muscle is required to produce the increased force necessary to fracture these 'harder' plants (Bernays, 1991). However, the force and velocity with which the mandibles close can also be influenced by differences in muscle physiology and biochemistry. Ant adductor muscles consist of two fibre types, fibres with either short or long sarcomeres. Fibres with short sarcomeres are fast contracting fibres whereas fibres with long sarcomeres are slow but forceful (Gronenberg and Ehmer, 1995; Gronenberg *et al.*, 1997; Paul and Gronenberg, 2002).

Despite mandible movement appearing mechanically very simple, variations in velocity and force are obtained by variations in the proportions of the two fibre types, how they are attached and their angle of attachment with respect to direction of pull (Paul and Gronenberg, 1999). Morphological comparisons of numerous ant species found correlations between the feeding habits and associated properties of the musculature. Species specialized for fast mandible movements (predators) generally had fast muscle fibres that attached to the apodeme at small angles, encompassed in long heads, and vice versa for ants that performed forceful mandible movements (e.g. cracking seeds or leaf harvesting) (Paul and Gronenberg, 1999; Paul, 2001).

Similarly detailed studies to those on ants have not been untaken on caterpillars or acridids that feed on stiff or tough diets to see if there are any patterns in adductor muscle physiology and/or mechanics. There is some evidence to suggest that exploiting foods with differing physical characteristics has been accompanied by selection of some common characters. Modelling the head capsules of different beetle larvae based on the design of a basic orthopterous feeding mechanism, showed that the spatial positions of the mandible axes and insertion points of the mandible muscles varied with feeding behaviour (Gorb and Beutel, 2000). Acridids and caterpillars adapted to feed on plants of differing biomechanical properties may not exhibit the same degree of sophisticated variation that has evolved in ants that feed on a wider variety of foods. The limited available data suggests that the speed with which the mandibles close may be important, as changes to the velocity at which leaf blades were sheared altered the work required to fracture them (Sanson, 2006, Clissold, personal observation).

5.2 INTEGRATION OF MANDIBULAR MOVEMENT DURING FEEDING

For both acridids and caterpillars, there appears to be a close correlation between mouthpart structure and feeding patterns as determined by leaf damage (Gangwere, 1960, 1966; Weller, 1987; Godfrey *et al.*, 1989; Dockter, 1993; Hochuli, 2001). However, the interaction of the mandibles with a leaf in the oral cavity has received little attention (Gangwere, 1960).

Locusts ingest leaf blades by cutting across the outer vascular bundles, followed by bites parallel to and between the vascular bundles, with the final bites severing the outer vascular bundles to completely excise a piece of plant tissue (Figs. 9, 10) (Gangwere, 1960). This sequence is repeated until the meal ends (Fig. 9). Given the structure of the mandible, consuming the grass blade in this manner means that the strip being excised by the incisors passes over the molar region, with the vascular bundles running parallel to the molar ridges (Figs. 10, 11a). Locusts appear to 'chew' the excised strip before commencing biting to initiate a new strip (Simpson *et al.*, 1988b; Bernays, 1991; Clissold, 2003).

Fracture is initiated in a leaf blade when the incisor regions of opposing mandibles are driven through the leaf (Gangwere, 1960; Chapman, 1964;

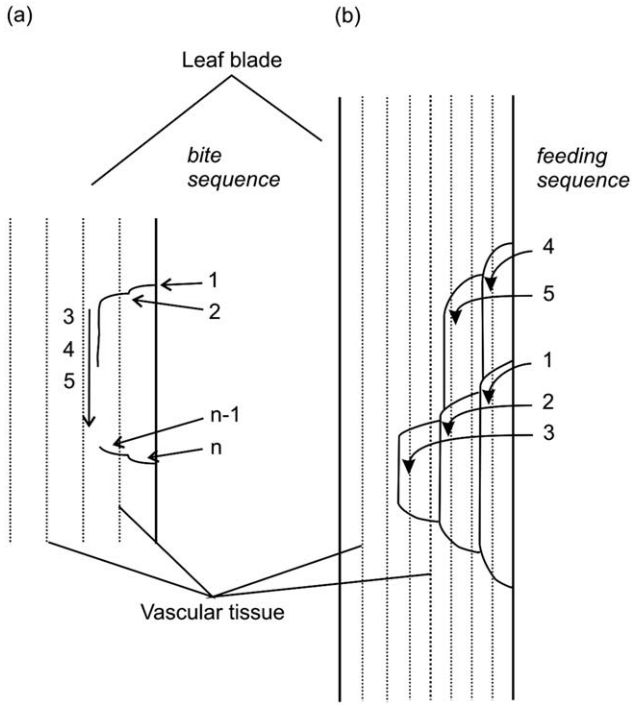

FIG. 9 Diagram illustrating (a) the typical bite sequence and (b) the feeding sequence of locusts consuming grass. (a) Locusts initially sever the outer vascular bundles (bites 1 and 2) and then proceed to fracture between the vascular bundles (bites 3, 4, 5, etc.) and finish by severing the outer vascular bundles (bites $n-1$, n) to form feeding sequence 1. (b) this sequence of bites is repeated following the feeding sequence outlined until the meal is completed. The solid arrows indicate the direction of bites, and the dotted arrows indicate the direction of feeding sequences. The number of vascular bundles per strip is dependent on the age (size) of the locust consuming the grass blade.

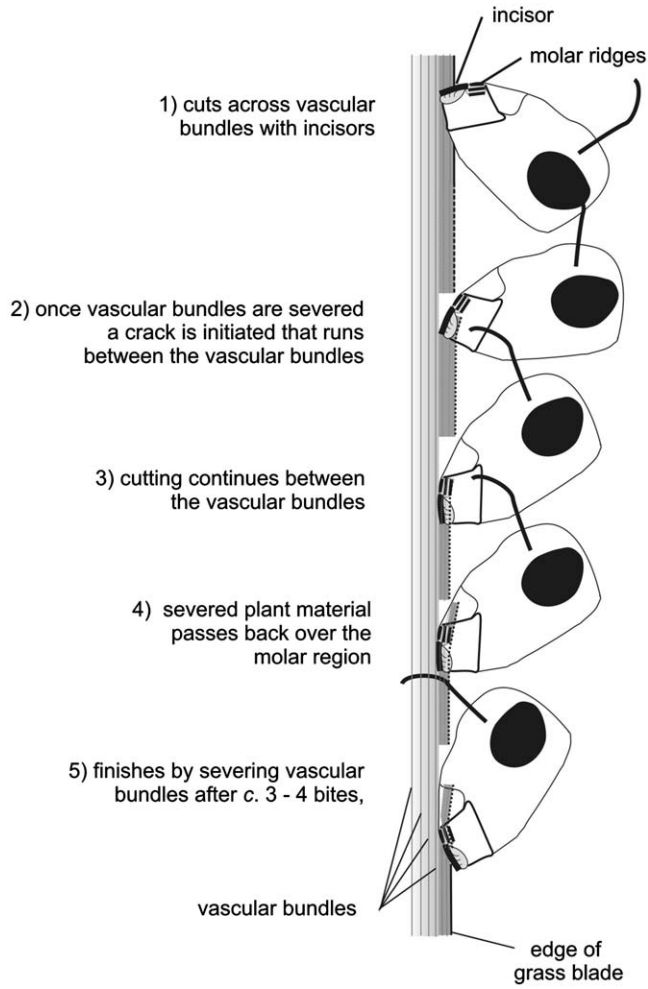

FIG. 10 Reconstruction of a locust consuming a blade of grass.

Hillerton, 1980). Modelling the closing sequence of the incisor region from a locust with 'graminivorous' mandibles, suggests that the tip of the left mandible passes along the outer surface of the right mandible, like two blades passing each other (Fig. 12) (Clissold, personal observation). This generates the characteristic wear pattern and flattened outer side of the right mandible that characterizes 'graminivorous' mandibles (Fig. 6). This observation strongly suggests that the incisors act as double blades (Fig. 5) that tend to control the fracture path and are the best to fracture tough materials (Sanson, 2006).

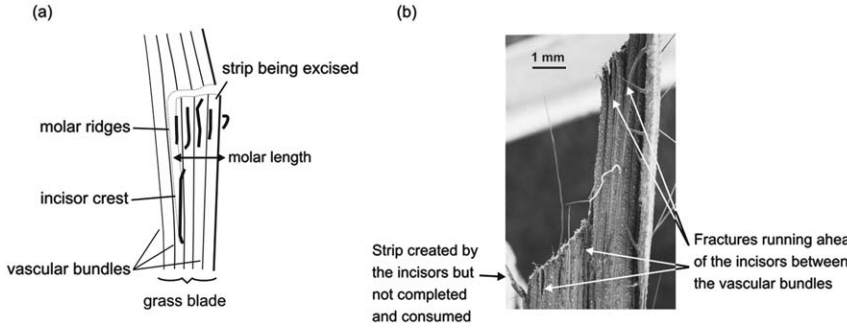

FIG. 11 (a) Alignment of the incisor and molar ridges from the right mandible superimposed on a grass blade. The left mandible closes over the right. The molar ridges and incisor crest are drawn to scale, the plant is not. Mandible size increases linearly with age, i.e. a second instar mandible is a proportionately smaller fifth instar mandible. The number of vascular bundles trapped between the molar ridges depends on the age (size) of the locust. There is no advantage in the locust incising the leaf blade deeper than the molar length, as the piece of excised leaf would not be processed as it passes over the molar ridges. (b) Image showing (i) fractures running ahead of the path of the incisors between the vascular bundles and (ii) a strip created on the edge of the grass blade by the incisors but not completed and consumed. These fractures were created by an adult male *C. terminifera* feeding on *Astrebla* (Mitchell) grass.

The curvature of the incisors appears to maximize the force that can be loaded onto the tip of the mandible and minimize the contact between the two incisor surfaces. This results in reduced friction and maximizes the force that can be concentrated onto the tips (Sibbing, 1991). Blades are the best shape to promote elastic fracture over plastic deformation cheaply in plants with high toughness (Lucas, 2004; Sanson, 2006). The wear patterns on the 'mixed-feeder' mandibles (Fig. 7) suggest they may initiate fracture in a similar way. However, the sharply pointed incisor cusps of the 'forbivorous' mandibles and the lack of wear on the occluding surfaces suggests they may operate differently. The sharply pointed incisor cusps of 'forbivorous' mandibles may simply be forced into a leaf to generate a fracture (Mode I), and thus occlusion is not important. This difference in wear between 'graminivorous' and 'forbivorous' mandibles has also been noted for lepidopterans (Hochuli, 1994).

Locusts appear to minimize energy and force expenditure in obtaining leaf material by making the majority of the fractures required to ingest leaf material between the vascular bundles. Wright (1992) found that fracture across the vascular bundles of a grass blade required 69 times less energy per unit area than fracturing across the vascular bundles. The uncontrolled fractures between the vascular bundles observed running ahead of the incisors suggests the locusts were supplying excess energy (Fig. 11b).

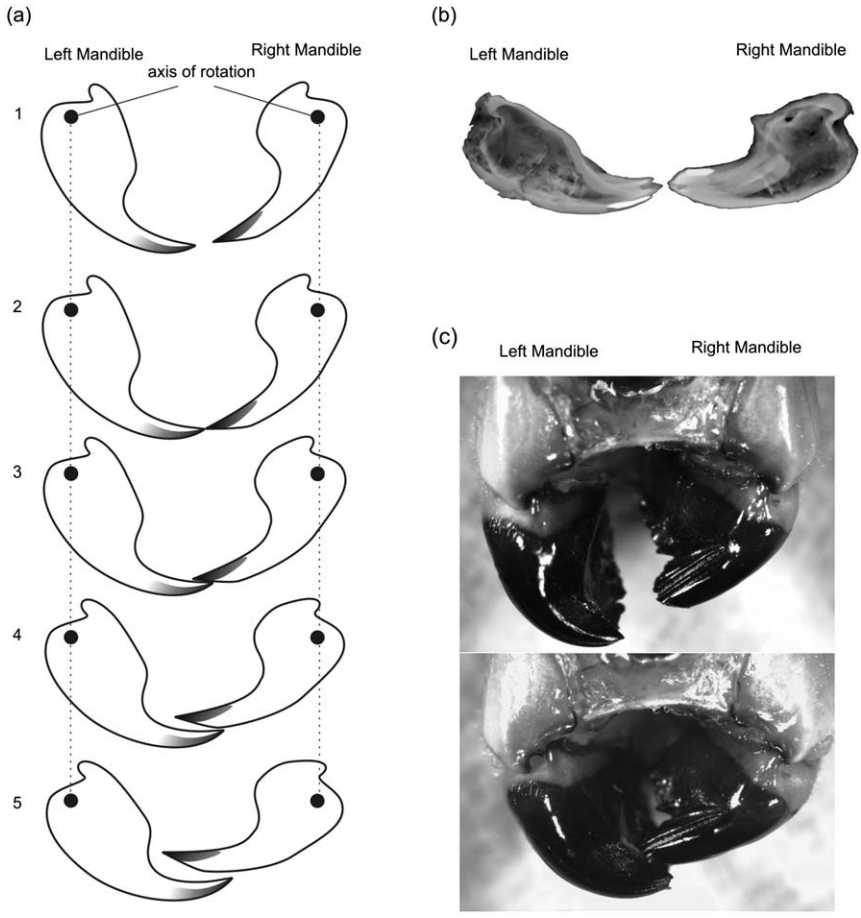

FIG. 12 (a) Proposed occlusion during the closing sequence (1–5) of the incisors from a locust with 'graminivorous' mandibles. The shaded areas give the location of the densest material. The two vertical dashed lines run through the axis of rotation. (b) This model was generated from the cross-section taken from X-ray microtomography analysis of mandibles from freshly moulted fifth instar, *C. terminifera* and the axis of rotation from (c) the mandibles viewed *in situ* ventrally with all the appendages posterior to the mandibles removed. The tip of the left mandible passes along the outer surface of the right mandible generating the characteristic wear patterns (Fig. 6). See text for further details.

Acridids with 'forbivorous' type mandibles are unable to split grass leaves between the vascular bundles (Gangwere, 1966). Instead, these mandibles make little bites, which when feeding on plants with parallel venation means they are always trying to fracture the vascular bundles. For an acridid that feeds exclusively on creosote bush (and presumably has

'forbivorous' mandibles), *Bootettix argentatus*, was unable to feed on a grass as it could not cut through the vascular bundles (Chapman *et al.*, 1988).

The model of incisor occlusion illustrated in Fig. 12 suggests that the shape of the mandibles allows the molars to work separately from the incisors. Once the incisor tips have passed each other they no longer touch (Fig. 12a, c). The force generated by the adductor muscle will then act on the tips of the molar ridges. The tips of the molar ridges are closer to the condyl than the incisor tips (Fig. 8c). Therefore, the length of the out-lever arm is decreased resulting in increased mechanical advantage and subsequent out force. However, the area of the molar tips in contact with the food will also influence the force acting on a food particle. No studies to measure this have been undertaken.

The molar ridges of the 'graminivorous' mandible align with the vascular bundles of a grass blade (Fig. 11) and the number of vascular bundles trapped between the molar ridges will depend on the age (size) of the locust. The molar ridges in 'graminivorous' mandibles are very hard; whether they act as blades, flattened cusps or wedges has not been ascertained (Fig. 13). While vascular bundles increase the force and energy required to fracture a leaf blade (Vincent, 1982; Wright, 1992), they also may 'act like sand in a pestle and mortar during chewing, providing a stiff material against which cells are pressed to cause rupture' (Wright and Vincent, 1996). It is not known how the molar region of 'forbivorous' or 'mixed-feeder' type mandibles interact with leaves of differing venation patterns.

It is thought that movement of food through the mouth is a mechanical process and there is no evidence for the existence of a distinct swallowing process (Chapman, 1995). However, both acridids and caterpillars can ingest fluids without the use of their mandibles (Sasaki and Asaoka, 2006). Locusts have been seen to pause and 'chew' during a meal (Simpson *et al.*, 1988b) and this chewing behaviour varies with diet and the internal state of the insect (Simpson *et al.*, 1988b; Bernays, 1991; Clissold, 2003). It is unknown whether this is to manipulate the meal before it enters the digestive tract, whether the mandible movements are required to move the food into the digestive tract, or whether such 'chewing' is simply the mandibles rhythmically opening and closing before receiving a signal to initiate a new biting sequence.

5.3 CHANGES IN FEEDING BEHAVIOUR WITH ONTOGENY

The mandibles of many caterpillars change with development and this is associated with altered feeding behaviour. For example, first instar notodontid caterpillars generally appear to scrape and skeletonize the leaves, leaving the epidermis intact, whereas the later instars cut through

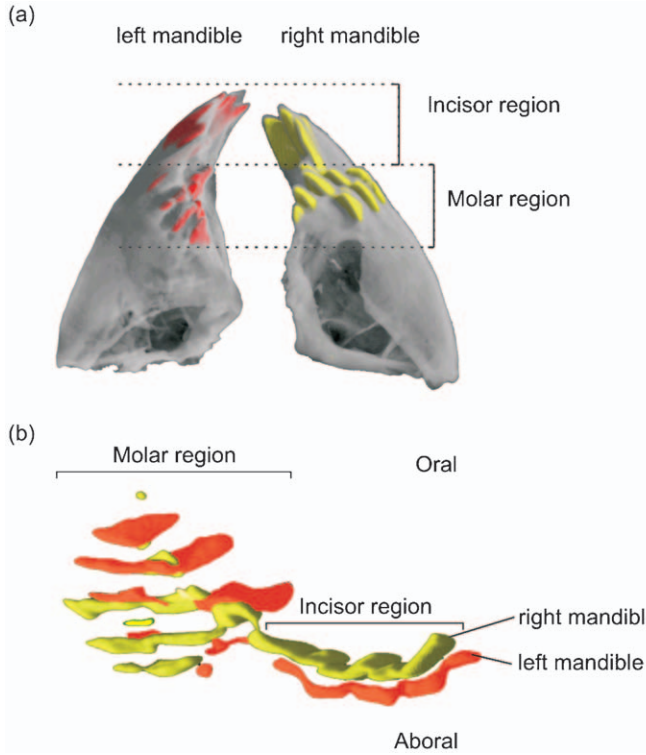

FIG. 13 (a) Incisor cusps and molar ridges of the right and left mandible of an acridid with 'graminivorous' mandibles (fifth instar, *C. terminifera*). The densest parts of the mandibles are represented by the coloured regions. This most likely represents the location of the 'harder' type of cuticle identified by Gardiner and Khan (1979) and that cuticle impregnated with zinc (Hillerton and Vincent, 1982). (b) Removing the less dense material leaving only the densest material that forms the ridges and cusps suggests the molars may create fractures in grasses using a combination of methods, cusps and blades (see Fig. 5). The incisors of the left mandible (red) overlap the right mandible (yellow) incisors. The images were generated by X-ray microtomography.

the entire leaf (Godfrey *et al.*, 1989; Dockter, 1993). This change in feeding behaviour correlates with a change in mandible morphology that occurs with successive moults, from having a toothed incisor in the early instars to a smooth incisor in the later instars. This change in morphology with ontogeny has been recorded in many caterpillar species and often involves the development of dentes (known as retinaculum) or blades on the oral surfaces (reviewed by Hochuli, 2001).

The effect of mandible size on the ability to initiate fracture is probably great, and leaves that have properties that make them stress-limited or

tough (refer Section 3.1) will likely impose limitations on feeding for small insects. Rather than sever their host grasses between the vascular bundles, adult *C. terminifera* often sever across the grass blades (Clissold, personal observation). Such behaviour has also been observed for the larger species, *L. migratoria*, but at an earlier stage of development. Younger *C. terminifera* nymphs have been observed to fracture across the blades of less tough grasses although this did not appear to improve nutrient assimilation (Clissold unpublished data).

Early instar locusts often appear to struggle to initiate fracture of tougher leaves across the outermost edge of a leaf blade, where typically the vascular bundles are closest together and/or sclerenchyma cells are densely packed (Clissold, 2003, personal observation). The high mortality of solitary first instar beetle larvae, *Chrysophtharta agricola*, feeding on older leaves decreased significantly when the margin of their host leaves was artificially damaged (Nahrung *et al.*, 2001). These beetle larvae initiate feeding at the leaf margin, which is thicker than the lamina and this becomes more pronounced as the leaves mature. The thickness of the leaf margins appears to prevent many of the first instar beetle larvae initiating a fracture, but once the leaf margin has been fractured, access to the thinner leaf margin can be gained. It is thought that one of the advantages of living in a large group is that it increases the likelihood that one member of the group will be able to initiate a feeding site thus ensuring the survival of the cohort (Hochuli, 2001; Nahrung *et al.*, 2001).

Scale or the size of the locust will not only affect feeding behaviour by the forces that the mandibles can generate but also the size of each 'bite'. The digestibility of two grasses decreased with increasing age of *C. terminifera* nymphs (Clissold *et al.*, 2006). This may be due to larger particles, or strips, being produced by the larger mandibles of older nymphs. As the size of the excised fragment increases, the ratio of cells fractured by the incisors to those remaining intact would decrease. The number of vascular bundles trapped between the molar ridges will depend on the age (size) of the locust (Fig. 14). Although there is only a relatively small increase in the distance between the molar ridges and incisor length with development across instars, nutrient assimilation efficiency decreased significantly. Increased nutrient assimilation efficiency by the younger instars may be due to smaller 'bites' and that relatively more time was spent fractionating a meal (chewing and biting) (Fig. 15a) (Clissold, 2003). Perhaps to compensate for the increase in mandible size with age, chewing behaviour changed as the locusts aged. Second instar locusts made the same number of chews per bite, approximately one chew was made for four bites, when feeding on either of two grasses, *Dactyloctenium radulans* and *Astrebla lappacea* (Fig. 15b) (Clissold, 2003). These grasses were chemically similar but biomechanically and anatomically different (Clissold *et al.*, 2006). Feeding on both diets, all nymphs as they aged increased the

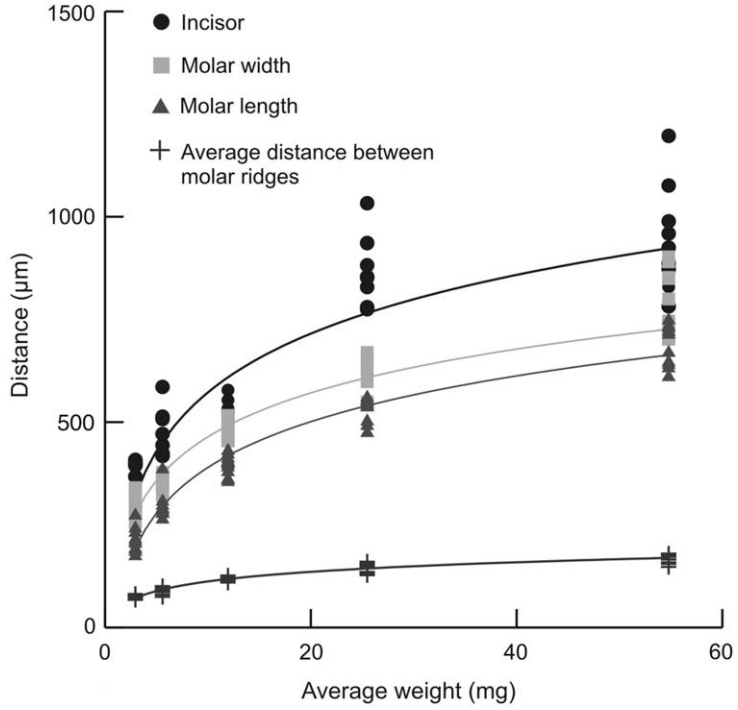

FIG. 14 Relationship between the length of incisor, molar width, molar length and average distance between molar ridges for the average weight of second to fifth Instar and adult male Australian plague locusts. The fitted lines are log smoothed.

number of chews per bite. However, for nymphs feeding on the tougher diet, *A. lappacea*, the change was greater so that by the final nymphal instar they were making almost one chew for each bite. Increases in the number of chews per bite have been reported for other locust species that consume tough diets (Bernays, 1991). However, which of the neural mechanisms (discussed in Section 6) that influence mandible movements causes the change in the proportions of chews to bites is unknown. It is unlikely foods need to be fractionated to a specific size before being passed to the foregut, as dissection of the gut on many occasions has revealed seedling wheat blades in the gut longer than the insect itself (Clissold, personal observation). And, chemostimulation from the major macronutrients would be the same. Equal meal sizes (on a dry weight basis) were ingested by nymphs feeding on both grasses, resulting in the same proportion of protein and carbohydrate being consumed per meal. Therefore, the altered pattern of chewing may have resulted from differences in mechanoreception as one grass, *A. lappacea*, was twice as tough as the other, *D. radulans*.

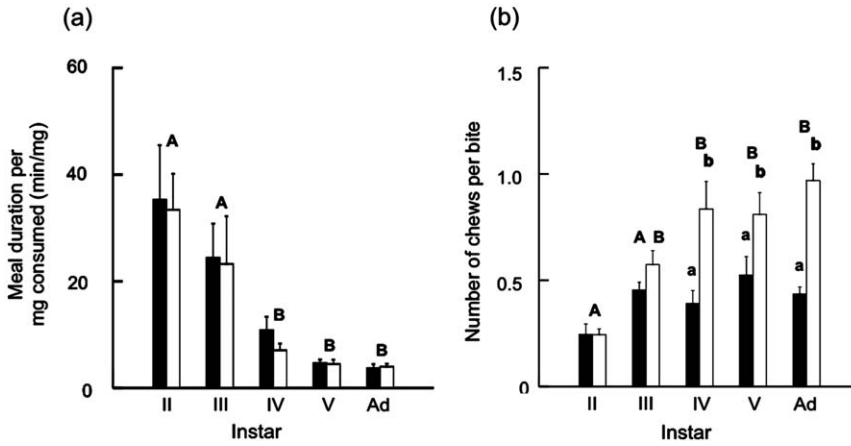

FIG. 15 Relationship between instar and the (a) time taken to consume 1 mg of two different grasses and, (b) ratio of chews per bite when consuming two grasses, *D. radulans*, solid bars and *A. lappacea*, open bars. Different letters above the bars represent differences ($P < 0.05$). Capital letters represent differences between ages and small letters between diets at each age.

6 Neural control of mandibular movements

Feeding is a complex behaviour resulting from the coordination of a suite of activities; it requires food to be located, a 'decision' made whether to reject or accept it, and if accepted, how much to consume. The mouthparts of acridids and caterpillars have many sensilla that typically contain both mechanosensory and chemosensory neurons (reviewed by Rogers and Newland, 2003). The inputs from these receptors mostly project onto the subesophageal ganglion where the motor neurons of the mandibular muscle reside (Kent and Hildebrand, 1987). An early stage of the feeding process involves contacting the food with the sensilla on the outer mouthparts and if the food is not rejected the insect will proceed to bite it (reviewed by Rogers and Newland, 2003). Rejection of leaves after biting may be due either to insufficient levels of phagostimulants, or to presence of deterrent chemicals, detected by chemoreceptors within the preoral cavity, or learned associations (Chapman, 1995). However, for an acridid, *Chorthippus parallelus*, leaf rejection at this stage was also correlated with increased leaf hardness (Bernays and Chapman, 1970). The mandibles of acridids and caterpillars contain scolopodial receptors (proprioreceptors) located at the tips of the incisor cusps and between the molar cusps, and mechanosensors in the hinge region. Locusts additionally possess campaniform sensors at the bases of the adductor muscle apodeme, which may be responsible for detecting food hardness (reviewed by Chapman, 1995).

Whereas the outer surface of the leaves may give the insect some information regarding internal chemical concentrations (Fiala *et al.*, 1990; Derridji *et al.*, 1996) on initial contact, once fracture of that leaf tissue has occurred, nutrients leak over the numerous sensilla located on the hydrophilic inner surfaces of the mouthparts (Chapman, 1982). The continued feeding on a leaf is a function of the balance between positive chemosensory inputs and negative feedbacks which accrue during feeding. The 'chemostimulatory power' of the food is an integration of the chemical nature of the food with the nutritional state of the insect, mediated by haemolymph-borne nutritional feedbacks and learning (Simpson, 1995; Simpson and Raubenheimer, 1996; Simpson and Raubenheimer, 2000; Ayali *et al.*, 2002). Negative feedbacks include inhibition from stretch receptors in the gut (Bernays and Chapman, 1973; Simpson, 1983b; Roessingh and Simpson, 1984).

A chewing cycle consists of the mandibles opening when the abductor muscles contract followed by a closing movement when the adductor muscle contracts. The contraction of the muscles on the left and right side are synchronized (Seath, 1977b). The abductor muscles contract in response to mechanical stimulation to the labrum (Chapman, 1995). The act of opening the mandibles triggers the adductor muscles to contract. For the mandibles to detach and fragment leaf material, feeding requires coordination of all the mouthparts. For example, the labrum and labium need to rise and fall in time with the opening and closing of the mandibles. For locusts, the muscles controlling the mouthparts and salivary glands, except for the muscles to the labial palps, appears to be strongly coupled to the mandibular motor pattern (Rast and Braunig, 2001).

The rhythmic opening and closing of the mandibles occurs spontaneously in the absence of inputs from the brain and central nervous system posterior to the subesophageal ganglion for a caterpillar (Griss *et al.*, 1991; Rowell and Simpson, 1992; Rast and Braunig, 2001) but not a grasshopper (Rast and Braunig, 1997, Simpson, personal communication). During feeding these rhythmic mandible movements are generated by premotor central pattern generating circuits (Rohrbacher, 1994a,b), the output of which is modulated by mechanosensory input from food (Seath, 1977a,b; Griss *et al.*, 1991; Simpson, 1992), chemosensory input from an interaction of diet and the internal nutritional state (Barton Browne *et al.*, 1975; Simpson *et al.*, 1988a; Simpson *et al.*, 1988b; Rowell and Simpson, 1992; Bowdan, 1995; Ayali *et al.*, 2002), and in *Manduca sexta*, input from unidentified receptors in the thorax (Griss *et al.*, 1991; Rowell and Simpson, 1992). While chemosensory input does not appear necessary for rhythmic chewing in caterpillars (Rowell and Simpson, 1992), it modifies the motor output which produces changes in the rate of chewing (or bite frequency) (Bowdan, 1995; Bowden and Wyse, 1997).

The muscle fibres in larval *M. sexta* are all the 'fast' type (Griss, 1990) and variations in output occur by differences in the number of muscle units activated rather than through inhibition (Griss, 1990). Recently, it was found that the pool of mandibular closer muscle neurons in *Bombyx mori* consisted of different functional types; slow or fast neurons (Sasaki and Asaoka, 2005). These researchers suggest that this may allow the mandibular muscles to produce different mandibular movements. In ants, forceful, fast or precise movement of the mandibles occurs from differential activation of the number and type of motor neurons (Paul and Gronenberg, 2002). Activation of fast motor neurons resulted in high-velocity mandible movements, while forceful movements occurred when all motor neurons were activated (Paul and Gronenberg, 2002). The presence of neuromodulators, e.g. serotonin, is also thought to be able to modify neural output, both centrally and peripherally (reviewed by Chapman, 1995).

6.1 RELATIONSHIP BETWEEN CHEWING RATE AND MEAL SIZE

For locusts, the amount eaten and the rate at which food is ingested are determined by the level of excitation provided by the interaction of the food and the internal physiological state of the locust (Bernays and Chapman, 1974; Barton Browne *et al.*, 1976; Simpson, 1983a,b; Abisgold and Simpson, 1987; Simpson *et al.*, 1988b; Simpson and Simpson, 1992; Simpson and Raubenheimer, 1993a; Simpson and Raubenheimer, 1996). Meal size and ingestion rate are positively correlated (Simpson *et al.*, 1988b). Locusts exhibit numerous behaviours during a meal; these being ingestion, chewing, pausing and locomotion. An increase in ingestion rate by a locust resulted from not only spending more time ingesting food but also by increasing the amount eaten during a period of ingestion. The latter occurred because the locusts increased the rate of mandibular movements (Simpson *et al.*, 1988b). Changes in frequency of mandibular movements in response to internal state and the phagostimulatory power of the food have also been recorded for the lepidopteran, *M. sexta* (Bowdan, 1995). In *L. migratoria*, intake rate is uniformly maximal at the start of the meal and then declines (Simpson *et al.*, 1988b). The rate of decline is a function of the size of the meal, i.e. ingestion rate declines rapidly when a small meal is ingested and is maintained longer for large meals (Fig. 16). Simpson *et al.* (1988b) reported finding smaller particles in the gut towards the end of a meal, although data were not presented. This observation may provide an answer to the question raised by optimality theory as to why ingestion rate is not uniformly fast at all times, both from meal to meal and throughout the course of a meal (Simpson *et al.*, 1988b). Faster chewing at the start of a meal provides a rapid rate of food intake, but it yields large particles that are less well assimilated, whereas slower chewing as the meal

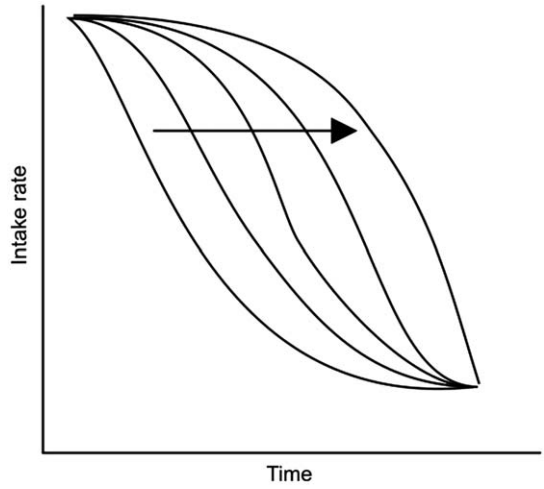

FIG. 16 Diagrammatic representation of the change in intake rate over the duration of a meal for meals of different sizes. The arrow indicates increasing meal size. Thus intake rate is maximal at the start of the meal and then declines. The rate of decline is a function of the size of the meal. This is determined by the levels of excitation that are the product of the meal itself and the internal state of the locust. Based on Simpson *et al*. (1988b).

progresses provides smaller, better assimilated particles. This same model of decline in ingestion rate with meal size also appears to occur in caterpillars: the rate of mandibular movement was uniformly high at the start of any meal, but the initial high rate of chewing was maintained for longer as meal size increased (Bowdan, 1995). Bowdan (1987, 1988) found that larger caterpillars ate larger meals relatively faster than smaller caterpillars. A similar pattern might explain the decreased assimilation efficiency found for older instar acridids, i.e. they make larger 'bites' and spend relatively less time fractionating each meal (Fig. 15a) (Clissold, 2003).

6.2 BEHAVIOURAL PLASTICITY

Fractionation of leaves by a given mandible morphology can be increased by changing either the rate of chewing or the time spent chewing or both. For mammals, differences in chewing behaviour are strongly correlated with food traits (reviewed by Perez-Barberia and Gordon, 1998). As discussed earlier, for caterpillars and acridids the rate of biting and chewing varies (Fig. 15b; Bernays, 1991). However, can a caterpillar or acridid actively control this as a means of adjusting nutrient supply rate

and ratio? If the degree to which a plant is fragmented affects the degree to which total nutrients are assimilated and the relative proportion of carbohydrate made available for assimilation (see Section 2), then being able to adjust the rate at which a meal is ingested may be important to achieving nutrient balance.

7 Costs of consuming tough diets

The mechanisms that make tougher or stiffer leaves a poor food source are likely to be complex. Such leaves may prevent physical access to enclosed nutrients (Clissold *et al.*, 2006), or provide a physiological barrier, through indigestible cell walls diluting nutrients (Clissold *et al.*, 2004; Lee *et al.*, 2004), or increased metabolic costs required to gain those nutrients (Roces and Lighton, 1995).

7.1 METABOLIC COST OF CHEWING

The process of ingesting and digesting food increases respiration in insects (e.g. Aidley, 1976; McEvoy, 1984; Zanotto *et al.*, 1997; Gouveia *et al.*, 2000). How variations in the physical properties of the diet contribute to this cost has received little attention in insects. Many nutritional ecology studies have reported differences in the efficiency with which insects convert assimilated nutrients to body mass when feeding on different plant species, but there are numerous possible causes of these differences. The properties of leaf tissues are likely to influence metabolic costs when nutrients are diluted through increased consumption (Trier and Mattson, 2003; Lee *et al.*, 2004; Clissold, personal observation) and/or via diet-induced thermogenesis used to balance nutrient supply post-ingestively when excessive carbohydrate is assimilated (Zanotto *et al.*, 1997). Although the ratio of 'bites to chews' have been shown to change when feeding on different diets (Fig. 15b), it is not thought that the muscular effort of feeding *per se* will contribute substantially to altered oxygen consumption (Zanotto *et al.*, 1997; Gouveia *et al.*, 2000). Oxygen consumption for a locust increased rapidly at the onset of feeding (Zanotto *et al.*, 1997; Gouveia *et al.*, 2000) but this was attributed to a state of arousal rather than to the metabolic demands of chewing. Hence, a similar rapid rise in oxygen consumption occurred when food odour was blown into the chamber (Gouveia *et al.*, 2000). The only study where the act of leaf snipping was uncoupled from ingestion was that by Roces and Lighton (1995), where they recorded a 30-fold increase in oxygen consumption for the leaf-cutting ant, *Atta sexdens* cutting artificial leaves made of parafilm.

7.2 COSTS OF NUTRIENT DILUTION AND IMBALANCE

For both caterpillars and acridids, the indigestible cell wall dilutes the primary macromolecules. Decreased efficiency in converting assimilate to body mass occurs in insects when feeding on diluted diets, through either increased costs of compensatory feeding to gain limiting nutrients and/or because instar durations are lengthened. Various studies have shown that locusts and caterpillars are able to compensate to varying degrees by increasing consumption for a diet that is diluted with an indigestible component (McGinnis and Kasting, 1967; Timmins *et al.*, 1988; Raubenheimer and Simpson, 1993; Yang and Joern, 1994; Joern and Behmer, 1997). In some cases, the capacity to increase consumption is greater than the extent to which dilution by cell walls occurs in plants (Van Soest, 1994). However, plants where the nutrients are diluted by increased cell wall also generally have lower water content, which increases the time that food is resident in the gut (Baines *et al.*, 1973; Clissold *et al.*, 2006) and consequently the rate of nutrient assimilation is reduced.

The degree to which the diet is fractionated will affect not only the rates of absolute nutrient transfer across the gut wall but increased gut passage rate can also alter the ratio of protein:carbohydrate assimilated (Raubenheimer and Simpson, 1996; Raubenheimer and Simpson, 1998; Clissold *et al.*, 2006). Fitness costs are incurred when insects are unable to match their requirements from that supplied (e.g. Simpson *et al.*, 2004) and this is exacerbated when the protein:carbohydrate ratio is unbalanced with respect to requirements. Lee *et al.* (2004) found that although a generalist caterpillar was able to increase ingestion to compensate for nutrient dilution, growth and development were reduced when feeding on highly diluted foods, especially those where the ratio of protein:carbohydrate was unbalanced with respect to optimal requirement because nutrient intake was reduced and utilization efficiency of ingested nutrients was decreased. The physical characteristics of the diet influenced food retention time for a locust fed one of two grass species (Clissold *et al.*, 2006). These two grasses had the same concentrations of protein and carbohydrate, but relatively more carbohydrate was assimilated from the grass that was retained within the gut for the shorter period of time. This grass was less tough and had higher water content; both factors that increased movement of food through the gut (Clissold *et al.*, 2006).

7.3 MANDIBLE WEAR

Given that fractionation of the diet depends on the morphology of the mandibles, it follows that anything that alters the shape of the mandibles may affect nutrient assimilation. Changes to the shape of mandibles (wear) can occur from mandible–mandible and mandible–food contact. To produce

fracture the mandibles need to be harder than the diet and thus the way they occlude will affect how they wear. A second cause of wear is hard materials in and/or on the diet, e.g. endogenous silica or grit ingested with the diet. For insects, increased wear has also been associated with the toughness of the diet (Raupp, 1985) but whether this was a result of factors causing toughness *per se* or compensatory increases in amounts eaten is not known.

For mammals, wear is thought to be a major factor affecting the effectiveness of teeth in fractionating leaves. The evolution in mammals of the capacity to exploit grasses gave rise to numerous strategies to prevent tooth wear; such as hypsodonty (high crowns), molar progression, or in a few species continually growing teeth (Sanson, 2006). Insects that chew grasses also appear to show at least one similar morphological strategy to those seen in some mammals – the incisors of 'graminivorous' type mandibles are relatively longer, as they arise closer to the base of the mandible than those of 'forbivorous' types. It is unknown if there are differences in the hardness or differences in thickness of the molar region of 'graminivorous' and 'forbivorous' type mandibles.

The determination of loss of tooth effectiveness with wear has been difficult to ascertain for mammals. Loss of tooth effectiveness is often measured by changes to chewing behaviour, as it is assumed that animals will compensate for reduced tooth function. However, chewing behaviour appears to be more closely related to food traits than loss of tooth shape (reviewed by Perez-Barberia and Gordon, 1998; Sanson, 2006). Natural wear has been associated with an increase in the proportion of larger particles in the guts, altered chewing rates and patterns of feeding (reviewed by Perez-Barberia and Gordon, 1998; Sanson, 2006). The interpretations of these differences in feeding behaviour with natural wear are, however, confounded by other consequences of aging. Experiments that attempt to manipulate wear on comparably aged animal generally cannot reproduce naturally occurring wear. Experimental manipulations of morphology generally decrease the area of occlusal contact, which does not occur with natural wear. In fact, wear may improve the effectiveness of mammalian teeth, after which further wear decreases tooth effectiveness (Perez-Barberia and Gordon, 1998). Sharpness of blades or cusps is a small-scale effect occurring at or close to the tip of a tooth, i.e. at the tooth–food interface (Sanson, 2006). It is logical to assume that sharp blades or cusps would be best at promoting fracture. However, better fracture occurs with blunter cusps (Lucas, 2004).

Compared with mammals, changes to mandible morphology with wear are not considered to affect insect nutrition. Although insect cuticle is generally significantly softer than enamel, the impregnation of metals (Hillerton *et al.*, 1984) in the cutting edges of the incisors makes them almost as hard as enamel (Vincent and Wegst, 2004; Schoberl and Jager,

2006). Insects are not particularly long-lived and for a large proportion of their life, mandibles are replaced at frequent intervals, upon each moult. Therefore, wear may not affect developing insects. Arens (1990) reported that stream-dwelling insect larvae (from the Ephemeroptera, Plecoptera, Coleoptera, Diptera) have high levels of mandible wear due to the ingestion of particles of rock and sand associated with scraping algae from rocks. However, when different levels of mandible wear were induced by allowing nymphs to feed from algae growing on different grades of sand paper, nymphs from all treatments grew at the same rate for three generations (Arens, 1990). Some researchers (Houston, 1981; Arens, 1990) have speculated that frequent moulting exhibited by some insect groups may be an adaptation to offset mandible wear. However, there is no evidence to support that view (Slansky and Scriber, 1985).

The other few studies investigating wear on insect mouthparts are difficult to interpret. While a decrease in intake rate has been observed with insects with worn mandibles (Chapman, 1964; Raupp, 1985), in one case this decrease was also associated with a difference in meal size (Chapman, 1964). However, it is predicted that intake rate may decrease because smaller 'bites' are taken when the length of the incisor is reduced (Hochuli, 1994). In neither case was the effect on nutritional gain reported. Taking 'smaller' bites may increase fractionation of cell walls, which may increase the efficiency of nutrient assimilation (see Section 2). Thus, whether reduced intake rate was a result of smaller meals being consumed due to nutritional factors regulating intake or limitations on intake imposed by the mandibles cannot be determined. Chapman (1964) hypothesized that as the reduction in intake rate was so small, it would be unlikely significantly to affect a grasshopper's fitness. One situation where altered mandible morphology may be a factor influencing fitness is for long-lived adults, e.g. those that overwinter as adults.

8 Conclusions

Chapman (1995) concluded his review of the mechanics of food handling by chewing insects by saying that 'much of our present understanding is based on the morphology of the mouthparts and foregut, with little rigorous analysis of the mechanical processes involved'. The detailed studies on ant mandible movements by Jurgen Paul, Wulfila Gronenberg and associates have demonstrated how small changes to a relatively simple biomechanical system can elicit a variety of movements. The key to the versatility of movements observed across ant species is the adductor muscle. Differences in its physiology, biochemistry, angle and mode of attachment alter the force, velocity and precision of movement. Differences

in the biomechanics of ant mandible movements coupled with differences in mandible morphology have enabled ants to exploit a wide variety of feeding niches. Herbivorous insects may also have evolved a variety of mechanisms to detach leaf fragments. The differences in morphology between acridid and caterpillar mandibles suggest that they may use different strategies to generate fractures. Acridids seem to have two distinct behaviours to process foods; biting to detach a leaf fragment and then post-bite processing ('chewing') to fractionate the food further. Acridid mandibles have a complex molar region, whereas that of caterpillars has at most a few cusps. Insects are small, but the changes in size from first to last instar are relatively large. The effects of this change in scale have received little attention. The forces generated and the velocities mandibles move is likely to vary both with instar (age) and will most likely differ between insect species.

Biomechanical models are valuable in that they provide testable hypotheses of the relationship between form and function. Although models can oversimplify the actual mechanics and forces to some degree, they provide a framework for the collection of physiological and morphological data. Apart from the detailed, elegant studies of variations in ant mandible musculature morphology and kinetics, variations across a group of chewing herbivorous mandibulate insects have not been quantified. Only Patterson (1983, 1984) has attempted to quantify the original descriptions of relative mandible lengths (e.g. Isely, 1944; Chapman, 1964). Visual descriptions form the bulk of our knowledge of insect mandibles and associated musculature and mouthparts. Promising new techniques may allow valuable insights into the characterization of mandible surface morphology independently of scale, as has been the case for mammalian teeth (Evans *et al.*, 2007). This together with the development of the use of synchrotron X-rays to investigate the structure and dynamics of the internal anatomy of insects will allow the *in situ* analysis of the interaction of insect mandibles and their food (Socha *et al.*, 2007).

Leaves have evolved to withstand many stresses, both abiotic and biotic (Read and Stokes, 2006). Herbivores have thus had to evolve mechanisms to propagate fractures through materials and structures that have evolved to oppose this. Many ecological studies suggest the physical characteristics of leaves may be a major factor limiting host use by insects rather than the concentration of macronutrients *per se*. Rather it may be the availability of macronutrients and the cost in obtaining them which drives ecological patterns. However, disentangling the multiple factors that vary between leaves will require careful detailed studies before any generalizations can be drawn. The prevention of leaf detachment by spines or hairs is well known, but structural characters of leaf material that may restrict nutrient

assimilation, or make one plant a poorer host than another, mostly comes from correlations of patterns of herbivore association or conversely the amount of damage with leaf properties (e.g. Feeny, 1970; Coley, 1983; Lowman and Box, 1983; Ohmart *et al.*, 1987; Larsson and Ohmart, 1988; Nichols-Orians and Schultz, 1990; Ohmart and Edwards, 1991; Stevenson *et al.*, 1993; Casher, 1996; Choong, 1996; Peeters *et al.*, 2007). The conclusions drawn from such studies are restricted by the multiplicity of correlated plant traits. Although correlative studies are useful for suggesting avenues for future research, correlations between form and function are exactly that, a correlation, and should not be regarded as an adaptation or mechanism until a link can be demonstrated.

Correlations that transcend phylogeny suggest leaf venation appears to have influenced the morphology of the mandibles and associated musculature. But the relationship between acridid mandible morphology and food types eaten is far from precise (Chapman, 1964; Mulkern, 1967). However, it is more important to know the nutritional implication of processing grasses or non-grasses with different mandible morphologies, as this is what will affect ecological processes. It is known that vegetation patterns affect acridid population densities (Joern, 2004) and although the reasons for this are likely to be complex, nutrition may be a partial explanation. Recent work demonstrated a link between host choice and head morphometry for male and female Eastern lubber grasshoppers (Vincent, 2006). Acridids and caterpillars actively regulate their intake of macronutrients and their foraging patterns are linked to the relative frequency and distribution of foods in their environment (Behmer *et al.*, 2001; van der Zee *et al.*, 2002; Behmer *et al.*, 2003).

Nutrition is the outcome of feeding. Food choice, amount ingested and the rate of ingestion all affect the degree to which a food is fragmented, which in turn determines how well nutrients are assimilated post-ingestively. Compared to the mammalian literature, mostly from studies on humans and ruminants, the insect literature is relatively sparse. However, very little correlation has been found between the morphological characters of teeth, chewing behaviour and the fragmentation of leaves for mammals. There is a lack of agreement on what are the key morphological characters determining the effectiveness of a particular morphology for a given diet (reviewed by Perez-Barberia and Gordon, 1998). Such studies have not measured the nutritional outcome for the organism. Rather they correlated aspects of tooth morphology and/or diet with chewing behaviour or food intake rate in an attempt to find parameters that scale.

The degree to which leaves are fractionated is the consequence of the 'hardware' (teeth) and amount of processing (chewing behaviour). As our knowledge of how organisms maintain nutritional homoeostasis increases, it is becoming apparent that animals are characterized by obtaining

variable ends using a variety of means. Therefore, each step in the process needs to be understood, and as such, studies that use, for example, intake rate as a measure of performance may in fact be measuring nutritionally one thing in one animal and quite another thing for others. Thus, understanding nutrient gain should underpin any study of the effectiveness of processing leaves by insects.

The small size of insects compared to mammals makes them ideal study animals. Digestibility of food can be determined from a single meal, as a meal flows through the gut of an insect as a unit (Yang, 1993; Yang and Joern, 1994; Wolesensky *et al.*, 2005). Changes in feeding behaviour of acridids and caterpillars can be induced quite rapidly (within 1–2 h) by altering their internal nutritional state, and feeding behaviour can be linked directly to post-ingestive nutrient utilization (Simpson *et al.*, 1995; Simpson and Raubenheimer, 2000).

Increasingly, insights into ecological and evolutionary patterns and processes are being gained from an understanding of animal physiology and behaviour. The ability of organisms to balance nutrient supply with demand is constrained by evolutionary processes that have shaped morphology and behaviour and the plasticity of these traits. The development of the geometric framework (Raubenheimer and Simpson, 1993; Simpson and Raubenheimer, 1993b) has provided a means to explore and unite feeding and nutrition. How nutrition is affected by a particular mandible morphology, and the degree of behavioural flexibility that an insect can employ to assist in overcoming these limitations, are not known and worthy of future study. To understand the nutritional ecology of herbivores, studies investigating feeding behaviour and nutrition need to consider intake and assimilation of multiple nutrients and their subsequent allocation to biomass. A recent study demonstrated that the relationship between plant macronutrients, water and physical structure is complex, changes over ontogenetic development and has important implications for population dynamics of an outbreaking locust species (Clissold *et al.*, 2006). Studies of behaviour at the level of individuals are required to understand how host plant availability, chemistry and physical properties drive correlations between insect herbivores and their host plants evident at the community, ecosystem and evolutionary levels.

Increased understanding of what causes some plants to make better hosts than others, and the capacities that insects have to overcome limiting plant traits will come from studies that account for effects of plant primary and secondary chemistry, along with:

i. Measures of mechanical properties of leaves that are most likely to influence fracture by herbivores, namely toughness and stiffness;

ii. Models of the kinetics of mandibles and their associated musculature, to compare quantitatively differences in morphology amongst feeding types;
iii. Measures of developmental plasticity in mandible, head and body size in response to diet; and
iv. Understanding whether insects can adjust biting and chewing to alter rates and ratios of nutrients assimilated.

Acknowledgements

Thanks to Professor Stephen Simpson and two anonymous reviewers for comments and critique on earlier drafts of this manuscript. Dr Allan Jones, from The Electron Microscope Unit, Australian Key Centre for Microscopy and Microanalysis, The University of Sydney made possible the three-dimensional visualization of the mandibles.

References

Abe, T. and Higashi, M. (1991). Cellulose centered perspective on terrestrial community structure. *Oikos* **60**, 127–133.
Abisgold, J. D. and Simpson, S. J. (1987). The physiology of compensation by locusts for changes in dietary protein. *J. Exp. Biol.* **129**, 329–346.
Aidley, D. J. (1976). Increase in respiratory rate during feeding in larvae of the armyworm, *Spodoptera exempta*. *Physiol. Entomol.* **1**, 73–75.
Aranwela, N., Sanson, G. and Read, J. (1999). Methods of assessing leaf-fracture properties. *New Phytol.* **144**, 369–383.
Arens, W. (1990). Wear and tear of mouthparts: a critical problem in stream animals feeding on epilithic algae. *Can. J. Zool.* **68**, 1896–1914.
Ashby, M. F. (1999). *Materials Selection in Mechanical Design*, 2nd ed. Oxford: Butterworth-Heinemann.
Atkins, A. G. and Mai, Y. W. (1985). *Elastic and Plastic Fracture: Metals, Polymers, Ceramics, Composites, Biological Materials*. New York: Halsted Press.
Ayali, A., Zilberstein, Y. and Cohen, N. (2002). The locust frontal ganglion: a central pattern generator network controlling foregut rhythmic motor patterns. *J. Exp. Biol.* **205**, 2825–2832.
Bacic, A., Harris, P. J. and Stone, B. A. (1988). Structure and function of plant cell walls. In: *The Biochemistry of Plants: A Comprehensive Treatise*, Vol. 14 (ed. Preiss, J.), pp. 297–371. New York: Academic Press
Baines, D. M., Bernays, E. A. and Leather, E. M. (1973). Movement of food through the gut of fifth-instar males of *Locusta migratoria migratorioide*s (R. & F.). *Acrida* **2**, 319–332.
Barbehenn, R. (1989). *The Nutrional Ecology and Mechanism of Digestion of C3 and C4 Grass-Feeding Lepidoptera*. Berkeley: University of California.
Barbehenn, R. V. (1992). Digestion of uncrushed leaf tissues by leaf-snipping larval Lepidoptera. *Oecologia (Berlin)* **89**, 229–235.

Barbehenn, R. V. (2005). Grasshoppers efficiently process C-4 grass leaf tissues: implications for patterns of host-plant utilization. *Entomol. Exp. Appl.* **116**, 209–217.

Baron-Epel, O., Gharyal, P. K. and Schindler, M. (1988). Pectins as mediators of wall porosity in soybean cells. *Planta* **175**, 389–395.

Barton Browne, L., Moorhouse, J. E. and van Gerwen, A. C. M. (1976). A relationship between weight loss during food deprivation and subsequent meal size in the locust, *Chortoicetes terminifera*. *J. Insect Physiol.* **22**, 89–94.

Barton Browne, L., Moorhouse, J. E. and van Gerwin, A. C. M. (1975). An excitatory state generated during feeding in the locust, *Chortoicetes terminifera*. *J. Insect Physiol.* **21**, 1731–1736.

Behmer, S. T., Cox, E., Raubenheimer, D. and Simpson, S. J. (2003). Food distance and its effect on nutrient balancing in a mobile insect herbivore. *Anim. Behav.* **66**, 665–675.

Behmer, S. T., Raubenheimer, D. and Simpson, S. J. (2001). Frequency-dependent food selection in locusts: a geometric analysis of the role of nutrient balancing. *Anim. Behav.* **61**, 995–1005.

Bennack, D. E. (1981). The effects of mandible morphology and photosynthetic pathway on selected herbivory in grasshoppers. *Oecologia* **51**, 281–283.

Bernays, E. A. (1986). Diet-induced head allometry among foliage-chewing insects and its importance for graminivores. *Science* **231**, 495–497.

Bernays, E. A. (1991). Evolution of insect morphology in relation to plants. *Philos. Trans. R. Soc. Lond. B* **333**, 257–264.

Bernays, E. A. and Barbehenn, R. (1987). Nutritional ecology of grass foliage-chewing insects. In: *Nutritional Ecology of Insects, Mites, Spiders, and Related Invertebrates* (eds Slansky, F. Jr. and Rodriguez, J. G.). New York: Wiley.

Bernays, E. A. and Chapman, R. F. (1970). Experiments to determine the basis of food selection by *Chorthippus parallelus* (Zetterstedt) (Orthoptera: Acrididae) in the field. *J. Anim. Ecol.* **39**, 383–394.

Bernays, E. A. and Chapman, R. F. (1973). The regulation of feeding in *Locusta migratoria*: internal inhibitory mechanisms. *Entomol. Exp. Appl.* **16**, 329–342.

Bernays, E. A. and Chapman, R. F. (1974). The effect of haemolymph osmotic pressure on the meal size of nymphs of *Locusta migratoria* L. *J. Exp. Biol.* **61**, 473–480.

Bernays, E. A. and Hamai, J. (1987). Head size and shape in relation to grass feeding in Acridoidea (Orthoptera). *Int. J. Insect Morph. Embryol.* **16**, 323–330.

Bernays, E. A. and Janzen, D. H. (1988). Saturniid and sphingid caterpillars: two ways to eat leaves. *Ecology* **69**, 1153–1160.

Bowdan, E. (1987). Feeding regulation and the microstructure of eating tomato leaf by tobacco hornworm caterpillars. *Ann. N. Y. Acad. Sci.* **510**, 190–192.

Bowdan, E. (1988). Microstructure of feeding by tobacco hornworm caterpillars, *Manduca sexta*. *Entomol. Exp. Appl.* **47**, 127–136.

Bowdan, E. (1995). The effects of a phagostimulant and a deterrent on the microstructure of feeding by *Manduca sexta* caterpillars. *Entomol. Exp. Appl.* **77**, 297–306.

Bowden, E. and Wyse, G. A. (1997). Removing antennae and maxillae has little effect on feeding on normal host plants by two species of caterpillar. *J. Insect Physiol.* **43**, 1053–1063.

Boys, H. A. (1981). Food selection by some graminivorous Acrididae. Doctor of Philosophy, Oxford University, Oxford, UK.

Braby, M. F. (1994). The significance of egg size variation in butterflies in relation to host plant quality. *Oikos* **71**, 119–129.

Brett, C. T. and Waldron, K. W. (1996). *Physiology and Biochemistry of Plant Cell Walls*, 2nd ed. London: Chapman & Hall.
Brown, E. S. and Dewhurst, C. F. (1975). Genus Spodoptera (Lepidoptera, Noctuidae) in Africa and near East. *Bull. Entomol. Res.* **65**, 221–262.
Carpita, N., Sabularse, D., Montezinos, D. and Delmer, D. P. (1979). Determination of the pore-size of cell-walls of living plant-cells. *Science* **205**, 1144–1147.
Casher, L. E. (1996). Leaf toughness in *Quercus agrifolia* and its effects on tissue selection by first instars of *Phryganidia californica* (Lepidoptera: Dioptidae) and *Bucculatrix albertiella* (Lepidoptera: Lyonetiidae). *Ann. Entomol. Soc. Am.* **89**, 109–121.
Cazemier, A. E., OpdenCamp, H. J. M., Hackstein, J. H. P. and Vogels, G. D. (1997). Fibre digestion in arthropods. *Comp. Biochem. Physiol. A* **118**, 101–109.
Chambers, P. G., Simpson, S. J. and Raubenheimer, D. (1995). Behavioural mechanisms of nutrient balancing in *Locusta migratoria* nymphs. *Anim. Behav.* **50**, 1513–1523.
Chapman, R. F. (1964). The structure and wear of the mandibles in some African grasshoppers. *Proc. Zool. Soc. Lond.* **142**, 107–121.
Chapman, R. F. (1982). Chemoreception-the significance of receptor numbers. *Adv. Insect Physiol.* **16**, 247–356.
Chapman, R. F. (1995). Mechanics of food handling by chewing insects. In: *Regulatory Mechanisms in Insect Feeding* (eds Chapman, R. F. and de Boer, G.), pp. 3–31. New York: Chapman & Hall
Chapman, R. F., Bernays, E. A. and Wyatt, T. (1988). Chemical aspects of host-plant specificity in 3 larrea-feeding grasshoppers. *J. Chem. Ecol.* **14**, 561–579.
Charnley, A. K., Hunt, J. and Dillon, R. J. (1985). The germ-free culture of desert locusts, *Schistocerca gregaria*. *J. Insect Physiol.* **31**, 477–485.
Choong, M. F. (1996). What makes a leaf tough and how this affects the pattern of *Castanopsis fissa* leaf consumption by caterpillars. *Funct. Ecol.* **10**, 668–674.
Clissold, F. J. (2003). Nutritional ecology of the Australian plague locust. *Chortoicetes terminifera*, PhD, Monash University, Victoria, Australia.
Clissold, F. J., Sanson, G. D. and Read, J. (2004). Indigestibility of plant cell wall by the Australian plague locust, *Chortoicetes terminifera*. *Entomol. Exp. Appl.* **112**, 159–168.
Clissold, F. J., Sanson, G. D. and Read, J. (2006). The paradoxical effects of nutrient ratios and supply rates on an outbreaking insect herbivore, the Australian plague locust. *J. Anim. Ecol.* **75**, 1000–1013.
Coley, P. D. (1980). Effects of leaf age and plant life history patterns on herbivory. *Nature* **284**, 545–546.
Coley, P. D. (1983). Herbivory and defensive characteristics of tree species in a lowland tropical environment. *Ecol. Monogr.* **53**, 209–233.
Dadd, R. H. (1960). The nutritional requirements of locusts-III carbohydrate requirements and utilization. *J. Insect Physiol.* **5**, 301–316.
Derridji, S., Wu, B. R., Stammitti, L., Garrec, J. P. and Derrien, A. (1996). Chemicals on the leaf surface, information about the plant available to insects. *Entomol. Exp. Appl.* **80**, 197–201.
Dockter, D. E. (1993). Developmental changes and wear of larval mandibles in *Heterocampa guttivitta* and *H. subrotata* (Notodontidae). *J. Lepid. Soc.* **47**, 32–48.
Evans, W. A. L. and Payne, D. W. (1964). Carbohydrases of the alimentary tract of the desert locust, *Schistocerca gregaria* Forsk. *J. Insect Physiol.* **10**, 657–674.
Evans, A. R., Wilson, G. P., Fortelius, M. and Jernvall, J. (2007). High-level similarity of dentitions in carnivorans and rodents. *Nature* **445**, 78–81.

Farquhar, T. and Zhao, Y. (2006). Fracture mechanics and its relevance to botanical structures. *Am. J. Bot.* **93**, 1449–1454.
Feeny, P. (1970). Seasonal changes in oak leaf tannins and nutrients as a cause of spring feeding by winter caterpillars. *Ecology* **51**, 565–581.
Ferreira, C., Oliveira, M. C. and Terra, W. R. (1990). Compartmentalization of the digestive process in *Abracris flavolineata* (Orthoptera: Acrididae) adults. *Insect Biochem.* **20**, 267–274.
Fiala, V., Glad, C., Martin, M., Jolivet, E. and Derridj, S. (1990). Occurrence of soluble carbohydrates on the phylloplane of maize (*Zea mays L.*) – variations in relation to leaf heterogeneity and position on the plant. *New Phytol.* **115**, 609–615.
Gangwere, S. K. (1960). The use of the mouthparts of orthoptera during feeding. *Entomol. News* **71**, 193–206.
Gangwere, S. K. (1966). Relationships between the mandibles, feeding behaviour, and damage inflicted on plants by the feeding of certain acridids (Orthoptera). *Mich. Entomol.* **1**, 13–16.
Gardiner, B. G. and Khan, M. F. (1979). A new form of insect cuticle. *Zool. J. Linn. Soc.* **66**, 91–94.
Geitmann, A. (2006). Experimental approaches used to quantify physical parameters at cellular and subcellular levels. *Am. J. Bot.* **93**, 1380–1390.
Godfrey, G. L., Miller, J. S. and Carter, D. J. (1989). 2 mouthpart modifications in larval notodontidae (Lepidoptera) – their taxonomic distributions and putative functions. *J. N. Y. Entomol. Soc.* **97**, 455–470.
Gorb, S. and Beutel, R. G. (2000). Head-capsule design and mandible control in beetle larvae: a three-dimensional approach. *J. Morphol.* **244**, 1–14.
Gordon, I. J. (2003). Browsing and grazing ruminants: are they different beasts?. *For. Ecol. Manage.* **181**, 13–21.
Gouveia, S. M., Simpson, S. J., Raubenheimer, D. and Zanotto, F. P. (2000). Patterns of respiration in *Locusta migratoria* nymphs when feeding. *Physiol. Entomol.* **25**, 88–93.
Greene, E. (1989). A diet-induced developmental polymorphism in a caterpillar. *Science* **243**, 643–646.
Griffiths, W. M. (2006). Plant–animal mechanics and bite procurement in grazing ruminants. In: *Ecology and Biomechanics. A Mechanical Approach to the Ecology of Plants and Animals* (eds Herrel, A., Speck, T. and Rowe, N. P.), pp. 101–122. Boca Raton, FL: CRC Press
Griss, C. (1990). Mandibular motor neurons of the caterpillar of the hawk moth *Manduca sexta*. *J. Comp. Neurol.* **296**, 393–402.
Griss, C., Simpson, S., Rohrbacher, J. and Rowell, C. (1991). Localization of the central nervous system of larval *Manduca sexta* (Lepidoptera: Sphingidae) of areas responsible for aspects of feeding behaviour. *J. Insect Physiol.* **7**, 477–482.
Gronenberg, W. and Ehmer, B. (1995). Tubular muscle-fibers in ants and other insects. *Zool. Anal. Complex Syst.* **99**, 68–80.
Gronenberg, W., Paul, J., Just, S. and Holldobler, B. (1997). Mandible muscle fibers in ants: fast or powerful?. *Cell Tissue Res.* **289**, 347–361.
Hairston, N. G., Smith, F. E. and Slobodkin, L. B. (1960). Community structure, population control, and competition. *Am. Nat.* **94**, 421–425.
Hillerton, J. E. (1980). The hardness of locust incisors. *Symp. Soc. Exp. Biol.* **34**, 483–484.
Hillerton, J. E. (1986). Basis of overlap of mandibles of chewing insects. *Entomol. Mon. Mag.* **122**, 229–232.
Hillerton, J. E., Reynolds, S. E. and Vincent, J. F. V. (1982). On the indentation hardness of insect cuticle. *J. Exp. Biol.* **96**, 45–52.

Hillerton, J. E., Robertson, B. and Vincent, J. F. V. (1984). The presence of zinc or manganese as the pedominant metal in the mandibles of adult, stored-product beetles. *J. Stored Prod. Res.* **20**, 133–137.

Hillerton, J. E. and Vincent, J. F. V. (1982). The specific location of zinc in insect mandibles. *J. Exp. Biol.* **101**, 333–336.

Hochuli, D. F. (1994). *Nutritional ecology of herbivorous insects: studies on their functional morphology and the mechanical properties of plants*. Bundoora, Victoria, Australia: La Trobe University.

Hochuli, D. F. (2001). Insect herbivory and ontogeny: how do growth and development influence feeding behaviour, morphology and host use? *Austral. Ecol.* **26**, 563–570.

Hochuli, D. F., Roberts, B. and Sanson, G. D. (1992). Anteriorly directed microspines in the foregut of L*ocusta migratoria* (Orthoptera: Acrididae). *Int. J. Insect Morph. Embryol.* **21**, 95–97.

Hochuli, D. F., Roberts, B. and Sanson, G. D. (1994). Foregut morphology of *Locusta migratoria* (L.) (Orthoptera: Acrdidae). *J. Aust. Entomol. Soc.* **33**, 65–69.

Hochuli, D. F., Sanson, G. D. and Roberts, B. (1993). Approximate digestibility of fibre for two locusts. *Entomol. Exp. Appl.* **66**, 187–190.

Houston, W. W. K. (1981). The life-cycles and age of *Carabus glabratus* Paykull and *Carabus problematicus* Herbst (Col, Carabidae) on Moorland in Northern England. *Ecol. Entomol.* **6**, 263–271.

Hunt, J. and Charnley, A. K. (1981). Abundance and distribution of the gut flora of the desert locust, *Schistocerca gregaria*. *J. Invertebr. Pathol.* **38**, 378–385.

Isely, F. B. (1944). Correlation between mandibular morphology and food specificity in grasshoppers. *Ann. Entomol. Soc. Am.* **37**, 47–67.

Jablonka, E. and Lamb, M. (2005). *Evolution in four dimensions – genetic, epigentic, behavioural, and symbolic variation in the history of life*. Cambridge, MA: MIT Press.

Jeronimidis, G. (1991). Mechanical and fracture properties of cellular and fibrous materials. In: *Feeding and the Texture of Food*, Vol. 44 (eds Vincent, J. F. V. and Lillford, P. J.), pp. 1–17. Cambridge, UK: Cambridge University Press

Joern, A. (2004). Variation in grasshopper (Acrididae) densities in response to fire frequency and bison grazing in tallgrass prairie. *Environ. Entomol.* **33**, 1617–1625.

Joern, A. and Behmer, S. T. (1997). Importance of dietary nitrogen and carbohydrates to survival, growth, and reproduction in adults of the grasshopper *Ageneotettix deorum* (Orthoptera: Acrididae). *Oecologia* **112**, 201–208.

Joern, A. and Gaines, S. B. (1990). Population dynamics and regulation in grasshoppers. In: *Biology of Grasshoppers* (eds Chapman, R. F. and Joern, A.), pp. 415–482. New York, USA: Wiley

Kent, K. S. and Hildebrand, J. G. (1987). Cephalic sensory pathways in the central-nervous-system of larval *Manduca sexta* (Lepidoptera, Sphingidae). *Philos. Trans. R. Soc. Lond. B* **315**, 1–36.

Larsson, S. and Ohmart, C. P. (1988). Leaf age and larval performance of the leaf beetle *Paropsis atomaria*. *Ecol. Entomol.* **13**, 19–24.

Lee, K. P., Raubenheimer, D., Behmer, S. T. and Simpson, S. J. (2003). A correlation between macronutrient balancing and insect host-plant range: Evidence from the specialist caterpillar *Spodoptera exempta* (Walker). *J. Insect Physiol.* **49**, 1161–1171.

Lee, K. P., Raubenheimer, D. and Simpson, S. J. (2004). The effects of nutritional imbalance on compensatory feeding for cellulose-mediated dietary dilution in a generalist caterpillar. *Physiol. Entomol.* **29**, 108–117.

Lentle, R. G., Hemar, Y. and Hall, C. E. (2006). Viscoelastic behaviour aids extrusion from and reabsorption of the liquid phase into the digesta plug: creep rheometry of hindgut digesta in the common brushtail possum *Trichosurus vulpecula*. *J. Comp. Physiol. B* **176**, 469–475.

Lentle, R. G., Hemar, Y., Hall, C. E. and Stafford, K. J. (2005). Periodic fluid extrusion and models of digesta mixing in the intestine of a herbivore, the common brushtail possum (*Trichosurus vulpecula*). *J. Comp. Physiol. B.* **175**, 337–347.

Lowman, M. D. and Box, J. D. (1983). Variation in leaf toughness and phenolic content among 5 species of Australian rain-forest trees. *Aust. J. Ecol.* **8**, 17–25.

Lucas, P., Choong, M. F., Tan, T. W., Turner, I. M. and Berrick, A. J. (1991). The fracture toughness of the leaf of the dicotyledon *Calophyllum inophyllum* L. (Guttiferae). *Philos. Trans. R. Soc. Lond. B* **334**, 95–106.

Lucas, P. W. (1994). Categorisation of food items relevant to oral processing. In: *The Digestive System in Mammals: Food, Form and Function* (eds Chivers, D. J. and Langer, P.). Cambidge, UK: Cambidge University Press.

Lucas, P. W. (2004). *Dental Functional Morphology. How Teeth Work*. New York: Cambridge University Press.

Lucas, P. W., Darvell, B. W., Lee, P. K. D., Yuen, T. D. B. and Choong, M. F. (1995). The toughness of plant cell walls. *Philos. Trans. R. Soc. Lond. B* **348**, 363–372.

Lucas, P. W. and Pereira, B. (1990). Estimation of the fracture toughness of leaves. *Funct. Ecol.* **4**, 819–822.

Lucas, P. W., Turner, I. M., Dominy, N. J. and Yamashita, N. (2000). Mechanical defenses to herbivory. *Ann. Bot.* **86**, 913–920.

Martin, M. M. (1983). Cellulose digestion in insects. *Comp. Biochem. Physiol. A* **75**, 313–324.

Martin, M. M. (1991). The evolution of cellulose digestion in insects. *Philos. Trans. R. Soc. Lond. B* **333**, 281–288.

Martin, M. M. and Martin, J. S. (1984). Surfactants: their role in preventing the precipitation of proteins by tannins in insect guts. *Oecologia* **61**, 342–345.

McEvoy, P. B. (1984). Increase in respiratory rate during feeding in larvae of the cinnabar moth *Tyria jacobaeae*. *Physiol. Entomol.* **9**, 191–195.

McGinnis, A. J. and Kasting, R. (1967). Dietary cellulose: effect on food consumption and growth of a grasshopper. *Can. J. Zool.* **45**, 365–367.

McGinnis, A. J. and Kasting, R. (1969). Digestibility studies with cellulose-U-C^{14} on larvae of the pale western cutworm, *Agrotis orthogona*. *J. Insect Physiol.* **15**, 5–10.

Morgan, M. R. J. (1975). A qualitative survey of the carbohydrases of the alimentary tract of the migratory locust, *Locusta migratoria migratorioides*. *J. Insect Physiol.* **21**, 1045–1053.

Morgan, M. R. J. (1976). Gut carbohydrases in locusts and grasshoppers. *Acrida* **5**, 45–58.

Mulkern, G. B. (1967). Food selection by grasshoppers. *Annu. Rev. Entomol.* **12**, 59–78.

Murdoch, W. W. (1966). Community structure, population control, and competition-a critique. *Am. Nat.* **100**, 219–226.

Nahrung, H. F., Dunstan, P. K. and Allen, G. R. (2001). Larval gregariousness and neonate establishment of the eucalypt-feeding beetle *Chrysophtharta agricola* (Coleoptera: Chrysomelidae: Paropsini). *Oikos* **94**, 358–364.

Nichols-Orians, C. M. and Schultz, J. C. (1990). Interactions among leaf toughness, chemistry, and harvesting by attine ants. *Ecol. Entomol.* **15**, 311–320.

Ohmart, C. P. and Edwards, P. B. (1991). Insect herbivory on eucalyptus. *Annu. Rev. Entomol.* **36**, 637–657.
Ohmart, C. P., Thomas, J. R. and Stewart, L. G. (1987). Nitrogen, leaf toughness and the population dynamics of *Paropsis atomaria* Oliver (Coleoptera: Chrysomelidae). *J. Aust. Entomol. Soc.* **26**, 203–207.
Pappers, S. M., van Dommelen, H., van der Velde, G. and Ouborg, N. J. (2001). Differences in morphology and reproductive traits of *Galerucella nymphaeae* from four host plant species. *Entomol. Exp. Appl.* **99**, 183–191.
Parker, R. and Ring, S. G. (2001). Aspects of the physical chemistry of starch. *J. Cereal Sci.* **34**, 1–17.
Patterson, B. D. (1983). Grasshopper mandibles and the niche variation hypothesis. *Evolution* **37**, 375–388.
Patterson, B. D. (1984). Correlation between mandibular morphology and specific diet of some desert grassland Acrididae (Orthoptera). *Am. Midl. Nat.* **111**, 296–303.
Paul, J. (2001). Mandible movements in ants. *Comp. Biochem. Physiol. A* **131**, 7–20.
Paul, J. and Gronenberg, W. (1999). Optimizing force and velocity: mandible muscle fibre attachments in ants. *J. Exp. Biol.* **202**, 797–808.
Paul, J. and Gronenberg, W. (2002). Motor control of the mandible closer muscle in ants. *J. Insect Physiol.* **48**, 255–267.
Peeters, P. J. (2002a). Correlations between leaf constituent levels and the densities of herbivorous insect guilds in an Australian forest. *Austral. Ecol.* **27**, 658–671.
Peeters, P. J. (2002b). Correlations between leaf structural traits and the densities of herbivorous insect guilds. *Biol. J. Linn. Soc.* **77**, 43–65.
Peeters, P. J., Sanson, G. and Read, J. (2007). Leaf biomechanical properties and the densities of herbivorous insect guilds. *Funct. Ecol.* **21**, 246–255.
Perez-Barberia, F. J. and Gordon, I. J. (1998). Factors affecting food comminution during chewing in ruminants: a review. *Biol. J. Linn. Soc.* **63**, 233–256.
Peterson, S. S., Scriber, J. M. and Coors, J. G. (1988). Silica, cellulose and their interactive effects on the feeding performance of the Southern Armyworm, *Spodoptera eridania* (Cramer)(Lepidoptera: Noctuidae). *J. Kansas Entomol. Soc.* **61**, 169–177.
Popadic, A., Panganiban, G., Rusch, D., Shear, W. A. and Kaufman, T. C. (1998). Molecular evidence for the gnathobasic derivation of arthropod mandibles and for the appendicular origin of the labrum and other structures. *Dev. Genes Evol.* **208**, 142–150.
Price, P. W. and Hunter, D. M. (2005). Long-term population dynamics of a sawfly show strong bottom-up effects. *J. Anim. Ecol.* **74**, 917–925.
Rast, G. F. and Braunig, P. (1997). Pilocarpine-induced motor rhythms in the isolated locust suboesophageal ganglion. *J. Exp. Biol.* **200**, 2197–2207.
Rast, G. F. and Braunig, P. (2001). Insect mouthpart motor patterns: central circuits modified for highly derived appendages. *Neuroscience* **108**, 167–176.
Raubenheimer, D. and Jones, S. A. (2006). Nutritional imbalance in an extreme generalist omnivore: tolerance and recovery through complementary food selection. *Anim. Behav.* **71**, 1253–1262.
Raubenheimer, D. and Simpson, S. J. (1993). The geometry of compensatory feeding in the locust. *Anim. Behav.* **45**, 953–964.
Raubenheimer, D. and Simpson, S. J. (1996). Meeting nutrient requirements: the roles of power and efficiency. *Ent. Exp. Appl.* **80**, 65–68.
Raubenheimer, D. and Simpson, S. J. (1997). Integrative models of nutrient balancing: application to insects and vertebrates. *Nutr. Res. Rev.* **10**, 151–179.

Raubenheimer, D. and Simpson, S. J. (1998). Nutrient transfer functions: the site of integration between feeding behaviour and nutritional physiology. *Chemoecology* **8**, 61–68.
Raubenheimer, D. and Simpson, S. J. (1999). Integrating nutrition: a geometrical approach. *Entomol. Exp. Appl.* **91**, 67–82.
Raubenheimer, D. and Simpson, S. J. (2003). Nutrient balancing in grasshoppers: behavioural and physiological correlates of dietary breadth. *J. Exp. Biol.* **206**, 1669–1681.
Raupp, M. J. (1985). Effects of leaf toughness on mandibular wear of the leaf beetle, *Plagiodera versicolora*. *Ecol. Entomol.* **10**, 73–79.
Read, S. M. and Bacic, A. (1996). Cell wall porosity and its determination. In: *Plant Cell Wall Analysis*, Vol. 17 (eds Linskens, H. F. and Jackson, J. F.), pp. 63–80. Berlin: Springer
Read, J. and Sanson, G. D. (2003). Characterizing sclerophylly: the mechanical properties of a diverse range of leaf types. *New Phytol.* **160**, 81–99.
Read, J. and Stokes, A. (2006). Plant biomechanics in an ecological context. *Am. Bot.* **93**, 1546–1565.
Roberts, A. G. and Oparka, K. J. (2003). Plasmodesmata and the control of symplastic transport. *Plant Cell Environ.* **26**, 103–124.
Roces, H. and Lighton, J. R. B. (1995). Larger bites of leaf-cutting ants. *Nature* **373**, 392–393.
Roessingh, P. and Simpson, S. J. (1984). Volumetric feedback and the control of meal size in *Schistocerca gregaria*. *Entomol. Exp. Appl.* **36**, 279–286.
Rogers, S. M. and Newland, P. L. (2003). The neurobiology of taste in insects. *Adv. Insect Physiol.* **31**, 141–204.
Rohrbacher, J. (1994a). Fictive chewing activity in motor neurons and interneurons of the suboesophageal ganglion of *Manduca sexta* larvae. *J. Comp. Physiol. A* **175**, 629–637.
Rohrbacher, J. (1994b). Mandibular premotor interneurons of larval *Manduca sexta*. *J. Comp. Physiol. A* **175**, 619–628.
Rowell, C. H. F. and Simpson, S. J. (1992). A peripheral input of thoracic origin inhibits chewing movements in the larvae of *Manduca sexta*. *J. Insect Physiol.* **38**, 475–483.
Sanson, G. (2006). The biomechanics of browsing and grazing. *Am. Bot.* **93**, 1531–1545.
Sanson, G., Read, J., Aranwela, N., Clissold, F. and Peeters, P. (2001). Measurement of leaf biomechanical properties in studies of herbivory: opportunities, problems and procedures. *Austral. Ecol.* **26**, 535–546.
Sasaki, K. and Asaoka, K. (2005). Different physiological properties in a pool of mandibular closer motor neurons in a caterpillar, *Bombyx mori*. *Neurosci. Lett.* **374**, 166–170.
Sasaki, K. and Asaoka, K. (2006). Swallowing motor pattern triggered and modified by sucrose stimulation in the larvae of the silkworm, *Bombyx mori*. *J. Insect Physiol.* **52**, 528–537.
Schoberl, T. and Jager, I. L. (2006). Wet or dry-hardness, stiffness and wear resistance of biological materials on the micron scale. *Adv. Eng. Mater.* **8**, 1164–1169.
Schofield, R. M. S., Nessen, M. H. and Richardson, K. A. (2002). Tooth hardness increases with zinc-content in mandibles of young adult leaf-cutter ants. *Naturwissenschaften* **89**, 579–583.
Schoonhoven, L. M., Jermy, T. and van Loon, J. J. A. (1998). *Insect-Plant Biology. From Physiology to Evolution*. London, UK: Chapman & Hall.

Scrivener, A. M., Slaytor, M. and Rose, H. A. (1989). Symbiont-independent digestion of cellulose and starch in *Panesthia cribrata* Saussure, an Australian wood-eating cockroach. *J. Insect Physiol.* **35**, 935–941.

Seath, I. (1977a). The effects of increasing mandibular load on electrical activity in the mandibular closer muscles during feeding in the desert locust, *Schistocerca gregaria*. *Physiol. Entomol.* **2**, 237–240.

Seath, I. (1977b). Sensory feedback in the control of mouthpart movements in the desert locust *Schistocerca gregaria*. *Physiol. Entomol.* **2**, 147–156.

Sibbing, F. A. (1991). Food processing by mastication in cyprinid fish. In: *Feeding and the Texture of Food* (eds Vincent, J. F. V. and Lillford, P. J.), pp. 57–92. Cambridge, UK: Cambridge University Press

Simpson, S. J. (1983a). Changes during the fifth-instar of *Locusta migratoria* in the rate of crop emptying and their relationship to feeding and food utilization. *Entomol. Exp. Appl.* **33**, 235–243.

Simpson, S. J. (1983b). The role of volumetric feedback from the hindgut in the regulation of meal size in fifth-instar *Locusta migratoria* nymphs. *Physiol. Entomol.* **8**, 451–467.

Simpson, S. J. (1992). Mechanoresponsive neurons in the suboesophageal ganglion of the locust. *Physiol. Entomol.* **17**, 351–369.

Simpson, S. J. (1995). Regulation of a meal: chewing insects. In: *Regulatory Mechanisms in Insect Feeding* (eds Chapman, R. F. and de Boer, G.), pp. 137–156. New York: Chapman & Hall

Simpson, S. J. and Raubenheimer, D. (1993a). The central role of the haemolymph in the regulation of nutrient intake in insects. *Physiol. Entomol.* **18**, 395–403.

Simpson, S. J. and Raubenheimer, D. (1993b). A multi-level analysis of feeding behaviour: the geometry of of nutritional decisions. *Philos. Trans. R. Soc. Lond. B* **342**, 381–402.

Simpson, S. J. and Raubenheimer, D. (1996). Feeding behaviour, sensory physiology and nutrient feedback: a unifying model. *Ent. Exp. Appl.* **80**, 55–64.

Simpson, S. J. and Raubenheimer, D. (2000). The hungry locust. *Adv. Study Behav.* **29**, 1–44.

Simpson, S. J., Raubenheimer, D. and Chambers, P. G. (1995). The mechanisms of nutritional homeostasis. In: *Regulatory Mechanisms in Insect Feeding* (eds Chapman, R. F. and de Boer, G.), pp. 251–278. New York: Chapman & Hall

Simpson, S. J., Sibly, R. M., Lee, K. P., Behmer, S. T. and Raubenheimer, D. (2004). Optimal foraging when regulating intake of multiple nutrients. *Anim. Behav.* **68**, 1299–1311.

Simpson, S. J., Simmonds, M. S. J. and Blaney, W. M. (1988a). A comparison of dietary selection behaviour in larval *Locusta migratoria* and *Spodoptera littoralis*. *Physiol. Entomol.* **13**, 225–238.

Simpson, S. J., Simmonds, M. S. J., Wheatley, A. R. and Bernays, E. A. (1988b). The control of meal termination in the locust. *Anim. Behav.* **36**, 1216–1227.

Simpson, S. J. and Simpson, C. L. (1992). Mechanisms controlling modulation by haemolymph amino acids of gustatory responsiveness in the locust. *J. Exp. Biol.* **168**, 269–287.

Slansky, F. (1993). Nutritional ecology: the fundamental quest for nutrients. In: *Caterpillars. Ecological and Evolutionary Constraints on Foraging* (eds Stamp, N. E. and Casey, T. M.). New York: Chapman and Hall.

Slansky, F. and Scriber, J. M. (1985). Food consumption and utilization. In: *Comprehensive insect physiology, biochemistry and pharmacology*, Vol. 4 (eds Kerkut, G. A. and Gilbert, L. I.). Oxford: Pergamon Press.

Slaytor, M. (1992). Cellulose digestion in termites and cockroaches: what role do symbionts play? *Comp. Biochem. Physiol. B* **103**, 775–784.
Smith, T. R. and Capinera, J. L. (2005). Mandibular morphology or some Floridian grasshoppers (Orthoptera: Acrididae). *Fla. Entomol.* **88**, 204–207.
Snodgrass, R. E. (1935). *Principles of Insect Morphology*. New York, USA: Cornall University Press.
Socha, J. J., Westneat, M. W., Harrison, J. F., Waters, J. S. and Lee, W. K. (2007). Real-time phase-contrast X-ray imaging: a new technique for the study of animal form and function. *BMC Biology*, doi:10.1186/1741-7007-5-6.
Stevenson, J. P. (1966). The normal bacterial flora of laboratory stocks of the desert locust, *Schistocerca gregaria* Forskal. *J. Invertebr. Pathol.* **8**, 205–211.
Stevenson, P. C., Blaney, W. M., Simmonds, M. J. S. and Wightman, J. A. (1993). The identification and characterization of resistance in wild-species of Arachis to Spodoptera-Litura (Lepidoptera, Noctuidae). *Bull. Entomol. Res.* **83**, 421–429.
Strong, D. R., Lawton, J. H. and Southwood, T. R. E. (1984). *Insect on Plants. Community Patterns and Mechanisms*. Oxford: Blackwell Scientific Publications.
Tepfer, M. and Taylor, I. E. P. (1981). The permeability of plant cell walls as measured by gel filtration chromatography. *Nature* **213**, 761–763.
Thompson, D. B. (1992). Consumption rates and the evolution of diet-induced plasticity in the head morphology of *Melanoplus femurrubrum* (Orthoptera: Acrididae). *Oecologia* **89**, 204–213.
Thompson, D. B. (1999). Genotype-environment interaction and the ontogeny of diet-induced phenotypic plasticity in size and shape of *Melanoplus femurrubrum* (Orthoptera: Acrididae). *J. Evol. Biol.* **12**, 38–48.
Thompson, S. N. and Redak, R. A. (2000). Interactions of dietary protein and carbohydrate determine blood sugar level and regulate nutrient selection in the insect *Manduca sexta* L. *Biochim. Biophys. Acta – General Subjects* **1523**, 91–102.
Timmins, W. A., Bellward, K., Stamp, A. J. and Reynolds, S. E. (1988). Food intake, conversion efficiency, and feeding behaviour of tobacco hornworm caterpillars given artificial diet of varying nutrient and water content. *Physiol. Entomol.* **13**, 303–314.
Trier, T. M. and Mattson, W. J. (2003). Diet-induced thermogenesis in insects: a developing concept in nutritional ecology. *Environ. Entomol.* **32**, 1–8.
Tscharntke, T. and Greiler, H.-J. (1995). Insect communities, grasses, and grasslands. *Annu. Rev. Entomol.* **40**, 535–558.
Uvarov, B. (1966). *Grasshoppers and Locusts. A Handbook of General Acridology*. Cambridge, UK: Cambridge University Press.
Van Soest, P. J. (1994). *Nutritional Ecology of the Ruminant*, 2nd ed. Ithaca, NY: Cornell University Press.
Vincent, J. F. V. (1982). The mechanical design of grass. *J. Mat. Sci.* **17**, 856–860.
Vincent, J. F. V. (1990). Fracture properties of plants. *Adv. Bot. Res.* **17**, 235–287.
Vincent, J. F. V. (1991). Strength and fracture of grasses. *J. Mat. Sci.* **26**, 1947–1950.
Vincent, J. F. V. (1992a). Introduction. In: *Biomechanics-Materials: A Practical Approach* (ed. Vincent, J. F. V.), pp. 1–8. Oxford, UK: Oxford University Press.
Vincent, J. F. V. (1992b). Plants. In: *Biomechanics-Materials: A Practical Approach* (ed. Vincent, J. F. V.), pp. 165–191. Oxford, UK: Oxford University Press.
Vincent, J. F. V. (1992c). Fracture. In: *Biomechanics-Materials: A Practical Approach* (ed. Vincent, J. F. V.), pp. 193–217. Oxford, UK: Oxford University Press.

Vincent, S. E. (2006). Sex-based divergence in head shape and diet in the Eastern lubber grasshopper (*Romalea microptera*). *Zoology* **109**, 331–338.
Vincent, J. F. V. and Wegst, U. G. K. (2004). Design and mechanical properties of insect cuticle. *Arthropod Struct. Dev.* **33**, 187–199.
Weller, S. J. (1987). *Litodonta hydromeli* Harvey (Notodontidae): description of life stages. *J. Lepid. Soc.* **41**, 187–194.
West-Eberhard, M. J. (2003). *Developmental Plasticity and Evolution*. New York: Oxford University Press.
Westneat, M. W. (2003). A biomechanical model for analysis of muscle force, power output and lower jaw motion in fishes. *J. Theor. Biol.* **223**, 269–281.
Westneat, M. W. (2004). Evolution of levers and linkages in the feeding mechanisms of fishes. *Integ. Comp. Biol*. **44**, 378–389.
Wheater, C. P. and Evans, M. E. G. (1989). The mandibular forces and pressures of some predacious coleoptera. *J. Insect Physiol.* **35**, 815–820.
Wilkie, K. C. B. (1979). The hemicelluloses of grasses and cerals. *Adv. Carbohyd. Chem. Biochem.* **36**, 215–264.
Williams, L. H. (1954). The feeding habits and food preferences of Acrididae and the factors which determine them. *Philos. Trans. R. Ent. Soc. Lond. B* **105**, 423–454.
Wilson, J. R. (1993). Organization of forage plant tissues. In: *Forage Cell Wall Structure and Digestibility*, pp. 1–32. Madison, WI, USA: American Society of Agronomy, Inc., Crop Science Society of America, Inc., Soil Science Society of America, Inc.
Wolesensky, W., Joern, A. and Logan, J. D. (2005). A model of digestion modulation in grasshoppers. *Ecol. Model.* **188**, 358–373.
Wright, I. J., Reich, P. B., Westoby, M., Ackerly, D. D., Baruch, Z., Bongers, F., Cavender-Bares, J., Chapin, T., Cornelissen, J. H. C., Diemer, M., Flexas, J., Garnier, E., Groom, P. K., Gulias, J., Hikosaka, K., Lamont, B. B., Lee, T., Lee, W., Lusk, C., Midgley, J. J., Navas, M. L., Niinemets, U., Oleksyn, J., Osada, N., Poorter, H., Poot, P., Prior, L., Pyankov, V. I., Roumet, C., Thomas, S. C., Tjoelker, M. G., Veneklaas, E. J. and Villar, R. (2004). The worldwide leaf economics spectrum. *Nature* **428**, 821–827.
Wright, W. (1992). The fracture properties of grasses and their relevance to feeding in herbivores. PhD, University of Reading.
Wright, W. and Illius, A. W. (1995). A comparative study of the fracture properties of five grasses. *Funct. Ecol.* **9**, 269–278.
Wright, W. and Vincent, J. F. V. (1996). Herbivory and the mechanics of fracture in plants. *Biol. Rev.* **71**, 401–413.
Yang, Y. (1993). The insect herbivore gut as a series of chemical reactors: mathematical modelling and empirical evaluation. PhD, University of Nebraska, Lincoln.
Yang, Y. and Joern, A. (1994). Influence of diet quality, developmental stage, and temperature on food residence time in the grasshopper *Melanoplus differentialis*. *Physiol. Zool.* **67**, 598–616.
Ylioja, T., Roinninen, H., Ayres, M. P., Rousi, M. and Price, P. W. (1999). Host-driven population dynamics in an herbivorous insect. *Proc. Natl. Acad. Sci. USA* **96**, 10735–10740.
Zanotto, F. P., Gouveia, S. M., Simpson, S. J., Raubenheimer, D. and Calder, P. C. (1997). Nutritional homeostasis in locusts: Is there a mechanism for increased energy expenditure during carbohydrate overfeeding? *J. Exp. Biol.* **200**, 2437–2448.

Zanotto, F. P., Simpson, S. J. and Raubenheimer, D. (1993). The regulation of growth by locusts through post-ingestive compensation for variation in the levels of dietary protein and carbohydrate. *Physiol. Entomol.* **18**, 425–434.

van der Zee, B., Behmer, S. T. and Simpson, S. J. (2002). Food mixing strategies in the desert locust: effects of phase, distance between foods, and food nutrient content. *Entomol. Exp. Appl.* **103**, 227–237.

Zemke-White, W. L., Clements, K. D. and Harris, P. J. (2000). Acid lysis of macroalgae by marine herbivorous fishes: effects of acid pH on cell wall porosity. *J. Exp. Mar. Biol. Ecol.* **245**, 57–68.

Index

Absolute quantities, measurement of 289–292
Acheta domesticus 5
Acrobates pygmaeus 108
Active reaction 202
Adductor muscles, mandibles 337–341
Adhesion forces, smooth attachment pads 95
Aglais 260, 263
Airflow sensors, *see* Flight stabilisation; Flow-sensing hairs
Alphelocheirus 153
Amolops frogs 104
Amphibian smooth attachment pads 108
Anisops 164
Anisotropy 110
  in smooth attachment pad fibre orientation 106
Antennae 260–272, 291
  anatomy 261–264
  function 260–261, 268–272
  oscillations 266–268
  positioning reaction 264–266, 270–272, 291
Antennal mechanosensory and motor centre (AMMC) 265–266, 271
Anurida 165, 166
Aphis fabae 95
Apis 265
Argyroneta aquatica 162
Artificial motion sensors, *see* Bio-inspired artificial motion sensors
Atomic Force Microscopy (AFM) 176
  Fluid-Interface AFM 176–177
Atractocerus brevicornis 285
Atta sexdens 354
Attachment pads 82–83
  see also Smooth attachment devices

Bees, smooth attachment pads 87
Bio-inspired artificial motion sensors 63–69
  applications 63–64
  enabling materials 64–68
  fabrication technologies 64–68
  practical considerations 68–69
Böhm's bristles 263
Bolitoglossa 108
Bombyx mori 352
Bootettix argentatus 346
Brittleness 325

Calliphora:
  airflow sensors 261–269, 272
  inertial sensors 280, 281–282, 284
  vicina 95, 281
  visual sensors 237–239, 247, 250, 253, 256, 300
  wing-load sensors 287, 288
Camnula pellucida 335
Campaniform sensilla (CS):
  antennal 263, 270–271
  halteres 281
  mechanosensory feedback in walking 195, 197–198, 209–210, 213, 216–218
  wing 287–289
    anatomy 287
    function 287–288
    role in flight stabilisation 287
Capillary attraction 128–130
Cassie–Baxter relation 137–139, 141, 158
Central pattern generators (CPGs) 203, 204–209, 216–218
Chewing, *see* Leaf chewing
Chlorophanus viridis 242
Chordotonal organs (COs) 195
  femoral (fCO) 197–199, 209, 213
Chorthippus parallelus 350
Chortoicetes terminifera 322, 336, 348
Chrysophtharta agricola 348
Cockroach:
  flow-sensing hairs 5, 13, 15, 23
  mechanosensory control of walking 201, 210, 214, 218–219
  see also Periplaneta americana
Compound eyes 245–256
  fusion of inputs from compound eyes and ocelli 259

lobula plate tangential cells (LPTCs) 246–256
adaptation and gain control 253–255
directional sensitivity 246–247, 292–294
horizontal system (HS) and vertical system (VS) cells 247–250
information provided by 255–256
optic flow parameter estimation 250–253
organisation of motion–vision pathways 246–247
significance in flight stabilisation 245
Contact angle 132–133, 134–136, 150, 168
hysteresis 139–142, 145
Coordination rules in walking 211–213
Coreus marginatus 93, 98
Coriolis force 282–283, 284, 285–286
Cupiennius salei:
flow-sensing hairs 5–7, 9–11, 53
hair arrays 13–15
hair motion models 17, 21, 26, 30–40, 59
Cuticle 144–147
composition 144–145
elastic deformation 179–180
function in water-walking insects 157–169
clasping the free surface 165–167
drag reduction and thrust generation 167–169
plastron respiration 161–165
water- and rain-proofing 158–161
morphology 145–153
stability 153–157

Damping constant R 4–5, 52
determination of 28–31
Descending interneurons (DNs) 274, 277–278, 297
Directional motion sensing 239–245, 292–295
Drag reduction, water-walking arthropods 167–169
Drosophila 250, 288, 297

Echinoderm tube feet 107
Effective elasticity module (EEM) 90–91
Elasticity, smooth attachment devices 90–92
Electrostatic forces 156
Elementary Movement Detector (EMD) model 242–244, 290
Euscorpius italicus 5
Evaporation of water drops 160
Evolution:
flow-sensing hairs 61–62
smooth attachment devices 83–86

Fabrication technologies 64–68
Feedback control 235–237
see also Mechanosensory feedback signals in walking
Femoral chordotonal organs (fCO) 197, 198, 199, 209, 213
Flagellum 263–264
Flight mechanics 234–235
Flight stabilisation 232–234, 289–301
airflow sensors 260–278
antennae 260–272
significance of 260
wind-sensitive hairs 272–278, 294–295
directional sensitivity 239–245, 292–295
feedback control 235–237
inertial sensors 278–286
haltere analogues 285–286
halteres 279–285, 292, 294, 297
significance of 278
integration of multimodal sensory inputs 295–297
measurement of disturbances not absolutes 289–292
natural-mode sensing hypothesis 297–301
visual sensors 237–259
compound eyes 245–256, 259, 292–294
directional motion sensing 239–245, 292–294
ocelli 256–258, 259
significance of 237–239
wing-load sensors 286–289
significance of 286–287
wing campaniform sensilla 287–289
Flow-sensing hairs 2–4, 272–278
absolute sensitivity 4
boundary layer thickness 9–11, 52–53

damping constant *R* 4–5, 52
determination of 28–31
dendrite coupling 8–9
evolution 61–62
flight stabilisation role 272–273
cephalic hairs 273–278, 294–295
directional sensitivity 294–295
hair arrays 11–15
viscosity-mediated coupling 36–40
length 9–11, 51–52
lever system 5–7
mass 7
modelling responses to natural flows 58–61
motion sensing in air and water 54–58
resonance frequency determination 77–78
response to transient pulsating boundary layer flow 78–80
selectivity 51–54
sensitivity 4, 51–54
sensory ecology 54–61
surface 7
surface area 51–52
torsional restoring constant *S* 4–5, 52
determination of 28–31
see also Bio-inspired artificial motion sensors; Flight stabilisation; Hair motion models
Fluid-Interface Atomic Force Microscopy 176–177
Fracture stress 326
Friction, smooth attachment devices 99–101

Gaze stabilisation 238–239, 259
Grooming 156
Gryllus bimaculatus, flow-sensing hairs 7, 9, 21
hair motion models 30–40

Hair motion models 15–40
determination of constants 28–31
hair arrays 36–40
hair geometry and physical property effects 43–50
in air 36
in water 36
medium density and viscosity effects 40–43
modelling hair responses to natural flows 58–61
physically approximate model (PAM) 15, 25–28, 43–44, 56
validation 34–36
physically exact model (PEM) 15, 17–25, 45–50, 56
validation 32–34
resonance frequency determination 77–78
single hairs 16–28
see also Flow-sensing hairs
Hairs:
macrotrichia 148–150, 151–153, 161, 168–169, 177–178
mechanosensory feedback in walking 195–198
campaniform sensilla (CS) 195, 197–198, 209–210, 213, 216–218
posture control 199
ventral coxal hair plate (vcxHP) 195–196, 198
water-walking arthropods 146–157, 162, 179
see also Flow-sensing hairs; Hair motion models
Hairy attachment pads 82
Halovelia 162
Haltere analogues 285–286
Halteres 279–285, 292
anatomy and physiology 281–282
directional sensitivity 294
function 282–285, 297
role in flight stabilisation 279–281
Hemisphaerota cyanea 102
High speed imaging 175–176
Homarus americanus 62
Horizontal system (HS) LPTCs 247–250
information provided by 255–256
optic flow parameter estimation 250–253
Hydrometra 167
Hydrophobicity 118, 142–144

Imaging techniques, solid–fluid interface 169–177
optical microscopy 173–176

scanning electron microscopy (SEM) 170–172
environmental SEM 172
wet-SEM 171–172, 180
scanning probe microscopy 176–177
Inertial sensors, *see* Flight stabilisation
Insect cuticle, *see* Cuticle
Inter-leg coordination in walking 211–213
Inverted microscopy 174, 180

Johnston's organ 264, 266, 268, 270–272, 286

L-neurons 256–257, 258
Laser-scanning-based confocal microscopy 173
Leaf chewing 319–320, 367–361
behavioural plasticity 353–354
chewing rate related to meal size 352–353
costs of consuming tough diets 354–357
mandible wear 355–357
metabolic cost of chewing 354
nutrient dilution and imbalance 355
mandible movement 337–354
changes with ontogeny 346–349
integration of during feeding 341–346
neural control of 350–354
plant fracture 322–323, 324–330, 342–346
mechanics 325–330
morphology and 328–330
plant defences 326
see also Mandible morphology
Levers 339–340
Lichao's surface 139
Load sensing, *see* Wing-load sensors
Lobula plate tangential cells (LPTCs) 244, 246–256
adaptation and gain control 253–255
directional sensitivity 246–247
horizontal system (HS) and vertical system (VS) cells 247–250
information provided by 255–256
optic flow parameter estimation 250–253
Locusta:
flight stabilisation 260–261, 263–265, 267, 273, 275–276
migratoria, leaf chewing 336, 348, 352
smooth attachment pads 86–88, 92, 96–97, 102, 105, 107

M-neurons 256
Macrotrichia 148–150, 151–152, 161, 168–169, 177–178
nanogrooves 150, 152–153, 161, 168–169, 178
Mandible morphology 323–324, 330–337
changes with ontogeny 347
nutrient assimilation and 334–336
phenotype plasticity 336–337
plant anatomy relationship 331–334
see also Leaf chewing
wear 355–357
Manduca 263, 264, 267, 285
sexta 206, 351–352
Marangoni propulsion 123
Mechanosensory feedback signals in walking 195–198, 201–204
inter-leg coordination 211–213
modifications in locomotor output 213–221
turning 218–221
walking direction 216–218
walking speed 213–215
neural network organization 204–209
posture control 199
specificity of sensory–motor influences 209–211
Medium flow receptors 3
see also Flow-sensing hairs
Melanoplus sanguinipes 335
Meniscus climbing 129
Mesovelia 121–122, 146, 152, 165–166
Micro-Electro-Mechanical Systems (MEMS) 63, 65–66, 279, 283
Microfabrication 64–68
Microvelia 146, 151–152, 160, 165, 168, 174, 179
Musca 237, 250
Mycalesis 337

Nanotube forests 143
Natural-mode sensing hypothesis 297–301

Natural selection:
flow-sensing hairs 58, 61–62
see also Evolution
Nephila clavipes 7
Neural networks controlling single-leg stepping 204–209
Neuronal adaptation 291
Notonecta 145
Nutrient acquisition from plants 320–324
mandible morphology and 334–336
see also Leaf chewing

Ocelli 256–258
fusion of inputs from compound eyes and ocelli 259
information provided by 258
organisation of ocellar pathways 256–257
significance in flight stabilisation 256
spatial integration of light intensity changes 257
Optic flow 239–242
estimation of by HS- and VS-cells 250–253
Optical microscopy 173–176
Optomotor responses 237–238
Orthetrum 263

Pedicel 262–263
pedicel-flagellum joint 264
Periplaneta americana 5
Plants:
cell walls 320–321
fracture of 322–330, 342–346
mechanics 325–330
morphology and 328–330
plant defences 326
nutrient acquisition from 320–324
mandible morphology and 334–336
see also Leaf chewing
Plastic Deformation Magnetic Assembly (PDMA) 66
Plastron respiration 161–165
Podura aquatica 166
Polydimethylsiloxane (PDMS) 65, 67
Polyurethane 65
Possums, smooth attachment pads 108
Posture control 199
Procambarus clarkii 21, 33

Rain-proofing 157–161
Reflexes:
resistance 199
visual stabilisation 237–239
flight stabilisation 239
gaze stabilisation 238–239
Resistance reflexes 199
Resonance frequency, flow-sensing hairs 77–78
Rhodnius prolixus 95
Riblet technology 167
Roughness effects:
smooth attachment pads 96
wetting and 133–139, 177–178

S-neurons 256–257
"Sandwich" adhesives 108–109
Scanning electron microscopy (SEM) 170–172
environmental SEM 172
wet-SEM 171–172, 180
Scanning probe microscopy 176–177
Scape 261
head–scape joint 261–262, 264
scape–pedicel joint 262–264
Schistocerca 272–276, 288, 289, 299
gregaria 336, 340
Selectivity 51
flow-sensing hairs 51–54
Self-motion assessment 239–242, 250–253
Sensitivity 51
flow-sensing hairs 4, 51–54
Sensorimotor integration 295–297
Sericopelma 9
Sisyrphus schaefferi 285
Smooth attachment devices 83
adaptation to fractal surfaces 104–105
adhesion forces 95
anisotropy in fibre orientation 106
aquaplaning prevention 104, 106
biometric implications 108–110
anisotropy 110
"sandwich" adhesives 108–109
surface pattern of tyres 109
surface wrinkles 109–110
comparison to other animal groups 107–108
dependence on material stiffness 96–97

elasticity 90–92
evolution 83–86
fluid 102–104
chemical composition 102
role in adhesion 102–104
frictional properties 99–101
outlook 110
passive and active pads 89–90
physical forces contributing to adhesion 95–96
roughness effects 96
size effects 98
soft in compression, strong in tension 105–106
spring model 93
surface pattern 88–89, 106
thin surface layer role 106–107
ultrastructure 86–88
viscoelasticity 92–93
Spider:
flow-sensing hairs 5–11, 23
hair arrays 13–15
plastron respiration 165
see also Specific species
Spring model, smooth attachment pads 93
State feedback 236
Sternorca 180
Stick insect 195–198, 201–202, 206–210, 213–214, 216, 219, 221
Stiffness 325–328
Stochastic resonance 4
Superhydrophobic surfaces 119
Superhydrophobicity, drag reduction and 167
Surface tension 120–131
capillary attraction 128–130
propulsion 130–131
weight support 124–128
Surface wrinkles 109–110
Surfactants 123–124

Temperature sensitivity 291–292
Tetrapod gait 211
Tettigonia viridissima 86–96, 100, 104–105, 107
Thrust generation, water-walking arthropods 167–169
Torsional restoring constant *S* 4–5, 52
determination of 28–31
Toughness 326–327
Trichobothrium, *see* Flow-sensing hairs
Trichoid sensilla 273–274
Tripod gait 211, 214
Tyre surface pattern 109

Ungui 165–167
Unit-Burst-Generator (UBG) concept 211

Van der Waals forces 153–156
Ventral coxal hair plate (vcxHP) 195–196, 198
Vertical system (VS) LPTCs 247–250, 259
information provided by 255–256
optic flow parameter estimation 250–253
Viscoelasticity, smooth attachment devices 92–93
Viscosity-mediated coupling 36–40
Visual sensors, *see* Flight stabilisation; *Specific sensors*

Walking 194–195
changing direction 216–218
changing speed 213–216
gaits 211, 214
mechanosensory feedback signals 195–198, 201–204
inter-leg coordination 211–213
modifications in locomotor output 213–221
neural network organization 204–209
posture control 199
specificity of sensory–motor influences 209–211
see also Water-walking
turning 218–221
Water droplets:
adhesion forces 168
evaporation 160
Water-repellency 118, 142–144, 168, 177–178
cuticle 144
water- and rain-proofing 157–161
Water spider 162
Water strider 147–151, 160–162, 165

Water-walking 118–120
  cuticle function 157–169
    clasping the free surface 165–167
    drag reduction and thrust generation 167–169
    plastron respiration 161–165
    water- and rain-proofing 157–161
  cuticle properties and 144–157
    composition 144–145
    morphology 145–153
    stability 153–157
  detachment from free surface 179
  submergence 161–165
  surface tension 120–131
    capillary attraction 128–130
    propulsion 130–131
    weight support 124–128
  wetting 131–144
    contact angle 132–136
    contact angle hysteresis 139–142, 145
    surface roughening and 133–139, 177–178
    variable wetting properties 180
    water-repellency 142–144
Wenzel's relation 133–137, 158
Wetting 131–144, 158–160
  speeds and depths 159–160
  variable wetting properties 180
Wing-load sensors 286–289
  significance in flight stabilisation 286–287
Wind-sensitive hairs, *see* Flow-sensing hairs
  wing campaniform sensilla 287–289
    anatomy 287
    function 288–289
    role 287

Xenos vesparum 285

Yield strength 325–326
Young's relation 132